

Advanced Structured Materials

Holm Altenbach · Svetlana Bauer ·
Victor A. Eremeyev · Gennadi I. Mikhasev ·
Nikita F. Morozov *Editors*

Recent Approaches in the Theory of Plates and Plate-Like Structures

 Springer


Advanced Structured Materials

Volume 151

Series Editors

Andreas Öchsner, Faculty of Mechanical Engineering, Esslingen University of Applied Sciences, Esslingen, Germany

Lucas F. M. da Silva, Department of Mechanical Engineering, Faculty of Engineering, University of Porto, Porto, Portugal

Holm Altenbach , Faculty of Mechanical Engineering, Otto von Guericke University Magdeburg, Magdeburg, Sachsen-Anhalt, Germany

Common engineering materials reach in many applications their limits and new developments are required to fulfil increasing demands on engineering materials. The performance of materials can be increased by combining different materials to achieve better properties than a single constituent or by shaping the material or constituents in a specific structure. The interaction between material and structure may arise on different length scales, such as micro-, meso- or macroscale, and offers possible applications in quite diverse fields.

This book series addresses the fundamental relationship between materials and their structure on the overall properties (e.g. mechanical, thermal, chemical or magnetic etc.) and applications.

The topics of *Advanced Structured Materials* include but are not limited to

- classical fibre-reinforced composites (e.g. glass, carbon or Aramid reinforced plastics)
- metal matrix composites (MMCs)
- micro porous composites
- micro channel materials
- multilayered materials
- cellular materials (e.g., metallic or polymer foams, sponges, hollow sphere structures)
- porous materials
- truss structures
- nanocomposite materials
- biomaterials
- nanoporous metals
- concrete
- coated materials
- smart materials

Advanced Structured Materials is indexed in Google Scholar and Scopus.


More information about this series at <http://www.springer.com/series/8611>

Holm Altenbach · Svetlana Bauer ·
Victor A. Eremeyev · Gennadi I. Mikhasev ·
Nikita F. Morozov
Editors

Recent Approaches in the Theory of Plates and Plate-Like Structures

 Springer

Editors

Holm Altenbach 
Fakultät für Maschinenbau
Otto-von-Guericke-Universität
Magdeburg
Magdeburg, Germany


Victor A. Eremeyev
DICAAR
University of Cagliari
Cagliari, Italy

Faculty of Civil and Environmental
Engineering
Gdansk University of Technology
Gdansk, Poland

Research Institute for Mechanics
National Research Lobachevsky State
University of Nizhni Novgorod
Nizhni Novgorod, Russia

Nikita F. Morozov
Faculty of Mathematics and Mechanics
St. Petersburg State University
St. Petersburg, Russia

Svetlana Bauer
Faculty of Mathematics and Mechanics
St. Petersburg State University
St. Petersburg, Russia

Gennadi I. Mikhasev 
Faculty of Mechanics and Mathematics
Belarusian State University
Minsk, Belarus

ISSN 1869-8433

Advanced Structured Materials

ISBN 978-3-030-87184-0

<https://doi.org/10.1007/978-3-030-87185-7>

ISSN 1869-8441 (electronic)

ISBN 978-3-030-87185-7 (eBook)

© The Editor(s) (if applicable) and The Author(s), under exclusive license to Springer Nature Switzerland AG 2022

This work is subject to copyright. All rights are solely and exclusively licensed by the Publisher, whether the whole or part of the material is concerned, specifically the rights of translation, reprinting, reuse of illustrations, recitation, broadcasting, reproduction on microfilms or in any other physical way, and transmission or information storage and retrieval, electronic adaptation, computer software, or by similar or dissimilar methodology now known or hereafter developed.

The use of general descriptive names, registered names, trademarks, service marks, etc. in this publication does not imply, even in the absence of a specific statement, that such names are exempt from the relevant protective laws and regulations and therefore free for general use.

The publisher, the authors and the editors are safe to assume that the advice and information in this book are believed to be true and accurate at the date of publication. Neither the publisher nor the authors or the editors give a warranty, expressed or implied, with respect to the material contained herein or for any errors or omissions that may have been made. The publisher remains neutral with regard to jurisdictional claims in published maps and institutional affiliations.

This Springer imprint is published by the registered company Springer Nature Switzerland AG
The registered company address is: Gewerbestrasse 11, 6330 Cham, Switzerland

*To Petr Evgenievich Tovstik,
a prominent Russian scientist
in the field of thin-walled structures
— our teacher, colleague, collaborator,
and friend.*

Preface

On December 30, 2020 in only two days after his 85th anniversary professor P.E. Tovstik, outstanding researcher and teacher, died as a result of COVID-19.

All his life was inseparably linked with the Faculty of Mathematics and Mechanics of Leningrad, and then St. Petersburg State University. In 1958 P.E. Tovstik graduated with distinction from the faculty and started the postgraduate study. After defense in 1963 his Candidate (PhD) thesis he worked in laboratory of vibrations of the Scientific Research Institute of Mathematics and Mechanics (NIIMM) at Leningrad State University. Having defended in 1968 his doctoral dissertation (Graduation), he became the Associate Professor, and then Professor of the Department of Theoretical and Applied Mechanics. Since 1978 he headed this department.

The first research projects made by P.E. Tovstik in the Laboratory of Vibrations at NIIMM under supervision of the head of the laboratory Associate Professor G.N. Bukharinov were devoted to asymptotic analysis of equations of vibrations of

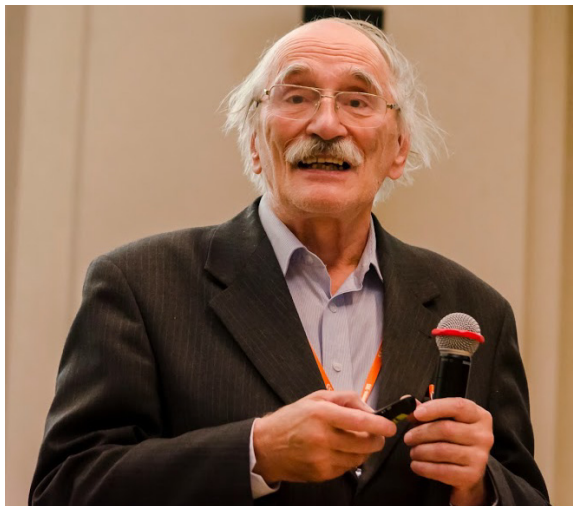


Fig. 1 Petr Evgenievich
Tovstik (1935-2020).

screw springs. The high scientific level of the young scientist research was recognized by the mathematical community in Fomin and Shilov (1970). Further he became interested in very difficult problems of thin shell theory, including problems on free vibrations of thin shells of revolution, which are described by ordinary differential equations with variable coefficients containing a small parameter at the highest derivative. For solutions of the whole class of such singularly perturbed differential equations containing turning point(s) he developed a new asymptotic method of integration. The obtained asymptotic expansions were used to find natural frequencies and modes of vibrations of shells of revolution. In 1968, these results were included into his doctoral thesis. Many of results of this research were later included in Goldeneizer et al (1979). In 1970, for a cycle of works on the theory of shells he got the first prize of Leningrad State University for scientific works.

In the mid-eighties P.E. Tovstik developed a new asymptotic method of approximate evaluation of the lower frequencies of vibrations and critical buckling loads for noncircular cylindrical and conic shells. By means of this method, simple approximate solutions for a large number of problems of the theory of vibrations and buckling of shells, for which vibrational and buckling modes are localized near so-called weakest generatrices, were obtained. Earlier for these problems only numerical results for special cases were known. In the doctoral dissertations (Dr.Sc.) of his pupils, G.I. Mikhasev and S.B. Filippov, this method was applied and developed.

Also other types of localization of vibrations were studied, including cases, when small pits are concentrated near the weakest point on a median surface or in the neighborhood of weakly supported edge. Main results of the research on the shell buckling theory, localized buckling and vibrational modes of thin elastic shells were included in Tovstik (1995); Tovstik and Smirnov (2001); Mikhasev and Tovstik (2009). In 1998, for a cycle of works "Fundamental problems of the theory of thin-walled structures" P.E. Tovstik, together with his co-authors, was awarded the State Prize of the Russian Federation in Science and Technology. In the same year he was awarded the title "Honored Scientist of the Russian Federation".

The error of the shell theory increases in nonlinear problems as deformations go up, and the main inaccuracy is associated with constitutive relations between stress-resultants/stress couples and deformations. In P.E. Tovstik works, refined elasticity relations were derived from 3D equations of the theory of elasticity. When these relations are used, the error of the non-linear shell theory has an order of the dimensionless thickness of a shell. The formulation of refined elasticity relations is a new fundamental result of the non-linear shell theory, which was included in Kabrits et al (2002). For this book the authors got the First Prize for Scientific Research from St. Petersburg State University in 2002.

In recent years, P.E. Tovstik paid attention to nonclassical problems of statics and dynamics of thin shells and plates:

1. problems of buckling and vibrations of multilayered shells and plates,
2. shells and plates lying on elastic foundations, and
3. beams, plates and shells, made of material with anisotropy of the general type, and others.

A large series of papers by P.E. Tovstik was devoted to beams, plates and shells made of linearly elastic homogeneous anisotropic materials of a general type, which elasticity relations contain 21 elastic modules. It is well known that theories of plates and shells are either based on some assumptions (hypotheses) or obtained by means of asymptotic methods permitted to derive equations for 2D structures from equations of 3D elasticity theory. P.E. Tovstik was one of the leading specialists among those, who used the last approach to derive asymptotically consistent equations for plates and shells. For anisotropic, inhomogeneous in thickness (in particular, multilayer) beams, plates and shells, the problem of constructing 2D models becomes much more complicated. Hypothesis-based methods become inapplicable or the area of their applicability narrowed significantly. At the same time, methods of asymptotic integration give reliable results confirming by test examples, for which 3D problems admit exact solutions.

Based on the generalized Timoshenko–Reissner hypotheses, free vibrations and buckling under uniform external pressure of thin elastic cylindrical shells made of material with general type anisotropy were studied and then using asymptotic method P.E. Tovstik derived approximate formulas for vibrational frequencies and modes, critical external pressure and buckling modes. The accuracy of asymptotic results was confirmed by numerical analysis with the help of finite element method. P.E. Tovstik together with N.F. Morozov solved the problems of free vibrations and buckling of the compressed transversely isotropic space, half-space and plate. Special attention was paid to analysis of buckling modes both a plate and its supporting foundation. The non-linear analysis of the energy of post-critical deformation resulted in conclusion that the buckling mode had the chess-board like form, which agreed with the experimental results.

Research interests of P.E. Tovstik was never limited to the field of thin-walled structures. For many years he headed numerous and varied industrial projects. Amazing intuition helped him to catch immediately the main features of the studied mechanical system and develop an adequate mathematical model for it. Here we mention only some of these projects.

The large cycle of applied research on analysis of lightweight metal mirrors of telescopes has been carried out in long-term cooperation with the State Optical Institute. The telescope mirror was simulated as an annular laminated plate of variable thickness. Main results of these studies were included in Bauer et al (1997).

Since 1994, P.E. Tovstik took an active part in the application of theory of shells and plates to problems of ophthalmology. Models proposed by him help in describing pathological changes in the sclera of an eye, as well as changes in the stress-strain state of eye shells after surgery. Some of the results he obtained were published in Bauer et al (2000).

In 2013–2015, P.E. Tovstik analyzed the classical Ishlinsky–Lavrentiev problem of dynamic behavior of a rod axially compressed by an applied force. Application of the two-scale asymptotic decomposition method allowed studying main and combination resonances for transverse rod vibrations caused by its axial vibrations, estimate the maximum deflection value, examine beat modes associated with transfer of energy from axial to transverse vibrations and back.

P.E. Tovstik also considered the influence of the form of initial imperfections on emergence and development of transverse vibrations. With the use of integral transforms he revealed the connection between the most dangerous imperfections and the fastest growing deflection modes found in the work by M.A. Lavrentiev and A.Yu. Ishlinsky. In 2015 for the series of papers entitled “Rod Dynamics under Axial Compression: the development of ideas by M.A. Lavrentiev and A.Yu. Ishlinsky” he (together with co-authors N.F. Morozov and A.K. Belyaev) was awarded the Lavrentiev prize of Russia Academy of Sciences for outstanding achievements in mathematics and mechanics.

Until his last days, P.E. Tovstik retained very high scientific potential, which many younger colleagues may just envy. In 2016–2020, he published more than 40 scientific paper including 27 publications in the most prestigious Russian and European journals. In addition, together with G.I. Mikhasev he published a book on localized dynamics of thin-walled structures (Mikhasev and Tovstik, 2020). In total he is the author of more than 270 scientific publications, including 11 monographs. These publications contain studies of actual and difficult problems in the most general formulations and their graceful solutions with the help of asymptotic methods, to which P.E. Tovstik made a great contribution. In all his researches, the general fundamental theoretical analyses are followed by considerations of actual examples, which he solved numerically writing and debugging computer codes. Since 1994, P.E. Tovstik was permanently a principal investigator in the team of his pupils working on a grant on thin-walled structures presented by Russian Foundation for Basic Research. Main results included in grant reports usually belonged to him.

P.E. Tovstik spared no time and efforts for the numerous pupils, among which there were 9 Doctors (Dr. Sc.) and more than 30 Candidates of Science (PhD) with whom he generously shared ideas. P.E. Tovstik founded a scientific school on application of asymptotic methods in theories of thin-walled structures. For many years P.E. Tovstik delivered a course on asymptotic methods in mechanics. Based on these lectures he and his pupils published textbooks on application of asymptotic methods in mechanics of solids (Vaillancourt and Smirnov, 1993; Bauer et al, 2007, 2015), which are widely used in Russian universities and abroad.

He headed the Department of Theoretical and Applied Mechanics of St. Petersburg State University for more than 42 years, longer, than any of his prominent predecessors. When taken the office he was the only Full Professor of the Department, but with time five more Full Professors joint the Department. The breadth of scientific interests allowed P.E. Tovstik to supervise research in all scientific areas those were studied under his predecessor Professor N.N. Polyakhov, who headed the department from 1952 till 1978. For decades P.E. Tovstik delivered a course on theoretical mechanics. He was one of the authors and the editor of the two-volume textbook on theoretical mechanics, that is planned to be published in 2021 by the St. Petersburg University Press in Russian and, simultaneously, by Springer in English.

P.E. Tovstik always successfully combined research and scientific and professional social work. He was the member of the Russian National Committee on Theoretical and Applied Mechanics, expert of the Russian Foundation for Basic Research, Editor-in-chief of the journals “Vestnik St. Petersburg University. Math-

ematics. Mechanics. Astronomy” (St. Petersburg University Press) and “Vestnik St. Petersburg University. Mathematics.” (Springer), the chairman the Dissertation Councils for Awarding Academic Degrees, the chairman of section of theoretical mechanics at St. Petersburg House of Scientists of Russian Academy of Science, the member of the Academic Council of St. Petersburg State University. He had encyclopedic knowledge in many sections of mechanics that permitted him to cope brilliantly with numerous duties.

The door to his office was always open to undergraduate and graduate students, employees of the department and colleagues from the faculty. He never refused to consult people who turned to him for help giving comprehensive, deep and clear answers and advice.

P.E. Tovstik was awarded the Order of Honor of the Russian Federation and Diploma of St. Petersburg State University “For pedagogical skill and teaching”. It should be noted that P.E. Tovstik never considered awards and prizes he got as his personal merit but as a positive assessment of the entire department.

P.E. Tovstik was a caring husband and father of two wonderful daughters. His wife Tatyana, Associate Professor at the Department of Statistical Modeling of St. Petersburg State University, was co-author of his papers on random effects. The family atmosphere of love and warmth created by her and the constant support of her husband helped his outstanding achievements in science.

The eldest daughter Tanya, PhD, Senior Researcher at the Institute of Problems in Mechanical Engineering of the Russian Academy of Science, always helped her father and was a co-author of many of his latest works. Junior, Sasha, chose a different path and became an artist.

P.E. Tovstik was a tireless traveler, and Tatyana was his indispensable companion. His other hobby was kayaking in northern rivers and lakes. Till his last days he spent hours walking through forests at the neighborhood of St. Petersburg. He was a devoted fan of Zenit, rejoicing at its victories and grieving at its losses. An avid chess player, Candidate for Master of Sport, P.E. Tovstik for forty years regularly three times a week played 12 chess blitz games with his former student S.B. Filippov and the score was always not in favor of the student.



Fig. 2 Petr Tovstik with his wife Tatyana.

Outstanding scientific achievements, high professionalism, exceptional human qualities of the excellent Russian intellectual won the honor, respect and love of his students and colleagues. We will miss P.E. Tovstik very much — a great scientist, a beloved teacher, a man of great talent. Bright and eternal memory to him.

July 2021

Magdeburg,
St. Petersburg,
Minsk,

*Holm Altenbach
Svetlana M. Bauer
Sergei B. Fillipov
Gennadi I. Mikhasev
Andrei L. Smirnov*

References

- Bauer SM, Kovalev AM, Petrov MB, Tikhomirov VV, Tovstik PE, Ulitin MI, Filippov SB (1997) Design and Optimization of Metal Mirrors for Telescopes (in Russ.). St. Petersburg University Press, St. Petersburg
- Bauer SM, Zimin BA, Tovstik PE (2000) Simplest Models of the Theory of Shells and Plates in Ophthalmology (in Russ.). St. Petersburg University Press, St. Petersburg
- Bauer SM, Filippov SB, Smirnov AL, Tovstik PE (2007) Asymptotic Methods in Mechanics of Solids (in Russ.). R&C Dynamics, Moscow-Izhevsk
- Bauer SM, Filippov SB, Smirnov AL, Tovstik PE, Vaillancourt R (2015) Asymptotic Methods in Mechanics of Solids, International Series of Numerical Mathematics, vol 167. Birkhäuser, Basel
- Fomin SV, Shilov GE (eds) (1970) Mathematics in the USSR (1958-1967), vol 2. Fizmatlit, Moscow
- Goldenevizer AL, Lidsky VB, Tovstik PE (1979) Free Vibrations of Thin Elastic Shells (in Russ.). Nauka, Moscow
- Kabrits SA, Mikhaylovsky EA, Tovstik PE, Chernykh KF, Shamina VA (2002) General Nonlinear Theory of Elastic Shells (in Russ.). St. Petersburg University Press, St. Petersburg
- Mikhasev GI, Tovstik PE (2009) Localized Vibrations and Waves in Thin Shells. Asymptotic Methods (in Russ.). Fizmatlit, Moscow
- Mikhasev GI, Tovstik PE (2020) Localized Dynamics of Thin-Walled Shells. Chapman & Hall/CRC Monographs and Research Notes in Mathematics, CRC Press. Taylor & Francis
- Tovstik PE (1995) Buckling of Thin Shells: Asymptotic Methods (in Russ.). Nauka, Moscow
- Tovstik PE, Smirnov AL (2001) Asymptotic Methods in the Buckling Theory of Elastic Shells, Series on Stability, Vibration and Control of Systems, Series A, vol 4. World Scientific, Singapore et al.
- Vaillancourt R, Smirnov AL (eds) (1993) Asymptotic Methods in Mechanics, CRM Proceedings and Lecture Notes, vol 3. American Mathematical Society, Providence, Rhode Island

Contents

| | | |
|----------|--|----|
| 1 | On one Class of Spatial Problems of Layered Plates and Applications in Seismology | 1 |
| | Mher L. Aghalovyan and Lenser A. Aghalovyan | |
| | 1.1 Introduction | 1 |
| | 1.2 Asymptotic Solutions of 3D Quasistatic Problem | 3 |
| | 1.3 Mathematically Precise Solutions | 8 |
| | 1.4 Investigation of Dynamic Processes | 10 |
| | 1.5 Conclusions | 15 |
| | References | 15 |
| 2 | Asymmetric Buckling of Heterogeneous Annular Plates | 17 |
| | Svetlana M. Bauer and Eva B. Voronkova | |
| | 2.1 Introduction | 17 |
| | 2.2 Problem Formulation | 18 |
| | 2.3 Equations for Buckling | 21 |
| | 2.4 Numerical Results | 22 |
| | 2.5 Conclusion | 24 |
| | References | 24 |
| | Appendix | 25 |
| 3 | Bending Stiffness of Multilayer Plates with Alternating Soft and Hard Layers | 27 |
| | Alexander K. Belyaev, Nikita F. Morozov, Petr E. Tovstik, and Tatiana P. Tovstik | |
| | 3.1 Introduction | 27 |
| | 3.2 Free Vibration and Bending of Multilayer Plate | 28 |
| | 3.3 Asymptotic Integration of Three-dimensional Equations | 29 |
| | 3.4 The Transverse Shear Stiffness | 31 |
| | 3.5 The Exact Value of the Shear Stiffness | 31 |
| | 3.6 About the TR Model for a Homogeneous Transversally Isotropic Plate | 32 |

| | | |
|----------|---|-----------|
| 3.7 | Other Ways to Calculate the Shear Parameter g | 32 |
| 3.8 | Numerical Results. Three-layer Plate Symmetrical in Thickness . . | 33 |
| 3.9 | Three-layer Plate Asymmetric in Thickness | 34 |
| 3.10 | Multilayer Plate | 35 |
| 3.11 | Buckling of a Multilayer Plate Under Uniform Compression | 36 |
| 3.12 | Discussion | 37 |
| | References | 38 |
| 4 | On the Bending of Multilayered Plates Considering Surface | |
| | Viscoelasticity | 39 |
| | Victor A. Eremeyev and Violetta Konopińska-Zmysłowska | |
| 4.1 | Introduction | 39 |
| 4.2 | Surface Viscoelasticity | 40 |
| 4.3 | Bending of a Plate-like Body | 42 |
| 4.4 | Conclusions | 45 |
| | References | 45 |
| 5 | Buckling of a Ring-stiffened Cylindrical Shell Under the External | |
| | Pressure | 49 |
| | Sergei B. Filippov and Grigory A. Nesterchuk | |
| 5.1 | Introduction | 49 |
| 5.2 | Formulation of the Problem | 50 |
| 5.3 | Calculation of Eigenvalues of a Beam Stiffened by Springs | 52 |
| 5.4 | Shell Parameters Optimization | 53 |
| 5.5 | Minimization of Mass | 55 |
| 5.6 | Results | 56 |
| 5.7 | Conclusion | 60 |
| | References | 61 |
| 6 | Free Vibration Corrugated Open Cylindrical Shells | 63 |
| | Alexander Ya. Grigorenko, Maksym Yu. Borysenko, Olena V. Boychuk, and Natalia P. Boreiko | |
| 6.1 | Introduction | 63 |
| 6.2 | Basic Relationships | 65 |
| 6.3 | Solution to the Test Problem | 67 |
| 6.4 | Construction of a Computational Model | 68 |
| 6.5 | Results of Numerical Calculations | 69 |
| 6.6 | Conclusion | 73 |
| | References | 73 |
| 7 | On a New Theory of the Cosserat Continuum with Applications in | |
| | Electrodynamics | 75 |
| | Elena A. Ivanova | |
| 7.1 | Introduction | 75 |
| 7.2 | Maxwell's Equations for Anisotropic Materials | 76 |
| 7.3 | A Cosserat Continuum of a Special Type: a Nonlinear Theory | 77 |

| | | |
|-----------|--|------------|
| 7.4 | A Cosserat Continuum of a Special Type: the Linear Theory | 78 |
| 7.5 | Mechanical Analogies of Physical Quantities in the Linear Theory | 79 |
| 7.6 | The Nonlinear Theory and Maxwell's Equations | 79 |
| 7.7 | On the Theories Based on Translational Degrees of Freedom | 82 |
| 7.8 | The Gauß Law for Gravitational Field | 83 |
| 7.9 | Conclusions | 85 |
| | References | 86 |
| 8 | Hierarchical Models of Conduction of Heat in Continua Contained in Prismatic Shell-like Domains | 89 |
| | George Jaiani | |
| 8.1 | Introduction | 89 |
| 8.2 | Governing System of Conduction of Heat | 90 |
| 8.3 | Mathematical Moments | 91 |
| 8.4 | Construction of Hierarchical Models | 96 |
| 8.5 | The $N = 0$ Approximation | 98 |
| 8.6 | Case of Cusped Bodies | 99 |
| 8.7 | Conclusions | 101 |
| | References | 101 |
| 9 | Dynamic Sliding Contact for a Thin Elastic Layer | 103 |
| | Julius Kaplunov, Danila A. Prikazchikov, and Tomaž Savšek | |
| 9.1 | Introduction | 104 |
| 9.2 | Two-Sided Sliding | 105 |
| 9.3 | One-Sided Sliding | 107 |
| 9.4 | Concluding Remarks | 112 |
| | References | 112 |
| 10 | Analytical Approach to the Derivation of the Stress Field of a Cylindrical Shell with a Circular Hole under Axial Tension | 115 |
| | Stanislava V. Kashtanova and Alexey V. Rzhonsnitskiy | |
| 10.1 | Introduction | 115 |
| 10.2 | Problem Formulation | 116 |
| 10.3 | Solution | 117 |
| 10.4 | New Approach | 119 |
| 10.5 | Boundary Conditions | 121 |
| 10.6 | System Investigation | 123 |
| 10.7 | Results | 125 |
| | References | 126 |
| | Appendix | 129 |
| 11 | Analysis of Solutions for Elliptic Boundary Layer in Cylindrical Shells at Edge Shock Loading | 131 |
| | Irina V. Kirillova and Leonid Y. Kossovich | |
| 11.1 | Introduction | 131 |
| 11.2 | Statement of the Problem | 132 |

| | | |
|-----------|--|------------|
| 11.3 | Equivalent Problem for the Infinite Shell | 134 |
| 11.4 | Solution of the Equivalent Problem for the Cylindrical Shell | 136 |
| | References | 139 |
| 12 | Dimension Reduction in the Plate with Tunnel Cuts | 141 |
| | Alexander G. Kolpakov and Sergei I. Rakin | |
| 12.1 | Introduction | 141 |
| 12.2 | Statement of the Problem | 142 |
| 12.3 | Problem 12.1 with Index $i = 2$ | 144 |
| | 12.3.1 In-plane Shift | 145 |
| | 12.3.2 Torsion | 145 |
| 12.4 | Problem 12.2 with Indices $i = \xi = 1, 3 = x, z$. Deformation in the Direction Perpendicular to the Fibers | 147 |
| | 12.4.1 Index $AB = 22$. Tension-compression and Bending Along the Fibers (in the $0xz$ -plane) | 148 |
| | 12.4.2 Index $AB = 11$. Tension-compression and Bending Perpendicular to the Fibers (in the $0yz$ -plane) | 149 |
| | 12.4.3 Index $AB = 12, 21$. Shift/Torsion Perpendicular to the Fibers (in the $0yz$ -plane) | 150 |
| 12.5 | Numerical Solutions | 150 |
| | 12.5.1 The Boundary Layers | 151 |
| | 12.5.2 Wrinkling of the Top and Bottom Surfaces of the Plate | 152 |
| 12.6 | The Macroscopic SSS of General Form | 152 |
| 12.7 | Conclusions | 152 |
| | References | 153 |
| 13 | Topological Optimization of Multilayer Structural Elements of MEMS/NEMS Resonators with an Adhesive Layer Subjected to Mechanical Loads | 155 |
| | Anton V. Krysko, Jan Awrejcewicz, Pavel V. Dunchenkin, Maxim V. Zhigalov, and Vadim A. Krysko | |
| 13.1 | Introduction | 155 |
| 13.2 | Statement of the Topological Optimization Problem | 157 |
| 13.3 | Case Study 1 | 158 |
| 13.4 | Case Study 2 | 161 |
| 13.5 | Concluding Remarks | 164 |
| | References | 165 |
| 14 | Forced Vibration Analysis of Laminated Piezoelectric Plates by a Strong Sampling Surfaces Formulation | 167 |
| | Gennady M. Kulikov and Svetlana V. Plotnikova | |
| 14.1 | Introduction | 167 |
| 14.2 | Basic Assumptions | 168 |
| 14.3 | Strong SAS Formulation | 169 |
| 14.4 | Free Vibrations of Simply Supported Piezoelectric Plates | 171 |
| 14.5 | Forced Vibrations of Simply Supported Piezoelectric Plates | 173 |

| | | |
|-----------|--|-----|
| 14.6 | Conclusions | 174 |
| | References | 177 |
| 15 | Asymptotic Analysis of Buckling of Layered Rectangular Plates Accounting for Boundary Conditions and Edge Effects Induced by Shears | 179 |
| | Gennadi Mikhasev and Rovshen Ataev | |
| 15.1 | Introduction | 179 |
| 15.2 | Governing Equations | 181 |
| 15.3 | Simply Supported Plate with the Edge Diaphragms | 185 |
| 15.4 | Buckling Modes Accounting for the Edge Effects | 186 |
| 15.4.1 | Layered Plates with the Reduced Young's and Shear Moduli of the same Order | 187 |
| 15.4.2 | Layered Plates with Small Reduced Shear Modulus | 195 |
| 15.5 | Analysis of Influence of Boundary Conditions and Edge Effects on Critical Force | 196 |
| 15.6 | Conclusions | 200 |
| | References | 200 |
| 16 | Semi-analytical Model for the Close-range Stress Analysis of Transverse Cracks in Composite Plates | 203 |
| | Clemens Peiler, Andreas Kappel, and Christian Mittelstedt | |
| 16.1 | Introduction | 203 |
| 16.2 | Structural Situation | 205 |
| 16.3 | Semi-analytical Approach | 206 |
| 16.3.1 | CLT Solution | 206 |
| 16.3.2 | Internal Solution | 207 |
| 16.4 | Results | 211 |
| 16.5 | Summary and Conclusions | 212 |
| | References | 212 |
| | Appendix | 215 |
| 17 | Shear Deformable Elastic Beam Models in Vibration and Sensitivity of Natural Frequencies to Warping Effects | 217 |
| | Castrenze Polizzotto, Isaac Elishakoff, and Paolo Fuschi | |
| 17.1 | Introduction | 218 |
| 17.2 | Kinematics, Stresses, and Warping Function | 220 |
| 17.3 | Equilibrium Equations and Governing Differential Equations | 223 |
| 17.4 | An Alternative Form of the Motion Equation | 225 |
| 17.4.1 | A Simplification: From Double Spectrum to Single Spectrum | 226 |
| 17.5 | Application to a Simply Supported Beam | 227 |
| 17.5.1 | Other Comments on the Obtained Numerical Results | 231 |
| 17.6 | Conclusion | 232 |
| | References | 234 |

18 Conceptual Approaches to Shells. Advances and Perspectives 237
 Oksana R. Polyakova and Tatiana P. Tovstik

18.1 Introduction 237

18.2 Historical Perspective 239

 18.2.1 On the Tension-torsion Test of Beams 239

 18.2.2 Beam Bending and Neutral Line Detection History 240

 18.2.3 To the History of the Derivation of the Shell Equations 240

18.3 Analytical Methods in the Shell Theory 242

18.4 A Mathematical View of Shells 244

18.5 On Forms of Shells 245

18.6 Problems of Modern Biomechanics 247

18.7 Micro- and Macro-scale Shells 248

18.8 The Role of Mechanics in the Development of Science 249

References 250

19 Necessary Conditions for Energy Minimizers in a Cosserat Model of Fiber-reinforced Elastic Solids 253
 Milad Shirani and David J. Steigmann

19.1 Introduction 253

19.2 Cosserat Elasticity of Fiber-reinforced Materials 254

 19.2.1 Kinematical and Constitutive Variables in Cosserat Elasticity 255

 19.2.2 Virtual Power and Equilibrium 256

 19.2.3 Fiber-matrix Interaction 257

19.3 Conservative Problems, Energy Minimizers and the Legendre-Hadamard Conditions 259

References 265

20 Vibration Control of a Non-homogeneous Circular Thin Plate 267
 Andrei L. Smirnov and Grigory P. Vasiliev

20.1 Introduction 267

20.2 Statement of the Problem 268

20.3 Boundary Eigenvalue Problem 270

20.4 Results 271

 20.4.1 Plate with the Variable Thickness 271

 20.4.2 Plate with the Variable Stiffness 272

20.5 Conclusions 275

References 275

Appendix 276

21 Modeling of an Inhomogeneous Circular Timoshenko Plate with an Elastically Supported Boundary 277
 Alexander O. Vatulyan, Olga A. Potetyunko, and Ivan V. Bogachev

21.1 Introduction 277

21.2 Statement of the Problem 279

21.3 Direct Problem Solving Method 280

- 21.4 Computational Experiments 280
- 21.5 Conclusion..... 285
- References 286

- 22 Effect of Distributed Dislocations on Large Deformations of
Cylindrical Tube made of Micropolar Elastic Material 287**
Leonid M. Zubov and Evgeniya V. Goloveshkina
- 22.1 Introduction 287
- 22.2 Input Relations 288
- 22.3 Cylindrical Tube with Distributed Dislocations 290
- 22.4 Distribution of Straight Edge Dislocations..... 293
- 22.5 Exact Solution 295
- 22.6 Conclusion..... 304
- References 304

List of Contributors

Lenser A. Aghalovyan

Institute of Mechanics of NAS of Armenia, Armeniya, e-mail: lagal@sci.am

Mher L. Aghalovyan

Institute of Mechanics of NAS of Armenia, Armeniya,

e-mail: mheraghalovyan@yahoo.com

Rovshen M. Ataev

Belarusian State University, 4 Nezavisimosti Avenue, 220030 Minsk, Belarus,

e-mail: at.rovshan@gmail.com

Jan Awrejcewicz

Department of Automation, Biomechanics and Mechatronics, Lodz University of Technology, 1/15 Stefanowskiego Str., 90-924 Łódź, Poland,

e-mail: jan.awrejcewicz@p.lodz.pl

Svetlana M. Bauer

St. Petersburg State University, 7/9 Universitetskaya nab., St. Petersburg, Russian

Federation, e-mail: s.bauer@spbu.ru

Alexander K. Belyaev

Institute for Problems in Mechanical Engineering RAS, Bolshoy pr. V. O., 61, St.

Petersburg, 199178, Russian Federation, e-mail: 13augen@mail.ru

Ivan V. Bogachev

SFU, Russian Federation, 344006, Rostov-on-Don, Bolshaya Sadovaya str., 105/42,

e-mail: bogachev89@yandex.ru

Natalia P. Boreiko

S.P. Timoshenko Institute of Mechanics, National Academy of Sciences of Ukraine,

3 Nesterova St., Kyiv, 03057 Ukraine, e-mail: nataliya.petrivna@ukr.net

Maksym Yu. Borysenko

S.P. Timoshenko Institute of Mechanics, National Academy of Sciences of Ukraine,
3 Nesterova St., Kyiv, 03057 Ukraine, e-mail: mechanics530@gmail.com

Olena V. Boychuk

Nikolaev National Agrarian University, 9 Georgy Gongadze St., Nikolaev, 54030,
Ukraine, e-mail: boychuklena27@gmail.com

Pavel V. Dunchenkin

Department of Mathematics and Modelling, Saratov State Technical University,
Politekhnikeskaya, 77, Saratov, 410054, Russian Federation,
e-mail: dunchenkin.pasha@yandex.ru

Isaac Elishakoff

Department of Ocean and Mechanical Engineering, Florida Atlantic University,
Boca Raton, FL 33431-0991, USA, e-mail: elishako@fau.edu

Victor A. Eremeyev

Gdańsk University of Technology, ul. Gabriela Narutowicza 11/12, 80-233 Gdańsk,
Poland & University of Cagliari, Via Marengo, 2, 09123 Cagliari, Italy & National
Research Lobachevsky State University of Nizhni Novgorod, 23 Prospekt Gagarina
(Gagarin Avenue) BLDG 6, Nizhni Novgorod, 603950, Russian Federation,
e-mail: vicereme@pg.edu.pl, victor.ermeev@unica.it, eremeyev.victor@gmail.com

Sergei B. Filippov

St. Petersburg State University, 7/9 University Embankment, St. Petersburg, 199034
Russian Federation, e-mail: s_b_filippov@mail.ru

Paolo Fuschi

Department PAU, University Mediterranea of Reggio Calabria, I-89124 Reggio
Calabria, Italy, e-mail: paolo.fuschi@unirc.it

Evgeniya V. Goloveshkina

Institute of Mathematics, Mechanics, and Computer Science of Southern Federal
University, Milchakova Str. 8a, Rostov-on-Don, 344090, Russian Federation,
e-mail: evgeniya.goloveshkina@yandex.ru

Alexander Ya. Grigorenko

S.P. Timoshenko Institute of Mechanics, National Academy of Sciences of Ukraine,
3 Nesterova St., Kyiv, 03057, Ukraine, e-mail: ayagrigorenko1991@gmail.com

Elena A. Ivanova

Higher School of Theoretical Mechanics, Peter the Great St.Petersburg Polytechnic
University, Polytechnicheskaya, 29, 195251, Saint-Petersburg & Institute for
Problems in Mechanical Engineering of Russian Academy of Sciences, Bolshoy pr.
V.O., 61, 199178, Saint-Petersburg, Russian Federation,
e-mail: elenaivanova239@gmail.com

George Jaiani

I. Vekua Institute of Applied Mathematics of I. Javakhishvili Tbilisi State University, 2, University Street, 0186, Tbilisi, Georgia, e-mail: george.jaiani@gmail.com

Julius Kaplunov

School of Computing and Mathematics, Keele University, Keele, Staffordshire, ST5 5BG, UK & Faculty of Industrial Engineering, 8000, Novo Mesto, Slovenia, e-mail: j.kaplunov@keele.ac.uk

Andreas Kappel

Technische Universität Darmstadt, Department of Mechanical Engineering, Institute for Lightweight Construction and Design, Germany, e-mail: andreas.kappel@klub.tu-darmstadt.de

Stanislava V. Kashtanova

Institute for Problems in Mechanical Engineering of the Russian Academy of Sciences, Russian Federation, e-mail: kastasya@yandex.ru

Irina V. Kirillova

Saratov State University, 83 Astrakhanskaya Street, Saratov, 410012, Russian Federation, e-mail: nano-bio@info.sgu.ru

Alexander G. Kolpakov

SysAn, A. Nevskogo str., 12a, 34, Novosibirsk, 630075 & Novosibirsk state university of architecture and civil engineering (Sibstrin) , 113 Leningradskay str., Novosibirsk, 630008, Russian Federation, e-mail: algk@ngs.ru

Violetta Konopińska-Zmysłowska

Gdańsk University of Technology, ul. Gabriela Narutowicza 11/12, 80-233 Gdańsk, Poland, e-mail: violetta.konopinska@pg.edu.pl

Leonid Y. Kossovich

Saratov State University, 83 Astrakhanskaya Street, Saratov, 410012, Russian Federation, e-mail: president@info.sgu.ru

Anton V. Krysko

Scientific and Educational Center of Department of Mathematics and Modelling, Saratov State Technical University, Politekhnicheskaya 77, Saratov, 410054, Russian Federation, e-mail: antonkrysko@gmail.com

Vadim A. Krysko

Department of Mathematics and Modelling, Saratov State Technical University, Politekhnicheskaya, 77, Saratov, 410054, Russian Federation, e-mail: tak@san.ru

Gennady M. Kulikov

Laboratory of Intelligent Materials and Structures, Tambov State Technical University, Sovetskaya Street, 106, Tambov 392000, Russian Federation, e-mail: gmkulikov@mail.ru

Gennady I. Mikhasev

Belarusian State University, 4 Nezavisimosti Avenue, 220030 Minsk, Belarus, e-mail: mikhasev@bsu.by

Christian Mittelstedt

Technische Universität Darmstadt, Department of Mechanical Engineering,
Institute for Lightweight Construction and Design, Germany,
e-mail: christian.mittelstedt@klub.tu-darmstadt.de

Nikita F. Morozov

Mathematics and Mechanics Faculty, St. Petersburg State University, Universitetsky
pr., 28, Stary Peterhof, 198504, Russian Federation,
e-mail: morozov@nm1016.spb.edu

Grigory A. Nesterchuk

St. Petersburg State University, 7/9 University Embankment, St. Petersburg, 199034
Russian Federation, e-mail: grigory_ne@mail.ru

Clemens Peiler

Technische Universität Darmstadt, Department of Mechanical Engineering,
Institute for Lightweight Construction and Design, Germany,
e-mail: clemens.peiler@klub.tu-darmstadt.de

Svetlana V. Plotnikova

Laboratory of Intelligent Materials and Structures, Tambov State Technical
University, Sovetskaya Street, 106, Tambov, 392000, Russian Federation,
e-mail: plotnikovasvetlana62@gmail.com

Castrenze Polizzotto

Department of Engineering, University of Palermo, I-90128 Palermo, Italy,
e-mail: castrenze.polizzotto@unipa.it

Oksana R. Polyakova

St. Petersburg State University of Architecture and Civil Engineering, 2ya
Krasnoarmejskaya ul., 4, St. Petersburg, 190005, Russian Federation,
e-mail: ksenpolyaor@yandex.ru

Olga A. Potetyunko

SFU, Rostov-on-Don, 344006, Bolshaya Sadovaya str., 105/42, Russian Federation,
e-mail: ol_potet73@mail.ru

Danila Prikazchikov

School of Computing and Mathematics, Keele University, Keele, Staffordshire, ST5
5BG, UK & Institute for Problems in Mechanical Engineering, Russian Academy
of Sciences, Saint-Petersburg, 199178, Russian Federation,
e-mail: d.prikazchikov@keele.ac.uk

Sergei I. Rakin

SysAn, A. Nevskogo str., 12a, 34, Novosibirsk, 630075 & Siberian Transport
University, 191 Dusi Kovalchuk str., Novosibirsk, 630049, Russian Federation,
e-mail: rakinsi@ngs.ru

Alexey V. Rzhonsnitskiy

Saint-Petersburg State Institute of Technology, Russian Federation,
e-mail: rzhonsnitskiy@yandex.ru

Tomaž Savšek

Faculty of Industrial Engineering, 8000, Novo Mesto, Slovenia,
e-mail: tomaz.savsek@fini-unm.si

Milad Shirani

Department of Mechanical Engineering, University of California, Berkeley, CA.
94720, USA,
e-mail: milad_shirani@berkeley.edu

Andrei L. Smirnov

St. Petersburg State University, 7/9 Universitetskaya nab., St. Petersburg, Russian
Federation, e-mail: a.l.smirnov@spbu.ru

David Steigmann

Department of Mechanical Engineering, University of California, Berkeley, CA.
94720, USA, e-mail: dsteigmann@berkeley.edu

Petr E. Tovstik

Mathematics and Mechanics Faculty, St. Petersburg State University, Universitetsky
pr., 28, Stary Peterhof, 198504, Russian Federation

Tatiana P. Tovstik

Institute for Problems in Mechanical Engineering RAS, Bolshoy pr. V. O., 61, St.
Petersburg, 199178, Russian Federation, e-mail: tovstik_t@mail.ru

Grigory P. Vasiliev

St. Petersburg State University, Russian Federation, e-mail: vasiliev.gregory@gmail.com

Alexander O. Vatulyan

SFU, Russian Federation, 344006, Rostov-on-Don, Bolshaya Sadovaya str., 105/42,
e-mail: vatulyan@aanet.ru

Eva B. Voronkova

St. Petersburg State University, 7/9 Universitetskaya nab., St. Petersburg, Russian
Federation, e-mail: e.voronkova@spbu.ru

Maxim V. Zhigalov

Department of Mathematics and Modelling, Saratov State Technical University,
Politekhnicheskaya, 77, Saratov 410054, Russian Federation, e-mail: zhi-
galovm@ya.ru

Leonid M. Zubov

Institute of Mathematics, Mechanics, and Computer Science of Southern Federal
University, Milchakova Str. 8a, Rostov-on-Don, 344090, Russian Federation,
e-mail: zubovl@yandex.ru



Chapter 1

On one Class of Spatial Problems of Layered Plates and Applications in Seismology

Mher L. Aghalovyan and Lenser A. Aghalovyan

Abstract The class of spatial nonclassical quasistatic and dynamic problems of the theory of elasticity for orthotropic layered plates was solved. We determined the stress-strain states (SSS) of Earth's Lithospheric plates and blocks of Earth's crust on the basis of data from inclinometers, strainmeters and other measuring instruments. Monitoring of changes in the stress-strain state of layered package with respect to the time makes it possible to trace the entire process of accumulation of critical deformation energy and the possibility of earthquakes occurrence.

Key words: 3D problems elasticity, Laminated plate, Asymptotic method, Seismology, Earthquake prediction

1.1 Introduction

The occurrence of strong earthquakes modern science associated with the tectonics of Lithospheric plates of planet Earth. It was established, that earthquake sources are located in narrow zones of Earth's crust (seismic zones), which are zones of tectonic interaction of adjacent Lithospheric plates (95% of earthquakes) (Pichon et al, 1973; Rikitake, 1976; Kasahara, 1981; Basar et al, 2015). Planet Earth ($R_{\text{Earth}} = 6378$ km) is nonhomogeneous and layered. It consists of Earth's Crust, Upper and Lower Mantle, Outer and Inner Cores. The distinctive feature of these layers, in particular, are significantly different velocities of propagation v_P, v_S of longitudinal (primary) P and transverse (secondary, shear) S waves in them. Earth's Crust is also layered with basic layers: sedimentary ($v_P = 2.0 \div 5.0$ km/s; $h_1 = 10 \div 25$ km), granite ($v_P = 5.5 \div 6.0$ km/s; $h_2 = 30 \div 40$ km), basaltic ($v_P = 6.5 \div 7.4$ km/s; $h_3 = 15 \div 20$ km). Part of Upper Mantle to the border with the Asthenosphere, where $v_S \approx 0$ km/s, to-

Mher L. Aghalovyan · Lenser A. Aghalovyan
Institute of Mechanics of NAS of Armenia, Armeniya,
e-mail: mheraghalovyan@yahoo.com, lagal@sci.am

gether with Earth's Crust, makes up Lithosphere. By the network of deep faults Lithosphere is divided into several large blocks which are called plates. The great Lithospheric plates of the Earths are: Euroasian, Antarctic, Pacific Ocean, Indo-Australian, South-American, North-American, African, Anatolian, Arabian, etc.

The process of earthquakes preparation includes two main stages of tectonic movements: slow (age-old) and fast (jump-like). Age-old movements may last decades, therefore they are quasistatic. Over the years, in Lithospheric plates and individual blocks of Earth's Crust deformations accumulate, which when having reached the critical value of the order 10^{-4} , and according to the data of Rikitake (1976) - the order 4.7×10^{-5} , leading to the global destruction (an earthquake). The main part of the accumulated huge potential energy of deformation is released in the form of volumetric elastic longitudinal P and shear S waves, as well as Rayleigh and Love surface waves. Always v_P speed is greater than v_S speed. By fixing the time of arrival of these waves at the given point (seismic station) by their difference, it is possible to establish the distance L of the earthquake source from the given station, and according to data of three stations, its location as the area (point) of intersection of three spheres with radii L_1, L_2, L_3 and centers at these stations. This is what most of seismic stations are doing, recording an event that has already occurred.

Fast movements are dynamic and arise as a result of the foreshock, the earthquake itself, and the aftershock. Thus, earthquakes are the result of global destruction. Consequently, for earthquakes prediction, it is necessary to determine the stress-strain states (SSS) of Lithospheric plates and blocks of the Earth's Crust and follow to their change during the time in order to identify critical states and places of their manifestation. Having values of stresses and displacements, according to known formulas, it is possible to determine the accumulated potential energy of deformation and the magnitude of the expected earthquake (Gutenberg and Richter, 1956; Kasahara, 1981).

In the twentieth century, seismologists recorded noticeable deformations (displacements of points) of Earth's surface before an earthquake (Rikitake, 1976). At the same time, the natural problem arose (Rikitake's problem) - is it possible to determine the SSS of the Lithospheric plate or the corresponding block of the Earth's Crust based on data of measured displacements of surface points and monitor its change over time, according to data of new measurements. The arose problem, however, turned out to be the non-classical problem of the theory of elasticity, since on the face surface of area the six conditions must be satisfied: the surface is free, i.e. three components of the stress tensor are equal to zero, but the values of displacements of points are known on this surface (three conditions) as a result of measurements. But in the classical theory of elasticity on the surface, three conditions are prescribed only. The asymptotic method of solving singularly perturbed differential equations made it possible to solve this problem.

First works on the asymptotic theory of plates and shells were carried out by Friedrichs (1955); Friedrichs and Dressler (1961); Gol'denveizer (1962); Green (1962); Gol'denveizer (1976). The further development of the asymptotic theory of plates and shells is associated with Bauer et al (1993); Kaplunov et al (1993); Tovstik (1995); Bauer et al (1997); Kaplunov et al (2000); Tovstik and Smirnov

(2001); Mikhasev and Tovstik (2009); Vilde et al (2010); Morozov and Tovstik (2011); Morozov et al (2016); Tovstik and Tovstik (2017). Long-term close scientific contacts of the author with Prof. A.L. Gol'denveizer contributed to the creation of the asymptotic theory of anisotropic plates and shells, the solution of fundamentally new classes of 3D problems of plates and shells (Aghalovyan, 2015a).

Returning to Rikitake's problem, we note that we have proved, that it has the unique solution, moreover, always exist the classical boundary value problem of the theory of elasticity (3 conditions on the top surface and 3 conditions on the lowest surfaces) for which it will be the solution (Aghalovyan, 2011). Rikitake's problem for the layered package of orthotropic plates, when the top surface of the package is free, but are known the values of the displacements of the points of this surface, was solved by the asymptotic method in Aghalovyan (2015a).

In order to reduce the influence of changes of external anomalous, in particular atmospheric factors, on the data caused by the truly proceeding processes inside the layered package (Lithospheric plate, block of Earth's Crust), seismologists began to place measuring instruments - inclinometers and strainmeters - inside the package at some distance from the face surface.

In this paper, asymptotic solutions of the corresponding 3D quasistatic and dynamic problems of elasticity theory are found. It is considered, that measuring instruments are located on the contact surface between second and third layers. Cases are established, when the solution becomes mathematically exact. Monitoring the solution in time, allows to identify situations when between individual layers of the package the separation (local destruction) is possible. Calculation of the potential energy of deformation makes it possible to predict global destruction - the earthquake and estimate the magnitude of the expected earthquake.

1.2 Asymptotic Solutions of 3D Quasistatic Problem

Lithospheric plates and blocks of Earth's Crust are layered, let them consist of N orthotropic layers (the case of isotropy is the special case of the considered one) and occupied the area

$$Z = \left\{ (x, y, z) : 0 \leq x \leq a, 0 \leq y \leq b, 0 \leq z \leq h, h = \sum_{j=1}^N h_j, \min(a, b) = l, h \ll l \right\},$$

where h_j is the thickness of plates (Fig. 1.1).

The process of the first stage of earthquake preparation, as it stated above, is quasi-static (age-old). For determination the stress-strain state of the package of plates, it is necessary to determine in the domain Z the solution of the equilibrium equations of the problem of the theory of elasticity:

$$\frac{\partial \sigma_{xx}^{(k)}}{\partial x} + \frac{\partial \sigma_{xy}^{(k)}}{\partial y} + \frac{\partial \sigma_{xz}^{(k)}}{\partial z} + F_x^{(k)} = 0, \quad (x, y, z), \quad k = 1, 2, \dots, N \quad (1.1)$$

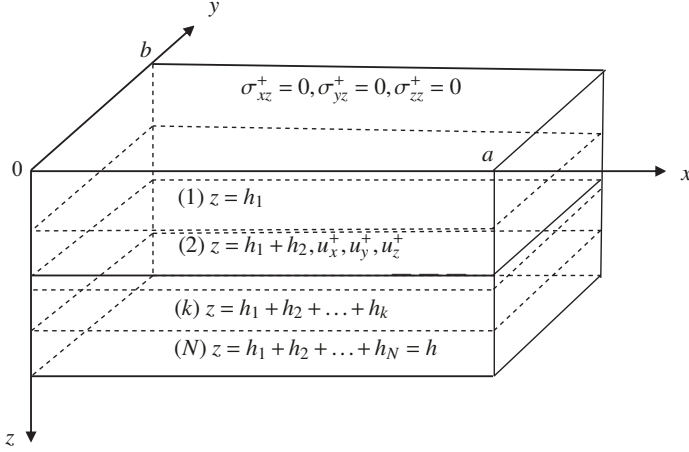


Fig. 1.1 Geometrical model of the lithospheric plates.

relations of the elasticity (generalized Hooke's law) taking into account the influence of the temperature field according to Duhamel-Neumann's model:

$$\begin{aligned} \frac{\partial u_x^{(k)}}{\partial x} &= a_{11}^{(k)} \sigma_{xx}^{(k)} + a_{12}^{(k)} \sigma_{yy}^{(k)} + a_{13}^{(k)} \sigma_{zz}^{(k)} + \alpha_{11}^{(k)} \theta^{(k)}, \quad (1, 2, 3; x, y, z), \\ \frac{\partial u_y^{(k)}}{\partial x} + \frac{\partial u_x^{(k)}}{\partial y} &= a_{66}^{(k)} \sigma_{xy}^{(k)}, \quad \frac{\partial u_y^{(k)}}{\partial z} + \frac{\partial u_z^{(k)}}{\partial y} = a_{44}^{(k)} \sigma_{yz}^{(k)}, \quad \frac{\partial u_x^{(k)}}{\partial z} + \frac{\partial u_z^{(k)}}{\partial x} = a_{55}^{(k)} \sigma_{xz}^{(k)}, \end{aligned} \quad (1.2)$$

where σ_{ij} – components of stress tensor, u_i – components of displacement vector, a_{ij} – constants of elasticity, α_{ij} – coefficients of thermal expansion, $\theta = T(x, y, z, t) - T_0(x, y, z, t)$ – temperature of field change, F_i – volumetric forces (weight).

The found solution has to satisfy free boundary conditions on the face surface $z = 0$ of the package

$$\sigma_{jz}^{(1)}(x, y, 0, t) = 0, \quad j = x, y, z \quad (1.3)$$

conditions for displacements on the plane of contact between second and third layers

$$u_j^{(2)}(x, y, \zeta_2, t_*) = u_j^{(3)}(x, y, \zeta_2, t_*) = u_j^+(x, y), \quad j = x, y, z, \quad \zeta_2 = (h_1 + h_2)/h, \quad (1.4)$$

where $u_j^+(x, y)$ – are known functions as a result of measurements carried out when $t = t_*$.

If for displacements numeric values are set, then the displacement surface have to be approximated by a polynomial, for example, Lagrange's polynomials. The solution has to satisfy the conditions for full contact between all adjacent layers:

$$\begin{aligned}\sigma_{jz}^{(n)}(x, y, \zeta_n, t) &= \sigma_{jz}^{(n+1)}(x, y, \zeta_n, t), \quad \zeta_n = \left(\sum_{i=1}^n h_i \right) / h, \\ u_j^{(n)}(x, y, \zeta_n, t_*) &= u_j^{(n+1)}(x, y, \zeta_n, t_*), \quad j = x, y, z, \quad n = 1, 2, \dots, N-1.\end{aligned}\quad (1.5)$$

For solving of this problem, in Eqs. (1.1) and relations (1.2) let we pass to dimensionless coordinates and displacements

$$\xi = x/l, \quad \eta = y/l, \quad \zeta = z/h = \varepsilon^{-1}z/l, \quad u = u_x/l, \quad v = u_y/l, \quad w = u_z/l. \quad (1.6)$$

As a result we will obtain a system singularly perturbed equations by a small parameter $\varepsilon = h/l$

$$\begin{aligned}\frac{\partial \sigma_{xx}^{(k)}}{\partial \xi} + \frac{\partial \sigma_{xy}^{(k)}}{\partial \eta} + \varepsilon^{-1} \frac{\partial \sigma_{xz}^{(k)}}{\partial \zeta} + lF_x^{(k)} &= 0, \quad (x, y, \xi, \eta), \\ \frac{\partial \sigma_{xz}^{(k)}}{\partial \xi} + \frac{\partial \sigma_{yz}^{(k)}}{\partial \eta} + \varepsilon^{-1} \frac{\partial \sigma_{zz}^{(k)}}{\partial \zeta} + lF_z^{(k)} &= 0, \\ \frac{\partial u^{(k)}}{\partial \xi} = e_1^{(k)} + \alpha_{11}^{(k)} \theta^{(k)}, \quad \frac{\partial v^{(k)}}{\partial \eta} = e_2^{(k)} + \alpha_{22}^{(k)} \theta^{(k)}, \quad \varepsilon^{-1} \frac{\partial w^{(k)}}{\partial \zeta} &= e_3^{(k)} + \alpha_{33}^{(k)} \theta^{(k)}, \\ \varepsilon^{-1} \frac{\partial v^{(k)}}{\partial \zeta} + \frac{\partial w^{(k)}}{\partial \eta} = a_{44}^{(k)} \sigma_{yz}^{(k)}, \quad \varepsilon^{-1} \frac{\partial u^{(k)}}{\partial \zeta} + \frac{\partial w^{(k)}}{\partial \xi} = a_{55}^{(k)} \sigma_{xz}^{(k)}, \\ \frac{\partial v^{(k)}}{\partial \xi} + \frac{\partial u^{(k)}}{\partial \eta} = a_{66}^{(k)} \sigma_{xy}^{(k)}, \quad e_m^{(k)} = a_{1m}^{(k)} \sigma_{xx}^{(k)} + a_{2m}^{(k)} \sigma_{yy}^{(k)} + a_{3m}^{(k)} \sigma_{zz}^{(k)}, \quad m = 1, 2, 3.\end{aligned}\quad (1.7)$$

The solution to the system (1.7) consists of solutions of the external problem I^{out} and the boundary layer (I_b) (Aghalovyan, 2015a,b). The solution to the external problem is sought in the form:

$$\begin{aligned}\sigma_{ij}^{(k)\text{out}} &= \varepsilon^{-1+s} \sigma_{ij}^{(k,s)}, \quad (i, j = x, y, z), \quad s = \overline{0, S}, \\ u^{(k)\text{out}} &= \varepsilon^s u^{(k,s)}, \quad (u, v, w), \quad k = 1, 2, \dots, N,\end{aligned}\quad (1.8)$$

where the notation $s = \overline{0, S}$ means, that by umbral (repeating) index s is taken place summed over all integer values from zero to S (Einstein's notation). By substituting (1.8) into system (1.7) and equating the corresponding coefficients in each equation at ε , we will obtain the new system, from which are uniquely determining $\sigma_{ij}^{(k,s)}$, $u^{(k,s)}$, $v^{(k,s)}$, $w^{(k,s)}$:

$$\begin{aligned}\sigma_{jz}^{(k,s)} &= \sigma_{jz0}^{(k,s)}(\xi, \eta) + \sigma_{jz*}^{(k,s)}(\xi, \eta, \zeta), \quad j = x, y, z, \\ \sigma_{xx}^{(k,s)} &= -\frac{A_{23}^{(k,s)}}{A_{11}^{(k)}} \sigma_{zz0}^{(k,s)} - \frac{\gamma_{11}^{(k,s)}}{A_{11}^{(k)}} \theta^{(k,s)} + \sigma_{xx*}^{(k,s)}(\xi, \eta, \zeta), \\ \sigma_{yy}^{(k,s)} &= -\frac{A_{13}^{(k,s)}}{A_{11}^{(k)}} \sigma_{zz0}^{(k,s)} - \frac{\gamma_{22}^{(k,s)}}{A_{11}^{(k)}} \theta^{(k,s)} + \sigma_{yy*}^{(k,s)}(\xi, \eta, \zeta),\end{aligned}$$

$$\begin{aligned}
\sigma_{xy}^{(k,s)} &= \frac{1}{a_{66}^{(k)}} \left[\frac{\partial v^{(k,s-1)}}{\partial \xi} + \frac{\partial u^{(k,s-1)}}{\partial \eta} \right], \\
u^{(k,s)} &= a_{55}^{(k)} \zeta \sigma_{xz0}^{(k,s)} + u_0^{(k,s)}(\xi, \eta) + u_*^{(k,s)}(\xi, \eta, \zeta), \\
v^{(k,s)} &= a_{44}^{(k)} \zeta \sigma_{yz0}^{(k,s)} + v_0^{(k,s)}(\xi, \eta) + v_*^{(k,s)}(\xi, \eta, \zeta), \\
w^{(k,s)} &= \frac{A_{33}^{(k)}}{A_{11}^{(k)}} \zeta \sigma_{zz0}^{(k,s)} + w_0^{(k,s)}(\xi, \eta) + \frac{B_{11}^{(k)}}{A_{11}^{(k)}} \int_{\xi_{k-1}}^{\zeta} \theta^{(k,s)} d\zeta + w_*^{(k,s)}(\xi, \eta, \zeta),
\end{aligned} \tag{1.9}$$

where

$$\begin{aligned}
\theta^{(k,0)} &= \varepsilon \theta^{(k)}, \quad \theta^{(k,0)} = 0 \quad \text{if } s \neq 0, \\
A_{11}^{(k)} &= a_{11}^{(k)} a_{22}^{(k)} - (a_{12}^{(k)})^2, \quad A_{13}^{(k)} = a_{11}^{(k)} a_{23}^{(k)} - a_{12}^{(k)} a_{13}^{(k)}, \quad A_{23}^{(k)} = a_{22}^{(k)} a_{13}^{(k)} - a_{12}^{(k)} a_{23}^{(k)}, \\
A_{33}^{(k)} &= a_{33}^{(k)} A_{11}^{(k)} - a_{13}^{(k)} A_{23}^{(k)} - a_{23}^{(k)} A_{13}^{(k)}, \quad \gamma_{11}^{(k)} = \alpha_{11}^{(k)} a_{22}^{(k)} - \alpha_{22}^{(k)} a_{12}^{(k)}, \\
\gamma_{22}^{(k)} &= \alpha_{22}^{(k)} a_{11}^{(k)} - \alpha_{11}^{(k)} a_{12}^{(k)}, \quad B_{11}^{(k)} = \alpha_{33}^{(k)} A_{11}^{(k)} - a_{13}^{(k)} \gamma_{11}^{(k)} - a_{23}^{(k)} \gamma_{22}^{(k)}, \\
\sigma_{jz*}^{(k,s)} &= - \int_{\xi_{k-1}}^{\zeta} \left[F_j^{(k,s)} + \frac{\partial \sigma_{jx}^{(k,s-1)}}{\partial \xi} + \frac{\partial \sigma_{jy}^{(k,s-1)}}{\partial \eta} \right] d\zeta, \quad j = x, y, z, \\
\sigma_{xx*}^{(k,s)} &= \frac{1}{A_{11}^{(k)}} \left[a_{22}^{(k)} \frac{\partial u^{(k,s-1)}}{\partial \xi} - a_{12}^{(k)} \frac{\partial v^{(k,s-1)}}{\partial \eta} - A_{23}^{(k)} \sigma_{zz*}^{(k,s)} \right], \\
\sigma_{yy*}^{(k,s)} &= \frac{1}{A_{11}^{(k)}} \left[a_{11}^{(k)} \frac{\partial v^{(k,s-1)}}{\partial \eta} - a_{12}^{(k)} \frac{\partial u^{(k,s-1)}}{\partial \xi} - A_{13}^{(k)} \sigma_{zz*}^{(k,s)} \right], \\
u_*^{(k,s)} &= \int_{\xi_{k-1}}^{\zeta} \left[a_{55}^{(k)} \sigma_{xz*}^{(k,s-1)} - \frac{\partial w^{(k,s-1)}}{\partial \xi} \right] d\zeta, \\
v_*^{(k,s)} &= \int_{\xi_{k-1}}^{\zeta} \left[a_{44}^{(k)} \sigma_{yz*}^{(k,s-1)} - \frac{\partial w^{(k,s-1)}}{\partial \eta} \right] d\zeta, \\
w_*^{(k,s)} &= \int_{\xi_{k-1}}^{\zeta} \left[a_{13}^{(k)} \sigma_{xx*}^{(k,s-1)} + a_{23}^{(k)} \sigma_{yy*}^{(k,s-1)} + a_{33}^{(k)} \sigma_{zz*}^{(k,s-1)} \right] d\zeta, \\
Q^{(k,m)} &= 0 \quad \text{if } m < 0.
\end{aligned} \tag{1.10}$$

The solution (1.8)-(1.10) contains unknown functions that are uniquely determined from conditions (1.3)-(1.5). Using (1.9) and satisfying conditions (1.3), we obtain:

$$\begin{aligned}
\sigma_{jz0}^{(1,s)} &= 0, \quad \sigma_{jz*}^{(1,s)} = \sigma_{jz*}^{(1,s)}(\xi, \eta, \zeta), j = x, y, z, \\
u^{(1,s)} &= u_0^{(1,s)}(\xi, \eta) + u_*^{(1,s)}(\xi, \eta, \zeta), \quad v^{(1,s)} = v_0^{(1,s)}(\xi, \eta) + v_*^{(1,s)}(\xi, \eta, \zeta), \\
w^{(1,s)} &= w_0^{(1,s)}(\xi, \eta) + w_*^{(1,s)}(\xi, \eta, \zeta) + \frac{B_{11}^{(1)}}{A_{11}^{(1)}} \int_0^\zeta \theta^{(1,s)} d\zeta.
\end{aligned} \tag{1.11}$$

In (1.11) the functions $u_0^{(1,s)}, v_0^{(1,s)}, w_0^{(1,s)}$ are for the present unknown. To determine them, we first have to satisfy conditions (1.4). According to (1.9), we will have

$$\begin{aligned}
u_0^{(2,s)}(\xi, \eta) &= u^{+(s)} - a_{55}^{(2)} \zeta_2 \sigma_{xz0}^{(2,s)} - u_*^{(2,s)}(\xi, \eta, \zeta_2), \quad (u, v; a_{55}, a_{44}; x, y) \\
u^{(2,s)}(\xi, \eta, \zeta) &= u^{+(s)} + a_{55}^{(2)} (\zeta - \zeta_2) \sigma_{xz0}^{(2,s)} + u_*^{(2,s)}(\xi, \eta, \zeta) - u_*^{(2,s)}(\xi, \eta, \zeta_2), \\
u_0^{(3,s)}(\xi, \eta) &= u^{+(s)} - a_{55}^{(3)} \zeta_2 \sigma_{xz0}^{(3,s)} - u_*^{(3,s)}(\xi, \eta, \zeta_2), \\
u^{(3,s)}(\xi, \eta, \zeta) &= u^{+(s)} + a_{55}^{(3)} (\zeta - \zeta_2) \sigma_{xz0}^{(3,s)} + u_*^{(3,s)}(\xi, \eta, \zeta) - u_*^{(3,s)}(\xi, \eta, \zeta_2), \\
&\quad (u, v; a_{55}, a_{44}; x, y), \\
w^{(2,s)}(\xi, \eta, \zeta) &= w^{+(s)} + \frac{A_{33}^{(2)}}{A_{11}^{(2)}} (\zeta - \zeta_2) \sigma_{zz0}^{(2,s)} + \frac{B_{11}^{(2)}}{A_{11}^{(2)}} \left(\int_{\zeta_1}^\zeta \theta^{(2,s)} d\zeta - \int_{\zeta_1}^{\zeta_2} \theta^{(2,s)} d\zeta \right) \\
&\quad + w_*^{(2,s)}(\xi, \eta, \zeta) - w_*^{(2,s)}(\xi, \eta, \zeta_2), \\
w^{(3,s)}(\xi, \eta, \zeta) &= w^{+(s)} + \frac{A_{33}^{(3)}}{A_{11}^{(3)}} (\zeta - \zeta_2) \sigma_{zz0}^{(3,s)} + \frac{B_{11}^{(3)}}{A_{11}^{(3)}} \left(\int_{\zeta_2}^\zeta \theta^{(3,s)} d\zeta \right) \\
&\quad + w_*^{(3,s)}(\xi, \eta, \zeta) - w_*^{(3,s)}(\xi, \eta, \zeta_2), \\
u^{+(0)} &= u_x^+ / l, \quad u^{+(s)} = 0, \quad s \neq 0 \quad (u, v, w, ; x, y, z)
\end{aligned} \tag{1.12}$$

Hence, become known all being sought values of second and third layers. Using the data (1.11), (1.12) and satisfying the contact conditions (1.5) between first and second layers let determine $u_0^{(1,s)}, v_0^{(1,s)}, w_0^{(1,s)}$ and displacements of points of the first layer:

$$\begin{aligned}
u_0^{(1,s)} &= u^{+(s)} + a_{55}^{(2)} (\zeta_1 - \zeta_2) \sigma_{xz0}^{(2,s)} + u_*^{(2,s)}(\xi, \eta, \zeta_1) - u_*^{(1,s)}(\xi, \eta, \zeta_1) - u_*^{(2,s)}(\xi, \eta, \zeta_2), \\
u^{(1,s)} &= u_0^{(1,s)} + u_*^{(1,s)}(\xi, \eta, \zeta), \quad (u, v; a_{55}, a_{44}; x, y), \\
w_0^{(1,s)} &= w^{+(s)} + \frac{A_{33}^{(2)}}{A_{11}^{(2)}} (\zeta_1 - \zeta_2) \sigma_{zz0}^{(2,s)} + w_*^{(2,s)}(\xi, \eta, \zeta_1) - w_*^{(2,s)}(\xi, \eta, \zeta_2) \\
&\quad - w_*^{(1,s)}(\xi, \eta, \zeta_1) - \frac{B_{11}^{(2)}}{A_{11}^{(2)}} \int_{\zeta_1}^{\zeta_2} \theta^{(2,s)} d\zeta, \\
w^{(1,s)} &= w_0^{(1,s)} + w_*^{(1,s)}(\xi, \eta, \zeta).
\end{aligned} \tag{1.13}$$

By satisfying the conditions (1.5) of full contact between adjacent layers, we will obtain following recurrent formulas for the consecutive determination of sought components of the stress tensor and the displacement vector of others layers:

$$\begin{aligned}
\sigma_{jz}^{(n+1,s)}(\xi, \eta, \zeta) &= \sigma_{jz0}^{(n,s)}(\xi, \eta) + \sigma_{jz^*}^{(n,s)}(\xi, \eta, \zeta_n) + \sigma_{jz^*}^{(n+1,s)}(\xi, \eta, \zeta) \\
&\quad - \sigma_{jz^*}^{(n+1,s)}(\xi, \eta, \zeta_n) \\
u^{(n+1,s)}(\xi, \eta, \zeta) &= a_{55}^{(n+1)}(\zeta - \zeta_n)\sigma_{xz0}^{(n+1,s)} + u^{(n,s)}(\xi, \eta, \zeta_n) + u_*^{(n+1,s)}(\xi, \eta, \zeta) \\
&\quad - u_*^{(n+1,s)}(\xi, \eta, \zeta_n) \\
v^{(n+1,s)}(\xi, \eta, \zeta) &= a_{44}^{(n+1)}(\zeta - \zeta_n)\sigma_{yz0}^{(n+1,s)} + v^{(n,s)}(\xi, \eta, \zeta_n) + v_*^{(n+1,s)}(\xi, \eta, \zeta) \quad (1.14) \\
&\quad - v_*^{(n+1,s)}(\xi, \eta, \zeta_n) \\
w^{(n+1,s)}(\xi, \eta, \zeta) &= \frac{A_{33}^{(n+1)}}{A_{11}^{(n+1)}}(\zeta - \zeta_n)\sigma_{zz0}^{(n+1,s)} + w^{(n,s)}(\xi, \eta, \zeta_n) + w_*^{(n+1,s)}(\xi, \eta, \zeta) \\
&\quad - w_*^{(n+1,s)}(\xi, \eta, \zeta_n) + \frac{B_{11}^{(n+1)}}{A_{11}^{(n+1)}} \int_{\zeta_n}^{\zeta} \theta^{(n+1,s)} d\zeta, n = 3, 4, \dots, N-1
\end{aligned}$$

We note, that when functions u_x^+, u_y^+, u_z^+ are polynomials from tangential coordinates ξ, η iteration process breaks at a certain approximation. As a result, we have a mathematically exact solution to the external problem.

By satisfying other conditions (1.5) of full contact between adjacent layers, we will obtain following recurrent formulas for the consecutive determination of sou The solution to the external problem, as a rule, would not satisfy boundary conditions on the lateral surface of the package. Arousing discrepancy is eliminated by solving the boundary layer. The boundary layer magnitudes exponentially decrease with removing from the lateral surface to the inside of the package. The solution to the boundary layer can be constructing and joining with the solution of the external problem by the method described in Aghalovyan (2015a). In seismology, since tangential dimensions of the package are much larger than its thickness, the boundary layer is usually neglected.

1.3 Mathematically Precise Solutions

As an illustration of the above-mentioned we present the solution of the external problem for the four-layered package, when

$$\begin{aligned} u_x^+ &= l(b_{1u} + \xi b_{2u} + \eta b_{3u}), \quad (x, y, z; u, v, w), \quad b_{ij} = \text{const}, \\ F_x^{(k)} = F_y^{(k)} = F_z^{(k)} &= 0, \quad \theta^{(k)} = 0. \end{aligned} \quad (1.15)$$

Iteration breaks after approximations $s = 0, 1$. As a result, on base of Eqs. (1.3)-(1.14), we have the mathematically precise solution:

- values for the first layer ($0 \leq \zeta \leq \zeta_1, \zeta_1 = h_1/h$)

$$\begin{aligned} u_x^{(1)} &= l(u^{(1,0)} + \varepsilon u^{(1,1)}) = u_x^+ + hb_{2w}(\zeta_2 - \zeta), \\ u_y^{(1)} &= l(v^{(1,0)} + \varepsilon v^{(1,1)}) = u_y^+ + hb_{3w}(\zeta_2 - \zeta), \\ u_z^{(1)} &= l(w^{(1,0)} + \varepsilon w^{(1,1)}) = u_z^+ + h\gamma_1(\zeta - \zeta_1) + h\gamma_2(\zeta_1 - \zeta_2), \\ \gamma_j &= \frac{1}{A_{11}^{(j)}} \left[(a_{13}^{(j)} a_{22}^{(j)} - a_{12}^{(j)} a_{23}^{(j)}) b_{2u} + (a_{23}^{(j)} a_{11}^{(j)} - a_{13}^{(j)} a_{12}^{(j)}) b_{3v} \right], \\ \sigma_{xx}^{(1)} &= \frac{1}{A_{11}^{(1)}} (a_{22}^{(1)} b_{2u} - a_{12}^{(1)} b_{3v}), \quad \sigma_{yy}^{(1)} = \frac{1}{A_{11}^{(1)}} (a_{11}^{(1)} b_{3v} - a_{12}^{(1)} b_{2u}), \\ \sigma_{xy}^{(1)} &= \frac{1}{a_{66}^{(1)}} (b_{3u} + b_{2v}), \quad \sigma_{xz}^{(1)} = \sigma_{yz}^{(1)} = \sigma_{zz}^{(1)} = 0 \end{aligned} \quad (1.16)$$

with $j = 1, 2, 3, 4$,

- values for the second layer ($\zeta_1 \leq \zeta \leq \zeta_2, \zeta_2 = (h_1 + h_2)/h$)

$$\begin{aligned} u_x^{(2)} &= u_x^+ + hb_{2w}(\zeta_2 - \zeta), \\ u_y^{(2)} &= u_y^+ + hb_{3w}(\zeta_2 - \zeta), \\ u_z^{(2)} &= u_z^+ + h\gamma_2(\zeta - \zeta_2), \\ \sigma_{xx}^{(2)} &= \frac{1}{A_{11}^{(2)}} (a_{22}^{(2)} b_{2u} - a_{12}^{(2)} b_{3v}), \quad \sigma_{yy}^{(2)} = \frac{1}{A_{11}^{(2)}} (a_{11}^{(2)} b_{3v} - a_{12}^{(2)} b_{2u}), \\ \sigma_{xy}^{(2)} &= \frac{1}{a_{66}^{(2)}} (b_{3u} + b_{2v}), \quad \sigma_{xz}^{(2)} = \sigma_{yz}^{(2)} = \sigma_{zz}^{(2)} = 0, \end{aligned} \quad (1.17)$$

- values for the third layer ($\zeta_2 \leq \zeta \leq \zeta_3, \zeta_3 = (h_1 + h_2 + h_3)/h$)

$$\begin{aligned} u_x^{(3)} &= u_x^+ + hb_{2w}(\zeta_2 - \zeta), \\ u_y^{(3)} &= u_y^+ + hb_{3w}(\zeta_2 - \zeta), \\ u_z^{(3)} &= u_z^+ + h\gamma_3(\zeta - \zeta_2), \\ \sigma_{xx}^{(3)} &= \frac{1}{A_{11}^{(3)}} (a_{22}^{(3)} b_{2u} - a_{12}^{(3)} b_{3v}), \quad \sigma_{yy}^{(3)} = \frac{1}{A_{11}^{(3)}} (a_{11}^{(3)} b_{3v} - a_{12}^{(3)} b_{2u}), \\ \sigma_{xy}^{(3)} &= \frac{1}{a_{66}^{(3)}} (b_{3u} + b_{2v}), \quad \sigma_{xz}^{(3)} = \sigma_{yz}^{(3)} = \sigma_{zz}^{(3)} = 0, \end{aligned} \quad (1.18)$$

- values for the fourth layer ($\zeta_3 \leq \zeta \leq 1$)

$$\begin{aligned}
u_x^{(4)} &= u_x^+ + hb_{2w}(\zeta_2 - \zeta), \\
u_y^{(4)} &= u_y^+ + hb_{3w}(\zeta_2 - \zeta), \\
u_z^{(4)} &= u_z^+ + h\gamma_3(\zeta_3 - \zeta_2) + h\gamma_4(\zeta - \zeta_3), \\
\sigma_{xx}^{(4)} &= \frac{1}{A_{11}^{(4)}}(a_{22}^{(4)}b_{2u} - a_{12}^{(4)}b_{3v}), \quad \sigma_{yy}^{(4)} = \frac{1}{A_{11}^{(4)}}(a_{11}^{(4)}b_{3v} - a_{12}^{(4)}b_{2u}), \\
\sigma_{xy}^{(4)} &= \frac{1}{a_{66}^{(4)}}(b_{3u} + b_{2v}), \quad \sigma_{xz}^{(4)} = \sigma_{yz}^{(4)} = \sigma_{zz}^{(4)} = 0.
\end{aligned} \tag{1.19}$$

Having the solution to the external problem, it is possible to monitor the change of the stress-strain states over the time, in accordance with regularly carried out measurements. It is possible to detect separation between some layers - when tangential stress becomes greater than the admissible value. It is possible to calculate the accumulated potential energy of deformation

$$E = \frac{1}{2} \int_V (\sigma_{xx}\varepsilon_{xx} + \sigma_{yy}\varepsilon_{yy} + \sigma_{zz}\varepsilon_{zz} + \sigma_{xy}\varepsilon_{xy} + \sigma_{xz}\varepsilon_{xz} + \sigma_{yz}\varepsilon_{yz}) dv \tag{1.20}$$

and trace when the huge potential deformation energy, accumulated during the years, reaches the critical value. At that time will arise the global destruction (earthquake). It is possible to predict the magnitude M of the expected earthquake by the formula (Kasahara, 1981; Gutenberg and Richter, 1956)

$$\lg E = 11,8 + 1,5M \tag{1.21}$$

1.4 Investigation of Dynamic Processes

To investigate related with earthquake, fast, having dynamic character processes (Foreshocks, Earthquakes, Aftershocks), it is necessary to solve in the area Z dynamic equations of the motion of the theory of elasticity:

$$\frac{\partial \sigma_{xx}^{(k)}}{\partial x} + \frac{\partial \sigma_{xy}^{(k)}}{\partial y} + \frac{\partial \sigma_{xz}^{(k)}}{\partial z} = \rho_k \frac{\partial^2 u_x^{(k)}}{\partial t^2}, \quad (x, y, z), k = 1, 2, \dots, N \tag{1.22}$$

under the elasticity relations (1.2) (usually without taking into account temperature) and conditions of full contact between adjacent layers. Let we will again assume, that the measurement data were taken from the contact surface between second and third layers. The case when data were taken from the contact surface between arbitrarily selected layers is considered in a similar way and does not cause any difficulties. The boundary conditions of the problem will be:

- the face surface of the package $z = 0$ is free

$$\sigma_{jz}^{(1)}(x, y, 0, t) = 0, \quad j = x, y, z, \quad (1.23)$$

- the values of displacement are known at $z = h_1 + h_2, \zeta = \zeta_2$

$$u_x^{(2)}(x, y, \zeta_2, t) = u_x^{(3)}(x, y, \zeta_2, t) = u_x^+(x, y) \exp(i\Omega t), \quad (x, y, z) \quad (1.24)$$

and must be satisfied conditions of full contact (1.5) between all adjacent layers. In (1.24) Ω - the frequency of oscillations of the surface of contact between second and third layers, which is registered by inclinometers, seismic stations, GPS.

The solution of the formulated problem we will find in the form:

$$\begin{aligned} \sigma_{\alpha\beta}^{(k)}(x, y, z, t) &= \sigma_{ij}^{(k)}(x, y, z) \exp(i\Omega t), \quad \alpha, \beta = x, y, z; \quad i, j = 1, 2, 3, \\ u_x^{(k)}(x, y, z, t) &= \bar{u}_x^{(k)}(x, y, z) \exp(i\Omega t), \quad (x, y, z). \end{aligned} \quad (1.25)$$

In corresponding Eqs. (1.22) and elasticity relations (1.2) dimensionless coordinates and displacements

$$\xi = \frac{x}{l}, \eta = \frac{y}{l}, \zeta = \varepsilon^{-1} \frac{z}{l}, U^{(k)} = \frac{\bar{u}_x^{(k)}}{l}, V^{(k)} = \frac{\bar{u}_y^{(k)}}{l}, W^{(k)} = \frac{\bar{u}_z^{(k)}}{l} \quad (1.26)$$

will be introduced and a system of differential equations singularly perturbed by the small parameter $\varepsilon = h/l$ can be obtained. The solution to this system is the sum of the solutions to the external problem ($I^{(k)\text{out}}$) and the boundary layer ($I_b^{(k)}$), where k - is the layer number.

The solution to the external problem is sought in the form

$$U^{(k)\text{out}} = \varepsilon^s U^{(k,s)}, \quad (U, V, W), \quad \sigma_{ij}^{(k)\text{out}} = \varepsilon^{-1+s} \sigma_{ij}^{(k,s)}, \quad s = \overline{0, S}. \quad (1.27)$$

After substituting (1.27) into the above mentioned transformed system and equating of corresponding coefficients at ε , we will get the system:

$$\frac{\partial \sigma_{11}^{(k,s-1)}}{\partial \xi} + \frac{\partial \sigma_{12}^{(k,s-1)}}{\partial \eta} + \frac{\partial \sigma_{13}^{(k,s)}}{\partial \zeta} + \Omega_*^2 \rho_k U^{(k,s)} = 0,$$

$$\frac{\partial \sigma_{12}^{(k,s-1)}}{\partial \xi} + \frac{\partial \sigma_{22}^{(k,s-1)}}{\partial \eta} + \frac{\partial \sigma_{23}^{(k,s)}}{\partial \zeta} + \Omega_*^2 \rho_k V^{(k,s)} = 0,$$

$$\frac{\partial \sigma_{13}^{(k,s-1)}}{\partial \xi} + \frac{\partial \sigma_{23}^{(k,s-1)}}{\partial \eta} + \frac{\partial \sigma_{33}^{(k,s)}}{\partial \zeta} + \Omega_*^2 \rho_k W^{(k,s)} = 0,$$

$$\frac{\partial U^{(k,s-1)}}{\partial \xi} = a_{11}^{(k)} \sigma_{11}^{(k,s)} + a_{12}^{(k)} \sigma_{22}^{(k,s)} + a_{13}^{(k)} \sigma_{33}^{(k,s)},$$

$$\frac{\partial V^{(k,s-1)}}{\partial \xi} = a_{12}^{(k)} \sigma_{11}^{(k,s)} + a_{22}^{(k)} \sigma_{22}^{(k,s)} + a_{23}^{(k)} \sigma_{33}^{(k,s)}, \quad (1.28)$$

$$\frac{\partial W^{(k,s)}}{\partial \zeta} = a_{13}^{(k)} \sigma_{11}^{(k,s)} + a_{23}^{(k)} \sigma_{22}^{(k,s)} + a_{33}^{(k)} \sigma_{33}^{(k,s)},$$

$$\frac{\partial W^{(k,s-1)}}{\partial \xi} + \frac{\partial U^{(k,s)}}{\partial \zeta} = a_{55}^{(k)} \sigma_{13}^{(k,s)},$$

$$\frac{\partial W^{(k,s-1)}}{\partial \eta} + \frac{\partial V^{(k,s)}}{\partial \zeta} = a_{44}^{(k)} \sigma_{23}^{(k,s)},$$

$$\frac{\partial V^{(k,s-1)}}{\partial \xi} + \frac{\partial U^{(k,s-1)}}{\partial \eta} = a_{66}^{(k)} \sigma_{12}^{(k,s)},$$

where $\Omega_* = h\Omega$, values of the type of $Q^{(k,m)} = 0$ at $m < 0$. From the system (1.28), stresses can be expressed through displacements according to formulas

$$\begin{aligned} \sigma_{11}^{(k,s)} &= -B_{23}^{(k)} \frac{\partial W^{(k,s)}}{\partial \zeta} + B_{22}^{(k)} \frac{\partial U^{(k,s-1)}}{\partial \xi} - B_{12}^{(k)} \frac{\partial V^{(k,s-1)}}{\partial \eta}, \\ &\quad (1, 2, ; \xi, \eta; 22, 33; U, V), \\ \sigma_{33}^{(k,s)} &= B_{11}^{(k)} \frac{\partial W^{(k,s)}}{\partial \zeta} - B_{23}^{(k)} \frac{\partial U^{(k,s-1)}}{\partial \xi} - B_{13}^{(k)} \frac{\partial V^{(k,s-1)}}{\partial \eta}, \\ \sigma_{12}^{(k,s)} &= \frac{1}{a_{66}^{(k)}} \left(\frac{\partial U^{(k,s-1)}}{\partial \eta} + \frac{\partial V^{(k,s-1)}}{\partial \xi} \right), \\ \sigma_{13}^{(k,s)} &= \frac{1}{a_{55}^{(k)}} \left(\frac{\partial W^{(k,s-1)}}{\partial \xi} + \frac{\partial U^{(k,s)}}{\partial \zeta} \right), \quad (\xi, \eta; 1, 2; U, V; a_{55}, a_{44}), \end{aligned} \quad (1.29)$$

and $B_{ij}^{(k)}$, expressed through $a_{ij}^{(k)}$ by formulas:

$$\begin{aligned} B_{11}^{(k)} &= \frac{a_{11}^{(k)} a_{22}^{(k)} - (a_{12}^{(k)})^2}{\Delta}, & B_{22}^{(k)} &= \frac{a_{22}^{(k)} a_{33}^{(k)} - (a_{23}^{(k)})^2}{\Delta}, \\ B_{33}^{(k)} &= \frac{a_{11}^{(k)} a_{33}^{(k)} - (a_{13}^{(k)})^2}{\Delta}, & B_{13}^{(k)} &= \frac{a_{11}^{(k)} a_{23}^{(k)} - a_{12}^{(k)} a_{13}^{(k)}}{\Delta}, \\ B_{23}^{(k)} &= \frac{a_{22}^{(k)} a_{13}^{(k)} - a_{12}^{(k)} a_{23}^{(k)}}{\Delta}, & B_{12}^{(k)} &= \frac{a_{12}^{(k)} a_{33}^{(k)} - a_{13}^{(k)} a_{23}^{(k)}}{\Delta}, \\ \Delta &= a_{11}^{(k)} a_{22}^{(k)} a_{33}^{(k)} + 2a_{12}^{(k)} a_{23}^{(k)} a_{13}^{(k)} - a_{11}^{(k)} (a_{23}^{(k)})^2 - a_{33}^{(k)} (a_{12}^{(k)})^2. \end{aligned} \quad (1.30)$$

For determining displacements $U^{(k,s)}$, $V^{(k,s)}$, $W^{(k,s)}$, it is necessary to substitute values $\sigma_{13}^{(k,s)}$, $\sigma_{23}^{(k,s)}$, $\sigma_{33}^{(k,s)}$, from (1.29) into the first three equations of the system (1.28). As the result we will have

$$\frac{\partial^2 U^{(k,s)}}{\partial \zeta^2} + a_{55}^{(k)} \rho_k \Omega_* U^{(k,s)} = R_u^{(k,s)}, \quad \left(U, V, W; a_{55}^{(k)}, a_{44}^{(k)}, \frac{1}{B_{11}^{(k)}} \right), \quad (1.31)$$

where

$$\begin{aligned} R_u^{(k,s)} &= -\frac{\partial^2 W^{(k,s)}}{\partial \xi \partial \zeta} - a_{55}^{(k)} \left(\frac{\partial \sigma_{11}^{(k,s-1)}}{\partial \xi} + \frac{\partial \sigma_{12}^{(k,s-1)}}{\partial \eta} \right), \quad (U, V, 1, 2; \xi, \eta; a_{55}^{(k)}, a_{44}^{(k)}), \\ R_w^{(k,s)} &= \frac{1}{B_{11}^{(k)}} \left(B_{23}^{(k)} \frac{\partial^2 U^{(k,s-1)}}{\partial \xi \partial \zeta} + B_{13}^{(k)} \frac{\partial^2 V^{(k,s-1)}}{\partial \eta \partial \zeta} - \frac{\partial \sigma_{13}^{(k,s-1)}}{\partial \xi} - \frac{\partial \sigma_{23}^{(k,s-1)}}{\partial \eta} \right). \end{aligned} \quad (1.32)$$

Solutions to Eqs. (1.31) are

$$U^{(k,s)} = C_{u1}^{(k,s)}(\xi, \eta) \sin \Omega_* \sqrt{a_{55}^{(k)}} \rho_k \zeta + C_{u2}^{(k,s)}(\zeta, \eta) \cos \Omega_* \sqrt{a_{55}^{(k)}} \rho_k \zeta + \bar{u}^{(k,s)}(\xi, \eta, \zeta) \quad (1.33)$$

$(U, V, W; a_{55}^{(k)}, a_{44}^{(k)}, \frac{1}{B_{11}^{(k)}}), \bar{u}, \bar{v}, \bar{w}$ - particular solutions to equations (1.31).

For determining included in (1.33) unknown functions $C_{u1}^{(k,s)}, C_{u2}^{(k,s)}(u, v, w)$ it is necessary to satisfy conditions (1.23), (1.24), (1.5). According to (1.29), (1.33)

$$\begin{aligned} \sigma_{13}(k, s) &= \sqrt{\frac{\rho_k}{a_{55}^{(k)}}} \left(C_{u1}^{(k,s)} \cos \Omega_* \sqrt{a_{55}^{(k)}} \rho_k \zeta - C_{u2}^{(k,s)} \sin \Omega_* \sqrt{a_{55}^{(k)}} \rho_k \zeta \right) + \sigma_{13*}^{(k,s)}, \\ \sigma_{13*}^{(k,s)}(\xi, \eta, \zeta) &= \frac{1}{a_{55}^{(k)}} \left(\frac{\partial W^{(k,s)}}{\partial \xi} + \frac{\partial \bar{U}^{(k,s)}}{\partial \zeta} \right). \end{aligned} \quad (1.34)$$

Satisfying condition (1.23) for $\sigma_{xz}^{(1)}$, we will obtain

$$C_{u1}^{(1,s)} = -\sqrt{\frac{a_{55}^{(1)}}{\rho_1}} \sigma_{13*}^{(1,s)}(\xi, \eta, 0). \quad (1.35)$$

Satisfying conditions of full contact (1.5) between first and second layers for determination $C_{u2}^{(1,s)}, C_{u1}^{(2,s)}, C_{u2}^{(2,s)}$ taking into account (1.24), we will obtain the algebraic system

$$\begin{aligned} d_{1u}^{(s)} &= b_{1u}^{(1,1)} C_{u2}^{(1,s)} + b_{2u}^{(2,1)} C_{u1}^{(2,s)} - b_{1u}^{(2,1)} C_{u2}^{(2,s)}, \\ d_{2u}^{(s)} &= a_{2u}^{(1,1)} C_{u2}^{(1,s)} - a_{1u}^{(2,1)} C_{u1}^{(2,s)} - a_{2u}^{(2,1)} C_{u2}^{(2,s)}, \\ d_{3u}^{(s)} &= a_{1u}^{(2,2)} C_{u1}^{(2,s)} + a_{2u}^{(2,2)} C_{u2}^{(2,s)}, \end{aligned} \quad (1.36)$$

where

$$\begin{aligned}
a_{1u}^{(k,j)} &= \sin \Omega_* \sqrt{a_{55}^{(k)} \rho_k \zeta_j}, \quad k = 1, 2, 3; j = 1, 2, \\
a_{2u}^{(k,j)} &= \cos \Omega_* \sqrt{a_{55}^{(k)} \rho_k \zeta_j}, \\
b_{1u}^{(k,j)} &= \sqrt{\frac{\rho_k}{a_{55}^{(k)}}} \sin \Omega_* \sqrt{a_{55}^{(k)} \rho_k \zeta_j}, \\
b_{2u}^{(k,j)} &= \sqrt{\frac{\rho_k}{a_{55}^{(k)}}} \cos \Omega_* \sqrt{a_{55}^{(k)} \rho_k \zeta_j}, \\
d_{1u}^{(s)} &= b_{2u}^{(1,1)} C_{u1}^{(1,s)} + \sigma_{13*}^{(1,s)}(\xi, \eta, \zeta_1) - \sigma_{13*}^{(2,s)}(\xi, \eta, \zeta_1), \\
d_{2u}^{(s)} &= \bar{u}^{(2,s)}(\xi, \eta, \zeta_1) - \bar{u}^{(1,s)}(\xi, \eta, \zeta_1) - a_{1u}^{(1,1)} C_{u1}^{(1,s)}, \\
d_{3u}^{(s)} &= u_x^{+(s)} - \bar{u}^{(2,s)}(\xi, \eta, \zeta_2), \quad u_x^{+(0)} = \frac{u_x^+}{l}, \quad u_x^{+(s)} = 0, s \neq 0.
\end{aligned} \tag{1.37}$$

From the system (1.36) by Cramer's formula

$$C_{u2}^{(1,s)} = \frac{\Delta_1^{(s)}}{\Delta}, \quad C_{u1}^{(2,s)} = \frac{\Delta_2^{(s)}}{\Delta}, \quad C_{u2}^{(2,s)} = \frac{\Delta_3^{(s)}}{\Delta}, \tag{1.38}$$

where

$$\Delta = \begin{vmatrix} b_{1u}^{(1,1)} & b_{2u}^{(2,1)} & -b_{1u}^{(2,1)} \\ a_{2u}^{(1,1)} & -a_{1u}^{(2,1)} & -a_{2u}^{(2,1)} \\ 0 & a_{1u}^{(2,2)} & a_{2u}^{(2,2)} \end{vmatrix}, \quad \delta^{(s)} = \begin{vmatrix} d_{1u}^{(s)} \\ d_{2u}^{(s)} \\ d_{3u}^{(s)} \end{vmatrix} \tag{1.39}$$

$\Delta_j^{(s)}$ is obtained from Δ by replacing the j -th column with $\delta^{(s)}$. Data for the values of the third layer could be obtained from conditions

$$\sigma_{13}^{(2,s)}(\xi, \eta, \zeta_2) = \sigma_{13}^{(3,s)}(\xi, \eta, \zeta_2), \quad U^{(3,s)}(\xi, \eta, \zeta_2) = u_x^{+(s)} \tag{1.40}$$

according to condition (1.24).

After satisfying conditions (1.40), for determining $C_{u1}^{(3,s)}, C_{u2}^{(3,s)}$ we will obtain the system

$$\begin{aligned}
d_{4u}^{(s)} &= b_{2u}^{(3,2)} C_{u1}^{(3,s)} - b_{1u}^{(3,2)} C_{u2}^{(3,s)}, \\
d_{5u}^{(s)} &= a_{1u}^{(3,2)} C_{u1}^{(3,s)} + a_{2u}^{(3,2)} C_{u2}^{(3,s)}, \\
d_{4u}^{(s)} &= b_{2u}^{(2,2)} C_{u1}^{(2,1)} - b_{1u}^{(2,2)} C_{u2}^{(2,s)} + \sigma_{13*}^{(2,s)}(\xi, \eta, \zeta_2) - \sigma_{13*}^{(3,s)}(\xi, \eta, \zeta_2), \\
d_{5u}^{(s)} &= u_x^{+(s)} - \bar{u}^{(3,s)}(\xi, \eta, \zeta_2)
\end{aligned} \tag{1.41}$$

consequently

$$\begin{aligned}
 C_{u1}^{(3,s)} &= \frac{\Delta_1^{(s)}}{\Delta}, & C_{u2}^{(3,s)} &= \frac{\Delta_2^{(s)}}{\Delta}, \\
 \Delta &= \begin{vmatrix} b_{2u}^{(3,2)} & -b_{1u}^{(3,2)} \\ a_{1u}^{(3,2)} & a_{2u}^{(3,2)} \end{vmatrix}, & \delta^{(s)} &= \begin{vmatrix} d_{4u}^{(s)} \\ d_{5u}^{(s)} \end{vmatrix}
 \end{aligned}
 \tag{1.42}$$

Data for subsequent layers with numbers $n > 3$ are sequentially determined from conditions of full contact between adjacent layers. Since data for the previous layer are already known, formulas similar to (1.41), (1.42) are obtained.

Data corresponding to other groups of conditions (1.23), (1.24):

$$\begin{aligned}
 \sigma_{23}^{(1)}(x, y, 0, t) &= 0, \\
 u_y^{(2)}(x, y, h_1 + h_2, t) &= u_y^{(3)}(x, y, h_1 + h_2, t) = u_y^+(x, y) \exp(i\Omega t), \\
 \sigma_{33}^{(1)}(x, y, 0, t) &= 0, \\
 u_z^{(2)}(x, y, h_1 + h_2, t) &= u_z^{(3)}(x, y, h_1 + h_2, t) = u_z^+(x, y) \exp(i\Omega t)
 \end{aligned}
 \tag{1.43}$$

could be obtained from the above-mentioned by cyclic permutation

$$\left(u_x, u_y, u_z; u, v, w; a_{55}, a_{44}, \frac{1}{B_{11}}; 13, 23, 33 \right)
 \tag{1.44}$$

1.5 Conclusions

The asymptotic solution is found for a new class of quasistatic and dynamic problems of the theory of elasticity for the layered package from orthotropic plates. It describes the behavior of Lithospheric plates and blocks of Earth’s Crust during the preparation and occurrence of earthquakes. Based on the measurement data of inclinometers and seismographs, located at a some depth from the face surface of the layered package, the stress-strain state of the layered package is found. Slow (age-old) and fast (jump-like) movements of Lithospheric plates and blocks of the Earth’s Crust, inherent to the preparation of earthquakes are considered. Based on the obtained solution, it is possible to determine the accumulated potential deformation energy, trace the entire process of earthquake preparation and predict the magnitude of the expected earthquake.

References

Aghalovyan LA (2011) On one class of three-dimensional problems of elasticity theory for plates. Proc of A Razmadze Mathematical Institute 155(1):3–10
 Aghalovyan LA (2015a) Asymptotic Theory of Anisotropic Plates and Shells. World Scientific, Singapore

- Aghalovyan LA (2015b) On some classes of 3d boundary-value problems of statics and dynamics of plates and shells. In: Altenbach H, Mikhasev GI (eds) *Shell and Membrane Theories in Mechanics and Biology*, Cham, Advanced Structured Materials, vol 45, pp 1–23
- Basar S, Coupland D, Obrist HU (2015) *The Age of Earthquakes*. Penguin Random House
- Bauer SM, Filippov SB, Smirnov AL, Tovstik PE (1993) Asymptotic methods in mechanics with applications to thin shells and plates. In: Vaillancourt R, Smirnov AL (eds) *Asymptotic Methods in Mechanics*, American Mathematical Society, Providence, Rhode Island, CRM Proceedings and Lecture Notes, vol 3, pp 3–140
- Bauer SM, Smirnov AL, Tovstik PE, Filippov SB (1997) *Asymptotic methods in examples and problems (in Russ.)*. St. Petersburg University Press, St. Petersburg
- Friedrichs KO (1955) Asymptotic phenomena in mathematical physics. *Bulletin of the American Mathematical Society* 61(6):485–504
- Friedrichs KO, Dressler RF (1961) A boundary-layer theory for elastic plates. *Communications on Pure and Applied Mathematics* 14(1):1–33
- Gol'denveizer AL (1962) Derivation of an approximate theory of bending of a plate by the method of asymptotic integration of the equations of the theory of elasticity. *Journal of Applied Mathematics and Mechanics* 26(4):1000–1025
- Gol'denveizer AL (1976) *Theory of Thin Ellastic Shells (in Russ.)*. Nauka, Moscow
- Green AE (1962) On the linear theory of thin elastic shells. *Proceedings of the Royal Society of London Series A Mathematical and Physical Sciences* 266(1325):143–160
- Gutenberg B, Richter C (1956) Earthquake magnitude, intensity, energy, and acceleration. *Bulletin of the Seismological Society of America* 46(2):105–145
- Kaplunov JD, Kossovich LY, Rogerson GA (2000) Direct asymptotic integration of the equations of transversely isotropic elasticity for a plate near cut-off frequencies. *The Quarterly Journal of Mechanics and Applied Mathematics* 53(2):323–341
- Kaplunov YD, Kirillova IV, Kossovich LY (1993) Asymptotic integration of the dynamic equations of the theory of elasticity for the case of thin shells. *Journal of Applied Mathematics and Mechanics* 57(1):95–103
- Kasahara K (1981) *Earthquake Mechanics*. Cambridge University Press, Cambridge
- Mikhasev GI, Tovstik PE (2009) *Localized Vibrations and Waves in Thin Shells. Asymptotic Methods (in Russ.)*. Fizmatlit, Moscow
- Morozov NF, Tovstik PY (2011) Bending of a two-layer beam with non-rigid contact between the layers. *Journal of Applied Mathematics and Mechanics* 75(1):77–84
- Morozov NF, Tovstik PE, Tovstik TP (2016) A continuum model of a multilayer nanosheet. *Doklady Physics* 62(11):567–570
- Pichon XL, Francheteau J, Bonnin J (1973) *Plate Tectonics*. Elsevier, Amsterdam
- Rikitake T (1976) *Earthquake Prediction*. Elsevier, Amsterdam
- Tovstik PE (1995) *Stability of Thin Shells: Asymptotic Methods (in Russ.)*. Nauka, Moscow
- Tovstik PE, Smirnov AL (2001) *Asymptotic Methods in the Buckling Theory of Elastic Shells (in Russ.)*. World Scientific, Singapore et al.
- Tovstik PE, Tovstik TP (2017) Two-dimensional model of plate made of an anisotropic inhomogeneous material. *Mechanics of Solids* 52(2):144–154
- Vilde MV, Kaplunov JD, Kossovich LY (2010) *Edge and Interface Resonance Phenomena in Elastic Bodies (in Russ.)*. Fizmatlit, Moscow



Chapter 2

Asymmetric Buckling of Heterogeneous Annular Plates

Svetlana M. Bauer and Eva B. Voronkova

Abstract Nonaxisymmetrical buckling of inhomogeneous annular plates subjected to normal pressure is studied. The effect of material heterogeneity and ratio of inner to outer radii on the buckling load is examined. The unsymmetric part of the solution is sought in terms of multiples of the harmonics of the angular coordinate. A numerical method is employed to obtain the lowest load value, which leads to the appearance of waves in the circumferential direction. For an annular plate with a small inner radius of a plate and Young's modulus, decreasing towards the outer edge, the critical pressure for unsymmetrical buckling is sufficiently lower than for a plate with constant mechanical properties. For an annulus with large inner radius, the buckling pressure and the buckling mode number increases as the Young modulus decreases towards to outer edge of a plate.

2.1 Introduction

Wrinkling of circular and annular plates and spherical shells appears in various engineering and biomechanical applications and has been studied by Adachi and Benicek (1964); Bushnell (1981); Panov and Feodosiev (1948). Under some loading types and boundary conditions a ring of large circumferential compressive stress develops near the edge of the plate (or shell) and may cause asymmetrical buckling (Cheo and Reiss, 1973; Bauer and Voronkova, 2018, 2020)).

Nonaxisymmetric buckling of circular plates subjected to surface load was first formulated and studied in Panov and Feodosiev (1948), and, later, existence and uniqueness of unsymmetric equilibrium states were proved by Morozov (1961); Piechocki (1969)). The buckling load for a clamped circular plate subjected to normal pressure load in the case of nonaxisymmetrical buckling was found numeri-

Svetlana M. Bauer · Eva B. Voronkova
St. Petersburg State University, 7/9 Universitetskaya nab., St. Petersburg, Russian Federation
e-mail: s.bauer@spbu.ru, e.voronkova@spbu.ru

cally in Cheo and Reiss (1973). The authors suspected that Panov and Feodos'ev had found unstable unsymmetric state in Panov and Feodosiev (1948), and underlined that a precise approximation of a plate under large deformations is crucial in predicting of buckling load and buckling mode shape.

The unsymmetrical buckling of a uniformly stretched circular plate under transverse pressure was investigated in Coman (2013). The author compared the asymptotic predictions for the buckling load and the corresponding wave number with numerical calculations.

Mansfield (1960) examined the buckling of an annular plate subjected to compressive or tensile radial load acting along the inner edge. Results are presented for different boundary conditions along the plate edges. The postbuckling behaviour of annular plates was studied in Radwańska and Waszczyszyn (1980). The authors reported that the buckling load and buckling mode depended on the boundary conditions, the ratio between the inner and outer radii and the loads applied. Lepik studied the effect of a circular rigid support on increase of buckling strength of an annulus (Lepik, 2002).

Coman (2010) investigated the role of polar orthotropy in relation to a wrinkling problem for annular thin plates in tension. The author identified three parameters responsible for the wrinkling mechanism. Asymmetric buckling of buckling of circular and annular plates which are stiffened by a cylindrical shell examined in Burmeister (2018).

Stability of axisymmetric equilibrium states for nonuniform circular plates and spherical caps was studied in Bauer and Voronkova (2018, 2020). This paper deals with buckling of an annular plates with nonuniform mechanical characteristics. The effect of spatially varying elastic properties and geometry of an annulus (the ratio between the inner and outer radii) is examined.

2.2 Problem Formulation

Consider an annular plate of inner radius R_m , outer radius R , and thickness h ($h/R \ll 1$), subjected to normal pressure P , as illustrated in Fig. 2.1. The plate material is assumed to be linearly isotropic with spatially varying Young's modulus. The nonlinear governing system of equations for a plate with material inhomogeneity can be written in terms of the normal displacement w and the stress function F , namely

$$\begin{aligned} D\Delta\Delta w + \frac{\partial D}{\partial r} L_1^+(w) + \frac{\partial^2 D}{\partial r^2} L_2^+(w) &= P + L(w, F), \\ \frac{\Delta\Delta F}{E} + \frac{\partial}{\partial r} \left(\frac{1}{E} \right) L_1^-(F) + \frac{\partial^2}{\partial r^2} \left(\frac{1}{E} \right) L_2^-(F) &= -\frac{h}{2} L(w, w), \end{aligned} \quad (2.1)$$

$$(\cdot)' = \partial(\cdot)/\partial r, \quad (\dot{\cdot}) = \partial(\cdot)/\partial \theta,$$

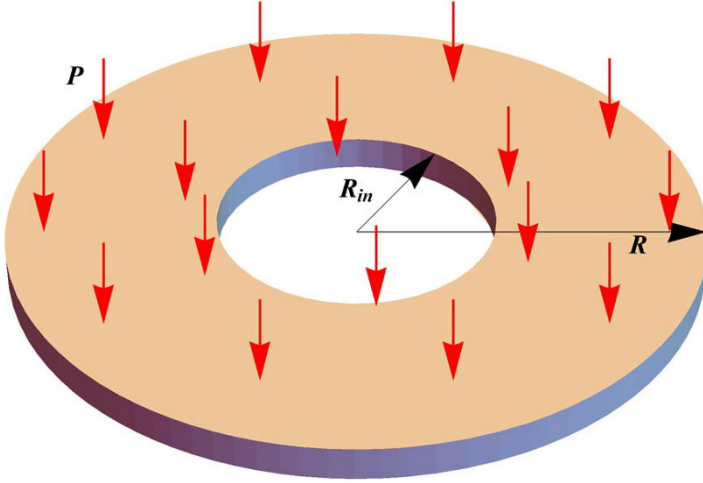


Fig. 2.1 Geometry of the annular plate.

where r and θ are polar coordinates, $D(r) = E(r)h^3/12(1 - \nu^2)$ is the bending stiffness, see Bauer and Voronkova (2018, 2020). The Laplacian is defined as

$$\Delta = \frac{\partial^2}{\partial r^2} + \frac{1}{r} \frac{\partial}{\partial r} + \frac{1}{r^2} \frac{\partial^2}{\partial \theta^2}.$$

The differential operators that appear in (2.1) are listed in Appendix.

We introduce the dimensionless quantities

$$r^* = \frac{r}{R}, \quad w^* = \beta \frac{w}{h}, \quad P^* = \beta^3 \frac{PR^4}{E_{av}h^4}, \quad F^* = \beta^2 \frac{F}{E_{av}h^3}, \quad \beta^2 = 12(1 - \nu^2), \quad (2.2)$$

here E_{av} is an average value of Young's modulus in the radial direction

$$E_{av} = \frac{1}{\pi(R^2 - R_{in}^2)} \int_0^{2\pi} \int_{R_{in}}^R E(r)r dr d\theta, \quad E(r) = E_0 f(r),$$

where $f(r)$ is a smooth position function. The dimensionless forms of Eqs. (2.1)

$$\begin{aligned} g_1(r)\Delta\Delta w + g'_1(r)L_1^+(w) + g''_1(r)L_2^+(w) &= P + L(w, F), \\ g_2(r)\Delta\Delta F + g'_2(r)L_1^-(F) + g''_2(r)L_2^-(F) &= -L(w, w)/2, \\ g_1(r) &= E_0 f(r)/E_{av}, \quad g_2(r) = 1/g_1(r). \end{aligned} \quad (2.3)$$

The plate is subjected to the following boundary conditions

$$w = w' = N_r = N_{r\theta} = 0 \quad \text{at } r = 1, \quad (2.4)$$

$$u = w' = N_{r\theta} = Q_r^* = 0 \quad \text{at } r = \delta. \quad (2.5)$$

Here $r = \delta = R_{in}/R$ is a dimensionless radial coordinate of the inner edge, u denotes the horizontal radial components of displacement, $N_r, N_{r\theta}$ are stress resultants, Q_r^* is the generalized shear force, that can be expressed via the shear force Q_r , the bending M_r, M_θ and twisting $M_{r\theta}$ moments as is stated below:

$$Q_r^* = Q_r + \dot{M}_{r\theta}/r = M_r' + (M_r - M_\theta)/r + 2\dot{M}_{r\theta}/r.$$

The physical interpretation of the boundary conditions (2.4)-(2.5) is as follows. The outer edge of the plate $r = 1$ is clamped but can move freely in the radial direction without rotation, while the inner contour $r = \delta$ is supported by roller that can slide along a vertical wall.

In the terms of the displacement component w and stress function F , the boundary conditions (2.4)-(2.5) are equivalent to

$$\begin{aligned} w(1) = w'(1) &= \left(\frac{F'}{r} + \frac{\ddot{F}}{r^2} \right) \Big|_{r=1} = 0, \\ -\left(\frac{\dot{F}}{r} \right)' \Big|_{r=1} &= 0, \\ w'(\delta) &= -\left(\frac{\dot{F}}{r} \right)' \Big|_{r=\delta} = 0, \\ g_1(\delta) \left((\Delta w)' + \frac{1-\nu}{r} \left(\frac{\ddot{w}}{r} \right)' \right) \Big|_{r=\delta} &+ g_1'(\delta) L_2^+(w) \Big|_{r=\delta} = 0, \\ g_2(\delta) \left((\Delta F)' - \frac{\Delta F}{r} + \frac{1+\nu}{r^2} (\dot{F} + F)' \right) \Big|_{r=\delta} &- g_2'(\delta) L_2^-(F) \Big|_{r=\delta} = 0. \end{aligned} \quad (2.6)$$

For the axisymmetrical problem Eqs. (2.3) are reduced to

$$\begin{aligned} g_1(r) \left(\Theta_0'' + \frac{\Theta_0'}{r} - \frac{\Theta_0}{r^2} \right) + g_1'(r) \left(\Theta_0' + \nu \frac{\Theta_0}{r} \right) &= \frac{Pr}{2} \left(1 - \frac{\delta^2}{r^2} \right) + \frac{\Theta_0 \Phi_0}{r}, \\ g_2(r) \left(\Phi_0'' + \frac{\Phi_0'}{r} - \frac{\Phi_0}{r^2} \right) + g_2'(r) \left(\Phi_0' - \nu \frac{\Phi_0}{r} \right) &= -\frac{\Theta_0^2}{2r}, \end{aligned} \quad (2.7)$$

where $\Theta_0(r) = w'(r)$, $\Phi_0(r) = F'(r)$. The system (2.7) needs to be solved together with the boundary conditions

$$\begin{aligned} \Theta_0(1) = \Phi_0(1) &= 0, \\ \Phi'(\delta) - \nu \Phi(\delta) &= \Theta(\delta) = 0. \end{aligned} \quad (2.8)$$

2.3 Equations for Buckling

Asymmetrical solutions of problem (2.3) with appropriate boundary conditions branch from a solution of axisymmetric states (Cheo and Reiss, 1973). To detect the occurrence of wrinkling we seek for a solution of Eqs. (2.3) in the form

$$\begin{aligned} w(r, \theta) &= w_s(r) + \varepsilon w_{ns} \cos(n\theta), \\ F(r, \theta) &= F_s(r) + \varepsilon F_{ns} \cos(n\theta), \end{aligned} \quad (2.9)$$

where $w_s(r)$, $F_s(r)$ describe prebuckling axisymmetric state, ε is infinitesimal parameter, n is a mode number and $w_n(r)$, $F_n(r)$ are the non-symmetrical components.

After substitution of (2.9) in (2.3), using Eqs. (2.7) and linearization with respect to ε we obtain

$$\begin{aligned} g_1 \Delta_n \Delta_n w_n + \mathcal{L}_1(g_1, w_n) &= \frac{w_n''}{r} \Phi_0 + \frac{F_n''}{r} \Theta_0 + \Theta_0' \left(\frac{F_n'}{r} - \frac{n^2}{r^2} F_n \right) - \Phi_0' \left(\frac{w_n'}{r} - \frac{n^2}{r^2} w_n \right), \\ g_2 \Delta_n \Delta_n F_n + \mathcal{L}_2(g_2, F_n) &= -\frac{w_n''}{r} \Theta_0 - \Theta_0' \left(\frac{w_n'}{r} - \frac{n^2}{r^2} w_n \right). \end{aligned} \quad (2.10)$$

The definitions of the operators \mathcal{L}_1 , \mathcal{L}_2 are listed in the Appendix.

Boundary conditions (2.4) are reduced to

$$w_n(1) = w_n'(1) = F_n(1) = F_n'(1) = 0. \quad (2.11)$$

For the inner edge of the plate we have

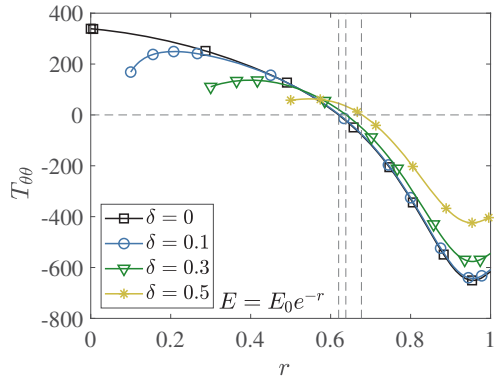
$$\begin{aligned} w_n'(\delta) &= 0, \\ F_n'(\delta) - \delta F_n(\delta) &= 0, \\ g_1(\delta) \left((\Delta_n w_n)' - \frac{n^2}{r} (1-\nu) \left(\frac{w_n}{r} \right)' \right) \Big|_{r=\delta} + g_1(\delta)' L_{2n}^+(w_n) \Big|_{r=\delta} &= 0, \\ g_2(\delta) \left((\Delta_n F_n)' - \frac{\Delta_n F_n}{r} - \frac{1+\nu}{r^2} (n^2-1) F_n' \right) \Big|_{r=\delta} - g_2'(\delta) L_{2n}^-(F_n) \Big|_{r=\delta} &= 0. \end{aligned} \quad (2.12)$$

Buckling equations (2.10) with boundary conditions (2.11), (2.12) constitute an eigenvalue problem, in which the parameter p is implicit and appears in the equations through the functions Θ_0 and Φ_0 . The axisymmetric problem (2.7)-(2.8) was solved by standart MATLAB functions. The value of P , for which (2.10) with (2.11), (2.12), have nontrivial solution, was found by using the finite difference method (Cheo and Reiss, 1973). We regard the smallest of these eigenvalues as the buckling load.

2.4 Numerical Results

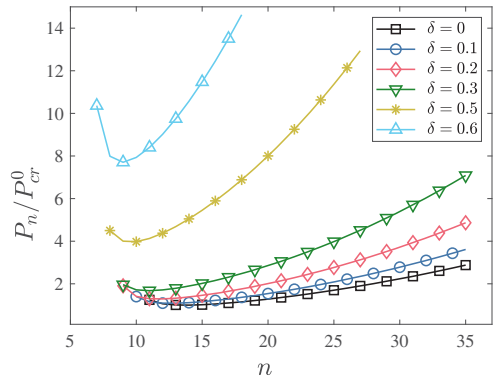
Figure 2.2 illustrates the dimensionless axisymmetrical circumferential stress that developed in a non-uniform circular or annular plate for different values of inner radii δ . A ring of large circumferential compressive stress develops near the edge of the plate and indicates possibility of wrinkling near the outer edge of a plate as it describes in Cheo and Reiss (1973). We assume exponential law for material inhomogeneity: $E = E_0 e^{qr}$ and perform calculations numerically over a large range of parameters E_0, q , but for constant average value of the elastic modulus (2.2).

Fig. 2.2 Dimensionless circumferential stress resultant $T_{\theta\theta}$ for the different values of inner radius δ . Black line with square marks corresponds to a circular plate ($\delta = 0$). Here load parameter $P = 30000$, Young's modulus $E(r) = E_0 e^{-r}$.



In Fig. 2.3, we illustrate dependence of the normalized critical load P_{cr}/P_{cr}^0 and the critical mode number n on inner radius δ for a homogeneous plate. The value P_{cr}^0

Fig. 2.3 Dependence of the normalized critical load P_{cr}/P_{cr}^0 and the critical mode number n on inner radius δ for a homogeneous plate. Black line with square marks corresponds to a circular plate ($\delta = 0$).



corresponds to the buckling load of axisymmetric equilibrium states of an isotropic homogeneous circular plate ($P_{cr}^0 = 64453, n = 14$). The normalized buckling pressure P_{cr}/P_{cr}^0 increases as the radius of the opening δ increases, while the buckling mode n has opposite behavior: it decreases when δ increases (see also, Table 2.1).

The effect of the varying rate of inhomogeneity on the critical load and buckling mode is showed in Figs. 2.4 and 2.5. When the inner radius is small, compared to the outer radius of the plate ($\delta = R_{in}/R = 0.05$), the behavior of the buckling curves for a nonuniform annular plate is similar to a circular plate with varying Young's modulus (Bauer and Voronkova, 2018, 2020): the normalized buckling pressure P_{cr}/P_{cr}^0 decreases, if Young's modulus of an annulus decreases towards the outer edge of the plate, and increases, if the Young modulus of a plate increases near the outer edge (see Table 2.1 for $\delta = 0$ and 0.05).

Table 2.1 Normalized buckling load (P_{cr}/P_{cr}^0) and corresponding wave numbers for a heterogeneous annular plate.

| $E(r) = E_0 e^{qr}$ | $q = 2$ | $q = 1$ | $q = 0$ | $q = -1$ | $q = -2$ |
|----------------------------|---------|---------|---------|----------|----------|
| $\delta = R_{in}/R = 0$ | | | | | |
| P_{cr}/P_{cr}^0 | 1.7 | 1.3 | 1 | 0.76 | 0.57 |
| Mode number, n | 14 | 14 | 14 | 14 | 14 |
| $\delta = R_{in}/R = 0.05$ | | | | | |
| P_{cr}/P_{cr}^0 | 1.42 | 1.2 | 1.03 | 0.88 | 0.75 |
| Mode number, n | 13 | 14 | 13 | 14 | 15 |
| $\delta = 0.1$ | | | | | |
| P_{cr}/P_{cr}^0 | 1.02 | 1.05 | 1.09 | 1.12 | 1.21 |
| Mode number, n | 15 | 14 | 13 | 12 | 12 |
| $\delta = 0.3$ | | | | | |
| P_{cr}/P_{cr}^0 | 0.76 | 1.03 | 1.68 | 2.58 | 4.97 |
| Mode number, n | 9 | 9 | 11 | 13 | 18 |

For the larger value of $\delta = 0.1$ and 0.3 we notice the opposite behavior: for the buckling load for the plate with weak outer edge ($q < 0$) becomes larger than the buckling load for the uniform plate. This phenomenon is relatively weak for a plate with $\delta = 0.1$: the difference between buckling pressures for a uniform plate ($q = 0$) and for plate with $q = -2$ is about 10% (Fig. 2.4 (left)). The tendency becomes more pronounced for a narrower plates: the buckling load for heterogeneous plate ($q = -2$) differs by factor of 3 from the uniform plate. This the situation depicted in Fig. 2.5 (right) for a plate with $\delta = 0.3$.

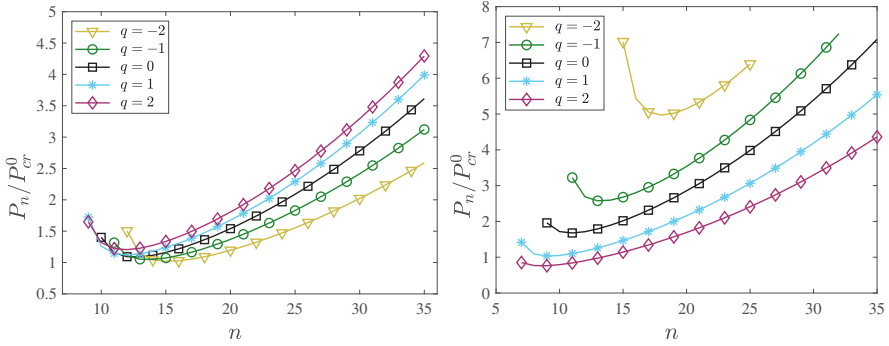
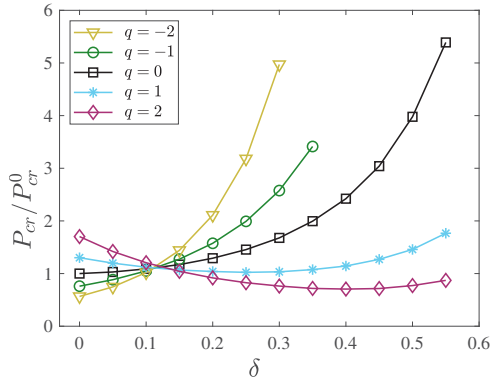


Fig. 2.4 Dependence of the normalized critical load P^{cr} on the mode number n for a different values of inhomogeneity parameter q . Left: $\delta = 0.1$, Right: $\delta = 0.3$.

Fig. 2.5 Change of the normalized buckling pressure P_{cr}/P_{cr}^0 when the degree of heterogeneity of the plate q changes for different values of the inner radius δ . P_{cr}^0 denotes the buckling pressure for a uniform circular plate.



2.5 Conclusion

In this article we have presented a wrinkling analysis of an annular plate with nonuniform mechanical characteristics subjected to normal pressure. For an annular plate with a small inner radius of a plate and Young’s modulus, decreasing towards the outer edge, the critical pressure for unsymmetrical buckling is sufficiently lower than for a plate with constant mechanical properties. For an annulus with large inner radius, the buckling pressure and the buckling mode number increases as the Young modulus decreases towards to outer edge of a plate.

References

Adachi J, Benicek M (1964) Buckling of torispherical shells under internal pressure. *Experimental Mechanics* 4(8):217–222
 Bauer SM, Voronkova EB (2018) On the unsymmetrical buckling of shallow spherical shells under internal pressure (in Russ.). *Izvestiya Saratovskogo Universiteta (Nvaya Seriya), Seriya*

- Matematika, Mekhanika, Informatika 18(4):390–396
- Bauer SM, Voronkova EB (2020) On buckling behavior of inhomogeneous shallow spherical caps with elastically restrained edge. In: Altenbach H, Chinchaladze N, Kienzler R, Müller W (eds) Analysis of Shells, Plates, and Beams, Springer, Cham, Advanced Structured Materials, vol 134, pp 65–74
- Burmeister D (2018) Asymmetric buckling of shell-stiffened annular plates. International Journal of Mechanics and Materials in Design 14(4):565–575
- Bushnell D (1981) Buckling of shells - pitfall for designers. AIAA Journal 19(9):1183–1226
- Cheo LS, Reiss EL (1973) Unsymmetric wrinkling of circular plates. Quarterly of Applied Mathematics 31(1):75–91
- Coman CD (2010) Global asymptotic approximations for wrinkling of polar orthotropic annular plates in tension. International Journal of Solids and Structures 47(11):1572–1579
- Coman CD (2013) Asymmetric bifurcations in a pressurised circular thin plate under initial tension. Mechanics Research Communications 47:11–17
- Lepik U (2002) Optimal location of a circular support for nonaxisymmetric buckling of annular plates. Structural and Multidisciplinary Optimization 23(3):252–256
- Mansfield EH (1960) On the buckling of an annular plate. The Quarterly Journal of Mechanics and Applied Mathematics 13(1):16–23
- Morozov NF (1961) On the existence of a non-symmetric solution in the problem of large deflections of a circular plate with a symmetric load (in Russ.). Izvestiya Vysshikh Uchebnykh Zavedenii Matematiky (2):126–129
- Panov DY, Feodosiev VI (1948) On the equilibrium and loss of stability of shallow shells in the case of large displacement. Prikladnaya Matematika i Mekhanika 12:389–406
- Piechocki W (1969) On the nonlinear theory of thin elastic spherical shells: Nonlinear partial differential equations solutions in theory of thin elastic spherical shells subjected to temperature fields and external loading. Archiwum mechaniki stosowanej 21(1):81–102
- Radwańska M, Waszczyszyn Z (1980) Numerical analysis of nonsymmetric postbuckling behaviour of elastic annular plates. Computer Methods in Applied Mechanics and Engineering 23(3):341–353

Appendix

The linear differential operators that appear in (2.1) are defined by

$$L(x, y) = x'' \left(\frac{y'}{r} + \frac{\ddot{y}}{r^2} \right) + y'' \left(\frac{x'}{r} + \frac{\ddot{x}}{r^2} \right) - 2 \left(\frac{\dot{x}}{r} \right)' \left(\frac{\dot{y}}{r} \right)',$$

$$L_1^\pm(y) = 2y'''' + (2 \pm \nu) \frac{y'''}{r} + 2 \frac{(\ddot{y})'}{r^2} - \frac{y'}{r^2} - 3 \frac{\ddot{y}}{r^3},$$

$$L_2^\pm(y) = y'' \pm \nu \left(\frac{y'}{r} + \frac{\ddot{y}}{r^2} \right).$$

The differential operators introduced in (2.10) are given by

$$\mathcal{L}_1(g_1, w_n) = g_1' L_{1n}^+(w_n) + g_1'' L_{2n}^+(w_n),$$

$$\mathcal{L}_2(g_2, F_n) = g_2' L_{1n}^-(F_n) + g_2'' L_{2n}^-(F_n),$$

where

$$L_1^\pm(y) = 2y''' + \frac{2 \pm \nu}{r} y'' - \frac{2n^2 + 1}{r^2} \ddot{y} + \frac{3n^2}{r^3} \dot{y},$$
$$L_2^\pm(y) = y'' \pm \nu \left(\frac{y'}{r} - \frac{n^2}{r^2} \dot{y} \right).$$



Chapter 3

Bending Stiffness of Multilayer Plates with Alternating Soft and Hard Layers

Alexander K. Belyaev, Nikita F. Morozov, Petr E. Tovstik, and Tatiana P. Tovstik

Abstract The bending stiffness of a multilayer plate with alternating soft and hard layers is considered under the assumption that the deformation wavelength is substantially greater than the plate thickness. We discuss the approximate methods for determining the shear compliance required for replacing a multilayer plate with an equivalent single-layer Timoshenko – Reissner plate. A comparison is made with the exact solution of the three-dimensional problem of the theory of elasticity. The dependence of shear compliance on the ratio of Young’s moduli of layers and on their location is investigated.

Key words: Plate vibrations and buckling, Multilayer plate, Long-wave deformation, Generalized Timoshenko – Reissner model, Transverse shear stiffness

3.1 Introduction

The approach to plate theory based on the hypothesis of a straight non-deformable normal, which was proposed and developed by Kirchhoff (1876) and then applied and improved for shells by Love (1927), is the main two-dimensional model of the theory of thin plates and shells. The range of applicability of this model is limited to single-layer plates made of a homogeneous isotropic material. However for anisotropic plates with low shear stiffness, for plates with oblique anisotropy, for

Alexander K. Belyaev · Tatiana P. Tovstik
Institute for Problems in Mechanical Engineering RAS, Bolshoy pr. V. O., 61, St. Petersburg, 199178, Russian Federation
e-mail: 13augen@mail.ru, tovtstik_t@mail.ru

Nikita F. Morozov · Petr E. Tovstik
Mathematics and Mechanics Faculty, St. Petersburg State University, Universitetsky pr., 28, Stary Peterhof, 198504, Russian Federation
e-mail: morozov@nm1016.spb.edu

multilayer plates with alternating soft and hard layers, the Kirchhoff – Love (KL) model leads to significant inaccuracies, that means, it becomes necessary to use refined models.

A more complex model was proposed in the first half of the 20th century by Timoshenko (1921); Reissner (2021). The Timoshenko – Reissner (TR) theory takes into account rotations of the mid surface normals, that is, includes the effect of transverse shear deformation. In this case, the plate can be considered as a material plane, the elements of which have translational and rotational degrees of freedom. In the limiting case, when the shear stiffness is equal to infinity, the TR model turns to the KL model.

The TR accounting for the transverse shear leads to a significant refinement of the results compared to the KL model for anisotropic plates with low transverse shear stiffness and for multilayer plates with alternating soft and hard layers. For multilayer plates, an equivalent single-layer TR plate made of a homogeneous material is introduced in Tovstik and Tovstik (2017a,b), which models a multilayer plate from a perspective of deflections, vibrations and buckling. The equivalent bending stiffness can be found using the same formulas as in the KL model, but determining the shear stiffness presents certain difficulties and is discussed in detail in what follows. In this paper, to determine this rigidity, we use an asymptotic expansion of the solution of a three-dimensional problem in a series in powers of a small dimensionless thickness (Tovstik and Tovstik, 2014; Morozov et al, 2016). Other methods for determining the shear stiffness are also discussed in Hill (1965); Grigolyuk and Kulikov (1988). These methods are discussed using the example of the problem of free vibrations of a multilayer plate with transversely isotropic layers. A comparison is made with the exact solution of the three-dimensional problem. The dependence of the shear compliance, bending stiffness, vibration frequency and buckling of a multilayer plate on the ratio of Young’s moduli of layers and on the arrangement of layers is investigated.

3.2 Free Vibration and Bending of Multilayer Plate

Let us first consider free bending vibrations of a transversely isotropic homogeneous plate with the deflection $w(x,y,t) = w_0 \sin px \sin qy \sin \omega t$. This deflection is typical for vibrating infinite plate, as well as vibration of a rectangular simply supported plate. In the latter case $p = p_m = m\pi/L_x$, $q = q_n = n\pi/L_y$, $m, n = 1, 2, \dots$, where L_x, L_y stand for length of the corresponding size. For the TR model, the vibration frequency ω is related to the dimensionless frequency parameter

$$\lambda = \frac{\rho h^2 \omega^2}{E_0}$$

and given by the equations (Tovstik and Tovstik, 2017a,b)

$$\lambda = \lambda^{TR} = \frac{\lambda^{KL}}{1+g}, \quad \lambda^{KL} = D\mu^4, \quad (3.1)$$

where $E_0 = E/(1-\nu^2)$, $\mu = rh = 2\pi h/L$, $r^2 = p^2 + q^2$. Here ρ is the material mass density, h is the plate thickness, $L = (L_x^{-2} + L_y^{-2})^{-\frac{1}{2}}$ is a typical wave length, E is the Young modulus, ν is the Poisson ratio, μ is a small parameter proportional to the ratio of the plate thickness to a typical wave length, $D = 1/12$ is a dimensionless parameter of the bending stiffness, $g = (E_0\mu^2)/(10G_{13})$ is a parameter of influence of transverse shear, G_{13} is the transverse shear modulus. For isotropic layers $G_{13} = E/(2(1+\nu))$, while for transversally isotropic layers G_{13} is an independent parameter. For thin plates ($\mu \ll 1$) when $E/G_{13} \sim 1$ the term g in (1) can be neglected whereas for $G_{13} \ll E$ the shear correction factor becomes considerable. When $g = 0$, i.e. when the shear is not taken into account, Eq. (3.1) yields the KL formula $\lambda^{KL} = D\mu^4$.

For KL model, the static deflection $w(x,y) = w_0 \sin px \sin qy$ of the plate under the normal load $f(x,y,t) = f_0 \sin px \sin qy$ is given by the equation

$$\frac{Dr^4 w_0}{1+g} = f_0, \quad (3.2)$$

cf. Tovstik and Tovstik (2017a,b), where the bending stiffness D and the shear compliance g are given by Eq. (3.1). The objective of the present work is to develop Eqs. (3.1) and (3.2) for multilayer plates.

3.3 Asymptotic Integration of Three-dimensional Equations

For a multilayer plate, the elastic moduli and the mass density become piecewise constant functions of the transverse coordinate z , $0 \leq z \leq h$. This parametrization is more convenient than the usual $-h/2 \leq z \leq h/2$, since for coordinates used here $z \neq 0$ at the neutral layer. We introduce dimensionless variables (with ^)

$$\begin{aligned} \{u_1, u_2, w, z\} &= h\{\hat{u}_1, \hat{u}_2, \hat{w}, \hat{z}\}, \quad \{x, y\} = L\{\hat{x}, \hat{y}\} \\ \{E, E_0, G_{13}, \sigma_{ij}\} &= E_*\{\hat{E}, \hat{E}_0, \hat{G}_{13}, \hat{\sigma}_{ij}\}, \quad i, j = 1, 2, 3, \end{aligned}$$

where u_1, u_2 are tangential displacements along the x, y axes, σ_{ij} are stress tensor components, E_* - thickness-average Young's modulus. Here and after we omit mark ^.

For a multilayer plate, the exact expression for the frequency parameter λ can be found from a three-dimensional boundary value problem, which for transverse vibrations in dimensionless variables is reduced to the form (Tovstik and Tovstik, 2014; Morozov et al, 2016; Tovstik and Tovstik, 2017a,b):

$$\begin{aligned}
\frac{dw}{dz} &= -\mu^2 c_v(z)u + \mu^4 c_3(z)\sigma_{33}, & \frac{du}{dz} &= w + \mu^2 c_g(z)\sigma, \\
\frac{d\sigma}{dz} &= E_0(z)u + \mu^2 c_v(z)\sigma_{33} - \mu^2 \lambda \rho(z)u, & \frac{d\sigma_{33}}{dz} &= -\sigma - \lambda \rho(z)w, \\
\sigma &= \sigma_{33} = 0, & z &= 0, 1.
\end{aligned} \tag{3.3}$$

Here the displacements and the z coordinate are related to the plate thickness, whereas the stresses and the elastic moduli are related to Young's modulus of the rigid layer, and the densities are related to the density of the rigid layer. Instead of tangential movements u_1 , u_2 and stresses σ_{13} , σ_{23} we introduce auxiliary unknowns quantities $u = \mu(pu_1 + qu_2)$, $\sigma = \mu^3(p\sigma_{13} + q\sigma_{23})$ and

$$c_v = \frac{\nu}{1-\nu}, \quad c_3 = \frac{(1+\nu)(1-2\nu)}{E(1-\nu)}, \quad c_g = \frac{1}{G_{13}}.$$

By asymptotic expansion of the solution to the boundary value problem (3.3) in powers of the small parameter μ in Timoshenko (1921); Reissner (2021); Tovstik and Tovstik (2017b), an expression for the frequency parameter λ was obtained in a form similar to (3.1):

$$\lambda = \frac{\rho_* h^2 \omega^2}{E_*} = \frac{\lambda^{KL}}{1+g}, \quad \lambda^{KL} = D_* \mu^4, \quad D_* = \frac{1}{E_*} \int_0^1 E_0(z)(z-a)^2 dz, \tag{3.4}$$

where

$$\begin{aligned}
g &= g^a + O(\mu^4), & g^a &= \mu^2(A_g + A_v + J + J_v), \\
\{E_*, \rho_*\} &= \int_0^1 \{E_0(z), \rho(z)\} dz, & a &= \frac{1}{E_*} \int_0^1 E_0(z)z dz, \\
A_g &= \frac{1}{E_* D_*} \int_0^1 \frac{\left(\int_0^z E_0(z_1)(z_1-a) dz_1 \right)^2}{G_{13}(z)} dz.
\end{aligned} \tag{3.5}$$

Here E_* , ρ_* is the thickness average tensile stiffness and density, D_* is the bending stiffness parameter and a is the coordinate of the neutral layer. The second order terms g^a take into account the lateral shear compliance (A_g), the Poisson tension of a normal fiber (A_v), the inertia of rotational motion (J) and the inertia of the Poisson extension (J_v). The quantities A_v , J and J_v are not shown here, cf. Tovstik and Tovstik (2017a,b).

For the problem of statics (3.2), the formula for deflection, accurate to terms of the second order of smallness, has the form:

$$w^{TR} = w^{KL}(1+g), \quad w^{KL} = \frac{f_0}{D_* \mu^4}, \quad g = g^a = \mu^2(A_g + A_v). \tag{3.6}$$

3.4 The Transverse Shear Stiffness

Calculations for multilayer plates by Eqs. (3.4)-(3.6) are associated with the calculation of iterated integrals of piecewise constant functions, and hence are rather cumbersome. That is why we will consider the possibility of simplifying them in what follows. Consider a plate with alternating isotropic hard and soft layers and denote by η the ratio of Young's moduli of hard and soft layers. If the parameter η increases, then the moduli G_{13} of the soft layers of the plate decrease and, by virtue of formula (3.4), the coefficient A_g also increases, while the remaining second-order coefficients A_v, J, J_v remain significantly smaller than A_g .

Consider, for example, a three-layer plate with the layer thicknesses $h_1 = 0.3, h_2 = 0.6, h_3 = 0.1$. Respectively, Young's moduli of hard and soft layers are equal to $E_1 = E_3 = 1, E_2 = 1/\eta$, Poisson's ratios $\nu_1 = \nu_3 = 0.3, \nu_2 = 0.35$. For a number of values of η , the coefficients of the second order of smallness are given in Table 3.1.

We put approximately $g^a = \mu^2 A_g$, thus returning to the TR model, which takes into account only the shear and ignores the other terms of the second order of smallness.

Calculations in Tovstik and Tovstik (2017a,b) showed that at $\eta \leq 1000, \mu = 0.1$ the error of Eq. (3.4) for $g = g^a = \mu^2 A_g$ does not exceed 4%. In what follows, the error of this replacement is discussed in more detail, cf. Hill (1965).

3.5 The Exact Value of the Shear Stiffness

By virtue of Eq. (3.5), we have the estimate

$$g^a = \mu^2 A_g = O(\mu^2 \eta). \tag{3.7}$$

For very large η , i.e., for a large ratio of the stiffness of the layers we have $g^a > 1$, Eq. (3.4) for $g = g^a$ becomes inaccurate and it is necessary to find the exact value $g = g^e$ for which Eq. (3.4) gives the exact value $\lambda = \lambda^e$. In order to find it we put $c_v = c_3 = 0$ in system (3.3) and omit the term $\mu^2 \lambda \rho(z)u$ in the third equation. We obtain $w = 1$ and the auxiliary boundary-value problem

$$\frac{du}{dz} = w + \mu^2 c_g(z)\sigma, \quad \frac{d\sigma}{dz} = E_0(z)u, \quad \sigma(0) = \sigma(1) = 0. \tag{3.8}$$

Table 3.1 Terms of the second order of smallness.

| η | A_g | A_v | J | J_v | a | D_* |
|--------|---------|--------|--------|--------|-------|--------|
| 1 | 0.299 | 0.0928 | 0.1150 | 0.0308 | 0.502 | 0.0824 |
| 10 | 1.461 | 0.0875 | 0.1114 | 0.0081 | 0.384 | 0.1202 |
| 100 | 12.921 | 0.0844 | 0.1149 | 0.0026 | 0.354 | 0.1253 |
| 1000 | 127.515 | 0.0840 | 0.1154 | 0.0019 | 0.350 | 0.1259 |

After solving it, from the compatibility condition of the fourth equation (3.3), we find $\lambda = -\int_0^1 \sigma(z) dz$ from Eq. (3.3) we have

$$g^e = \frac{1}{\mu^2} \left(\frac{D_*}{\lambda} - 1 \right). \quad (3.9)$$

Some examples of calculation are provided in Sect. 3.8.

Equation (3.9) is obtained from consideration of free vibrations. Calculation of the same value g^e from the statics problem is more difficult, because with an exact statement, the deflection depends on the distribution of the load over the thickness and the types of the layer, cf. Tovstik and Tovstik (2017a).

3.6 About the TR Model for a Homogeneous Transversally Isotropic Plate

According to the TR model, the frequency parameter λ for a homogeneous transversely isotropic plate is determined by Eq. (3.4), in which $g = g_0 = \frac{q}{10}$, $q = \frac{\mu^2 E_0}{G_{13}}$. Let us estimate the accuracy of this formula for $g_0 > 1$. For a homogeneous plate, problem (3.6) has a closed form solution

$$\sigma = \frac{G}{\mu^2} \left(\frac{\cosh(\sqrt{q}(z-0.5))}{\frac{\sqrt{q}}{2}} - 1 \right)$$

and Eq. (3.9) yields

$$g^e = \frac{q}{12(2 \cosh(\sqrt{q}/2) / \sqrt{q} - 1)} - 1. \quad (3.10)$$

Calculations using Eq. (3.10) gave the following results:

| | | | | | |
|----------|--------|-------|------|------|------|
| $q/10 =$ | 0.1 | 1 | 10 | 100 | 1000 |
| $g^e =$ | 0.0999 | 0.989 | 9.42 | 88.0 | 849 |

from which it follows that with an increase in q , the exact value of g^e deviates downward from the value $q/10$, recommended by the TR model.

3.7 Other Ways to Calculate the Shear Parameter g

In the classical paper by Hill (1965) two models, Voigt and Reuss, for estimating the transverse shear modulus of a composite material are given $G_V = \gamma_1 G_1 + \gamma_2 G_2$

and $G_R = \left(\frac{\gamma_1}{G_1} + \frac{\gamma_2}{G_2} \right)^{-1}$. The second formula for the plate with N layers takes the form of the sum of shear compliance of the layers

$$g = \sum_{n=1}^N \frac{\gamma_n}{G_n}, \quad (3.11)$$

where γ_n do not depend in transverse shear moduli of the layers G_n . G_n are the independent coefficients, the formulas for which are not given here. Note that Eq. (3.11) for A_g is reduced to (11) after calculating the integrals.

The monograph by Grigolyuk and Kulikov (1988) (GK) proposed an algorithm for taking into account the transverse shear effect for multilayer plates and shells. It is expedient to return to this algorithm, because the recent works (Mikhasev and Altenbach, 2019; Morozov et al, 2020), as well as a number of other works, reported application of this algorithm for solving some particular problems. This algorithm is based on the hypothesis of distribution of the transverse shear deformations over the plate thickness. According to Grigolyuk and Kulikov (1988), the formula for g can be written as:

$$\left(\left(\sum_{n=1}^N \frac{\alpha_n}{G_n} \right)^{-1} + \sum_{n=1}^N \beta_n G_n \right)^{-1}, \quad (3.12)$$

where α_n and β_n are G_n - independent coefficients. The explicit form of the formula for g is given in Grigolyuk and Kulikov (1988); Mikhasev and Altenbach (2019); Morozov et al (2020). Calculations have shown that the GK algorithm can be used only for plates with a small ratio η of Young's moduli of layers which is also discussed in Grigolyuk and Kulikov (1988). With an increase in η , the error of Eq. (3.10) for $\Delta(\eta)$ grows rapidly. For example, for the plate considered in Table 3.1, the error $\Delta(1) = 1.2\%$, $\Delta(10) = 42\%$ where at $\eta = 100$, the value of g given by Eq. (3.10) is 10 times greater than the exact value. Apparently, the hypotheses underlying the GK model and violating the continuity of shear stresses at the layer boundary need to be corrected.

3.8 Numerical Results. Three-layer Plate Symmetrical in Thickness

The shear parameter g and the associated vibration frequency ω depend on many parameters. A number of special cases are considered below.

Consider a plate with the parameters $h_1 = h_3 = 0.3$, $h_2 = 0.4$, $E_1 = E_3 = 1$, $E_2 = 1/\eta$, $\nu_1 = \nu_2 = \nu_3 = 0.3$, $\rho_1 = \rho_3 = 1$, $\rho_2 = 1/\eta$. There are two free parameters left: the thickness parameter μ and the Young's modulus ratio η . As follows from estimate 3.7, the allowance for the transverse shear is associated with the value $\mu^2\eta$; therefore, we introduce the combined parameter $p = \mu^2\eta$ and carry out the calculations at a fixed value of the parameter $\mu = 0.1$. Table 3.2 shows for a number of p

values: approximate values of the shear parameter $g^a = \mu^2 A_g$ found by asymptotic formula (3.4), and the exact values of g^e found by Eq. (3.7); the exact values of λ^e of the frequency parameter λ obtained by solving the three-dimensional problem (3.2). The remaining values of the parameter λ are approximate. They are obtained by formula (3), and the values of λ^{ap} , λ^{TR} , λ^{KL} are calculated for $g = g^e$, for $g = g^a = \mu^2 A_g$ and for $g = 0$, respectively. The λ^{TR} value corresponds to the TR model with allowance for the shear according to the approximate model (3.4). The λ^{KL} value corresponds to the KL model, which does not take into account the transverse shear.

Comparison of columns 3–4 and 5–8 allows us to judge the areas of applicability of the approximate models. The KL model is applicable only at $\eta \leq 10$ (or at $p \leq 0.1$). The asymptotic approach of the second order of accuracy which leads to the values of g^a and λ^{TR} is certainly applicable for $\eta \leq 100$ and gives a noticeable error for $100 < \eta \leq 1000$. In this case, parameter g^a exceeds the exact value g^e . Using the g^e value gives fairly accurate results over the entire considered range of $\eta \leq 10000$, as evidenced by the comparison of columns 5 and 6 (when calculating λ^{ap} only the shear is accurately taken into account while the other second-order effects are ignored).

Calculations were also carried out at $\mu = 0.316$ and at $\mu = 0.0316$ however, the numerical results are not presented, because they differ from those given in Table 3.2 by less than 1% (except for the parameter η which is 10 times less or more, respectively).

3.9 Three-layer Plate Asymmetric in Thickness

Consider a three-layer plate with a constant thickness of the soft layer $h_2 = 0.4$ and with variable thicknesses of the hard layers $0 < h_1 \leq 0.3$, $h_3 = 0.6 - h_1$. The rest of the parameters are the same as in Sect. 3.4. When $h_1 = 0.3$ the plate is symmetrical in thickness, and the difference $0.3 - h_1$ serves as a measure of asymmetry. Let us discuss function $\lambda^e(\eta, h_1)$. From the results of Table 3.3, it follows that at $1 < \eta \leq 100$ the frequency decreases with an increase in the asymmetry of the plate (with a

Table 3.2 Shear and frequency parameters depending on p at $\mu = 0.1$.

| 1 | 2 | 3 | 4 | 5 | 6 | 7 | 8 |
|------|--------|---------|---------|-------------|----------------|----------------|----------------|
| p | η | g^a | g^e | λ^e | λ^{ap} | λ^{TR} | λ^{KL} |
| 0.01 | 1 | 0.00286 | 0.00286 | 0.0913 | 0.0913 | 0.0913 | 0.0916 |
| 0.1 | 10 | 0.0174 | 0.0174 | 0.1321 | 0.1325 | 0.1325 | 0.1348 |
| 1 | 100 | 0.163 | 0.161 | 0.1222 | 0.1223 | 0.1224 | 0.1420 |
| 10 | 1000 | 1.62 | 1.47 | 0.0578 | 0.0578 | 0.0545 | 0.1432 |
| 100 | 10000 | 16.2 | 8.1 | 0.0157 | 0.0157 | 0.0083 | 0.1432 |

Table 3.3 The frequency parameter λ^e versus parameters η and h_1 at $\mu = 0.1$.

| h_1 | $\eta = 1$ | 10 | 100 | 1000 | 10000 |
|-------|------------|--------|--------|--------|--------|
| 0.3 | 0.0913 | 0.1321 | 0.1222 | 0.0578 | 0.0157 |
| 0.2 | 0.0913 | 0.1231 | 0.1141 | 0.0583 | 0.0183 |
| 0.1 | 0.0913 | 0.0953 | 0.0876 | 0.0575 | 0.0263 |
| 0.05 | 0.0913 | 0.0740 | 0.0652 | 0.0524 | 0.0320 |

decrease in the thickness h_1). At higher η , with increasing asymmetry, the frequency increases and reaches a maximum at a certain value of h_1 and then decreases. For a fixed value of h_1 and with increasing η , the frequency first increases and, upon reaching the maximum, decreases. At $h_1 = 0.05$, the maximum is reached at $\eta = 1.15$ and is not shown in Table 3.3.

3.10 Multilayer Plate

Consider a multilayer plate with an odd number $2n + 1$ of alternating hard and soft layers of the same thickness h_1 and h_2 with parameters $\mu = 0.1$, $\eta = 100$. Let ξ denote the fraction of the volume occupied by soft layers. Table 3.4 shows the values of the frequency parameter λ^e depending on the parameters n and ξ . It follows from the results presented in the table that the frequency decreases with an increase in the number of layers, approaching the limit corresponding to a transversely isotropic homogeneous plate. The last row of Table 3.4 was constructed according to Eq. (3.8) with $q = (1 - \xi + \eta\xi)(\eta(1 - \xi) + \xi)$, whence it follows that function $g^e(\xi)$ is even with respect to the point $\xi = 0.5$. The latter circumstance is associated with the peculiarity of specifying the density of the soft layers $\rho_2 = 1/\eta$.

With a small number of layers, the frequency increases with the fraction ξ of the soft material, whereas this regularity is violated with a large number of layers.

Table 3.4 Parameter λ^e depending on n and ξ at $\mu = 0.1$, $\eta = 100$.

| n | $\xi = 0.1$ | 0.3 | 0.5 | 0.7 | 0.9 |
|----------|-------------|--------|--------|--------|--------|
| 3 | 0.0962 | 0.1115 | 0.1354 | 0.1712 | 0.2190 |
| 5 | 0.0946 | 0.1024 | 0.1153 | 0.1338 | 0.1567 |
| 11 | 0.0915 | 0.0941 | 0.0991 | 0.1070 | 0.1169 |
| 21 | 0.0904 | 0.0904 | 0.0926 | 0.0970 | 0.1032 |
| 101 | 0.0893 | 0.0871 | 0.0868 | 0.0884 | 0.0919 |
| ∞ | 0.0891 | 0.0863 | 0.0854 | 0.0863 | 0.0891 |

3.11 Buckling of a Multilayer Plate Under Uniform Compression

Consider a multilayer simply supported rectangular plate with sides L_x , L_y which is uniformly compressed by tangential strain e . The following initial conditions accepted in the plane of the plate

$$T = T_1 = T_2 = eE_{1*}, \quad E_{1*} = \int_0^1 E_1(z)dz, \quad E_1 = \frac{E}{1-\nu}, \quad (3.13)$$

which upon the buckling $w(x,y) = w_0 \sin px \sin qy$ generate a load $f(x,y) = T\Delta w$ where Δ denotes the Laplace operator. Equation (3.2) in which D and g are calculated by Eqs. (3.4) and (3.5) after separation of variables $f_0 = eE_*r^2w$ yields the critical deformation

$$e = \frac{D_*\mu^2}{(1+g)E_{1*}}, \quad \mu = rh, \quad r^2 = \frac{\pi^2}{L_x^2} + \frac{\pi^2}{L_y^2}. \quad (3.14)$$

To estimate the error in Eq. (3.14), let us turn to the exact system (3.3). The last two equations of take the form

$$\frac{d\sigma}{dz} = E_0(z)u + \mu^2 c_\nu(z)\sigma_{33}, \quad \frac{d\sigma_{33}}{dz} = -\sigma - e\mu^2 E_1(z)w. \quad (3.15)$$

Let us consider the compression buckling of a plate asymmetric in thickness with the parameters $E_1 = E_3 = 1$, $E_2 = 1/\eta$, $h_1 = 0.1$, $h_2 = 0.6$, $h_3 = 0.3$, $\nu_1 = \nu_2 = \nu_3 = 0.3$. As in Table 3.2, parameter η will vary within wide limits $0 \leq \eta \leq 10000$. The calculations were carried out for the relative thickness $\mu = 0.1$. As in the vibration problem, the result depends on the combined parameter $p = \mu^2\eta$, so it can be used for other values of μ .

Table 3.5 shows the exact values of e_0^e found when integrating system (3.3) taking into account replacement (3.15); the values of e_0^{TR} found by Eq. (3.14) at $g = g^a$, along with the values of e_0^{KL} corresponding to the KL model and found by the same Eq. (3.14) at $g = 0$ (without taking into account the effect of transverse shear). As in the case of vibration, the KL model gives acceptable results only at $p \leq 0.1$ whereas the TR model using the second-order accuracy parameter $g = g^a$ gives good results

Table 3.5 Critical deformation $e = 10^{-3}e_0$ versus p for $\mu = 0.1$.

| p | η | g^a | e_0^e | e_0^{TR} | e_0^{KL} |
|------|--------|---------|---------|------------|------------|
| 0.01 | 1 | 0.00286 | 0.639 | 0.639 | 0.641 |
| 0.1 | 10 | 0.0141 | 0.914 | 0.914 | 0.926 |
| 1 | 100 | 0.124 | 0.858 | 0.857 | 0.960 |
| 10 | 1000 | 1.23 | 0.448 | 0.434 | 0.967 |
| 100 | 10000 | 12.3 | 0.111 | 0.073 | 0.967 |

at $p \leq 1$ and acceptable results at $p \leq 10$. For $p > 10$, the exact value $g = g^e$ should be used, the calculation of which is reduced to solving a simpler boundary value problem (3.8), otherwise it is necessary to solve the complete problem (3.3).

Note that the parameters g^a and g^e depend on the parameters of multilayer plate, but they are the same for the problems of vibration, statics, and buckling since boundary value problem (3.8) does not change when calculating g^e .

3.12 Discussion

The frequency of bending vibrations of a multilayer plate was found to be calculated by Eq. (3.4) corresponding to the TR model, in which the denominator $1 + g$ takes into account the effect of transverse shear. A combined parameter $p = \mu^2 \eta$ is introduced, which determines the range of applicability of various approaches in calculating g (μ is a small parameter of thickness and η is the ratio of Young's moduli of layers). When $p \leq 1$ for a homogeneous plate $g = \frac{E_0 \mu^2}{10G_{13}}$, and for a multilayer plate $g = g^a = \mu^2 A_g$, see (3.5). If $p > 1$ these formulas become inaccurate. For a homogeneous plate, g is calculated using the explicit formula (3.10). This gives an estimate of the error of the TR model for $g = \frac{E_0 \mu^2}{10G_{13}}$. For a multilayer plate, the value $g = g^e$ is calculated by Eq. (3.9). The use of this value of g gives fairly accurate results in the entire considered range of parameters $0.001 \leq \mu \leq 0.3$, $1 \leq \eta \leq 10000$ which is confirmed by comparison with the exact solution of the three-dimensional problem (3.3). A number of particular problems have been solved. For a three-layer plate, the influence of the location of the soft layer on the vibration frequencies is investigated. A multilayer plate with a constant fraction ξ of the volume occupied by soft layers is considered, and the influence of parameter ξ and the number of layers on the vibration frequency is investigated.

The results obtained for the factor $1 + g$ which takes into account the effect of transverse shear are also applicable without changes for the static problem of deflection of a multilayer plate under the action of a static harmonic load of the form $f = f_0 \sin px \sin qy$. These results are also used to solve the buckling problem for a multilayer plate under uniform compression in its plane. Equation (3.14) for critical deformation is a generalization of Eq. (3.4). In this case, the range of applicability of the approximate KL and TR models turns out to be the same as in the vibrational case.

For multilayer transversely isotropic plates, the presented results can be considered final. In Tovstik (2019), an asymptotic approximation of the second order of accuracy was constructed for a plate inhomogeneous in thickness with anisotropy of general form (with 21 elastic moduli), which leads to a rather cumbersome model that requires simplifications and a corresponding analysis of the error. In particular, a multilayer plate with orthotropic layers generally does not have a neutral layer. That is, the longitudinal and bending deformations are not separated and the calculation

becomes more complicated. Only partial results have been obtained in Belyaev et al (2019)¹ and the problem remains to be tackled.

Acknowledgements Financial support of Russian Foundation for Basic Research is acknowledged, projects, 19-01-00208a, 20-51-S52001 MHT-a.

References

- Belyaev AK, Morozov NF, Tovstik PE, Tovstik TP (2019) Two-dimensional linear models of multilayered anisotropic plates. *Acta Mechanica* 230(8):2891–2904
- Grigolyuk EI, Kulikov GM (1988) Multilayer reinforced shells (in Russ.). Mashinostroenie, Moscow
- Hill R (1965) A self-consistent mechanics of composite materials. *Journal of the Mechanics and Physics of Solids* 13(4):213–222
- Kirchhoff G (1876) *Vorlesungen über Mathematische Physik. Mechanik*. B.G. Teubner, Leipzig
- Love AEH (1927) *A Treatise on the Mathematical Theory of Elasticity*, 4th edn. Cambridge University Press, Cambridge
- Mikhasev G, Altenbach H (2019) Thin-walled Laminated Structures. Buckling, Vibrations, and Their Suppression, *Advanced Structured Materials*, vol 106. Springer, Cham
- Morozov NF, Tovstik PE, Tovstik TP (2016) The timoshenko–reissner generalized model of a plate highly nonuniform in thickness. *Doklady Physics* 61(8):394–398
- Morozov NF, Tovstik PE, Tovstik TP (2020) Bending vibrations of multilayered plates. *Doklady Physics* 65(8):17–21
- Reissner E (2021) The Effect of Transverse Shear Deformation on the Bending of Elastic Plates. *Journal of Applied Mechanics* 12(2):A69–A77
- Timoshenko SP (1921) LXVI. On the correction for shear of the differential equation for transverse vibrations of prismatic bars. *The London, Edinburgh, and Dublin Philosophical Magazine and Journal of Science* 41(245):744–746
- Tovstik PE (2019) Two-dimensional model of second-order accuracy for an anisotropic plate. *Vestnik St Petersburg University Mathematics* 52(1):112–121
- Tovstik PE, Tovstik TP (2014) A thin-plate bending equation of second-order accuracy. *Doklady Physics* 59(8):389–392
- Tovstik PE, Tovstik TP (2017a) An elastic plate bending equation of second-order accuracy. *Acta Mechanica* 228(10):3403–3419
- Tovstik PE, Tovstik TP (2017b) Generalized timoshenko-reissner models for beams and plates, strongly heterogeneous in the thickness direction. *ZAMM - Journal of Applied Mathematics and Mechanics / Zeitschrift für Angewandte Mathematik und Mechanik* 97(3):296–308

¹ Petr E. Tovstik wrote several papers together with the other authors - this is the last one of this series.



Chapter 4

On the Bending of Multilayered Plates Considering Surface Viscoelasticity

Victor A. Eremeyev and Violetta Konopińska-Zmysłowska

Abstract We discuss the bending resistance of multilayered plates taking into account surface/interfacial viscoelasticity. Within the linear surface viscoelasticity we introduce the surface/interfacial stresses linearly dependent on the history of surface strains. In order to underline the surface viscoelasticity contribution to the bending response we restrict ourselves to the elastic behaviour in the bulk. Using the correspondence principle of the theory of viscoelasticity we present an effective bending relaxation function.

Key words: Multilayered plate, Surface elasticity, Surface viscoelasticity, Bending, Effective properties

4.1 Introduction

Recently, various models of surface elasticity are widely applied to modelling of material behaviour at small scales, see Duan et al (2008); Wang et al (2011); Eremeyev (2016). Among the surface elasticity models it is worth to mention ones proposed by Gurtin and Murdoch (1975, 1978) and by Steigmann and Ogden (1997, 1999), see also Eremeyev (2016, 2020); Eremeev et al (2021) and the reference

Victor A. Eremeyev

Gdańsk University of Technology, ul. Gabriela Narutowicza 11/12, 80-233 Gdańsk, Poland,

e-mail: vicereme@pg.edu.pl

University of Cagliari, Via Marengo, 2, 09123 Cagliari, Italy

e-mail: victor.eremeev@unica.it

National Research Lobachevsky State University of Nizhni Novgorod, 23 Prospekt Gagarina (Gagarin Avenue) BLDG 6, Nizhni Novgorod, 603950, Russian Federation

e-mail: eremeyev.victor@gmail.com

Violetta Konopińska-Zmysłowska

Gdańsk University of Technology, ul. Gabriela Narutowicza 11/12, 80-233 Gdańsk, Poland

e-mail: violetta.konopinska@pg.edu.pl

therein. Within the surface elasticity one introduces additional constitutive equations which relates surface stresses, couples, and surface stresses of higher order as, for example, surface double and triple stresses, with surface strains and their gradients. Nowadays, the surface elasticity approach is successfully applied to modelling of composite materials with nanometer sized inclusions, pores, fibres, see e.g. Baranova et al (2020); Nazarenko et al (2017, 2021); Han et al (2018); Zemlyanova and Mogilevskaya (2018); Rahali et al (2020); Chen and Pindera (2020) and the references therein. It was shown that surface stresses may essentially affect the singularity of solutions in the vicinity of geometrical singularities such as crack tips, see Gorbushin et al (2020), or in the case of nanoindentation problems Li and Mi (2021). In addition, surface elasticity essentially changes the propagation of surface waves, see e.g. Eremeyev et al (2016, 2020); Eremeyev (2020); Chaki et al (2021); Mikhasev et al (2021). Some similarities between the surface elasticity and the strain gradient elasticity were firstly discussed by Mindlin (1965), see also Eremeyev et al (2019); Krawietz (2021a,b). The correspondence to lattice dynamics, i.e. to discrete models, was also studied by Eremeyev and Sharma (2019); Sharma and Eremeyev (2019).

Let us note that in the literature an elastic behaviour is mostly considered. For example, the surface elasticity was applied to modelling of plates and shells at the nanoscale by Altenbach and Eremeyev (2011); Ansari and Sahmani (2011); Ansari et al (2013, 2014); Shaat et al (2014); Sahmani et al (2015); Norouzzadeh and Ansari (2018); Ghorbani et al (2019); Ru (2016); Rouhi et al (2017). Nevertheless, an inelastic behavior at the nanoscale could be also observed. A viscoelastic extension of the surface elasticity was proposed by Ru (2009). Extending Ru's model to the case of plates and shells in Altenbach et al (2012) it was shown that the surface viscoelasticity could significantly change a viscoelastic response.

The aim of this chapter is to consider the influence of the surface/interfacial viscoelasticity on the effective bending parameters of multilayered plates. Using the correspondence principle of viscoelasticity here we extend the previous results on elastic plates towards viscoelastic ones.

4.2 Surface Viscoelasticity

Let us consider an elastic body \mathcal{B} which occupies a volume $V \subset \mathbb{R}^3$ with the smooth boundary $S = \partial V$. An infinitesimal deformation of \mathcal{B} is described through a displacement field vector \mathbf{u} given as a function of a position vector \mathbf{x} and time t

$$\mathbf{u} = \mathbf{u}(\mathbf{x}, t). \quad (4.1)$$

In the following we restrict ourselves to isotropic materials, so the constitutive relation in the bulk takes the form of Hooke's law

$$\boldsymbol{\sigma} = \lambda \text{tr} \boldsymbol{\epsilon} \mathbf{1} + 2\mu \boldsymbol{\epsilon} \quad (4.2)$$

with

$$\boldsymbol{\epsilon} = \frac{1}{2}(\nabla \mathbf{u} + \nabla \mathbf{u}^T),$$

where $\boldsymbol{\sigma}$ and $\boldsymbol{\epsilon}$ are the stress and strain tensors, respectively, λ and μ are Lamé elastic moduli, tr is the trace operator, $\mathbf{1}$ is the unit 3D tensor, and ∇ is the 3D nabla-operator.

In the bulk we have the equilibrium equations

$$\nabla \cdot \boldsymbol{\sigma} + \rho \mathbf{f} = \mathbf{0}, \quad (4.3)$$

where ρ is a mass density and \mathbf{f} is a vector of mass forces.

In addition to the stresses in the bulk, we assume the existence of surface stresses $\boldsymbol{\tau}$ acting on a surface $A \subset V$. This surface can be treated as a part of the boundary, $A \subset S$, and/or as an interface inside \mathcal{B} , and as an union of such surfaces, see Fig. 4.1 The latter case can describe an interface between parts of \mathcal{B} with different properties such as, for example, a thin polymeric layer between glass faces in the case of solar panels described by Naumenko and Eremeyev (2014).

Following Ru (2009); Altenbach et al (2012) we use the following constitutive relation for $\boldsymbol{\tau}$

$$\boldsymbol{\tau} = \boldsymbol{\tau}(\mathbf{x}, t) = \int_{-\infty}^t [\lambda_s(t-s) \text{tr} \dot{\boldsymbol{\epsilon}}(\mathbf{x}, s) \mathbf{A} + 2\mu_s(t-s) \dot{\boldsymbol{\epsilon}}(\mathbf{x}, s)] \Delta s, \quad (4.4)$$

$$\mathbf{e} = \frac{1}{2}(\nabla_s \mathbf{u} \cdot \mathbf{A} + \mathbf{A} \cdot \nabla_s \mathbf{u}^T),$$

where \mathbf{e} is the surface strain tensor, ∇_s is the surface nabla-operator defined as

$$\nabla_s = \mathbf{A} \cdot \nabla, \quad \mathbf{A} = \mathbf{1} - \mathbf{n} \otimes \mathbf{n},$$

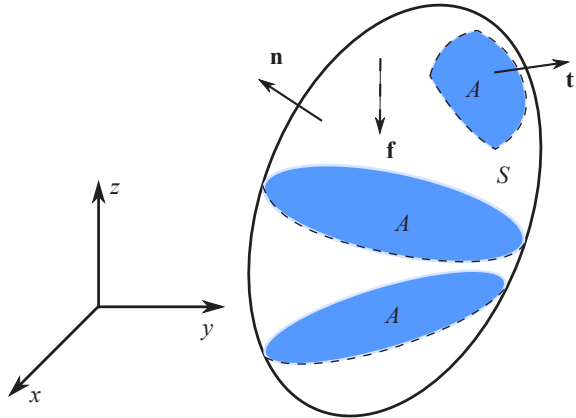


Fig. 4.1 A body \mathcal{B} with interfaces and a part of the boundary with prescribed surface stresses shown in blue color.

and λ_s and μ_s are surface relaxation functions, the overdot stands for the derivative with respect to t , \mathbf{A} is the surface (2D) unit tensor, \mathbf{n} is the unit vector of outward normal to A , and \cdot and \otimes denote the dot and dyadic products, respectively, see Simmonds (1994); Eremeyev et al (2018).

Using the Laplace transform of a function $f(t)$ defined as follows

$$\bar{f}(s) = \int_0^{\infty} f(t)e^{-st} dt$$

we can transform (4.4) into

$$\bar{\boldsymbol{\tau}} = \bar{\boldsymbol{\tau}}(\mathbf{x}, s) = s\lambda_s(s)\text{tr}\bar{\boldsymbol{\epsilon}}(\mathbf{x}, s)\mathbf{A} + 2s\mu_s(s)\bar{\boldsymbol{\epsilon}}(\mathbf{x}, s), \quad (4.5)$$

which coincides with the surface Hooke's law according to the Gurtin–Murdoch surface elasticity. So as in the case of linear viscoelasticity one can use the correspondence principle, see Christensen (1971). In other words, in the space of Laplace transforms one can use $s\lambda_s$ and $s\mu_s$ as surface Lamé moduli. Performing the inverse Laplace transform one comes to the relaxation functions. In particular, in the following with this principle we generalize effective properties to the case of viscoelastic behavior of n th-layered plates as was performed by Altenbach et al (2012).

Force balance on A results in the equations

$$\mathbf{n} \cdot \boldsymbol{\sigma} \Big|_A = \nabla_s \cdot \boldsymbol{\tau} + \mathbf{t}, \quad (4.6)$$

in the case of the boundary, $A \subset S$, here \mathbf{t} is an external traction, and/or

$$\mathbf{n} \cdot [[\boldsymbol{\sigma}]] \Big|_A = \nabla_s \cdot \boldsymbol{\tau}, \quad (4.7)$$

in the case of an interface. Here $[[\dots]]$ denotes the jump across the interface as by Eremeyev et al (2016); Eremeyev and Wiczenbach (2020). Here we assume the perfect interfacial contact, i.e. when

$$[[\mathbf{u}]] \Big|_A = \mathbf{0}. \quad (4.8)$$

For conditions on imperfect interfaces we refer to Placidi et al (2014); Eremeyev et al (2016).

4.3 Bending of a Plate-like Body

In order to discuss influence of surface/interfacial viscoelasticity on the bending of multilayered plates let us consider a plate-like body \mathcal{P} of thickness h as shown in Fig. 4.2. We assume that \mathcal{P} consists of n layers of thickness h_i , $i = 1, \dots, n$, so

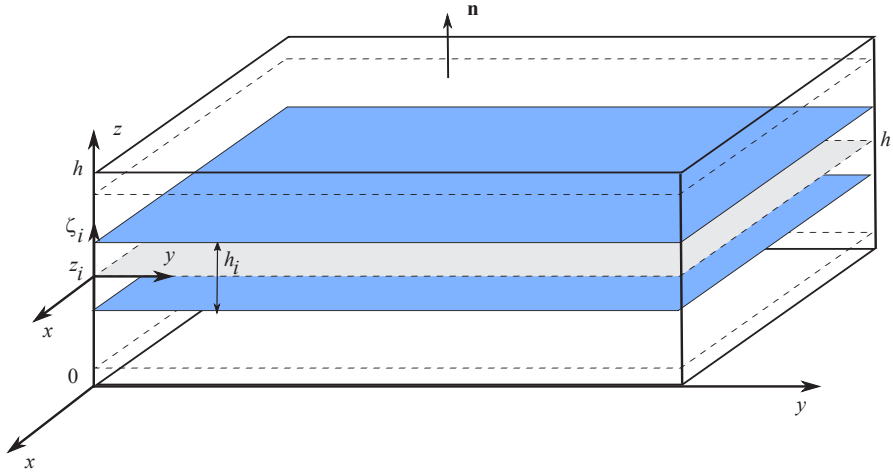


Fig. 4.2 A plate-like body \mathcal{P} which consists of n layers, the faces of i th layer of thickness h_i are shown in blue color whereas its midplane $z = z_i$ is marked in grey.

$h = h_1 + \dots + h_n$. We introduce the thickness coordinate z such that planes $z = 0$, $z = h$ correspond to faces of \mathcal{P} , whereas $z = h_i$, $i = 1, \dots, n-1$, describes the position of interfaces. Introducing two other Cartesian coordinates x and y we get the global coordinate system with the base vectors \mathbf{i}_1 , \mathbf{i}_2 , and \mathbf{i}_3 . Here in-plane coordinates belong to an area \mathcal{O} , so $\mathcal{P} = \mathcal{O} \oplus [0, h]$. In addition to (x, y, z) for i th layer we introduce the local thickness coordinates (x, y, ζ_i) with $\zeta_i \in [-h_i/2, h_i/2]$ as follows

$$\zeta_i = z - z_i, \quad z_1 = \frac{1}{2}h_1, \quad z_j = \frac{1}{2}h_j + \sum_{k=1}^{j-1} h_k, \quad i = 1, \dots, n, \quad j = 2, \dots, n.$$

Here $z = z_i$ describes the midplane of i th layer. Nevertheless, for each layer the differentiation operators do not depend on i

$$\nabla_i = \mathbf{i}_1 \frac{\partial}{\partial x} + \mathbf{i}_2 \frac{\partial}{\partial y} + \mathbf{i}_3 \frac{\partial}{\partial \zeta_i} = \mathbf{i}_1 \frac{\partial}{\partial x} + \mathbf{i}_2 \frac{\partial}{\partial y} + \mathbf{i}_3 \frac{\partial}{\partial z} = \nabla, \quad \nabla_s = \mathbf{i}_1 \frac{\partial}{\partial x} + \mathbf{i}_2 \frac{\partial}{\partial y}.$$

Considering bending deformations for i th layer we introduce the following approximation related to Kirchhoff hypothesis

$$\mathbf{u}_i(x, y, \zeta_i) = -\zeta_i \frac{\partial w_i}{\partial x} \mathbf{i}_1 - \zeta_i \frac{\partial w_i}{\partial y} \mathbf{i}_2 + w_i(x, y) \mathbf{i}_3. \quad (4.9)$$

As in the case of thin laminates we can assume that $w_i = w$, see Naumenko and Eremeyev (2014, 2017).

In the following we restrict ourselves to the analysis of the bending resistance. To this end we consider a deflection in the form of cylindrical bending, i.e.

$$w = w(x, t) = \frac{1}{2}\kappa(t)x^2.$$

Here $\kappa(t)$ describes the infinitesimal change of curvature. In this case we have

$$\mathbf{e} = \boldsymbol{\epsilon} = -z \frac{\partial^2 w}{\partial x^2} \mathbf{i}_1 \otimes \mathbf{i}_1 = -\kappa z \mathbf{i}_1 \otimes \mathbf{i}_1,$$

and

$$\boldsymbol{\kappa} = \frac{\partial^2 w}{\partial x^2} \mathbf{i}_1 \otimes \mathbf{i}_1 = \kappa \mathbf{i}_1 \otimes \mathbf{i}_1,$$

where $\boldsymbol{\kappa}$ is the tensor of change of curvature. For a viscoelastic behavior the bending moment has the form

$$M = \int_{-\infty}^t D_{\text{eff}}(t-s) \kappa(s) \Delta s, \quad (4.10)$$

where $D_{\text{eff}}(t)$ is the effective bending stiffness relaxation function.

For pure elastic materials it is constant, for example for a homogeneous elastic plate without surface stresses it takes the form

$$D = \frac{Eh^3}{12(1-\nu^2)},$$

so we came to the classic dependence $M = D\kappa$. Here E and ν are Young's modulus and Poisson's ratio, respectively.

For n th layered plate we introduce $n+1$ of pairs of relaxation functions $\lambda_s^{(i)}$ and $\mu_s^{(i)}$. Assuming for simplicity that the material in the bulk is homogeneous and has the same properties in the bulk, we get the formula for the Laplace transform

$$\bar{D}_{\text{eff}}(s) = D + \bar{D}_{\text{GM}}(s)$$

with

$$\bar{D}_{\text{GM}}(s) = (2s\bar{\mu}_s^{(0)} + s\bar{\lambda}_s^{(0)}) \frac{h^2}{4} + \sum_{i=1}^n (2s\bar{\mu}_s^{(i)} + s\bar{\lambda}_s^{(i)}) \frac{z^2}{4} \Big|_{z=-h/2+\sum_{k=1}^i h_k}.$$

Using the inverse transform we came to

$$D_{\text{eff}}(t) = D + (2\mu_s^{(0)}(t) + \lambda_s^{(0)}(t)) \frac{h^2}{4} + \sum_{i=1}^n (2\mu_s^{(i)}(t) + \lambda_s^{(i)}(t)) \frac{z^2}{4} \Big|_{z=-h/2+\sum_{k=1}^i h_k} \quad (4.11)$$

Let us assume that all faces and interface have the same properties and layers have the same thickness $\ell = h/n$. In this case the summation results in

$$D_{\text{GM}} = (2\mu_s(t) + \lambda_s(t)) \frac{\ell^2}{4} \sum_{i=0}^n (i-n/2)^2,$$

so we get

$$D_{\text{eff}} = \frac{Eh^3}{12(1-\nu^2)} + \frac{1}{n} \left(\frac{1}{6}n^2 + \frac{1}{2}n + \frac{1}{3} \right) [2\mu_s(t) + \lambda_s(t)] \frac{h^2}{8}, \quad (4.12)$$

where we perform the summation as in Eremeyev and Wiczenbach (2020).

Equation (4.12) shows an essential dependence of the bending stiffness parameter on the number of layers. So even being small in magnitude the surface viscoelasticity could be more pronounced for

- multilayered plates with $n \gg 1$;
- for plates of nanometer size, as the D_{GM} depends on h^2 whereas the classic stiffness depends on h^3 .

4.4 Conclusions

We discussed bending deformations of a n th-layered plate within the linear surface viscoelasticity theory. Using the through-the-thickness integration of equilibrium equations with kinematical approximations (4.9) we obtain the effective two-dimensional material properties. In other words, we derived the formula for effective relaxation function which corresponds to infinitesimal bending deformations. Here the effective viscoelastic properties are completely determined by viscoelastic properties of faces and interfaces as well as by through-the-thickness geometry. In a similar way, more general models of surface viscoelasticity based on the Steigmann–Ogden model could be also considered in future works as by Eremeyev and Wiczenbach (2020).

Let us note that the mechanics of layered plates was one of the corner stones of researches provided by Prof. Peter Tovstik to whom this paper is devoted, see, e.g. his recent papers (Belyaev et al, 2019; Morozov et al, 2020, 2021).

Acknowledgements Victor A. Eremeyev acknowledges the support from the RFBR under grant No. 12-01-00038.

References

- Altenbach H, Eremeyev VA (2011) On the shell theory on the nanoscale with surface stresses. *International Journal of Engineering Science* 49(12):1294–1301
- Altenbach H, Eremeyev VA, Morozov NF (2012) Surface viscoelasticity and effective properties of thin-walled structures at the nanoscale. *International Journal of Engineering Science* 59:83–89
- Ansari R, Sahmani S (2011) Surface stress effects on the free vibration behavior of nanoplates. *International Journal of Engineering Science* 49(11):1204–1215

- Ansari R, Gholami R, Faghih Shojaei M, Mohammadi V, Sahmani S (2013) Surface stress effect on the vibrational response of circular nanoplates with various edge supports. *Journal of Applied Mechanics* 80(2)
- Ansari R, Mohammadi V, Shojaei MF, Gholami R, Sahmani S (2014) On the forced vibration analysis of Timoshenko nanobeams based on the surface stress elasticity theory. *Composites Part B: Engineering* 60:158–166
- Baranova S, Mogilevskaya SG, Mantič V, Jiménez-Alfaro S (2020) Analysis of the antiplane problem with an embedded zero thickness layer described by the Gurtin-Murdoch model. *Journal of Elasticity* 140(2):171–195
- Belyaev AK, Morozov NF, Tovstik PE, Tovstik TP (2019) Two-dimensional linear models of multilayered anisotropic plates. *Acta Mechanica* 230(8):2891–2904
- Chaki MS, Eremeyev VA, Singh AK (2021) Surface and interfacial anti-plane waves in micropolar solids with surface energy. *Mathematics and Mechanics of Solids* 26(5):708–721
- Chen Q, Pindera MJ (2020) Homogenization and localization of elastic-plastic nanoporous materials with Gurtin-Murdoch interfaces: an assessment of computational approaches. *International Journal of Plasticity* 124:42–70
- Christensen RM (1971) *Theory of Viscoelasticity. An Introduction*. Academic Press, New York
- Duan HL, Wang J, Karihaloo BL (2008) Theory of elasticity at the nanoscale. In: *Advances in Applied Mechanic*, vol 42, Elsevier, pp 1–68
- Eremeev V, Lebedev L, Cloud M (2021) On weak solutions of boundary value problems within the surface elasticity of n th order. *ZAMM - Journal of Applied Mathematics and Mechanics / Zeitschrift für Angewandte Mathematik und Mechanik* 101(3):1–11
- Eremeyev VA (2016) On effective properties of materials at the nano- and microscales considering surface effects. *Acta Mechanica* 227(1):29–42
- Eremeyev VA (2020) Strongly anisotropic surface elasticity and antiplane surface waves. *Philosophical Transactions of the Royal Society A* 378(2162):20190,100
- Eremeyev VA, Sharma BL (2019) Anti-plane surface waves in media with surface structure: Discrete vs. continuum model. *International Journal of Engineering Science* 143:33–38
- Eremeyev VA, Wiczenbach T (2020) On effective bending stiffness of a laminate nanoplate considering Steigmann–Ogden surface elasticity. *Applied Sciences* 10(21):7402
- Eremeyev VA, Rosi G, Naili S (2016) Surface/interfacial anti-plane waves in solids with surface energy. *Mechanics Research Communications* 74:8–13
- Eremeyev VA, Cloud MJ, Lebedev LP (2018) *Applications of Tensor Analysis in Continuum Mechanics*. World Scientific, New Jersey
- Eremeyev VA, Rosi G, Naili S (2019) Comparison of anti-plane surface waves in strain-gradient materials and materials with surface stresses. *Mathematics and Mechanics of Solids* 24(8):2526–2535
- Eremeyev VA, Rosi G, Naili S (2020) Transverse surface waves on a cylindrical surface with coating. *International Journal of Engineering Science* 147:103,188
- Ghorbani K, Mohammadi K, Rajabpour A, Ghadiri M (2019) Surface and size-dependent effects on the free vibration analysis of cylindrical shell based on Gurtin-Murdoch and nonlocal strain gradient theories. *Journal of Physics and Chemistry of Solids* 129:140–150
- Gorbushin N, Eremeyev VA, Mishuris G (2020) On stress singularity near the tip of a crack with surface stresses. *International Journal of Engineering Science* 146:103,183
- Gurtin ME, Murdoch AI (1975) A continuum theory of elastic material surfaces. *Archive of Rational Mechanics and Analysis* 57(4):291–323
- Gurtin ME, Murdoch AI (1978) Surface stress in solids. *International Journal of Solids and Structures* 14(6):431–440
- Han Z, Mogilevskaya SG, Schillinger D (2018) Local fields and overall transverse properties of unidirectional composite materials with multiple nanofibers and Steigmann–Ogden interfaces. *International Journal of Solids and Structures* 147:166 – 182
- Krawietz A (2021a) Surface tension and reaction stresses of a linear incompressible second gradient fluid. *Continuum Mechanics and Thermodynamics* pp 1–24

- Krawietz A (2021b) Surface phenomena of gradient materials. *Continuum Mechanics and Thermodynamics* pp 1–10
- Li X, Mi C (2021) Nanoindentation of a half-space due to a rigid cylindrical roller based on Steigmann–Ogden surface mechanical model. *International Journal of Mechanics and Materials in Design* 17(1):25–40
- Mikhasev GI, Botogova MG, Eremyev VA (2021) On the influence of a surface roughness on propagation of anti-plane short-length localized waves in a medium with surface coating. *International Journal of Engineering Science* 158:103,428
- Mindlin RD (1965) Second gradient of strain and surface-tension in linear elasticity. *International Journal of Solids and Structures* 1(4):417–438
- Morozov N, Tovstik P, Tovstik T (2020) Flexural rigidity of multilayer plates. *Mechanics of Solids* 55(5):607–611
- Morozov NF, Belyaev AK, Tovstik PE, Tovstik TP (2021) Applicability ranges for four approaches to determination of bending stiffness of multilayer plates. *Continuum Mechanics and Thermodynamics* 33(4):1659–1673
- Naumenko K, Eremyev VA (2014) A layer-wise theory for laminated glass and photovoltaic panels. *Composite Structures* 112:283–291
- Naumenko K, Eremyev VA (2017) A layer-wise theory of shallow shells with thin soft core for laminated glass and photovoltaic applications. *Composite Structures* 178:434–446
- Nazarenko L, Bargmann S, Stolarski H (2017) Closed-form formulas for the effective properties of random particulate nanocomposites with complete gurtin–murdoch model of material surfaces. *Continuum Mechanics and Thermodynamics* 29(1):77–96
- Nazarenko L, Stolarski H, Altenbach H (2021) Effective properties of particulate nano-composites including Steigmann–Ogden model of material surface. *Computational Mechanics* pp 1–15
- Norouzzadeh A, Ansari R (2018) Nonlinear dynamic behavior of small-scale shell-type structures considering surface stress effects: An isogeometric analysis. *International Journal of Non-Linear Mechanics* 101:174–186
- Placidi L, Rosi G, Giorgio I, Madeo A (2014) Reflection and transmission of plane waves at surfaces carrying material properties and embedded in second-gradient materials. *Mathematics and Mechanics of Solids* 19(5):555–578
- Rahali Y, Eremyev VA, Ganghoffer JF (2020) Surface effects of network materials based on strain gradient homogenized media. *Mathematics and Mechanics of Solids* 25(2):389–406
- Rouhi H, Ansari R, Darvizeh M (2017) Size-dependent large amplitude vibration analysis of nanoshells using the Gurtin–Murdoch model. *International Journal of Nanoscience and Nanotechnology* 13(3):241–252
- Ru CQ (2009) Size effect of dissipative surface stress on quality factor of microbeams. *Applied Physics Letters* 94(5):051,905
- Ru CQ (2016) A strain-consistent elastic plate model with surface elasticity. *Continuum Mechanics and Thermodynamics* 28(1):263–273
- Sahmani S, Aghdam M, Bahrani M (2015) On the postbuckling behavior of geometrically imperfect cylindrical nanoshells subjected to radial compression including surface stress effects. *Composite Structures* 131:414–424
- Shaati M, Mahmoud F, Gao XL, Faheem AF (2014) Size-dependent bending analysis of Kirchhoff nano-plates based on a modified couple-stress theory including surface effects. *International Journal of Mechanical Sciences* 79:31–37
- Sharma BL, Eremyev VA (2019) Wave transmission across surface interfaces in lattice structures. *International Journal of Engineering Science* 145:103,173
- Simmonds JG (1994) *A Brief on Tensor Analysis*, 2nd edn. Springer, New York
- Steigmann DJ, Ogden RW (1997) Plane deformations of elastic solids with intrinsic boundary elasticity. *Proceedings of the Royal Society A* 453(1959):853–877
- Steigmann DJ, Ogden RW (1999) Elastic surface-substrate interactions. *Proceedings of the Royal Society A* 455(1982):437–474
- Wang J, Huang Z, Duan H, Yu S, Feng X, Wang G, Zhang W, Wang T (2011) Surface stress effect in mechanics of nanostructured materials. *Acta Mechanica Solida Sinica* 24:52–82

Zemlyanova AY, Mogilevskaya SG (2018) Circular inhomogeneity with Steigmann–Ogden interface: Local fields, neutrality, and Maxwell’s type approximation formula. *International Journal of Solids and Structures* 135:85–98



Chapter 5

Buckling of a Ring-stiffened Cylindrical Shell Under the External Pressure

Sergei B. Filippov and Grigory A. Nesterchuk

Abstract In this paper, the problem of buckling of a thin elastic cylindrical shell supported by the rings of various stiffness is considered. The Rayleigh–Ritz method is used to obtain the problem’s analytical solution for the case of the simply supported edges of the shell. The parameters of the optimal distribution of the structure mass between the shell and the stiffening ribs, which is required to maximize the critical pressure, have been found. The solution of the problem of minimizing the mass of a structure at a given critical pressure is obtained. Here are considered the rings with zero eccentricity. The approximate analytical solutions are compared with the numerical solutions obtained by the finite element method.

Key words: Ring-stiffened shell, Buckling, Optimal parameters, Asymptotic and Rayleigh–Ritz methods, Comsol software package

5.1 Introduction

Cylindrical shells are widely used in many industries. For example, in shipbuilding and rocketry, in the development of hulls, in the design of pipelines, industrial tanks (Lu et al, 2021), nuclear reactors and even in building of artificial islands (Verstov et al, 2020). Along with the use of smooth shells in order to increase the safety factor, reinforcement of shells with stiffening ribs (frames) is widely used. Depending on the formulation of the problem, this allows either to choose the optimal distribution of the structure weight between the shell and the ribs in order to maximize the critical pressure (Filippov, 1999), or to lighten the structure while maintaining its strength characteristics (Adamovich and Filippov, 2015).

Sergei B. Filippov · Grigory A. Nesterchuk
St. Petersburg State University, 7/9 University Embankment, St. Petersburg, 199034 Russian Federation
e-mail: s_b_filippov@mail.ru, grigory_ne@mail.ru

The paper reflects upon the problem of buckling of a thin elastic cylindrical shell under the uniform external pressure. In order to increase the critical pressure, the shell is stiffened with circular rings of different stiffness. Most of the works devoted to the theory of buckling consider the case of identical frames (Teng and Rotter, 2004), but – varying the parameters of each frame separately, the rigidity of the structure can be increased, making it possible to solve the problem of both increasing the critical pressure while maintaining the mass of the structure, and minimizing the weight of the structure while maintaining the critical pressure. Tian et al (1999) present the Ritz method for the buckling analysis of ring-stiffened cylindrical shell. In particular, ring with various size are considered, but the optimal parameters for this case are not found.

The paper considers the case of simple support of the shell edges, stiffened by ribs of the same width and different heights. The heights of the frames, characterizing their stiffness, are distributed along the generatrix of the shell according to a linear law. It is assumed that the reinforced and smooth shells buckle under the same critical pressure. Solving the problem of buckling is reduced to solving an eigenvalue problem of a system of equations describing the buckling of a cylindrical shell, boundary conditions at the edges of the shell, and conditions for coupling with stiffeners along parallels. The equations contain dimensionless thicknesses of the shell and frames, which are small parameters; therefore, asymptotic methods can be used to solve the buckling problem.

The obtained optimal parameters of the distribution function of the ring heights are used to design the shell and calculate its critical pressure by the finite element method. Comparison of the results shows that the method described in the paper can be used at the design stage of thin-walled structures.

5.2 Formulation of the Problem

Let us consider the problem of buckling of a thin-walled elastic cylindrical shell subjected to uniform external pressure p . The shell has n_r transverse stiffening ribs with zero eccentricity to increase the critical pressure. We consider the rings, whose stiffness is varied along the shell generatrix to maximize the critical pressure.

In order to describe the buckling, we use the following dimensionless equations of the technical shell theory (Tovstik, 1995):

$$\varepsilon^8 \Delta^2 w^{(i)} - \Delta_k \Phi^{(i)} - \lambda m^2 w^{(i)} = 0, \quad \Delta^2 \Phi^{(i)} + \Delta_k w^{(i)} = 0, \quad (5.1)$$

where

$$\Delta_k = \frac{d^2}{ds^2}, \quad \Delta = \Delta_k - m^2, \quad \sigma = 1 - \nu^2, \quad \lambda = \frac{p}{Eh}, \quad \varepsilon^8 = \frac{h^2}{12\sigma}. \quad (5.2)$$

Here, ε is a small parameter, $w^{(i)}$ is the displacement projection on the direction normal to the median surface for $s \in [s_{i-1}, s_i]$, $i = 1, 2, \dots, n$; $n = n_r + 1$; $s_0 = 0$, $s_n = l$; s

is the coordinate directed along the cylinder generatrix; $\Phi^{(i)}$ is the force function, m is the number of waves along the parallel; ν is the Poisson ratio; h is the dimensionless shell thickness; l is the dimensionless shell length; and E is Young modulus. Radius R of the cylinder base is taken as the unit length.

We represent the solution of system of equations (5.1) as a sum of solutions for the basic semi-membrane state, simple boundary effect near the shell edges and parallels stiffened by rings. In the first approximation, we obtain

$$\left(w_0^{(i)}\right)^{IV} - \alpha^4 w_0^{(i)} = 0, \quad \alpha^4 = m^6 \lambda_0 - \varepsilon^8 m^8, \quad (5.3)$$

where $w_0^{(i)}$ is the approximate solution of system (5.1) and λ_0 is the approximate value of λ (Filin, 1975). Hereinafter, only the approximate solution is considered, and notations $w^{(i)}$ and λ are used instead of $w_0^{(i)}$ and λ_0 .

In the case when the shell edges are simply supported, the boundary conditions for Eq. (5.3) can be written as:

$$w^{(1)}(0) = w^{(1)''}(0) = w^{(n)}(l) = w^{(n)''}(l) = 0. \quad (5.4)$$

Suppose that the typical dimension of the ring cross section $a \ll \varepsilon$. Then, the following matching conditions are fulfilled on the parallels stiffened by the rings (Filippov, 1999):

$$\begin{aligned} w^{(i)} &= w^{(i+1)}, & w^{(i)'} &= w^{(i+1)'}, & w^{(i)''} &= w^{(i+1)''}, \\ w^{(i)'''} - w^{(i+1)'''} &= -c_i w^{(i+1)}, & s &= s_i, & (i &= 1, 2, \dots, n_r), \end{aligned} \quad (5.5)$$

where

$$c_i = \frac{m^8 \varepsilon^8 l \eta_i}{n}, \quad \eta_i = \frac{12 \sigma n E_c J_i}{h^3 E l}, \quad J_i = \frac{a \cdot b_i^3}{12}.$$

Here, E_c is Young's modulus of the ring material, η_i is the effective stiffness of the ring placed in coordinate s_i (Alfutov, 2000), and J_i is the moment of inertia of the ring cross section with the respect to the cylinder generatrix. Index i indicates that the rings can differ from each other in height and thus in stiffness. For easier representation, the following notations are introduced: $c = c(\eta, m) = c_1$, $\eta = \eta_1$.

The approximate value of the critical pressure parameter $\lambda = p/(Eh)$ for a stiffened shell with simply supported edges is determined by the formula

$$\lambda(\eta) = \min_m \left[\frac{\alpha^4(c)}{m^6} + \varepsilon^8 m^2 \right], \quad (5.6)$$

where $\alpha(c)$ is the eigenvalue of the boundary problem (5.3–5.5).

5.3 Calculation of Eigenvalues of a Beam Stiffened by Springs

Eigenvalue problem (5.3)–(5.5) is equivalent to the problem of determining the vibration frequencies of a simply supported beam stiffened by springs with stiffness c_i at points s_i . In Sharypov (1997), the cases of the nonuniform arrangement of springs were analyzed. Exhaustive search method showed that the optimal arrangement of the springs is in the nodes of the vibration mode of an unsupported beam. In Lopatukhin and Filippov (2001), it was shown that in the case of simple support, zeros of the vibration mode of the unsupported beam coincided with the points of limiting optimal arrangement of the springs. In the case of simple support of a beam $s_i = il/n$ are the nodes of the vibration mode $w_n(s) = \sin(\alpha_n s)$, where $\alpha_n = \pi n/l$.

Let us consider the boundary value problem of buckling of a beam supported by springs. We apply the Rayleigh method to solve this problem. The Rayleigh formula for a spring-supported beam can be written in the following dimensionless form:

$$\alpha_1^4 = (I_1 + I_2)/I_0, \quad (5.7)$$

$$I_1 = \int_0^l (w'')^2 ds, \quad I_2 = \sum_{i=1}^{n-1} c_i w^2(s_i), \quad I_0 = \int_0^l w^2 ds,$$

In Fig. 5.1, a shell with rings is shown in the section along the shell generatrix. We equate Young's modulus of the rings with Young's modulus of the shell; hereinafter, we assume that the ring stiffness depends only on its physical dimensions. Suppose that all rings have the same width a , and the height of the first ring is $b = ka$. We also introduce $f(i)$ as a function of the ring height distribution along the cylinder generatrix: $b_i = bf(i) = kaf(i)$. Upon substituting the expressions for the ring dimensionless stiffness and the first vibration mode of the smooth shell into the Rayleigh formula, we obtain the following relation for :

$$\alpha_1^4(\eta, m) = \frac{\pi^4}{l^4} + \frac{2}{l} c(\eta, m) T(n), \quad J = \frac{ab^3}{12}, \quad (5.8)$$

$$J_i = \frac{a^4 k^3}{12} f^3(s_i) = J f^3(s_i), \quad T(n) = \sum_{i=1}^{n-1} f^3(i) \sin^2\left(\frac{\pi i}{n}\right).$$

Substituting the obtained α_1 into the formula for critical pressure parameter (5.6) we obtain

$$\lambda(\eta, m) = Xm^{-6} + Ym^2,$$

where

$$X = \frac{\pi^4}{l^4}, \quad Y = \left(1 + \frac{2T(n)}{n}\eta\right)\varepsilon^8.$$

Let us find the smallest value of frequency parameter λ_1 by minimizing the resulting function $\lambda(\eta, m)$ with respect to m :

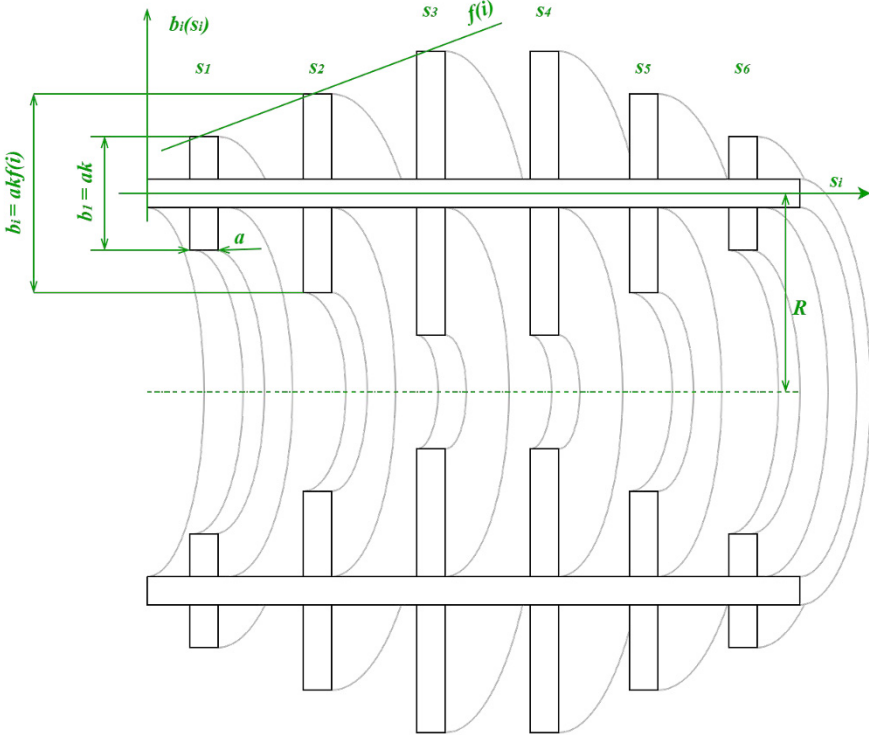


Fig. 5.1 Axial section of a ring-stiffened shell.

$$\lambda'_m(\eta, m) = -6Xm^{-7} + 2Ym = 0, \quad \lambda_1(\eta) = \sqrt[4]{\frac{256}{27}XY^3} = \varepsilon^6 \cdot \sqrt[4]{\frac{256}{27} \frac{\pi^4}{l^4} \left(1 + \frac{2T(n)}{n}\eta\right)^3}.$$

Since relation $\varepsilon^8 = h^2/(12\sigma)$ is satisfied for small parameter ε we write λ_1 in the following form:

$$\lambda_1(\eta) = \frac{\sqrt{6}\pi}{9l} \frac{h^{3/2}}{\sigma^{3/4}} \sqrt[4]{\left(1 + \frac{2T(n)}{n}\eta\right)^3}. \tag{5.9}$$

5.4 Shell Parameters Optimization

Let the mass of the stiffened shell be fixed. We consider the problem of determining the optimal mass distribution between the rings and the shell (coating), which corresponds to the highest value of the critical pressure.

Critical pressure p_0 for a smooth shell with length l and thickness h_0 can be found by the approximate Southwell–Papkovich formula taken from Filippov (1999):

$$\lambda = \frac{\sqrt{6}\pi}{9l} \frac{h_0^{3/2}}{\sigma^{3/4}}, \quad p_0 = \lambda E h_0 = \frac{4\pi E h_0^{5/2}}{6^{3/2} l \sigma^{3/4}}. \quad (5.10)$$

Suppose that n_r rings with rectangular cross section a in width and b_i in height are mounted on the shell due to reducing the shell thickness to h ; the ring-stiffened shell mass is

$$M_s = M(h) + M_r,$$

where $M(h) = 2\pi R \rho \cdot Rh \cdot Rl$ is the mass of the coating, while ring mass

$$M_r = \sum_{i=1}^{n-1} 2\pi R \rho \cdot Ra \cdot R a k f(i)$$

coincides with the smooth shell mass $M_0 = M(h_0)$.

In order to determine the critical pressure of the smooth and stiffened shells, we can use formulas (5.9) and (5.10). Those formulas can be used only when η is sufficiently small because the boundary problem (5.3)–(5.5) has a solution that is independent of the relative stiffness of rings:

$$w = \sin(\alpha x), \quad \alpha = \pi n / l.$$

This solution corresponds to $\lambda = n \cdot \lambda_1(0)$. Let us introduce a function of the ratio between the critical pressures of the stiffened and smooth shells and find its maximum value f_b^* :

$$f_b \simeq \frac{p_1}{p_0} = \begin{cases} d^{5/2} \sqrt[4]{\left(1 + \frac{2T(n)}{n} \eta\right)^3}, & 0 \leq \eta \leq \eta_*, \\ d^{5/2} n, & \eta_* < \eta, \end{cases}$$

where $d = h/h_0$, and parameter η_* is called the effective stiffness of the ring (Filippov, 1999; Alfutov, 2000) and can be found as the root of the following equation:

$$\left(1 + \frac{2T(n)}{n} \eta_*\right)^{3/4} = n, \quad \eta_* = \frac{n}{2T(n)} (n^{4/3} - 1).$$

Upon simplification, we obtain:

$$f_b = \begin{cases} d^{5/2} n, & 0 \leq d \leq d_*, \\ d^{5/2} \sqrt[4]{\left(1 + \frac{Ba^4}{d^3}\right)^3}, & d_* < d \leq 1, \end{cases} \quad (5.11)$$

where

$$B = \frac{2\sigma k^3}{lh_0^3} \cdot T(n), \quad A = \frac{k}{h_0 l} \cdot P(n), \quad P(n) = \sum_{i=1}^{n-1} f(i).$$

The condition of the equality of masses of ring-stiffened shell and smooth shell can be written as follows:

$$M(h_0) = M(h) + M_r, \quad a^4 = \frac{(1-d)^2}{A^2}.$$

Substituting the expression for a^4 into function $f_b(d)$, we obtain

$$f_b = \begin{cases} d^{5/2}n, & 0 \leq d \leq d_*, \\ d^{5/2} \left(1 + \frac{B}{A^2} \cdot \frac{(1-d)^2}{d^3} \right)^{3/4} & d_* < d \leq 1, \end{cases}$$

where d_* is the root of the cubic equation

$$d_*^3 - \frac{2\sigma kl}{h_0} \cdot \frac{T(n)}{P^2(n)(n^{4/3} - 1)} \cdot (d_* - 1)^2 = 0.$$

This equation has a single root on interval $(0, 1)$ that corresponds to the maximum critical pressure of a simply supported shell stiffened by rings with various stiffness. Here, a_* and f_b^* corresponding to d_* can be found by the following formulas:

$$a_* = \sqrt{\frac{1-d_*}{A}}, \quad f_b^* = n \cdot d_*^{5/2}.$$

5.5 Minimization of Mass

Consider a simply supported cylindrical shell with thickness h , length l and radius R stiffened by n_r uniformly spaced ribs of various height. We will look for the parameters of the shell with the lowest mass and critical pressure p . Then the mass of stiffened shell M_s and unstiffened M_0 shell can be expressed by the formulae:

$$M_s = 2\pi R^3 \rho \left(lh + \sum_{i=1}^{n-1} a \cdot akf(i) \right), \quad M_0 = 2\pi R^3 \rho lh_0, \quad (5.12)$$

where ρ is the density of the shell material. For convenience, we introduce the function $F(a, d)$, which will show the ratio of the mass of the stiffened shell to the mass of the smooth shell.

$$F(a, d) = \frac{M_s}{M_0} = d + Aa^2, \quad d = \frac{h}{h_0} \quad A = \frac{k}{h_0 l} \cdot P(n), \quad P(n) = \sum_{i=1}^{n-1} f(i).$$

Then the function showing the ratio of the critical pressures of the stiffened shell to the smooth shell is:

$$f_b \approx \frac{p_1}{p_0} = \begin{cases} d^{5/2} \sqrt[4]{\left(1 + \frac{2T(n)}{n}\eta\right)^3}, & 0 \leq \eta \leq \eta_*, \\ d^{5/2}n, & \eta_* < \eta, \end{cases}$$

substitution

$$B = \frac{2\sigma k^3}{lh_0^3} \cdot T(n), \quad T(n) = \sum_{i=1}^{n-1} f^3(i) \sin^2\left(\frac{\pi i}{n}\right).$$

drives the f_b function to

$$f_b = \frac{p_1}{p_0} = \begin{cases} d^{5/2}n, & 0 \leq d \leq d_* \\ d^{5/2} \left(1 + \frac{Ba^4}{d^3}\right)^{3/4}, & d_* < d \leq 1. \end{cases}$$

The condition of equality of the critical pressures of a smooth and a reinforced shell is reduced to solving the equation $f_b = 1$ for $\eta = \eta_*$. The corresponding parameters of the reinforced shell d_* and a_* can be found using the formulas

$$d_* = n^{-2/5}, \quad a_*^4 = \frac{(n^{4/3} - 1) \cdot d_*^3}{B}.$$

Which, when substituted into $F(a, d)$, reduce it to a function that depends on the number of rings n_r and the parameters of the distribution function of the heights of the rings k and u :

$$F(n) = n^{-2/5} + \frac{A}{\sqrt{B}} \cdot \sqrt{n^{2/15} - n^{-6/5}}.$$

5.6 Results

Some results for the copper ($\nu = 0.35$, $E = 110$ [GPa]) shell $R = 1$ [m], $l = 4$ [m], $h = 0.01$ [m], $k = 1$ and n_r rings obtained by the both described analytical method and finite element method (using Comsol software package) are driven. Table 5.1 shows the results for the critical pressure maximization problem and Table 5.2 shows the mass minimization problem. Both the cases of stiffening the shell by rings with equal heights and heights distributed according to the triangular law:

$$f(i) = (\kappa(i) - 1)(u - 1) + 1, \quad \kappa(i) = \begin{cases} i, & i < \frac{n}{2} \\ n - i, & i \geq \frac{n}{2} \end{cases},$$

are considered.

The buckling modes of a shell stiffened by even ribs (top) and uneven ribs (bottom) for three, four and five ribs are shown in Figs. 5.2-5.4.

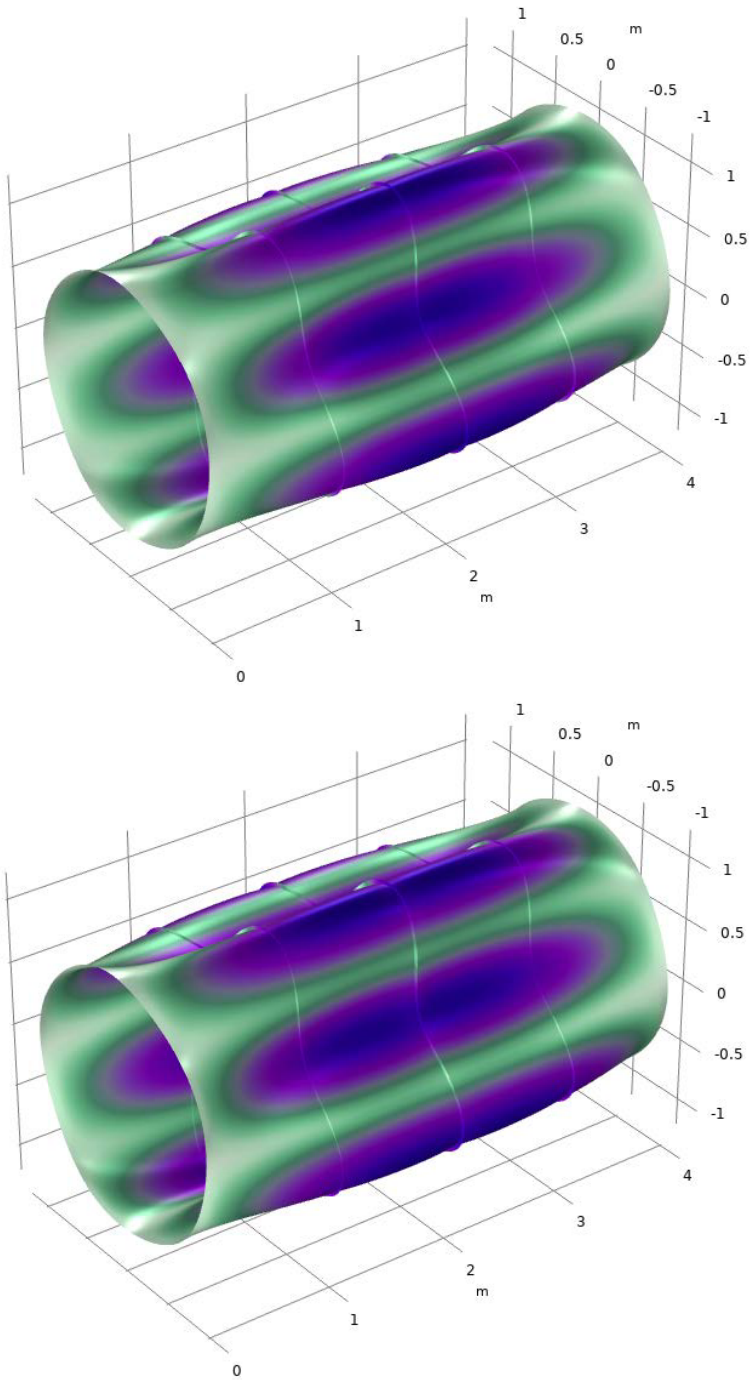


Fig. 5.2 Buckling of a shell stiffened by three ribs with even ribs (top) and uneven ribs (bottom).

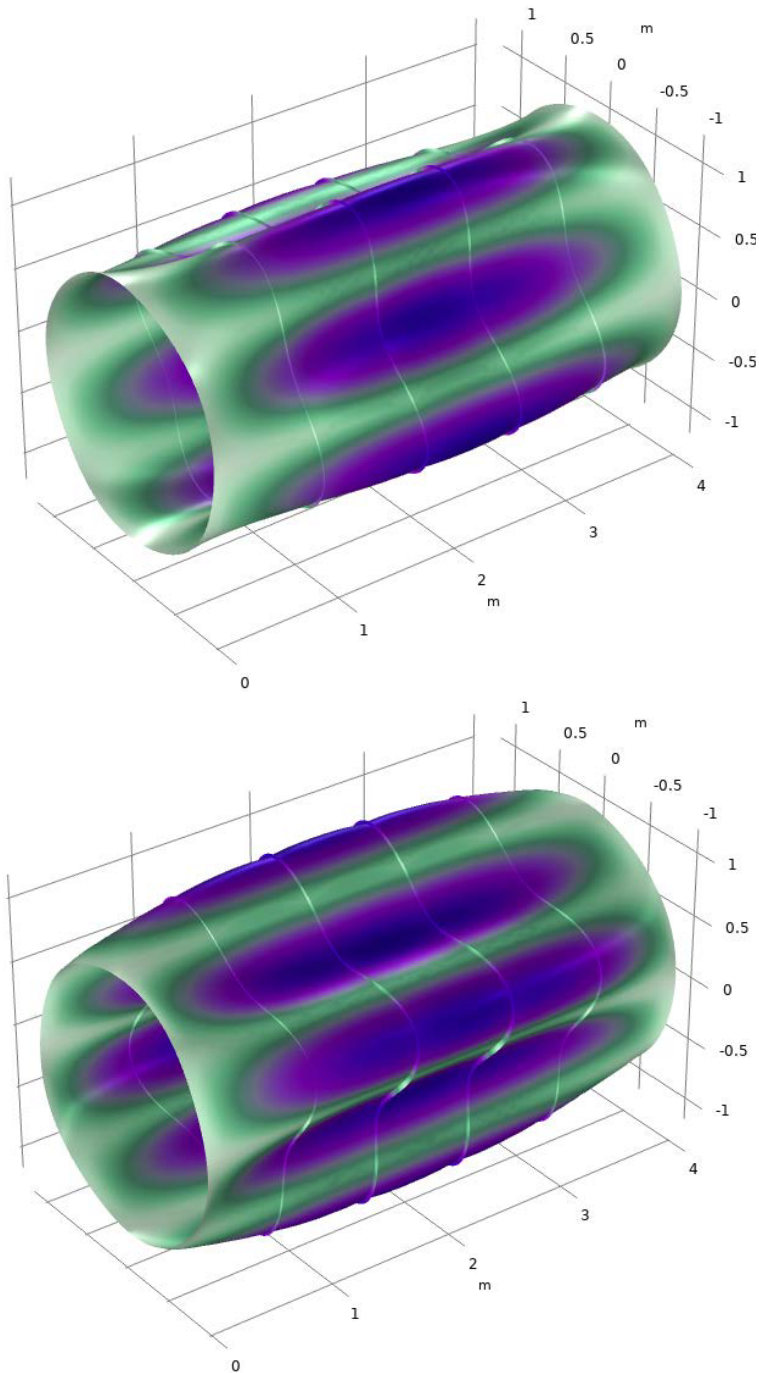


Fig. 5.3 Buckling of a shell stiffened by four ribs with even ribs (top) and uneven ribs (bottom).

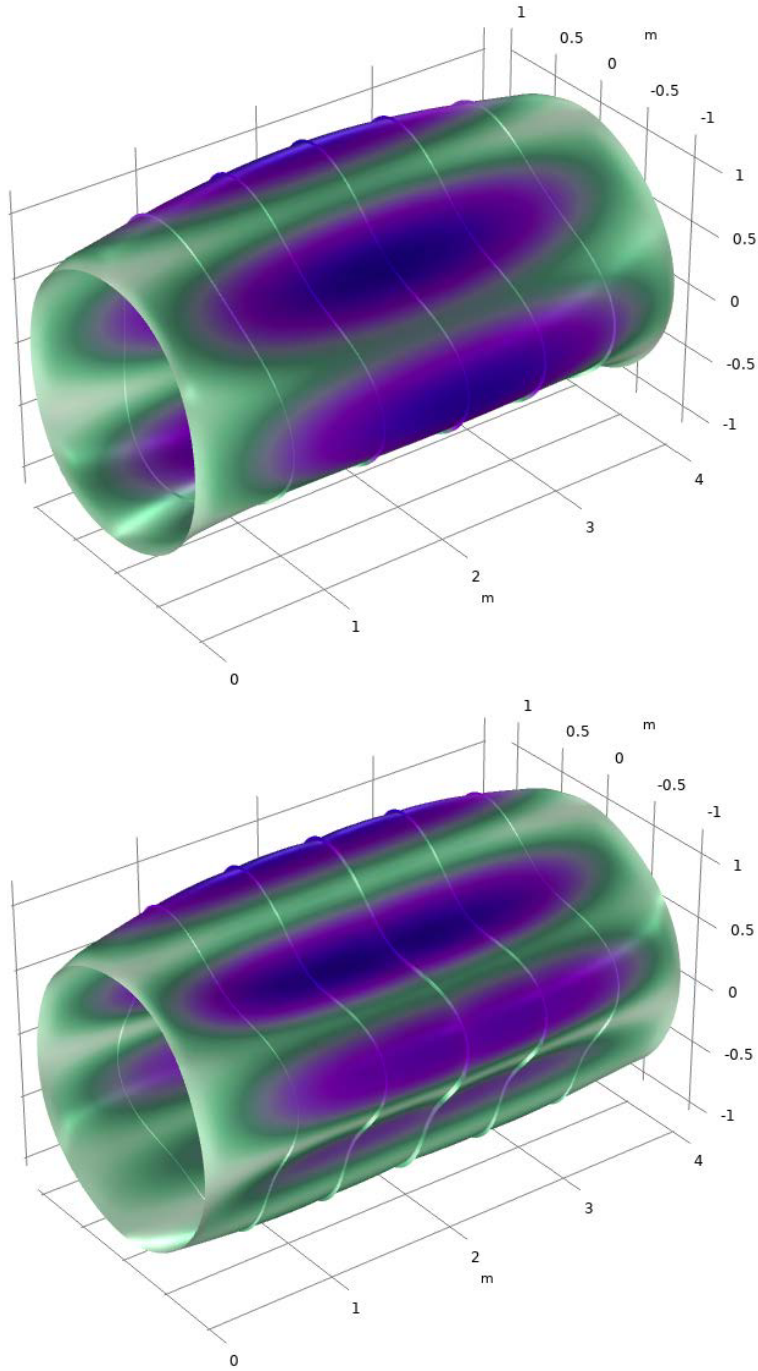


Fig. 5.4 Buckling of a shell stiffened by five ribs with even ribs(top) and uneven ribs(bottom).

Table 5.1 Pressure maximization problem.

| n_r | $u = 1$ | | | $u = 1.5$ | | |
|-------|---------|-----------------------|-----------------------------|-----------|-----------------------|-----------------------------|
| | f_b | p_{\max}, Pa | $p_{\text{fem}}, \text{Pa}$ | f_b | p_{\max}, Pa | $p_{\text{fem}}, \text{Pa}$ |
| 0 | 1 | 259346 | 281240 | | | |
| 1 | 1.79 | 464081 | 454120 | | | |
| 2 | 2.32 | 603640 | 610520 | | | |
| 3 | 2.69 | 698936 | 730570 | 2.9 | 752572 | 749210 |
| 4 | 2.94 | 786514 | 822300 | 3.29 | 852119 | 883650 |
| 5 | 3.11 | 806571 | 885130 | 3.76 | 975032 | 1000800 |

Table 5.2 Mass minimization problem.

| n_r | $u = 1$ | | | $u = 2$ | | |
|-------|---------|-------|-----------|---------|-------|-----------|
| | d_* | a_* | M_s/M_0 | d_* | a_* | M_s/M_0 |
| 0 | 1 | 0 | 1 | | | |
| 1 | 0.758 | 0.035 | 0.786 | | | |
| 2 | 0.644 | 0.034 | 0.703 | | | |
| 3 | 0.574 | 0.033 | 0.655 | 0.574 | 0.023 | 0.625 |
| 4 | 0.525 | 0.032 | 0.625 | 0.525 | 0.02 | 0.586 |
| 5 | 0.488 | 0.031 | 0.605 | 0.488 | 0.016 | 0.546 |

5.7 Conclusion

The application of asymptotic and Rayleigh–Ritz methods permits to obtain simple approximate formulas for evaluating of the critical external pressure and the optimal parameter for the cylindrical shell stiffened by rings with various heights.

The calculations showed that the shell of the fixed mass stiffened by rings with the various stiffness has a higher value of the critical pressure than the shell stiffened by identical rings. Also, if the critical pressure is set, then the minimal weight of the first shell is less than the minimal weight of the second one.

The relative error of approximate results in comparison with the results obtained by the finite element method is less than 9%. Hence, the approach described in this paper can be used for the approximate estimation of parameters before starting the design.

Acknowledgements This work was supported by RFBR (grant 19-01-00280) which is gratefully acknowledged.

References

- Adamovich IA, Filippov SB (2015) Optimal design of stiffened cylindrical shell (in russ.). *Vestnik Sankt-Peterburgskogo Universiteta Series 1 2* (60)(2):226–234
- Alfutov NA (2000) *Stability of Elastic Structures. Foundations of Engineering Mechanics*, Springer, Berlin, Heidelberg, New York
- Filin AP (1975) *Elements of the Theory of Shells* (in Russ.). Stroiizdat, Leningrad Division, Leningrad
- Filippov SB (1999) *Theory of connected and stiffened shells* (in Russ.). St. Petersburg State University Press, St. Petersburg
- Lopatukhin A, Filippov SB (2001) Low frequency vibration and buckling of the ring stiffened thin cylindrical shell (in russ.). *Vestnik Sankt-Peterburgskogo Universiteta Series 1* (2):84–90
- Lu Y, Wang L, Wang H, Chen G, Liu S, Yue H (2021) Experiments on active stiffness control of a thin-walled cylindrical shell with novel SMA driven screw-type actuators. *Thin-Walled Structures* 159:107,334
- Sharypov DV (1997) Low-frequency vibrations of the ring-stiffened thin cylindrical shell (in Russ.). *St Petersburg Univ Mech Bulletin* (3):29–34
- Teng JG, Rotter JM (2004) *Buckling of Thin Metal Shells*. CRC Press, London
- Tian J, Wang CM, Swaddiwudhipong S (1999) Elastic buckling analysis of ring-stiffened cylindrical shells under general pressure loading via the ritz method. *Thin-Walled Structures* 35(1):1–24
- Tovstik PE (1995) *Buckling of thin shells. Asymptotic methods* (in Russ.). Nauka, Nauka
- Verstov V, Yudina A, Gaido A (2020) Improving efficiency of arranging offshore cofferdams. *Soil Mechanics and Foundation Engineering* 57(1):73–76



Chapter 6

Free Vibration Corrugated Open Cylindrical Shells

Alexander Ya. Grigorenko, Maksym Yu. Borysenko, Olena V. Boychuk, and Natalia P. Boreiko

Abstract The problem of the free vibrations of the thin circular corrugated open cylindrical shells are presented. The finite element method was used. The frequencies and forms of free vibrations of the in circular corrugated open cylindrical under conditions of different longitudinal bisecting and different boundary conditions shells are calculated. The dependence of the frequency of free vibrations on the variant of longitudinal bisecting is analyzed.

Key words: Free vibrations, Corrugated circular cylindrical shell, Different boundary conditions, Rigid fixes, FEM

6.1 Introduction

The problem of the free vibrations of corrugated open cylindrical shells is very important for further basic research and for various practical problems. Solving such problems is associated with great computational difficulties. Therefore, the current problem of the mechanics and the applied mathematics of the free vibrations of corrugated open cylindrical is proposed to be solved based on FEM.

Cylindrical shells, due to their high strength and stability with relatively low weight, are widely used in various industries. Increasing the strength characteristics while maintaining mass can be achieved by changing the wall thickness of the shell or changing the shape of the cross section, for example, using corrugation. The

Alexander Ya. Grigorenko · Maksym Yu. Borysenko · Natalia P. Boreiko
S.P. Timoshenko Institute of Mechanics, National Academy of Sciences of Ukraine, 3 Nesterova St., Kyiv, 03057, Ukraine,
e-mail: ayagrigorenko1991@gmail.com, mechanics530@gmail.com, nataliya.petrivna@ukr.net

Olena V. Boychuk
Nikolaev National Agrarian University, 9 Georgy Gongadze St., Nikolaev, Ukraine, 54030,
e-mail: boychuklana27@gmail.com

design of the frames of various machines and mechanisms, and the shell elements of buildings, structures, and other constructions is dependent on a number of prior calculations. One of the important calculations is to determine the frequencies and forms of free vibrations, since when the frequency of the external force coincides with the frequency of free vibrations, resonance occurs, which can be destructive. In modern science, these problems of dynamics are commonly solved using a variety of computer-aided design software systems, which are based on various numerical methods such as the finite element method (FEM). One such software system is FEMAP with the NX Nastran solver. There arises an urgent problem of mechanics and applied mathematics about the extension of FEM to the study of frequencies and forms of free vibrations of corrugated open cylindrical shells.

Determination of the frequencies and forms of free vibrations of shells of a simple geometric shape is possible within the framework of the theory of thin shells (Arnold and Warburton, 1953; Baron and Bleich, 1954; Greenspon, 1959; Grigorenko et al, 2018b; Grigorenko and Rozhok, 2004; Grigorenko and Efimova, 2008). In the case of shells of a complex shape, which have non-circular cross-sections of constant (Budak et al, 2016) or variable (Budak et al, 2017) thickness, or open contours (Grigorenko et al, 2020a,b), or thick walls (Grigorenko et al, 2018a), it is advisable to use the FEM. In addition to numerical methods, there is the use of experimental methods for determining the frequencies and forms of free vibrations of shells of complex shapes, for example, the method of holographic interferometry (Grigorenko et al, 2013; Budak et al, 2014).

Let us consider some of the literature. In Puzyrev (2013), a study was carried out using the spline collocation method in combination with the method of discrete orthogonalization of resonance frequencies of noncircular cylindrical shells with an elliptical corrugated cross section. (Mousa Khalifa, 2015)) investigates the influence of the parameters of corrugation and material homogeneity on the vibration frequencies of isotropic and orthotropic oval cylindrical shells with a sinus-like contour. In Kim (2016), the free vibrations of longitudinally corrugated cylindrical shells are theoretically investigated, and the frequencies are calculated using the finite element method implemented in the ANSYS program. Nguyen et al (2021) present a semi-analytical approach to the study of vibration of corrugated functionally graded sandwich cylindrical shells. In Semenyuk et al (2005) investigates the influence of the length and amplitude of the corrugations on the fundamental frequency of corrugated non-circular cylindrical shells both while unloaded and while compressed along the axis. Xu et al (2008, 2010) investigate the dynamic characteristics of coupled longitudinal and bending vibrations of corrugated cylindrical piezoelectric shells. Yang et al (2015) study the vibration characteristics of corrugated composite cylindrical sandwich shells with free boundary conditions. Yuan and Liu (2007) investigate, on the basis of the equations covering the dynamics of large deflections of axisymmetric shallow shells in revolution, nonlinear forced vibrations of a corrugated shallow shell under a uniform load.

The purpose of this work is to determine by the finite element method (FEM) the frequencies and forms of free vibrations of thin circular open corrugated cylindrical

shells with variations in rigid fastening and to establish the effect of the method of longitudinal bisecting of the shell on the frequencies and forms of free vibrations.

6.2 Basic Relationships

The motion of a mechanical system with a finite number of degrees of freedom in the absence of external forces is described by a system of Lagrange equations of the second kind:

$$\frac{d}{dt} \left(\frac{\partial L}{\partial \dot{q}_j} \right) - \left(\frac{\partial L}{\partial q_j} \right) = 0, \quad j = 1, 2, \dots, s, \quad (6.1)$$

where $L = T - U$. Using the discrete form of the kinetic energy and deformation energy functionals:

$$T = \frac{1}{2} \dot{\bar{\Phi}}_i^T \mathbf{M}_i \dot{\bar{\Phi}}_i, \quad U = \frac{1}{2} \bar{\Phi}_i^T \mathbf{K}_i \bar{\Phi}_i, \quad (6.2)$$

where \mathbf{K}_i and \mathbf{M}_i are the stiffness matrix and the mass matrix of the i -th finite element, and $\bar{\Phi}_i$ is the vector of nodal displacements of the i -th element. From the Lagrange equation (6.1) we obtain the following equations of motion in the absence of damping

$$\mathbf{K} \bar{\Phi}_j + \mathbf{M} \ddot{\bar{\Phi}}_j = 0, \quad (6.3)$$

where \mathbf{K} and \mathbf{M} are the stiffness matrix and the mass matrix of the mechanical system, $\bar{\Phi}_j$ is the vector of displacements of the nodes of the system corresponding to the j -th degree of freedom, and reproduces the j -th mode of vibration.

With free vibrations of the shells, all nodal points carry out harmonic vibrations as a function of time

$$\bar{\Phi}_j(t) = \bar{\Phi}_j \sin(\omega_j t). \quad (6.4)$$

After substituting functions (6.4) into the equation of motion (6.3), the determination of natural frequencies and vibration modes is reduced to solving the system of algebraic equations

$$\mathbf{K} \bar{\Phi}_j - \omega_j^2 \mathbf{M} \bar{\Phi}_j = 0, \quad j = 1, 2, \dots, s, \quad (6.5)$$

where ω_j is the ripple or frequency of harmonic vibrations.

For determining the natural modes and vibration frequencies in the case when energy dissipation and damping is not taken into account NX Nastran primarily uses the Lanczos method, which requires fewer resources compared to other methods. The Lanczos method allows one to determine the n -th number of necessary eigen-

values and forms, while the results can be considered practically accurate for this discrete model, since the error is $\|\bar{\Phi}_j - \omega_j^2 \mathbf{K}^{-1} \mathbf{M} \bar{\Phi}_j\| / \|\bar{\Phi}_j\| \leq 10^{-7}$.

The Lanczos' method uses reduction to transform to the triodiagonal form of the matrix \mathbf{T}

$$\mathbf{T} = \mathbf{Q}_k^T \mathbf{M} \mathbf{K}^{-1} \mathbf{M} \mathbf{Q}_k, \quad (6.6)$$

where $\mathbf{Q}_k = \{\bar{q}_1, \bar{q}_2, \dots, \bar{q}_k\}$ is a rectangular matrix with elements $N_{eq} \times k$; N_{eq} is the number of equations; k is a step number according to the Lanczos method; \bar{q}_k is the k -th vector of Lanczos.

The formula

$$\beta_{k+1} \bar{q}_{k+1} = \mathbf{K}^{-1} \mathbf{M} \bar{q}_k - \alpha_k \bar{q}_k - \beta_k \bar{q}_k, \quad (6.7)$$

generates the next Lanczos vector and determines the current row of the matrix \mathbf{T}

$$\mathbf{T} = \begin{vmatrix} \alpha_1 & \beta_2 & & & \\ \beta_2 & \alpha_2 & \beta_3 & & \\ & \beta_3 & \alpha_3 & \beta_4 & \\ \cdot & \cdot & \cdot & \cdot & \\ & & \beta_k & \alpha_k & \end{vmatrix}. \quad (6.8)$$

Thus, we get the eigenvalue problem:

$$\mathbf{T} \bar{s}_h^k - \bar{\lambda}_h^k \bar{s}_h^k = 0, \quad h = 1, 2, \dots, k, \quad (6.9)$$

$$(\omega_h^k)^2 = 1/\lambda_h^k, \quad (6.10)$$

where ω_h^k is the k -th approximation of the circular frequency ω_h , $h = 1, 2, \dots, n$; n is the number of proper pairs.

The algorithm continues the calculations (for k increasing k , the step number of the Lanczos procedure) until the specified accuracy is achieved for all the necessary eigenvalues. The selective orthogonalization procedure maintains the required level of orthogonalization of Lanczos vectors q_k , which ensures the reliability and stability of the numerical calculation process. In this case, economical methods are used to implement the selectively orthogonalization procedure and to determine the eigenvalues (6.9) by using double QR – iterations with shifts. The output eigenvectors are determined by the formula

$$\bar{\Phi}_h^k = \mathbf{Q}_k \bar{s}_h^k = 0, \quad h = 1, 2, \dots, n. \quad (6.11)$$

6.3 Solution to the Test Problem

In the FEMAP program environment, the geometry of four corrugated cylindrical shells was built with corrugation densities $k = 4$, $k = 6$, $k = 8$ and $k = 10$ (Fig. 6.1), height $h = 120$ mm, thickness $d = 2$ mm and a median surface, given by the parametric equations:

$$x(\theta) = [a + r \cos(k\theta)] \cos\theta; \quad y(\theta) = [b + r \cos(k\theta)] \sin\theta; \quad (6.12)$$

where $a = b = 44$ mm are the semi-axes of the base ellipse of the cross-section, and $r = 2$ mm is the amplitude of the corrugation. The shell material was steel with Young’s modulus $E = 210$ GPa, Poisson’s ratio $\nu = 0.28$ and density $\rho = 7740$ kg/m³. The shell was rigidly fixed along all edges (CCCC).

As a result of solving test problems, the frequencies of free vibrations were obtained, which are presented in Table 6.1 together with the frequencies obtained by Puzyrev (2013) and with the given discrepancy in the calculations in percent. The resulting vibration modes are shown in Fig. 6.2.

Analyzing the obtained results of test problems, one can see agreement between the frequencies of free vibrations obtained using FEMAP and the frequencies calcu-

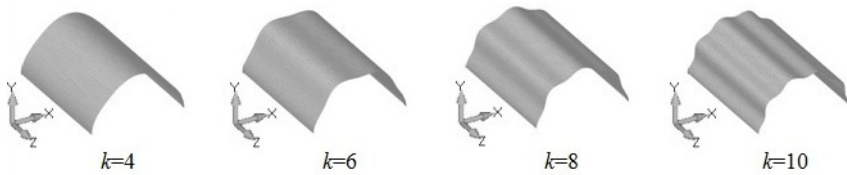


Fig. 6.1 Finite-element models of test corrugated shells.

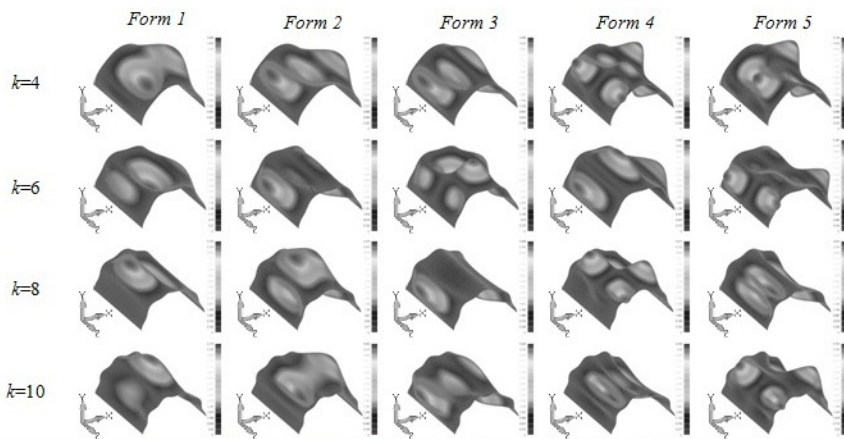


Fig. 6.2 Forms of free vibrations of test corrugated shells.

Table 6.1 Frequencies of free vibrations (f , Hz) of test corrugated shells.

| No. | $k = 4$ | | | No. | $k = 6$ | | |
|-----|---------|------|-------------------|-----|----------|------|-------------------|
| | Puzyrev | FEM | $\varepsilon, \%$ | | Puzyrev | FEM | $\varepsilon, \%$ |
| 1 | 4695 | 4668 | 0.58 | 1 | 3369 | 3269 | 3.06 |
| 2 | 4904 | 4880 | 0.49 | 2 | 4841 | 4681 | 3.42 |
| 3 | 6617 | 6581 | 0.55 | 3 | 4987 | 4827 | 3.31 |
| 4 | 6953 | 6897 | 0.81 | 4 | 6183 | 5962 | 3.71 |
| 5 | 7444 | 7391 | 0.72 | 5 | 6234 | 6011 | 3.71 |
| No. | $k = 8$ | | | No. | $k = 10$ | | |
| | Puzyrev | FEM | $\varepsilon, \%$ | | Puzyrev | FEM | $\varepsilon, \%$ |
| 1 | 4792 | 4753 | 0.82 | 1 | 5054 | 4879 | 3.59 |
| 2 | 5055 | 6581 | 0.55 | 3 | 4987 | 4827 | 3.31 |
| 4 | 6953 | 6897 | 0.81 | 4 | 6183 | 5962 | 3.71 |
| 5 | 7444 | 7391 | 0.72 | 5 | 6234 | 6011 | 3.71 |
| 3 | 6388 | 6294 | 1.49 | 3 | 6912 | 6643 | 4.05 |
| 4 | 6507 | 6433 | 1.15 | 4 | 7140 | 6778 | 5.34 |
| 5 | 7151 | 7001 | 2.14 | 5 | 8026 | 7676 | 4.56 |

lated by the spline collocation method in combination with the method of discrete orthogonalization, which indicates the correctness of the proposed method. At the same time, the discrepancy between the results increases with an increase in the number of corrugations. It's also possible to observe various wave forms for the same number of the mode.

6.4 Construction of a Computational Model

Using the FEMAP system, the geometry of a circular corrugated closed cylindrical shell was constructed with height $h = 120$ mm, thickness $d = 2$ mm, middle surface with parametric equations (6.12), where $a = b = 42.064$ mm, $r = 2$ mm, $k = 8$. Then the shell was cut in half at maxima points (Fig. 6.3a), midpoints (or 0) (Fig. 6.3b) or minima points (Fig. 6.3c) of corrugation waves. Steel with the following characteristics was set as the material: Young's modulus $E = 214$ GPa, Poisson's ratio $\nu = 0.32$ and density $\rho = 7820$ kg/m³. The shells were investigated with various rigidly fixed (C) and free edges (F) (Fig. 6.4). The calculation was carried out to determine the frequencies and forms of free vibrations.

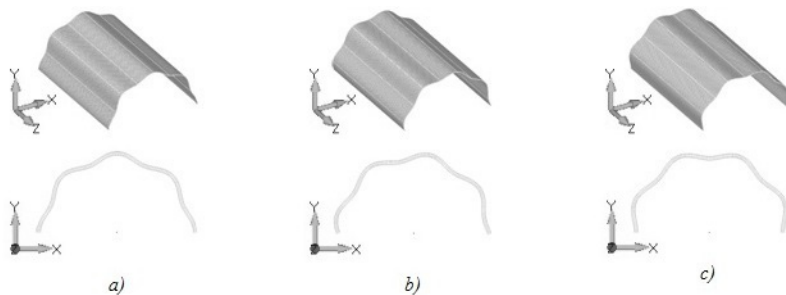


Fig. 6.3 Finite element models of corrugated shells with different locations of longitudinal bisecting.

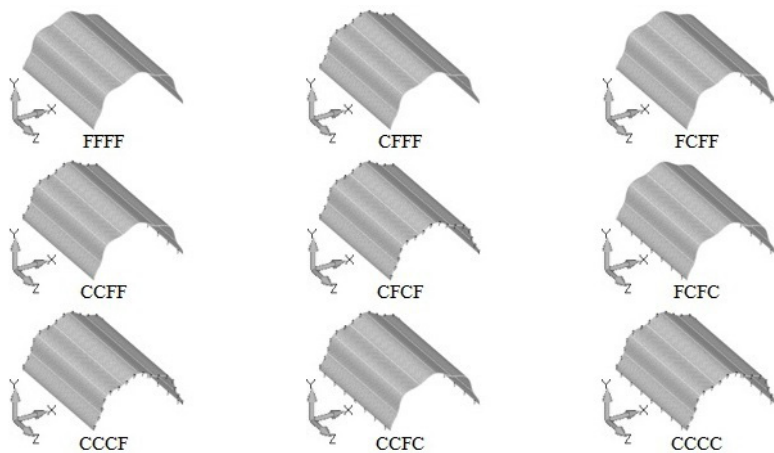


Fig. 6.4 Boundary conditions of the investigated corrugated shells.

6.5 Results of Numerical Calculations

As a result of calculations, we obtained the frequencies and forms of free vibrations of steel circular corrugated open cylindrical shells with different locations of longitudinal bisection and with $k = 8$ corrugations for all free edges and all rigidly fixed edges. The first ten frequencies of free vibrations of the three investigated corrugated shells of equivalent mass are presented in Table 6.2, where ε is the difference between the frequencies in percent. Analyzing the data in Table 6.2, one can see that for shells with the boundary conditions FFFF, the first five frequencies for shells with different bisecting locations have a small discrepancy compared to the next five frequencies. Starting from the sixth mode of vibration (Figs. 6.5 and 6.6), a different structural rigidity is manifested, which causes different shaping. That is, different modes of vibration or slightly distorted vibration modes correspond to the same shape number.

Table 6.2 Frequencies of free vibrations of corrugated open cylindrical shells with different locations of longitudinal bisection.

| No. | FFFF | | | | | CCCC | | | | |
|-----|------|------|------|---------------------|-------------------------|------|-------|-------|---------------------|-------------------------|
| | max | 0 | min | $\varepsilon_0, \%$ | $\varepsilon_{min}, \%$ | max | 0 | min | $\varepsilon_0, \%$ | $\varepsilon_{min}, \%$ |
| 1 | 428 | 429 | 430 | 0.23 | 0.47 | 5050 | 4801 | 4764 | 4.93 | 5.66 |
| 2 | 502 | 503 | 506 | 0.20 | 0.80 | 5193 | 5136 | 5123 | 1.10 | 1.35 |
| 3 | 842 | 849 | 852 | 0.83 | 1.19 | 6650 | 6668 | 6647 | 0.27 | 0.05 |
| 4 | 1430 | 1444 | 1463 | 0.98 | 2.31 | 6833 | 6705 | 6700 | 1.87 | 1.95 |
| 5 | 1771 | 1799 | 1821 | 1.58 | 2.82 | 7344 | 7205 | 7175 | 1.89 | 2.30 |
| 6 | 2087 | 2708 | 3146 | 29.76 | 50.74 | 7462 | 8105 | 8043 | 8.62 | 7.79 |
| 7 | 2154 | 2798 | 3518 | 29.90 | 63.32 | 8660 | 8195 | 8150 | 5.37 | 5.89 |
| 8 | 2868 | 2981 | 3846 | 3.94 | 34.10 | 8861 | 9279 | 9271 | 4.72 | 4.63 |
| 9 | 3113 | 3280 | 3921 | 5.36 | 25.96 | 9343 | 9732 | 9685 | 4.16 | 3.66 |
| 10 | 3786 | 4570 | 4577 | 20.71 | 20.89 | 9623 | 10312 | 10325 | 7.16 | 7.30 |

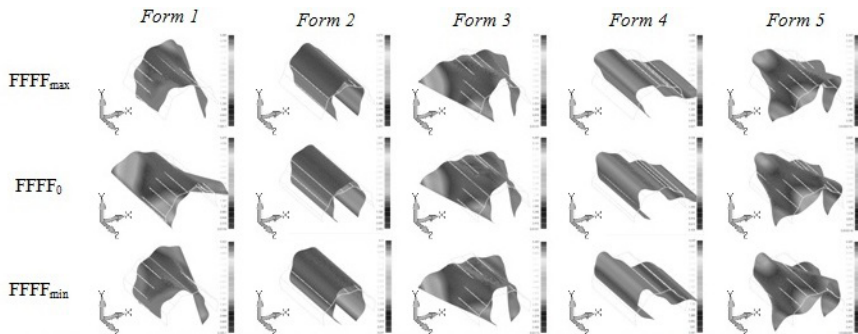


Fig. 6.5 Forms of free vibrations of corrugated open cylindrical shells with different profiles of longitudinal bisecting with all free edges.

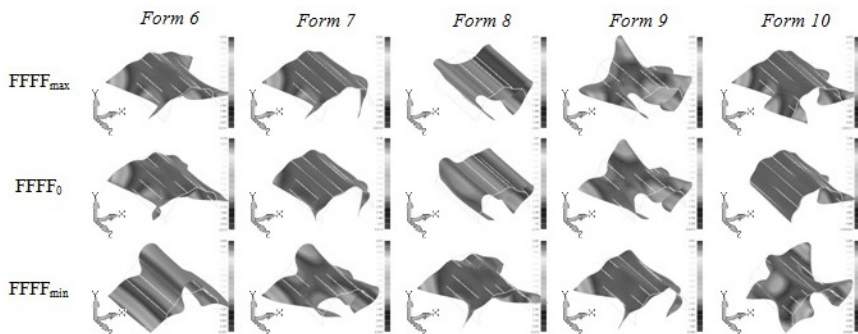


Fig. 6.6 Forms of free vibrations of corrugated open cylindrical shells with different profiles of longitudinal bisecting with all free edges.

For the shells with CCCC boundary conditions, the first ten frequencies have a discrepancy that does not exceed 9%, while there is a greater similarity of vibration modes for shells cut along the minima points and midpoints of corrugations (Figs. 6.7 and 6.8).

Further, the frequencies and forms of free vibrations of a steel circular corrugated ($k = 8$) open cylindrical shell cut in half along the maxima points of the corrugation waves with a variety of rigid fastening were calculated (Fig. 6.4). The first ten frequencies of free vibrations of the considered corrugated shell under nine different boundary conditions are presented in Table 6.3. The first five forms of free vibrations of the considered corrugated shell with a variety of rigid fastening are shown in Figs. 6.9-6.11, except for the cases of all free edges and rigid fastening along all edges, which are shown in Figs. 6.5 and 6.7 with max indices, respectively.

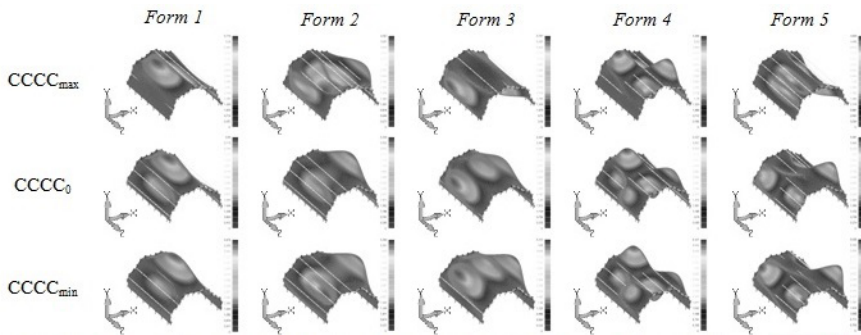


Fig. 6.7 Forms of free vibrations of corrugated open cylindrical shells with different profiles of longitudinal bisecting with all edges rigidly fixed.

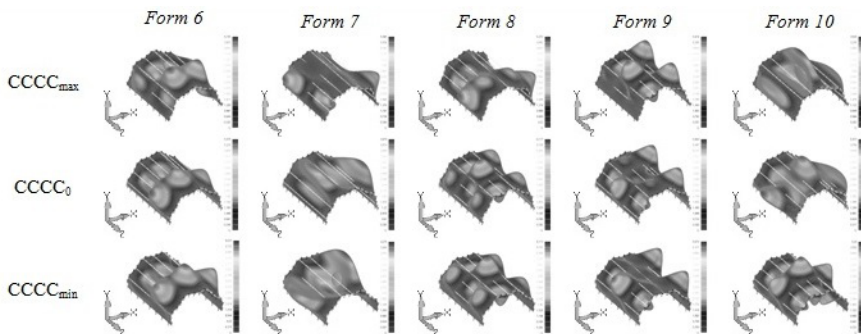


Fig. 6.8 Forms of free vibrations of corrugated open cylindrical shells with different profiles of longitudinal bisecting with all edges rigidly fixed.

Table 6.3 Frequencies of free vibrations of a corrugated shell with variations of rigid fastening.

| No. | FFFF | CFFF | FCFF | CCFF | CFCF | FCFC | CCCF | CCFC | CCCC |
|-----|------|------|------|------|------|------|------|------|------|
| 1 | 428 | 709 | 120 | 756 | 1549 | 1183 | 1572 | 2948 | 5050 |
| 2 | 502 | 752 | 216 | 1822 | 1595 | 2538 | 3250 | 3300 | 5193 |
| 3 | 842 | 1770 | 375 | 2024 | 3244 | 2612 | 4674 | 5421 | 6650 |
| 4 | 1430 | 1815 | 506 | 2961 | 3257 | 4295 | 5235 | 5490 | 6833 |
| 5 | 1771 | 1968 | 1269 | 3521 | 4442 | 5229 | 5642 | 5561 | 7344 |
| 6 | 2087 | 2226 | 1359 | 3991 | 5266 | 5680 | 6567 | 6853 | 7462 |
| 7 | 2154 | 3138 | 2120 | 5073 | 5638 | 5834 | 6745 | 7034 | 8660 |
| 8 | 2868 | 3520 | 2741 | 5449 | 5643 | 6039 | 6877 | 7288 | 8861 |
| 9 | 3113 | 3528 | 2860 | 5629 | 6128 | 6810 | 7460 | 7491 | 9343 |
| 10 | 3786 | 4558 | 3791 | 5897 | 6671 | 6889 | 8697 | 7826 | 9623 |

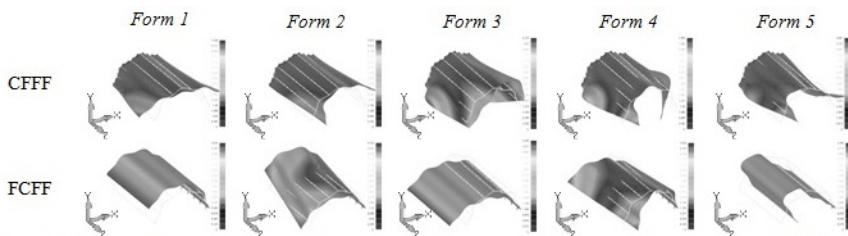


Fig. 6.9 Forms of free vibrations of a corrugated open cylindrical shell with one rigidly fixed edge and three free edges.

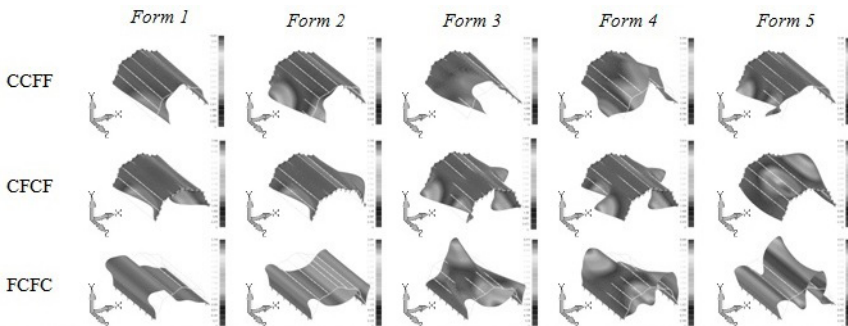


Fig. 6.10 Forms of free vibrations of a corrugated open cylindrical shell with two rigidly fixed edges and two free edges.

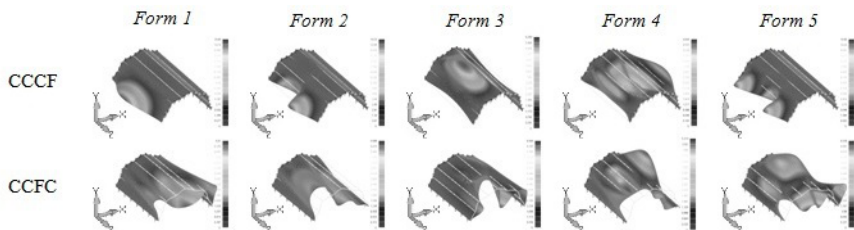


Fig. 6.11 Forms of free vibrations of a corrugated open cylindrical shell with three rigidly fixed edges and one free edge.

6.6 Conclusion

In this work, the frequencies and forms of free vibrations of thin circular corrugated open cylindrical shells with different locations of longitudinal bisecting and with different variations of the boundary conditions are determined based on the finite element method.

Test problems solved for open cylindrical shells with circular corrugated cross-sections show a strong agreement between the first five frequencies of free vibrations calculated by the proposed FEM and the frequencies calculated by another author, while the discrepancy between the results does not exceed 5.5% and increases with an increase in the number of corrugations. Forms of various wave are observed for the same number of the mode.

The dependence of the frequency of free vibrations on the location of longitudinal bisecting of the shell has been established. For example, for shells with the boundary conditions FFFF, the first five frequencies have a small discrepancy compared to the next five frequencies, where the discrepancy reaches almost 65%. This is due to a different structural rigidity from a different method of cutting the shell, which is well observed in different shapes, starting from the sixth form vibrations. That is, the same shape number corresponds to different vibration modes, or slightly distorted vibration modes. For shells with CCCC boundary conditions, the first ten frequencies have a discrepancy that does not exceed 9%, while a smaller divergence and uniformity of vibration modes is observed for shells with bisecting along the minima and along the middle of the corrugation waves.

For a corrugated open cylindrical shell cut in half along the maxima for all methods of boundary conditions, the first ten frequencies of free vibrations are calculated. The frequencies increase with an increase in the number of rigidly fixed ends, except for the FCFE fixing option. These are the first five modes of vibration.

References

- Arnold RN, Warburton GB (1953) The flexural vibrations of thin cylinders. Proceedings of the Institution of Mechanical Engineers 167(1):62–80

- Baron ML, Bleich HH (1954) Tables for Frequencies and Modes of Free Vibration of Infinitely Long Thin Cylindrical Shells. *Journal of Applied Mechanics* 21(2):178–184
- Budak VD, Grigorenko AY, Khorishko VV, Borisenko MY (2014) Holographic interferometry study of the free vibrations of cylindrical shells of constant and variable thickness. *International Applied Mechanics* 50(1):68–74
- Budak VD, Grigorenko AY, Borisenko MY, Boychuk EV (2016) Determination of eigenfrequencies of an elliptic shell with constant thickness by the finite-element method. *Journal of Mathematical Sciences* 201(2):182–192
- Budak VD, Grigorenko AY, Borisenko MY, Boichuk EV (2017) Natural frequencies and modes of noncircular cylindrical shells with variable thickness. *International Applied Mechanics* 53(2):167–172
- Greenspon JE (1959) Vibrations of thick cylindrical shells. *The Journal of the Acoustical Society of America* 31(12):1682–1683
- Grigorenko AY, Zolotoi YG, Prigoda AP, Zhuk IY, Khorishko VV, Ovcharenko AV (2013) Experimental investigation of natural vibrations of a thick-walled cylindrical shell by the method of holographic interferometry. *Journal of Mathematical Sciences* 194(3):239–244
- Grigorenko AY, Borisenko MY, Boychuk EV, Prigoda AP (2018a) Numerical determination of natural frequencies and modes of the vibrations of a thick-walled cylindrical shell. *International Applied Mechanics* 54(1):75–84
- Grigorenko AY, Borisenko MY, Boychuk EV (2020a) Free vibrations of an open elliptical cylindrical shell. *International Applied Mechanics* 56(4):389–401
- Grigorenko AY, Borysenko MY, Boychuk OV, Vasil'eva LY (2020b) Free vibrations of an open non-circular cylindrical shell of variable thickness. In: Altenbach H, Chinchaladze N, Kienzler R, Müller W (eds) *Analysis of Shells, Plates, and Beams*, Springer, Cham, *Advanced Structured Materials*, vol 134, pp 141–154
- Grigorenko OY, Parkhomenko OY, Vasil'eva LY, Borisenko MY (2018b) Solution of the problem of free vibrations of a nonthin orthotropic shallow shell of variable thickness in the refined statement. *Journal of Mathematical Sciences* 229(3):253–268
- Grigorenko YM, Efimova TL (2008) Using spline-approximation to solve problems of axisymmetric free vibration of thick-walled orthotropic cylinders. *International Applied Mechanics* 44(10):1137–1147
- Grigorenko YM, Rozhok LS (2004) Solving the stress problem for hollow cylinders with corrugated elliptical cross section. *International Applied Mechanics* 40(1):169–175
- Kim YW (2016) Vibration analysis of longitudinally corrugated cylindrical shells. *Transactions of the Korean Society for Noise and Vibration Engineering* 16(7):851–856
- Mousa Khalifa A (2015) Solving the vibration problem of inhomogeneous orthotropic cylindrical shells with hoop-corrugated oval cross section. *Comptes Rendus Mécanique* 343(9):482–494
- Nguyen TP, Nguyen-Thoi T, Tran DK, Ho DT, Vu HN (2021) Nonlinear vibration of full-filled fluid corrugated sandwich functionally graded cylindrical shells. *Journal of Vibration and Control* 27(9–10):1020–1035
- Puzyrev SV (2013) About free vibrations of non-circular cylindrical shells with a corrugated elliptical section. *Collection of scientific works NUS* 1:47–53
- Semenyuk NP, Babich IY, Zhukova NB (2005) Natural vibrations of corrugated cylindrical shells. *International Applied Mechanics* 41(5):512–519
- Xu L, Chen M, Du H, Hu H, Hu Y, Fan H, Yang J (2008) Vibration characteristics of a corrugated cylindrical shell piezoelectric transducer. *IEEE Transactions on Ultrasonics, Ferroelectrics, and Frequency Control* 55(11):2502–2508
- Xu L, Du H, Hu H, Shan X, Chen H, Hu Y, Chen X (2010) Study on the vibration characteristics of a finite-width corrugated cylindrical shell piezoelectric transducer. *IEEE Transactions on Ultrasonics, Ferroelectrics, and Frequency Control* 57(6):1460–1469
- Yang JS, Xiong J, Ma L, Feng LN, Wang SY, Wu LZ (2015) Modal response of all-composite corrugated sandwich cylindrical shells. *Composites Science and Technology* 115:9–20
- Yuan H, Liu RH (2007) Nonlinear vibration of corrugated shallow shells under uniform load. *Applied Mathematics and Mechanics* 28(5):573–580



Chapter 7

On a New Theory of the Cosserat Continuum with Applications in Electrodynamics

Elena A. Ivanova

Abstract We consider an elastic Cosserat continuum of a special type. Next we suggest analogies between quantities characterizing the stress–strain state of the continuum and quantities characterizing electrodynamic processes. Taking into account the suggested analogies, we interpret equations describing the continuum as equations of electrodynamics. We identify parameters of our model by comparing the obtained equations with Maxwell’s equations. As a result, in the framework of our model, we obtain a set of differential equations that coincide with Maxwell’s first equation (the one with the displacement current term), the Gauß law for electric field, the charge conservation law, a modification of the Maxwell–Faraday equation and a modification of the Gauß law for magnetic field. We also obtain the Gauß law for gravitational field and introduce the concept of gravitating mass.

Key words: Cosserat continuum, Micropolar continuum, Electrodynamics, Electromagnetic field, Gravitational field

7.1 Introduction

It is well known that, in the 19th century, mechanical models were used to describe all physical processes. These models are in large part based on the concept of the ether (Whittaker, 1910). For example, when describing electromagnetic processes, scientists of the 19th century were convinced that they were describing processes in the ether. The ether may be viewed as a substance that has the capacity to occupy

Elena A. Ivanova

Higher School of Theoretical Mechanics, Peter the Great St.Petersburg Polytechnic University, Polytechnicheskaya, 29, 195251, Saint-Petersburg & Institute for Problems in Mechanical Engineering of Russian Academy of Sciences, Bolshoy pr. V.O., 61, 199178, Saint-Petersburg, Russian Federation

e-mail: elenaivanova239@gmail.com

the whole free space and to penetrate into the material bodies endowing them with additional physical properties.

The ether theory, which initially met with general acceptance, subsequently fell into disuse. Now the interest in mechanical models of electromagnetic processes is renewed. A large number of review papers are published, see, e.g., Siegel (1991); Darrigol (2000); Chalmers (2001); Capria (2005); Silva (2007); Pietsch (2012); Longair (2015). Studies aimed at creating mechanical models of physical processes resume. Discussing the researches carried out at the turn of the 20th/21st centuries, we can refer to models based on translational degrees of freedom (Jaswon, 1969; Kelly, 1976; Zhilin, 1996b,a, 2006a,b; Larson, 1998; Zareski, 2001; Dmitriyev, 2003, 2008; Christov, 2007, 2009b,a, 2011; Wang, 2008; Lin and Lin, 2014) and models based on rotational degrees of freedom (Zhilin, 2006a; Dixon and Eringen, 1965a,b; Teregulov, 1989; Grekova and Zhilin, 2001; Grekova, 2001; Zhilin, 2012, 2013; Ivanova et al, 2007; Ivanova and Kolpakov, 2013; Ivanova, 2015; Ivanova and Kolpakov, 2016; Ivanova, 2019a,b; Ivanova and Matias, 2019; Müller et al, 2020; Ivanova, 2021). We are convinced that the models based on rotational degrees of freedom have several advantages over the models based on translational degrees of freedom. Below, we discuss this issue in detail.

The present study continues and develops the research carried out in Zhilin (2006a,b, 2012); Ivanova (2015, 2019a,b); Ivanova and Matias (2019); Ivanova (2021). Unlike our previous works, where we considered only isotropic media, in this study we focus on modeling electromagnetic processes in anisotropic materials. In addition, we draw an analogy between electrostatic interaction and gravitational interaction and propose an original model of the gravitational field.

7.2 Maxwell's Equations for Anisotropic Materials

Maxwell's equations can be written as

$$\nabla \times \mathcal{H} = \mathcal{J} + \frac{d\mathcal{D}}{dt}, \quad \nabla \times \mathcal{E} = -\frac{d\mathcal{B}}{dt}, \quad \nabla \cdot \mathcal{D} = \mathcal{Q}, \quad \nabla \cdot \mathcal{B} = 0, \quad (7.1)$$

where \mathcal{E} is the electric field vector, \mathcal{D} is the electric induction vector, \mathcal{H} is the magnetic field vector, \mathcal{B} is the magnetic induction vector, \mathcal{J} is the electric current density, and \mathcal{Q} is the electric charge density. We note that the first equation in (7.1) is known as the Maxwell's first equation, the second equation in (7.1) is usually called the Maxwell's second equation or the Maxwell–Faraday equation, the third and fourth equations in (7.1) are the Gauß laws for electric field and magnetic field, respectively. Equations (7.1) should be supplemented by material equations, which take the following form in the linear case:

$$\mathcal{D} = \varepsilon_0 \boldsymbol{\varepsilon} \cdot \mathcal{E}, \quad \mathcal{B} = \mu_0 \boldsymbol{\mu} \cdot \mathcal{H}. \quad (7.2)$$

where ε_0 and μ_0 are the permittivity and permeability of free space, $\boldsymbol{\varepsilon}$ and $\boldsymbol{\mu}$ are the tensors of the relative permittivities and the relative permeabilities of the material. It is well known that from Eq. (7.1) it follows the charge conservation law

$$\frac{dQ}{dt} + \nabla \cdot \boldsymbol{\mathcal{J}} = 0, \quad (7.3)$$

which, in fact, is a condition for the solvability of Eqs. (7.1) and (7.2).

7.3 A Cosserat Continuum of a Special Type: a Nonlinear Theory

Let vector \mathbf{r} identify the position of some point in space. For simplicity sake, we consider a continuum possessing only rotational degrees of freedom. To be exact, we assume that the translational velocity equals to zero and the strain measure associated with translational degrees of freedom equals to the unit tensor \mathbf{E} . We use the following notations: $\mathbf{P}(\mathbf{r}, t)$ is the rotation tensor, $\boldsymbol{\omega}(\mathbf{r}, t)$ is the angular velocity vector, $\boldsymbol{\Theta}(\mathbf{r}, t)$ is the angular strain tensor, $\rho(\mathbf{r})$ is the mass density of the continuum, $\mathbf{J}(\mathbf{r}, t)$ is the inertia tensor per unit mass. We note that the mass density does not depend on time since translational degrees of freedom are ignored. Angular velocity $\boldsymbol{\omega}$ and strain tensor $\boldsymbol{\Theta}$ are related to rotation tensor as

$$\frac{d\mathbf{P}}{dt} = \boldsymbol{\omega} \times \mathbf{P}, \quad \nabla \mathbf{P} = \boldsymbol{\Theta} \times \mathbf{P}. \quad (7.4)$$

From Eq. (7.4) it follows that

$$\frac{d\boldsymbol{\Theta}}{dt} = \nabla \boldsymbol{\omega} - \boldsymbol{\Theta} \times \boldsymbol{\omega}. \quad (7.5)$$

Kinetic energy per unit mass \mathcal{T} , linear momentum per unit mass $\boldsymbol{\mathcal{K}}_1$, and angular momentum per unit mass $\boldsymbol{\mathcal{K}}_2$ are

$$\mathcal{T} = \frac{1}{2} \boldsymbol{\omega} \cdot \mathbf{J} \cdot \boldsymbol{\omega}, \quad \boldsymbol{\mathcal{K}}_1 = 0, \quad \boldsymbol{\mathcal{K}}_2 = \mathbf{J} \cdot \boldsymbol{\omega}. \quad (7.6)$$

The equations of motion have the form

$$\nabla \cdot \boldsymbol{\tau} + \mathbf{f} = 0, \quad \nabla \cdot \mathbf{T} + \boldsymbol{\tau}_\times = \rho \frac{d(\mathbf{J} \cdot \boldsymbol{\omega})}{dt}, \quad (7.7)$$

where $\boldsymbol{\tau}$ is the stress tensor, \mathbf{T} is the moment stress tensor, \mathbf{f} is the external force per unit volume, $(\)_\times$ denotes the vector invariant of a tensor that is defined for an arbitrary dyad as $(\mathbf{ab})_\times = \mathbf{a} \times \mathbf{b}$.

Following Ivanova (2019a, 2021), we assume moment stress tensor \mathbf{T} to be an antisymmetric tensor:

$$\mathbf{T} = -\mathbf{M} \times \mathbf{E}, \quad (7.8)$$

where \mathbf{M} is the moment stress vector. Also following Ivanova (2019a, 2021), we accept the constitutive equation for vector \mathbf{M} :

$$\mathbf{M} = \rho^{-1} \mathbf{C}_\psi \cdot \boldsymbol{\theta}_\times, \quad (7.9)$$

where \mathbf{C}_ψ is the second rank stiffness tensor. As it has been shown in Ivanova (2019a, 2021), in the case of the considered continuum, the constitutive equation for the stress tensor has the form

$$\boldsymbol{\tau} = (\mathbf{M} \cdot \boldsymbol{\theta}_\times) \mathbf{E} + \mathbf{M} \times \boldsymbol{\theta}^T. \quad (7.10)$$

Substituting Eq. (7.8) and the first equation in (7.9) into the second equation in (7.7), we reduce Eq. (7.7) to the form

$$\nabla \times \mathbf{M} = \mathbf{M} \cdot (\boldsymbol{\theta} - \text{tr} \boldsymbol{\theta} \mathbf{E}) - \frac{d\mathcal{K}}{dt}, \quad (7.11)$$

where \mathcal{K} denotes

$$\mathcal{K} = \rho \mathbf{J} \cdot \boldsymbol{\omega}. \quad (7.12)$$

Thus, we arrive at the closed system of equations (7.5), (7.9), (7.11), (7.12) in four variables, namely vectors \mathbf{M} , \mathcal{K} , $\boldsymbol{\omega}$ and tensor $\boldsymbol{\theta}$. Further, we use the theory presented in this section to give a mechanical interpretation of Maxwell's equations written in the form of Eq. (7.1).

7.4 A Cosserat Continuum of a Special Type: the Linear Theory

In the linear approximation, the system of the basic equations can be written as two independent systems. The first system consists of the material equations

$$\mathbf{M} = \rho^{-1} \mathbf{C}_\psi \cdot \boldsymbol{\theta}_\times, \quad \mathcal{K} = \rho \mathbf{J} \cdot \boldsymbol{\omega}, \quad (7.13)$$

the angular momentum balance equation

$$\nabla \times \mathbf{M} = -\frac{d\mathcal{K}}{dt}, \quad (7.14)$$

and the vector invariant of the equation relating the strain tensor and the angular velocity

$$\nabla \times \boldsymbol{\omega} = \frac{d\boldsymbol{\theta}_\times}{dt}. \quad (7.15)$$

It is evident that Eqs. (7.13), (7.14), (7.15) are the closed system. If at the initial moment of time $\nabla \cdot \mathcal{K}$ and $\nabla \cdot \boldsymbol{\theta}_\times$ are equal to zero, from Eqs. (7.14), (7.15) it follows that

$$\nabla \cdot \mathcal{K} = 0, \quad \nabla \cdot \boldsymbol{\Theta}_\times = 0. \tag{7.16}$$

The second system includes the symmetric part of the relation between the strain tensor and the angular velocity:

$$\frac{d\boldsymbol{\Theta}^s}{dt} = (\nabla \boldsymbol{\omega})^s, \tag{7.17}$$

where s denotes the symmetric part of a tensor. Finding of the symmetric part of $\boldsymbol{\Theta}$ is not of interest to us. That is why, further we consider only the first system.

7.5 Mechanical Analogies of Physical Quantities in the Linear Theory

Following Ivanova (2021), we suppose that moment stress vector \mathbf{M} is the analogy of electric field vector $\boldsymbol{\mathcal{E}}$, vector invariant of the strain tensor $\boldsymbol{\Theta}_\times$ is the analogy of electric induction vector \mathcal{D} , angular velocity vector $\boldsymbol{\omega}$ is the analogy of magnetic field vector \mathcal{H} , and volume density of proper angular momentum \mathcal{K} is the analogy of magnetic induction vector \mathcal{B} :

$$\mathbf{M} = \chi \boldsymbol{\mathcal{E}}, \quad \boldsymbol{\Theta}_\times = \frac{1}{\chi} \mathcal{D}, \quad \boldsymbol{\omega} = \frac{1}{\chi} \mathcal{H}, \quad \mathcal{K} = \chi \mathcal{B}, \tag{7.18}$$

where χ is the normalization factor. Inserting Eq. (7.18) into Eqs. (7.14), (7.15), (7.16), we obtain Maxwell’s equations in the form of (7.1), but without electric charge density \mathcal{Q} and electric current density \mathcal{J} . Next, specifying the stiffness and inertia parameters as

$$\rho^{-1} \mathbf{C}_\psi = \chi^2 (\varepsilon_0 \boldsymbol{\mathcal{E}})^{-1}, \quad \rho \mathbf{J} = \chi^2 \mu_0 \boldsymbol{\mu}, \tag{7.19}$$

and substituting Eqs. (7.18), (7.19) into Eq. (7.13), we obtain the constitutive equations (7.2), which are appropriate for the linear anisotropic materials.

7.6 The Nonlinear Theory and Maxwell’s Equations

First of all, we note that, in contrast to the linear theory, the system of the basic equations of the nonlinear theory cannot be rewritten as two independent systems. Nevertheless, as in the linear theory, we consider the antisymmetric part of the equation relating the strain tensor and the angular velocity. As shown in Ivanova (2021), from Eq. (7.5) it follows a vector differential equation

$$\nabla \times \boldsymbol{\omega} = \boldsymbol{\omega} \cdot (\boldsymbol{\Theta} - \text{tr} \boldsymbol{\Theta} \mathbf{E}) + \frac{d\boldsymbol{\Theta}_\times}{dt}, \tag{7.20}$$

and also two scalar differential equations:

$$\nabla \cdot \boldsymbol{\theta}_\times = \frac{1}{2} \left((\text{tr} \boldsymbol{\theta})^2 - \boldsymbol{\theta} \cdot \boldsymbol{\theta} \right) \quad (7.21)$$

and

$$\frac{d}{dt} \left[\frac{1}{2} \left((\text{tr} \boldsymbol{\theta})^2 - \boldsymbol{\theta} \cdot \boldsymbol{\theta} \right) \right] + \nabla \cdot \left[\boldsymbol{\omega} \cdot (\boldsymbol{\theta} - \text{tr} \boldsymbol{\theta} \mathbf{E}) \right] = 0. \quad (7.22)$$

It is easy to see that Eq. (7.21) has the form of the Gauß law and Eq. (7.22) has the form of the balance law.

Now we turn to Eqs. (7.9), (7.11), (7.12), (7.20), (7.21), (7.22). It is evident that Eq. (7.11) contains nonlinear term $\mathbf{M} \cdot (\boldsymbol{\theta} - \text{tr} \boldsymbol{\theta} \mathbf{E})$ and Eqs. (7.20), (7.22) contain nonlinear term $\boldsymbol{\omega} \cdot (\boldsymbol{\theta} - \text{tr} \boldsymbol{\theta} \mathbf{E})$, neither of them can be expressed in terms of vectors \mathbf{M} , $\boldsymbol{\theta}_\times$, $\boldsymbol{\mathcal{K}}$, $\boldsymbol{\omega}$. That is why in order to close the system of Eqs. (7.9), (7.11), (7.12), (7.20), (7.21), (7.22) we should supplement it with the symmetric part of Eq. (7.5), namely

$$\frac{d\boldsymbol{\theta}^s}{dt} = (\nabla \boldsymbol{\omega})^s - \frac{1}{2} (\boldsymbol{\theta} \times \boldsymbol{\omega} - \boldsymbol{\omega} \times \boldsymbol{\theta}^T). \quad (7.23)$$

In the present paper, we are not aiming to give any physical interpretations of Eq. (7.23). Below, following ideas of Ivanova (2021) and making use of the analogies between the physical and mechanical quantities given by Eqs. (7.18), (7.19), we match Eqs. (7.9), (7.11), (7.12), (7.20), (7.21), (7.22) with Maxwell's equations (7.1), material equations (7.2) and the charge conservation law (7.3).

Inserting Eqs. (7.18), (7.19) into Eqs. (7.9), (7.12), we obtain the material equations (7.2). Next, inserting Eq. (7.18) into Eq. (7.11), we obtain a differential equation

$$\nabla \times \boldsymbol{\mathcal{E}} = -\boldsymbol{\mathcal{V}} - \frac{d\boldsymbol{\mathcal{B}}}{dt}, \quad (7.24)$$

where vector $\boldsymbol{\mathcal{V}}$ is calculated as

$$\boldsymbol{\mathcal{V}} = -\boldsymbol{\mathcal{E}} \cdot (\boldsymbol{\theta} - \text{tr} \boldsymbol{\theta} \mathbf{E}) \quad \Leftrightarrow \quad \boldsymbol{\mathcal{V}} = -\frac{1}{\chi} \mathbf{M} \cdot (\boldsymbol{\theta} - \text{tr} \boldsymbol{\theta} \mathbf{E}). \quad (7.25)$$

Equation (7.24) can be interpreted as the modified Maxwell–Faraday equation since it coincides with the classical Maxwell–Faraday equation if $\boldsymbol{\mathcal{V}}$ is assumed to be equal to zero. Following Ivanova (2021), we interpret vector $\boldsymbol{\mathcal{V}}$ as the electrical voltage density. A discussion of the physical meaning of this quantity is beyond the scope of this paper. This issue is covered in Ivanova (2021).

From Eq. (7.24) it follows that

$$\frac{d(\nabla \cdot \boldsymbol{\mathcal{B}})}{dt} = -\nabla \cdot \boldsymbol{\mathcal{V}}. \quad (7.26)$$

It is evident that the Gauß law for magnetic field $\nabla \cdot \boldsymbol{\mathcal{B}} = 0$ follows from Eq. (7.26) if $\nabla \cdot \boldsymbol{\mathcal{V}} = 0$ and $\nabla \cdot \boldsymbol{\mathcal{B}} = 0$ at the initial moment of time. Hence, Eq. (7.26) can be treated as a modified Gauß law for magnetic field. The physical meaning of this equation is discussed in Ivanova (2021).

Inserting Eq. (7.18) into Eq. (7.20) yields

$$\nabla \times \mathcal{H} = \mathcal{J} + \frac{d\mathcal{D}}{dt}, \quad (7.27)$$

where

$$\mathcal{J} = \mathcal{H} \cdot (\boldsymbol{\Theta} - \text{tr} \boldsymbol{\Theta} \mathbf{E}) \quad \Leftrightarrow \quad \mathcal{J} = \chi \boldsymbol{\omega} \cdot (\boldsymbol{\Theta} - \text{tr} \boldsymbol{\Theta} \mathbf{E}). \quad (7.28)$$

Equation (7.27) coincides with Maxwell's first equation if vector \mathcal{J} is interpreted as an analogy of the electric current density. Comparing the modified Maxwell–Faraday equation (7.24) with Maxwell's first equation (7.27) we deduce that these equations have the same structure. Furthermore, as it is seen from Eqs. (7.25), (7.28), the expressions for \mathcal{V} and \mathcal{J} contain the same tensor coefficient $(\boldsymbol{\Theta} - \text{tr} \boldsymbol{\Theta} \mathbf{E})$.

Next, following Ivanova (2021), we introduce an analogy of the electric charge density \mathcal{Q} as

$$\mathcal{Q} = \frac{\chi}{2} \left((\text{tr} \boldsymbol{\Theta})^2 - \boldsymbol{\Theta} \cdot \cdot \boldsymbol{\Theta} \right). \quad (7.29)$$

It is evident that, taking into account Eqs. (7.18), (7.29), we can rewrite Eq. (7.21) as the Gauß law for electric field $\nabla \cdot \mathcal{D} = \mathcal{Q}$. In view of Eqs. (7.18), (7.28), (7.29), the balance equation (7.22) takes the form of the charge conservation law (7.3). We note that due to the properties of the second principal invariant of tensor, we can represent the electric charge density (7.29) as the sum of two terms, one of which is always positive, and the other is always negative, namely

$$\mathcal{Q} = \mathcal{Q}^+ + \mathcal{Q}^-, \quad (7.30)$$

where the positive charge per unit volume \mathcal{Q}^+ is defined as

$$\mathcal{Q}^+ = \frac{\chi}{2} \left(\frac{1}{2} \boldsymbol{\Theta}_x \cdot \boldsymbol{\Theta}_x + (\text{tr} \boldsymbol{\Theta})^2 \right) \geq 0, \quad (7.31)$$

and the negative charge per unit volume \mathcal{Q}^- is defined as

$$\mathcal{Q}^- = -\frac{\chi}{2} \boldsymbol{\Theta}^s \cdot \cdot \boldsymbol{\Theta}^s \leq 0. \quad (7.32)$$

Thus, in the framework of the nonlinear theory, we have introduced the analogies of all quantities contained in Maxwell's equations. Using these analogies we have obtained: the material equations relating vector \mathcal{D} to vector \mathcal{E} and vector \mathcal{H} to vector \mathcal{B} ; Maxwell's first equation, the Gauß law for electric field and the charge conservation law; the modified Maxwell–Faraday equation and the modified Gauß law for magnetic field. If quantity \mathcal{V} vanishes, the last two modified equations become indistinguishable from the classical ones. That is why we are convinced that the proposed analogies can actually be considered as analogies. In fact, in the present paper, we have generalized the theory developed in Ivanova (2021) for isotropic materials to the case of anisotropic materials.

7.7 On the Theories Based on Translational Degrees of Freedom

It is well known that the mechanical models of the ether constructed in the 19th century are based on translational degrees of freedom (Whittaker, 1910). It is also known that the use of these models gave many interesting results, but at the same time, raised questions that were not answered by scientists of that time. Eventually, a number of 19th century scientists, namely Kelvin, Fitzgerald and Maxwell, came up with an idea that mechanical models of electromagnetism should be based upon rotational degrees of freedom (Whittaker, 1910). Nevertheless, models based on translational degrees of freedom are still in use today. The question arises: What is the reason? We believe that the main dominant reason is that the models based on translational degrees of freedom are visual, intuitive, and familiar. But let us look at the facts.

- It is not difficult to obtain Maxwell's equations for isotropic media without currents and charges by means of a model similar to classical solids. But in order to make the longitudinal wave velocity to be equal to zero, or at least, to be smaller than the transverse wave velocity, we have to assume that the bulk modulus is negative. The negative bulk modulus does not seem to be something intuitive, since it is inherent only in some artificial structures, but not in the natural materials. On the contrary, using models based on rotational degrees of freedom, an arbitrary ratio of the transverse and longitudinal wave velocities can be obtained without any unnatural assumptions.
- If we use a model similar to classical solids in the case of an anisotropic medium, we are forced to assume that the inertia properties of the model are characterised by a mass density tensor. Such a model does not seem to be something familiar. The tensor of inertia in a model based on rotational degrees of freedom is much more familiar than the mass density tensor in a model based on translational degrees of freedom.
- In the framework of a theory, based on translational degrees of freedom, it is impossible to introduce an analogy of the electric charge density in the same way as it is done in the framework of the proposed theory based on rotational degrees of freedom. Our concept of the electric charge is in a large part based upon the compatibility equation for angular strains in the ether. This equation has the form

$$\nabla \times \boldsymbol{\theta} = \frac{1}{2} \boldsymbol{\theta}^T \times \times \boldsymbol{\theta}. \quad (7.33)$$

Taking the trace of the both sides of Eq. (7.33), we arrive at the following equation

$$\nabla \cdot \boldsymbol{\theta}_\times = \frac{1}{2} [(\text{tr} \boldsymbol{\theta})^2 - \boldsymbol{\theta} \cdot \cdot \boldsymbol{\theta}], \quad (7.34)$$

which is an analogy of the Gauß law for electric field $\nabla \cdot \mathcal{D} = \Omega$, where the electric induction vector and the electric charge density are determined by Eq. (7.18) and Eq. (7.29), respectively. Let us turn to strain measure \mathbf{g} , which is associated with translational degrees of freedom and defined as $\mathbf{g} = \mathbf{E} - \nabla \mathbf{u}$, where \mathbf{u} is the

displacement vector. It is evident that we cannot introduce a mechanical analogy of the electric charge based on the compatibility equation for linear strains in the ether

$$\nabla \times \mathbf{g} = 0, \quad (7.35)$$

since the right-hand side of this equation is zero. Indeed, taking the trace of Eq. (7.35), we obtain $\nabla \cdot \mathbf{g}_x = 0$.

We believe that in the late 19th century a mathematical model of a micropolar continuum could be the long sought mechanical foundation for the ether theory. Unfortunately, the advent of the model proposed by the Cosserat brothers in 1909 was somewhat belated. By that time, interest in the ether models was almost completely lost and physics was developing in a different direction. Studies aimed at creating the ether theories have been renewed only at the turn of the 20th/21st centuries. We are convinced that the use of the ether models based on rotational degrees of freedom can propel the inflow of new ideas regarding to the further development of electrodynamics. At the same time, we do not deny the important role of translational degrees of freedom for modeling processes in the ether. For example, in Ivanova (2019a), we discuss the possibility of formation of matter particles from the ether. In the cited paper, we describe the formation of matter particles by means of a model taking both rotational and translational degrees of freedom. In addition, we suppose that a model with rotational and translational degrees of freedom can bring together electromagnetism and gravitation. This subject matter goes a lot further than the topic of the present paper. Nevertheless, in the next section, we provide groundwork for the model of gravitation.

7.8 The Gauß Law for Gravitational Field

It is well known that Newton's law of universal gravitation is similar to Coulomb's inverse-square law for electric charges. It is also known that Coulomb's law can be derived from the Gauß law for electric field if a number of additional assumptions are taken into account, namely: the postulate that the force acting on a charged particle is proportional to the electric field vector; the assumption of spherical symmetry; the assumption that the interacting charges are point charges. Hence, Newton's law can be derived from the Gauß law for gravitational field. The latter can be formulated as

$$\nabla \cdot \mathfrak{G} = \rho_m, \quad (7.36)$$

where ρ_m is the gravitating mass per unit volume, vector \mathfrak{G} plays the same role as the electric induction vector \mathfrak{D} in the Gauß law for electric field. It seems logical to call vector \mathfrak{G} the gravitational induction vector.

Above, in the framework of the Cosserat continuum, we have obtained an analogy of the Gauß law for electric field, see Eq. (7.34). Now, also in the framework of the Cosserat continuum, we are going to obtain an analogy of the Gauß law for gravitational field. We start with Eq. (7.33). Multiplying it by tensor \mathbf{g}^T and taking

the trace of the obtained equation, we have

$$\text{tr}[(\nabla \times \boldsymbol{\theta}) \cdot \mathbf{g}^T] = \frac{1}{2} \text{tr}[(\boldsymbol{\theta}^T \times \times \boldsymbol{\theta}) \cdot \mathbf{g}^T]. \quad (7.37)$$

It is not difficult to show that Eq. (7.37) can be rewritten as

$$\text{tr}[\nabla \times (\boldsymbol{\theta} \cdot \mathbf{g}^T)] + \boldsymbol{\theta}^T \cdot (\nabla \times \mathbf{g}) = (\det \mathbf{g}) \frac{1}{2} \text{tr}[(\boldsymbol{\theta} \cdot \mathbf{g}^{-1})^T \times \times (\boldsymbol{\theta} \cdot \mathbf{g}^{-1})]. \quad (7.38)$$

Taking into account Eq. (7.35) and performing a number of simple transformations, we reduce Eq.(7.38) to the form

$$\nabla \cdot (\boldsymbol{\theta} \cdot \mathbf{g}^T)_{\times} = (\det \mathbf{g}) \frac{1}{2} \left[(\text{tr} [\boldsymbol{\theta} \cdot \mathbf{g}^{-1}])^2 - (\boldsymbol{\theta} \cdot \mathbf{g}^{-1}) \cdot (\boldsymbol{\theta} \cdot \mathbf{g}^{-1}) \right]. \quad (7.39)$$

If tensor \mathbf{g} equals to the unit tensor, Eq. (7.39) reduces to Eq. (7.34). In the general case, Eq. (7.39) can be treated as the Gauß law for electric and gravitational fields. We emphasize that tensor \mathbf{g} determines the strain state of the ether, not the ponderable matter.

It is well known that, at interatomic distances, the gravitational interactions are negligible. It is also known that, at intergalactic distances, the electrical interactions are negligible since the matter is electrically neutral on average. That is why, it seems logical to introduce the strain tensor

$$\mathbf{e} = \mathbf{g} - \mathbf{E}, \quad (7.40)$$

and consider the difference of Eqs. (7.39) and (7.34). As a result, after simple transformations, we arrive at the following equation

$$\nabla \cdot (\boldsymbol{\theta} \cdot \mathbf{e}^T)_{\times} = (\det \mathbf{e}) \frac{1}{2} \left[(\text{tr} [\boldsymbol{\theta} \cdot \mathbf{e}^{-1}])^2 - (\boldsymbol{\theta} \cdot \mathbf{e}^{-1}) \cdot (\boldsymbol{\theta} \cdot \mathbf{e}^{-1}) \right]. \quad (7.41)$$

In our opinion, Eq. (7.41) can be interpreted as the Gauß law for gravitational field, i.e., Eq. (7.41) is an analogy of (7.36). This means that vector $(\boldsymbol{\theta} \cdot \mathbf{e}^T)_{\times}$ matches gravitational induction vector \mathfrak{G} :

$$\mathfrak{G} \leftrightarrow (\boldsymbol{\theta} \cdot \mathbf{e}^T)_{\times}, \quad (7.42)$$

and the scalar quantity on the right-hand side of Eq. (7.41) matches the gravitating mass per unit volume ρ_m :

$$\rho_m \leftrightarrow (\det \mathbf{e}) \frac{1}{2} \left[(\text{tr} [\boldsymbol{\theta} \cdot \mathbf{e}^{-1}])^2 - (\boldsymbol{\theta} \cdot \mathbf{e}^{-1}) \cdot (\boldsymbol{\theta} \cdot \mathbf{e}^{-1}) \right]. \quad (7.43)$$

Comparing Eq. (7.41) with Eq. (7.34), we infer that although these equations are similar, there are still some differences between them. Indeed, Eq. (7.34) includes the vector invariant and the second principal invariant of the same tensor, whereas

Eq. (7.41) includes the vector invariant and the second principal invariant of different tensors. In addition, Eq. (7.41) contains the determinant of strain tensor \mathbf{e} .

According to Eq. (7.43), the gravitating mass can be both positive and negative. The question arises whether this is something contrary to common sense and everyday experience. To answer this question, first of all, we refer to the well-known gravitational paradox. It consists in the fact that the Newtonian theory of gravitation leads to infinite values of the gravitational potential. Within the framework of the Newtonian theory of gravitation, models of the Universe free from the gravitational paradox could be constructed only under the assumption that the average density of matter in the Universe is equal to zero. We are not able to understand the deeper physical reason of why negative masses could exist, because we live in the world where all masses are positive. Nevertheless, the idea of matter with negative mass is not new in physics. We can refer to Huang et al (2009); Wang (2014) that construct models of metamaterials with negative mass, to experimental works (Tajmar and Assis, 2015; Khomehchi et al, 2017) studying particles with negative mass, and to cosmological theories (Farnes, 2018; Socas-Navarro, 2019) that use the concept of negative-mass matter. In order to clarify our concept of negative mass, we note that positive and negative mass can be distributed in the Universe in the same way as the positive and negative charges are distributed in matter. The only difference is that the characteristic size of regions containing only positive mass or only negative mass is comparable to the size of galaxies.

7.9 Conclusions

In this paper, we discuss the mechanical analogies of the following quantities: the electric field vector, the electric induction vector, the magnetic field vector, the magnetic induction vector, the electric current density, and the electric charge density. We have obtained the set of differential equations that coincide with the following ones: Maxwell's equation with the displacement current, the Gauß law for electric field and the charge conservation law. We have also obtained the modified Maxwell-Faraday equation and the modified Gauß law for magnetic field. These equations differ from the well-known ones by the presence of additional quantity \mathcal{V} , which is treated as the electric voltage density. In addition, we obtain the Gauß law for gravitational field and introduce the concept of gravitating mass. Certainly, it is impossible to develop a theory of gravity within the framework of the model discussed in this paper. To construct the theory of gravity, it is necessary not only to take into account translational velocities, but also to consider a two-component model, which includes the ether and the ponderable matter. The development of such a theory will be the subject of further researches.

Acknowledgements The author is deeply grateful to M. B. Babenkov and E. N. Vilchevskaya for useful discussions on the paper.

References

- Capria MM (ed) (2005) *Physics before and after Einstein*. IOS Press, Amsterdam
- Chalmers A (2001) Maxwell, mechanism, and the nature of electricity. *Physics in Perspective* 3(4):425–438
- Christov CI (2007) Maxwell–Lorentz electrodynamics as a manifestation of the dynamics of a viscoelastic metacontinuum. *Mathematics and Computers in Simulation* 74(2):93–104
- Christov CI (2009a) The concept of a quasi-particle and the non-probabilistic interpretation of wave mechanics. *Mathematics and Computers in Simulation* 80(1):91–101
- Christov CI (2009b) On the nonlinear continuum mechanics of space and the notion of luminiferous medium. *Nonlinear Analysis: Theory, Methods & Applications* 71(12):e2028–e2044
- Christov CI (2011) Frame indifferent formulation of Maxwell’s elastic-fluid model and the rational continuum mechanics of the electromagnetic field. *Mechanics Research Communications* 38(4):334–339
- Darrigol O (2000) *Electrodynamics from Ampère to Einstein*. Oxford University Press, New York
- Dixon RC, Eringen AC (1965a) A dynamical theory of polar elastic dielectrics — I. *International Journal of Engineering Science* 3(3):359–377
- Dixon RC, Eringen AC (1965b) A dynamical theory of polar elastic dielectrics — II. *International Journal of Engineering Science* 3(3):379–398
- Dmitriyev V (2008) Mechanical model of the Lorentz force and Coulomb interaction. *Central European Journal of Physics* 6(3):711–716
- Dmitriyev VP (2003) Electrodynamics and elasticity. *American Journal of Physics* 71(9):952–953
- Farnes JS (2018) A unifying theory of dark energy and dark matter: Negative masses and matter creation within a λ cdm modified framework. *Astronomy & Astrophysics* 620:A92
- Grekova E, Zhilin P (2001) Basic equations of Kelvin’s medium and analogy with ferromagnets. *Journal of Elasticity* 64(1):29–70
- Grekova EF (2001) Ferromagnets and Kelvin’s medium: Basic equations and wave processes. *Journal of Computational Acoustics* 9(2):427–446
- Huang HH, Sun CT, Huang GL (2009) On the negative effective mass density in acoustic metamaterials. *International Journal of Engineering Science* 47(4):610–617
- Ivanova EA (2015) A new model of a micropolar continuum and some electromagnetic analogies. *Acta Mechanica* 226(3):697–721
- Ivanova EA (2019a) On a micropolar continuum approach to some problems of thermo- and electrodynamic. *Acta Mechanica* 230(5):1685–1715
- Ivanova EA (2019b) Towards micropolar continuum theory describing some problems of thermo and electrodynamics. In: Altenbach H, Irschik H, Matveenko VP (eds) *Contributions to Advanced Dynamics and Continuum Mechanics*, Springer, Cham, *Advanced Structured Materials*, vol 114, pp 111–129
- Ivanova EA (2021) Modeling of electrodynamic processes by means of mechanical analogies. *ZAMM - Journal of Applied Mathematics and Mechanics / Zeitschrift für Angewandte Mathematik und Mechanik* 101(4):e202000,076
- Ivanova EA, Kolpakov YE (2013) Piezoeffect in polar materials using moment theory. *Journal of Applied Mechanics and Technical Physics* 54(6):989–1002
- Ivanova EA, Kolpakov YE (2016) A description of piezoelectric effect in non-polar materials taking into account the quadrupole moments. *ZAMM - Journal of Applied Mathematics and Mechanics / Zeitschrift für Angewandte Mathematik und Mechanik* 96(9):1033–1048
- Ivanova EA, Matias DV (2019) Coupled problems in thermodynamics. In: Altenbach H, Öchsner A (eds) *State of the Art and Future Trends in Material Modeling*, Springer, Cham, *Advanced Structured Materials*, vol 114, pp 151–172
- Ivanova EA, Krivtsov AM, Zhilin PA (2007) Description of rotational molecular spectra by means of an approach based on rational mechanics. *ZAMM - Journal of Applied Mathematics and Mechanics / Zeitschrift für Angewandte Mathematik und Mechanik* 87(2):139–149

- Jaswon MA (1969) Mechanical interpretation of Maxwell's equations. *Nature* 224(5226):1303–1304
- Kelly EM (1976) Vacuum electromagnetics derived exclusively from the properties of an ideal fluid. *II Nuovo Cimento B* 32(1):117–137
- Khamehchi MA, Hossain K, Mossman ME, Zhang Y, Busch T, Forbes MM, Engels P (2017) Negative-mass hydrodynamics in a spin-orbit-coupled Bose-Einstein condensate. *Physical Review Letter* 118(15):155,301
- Larson D (1998) A derivation of Maxwell's equations from a simple two component solid mechanical aether. *Physics Essays* 11(4):524–530
- Lin TW, Lin H (2014) Newton's laws of motion based substantial aether theory for electromagnetic wave. *Journal of Mechanics* 30(4):435–442
- Longair M (2015) '... a paper ... I hold to be great guns': a commentary on Maxwell (1865) 'a dynamical theory of the electromagnetic field'. *Philosophical Transactions of the Royal Society A: Mathematical, Physical and Engineering Sciences* 373(2039):20140,473
- Müller WH, Rickert W, Vilchevskaya EN (2020) Thence the moment of momentum. *ZAMM - Journal of Applied Mathematics and Mechanics / Zeitschrift für Angewandte Mathematik und Mechanik* 100(5):e202000,117
- Pietsch W (2012) Hidden underdetermination: A case study in classical electrodynamics. *International Studies in the Philosophy of Science* 26(2):125–151
- Siegel DM (1991) *Innovation in Maxwell's Electromagnetic Theory: Molecular Vortices, Displacement Current, and Light*. Cambridge University Press, New York
- Silva CC (2007) The role of models and analogies in the electromagnetic theory: A historical case study. *Science & Education* 16(7):835–848
- Socas-Navarro H (2019) Can a negative-mass cosmology explain dark matter and dark energy? *Astronomy & Astrophysics* 626:A5
- Tajmar M, Assis A (2015) Particles with negative mass: Production, properties and applications for nuclear fusion and self-acceleration. *Journal of Advanced Physics* 4(1):77–82
- Teregulov IG (1989) Moment theory of electromagnetic effects in anisotropic solids. *Journal of Applied Mathematics and Mechanics* 53(6):786–790
- Wang X (2014) Dynamic behaviour of a metamaterial system with negative mass and modulus. *International Journal of Solids and Structures* 51(7):1534–1541
- Wang XS (2008) Derivation of the Maxwell's equations based on a continuum mechanical model of vacuum and a singularity model of electric charges. *Progress in Physics* 2:111–120
- Whittaker E (1910) *A History of the Theories of Aether and Electricity. The Classical Theories*. Thomas Nelson and Sons Ltd, London et al.
- Zareski D (2001) The elastic interpretation of electrodynamics. *Foundations of Physics Letters* 14(5):447–469
- Zhilin PA (1996a) Classical and Modified Electrodynamics (in Russ.). In: *Proceedings of International Conference "New Ideas in Natural Sciences"*. Part I - Physics, St. Petersburg, pp 73–82
- Zhilin PA (1996b) Reality and Mechanics (in Russ.). In: *Proc. of XXIII Summer School "Analysis and synthesis of nonlinear mechanical oscillatory systems"*, St. Petersburg, pp 6–49
- Zhilin PA (2006a) *Advanced Problems in Mechanics*. In: Indeitsev DA, Ivanova EA, Krivtsov AM (eds) Selection of articles presented at the Annual International Summer School – Conference *Advanced Problems in Mechanics*, Institute for Problems in Mechanical Engineering of Russian Academy of Sciences, St. Petersburg, vol 2
- Zhilin PA (2006b) *Advanced Problems in Mechanics (in Russ.)*. In: Indeitsev DA, Ivanova EA, Krivtsov AM (eds) Selection of articles presented at the Annual International Summer School – Conference *Advanced Problems in Mechanics*, Institute for Problems in Mechanical Engineering of Russian Academy of Sciences, St. Petersburg, vol 1
- Zhilin PA (2012) *Rational Continuum Mechanics*. Polytechnic University Publishing House, St. Petersburg
- Zhilin PA (2013) Construction of a model of an electromagnetic field from the standpoint of rational mechanics (in Russ.). *RENSIT* 5(1):77–97



Chapter 8

Hierarchical Models of Conduction of Heat in Continua Contained in Prismatic Shell-like Domains

George Jaiani

Abstract We construct hierarchical models for the heat conduction in standard and prismatic shell-like and rod-like 3D domains with non-Lipschitz boundary, in general.

Key words: Hierarchical models, Heat conduction equations, Prismatic shell-like and rod-like 3D domains with non-Lipschitz boundaries

8.1 Introduction

If the quantities, causing deformation and temperature, vary sufficiently slowly from zero to their finite values and remain in such a state, then we have a steady process, i.e., static process as $t \rightarrow \infty$. Therefore, displacements and temperature become independent of time and are functions only of the state. Thus, in the equation of conduction of Heat disappear derivatives with respect to time, in particular deformation tensor velocity $\dot{\varepsilon}_{ij}(x, t) \equiv 0$. So, the governing system of thermoelasticity will be split and after solving the independent BVPs for temperature change θ and substituting the found temperature change into governing system of thermoelasticity we arrive at independent BVP of elasticity with the additional (caused by temperature) member. In the theory of temperature stresses, which studies influence of heating the body surfaces and heat sources on the stress state of body it is assumed that the influence of $\dot{\varepsilon}_{kk}$ involved in the equation of heat conduction on body deformation is negligible (see Nowacki, 1975, pp. 90, 92, 93, 764).

Thus, for the above-mentioned and for analogous cases it is important to have hierarchical models separately for the heat conduction in standard and prismatic

George Jaiani

I. Vekua Institute of Applied Mathematics of I. Javakhishvili Tbilisi State University, 2, University Street, 0186, Tbilisi, Georgia
e-mail: george.jaiani@gmail.com

shell-like and rod-like 3D domains with non-Lipschitz boundaries, in general, occupied by a continuum. In the present paper our purpose is to construct hierarchical models for heat conduction in prismatic shell-like 3D domains Ω with non-Lipschitz boundaries, in general. To this end we use I. Vekua's dimension reduction method (Vekua, 1955, 1965, 1973, 1985). We have a definite experience of application of this method, we have constructed hierarchical models: for micropolar elastic cusped prismatic shells (Jaiani, 2016b), elastic prismatic shells with microtemperatures (Jaiani, 2015), piezoelectric viscoelastic Kelvin-Voigt prismatic shells with voids (Jaiani, 2018b) for prismatic shells with mixed conditions on face surfaces (Jaiani, 2016c), layered prismatic shells (Jaiani, 2016a). The above-mentioned hierarchical models we easily reformulate from elastic to thermoelastic if in the constitutive relations, namely, in expression of stress tensor, to the right-hand side we add

$$-\gamma T \delta_{ij}, \quad \gamma = \frac{\alpha E}{1 - 2\nu}$$

with the linear thermal definition coefficient α .

Now, within the framework of the last hierarchical models we may consider the states described at the beginning of the present section and handle them with the way indicated there.

8.2 Governing System of Conduction of Heat

The conservation of energy equation has the form (see, e.g., Dautray and Lions (1990, Chapter 1, Section 2, Subsection 6, Point 6.3 General Equations of Classical Thermoelasticity) and also Nowacki (1975, Chapter 3, Section 3.3; Section 3.4, Point 4))

$$\rho \theta \frac{ds}{dt} + \operatorname{div} \mathbf{q} = f, \quad \theta := T(\mathbf{x}, t) - T_0, \quad \text{in } \Omega, \quad (8.1)$$

provided the intrinsic energy is zero, where T_0 is the absolute temperature in a natural state $t = t_0$, T is the absolute temperature at the moment t , s is the specific entropy, $\mathbf{q}(\mathbf{x}, t)$ is the heat flux vector (with components q_i in the considered reference frame, heat is crossing a unit element of fictitious surface $\partial\Omega$ passing through \mathbf{x} and perpendicular to a unit outward normal \mathbf{n} . The passage being made in the sense and direction of the vector \mathbf{q}); here, it is the question of heat transmitted by conduction of the interior of Ω , $f(\mathbf{x}, t)$ is density per unit volume defining a rate of heat supplied by external elements in the medium under consideration, e.i., so called "source" function is supposed to be given and is in fact zero in a certain number of applications. Fourier's law in the isotropic case looks like (see, e.g., Dautray and Lions (1990, Chapter 1, Section 2, Subsection 6, Point 6.3 General Equations of Classical Thermoelasticity)

$$\mathbf{q} = -k \operatorname{grad} \theta, \quad (8.2)$$

where k is the thermal conduction coefficient. In the steady case, from (8.1) we get

$$\operatorname{div} \mathbf{q} = f. \quad (8.3)$$

Now, about boundary conditions (BC):

(i) if the temperature \bar{T} is prescribed on a part at the boundary $\partial\omega$, then we have

$$\theta = \bar{T} - T_0; \quad (8.4)$$

(ii) if the flux of heat across a part of the boundary is imposed, then we have BC of the type

$$-q_i n_i = \bar{q}_n \text{ given}, \quad (8.5)$$

which because of (8.2) becomes

$$\frac{\partial \theta}{\partial n} = \bar{g} \text{ given}. \quad (8.6)$$

Let the body occupy a prismatic 3D domain Ω with a non-Lipschitz boundary, in general, and the upper and lower face surfaces of the prismatic 3D domain be given by $x_3 = \overset{(+)}{h}(x_1, x_2)$ and $x_3 = \overset{(-)}{h}(x_1, x_2)$, respectively. Let further

$$2h(x_1, x_2) := \overset{(+)}{h}(x_1, x_2) - \overset{(-)}{h}(x_1, x_2), \quad (x_1, x_2) \in \omega,$$

denote the thickness of the domain occupied by the body, ω is a projection of the 3D domain on the plane $x_3 = 0$, a part of the boundary $\partial\omega$ is called a cusped edge if $2h = 0$ there (see also the beginning of Sect. 3 of Jaiani, 2018b).

$$\widetilde{2h}(x_1, x_2) := \overset{(+)}{h}(x_1, x_2) + \overset{(-)}{h}(x_1, x_2), \quad (x_1, x_2) \in \omega.$$

Substituting (8.2) into (8.3) we obtain the heat equation

$$-(k(x_1, x_2)\theta_{,j})_{,j} = f \quad (8.7)$$

in the steady case.

8.3 Mathematical Moments

For the convenience of the reader we repeat the relevant material from Sect. 10 of Jaiani (2018b). Let $f(x_1, x_2, x_3)$ be a given function in $\bar{\Omega}$ having integrable partial derivatives, let f_r be its r -th order moment defined as follows

$$f_r(x_1, x_2) := \int_{\overset{(-)}{h}(x_1, x_2)}^{\overset{(+)}{h}(x_1, x_2)} f(x_1, x_2, x_3) P_r(ax_3 - b) dx_3,$$

where (see the end of Sect. 2 and the beginning of Sect. 3 of Jaiani, 2018b)

$$a(x_1, x_2) := \frac{1}{h(x_1, x_2)}, \quad b(x_1, x_2) := \frac{\widetilde{h}(x_1, x_2)}{h(x_1, x_2)},$$

$$2h(x_1, x_2) = \overset{(+)}{h}(x_1, x_2) - \overset{(-)}{h}(x_1, x_2) > 0,$$

$$\widetilde{2h}(x_1, x_2) = \overset{(+)}{h}(x_1, x_2) + \overset{(-)}{h}(x_1, x_2) > 0,$$

and

$$P_r(\tau) = \frac{1}{2^r r!} \frac{d^r(\tau^2 - 1)^r}{d\tau^r}, \quad r = 0, 1, \dots,$$

are the r -th order Legendre polynomials with the orthogonality property

$$\int_{-1}^{+1} P_m(\tau)P_n(\tau)d\tau = \frac{2}{2m+1}\delta_{mn}.$$

From here, substituting

$$\tau = ax_3 - b = \frac{2}{\overset{(+)}{h}(x_1, x_2) - \overset{(-)}{h}(x_1, x_2)}x_3 - \frac{\overset{(+)}{h}(x_1, x_2) + \overset{(-)}{h}(x_1, x_2)}{\overset{(+)}{h}(x_1, x_2) - \overset{(-)}{h}(x_1, x_2)},$$

we have

$$\left(m + \frac{1}{2}\right)a \int_{\overset{(-)}{h}(x_1, x_2)}^{\overset{(+)}{h}(x_1, x_2)} P_m(ax_3 - b)P_n(ax_3 - b)dx_3 = \delta_{mn}.$$

Using the well-known formulas of integration by parts (with respect to x_3) and differentiation with respect to a parameter of integrals depending on parameters (x_α) , taking into account $P_r(1) = 1, P_r(-1) = (-1)^r$, we deduce

$$\int_{\overset{(-)}{h}(x_1, x_2)}^{\overset{(+)}{h}(x_1, x_2)} P_r(ax_3 - b)f_{,3} dx_3 = -a \int_{\overset{(-)}{h}(x_1, x_2)}^{\overset{(+)}{h}(x_1, x_2)} P'_r(ax_3 - b)fdx_3 + f \overset{(+)}{h} - (-1)^r \overset{(-)}{h} f, \quad (8.8)$$

$$\int_{\overset{(-)}{h}(x_1, x_2)}^{\overset{(+)}{h}(x_1, x_2)} P_r(ax_3 - b)f_{,\alpha} dx_3 = f_{r,\alpha} - f \overset{(+)(+)}{h}_{,\alpha} + (-1)^r f \overset{(-)(-)}{h}_{,\alpha}$$

$$- \int_{\overset{(+)}{h}(x_1, x_2)}^{\underset{(-)}{h}(x_1, x_2)} P_r'(ax_3 - b)(a_{,\alpha} x_3 - b_{,\alpha}) f dx_3, \quad \alpha = 1, 2, \tag{8.9}$$

where superscript prime means differentiation with respect to the argument $ax_3 - b$, subscripts preceded by a comma mean partial derivatives with respect to the corresponding variables, $f := f[x_1, x_2, \overset{(\pm)}{h}(x_1, x_2)]$. Applying the following relations from the theory of the Legendre polynomials (see e.g. Jaiani, 2018a, pp. 338-339)

$$P_r'(\tau) = \sum_{s=0}^r (2s+1) \frac{1 - (-1)^{r+s}}{2} P_s(\tau) \tag{1}$$

$$\tau P_r'(\tau) = r P_r(\tau) + P_{r-1}'(\tau) = r P_r(\tau) + \sum_{s=0}^{r-1} (2s+1) \frac{1 + (-1)^{r+s}}{2} P_s(\tau) \tag{2}$$

and, in view of $\frac{a_{,\alpha}}{a} = (\ln a)_{,\alpha} = -\frac{h_{,\alpha}}{h}$, $\frac{a_{,\alpha}}{a} b = \widetilde{h} a_{,\alpha}$, $b_{,\alpha} = (\widetilde{h} a)_{,\alpha}$, it is easily seen that

$$\begin{aligned} P_r'(ax_3 - b)(a_{,\alpha} x_3 - b_{,\alpha}) &= \frac{a_{,\alpha}}{a} (ax_3 - b) P_r'(ax_3 - b) + \left(\frac{a_{,\alpha}}{a} b - b_{,\alpha}\right) P_r'(ax_3 - b) \\ &= -h_{,\alpha} h^{-1} (ax_3 - b) P_r'(ax_3 - b) - \widetilde{h}_{,\alpha} h^{-1} P_r'(ax_3 - b) \\ &= -\overset{r}{a_{\alpha r}} P_r(ax_3 - b) - \sum_{s=0}^{r-1} \overset{r}{a_{\alpha s}} P_s(ax_3 - b) \tag{3} \end{aligned} \tag{8.11}$$

where

¹ On the top of the symbol \sum both $r - 1$ and r are true since the last term equals zero.
² On the top of the symbol \sum both $r - 2$ and $r - 1$ are true since the last term equals zero.
³ The following relations are valid

$$\begin{aligned} &\sum_{s=0}^{r-1} (2s+1) \left[\frac{h_{,\alpha} + (-1)^{r+s} h_{,\alpha}}{2h} + \frac{\widetilde{h}_{,\alpha} - (-1)^{r+s} \widetilde{h}_{,\alpha}}{2h} \right] P_s(ax_3 - b) \\ &= \sum_{s=0}^{r-1} \frac{(2s+1)}{2h} \left(\frac{\overset{(+)}{h}_{,\alpha} - \overset{(-)}{h}_{,\alpha} + \overset{(+)}{h}_{,\alpha} (-1)^{r+s} - \overset{(-)}{h}_{,\alpha} (-1)^{r+s}}{2} \right. \\ &\quad \left. + \frac{\overset{(+)}{h}_{,\alpha} + \overset{(-)}{h}_{,\alpha} - \overset{(+)}{h}_{,\alpha} (-1)^{r+s} - \overset{(-)}{h}_{,\alpha} (-1)^{r+s}}{2} \right) P_s(ax_3 - b) \\ &= \sum_{s=0}^{r-1} (2s+1) \frac{\overset{(+)}{h}_{,\alpha} - (-1)^{r+s} \overset{(-)}{h}_{,\alpha}}{2h} P_s(ax_3 - b) \end{aligned}$$

because of $h = \frac{\overset{(+)}{h} - \overset{(-)}{h}}{2}$, $\widetilde{h} = \frac{\overset{(+)}{h} + \overset{(-)}{h}}{2}$.

$${}^r a_{\alpha r} := r \frac{h_{,\alpha}}{h}, \quad {}^r a_{\alpha s} := (2s+1) \frac{{}^{(+)}h_{,\alpha} - (-1)^{r+s} {}^{(-)}h_{,\alpha}}{2h}, \quad s \neq r. \tag{8.12}$$

Now, bearing in mind (8.11) and (8.10), from (8.9) and (8.8) we have

$$\begin{aligned} & \int_{{}^{(+)}h(x_1, x_2)} P_r(ax_3 - b) f_{,\alpha} dx_3 \\ & \int_{{}^{(-)}h(x_1, x_2)} P_r(ax_3 - b) f_{,\alpha} dx_3 \\ & = f_{r,\alpha} + \sum_{s=0}^r {}^r a_{\alpha s} f_s - f {}^{(+)(+)}h_{,\alpha} + (-1)^r f {}^{(-)(-)}h_{,\alpha}, \quad \alpha = 1, 2, \end{aligned} \tag{8.13}$$

$$\int_{{}^{(+)}h(x_1, x_2)} P_r(ax_3 - b) f_{,3} dx_3 = \sum_{s=0}^r {}^r a_{3s} f_s + f {}^{(+)} - (-1)^r f {}^{(-)} \int_{{}^{(-)}h(x_1, x_2)} P_r(ax_3 - b) f_{,3} dx_3 = \sum_{s=0}^r {}^r a_{3s} f_s + f {}^{(+)} - (-1)^r f {}^{(-)} \tag{8.14}$$

respectively. Here

$${}^r a_{3s} := -(2s+1) \frac{1 - (-1)^{s+r}}{2h}, \tag{8.15}$$

clearly,

$${}^r a_{3r} = 0. \tag{8.16}$$

Let

$$f(x_1, x_2, x_3) = \sum_{r=0}^{\infty} a\left(r + \frac{1}{2}\right) f_r(x_1, x_2) P_r(ax_3 - b), \tag{8.17}$$

then

$$\begin{aligned} f^{(\pm)} & := f(x_1, x_2, {}^{(\pm)}h(x_1, x_2)) = \sum_{s=0}^{\infty} a\left(s + \frac{1}{2}\right) f_s(\pm 1)^s \\ & = \sum_{s=0}^{\infty} \frac{(\pm 1)^s (2s+1)}{2h} f_s, \quad i = \overline{1, 3}, \end{aligned} \tag{8.18}$$

whence

$$f^{(+)} - (-1)^r f^{(-)} = - \sum_{s=0}^{\infty} {}^r a_{3s} f_s, \quad i = \overline{1, 3}, \tag{8.19}$$

$$f {}^{(+)(+)}h_{,\alpha} - (-1)^r f {}^{(-)(-)}h_{,\alpha} = \sum_{s=0}^{\infty} {}^r a_{\alpha s}^* f_s, \quad i = \overline{1, 3}, \quad \alpha = 1, 2, \tag{8.20}$$

where

$$a_{\alpha s}^* = a_{\alpha s}^r, \quad s \neq r, \quad a_{\alpha r}^* = (2r+1) \frac{h_{r,\alpha}}{h}. \quad (8.21)$$

Substituting (8.20) and (8.19) into (8.13) and (8.14), respectively, we get

$$\begin{aligned} \int_{\overset{(+)}{h}(x_1, x_2)}^{\overset{(-)}{h}(x_1, x_2)} P_r(ax_3 - b) f_{,\alpha} dx_3 &= f_{r,\alpha} + \sum_{s=0}^r a_{\alpha s}^r f_s - \sum_{s=0}^{\infty} a_{\alpha s}^* f_s \\ &= f_{r,\alpha} + \sum_{s=r}^{\infty} b_{\alpha s}^r f_s, \end{aligned} \quad (8.22)$$

where

$$b_{js}^r := -a_{js}^r, \quad s > r; \quad b_{js}^r = 0, \quad s < r; \quad (8.23)$$

$$b_{\alpha r}^r := a_{\alpha r}^r - a_{\alpha r}^* = -(r+1) \frac{\overset{(+)}{h}_{,\alpha} - \overset{(-)}{h}_{,\alpha}}{2h}, \quad b_{3r}^r = -a_{3r}^r = 0, \quad (8.24)$$

and

$$\begin{aligned} \int_{\overset{(+)}{h}(x_1, x_2)}^{\overset{(-)}{h}(x_1, x_2)} P_r(ax_3 - b) f_{,3} dx_3 &= \sum_{s=0}^r a_{3s}^r f_s - \sum_{s=0}^{\infty} a_{3s}^* f_s \\ &= - \sum_{s=r+1}^{\infty} a_{3s}^r f_s = \sum_{s=r+1}^{\infty} b_{3s}^r f_s, \end{aligned} \quad (8.25)$$

respectively.

If f and f are known (prescribed), then from (8.13) and (8.14), correspondingly, we obtain

$$\begin{aligned} \int_{\overset{(+)}{h}(x_1, x_2)}^{\overset{(-)}{h}(x_1, x_2)} P_r(ax_3 - b) f_{,\alpha} dx_3 &= f_{r,\alpha} + \sum_{s=0}^r a_{\alpha s}^r f_s \\ + f n_{\alpha} \sqrt{1 + \overset{(+)}{h}_{,1}^2 + \overset{(+)}{h}_{,2}^2} + (-1)^r f n_{\alpha} \sqrt{1 + \overset{(-)}{h}_{,1}^2 + \overset{(-)}{h}_{,2}^2} \end{aligned} \quad (8.26)$$

and

$$\int_{\overset{(-)}{h}(x_1, x_2)}^{\overset{(+)}{h}(x_1, x_2)} P_r(ax_3 - b) f_{,3} dx_3 = \sum_{s=0}^r a_{3s}^r f_s$$

$$+ f \overset{(+)}{n}_3 \sqrt{1 + (\overset{(+)}{h}_{,1})^2 + (\overset{(+)}{h}_{,2})^2} + (-1)^r f \overset{(-)}{n}_3 \sqrt{1 + (\overset{(-)}{h}_{,1})^2 + (\overset{(-)}{h}_{,2})^2}, \quad (8.27)$$

since

$$\overset{(\pm)}{n}_\alpha = \frac{\mp \overset{(\pm)}{h}_{,\alpha}}{\sqrt{1 + (\overset{(\pm)}{h}_{,1})^2 + (\overset{(\pm)}{h}_{,2})^2}}, \quad \overset{(\pm)}{n}_3 = \frac{\pm 1}{\sqrt{1 + (\overset{(\pm)}{h}_{,1})^2 + (\overset{(\pm)}{h}_{,2})^2}}.$$

8.4 Construction of Hierarchical Models

To this end, applying Vekua’s dimension reduction method (Vekua, 1955, 1965, 1973, 1985), we multiply (8.1), (8.2), (8.4), and (8.6) by $P_r(ax_3 - b)$ and then integrate within the limits $\overset{(-)}{h}(x_1, x_2)$ and $\overset{(+)}{h}(x_1, x_2)$. Using formulas (8.6), (8.7), (8.15), and (8.18), we assume the heat flux vector normal component $q(\mathbf{x}, t, \mathbf{n})$ to be prescribed on the face surfaces, while on the lateral boundary of the body we assume to be hold either BC (8.4) or BC (8.6). Besides, we consider $\rho = \rho(x_1, x_2)$ and by calculations for temperature change θ on the face surfaces we employ (8.19), (8.20).

Thus, in the steady case: from (8.3), by virtue of (8.26), (8.27), we have

$$\int_{\overset{(-)}{h}}^{\overset{(+)}{h}} q_{k,k} P_r(ax_3 - b) dx_3 = \int_{\overset{(-)}{h}}^{\overset{(+)}{h}} q_{\gamma,\gamma} P_r(ax_3 - b) dx_3 + \int_{\overset{(-)}{h}}^{\overset{(+)}{h}} v_{3,3} P_r(ax_3 - b) dx_3$$

$$= q_{\gamma r, \gamma} + \sum_{s=0}^r a_{\gamma s}^r q_{\gamma s} - q_{\gamma} \overset{(+)}{h}_{,\gamma} + (-1)^r q_{\gamma} \overset{(-)}{h}_{,\gamma} + \sum_{s=0}^r a_{3s}^r q_{3s} + q_3 - (-1)^r q_3$$

$$= q_{\gamma r, \gamma} + \sum_{s=0}^r a_{\gamma s}^r q_{\gamma s} + q_{\overset{(+)}{n}} \sqrt{1 + \overset{(+)}{h}_{,\gamma} \overset{(+)}{h}_{,\gamma}} + (-1)^r q_{\overset{(-)}{n}} \sqrt{1 + \overset{(-)}{h}_{,\gamma} \overset{(-)}{h}_{,\gamma}} = f_r, \quad (8.28)$$

$$r = 0, 1, 2, \dots,$$

because of

$$\overset{(\pm)}{n}_\gamma = \frac{\mp \overset{(\pm)}{h}_{,\gamma}}{\sqrt{\overset{(\pm)}{h}_{,\alpha} \overset{(\pm)}{h}_{,\alpha} + 1}}, \quad \overset{(\pm)}{n}_3 = \frac{\pm 1}{\sqrt{\overset{(\pm)}{h}_{,\alpha} \overset{(\pm)}{h}_{,\alpha} + 1}}$$

from (8.2), provided $k = k(x_1, x_2)$, by virtue of (8.22)-(8.24), we get

$$\begin{aligned}
q_{\gamma r} &= k(x_1, x_2) \int_{\overset{(-)}{h}(x_1, x_2)}^{\overset{(+)}{h}(x_1, x_2)} \theta_{,\gamma}(x_1, x_2, x_3) P_r(ax_3 - b) dx_3 \\
&= k(x_1, x_2) \left[\theta_{r,\gamma} + \sum_{s=0}^r a_{\gamma s}^r \theta_s - \overset{(+)(+)}{\theta} h_{,\gamma} + (-1)^r \overset{(-)(-)}{\theta} h_{,\gamma} \right] \\
&= k(x_1, x_2) \left[\theta_{r,\gamma} + \sum_{s=0}^r a_{\gamma s}^r \theta_s - \sum_{s=0}^r a_{\gamma s}^{*r} \theta_s \right] \\
&= k(x_1, x_2) \left[\theta_{r,\gamma} + \sum_{s=r}^{\infty} b_{\gamma s}^r \theta_s \right] \\
&= k(x_1, x_2) h^{r+1} (\tilde{\theta}_r)_{,\gamma} + \sum_{s=r+1}^{\infty} b_{\gamma s}^r h^{s+1} \tilde{\theta}_s, \tag{8.29} \\
&\quad \gamma = 1, 2, \quad r = 0, 1, 2, \dots,
\end{aligned}$$

because of $\theta_{r,\gamma} + b_{\gamma r}^r \theta_r = h^{r+1} (\tilde{\theta}_r)_{,\gamma}$, $\tilde{\theta}_r := \frac{\theta_r}{h^{r+1}}$

$$\begin{aligned}
q_{3r}(x_1, x_2) &= k(x_1, x_2) \left[\sum_{s=0}^r a_{3s}^r q_{3s} + \overset{(+)}{\theta} + (-1)^r \overset{(-)}{\theta} \right] \\
&= k(x_1, x_2) \sum_{s=r}^{\infty} b_{3s}^r \theta_s, \quad r = 0, 1, 2, \dots \tag{8.30}
\end{aligned}$$

If we multiply by h^r the last equality in (8.28), the obtained equation

$$h^r q_{\gamma r,\gamma} + h^r \sum_{s=0}^r a_{\gamma s}^r q_{\gamma s} + h^r \overset{r}{Q} = h^r f_r, \quad r = 0, 1, \dots, \tag{8.31}$$

where

$$\overset{r}{Q} := q_{\overset{(+)}{n}}^r \sqrt{1 + \overset{(+)}{h_{,\gamma}} \overset{(+)}{h_{,\gamma}}} + (-1)^r q_{\overset{(-)}{n}}^r \sqrt{1 + \overset{(-)}{h_{,\gamma}} \overset{(-)}{h_{,\gamma}}} \tag{8.32}$$

we can rewrite as

$$(h^r q_{\gamma r,\gamma} + h^r \sum_{s=0}^{r-1} a_{\gamma s}^r q_{\gamma s} + h^r \overset{r}{Q} = h^r f_r, \quad r = 0, 1, \dots, \tag{8.33}$$

because of

$$h^r q_{\gamma r,\gamma} + h^r a_{\gamma r}^r q_{\gamma r} = h^r q_{\gamma r,\gamma} + h^r r \frac{h_{,\gamma}}{h} = (h^r q_{\gamma r})_{,\gamma}. \tag{8.34}$$

Now, considering weighted moments

$$\tilde{q}_{jr} := \frac{q_{jr}}{h^{r+1}}, \quad j = \overline{1,3}, \quad \tilde{\theta}_r := \frac{\theta_r}{h^{r+1}} \quad (8.35)$$

from (8.33) we get the following equations

$$(h^{2r+1} \tilde{q}_{\gamma r})_{,\gamma} + h^r \sum_{s=0}^{r-1} a_{\gamma s} h^{s+1} \tilde{q}_{\gamma s} + h^r Q = h^r f_r, \quad (8.36)$$

$$\gamma = 1, 2, \quad r = 0, 1, \dots,$$

with respect to weighted moments $\tilde{q}_{\gamma r}$, inserting (8.29) into (8.33) we derive hit equation in terms of weighted moments of θ :

$$\left[k(x_1, x_2) h^{2r+1} (x_1, x_2) \tilde{\theta}_{r,\gamma} \right]_{,\gamma} + \left[k(x_1, x_2) \sum_{s=r+1}^{\infty} b_{\gamma s} h^{s+1} \tilde{\theta}_s \right]_{,\gamma} = f_r, \quad (8.37)$$

$$r = 0, 1, 2, \dots$$

In other words we have rewritten heat equation (8.7) in terms of moments $\tilde{\theta}_s$, $s = r, r+1, \dots$. If we neglect moments of order $r > N$, we get N th order approximation, i.e., N th hierarchical model of heat transfer with the following BCs in moments

$$\theta_r = \bar{\theta}_r, \quad r = 0, 1, 2, \dots, N, \quad q_{nr} = \bar{q}_{nr}, \quad r = 0, 1, 2, \dots, N, \quad (8.38)$$

where $\bar{\theta}_r$, \bar{q}_{nr} we calculate from prescribed $\bar{\theta}$ and \bar{q}_n after multiplying them by $P_r(ax_3 - b)$ and then integrating within the limits $\overset{(-)}{h}(x_1, x_2)$ and $\overset{(+)}{h}(x_1, x_2)$. In the case of cusped edges they should be calculated as limits from the inside of domain.

The last, according to (8.29) may be rewritten as weighted Neumann BC

$$kh^{r+1} \frac{\partial \bar{\theta}_r}{\partial n} = \bar{g}_r, \quad r = 0, 1, \dots, N, \quad (8.39)$$

Concentrated at point and at cusped edge (line) heat flux we define similar to definition of concentrated at point and at cusped edge (line) force (see Jaiani, 2008)

8.5 The $N = 0$ Approximation

In this case from (8.37)-(8.39) we get the following two BVPs:

Find $\theta_0 \in C^2$, satisfying equation

$$\left[k(x_1, x_2) h(x_1, x_2) \tilde{\theta}_{0,\gamma} \right]_{,\gamma} = f_0(x_1, x_2) \quad (8.40)$$

under either BC

$$\theta_0 = \bar{\theta}_0 \quad (8.41)$$

or BC

$$q_{n0} = \bar{q}_{n0}, \text{ i.e., } kh \frac{\partial \tilde{\theta}_0}{\partial n} = \bar{g}_0 \quad (8.42)$$

with prescribed $\tilde{\theta}_0$ and \bar{g}_0 .

8.6 Case of Cusped Bodies

Let now, in the $N = 0$ approximation (model) consider the body Ω with the half-thickness

$$h = h_0 x_2^\kappa, \quad h_0, \kappa = \text{const} > 0, \quad (8.43)$$

whose projection ω on plane $x_3 = 0$ is a strip

$$\{(x, y) : -\infty < x < +\infty, \quad 0 < y < L, \quad L = \text{const} > 0\},$$

Eq. (8.40) will get the form:

$$x_2^\kappa (k \tilde{\theta}_{0,1})_{,1} + (k x_2^\kappa \tilde{\theta}_{0,2})_{,2} = \frac{f_0(x_1, x_2)}{h_0}.$$

First we assume $k = k_0 = \text{const}$, then Eq. (8.40) looks like the following singular differential equation

$$u_{,11} + u_{,22} + \frac{\kappa}{x_2} u_{,2} = \frac{x_2^{-\kappa}}{k h_0} f_0(x_1, x_2), \quad (8.44)$$

i.e.,

$$x_2 \Delta u + \kappa u_{,2} = \frac{x_2^{1-\kappa}}{k_0 h_0} f_0(x_1, x_2). \quad (8.45)$$

Let us consider the rectangular part of the cusped strip bounded by lines $x = a$, $x = b$, $a < b$. From the main theorem (Jaiani, 1995) it immediately follows:

Theorem 8.1. *If $f_0(x_1, x_2) \equiv 0$, then for $\kappa < 1$ the Dirichlet Problem is well-posed, i.e. the weighted temperature $\tilde{\theta}_0$ should be prescribed on the whole boundary $\partial\omega$, while for $\kappa \geq 1$ the Keldysh Problem is well-posed, i.e., on the three non-cusped edges of the rectangular boundary weighted temperature $\tilde{\theta}_0$ should be prescribed but cusped edge $y = 0$, $a < x < b$ should be left without BC, provided solution $\tilde{\theta}_0$ is bounded.*

Now, we consider particular case when $\tilde{\theta}_0 = \tilde{\theta}_0(x_2)$, $f_0 = f_0(x_2)$, $k = k(x_2)$ and $k(x_2)h(x_2) > 0$ as $x_2 \in]0, L[$, $k(0)h(0) = 0$, then the general solution of equation (8.40), which takes the form of the following degenerate partial differential equation

$$\left[k(x_2)h(x_2)\tilde{\theta}_{0,2}(x_2) \right]_{,2} = f_0(x_2), \quad (8.46)$$

has the form

$$\tilde{\theta}_0(x_2) = c_1 \int_L^{x_2} \frac{d\tau}{k(\tau)h(\tau)} + \int_L^{x_2} \frac{d\tau}{k(\tau)h(\tau)} \int_L^{\tau} f_0(t)dt + c_2. \quad (8.47)$$

Whence, the Dirichlet problem is well-posed, i.e., the weighted temperature should be prescribed on both the edges $y = 0$ and $y = L$ if and only if

$$\int_0^{x_2^0} \frac{d\tau}{k(\tau)h(\tau)} < \infty, \quad (8.48)$$

for Keldysh type problem we have the condition

$$\int_0^{x_2^0} \frac{d\tau}{k(\tau)h(\tau)} = +\infty, \quad (8.49)$$

therefore, only at the edge $y = L$ should be prescribed the weighted temperature and the edge $y = 0$ should be freed from BC, provided we are looking for bounded solutions, i.e. we have the Keldysh type BVP. Moreover, both the BVP we solve in the explicit form under BCs

$$\tilde{\theta}_0(0) = \bar{\theta}_0, \quad (8.50)$$

$$\tilde{\theta}_0(L) = \bar{\theta}_L, \quad (8.51)$$

in the case of the Dirichlet type BVP and under BC (8.51) in the case of the Keldysh type BVP. The unique solutions have the form (8.47), where

$$c_2 = \bar{\theta}_0, \quad (8.52)$$

$$c_1 = \left[\int_L^0 \frac{d\tau}{k(\tau)h(\tau)} \right]^{-1} \left[\bar{\theta}_0 - \bar{\theta}_L - \int_L^0 \frac{d\tau}{k(\tau)h(\tau)} \int_L^{\tau} \frac{dt}{k(t)h(t)} \right]$$

for the Dirichlet type BVP and with $c_1 = 0$ and (8.52) for the Keldysh type BVP (clearly in the particular case (8.43), when $k(\tau) = k_0 \neq 0$ we again obtain the condition $\kappa < 1$ for the Dirichlet Problem and the condition $\kappa \geq 1$ for the Keldysh problem).

The mixed BVP under BC (8.51) and the weighted Neumann condition (8.42) has a unique explicit solution (8.47), where

$$c_1 = \bar{g}_0 - \int_L^0 f_0(t)dt - \bar{\theta}_L,$$

$$c_2 = \bar{\theta}_L.$$

Indeed, from (8.42), bearing in mind (8.49) we obtain

$$\bar{g}_0 = c_1 + \int_L^0 f_0(t) dt + \bar{\theta}_L.$$

8.7 Conclusions

Differential hierarchical models for the heat condition equation in prismatic shell-like domains non-Lipschitz, in general, are constructed and the peculiarities of setting of boundary conditions in the case of cusped domains are discussed. These results allow to investigate well-posedness of boundary value problems for thermoelastic bodies with non-Lipschitz boundaries, in general when deformation and temperature vary sufficiently slowly and the governing system of thermoelasticity will be split into two independent BVPs for temperature and the deformed state of the body.

The peculiarities of nonclassical setting of BCs when either the thickness, or thermal conduction coefficient, or both ones vanish at the edge of prismatic shells are discussed, criteria of setting the Dirichlet and Keldysh type BVPs are established. Some concrete BVPs are solved in the explicit form.

In the $N = 0$ approximation a mixed BVP, when at non-cusped edge the weighted temperature and at cusped edge the concentrated at edge heat flux are prescribed, is solved.

References

- Dautray R, Lions JL (1990) *Mathematical Analysis and Numerical Methods for Science and Technology*, vol 1 - Physical Origins and Classical Methods. Springer, Berlin, Heidelberg
- Jaiani G (1995) On a generalization of the Keldysh theorem. *Georgian Mathematical Journal* 2(3):291–297
- Jaiani G (2008) On physical and mathematical moments and setting of boundary conditions for cusped prismatic shells and beams. In: Jaiani G, Podio-Guidugli P (eds) *IUTAM Symposium on Relations of Shell Plate Beam and 3D Models*, Springer, Dordrecht, IUTAM Bookseries, vol 9, pp 133–147
- Jaiani G (2015) Differential hierarchical models for elastic prismatic shells with microtemperatures. *ZAMM - Journal of Applied Mathematics and Mechanics / Zeitschrift für Angewandte Mathematik und Mechanik* 95(1):77–90
- Jaiani G (2016a) A model of layered prismatic shells. *Continuum Mechanics and Thermodynamics* 28(3):765–784
- Jaiani G (2016b) On micropolar elastic cusped prismatic shells. *Transactions of A Razmadze Mathematical Institute* 170:376–384
- Jaiani G (2016c) Vekua type hierarchical models for prismatic shells with mixed conditions on face surfaces. *Composite Structures* 152:226–238
- Jaiani G (2018a) *Mathematical Models of Mechanics of Continua* (in Georgian), 2nd edn. Tbilisi University Press, Tbilisi
- Jaiani G (2018b) Piezoelectric viscoelastic Kelvin-Voigt cusped prismatic shells. *Lecture Notes of TICMI* 19:83

- Nowacki W (1975) *Theory of Elasticity* (in Russ.). Mir, Moscow
- Vekua I (1955) On one method of calculating of prismatic shells (in Russ.). *Trudy Tbilis Mat Inst* 21:191–259
- Vekua I (1965) The theory of thin shallow shells of variable thickness (in Russ.). *Proceedings of A Razmadze Institute of Mathematics of Georgian Academy of Sciences* 30:5–103
- Vekua I (1973) On two ways of constructing the theory of elastic shells (in Russ.). In: Becker E, Mikhailov GK (eds) *Proceedings of XIII International Congress of Theoretical and Applied Mechanics*, Moscow, August 16-21, 1972, Springer-VerlagSpringer-Verlag, Berlin, Heidelberg, New York, pp 322–339
- Vekua I (1985) *Shell Theory: General Methods of Construction*. Advanced Publishing Program, Pitman, Boston, London, Melbourne



Chapter 9

Dynamic Sliding Contact for a Thin Elastic Layer

Julius Kaplunov, Danila A. Prikazchikov, and Tomaž Savšek

Abstract The contribution is concerned with dynamics of a thin elastic layer, subject to sliding contact. Both one- and two-sided sliding contact are studied, revealing the presence of the fundamental vibration modes. First, mixed boundary conditions modelling two-sided sliding are addressed, allowing a factorisation of the dispersion relation. Then, the asymmetric problem of one-sided sliding contact is tackled, with mixed conditions along the contact surface and prescribed normal stress on the opposite face. Using symmetry, this problem is found to be related to that for a layer of a double thickness, with classical boundary conditions in terms of stresses. In this case, the fundamental mode of interest coincides with the zero-order Rayleigh-Lamb symmetric wave. A long-wave low-frequency perturbation scheme is implemented for the forced problem.

Key words: Sliding contact, Thin layer, Elastic, Waves

Julius Kaplunov

School of Computing and Mathematics, Keele University, Keele, Staffordshire, ST5 5BG, UK & Faculty of Industrial Engineering, 8000, Novo Mesto, Slovenia

e-mail: j.kaplunov@keele.ac.uk

Danila Prikazchikov

School of Computing and Mathematics, Keele University, Keele, Staffordshire, ST5 5BG, UK & Institute for Problems in Mechanical Engineering, Russian Academy of Sciences, Saint-Petersburg, 199178, Russian Federation

e-mail: d.prikazchikov@keele.ac.uk

Tomaž Savšek

Faculty of Industrial Engineering, 8000, Novo Mesto, Slovenia

e-mail: tomaz.savsek@fini-unm.si

© The Author(s), under exclusive license to Springer Nature Switzerland AG 2022

H. Altenbach et al. (eds.), *Recent Approaches in the Theory of Plates and Plate-Like Structures*, Advanced Structured Materials 151,

https://doi.org/10.1007/978-3-030-87185-7_9

9.1 Introduction

Usually, within the mathematical theories of thin plates and shells theories the face boundary conditions are either traction-free or contain prescribed stresses, see e.g. Goldenveizer et al (1979); Kaplunov et al (1998); Le (1999); Mikhasev and Tovstik (2020). In case of layered structures, these boundary conditions are accompanied by continuity conditions along the interfaces which often model a perfect contact, see Belyaev et al (2019, 2021); Nolde et al (2004) and containing asymptotic treatments for various material models. This type of boundary conditions supports fundamental vibration modes over the low-frequency range.

At the same time, for both or one faces fixed only the high-frequency harmonics may propagate, see e.g. Kaplunov (1995); Kaplunov and Nolde (2002); Kaplunov et al (2005); Aghalovyan (2015), and also Nolde and Rogerson (2002); Rogerson et al (2007); Lashhab et al (2015) dealing with pre-stressed elastic solids. The exception is a special setup of layered elastic structures with a strong vertical inhomogeneity, for which the lowest harmonics may also emerge in the low-frequency region, see Prikazchikova et al (2020). In addition, we cite the observation of transition between the boundary conditions corresponding to fixed and free faces in Moukhomodiarov et al (2010).

It is worth mentioning that the contact problems involve two limiting scenarios for interaction between a coating layer and a half-space, which may be regarded as "soft" and "stiff" contact. The first scenario is associated with plate bending, with the layer being much stiffer than the substrate, see asymptotic analysis in Erbaş et al (2018); Kaplunov et al (2019), whereas the second one corresponds to a Winkler-Fuss foundation, see Kaplunov et al (2018); Kudish et al (2021) for classifications of possible regimes. We also note an asymptotic consideration in Erbaş et al (2011), as well as related problems in lubrication (Kudish et al, 2020) and nanoindentation (Borodich, 2014; Borodich et al, 2019; Argatov and Mishuris, 2011, 2018), including bio-mechanical applications, e.g. Argatov and Mishuris (2016) and references therein.

An important sub-class of problems is concerned with sliding contact between elastic solids, which has received relatively less attention compared to other types of contact beginning with the perfect one, see references above. Among the contributions analysing sliding contact we mention Barnett et al (1988); Darinskii and Weihnacht (2005); Vinh and Ngoc Anh (2014). However, further insight into the peculiarities of dynamic behaviour of thin layers subject to a sliding contact seems to be of interest.

In this chapter, a simple manifestation of sliding contact is studied, including both one-sided and two-sided sliding. It is revealed that even for an absolutely rigid substrate, precluding vertical displacements of the layer, the fundamental vibration modes may occur, however, the situations for one- and two-sided sliding are quite different. For a two-sided sliding the transverse coordinate may be separated, see e.g. a similar technique implemented for 3D edge waves (Kaplunov et al, 2005), leading to straightforward factorisation of the dispersion relation. As for one-sided

sliding, using symmetry, the problem is transformed to plane stress at long-wave low-frequency limit.

The layout of the chapter is as follows. In Sect. 9.2 the problem for two-sided sliding of elastic layer is treated. It is observed that for the fundamental mode the problem is equivalent to plane-strain one. In Sect. 9.3 one-sided sliding is investigated. For traction-free upper face it is shown that the vibration phenomena is governed by the classical Rayleigh-Lamb dispersion relation. A forced vibration problem with the opposite side subject to prescribed normal stress is analysed in more detail. It is demonstrated that the problem is reduced to transverse compression for a thin layer earlier treated in Kaplunov et al (1998). Leading order and refined equations of motion are presented.

9.2 Two-Sided Sliding

Consider a thin elastic layer of thickness $2h$, occupying the domain $-\infty < x_1, x_2 < \infty$, $-h \leq x_3 \leq h$. In absence of the body forces, the governing equations of motion are conventionally given by

$$\frac{\partial \sigma_{ij}}{\partial x_j} = \rho \frac{\partial^2 u_i}{\partial t^2}, \quad i, j = 1, 2, 3, \tag{9.1}$$

with comma in the subscript denoting differentiation with respect to associated variable, σ_{ij} and u_i being the stress tensor and displacement components, respectively, and ρ standing for the volume mass density. The constitutive relations of linear isotropic elasticity are taken in standard form as

$$\sigma_{ij} = \frac{E}{2(1+\nu)} \left[\frac{2\nu}{1-2\nu} \delta_{ij} \left(\frac{\partial u_1}{\partial x_1} + \frac{\partial u_2}{\partial x_2} + \frac{\partial u_3}{\partial x_3} \right) + \left(\frac{\partial u_i}{\partial x_j} + \frac{\partial u_j}{\partial x_i} \right) \right], \tag{9.2}$$

where E and ν are the Young’s modulus and the Poisson’s ratio, respectively. The mixed boundary conditions on the faces $x_3 = \pm h$, considered in this section, are written as

$$u_3 = \sigma_{13} = \sigma_{23} = 0, \tag{9.3}$$

corresponding to motion of sliding type, see Fig. 9.1.

It is known that the transverse variable x_3 may be separated as



Fig. 9.1 Schematic of a sliding layer.

$$u_p = U_p(x_1, x_2, t) \cos(\Lambda_n x_3), \quad u_3 = U_3(x_1, x_2, t) \sin(\Lambda_n x_3), \quad p = 1, 2, \quad (9.4)$$

so that the boundary conditions (9.3) are satisfied automatically. In above

$$\Lambda_n = \frac{\Omega_n}{h}, \quad \Omega_n = n\pi, \quad n = 0, 1, 2, 3, \dots, \quad (9.5)$$

corresponding to thickness resonance frequencies. In view of (9.4), the equations of motion (9.1), rewritten in terms of displacements, take the form

$$\begin{aligned} \gamma^2 \frac{\partial^2 U_1}{\partial x_1^2} + \frac{\partial^2 U_1}{\partial x_2^2} - \Lambda_n^2 U_1 + (\gamma^2 - 1) \left(\frac{\partial^2 U_2}{\partial x_1 \partial x_2} + \Lambda_n \frac{\partial U_3}{\partial x_1} \right) &= \frac{1}{c_2^2} \frac{\partial^2 U_1}{\partial t^2}, \\ \frac{\partial^2 U_2}{\partial x_1^2} + \gamma^2 \frac{\partial^2 U_2}{\partial x_2^2} - \Lambda_n^2 U_2 + (\gamma^2 - 1) \left(\frac{\partial^2 U_1}{\partial x_1 \partial x_2} + \Lambda_n \frac{\partial U_3}{\partial x_2} \right) &= \frac{1}{c_2^2} \frac{\partial^2 U_2}{\partial t^2}, \\ \frac{\partial^2 U_3}{\partial x_1^2} + \frac{\partial^2 U_3}{\partial x_2^2} - \gamma^2 \Lambda_n^2 U_3 - \Lambda_n (\gamma^2 - 1) \left(\frac{\partial U_1}{\partial x_1} + \frac{\partial U_2}{\partial x_2} \right) &= \frac{1}{c_2^2} \frac{\partial^2 U_3}{\partial t^2}, \end{aligned} \quad (9.6)$$

where

$$\gamma = \frac{c_1}{c_2} = \sqrt{\frac{2-2\nu}{1-2\nu}}, \quad (9.7)$$

with

$$c_1 = \sqrt{\frac{E(1-\nu)}{(1+\nu)(1-2\nu)\rho}}, \quad c_2 = \sqrt{\frac{E}{2(1+\nu)\rho}} \quad (9.8)$$

denoting the conventional longitudinal and transverse wave speeds, respectively.

Next, we adopting the ansatz of travelling harmonic waves

$$U_i = A_i e^{ik(n_1 x_1 + n_2 x_2 - ct)}, \quad i = 1, 2, 3, \quad (9.9)$$

where k is wave number, and $\mathbf{n} = (n_1, n_2)$ is a 2D unit vector associated with wave propagation in (x_1, x_2) plane. Now, substituting (9.9) into (9.6), from solvability of the resulting algebraic system in A_1, A_2 and A_3 we deduce the dispersion relation in the form

$$(k^2 c^2 - c_1^2(k^2 + \Lambda_n^2))(k^2 c^2 - c_2^2(k^2 + \Lambda_n^2)) = 0. \quad (9.10)$$

Introducing the dimensionless wave number K , speed C and frequency Ω as

$$K = kh, \quad C = \frac{c}{c_2}, \quad \Omega = KC, \quad (9.11)$$

the relation (9.10) transforms to

$$(\Omega^2 - \gamma^2(K^2 + \Omega_n^2))(\Omega^2 - (K^2 + \Omega_n^2)) = 0. \quad (9.12)$$

It may be observed that the dispersion branches originate from the two families of thickness resonance frequencies, namely the thickness shear $\Omega = \Omega_n$ and thickness stretch frequencies $\Omega = \gamma \Omega_n$, following from (9.12) on setting $K = 0$.

The dispersion curves illustrating the relation (9.12) are shown in Fig. 9.2, for the Poisson’s ratio $\nu = 0.25$. The branches associated with thickness shear frequencies are depicted by solid lines, whereas the ones related to thickness stretch frequencies are presented as dotted lines. Clearly, since $\gamma > 1$, there are fewer dotted curves than solid ones over in the illustrated frequency domain.

Note that in case of the first mode ($n = 0$) the problem degenerates, implying $\Omega_n = 0$, hence, as follows from (9.4), $u_3 = 0$, and equations (9.6) become

$$\gamma^2 \frac{\partial^2 U_1}{\partial x_1^2} + \frac{\partial^2 U_1}{\partial x_2^2} + (\gamma^2 - 1) \frac{\partial^2 U_2}{\partial x_1 \partial x_2} = \frac{1}{c_2^2} \frac{\partial^2 U_1}{\partial t^2}, \tag{9.13}$$

$$\frac{\partial^2 U_2}{\partial x_1^2} + \gamma^2 \frac{\partial^2 U_2}{\partial x_2^2} + (\gamma^2 - 1) \frac{\partial^2 U_1}{\partial x_1 \partial x_2} = \frac{1}{c_2^2} \frac{\partial^2 U_2}{\partial t^2}, \tag{9.14}$$

with the problem being equivalent to plane-strain formulation. Thus, for frequencies below the first thickness shear resonance ($\Omega < \Omega_1$), the branches demonstrate non-dispersive behaviour.

9.3 One-Sided Sliding

In this section we deal with one-sided sliding for an elastic layer occupying the domain $-\infty < x_1, x_2 < \infty, 0 \leq x_3 \leq h$, with boundary conditions taking the form

$$\sigma_{13} = \sigma_{23} = \sigma_{33} = 0, \quad \text{at } x_3 = h, \tag{9.15}$$

$$\sigma_{13} = \sigma_{23} = 0, \quad u_3 = 0, \quad \text{at } x_3 = 0. \tag{9.16}$$

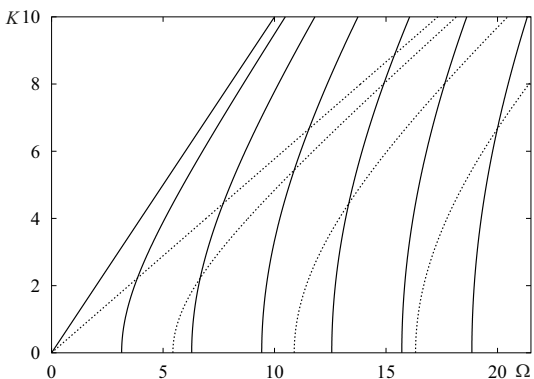


Fig. 9.2 Dispersion curves corresponding to relation (9.12) for $\nu = 0.25$.

In view of the symmetry it may be observed that the problem is closely related to symmetric motions of a layer of double thickness $-h \leq x_3 \leq h$ with traction-free faces, for which the conditions (9.16) are satisfied on the middle surface. Therefore, the dispersion relation will be the conventional symmetric Rayleigh-Lamb one (Rayleigh, 1888; Achenbach, 1973). In this case, the fundamental mode corresponds to classical theory for plate extension within leading order of the long-wave low-frequency approximation, see Kaplunov et al (1998).

Below, we consider in greater detail the associated forced vibration problem, which appears to be relevant for various applications, with the transverse loading imposed on the upper face.

$$\sigma_{13} = \sigma_{23} = 0, \quad \sigma_{33} = P, \quad \text{at } x_3 = h, \quad (9.17)$$

and the same boundary conditions (9.16) along the sliding contact surface $x_3 = 0$. Here $P = P(x_1, x_2, t)$ is a prescribed loading, see Fig. 9.3.

In view of the symmetry of the problem, it may be reformulated. It is possible to add a fictitious domain $-h \leq x_3 \leq 0$, and prescribe a symmetrical loading at $x_3 = -h$ as

$$\sigma_{13} = \sigma_{23} = 0, \quad \sigma_{33} = P, \quad \text{at } x_3 = -h. \quad (9.18)$$

Then, it would be possible to modify the results presented in Kaplunov et al (1998) for a refined asymptotic theory for transverse compression of a plate. We introduce the dimensionless variables

$$\xi_i = \frac{x_i}{\lambda}, \quad \zeta = \frac{x_3}{h}, \quad (9.19)$$

and a small parameter associated with the long-wave limit

$$\epsilon = \frac{h}{\lambda} \ll 1, \quad (9.20)$$

with λ denoting the typical wave length. Then, the asymptotic expansions for the components of the displacement and stress fields demonstrate polynomial dependence on ζ , i.e.

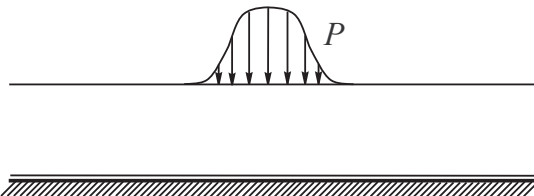


Fig. 9.3 Schematic: transverse compression of a sliding layer.

$$\begin{aligned}
u_i &= \lambda \left[u_i^{(0)} + \epsilon^2 \left(\zeta^2 u_i^{(1)} + U_i^{(1)} \right) \right], \\
u_3 &= \lambda \epsilon \zeta \left[u_3^{(0)} + \epsilon^2 \left(\zeta^2 u_3^{(1)} + U_3^{(1)} \right) \right], \\
\sigma_{ii} &= E \left[\sigma_{ii}^{(0)} + \epsilon^2 \left(\zeta^2 \sigma_{ii}^{(1)} + S_{ii}^{(1)} \right) \right], \\
\sigma_{ij} &= E \left[\sigma_{ij}^{(0)} + \epsilon^2 \left(\zeta^2 \sigma_{ij}^{(1)} + S_{ij}^{(1)} \right) \right], \\
\sigma_{3i} &= E \epsilon^3 \zeta \left[\zeta^2 \sigma_{3i}^{(0)} + S_{3i}^{(0)} \right], \\
\sigma_{33} &= E \left[\sigma_{33}^{(0)} + \epsilon^2 \left(\zeta^2 \sigma_{33}^{(1)} + S_{33}^{(1)} \right) \right],
\end{aligned} \tag{9.21}$$

Here and below $1 \leq i \neq j \leq 2$, and quantities with brackets in the superscript are assumed independent of the transverse variable.

At leading order, using the equations of motion (9.1) and the constitutive relations (9.2), we have

$$\sigma_{33}^{(0)} = \frac{P}{E}, \tag{9.22}$$

$$\sigma_{ii}^{(0)} = \frac{1}{1-\nu^2} \left(\frac{\partial u_i^{(0)}}{\partial \xi_i} + \nu \frac{\partial u_j^{(0)}}{\partial \xi_j} \right) + \frac{\nu}{1-\nu} \frac{P}{E}, \tag{9.23}$$

$$\sigma_{ij}^{(0)} = \frac{1}{2(1+\nu)} \left(\frac{\partial u_i^{(0)}}{\partial \xi_j} + \frac{\partial u_j^{(0)}}{\partial \xi_i} \right), \tag{9.24}$$

$$\frac{\partial \sigma_{ii}^{(0)}}{\partial \xi_i} + \frac{\partial \sigma_{ij}^{(0)}}{\partial \xi_j} - \frac{1}{2(1+\nu)} \frac{\partial^2 u_i^{(0)}}{\partial \tau^2} = 0, \tag{9.25}$$

$$\sigma_{3i}^{(0)} + S_{3i}^{(0)} = 0, \tag{9.26}$$

$$u_3^{(0)} = \sigma_{33}^{(0)} - \nu (\sigma_{ii}^{(0)} + \sigma_{jj}^{(0)}). \tag{9.27}$$

On substituting (9.23) and (9.24) into (9.25), we deduce

$$E \left(\frac{1}{1-\nu} \text{grad div } \mathbf{u}^{(0)} + \frac{1}{1+\nu} \Delta \mathbf{u}^{(0)} \right) - 2\rho \frac{\partial^2 \mathbf{u}^{(0)}}{\partial t^2} = -\frac{2\nu}{1-\nu} \text{grad } P, \tag{9.28}$$

where grad, div and Δ are standard two-dimensional gradient, divergence and Laplace operators in x_1, x_2 , and $\mathbf{u}^{(0)}$ is the leading order approximation for the in-plane displacement field $\mathbf{u}^{(0)} = \lambda (u_1^{(0)}, u_2^{(0)})$. In addition, (9.27) may be rewritten as

$$u_3^{(0)} = \frac{(1-2\nu)(1+\nu)}{1-\nu} \frac{P}{E} - \frac{\nu}{1-\nu} \left(\frac{\partial u_i^{(0)}}{\partial \xi_i} + \frac{\partial u_j^{(0)}}{\partial \xi_j} \right). \tag{9.29}$$

At next order,

$$\begin{aligned}
u_i^{(1)} &= -\frac{1}{2} \frac{\partial u_3^{(0)}}{\partial \xi_i}, \\
\sigma_{33}^{(1)} &= \frac{1}{4(1+\nu)} \frac{\partial^2 u_3^{(0)}}{\partial \tau^2}, \\
\sigma_{33}^{(1)} + S_{33}^{(1)} &= 0, \\
\sigma_{ii}^{(1)} &= \frac{1}{1-\nu^2} \left(\frac{\partial u_i^{(1)}}{\partial \xi_i} + \nu \frac{\partial u_j^{(1)}}{\partial \xi_j} \right) + \frac{\nu}{1-\nu} \sigma_{33}^{(1)}, \\
S_{ii}^{(1)} &= \frac{1}{1-\nu^2} \left(\frac{\partial U_i^{(1)}}{\partial \xi_i} + \nu \frac{\partial U_j^{(1)}}{\partial \xi_j} \right) + \frac{\nu}{1-\nu} S_{33}^{(1)}, \\
\sigma_{ij}^{(1)} &= \frac{1}{2(1+\nu)} \left(\frac{\partial u_i^{(1)}}{\partial \xi_j} + \frac{\partial u_j^{(1)}}{\partial \xi_i} \right), \tag{9.30} \\
S_{ij}^{(1)} &= \frac{1}{2(1+\nu)} \left(\frac{\partial U_i^{(1)}}{\partial \xi_j} + \frac{\partial U_j^{(1)}}{\partial \xi_i} \right), \\
\sigma_{3i}^{(0)} &= -\frac{1}{3} \left(\frac{\partial \sigma_{ii}^{(1)}}{\partial \xi_i} + \frac{\partial \sigma_{ij}^{(1)}}{\partial \xi_j} \right) + \frac{1}{6(1+\nu)} \frac{\partial^2 u_i^{(1)}}{\partial \tau^2}, \\
S_{3i}^{(0)} &= -\left(\frac{\partial S_{ii}^{(1)}}{\partial \xi_i} + \frac{\partial S_{ij}^{(1)}}{\partial \xi_j} \right) + \frac{1}{2(1+\nu)} \frac{\partial^2 U_i^{(1)}}{\partial \tau^2}, \\
u_3^{(1)} &= \sigma_{33}^{(1)} - \nu (\sigma_{ii}^{(1)} + \sigma_{jj}^{(1)}), \\
U_3^{(1)} &= S_{33}^{(1)} - \nu (S_{ii}^{(1)} + S_{jj}^{(1)}).
\end{aligned}$$

Using (9.30), we deduce from (9.30), (9.30), (9.31) and (9.31)

$$\begin{aligned}
\sigma_{ii}^{(1)} &= \frac{1}{4(1-\nu^2)} \left(\nu \frac{\partial^2 u_3^{(0)}}{\partial \tau^2} - 2 \frac{\partial^2 u_3^{(0)}}{\partial \xi_i^2} - 2\nu \frac{\partial^2 u_3^{(0)}}{\partial \xi_j^2} \right), \\
\sigma_{ij}^{(1)} &= -\frac{1}{2(1+\nu)} \frac{\partial^2 u_3^{(0)}}{\partial \xi_i \partial \xi_j} \\
\sigma_{3i}^{(0)} &= \frac{1}{12(1-\nu^2)} \left(2 \frac{\partial^3 u_3^{(0)}}{\partial \xi_i^3} + 2 \frac{\partial^3 u_3^{(0)}}{\partial \xi_i \partial \xi_j^2} - \frac{\partial^3 u_3^{(0)}}{\partial \xi_i \partial \tau^2} \right), \\
u_3^{(1)} &= \frac{1-2\nu}{4(1-\nu)} \frac{\partial^2 u_3^{(0)}}{\partial \tau^2} - \frac{\nu}{2(1-\nu)} \left(\frac{\partial^2 u_3^{(0)}}{\partial \xi_i^2} + \frac{\partial^2 u_3^{(0)}}{\partial \xi_j^2} \right),
\end{aligned} \tag{9.31}$$

where $u_3^{(0)}$ is defined in (9.29).

On substituting (9.32) and (9.31) into (9.26), and using (9.28), we obtain the refined 2D equation for the two-term approximate displacement

$$\mathbf{u} \approx \lambda \left(u_1^{(0)} + \varepsilon^2 U_1^{(1)}, u_2^{(0)} + \varepsilon^2 U_2^{(1)} \right), \tag{9.32}$$

namely

$$\begin{aligned}
&E \left(\frac{1}{1-\nu} \text{grad div } \mathbf{u} + \frac{1}{1+\nu} \Delta \mathbf{u} \right) - 2\rho \frac{\partial^2}{\partial t^2} \left[\mathbf{u} - \frac{\nu^2}{3(1-\nu)^2} h^2 \text{grad div } \mathbf{u} \right] \\
&= \text{grad} \left[\frac{1}{3} h^2 \Delta P - \frac{2\nu}{1-\nu} P - \frac{(1+\nu)(1-2\nu)(1-3\nu)}{3(1-3\nu)^2 E} \rho h^2 \frac{\partial^2 P}{\partial t^2} \right].
\end{aligned} \tag{9.33}$$

This equation may be recognised as that of the refined plane-stress state, arising in the case of transverse compression, see Kaplunov et al (1998). It contains corrections to both 2D inertia of the layer and the expression of the external loading. It is remarkable that transverse compression is usually not a feature of engineering plate models. It also should be noted that at vanishing Poisson's ratio ($\nu = 0$) the last equation reduces to

$$E(\text{grad div } \mathbf{u} + \Delta \mathbf{u}) - 2\rho \frac{\partial^2 \mathbf{u}}{\partial t^2} = \frac{h^2}{3} \left[\Delta - \frac{\rho}{E} \frac{\partial^2}{\partial t^2} \right] \text{grad } P, \tag{9.34}$$

where the left hand side corresponds to the leading order equation, whereas the right hand is two orders of magnitude smaller than the loading term in equation (9.28).

The analysis in this chapter helps to further interpret the results for a thin plate supported by a relatively soft Winkler foundation presented in Erbaş et al (2018, 2021). In the latter case, a bending mode arises, demonstrating veering with the extensional mode, which is very similar to that analysed within the consideration above. Such interaction restricts considerably the range of validity of the famous 2D engineering model of an elastically supported Kirchhoff plate.

9.4 Concluding Remarks

In this chapter, elastodynamics of a thin layer subject to sliding contact has been studied, revealing that the fundamental symmetric vibration modes are supported. It has been demonstrated that for one- and two-sided sliding, the fundamental modes correspond to the Rayleigh-Lamb dispersion relation for a layer of double thickness with traction-free faces, and to longitudinal and shear bulk waves, respectively.

The results of asymptotic analysis of a forced problem for the one-sided scenario with prescribed normal stress along the upper face are presented. In particular, a refined long-wave low-frequency 2D equation on the surface of contact, earlier derived for transverse compression of a thin layer, is adapted.

The proposed approach may be developed further to incorporate more general types of contact, as well as take into consideration curvature, the effect of edge boundary conditions, and also more advanced material properties, including anisotropy, pre-stress and viscosity.

Acknowledgements TS acknowledges support by the European Union, European Regional Development Fund, within the scope of the framework of the programme for investments in growth and jobs 2014-2020, contract No. C3330-18-952007 (EAGLE), in Sect. 9.2. JK and DAP acknowledge support from the Russian Science Federation, Grant No. 20-11-20133, in Sects. 9.1, 9.3 and 9.4.

References

- Achenbach J (1973) *Wave Propagation in Elastic Solids*. North Holland, Amsterdam
- Aghalovyan LA (2015) *Asymptotic Theory of Anisotropic Plates and Shells*. World Scientific, Singapore
- Argatov I, Mishuris G (2011) Frictionless elliptical contact of thin viscoelastic layers bonded to rigid substrates. *Applied Mathematical Modelling* 35(7):3201–3212
- Argatov I, Mishuris G (2016) *Contact Mechanics of Articular Cartilage Layers*. Springer, Cham
- Argatov I, Mishuris G (2018) Cylindrical lateral depth-sensing indentation of anisotropic elastic tissues: Effects of adhesion and incompressibility. *The Journal of Adhesion* 94(8):583–596
- Barnett DM, Gavazza SD, Lothe J, Chadwick P (1988) Slip waves along the interface between two anisotropic elastic half-spaces in sliding contact. *Proceedings of the Royal Society of London A Mathematical and Physical Sciences* 415(1849):389–419
- Belyaev AK, Morozov NF, Tovstik PE, Tovstik TP (2019) Two-dimensional linear models of multilayered anisotropic plates. *Acta Mechanica* 230(8):2891–2904
- Belyaev AK, Morozov NF, Tovstik PE, Tovstik TP (2021) Applicability ranges for four approaches to determination of bending stiffness of multilayer plates. *Continuum Mechanics and Thermodynamics* 33(4):1659–1673
- Borodich FM (2014) The Hertz-Type and Adhesive Contact Problems for Depth-Sensing Indentation. In: Bordas SPA (ed) *Advances in Applied Mechanics*, Elsevier, vol 47, pp 225–366
- Borodich FM, Galanov BA, Perepelkin NV, Prikazchikov DA (2019) Adhesive contact problems for a thin elastic layer: Asymptotic analysis and the JKR theory. *Mathematics and Mechanics of Solids* 24(5):1405–1424
- Darinskii AN, Weihnacht M (2005) Interface waves on the sliding contact between identical piezoelectric crystals of general anisotropy. *Wave Motion* 43(1):67–77

- Erbaş B, Yusufoglu E, Kaplunov J (2011) A plane contact problem for an elastic orthotropic strip. *Journal of Engineering Mathematics* 70(4):399–409
- Erbaş B, Kaplunov J, Nobili A, Kılıç G (2018) Dispersion of elastic waves in a layer interacting with a winkler foundation. *The Journal of the Acoustical Society of America* 144(5):2918–2925
- Erbaş B, Kaplunov J, Elishakoff I (2021) Asymptotic derivation of a refined equation for an elastic beam resting on a Winkler foundation. *Mathematics and Mechanics of Solids* DOI 10.1177/10812865211023885
- Goldenevizer AL, Lidsky VB, Tovstik PE (1979) *Free Vibrations of Thin Elastic Shells* (in Russ.). Nauka, Moscow
- Kaplunov J, Prikazchikov DA, Rogerson GA (2005) On three-dimensional edge waves in semi-infinite isotropic plates subject to mixed face boundary conditions. *Acoustical Society of America Journal* 118(5):2975–2983
- Kaplunov J, Prikazchikov D, Sultanova L (2018) Justification and refinement of Winkler-Fuss hypothesis. *Zeitschrift für Angewandte Mathematik und Physik* 69(3):80
- Kaplunov J, Prikazchikov D, Sultanova L (2019) Elastic contact of a stiff thin layer and a half-space. *Zeitschrift für Angewandte Mathematik und Physik* 70(1):22
- Kaplunov JD (1995) Long-wave vibrations of a thinwalled body with fixed faces. *The Quarterly Journal of Mechanics and Applied Mathematics* 48(3):311–327
- Kaplunov JD, Nolde EV (2002) Long-wave vibrations of a nearly incompressible isotropic plate with fixed faces. *The Quarterly Journal of Mechanics and Applied Mathematics* 55(3):345–356
- Kaplunov JD, Kossovich LY, Nolde EV (1998) *Dynamics of Thin Walled Elastic Bodies*. Academic Press, San Diego
- Kaplunov JD, Rogerson GA, Tovstik PE (2005) Localized vibration in elastic structures with slowly varying thickness. *The Quarterly Journal of Mechanics and Applied Mathematics* 58(4):645–664
- Kudish II, Pashkovski E, Volkov SS, Vasiliev AS, Aizikovich SM (2020) Heavily loaded line EHL contacts with thin adsorbed soft layers. *Mathematics and Mechanics of Solids* 25(4):1011–1037
- Kudish II, Volkov SS, Vasiliev AS, Aizikovich SM (2021) Characterization of the behavior of different contacts with double coatings. *Mathematics and Mechanics of Complex Systems* 9(2):179–202
- Lashhab MI, Rogerson GA, Prikazchikova LA (2015) Small amplitude waves in a pre-stressed compressible elastic layer with one fixed and one free face. *Zeitschrift für Angewandte Mathematik und Physik* 66(5):2741–2757
- Le KC (1999) *Vibrations of Shells and Rods*. Springer, Berlin
- Mikhasev GI, Tovstik PE (2020) *Localized Dynamics of Thin-Walled Shells*. Chapman & Hall/CRC Monographs and Research Notes in Mathematics, CRC Press. Taylor & Francis
- Moukhomodiarov RR, Pichugin AV, Rogerson GA (2010) The transition between neumann and dirichlet boundary conditions in isotropic elastic plates. *Mathematics and Mechanics of Solids* 15(4):462–490
- Nolde EV, Rogerson GA (2002) Long wave asymptotic integration of the governing equations for a pre-stressed incompressible elastic layer with fixed faces. *Wave Motion* 36(3):287–304
- Nolde EV, Prikazchikova LA, Rogerson GA (2004) Dispersion of small amplitude waves in a pre-stressed, compressible elastic plate. *Journal of Elasticity* 75(1):1–29
- Prikazchikova L, Aydın YE, Erbaş B, Kaplunov J (2020) Asymptotic analysis of an anti-plane dynamic problem for a three-layered strongly inhomogeneous laminate. *Mathematics and Mechanics of Solids* 25(1):3–16
- Rayleigh L (1888) On the free vibrations of an infinite plate of homogeneous isotropic elastic matter. *Proceedings of the London Mathematical Society* s1-20(1):225–237
- Rogerson GA, Sandiford KJ, Prikazchikova LA (2007) Abnormal long wave dispersion phenomena in a slightly compressible elastic plate with non-classical boundary conditions. *International Journal of Non-Linear Mechanics* 42(2):298–309, special Issue in Honour of Dr. Ronald S. Rivlin

Vinh PC, Ngoc Anh VT (2014) Rayleigh waves in an orthotropic half-space coated by a thin orthotropic layer with sliding contact. *International Journal of Engineering Science* 75:154–164



Chapter 10

Analytical Approach to the Derivation of the Stress Field of a Cylindrical Shell with a Circular Hole under Axial Tension

Stanislava V. Kashtanova and Alexey V. Rzhonsnitskiy

Abstract A new analytical approach to the stress field problem of the cylindrical shell with a circular cutout under axial tension is proposed. Classical models because of an expansion into small parameter have narrow range of applicability and almost do not differ from Kirsch case for plate. The new approach opens up opportunities for the analytical study of the stress field. The idea is to decompose each basis function into a Fourier series by separating the variables, which allows us to obtain an infinite system of algebraic equations for finding coefficients. One of the important steps of the study is that the authors were able to prove which of the equations of the system is a linear combination of several others. Excluding it made it possible to create a reduced system for finding unknown coefficients. The proposed approach does not impose mathematical restrictions on the values of the main parameter that characterizes the cylindrical shell.

Key words: Cylindrical Shell, Circular cutout, Elasticity theory

10.1 Introduction

In this paper¹, we propose a new analytical approach to the derivation of the stresses of a cylindrical shell with a circular hole under tension along forming axis. The state-

Stanislava V. Kashtanova

Institute for Problems in Mechanical Engineering of the Russian Academy of Sciences, Russian Federation,

e-mail: kastasya@yandex.ru

Alexey V. Rzhonsnitskiy

Saint-Petersburg State Institute of Technology, Russian Federation,

e-mail: rzhonsnitskiy@yandex.ru

¹ Dedicated to my teacher Prof. Peter Tovstik. Our last call was 13th of November 2020 when we discussed this article. Thank you that always believed in me, R.I.P.

© The Author(s), under exclusive license to Springer Nature Switzerland AG 2022

115

H. Altenbach et al. (eds.), *Recent Approaches in the Theory of Plates*

and *Plate-Like Structures*, Advanced Structured Materials 151,

https://doi.org/10.1007/978-3-030-87185-7_10

ment of the problem and the solution by the method of decomposition in the small parameter belongs to Lurie (1946). This parameter β characterizes the ratio of the radius of the hole, the thickness of the shell and the radius of curvature. Later, in the mid-1960s-70s, a surge of interest in this problem occurred not only among Soviet researchers, but also among foreign scientists who found an error in setting the boundary conditions at the boundary of a circular hole. Some of them reconsidered it by the same method (Houghton, 1961; Naghdi and Eringen, 1965; Pirogov and Iumatov, 1968; Murthy, 1969), others by numerical method of collocation (Eringen et al, 1965; Lekkerkerker, 1965; van Dyke, 1965). However, the proposed analytical approach was extremely cumbersome and worked for a very small range of values of the parameter β , which differed a little from the plane Kirsch problem, and the results obtained by the collocation method differed (Kashtanova et al, 2021). There were also attempts to solve this problem using the energy method (Pirogov and Iumatov, 1968; Adams, 1971) and the method of complex variables for arbitrary holes (Chekhov and Zakora, 1972; Hu et al, 1998). The resources of the considered methods have exhausted themselves without providing a convenient solution but no alternative methods have yet been proposed. Follow-up works rely on computer modelling, in particular, based on the finite element method (Yu et al, 2015; Chowdhury et al, 2016; Celebi et al, 2017; Storozhuk et al, 2018; Russo et al, 2019).

However, until now, the relevance and applicability of this problem remain high (Wu and Mu, 2003; Oterkus et al, 2007; Zhuang et al, 2015; Ray-Chaudhuri and Chawla, 2018), especially in the field of the aviation industry. And the analytical solution for the stress field in the hole area can give an impetus to the fundamental study of the issues of fracture and stability. This paper presents a new idea that makes it easy to find numerical values of stresses and opens up prospects for their analytical study. In this way, there are no mathematical restrictions on the values of the parameter β as it was before. In this paper, special attention is paid to the technique of solving the problem and a strict mathematical formulation.

10.2 Problem Formulation

We consider a cylindrical shell with a circular hole under tension p applied at infinity along forming axis x . The following symbols are used: parameter

$$\beta^2 = r_0^2 \frac{\sqrt{3(1-\nu^2)}}{4Rh},$$

where r_0 – the radius of the hole (without belittling the generality, we can take r_0 as a unit of measurement, i.e. $r_0 = 1$), R, h – the radius of curvature and the thickness of the shell, respectively, ν – Poisson's ratio. Parameter β is the main parameter responsible for the ratio of geometric parameters, including the curvature of the shell.

Note that the limiting case for $\beta \rightarrow 0$ leads us to the Kirsch problem. As it offered in Lurie (1946) we also introduce the function

$$\Phi = \frac{Eh}{8\beta^2 R} w - iU,$$

which depends on the deflection w and the stress function U . The relationship between the effort T and the function U is given as follows

$$\begin{pmatrix} T_x & T_{xy} \\ T_{xy} & T_y \end{pmatrix} = \begin{pmatrix} \frac{\partial^2 U}{\partial y^2} & -\frac{\partial^2 U}{\partial x \partial y} \\ -\frac{\partial^2 U}{\partial x \partial y} & \frac{\partial^2 U}{\partial y^2} \end{pmatrix}$$

The stress of the median surface of the thin shell is $\sigma = T/h$.

It is shown in Lurie (1946), Guz (1974), that the system of shell equilibrium equations reduces to the following equation

$$\Delta \Delta \Phi + 8i\beta^2 \frac{\partial^2 \Phi}{\partial x^2} = 0. \quad (10.1)$$

The full problem statement is to find a function that satisfies equation (10.1) and next boundary conditions

- at infinity

$$T_x = p, \quad T_{xy} = 0, \quad T_y = 0, \quad w = 0; \quad (10.2)$$

- at the boundary of a circular hole in the polar coordinate system (r, ϑ)

$$\begin{cases} T_{rr}|_{r=r_0} = 0, \\ T_{r\vartheta}|_{r=r_0} = 0, \\ M_r|_{r=r_0} = 0, \\ Q_r|_{r=r_0} = 0. \end{cases} \quad (10.3)$$

Here M_r is the moment, Q_r is the generalized boundary condition on a free edge (Lurie, 1946).

10.3 Solution

Despite the fact that the method for solving equation (10.1) is well known (Lurie, 1946; Naghdi and Eringen, 1965; Pirogov and Iumatov, 1968; Murthy, 1969; Guz, 1974; Kashtanova et al, 2021), some technical details were not given due attention. Consider two commuting linear operators

$$L_1 = \left(\Delta - 2i\alpha \frac{\partial}{\partial x} \right) \quad \text{and} \quad L_2 = \left(\Delta + 2i\alpha \frac{\partial}{\partial x} \right),$$

where $\alpha = (1 + i)\beta$. Then Eq. (10.1) can be written as

$$L_1 L_2 \Phi = 0 \Leftrightarrow \Phi \in \text{Ker} L_1 L_2.$$

That is, the problem is reduced to finding the kernel of the product $L_1 L_2$. From the fact that the operators commute, it follows that

$$\text{Ker} L_1 + \text{Ker} L_2 \subset \text{Ker} L_1 L_2.$$

Finding the solutions of the equations $L_1 \Phi = 0$ and $L_2 \Phi = 0$ separately with the subsequent possibility of finding their sum greatly simplifies the solution of the original equation, since lowers its order. However, it is important to note that the sum of kernels $\text{Ker} L_1 + \text{Ker} L_2$ does not coincide with the set of all solutions of equation (10.1), which can lead to the loss of solutions. Therefore, this method can be used to prove the existence of a solution and find it constructively, but the study of uniqueness should be carried out separately.

By replacing and separating variables, it is easy to establish (Lurie, 1946; Guz, 1974) that the solutions of $L_{1,2} \Phi = 0$ are functions $e^{\pm i\alpha x} H_n^{(1)}(\alpha r) e^{\pm in\vartheta}$, where $n \in \mathbb{Z}_+$. The choice of Hankel functions in the construction of the solution is due to the fact that these are the only Bessel functions that tend to zero at an infinitely distant complex point (Watson, 1945):

$$\lim_{\rho \rightarrow +\infty} H_n^{(1)}(\rho e^{i\varphi}) = \lim_{\rho \rightarrow +\infty} H_n^{(2)}(\rho e^{-i\varphi}) = 0, \quad \varphi \in [\varepsilon; \pi - \varepsilon].$$

Since $\alpha = (1 + i)\beta$ has the argument $\pi/4 \in [\varepsilon; \pi - \varepsilon]$, functions $e^{\pm i\alpha x} H_n^{(2)}(\alpha r) e^{\pm in\vartheta}$ obviously do not satisfy the boundary conditions, since the deflection $w \neq 0$ at infinity. At the same time, guided by Watson (1945), we can deduce that

$$|e^{\pm i\alpha x} H_n^{(1)}(\alpha r) e^{\pm in\vartheta}| \leq \frac{\tilde{C}}{\sqrt{r}} e^{-\beta r(1 - |\cos \vartheta|)}.$$

Note that the first three boundary conditions of system (10.2) are set not with respect to the function U , but with respect to its second derivatives. Therefore, it is necessary to make sure that not only the potential, but also the stresses tend to zero at large r . This is true, since it follows from the recurrence relations for the Bessel functions (Watson, 1945) that

$$\frac{\partial}{\partial r} \left(e^{\pm i\alpha x} H_n^{(1)}(\alpha r) e^{\pm in\vartheta} \right)$$

is a linear combination of functions of the same type $e^{\pm i\alpha x} H_m^{(1)}(\alpha r) e^{\pm in\vartheta}$. Moreover, calculations show that

$$\frac{1}{r} \frac{\partial}{\partial \vartheta} \left(e^{\pm i\alpha x} H_n^{(1)}(\alpha r) e^{\pm in\vartheta} \right)$$

is a linear combination of functions

$$e^{\pm i\alpha x} H_n^{(1)}(\alpha r) e^{\pm in\vartheta} \quad \text{and} \quad \frac{e^{\pm i\alpha x} H_n^{(1)}(\alpha r) e^{\pm in\vartheta}}{r}.$$

Thus, the solution $e^{\pm i\alpha x} H_n^{(1)}(\alpha r) e^{\pm in\vartheta}$ satisfies all boundary conditions at infinity.

Using trigonometric form for $e^{\pm i\alpha x} H_n^{(1)}(\alpha r) e^{\pm in\vartheta}$ and taking into account the circular hole symmetry we get that the solution of the problem (10.1)-(10.3) is possible to find in following form for even and odd n (Lurie, 1946; Chowdhury et al, 2016):

$$\Phi = -i \frac{p y^2}{2} + \sum_{n=0}^{\infty} (A_n + iB_n) \begin{bmatrix} \cos(\alpha x) \cdot H_n^{(1)}(\alpha r) \cdot \cos(n\vartheta) \\ \sin(\alpha x) \cdot H_n^{(1)}(\alpha r) \cdot \cos(n\vartheta) \end{bmatrix}. \quad (10.4)$$

The function Φ is the solution of the equation of mathematical physics (10.1), while Φ satisfies the boundary conditions (10.2). It remains only to find the coefficients A_n and B_n from the boundary conditions (10.3). Namely at this step the authors of previous works faced the greatest difficulties (for more information, see Kashtanova et al, 2021). Therefore, the main content part of the present paper is the method of searching for unknown coefficients.

10.4 New Approach

The main idea is to separate the variables r and ϑ in each basic function. Only in contrast to Lurie (1946), to achieve this goal, an expansion in the trigonometric Fourier series is proposed. The known Laurent series expansion $e^{\frac{z}{2}(t-\frac{1}{t})}$ (Watson, 1945) of

$$e^{\frac{z}{2}(t-\frac{1}{t})} = \sum_{m=-\infty}^{\infty} t^m J_m(z)$$

for $e^{i\alpha x} e^{in\vartheta}$ leads us to

$$\begin{aligned} e^{i\alpha x} e^{in\vartheta} &= e^{\frac{\beta(1+i)r}{2} \left(2i \frac{e^{i\vartheta} + e^{-i\vartheta}}{2} \right)} e^{in\vartheta} = e^{\frac{\beta(1+i)r}{2} \left(ic^{i\vartheta} - \frac{1}{ic^{i\vartheta}} \right)} e^{in\vartheta} \\ &= \left(\sum_{m=-\infty}^{\infty} \left(ic^{i\vartheta} \right)^m J_m((1+i)\beta r) \right) e^{in\vartheta} \\ &= \sum_{m=-\infty}^{\infty} i^m e^{i(n+m)\vartheta} J_m((1+i)\beta r) \\ &= \sum_{m=-\infty}^{\infty} i^{k-n} J_{k-n}((1+i)\beta r) e^{ik\vartheta} = \sum_{m=-\infty}^{\infty} (-i)^{k-n} J_{n-k}((1+i)\beta r) e^{ik\vartheta} \end{aligned}$$

Replacing n with \check{n} results in

$$e^{i\alpha x} e^{-in\vartheta} = \sum_{m=-\infty}^{\infty} i^{k+n} J_{k+n}((1+i)\beta r) e^{ik\vartheta}$$

If we add both equalities obtained, we get

$$e^{i\alpha x} (e^{in\vartheta} + e^{-in\vartheta}) = \sum_{m=-\infty}^{\infty} \left[(-i)^{k-n} J_{n-k}((1+i)\beta r) + i^{k+n} J_{k+n}((1+i)\beta r) \right] e^{ik\vartheta}$$

Now we can replace α by $\check{\alpha}$ in the last formula and add both equalities for even n , and for odd n subtract the other from one:

$$\begin{aligned} \cos \alpha x \cdot \cos n\vartheta &= \frac{1}{4} (e^{i\alpha x} + e^{-i\alpha x}) (e^{in\vartheta} + e^{-in\vartheta}) \\ &= (-1)^{n/2} J_n((1+i)\beta r) \\ &\quad + \sum_{l=1}^{\infty} (-1)^{l+(n/2)} (J_{n-2l}((1+i)\beta r) + J_{n+2l}((1+i)\beta r)) \cos 2l\vartheta \\ \sin \alpha x \cdot \cos n\vartheta &= \frac{1}{4i} (e^{i\alpha x} - e^{-i\alpha x}) (e^{in\vartheta} + e^{-in\vartheta}) \\ &= (-1)^{(n-1)/2} J_n((1+i)\beta r) \\ &\quad + \sum_{l=1}^{\infty} (-1)^{l+(n-1)/2} (J_{n-2l}((1+i)\beta r) + J_{n+2l}((1+i)\beta r)) \cos 2l\vartheta \end{aligned}$$

As a result, even and odd basis functions can be written in one general formula

$$\begin{aligned} \left[\begin{array}{l} \cos(\alpha x) \cdot H_n^{(1)}(\alpha r) \cdot \cos n\vartheta \\ \sin(\alpha x) \cdot H_n^{(1)}(\alpha r) \cdot \cos n\vartheta \end{array} \right] &= f_n(r, \vartheta) = (-1)^{\lfloor \frac{n}{2} \rfloor} \frac{H_n^{(1)}((1+i)\beta r)}{H_n^{(1)}((1+i)\beta)} [J_n((1+i)\beta r) \\ &\quad + \sum_{l=1}^{\infty} (-1)^l (J_{n+2l}((1+i)\beta r) + J_{n-2l}((1+i)\beta r)) \cos 2l\vartheta], \end{aligned} \tag{10.5}$$

where $\lfloor \frac{n}{2} \rfloor$ is an integer part of the number. In the denominator a normalizing factor $H_n^{(1)}((1+i)\beta)$ is introduced. The latter is done so that the numerical values of the unknown coefficients have moderate values, with which it is convenient to work.

Further, for convenience, we introduce the notation for the Fourier coefficients in the trigonometric expansion of the basis function $g(r, n, l)$:

$$g(r, n, l) = (-1)^{\lfloor \frac{n}{2} \rfloor + l} \frac{H_n^{(1)}((1+i)\beta r)}{H_n^{(1)}((1+i)\beta)} (J_{n+2l}((1+i)\beta r) + J_{n-2l}((1+i)\beta r))$$

with $n = 0, 1, \dots, \infty, l = 0, 1, \dots, \infty$. Then (10.5) takes the form

$$f_n(r, \vartheta) = \frac{g(r, n, 0)}{2} + \sum_{l=1}^{\infty} g(r, n, l) \cos 2l\vartheta. \tag{10.6}$$

Now solution (10.4) can be written as

$$\Phi(r, \vartheta) = -i \frac{py^2}{2} + \sum_{n=0}^{\infty} (a_n + ib_n) f_n(r, \vartheta) \tag{10.7}$$

That is convenient for substitution into the boundary conditions (10.3).

10.5 Boundary Conditions

First boundary condition $\sigma_{rr} = 0$ in polar coordinates

$$\mathcal{L}_1(U) = \mathcal{L}_1(-\text{Im}\Phi) = 0, \quad \mathcal{L}_1 = \frac{1}{r^2} \frac{\partial^2}{\partial \vartheta^2} + \frac{1}{r} \frac{\partial}{\partial r}$$

leads us to the equation

$$\frac{P}{2} + \frac{P}{2} \cos 2\vartheta - \text{Im} \sum_{n=0}^{\infty} (a_n + ib_n) \left(\frac{g'(r, n, 0)}{2} + \sum_{l=1}^{\infty} (-4l^2 g(r, n, l) + g'(r, n, l)) \cos 2l\vartheta \right) = 0. \quad (10.8)$$

The cosine coefficients give us the following system:

$$\left\{ \begin{array}{l} \cos 0 : \quad \frac{P}{2} - \text{Im} \sum_{n=0}^{\infty} (a_n + ib_n) \cdot \frac{g'(r, n, 0)}{2} = 0 \\ \cos 2\vartheta : \quad \frac{P}{2} + \text{Im} \sum_{n=0}^{\infty} (a_n + ib_n) \cdot (4g(r, n, 1) - g'(r, n, 1)) = 0 \\ \cos 4\vartheta : \quad \text{Im} \sum_{n=0}^{\infty} (a_n + ib_n) \cdot (16g(r, n, 2) - g'(r, n, 2)) = 0 \\ \dots \\ \cos 2l\vartheta : \quad \text{Im} \sum_{n=0}^{\infty} (a_n + ib_n) \cdot (4l^2 g(r, n, l) - g'(r, n, l)) = 0 \end{array} \right. \quad (10.9)$$

Second boundary condition $\sigma_{r\vartheta} = 0$

$$\mathcal{L}_2(U) = \mathcal{L}_2(-\text{Im}\Phi) = 0, \quad \mathcal{L}_2 = \frac{1}{r^2} \frac{\partial}{\partial \vartheta} - \frac{1}{r} \frac{\partial^2}{\partial r \partial \vartheta}$$

give us

$$-\frac{P}{2} \sin 2\vartheta - \text{Im} \sum_{n=0}^{\infty} (a_n + ib_n) 2 \sum_{l=1}^{\infty} l \cdot (g'(r, n, l) - g(r, n, l)) \sin 2l\vartheta = 0. \quad (10.10)$$

The sine coefficients are:

$$\left\{ \begin{array}{l} \sin 2\vartheta : -\frac{P}{2} - \operatorname{Im} \sum_{n=0}^{\infty} 2(a_n + ib_n) \cdot (g'(r, n, 1) - g(r, n, 1)) = 0 \\ \sin 4\vartheta : -\operatorname{Im} \sum_{n=0}^{\infty} 4(a_n + ib_n) \cdot (g'(r, n, 2) - g(r, n, 2)) = 0 \\ \dots \\ \sin 2l\vartheta : -\operatorname{Im} \sum_{n=0}^{\infty} 2l(a_n + ib_n) \cdot (g'(r, n, l) - g(r, n, l)) = 0 \end{array} \right. \quad (10.11)$$

From the third boundary condition $M_{rr} = 0$

$$\mathcal{L}_3(\operatorname{Re}\Phi) = 0, \quad \mathcal{L}_3 = -D \left(\frac{\partial^2}{\partial r^2} + \frac{\nu}{r} \frac{\partial}{\partial r} + \frac{\nu}{r^2} \frac{\partial^2}{\partial \vartheta^2} \right), \quad D = \frac{Eh^3}{12(1-\nu^2)},$$

where E – Young modulus and ν – Poisson ratio, we get

$$\left(\operatorname{Re} \sum_{n=0}^{\infty} (a_n + ib_n) \left(\frac{g''(r, n, 0)}{2} + \nu \frac{g'(r, n, 0)}{2} + \sum_{l=1}^{\infty} [g''(r, n, l) + \nu(g'(r, n, l) - 4l^2 g(r, n, l))] \cos 2l\vartheta \right) \right) = 0. \quad (10.12)$$

The cosine coefficients:

$$\left\{ \begin{array}{l} \cos 0 : \operatorname{Re} \sum_{n=0}^{\infty} (a_n + ib_n) \cdot \frac{\nu g'(r, n, 0) + g''(r, n, 0)}{2} = 0 \\ \cos 2\vartheta : \operatorname{Re} \sum_{n=0}^{\infty} (a_n + ib_n) \cdot (-4\nu g(r, n, 1) + \nu g'(r, n, 1) + g''(r, n, 1)) = 0 \\ \cos 4\vartheta : \operatorname{Re} \sum_{n=0}^{\infty} (a_n + ib_n) \cdot (-16\nu g(r, n, 2) + \nu g'(r, n, 2) + g''(r, n, 2)) = 0 \\ \dots \\ \cos 2l\vartheta : \operatorname{Re} \sum_{n=0}^{\infty} (a_n + ib_n) \cdot (-4l^2 \nu g(r, n, l) + \nu g'(r, n, l) + g''(r, n, l)) = 0 \end{array} \right. \quad (10.13)$$

From the fourth boundary condition $Q_r^* = 0$

$$\mathcal{L}_4(\operatorname{Re}\Phi) = 0, \quad \mathcal{L}_4 = -D \left(\frac{\partial}{\partial r} \Delta + (1-\nu) \frac{1}{r} \frac{\partial}{\partial r} \frac{1}{r} \frac{\partial}{\partial \vartheta^2} \right), \quad \Delta = \frac{\partial^2}{\partial r^2} + \frac{1}{r} \frac{\partial}{\partial r} + \frac{1}{r^2} \frac{\partial^2}{\partial \vartheta^2}$$

we find

$$\operatorname{Re} \sum_{n=0}^{\infty} (a_n + ib_n) \left[\frac{-g'(r, n, 0) + g''(r, n, 0) + g'''(r, n, 0)}{2} + \sum_{l=1}^{\infty} \left[4l^2(3 - \nu)g(r, n, l) - (1 + 4l^2(2 - \nu))g'(r, n, l) + g''(r, n, l) + g'''(r, n, l) \right] \cos 2l\vartheta \right] = 0. \quad (10.14)$$

The cosine coefficients:

$$\left\{ \begin{array}{l} \cos 0: \operatorname{Re} \sum_{n=0}^{\infty} (a_n + ib_n) \cdot \left(\frac{-g'(r, n, 0) + g''(r, n, 0) + g'''(r, n, 0)}{2} \right) = 0 \\ \cos 2\vartheta: \operatorname{Re} \sum_{n=0}^{\infty} (a_n + ib_n) \cdot (4(3 - \nu)g(r, n, 1) - (9 - 4\nu)g'(r, n, 1) + g''(r, n, 1) + g'''(r, n, 1)) = 0 \\ \cos 4\vartheta: \operatorname{Re} \sum_{n=0}^{\infty} (a_n + ib_n) \cdot (16(3 - \nu)g(r, n, 2) - (33 - 16\nu)g'(r, n, 2) + g''(r, n, 2) + g'''(r, n, 2)) = 0 \\ \dots \\ \cos 2l\vartheta: \operatorname{Re} \sum_{n=0}^{\infty} (a_n + ib_n) \cdot (4l^2(3 - \nu)g(r, n, l) - (1 + 4l^2(2 - \nu))g'(r, n, l) + g''(r, n, l) + g'''(r, n, l)) = 0 \end{array} \right. \quad (10.15)$$

10.6 System Investigation

In the second pair of systems (10.13)–(10.15), the expressions under the sum sign can be multiplied by i . Then all the equations of the four systems will include only the imaginary part of the sum. From all the systems obtained, we compose a general linear system with an infinite number of unknowns and equations. Firstly, let us do some elementary transformations:

1. for $l > 1$, the equations of systems (10.9) and (10.11) can be written as follows:

$$\left\{ \begin{array}{l} 4l^2 \operatorname{Im} \sum_{n=0}^{\infty} (a_n + ib_n)g(n, l) + (-1) \operatorname{Im} \sum_{n=0}^{\infty} (a_n + ib_n)g'(n, l) = 0 \\ 2l \cdot \operatorname{Im} \sum_{n=0}^{\infty} (a_n + ib_n)g(n, l) - 2l \cdot \operatorname{Im} \sum_{n=0}^{\infty} (a_n + ib_n)g'(n, l) = 0 \end{array} \right.$$

The result is a homogeneous system with respect to unknowns $\sum_{n=0}^{\infty} (a_n + ib_n)g(n, l)$ and $\sum_{n=0}^{\infty} (a_n + ib_n)g'(n, l)$ with a determinant different from zero

$$\begin{vmatrix} 4l^2 & -1 \\ 2l & -2l \end{vmatrix} \neq 0,$$

and consequently, it has only a trivial solution

$$\begin{cases} \operatorname{Im} \sum_{n=0}^{\infty} (a_n + ib_n)g(n, l) = 0 \\ \operatorname{Im} \sum_{n=0}^{\infty} (a_n + ib_n)g'(n, l) = 0 \end{cases} \quad (10.16)$$

2. for $l = 1$ the same equations give an inhomogeneous system

$$\begin{cases} 4\operatorname{Im} \sum_{n=0}^{\infty} (a_n + ib_n)g(n, 1) + (-1)\operatorname{Im} \sum_{n=0}^{\infty} (a_n + ib_n)g'(n, 1) = -\frac{p}{2} \\ 2\operatorname{Im} \sum_{n=0}^{\infty} (a_n + ib_n)g(n, 1) - 2\operatorname{Im} \sum_{n=0}^{\infty} (a_n + ib_n)g'(n, 1) = \frac{p}{2} \end{cases}$$

Solving it with respect to unknowns, we obtain

$$\begin{cases} \operatorname{Im} \sum_{n=0}^{\infty} (a_n + ib_n)g(n, 1) = -\frac{p}{4} \\ \operatorname{Im} \sum_{n=0}^{\infty} (a_n + ib_n)g'(n, 1) = -\frac{p}{2} \end{cases} \quad (10.17)$$

3. Let introduce the notation

$$\begin{aligned} t_3(n, l) &= i(-4l^2 \nu g(n, l) + \nu g'(n, l) + g''(n, l)), \\ t_4(n, l) &= i(12l^2 g(n, l) - (1 + \nu + 4l^2(2 - \nu))g'(n, l) + g'''(n, l)). \end{aligned}$$

In order to get rid of $g''(n, l)$ in the expression $t_4(n, l)$, we can subtract from the last equation of system (10.15) the last equation (10.13):

$$\begin{cases} \operatorname{Im} \sum_{n=0}^{\infty} (a_n + ib_n)t_3(n, l) = 0 \\ \operatorname{Im} \sum_{n=0}^{\infty} (a_n + ib_n)t_4(n, l) = 0 \end{cases} \quad (10.18)$$

It is important to note that the first equation of system (10.9), as proved by the authors, is a consequence of four equations: two equations of system (10.17) and

two equations of system (10.18) at $l = 0$. The proof is based on the properties of the Bessel functions (Watson, 1945) and the idea is presented in the Appendix. The fact of linear dependence of the equations, but the lack of understanding of which ones perplexed the author of a previous work (Murthy, 1969; Pirogov and Iumatov, 1968; Naghdi and Eringen, 1965).

All equations of systems (10.16) - (10.18) can be written in matrix form (see Table 10.6). Thus, a linear system with an infinite number of equations and unknowns is obtained. In this case, the elements of the infinite matrix of the system, which differ significantly from zero, are located near the main diagonal. This is due to the values $J_k((1+i)\beta)$, on which all elements of the matrix of the system depend, become very small with increasing k , namely, next to the main diagonal there are elements whose index $k = n - 2l$ is close to zero. The submatrix composed of the first $4N$ rows and columns will have a nonzero determinant. The solving the system allows to find uniquely the coefficients for the first $2N$ basis functions. At the same time, as calculations show, with an increase in N , the first found coefficients practically do not change, and the coefficients at basis functions with large indexes tend to zero. This method has no mathematical restrictions on the values of the main parameter β . From the point of view of mechanics, this model is applicable for the range $0 \leq \beta \leq 3,5 - 4,5$ (Guz, 1974).

10.7 Results

The found coefficients a_n and b_n can be substituted into (10.4). Herewith, any finite partial sum

Table 10.1 System (10.16) - (10.18) in matrix form.

| n | 0 | | 1 | | 2 | | 3 | | | unknown | free terms |
|-----|------------|------------|------------|------------|------------|------------|------------|------------|---|---------|----------------|
| | Im | Re | Im | Re | Im | Re | Im | Re | | | |
| l | | | | | | | | | | | |
| 0 | $t_3(0,0)$ | $t_3(0,0)$ | $t_3(1,0)$ | $t_3(1,0)$ | $t_3(2,0)$ | $t_3(2,0)$ | $t_3(3,0)$ | $t_3(3,0)$ | : | a_0 | 0 |
| 0 | $t_4(0,0)$ | $t_4(0,0)$ | $t_4(1,0)$ | $t_4(1,0)$ | $t_4(2,0)$ | $t_4(2,0)$ | $t_4(3,0)$ | $t_4(3,0)$ | | b_0 | 0 |
| 1 | $g(0,1)$ | $g(0,1)$ | $g(1,1)$ | $g(1,1)$ | $g(2,1)$ | $g(2,1)$ | $g(3,1)$ | $g(3,1)$ | | a_1 | $-\frac{P}{4}$ |
| 1 | $g'(0,1)$ | $g'(0,1)$ | $g'(1,1)$ | $g'(1,1)$ | $g'(2,1)$ | $g'(2,1)$ | $g'(3,1)$ | $g'(3,1)$ | | b_1 | $-\frac{P}{2}$ |
| 1 | $t_3(0,1)$ | $t_3(0,1)$ | $t_3(1,1)$ | $t_3(1,1)$ | $t_3(2,1)$ | $t_3(2,1)$ | $t_3(3,1)$ | $t_3(3,1)$ | | a_2 | 0 |
| 1 | $t_4(0,1)$ | $t_4(0,1)$ | $t_4(1,1)$ | $t_4(1,1)$ | $t_4(2,1)$ | $t_4(2,1)$ | $t_4(3,1)$ | $t_4(3,1)$ | | b_2 | 0 |
| 2 | $g(0,2)$ | $g(0,2)$ | $g(1,2)$ | $g(1,2)$ | $g(2,2)$ | $g(2,2)$ | $g(3,2)$ | $g(3,2)$ | | a_3 | 0 |
| 2 | $g'(0,2)$ | $g'(0,2)$ | $g'(1,2)$ | $g'(1,2)$ | $g'(2,2)$ | $g'(2,2)$ | $g'(3,2)$ | $g'(3,2)$ | | b_3 | 0 |

...

$$\Phi = -i \frac{py^2}{2} + \sum_{n=0}^{\infty} \frac{a_n + ib_n}{H_n^{(1)}[(1+i)\beta]} \begin{bmatrix} \cos(\alpha x) \cdot H_n^{(1)}(\alpha r) \cdot \cos(n\theta) \\ \sin(\alpha x) \cdot H_n^{(1)}(\alpha r) \cdot \cos(n\theta) \end{bmatrix}.$$

is an exact solution of the mathematical physics equation in the domain (in contrast, for example, from the solution of this problem by the Ritz method) and satisfies the boundary conditions at infinity. As calculations show, the boundary conditions on the hole boundary are satisfied quite accurately for any $\beta \in (0;4]$ for 18 basis functions, the coefficients of which are found from the reduced system. E.g., the maximum deviation of the boundary conditions from zero for $\beta = 0.212$ is no more than 10^{-14} , and for $\beta = 4$ no more than $6 \cdot 10^{-3}$. With increasing β , the maximum deviation increases: for greater accuracy, you can take 24 basis functions for large values of β , and then the deviation will be no more than $5 \cdot 10^{-6}$. As β increases, the number of basis functions that significantly affect the response increases, i.e., the basis coefficients increase for large n . The results shown in the graph (Fig. 10.1a) completely coincide with the results obtained in van Dyke (1965) by the collocation method. In the works of different authors were different the results, and it remained unclear what results to rely on. Now it has been possible to find an analytical method that is easy to implement and gives reliable results and the possibility of further investigation of stresses.

Acknowledgements The reported study was funded by RFBR, project number 19-31-60008.

References

- Adams NJI (1971) Stress Concentration in a Cylindrical Shell Containing a Circular Hole. *Journal of Engineering for Industry* 93(4):953–961
- Celebi M, Gürdal Z, Tatting B, Blom-Schieber A, Rassaian M, Wanthal SP (2017) Effects of Size and Location of a Circular Cutout on Buckling and Failure of a Cylindrical Shell in Bending. *American Institute of Aeronautics and Astronautics*, pp 1–18. DOI 10.2514/6.2017-0433
- Chekhov VN, Zakora SV (1972) Numerical determination of the stress concentration around a hole in a circular cylindrical shell. *Soviet Applied Mechanics* 8(7):785–788
- Chowdhury R, Saiteja Reddy M, Jain PC, Bangaru Babu P (2016) Stress concentration around cut-outs in plates and cylindrical shells. *ARPJ Journal of Engineering and Applied Sciences* 11(18):11,074–11,084
- Eringen AC, Naghdi AK, Thiel CC (1965) *State of Stress in a Circular Cylindrical Shell with a Circular Hole*. Welding Research Council, New York
- Guz AN (1974) *Cylindrical Shells with Cutouts* (in Russ.). Naukova Dumka, Kiev
- Houghton DS (1961) Stress concentrations around cut-outs in a cylinder. *The Journal of the Royal Aeronautical Society* 65(603):201–204
- Hu C, Liu D, Ma X, Wang B (1998) On the stress concentration in thick cylindrical shells with an arbitrary cutout. *Applied Mathematics and Mechanics* 19(5):373–384
- Kashtanova SV, Rzhonsnitskiy AV, Gruzdkov AA (2021) On the issue of analytical derivation of stress state in a cylindrical shell with a circular hole under axial tension. *Materials Physics and Mechanics* 47:186–195
- Lekkerkerker JG (1965) On the stress distribution in cylindrical shells weakened by a circular hole. *Uitgeverij Waltman, Delft*

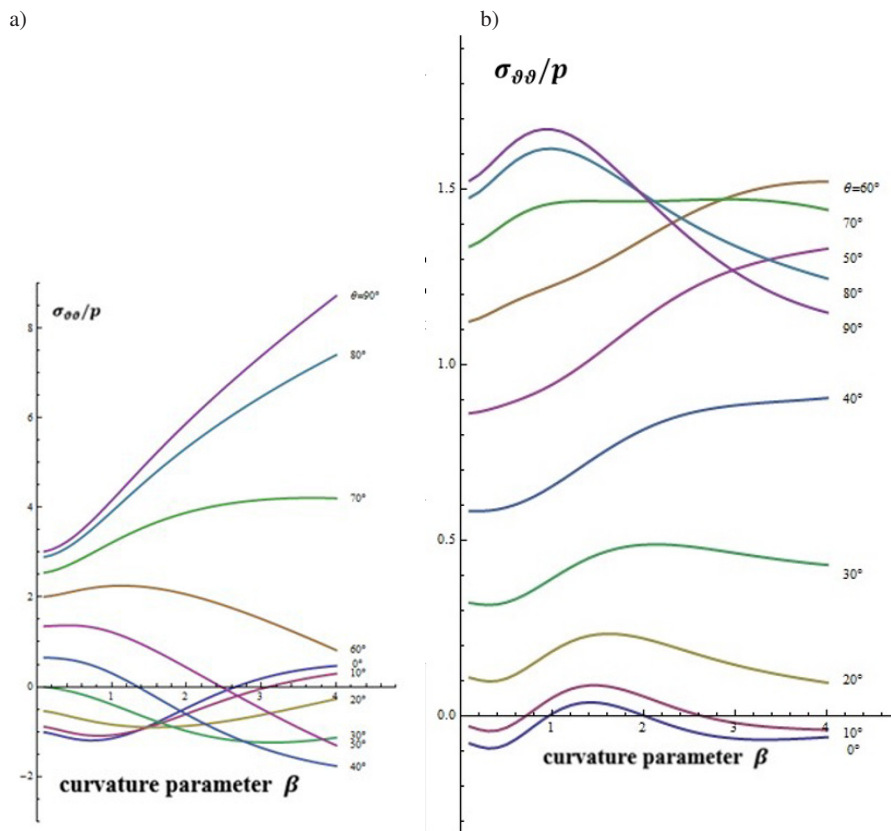


Fig. 10.1 Stress $\sigma_{\theta\theta}/p$ for all range of values $\beta \in (0; 4]$ for $r = 1$ (left) – on the boarder and $r = 1.5$ (right).

- Lurie AI (1946) Concentration of stresses in the vicinity of an aperture in the surface of a circular cylinder (in Russ.). *Prikladnaya Matematika i Mekhanika* 10:937, english transl. by N. Brunswick, New York University, Inst. of Math. Sci., 1960
- Murthy MVV (1969) Stresses Around an Elliptic Hole in a Cylindrical Shell. *Journal of Applied Mechanics* 36(1):39–46
- Naghdi AK, Eringen AC (1965) Stress distribution in a circular cylindrical shell with a circular cutout. *Ingenieur-Archiv* 34(3):161–172
- Oterkus E, Madenci E, Nemeth MP (2007) Stress analysis of composite cylindrical shells with an elliptical cutout. *Journal of Mechanics of Materials and Structures* 2(4):695–727
- Pirogov IM, Iumatov VP (1968) O napriazheniakh v cilindricheskoi obolochke oslablennoi krugovym otverstiem. In: *Sb. trudov Vsesoiuzn. zaochnoi politekh. int-ta, Vysshaya shkola, Moscow*, 51
- Ray-Chaudhuri S, Chawla K (2018) Stress and strain concentration factors in orthotropic composites with hole under uniaxial tension. *Curved and Layered Structures* 5(1):213–231
- Russo A, Sellitto A, Saputo S, Acanfora V, Riccio A (2019) A numerical–analytical approach for the preliminary design of thin-walled cylindrical shell structures with elliptical cut-outs. *Aerospace* 6(5):52

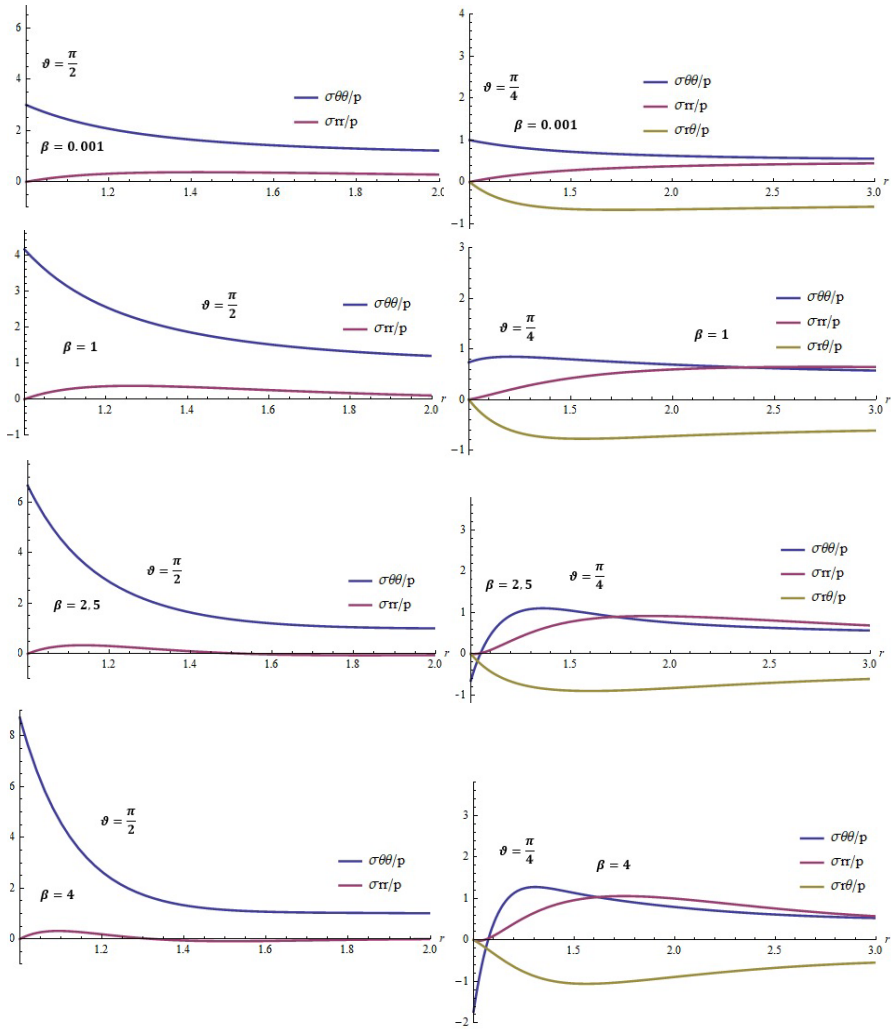


Fig. 10.2 Stresses for $\beta = 0,001; 1; 2,5; 4$ depending on r .

Storozhuk EA, Chernyshenko IS, Yatsura AV (2018) Stress-Strain State Near a Hole in a Shear-Compliant Composite Cylindrical Shell with Elliptical Cross-Section. *International Applied Mechanics* 54(5):559–567

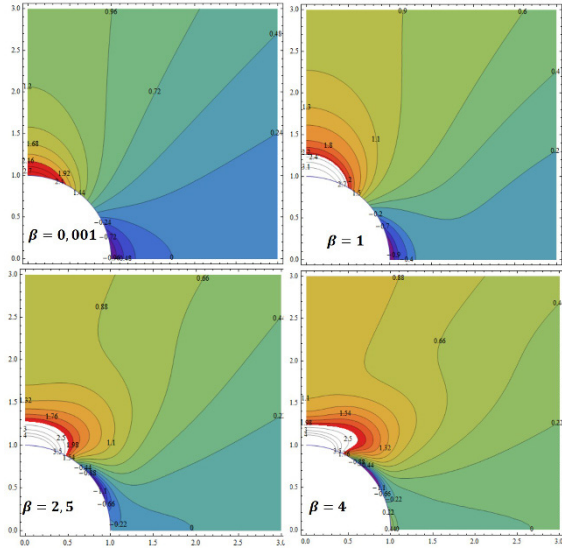
van Dyke P (1965) Stresses about a circular hole in a cylindrical shell. *AIAA Journal* 3(9):1733–1742

Watson GN (1945) *A Treatise on the Theory of Bessel Functions*. Cambridge University Press, Cambridge

Wu HC, Mu B (2003) On stress concentrations for isotropic/orthotropic plates and cylinders with a circular hole. *Composites Part B: Engineering* 34(2):127–134

Yu BH, Ma JJ, Liu Y (2015) Finite element analysis of cylindrical shell with a circular cutout using combination model of solid element and shell element. In: *Mechanical and Electrical*

Fig. 10.3 Stress field for $\sigma_{\theta\theta}/p$.



Technology VII, Trans Tech Publications Ltd, Applied Mechanics and Materials, vol 799, pp 739–745

Zhuang L, Su B, Lin M, Liao Y, Peng Y, Zhou Y, Luo D (2015) Influence of the property of hole on stress concentration factor for isotropic plates. In: Araújo AL, Correia JR, Mota Soares CM (eds) 10th International Conference on Composite Science and Technology, Lisboa, pp 1–5

Appendix

Statement: the first equation in (10.9) is a consequence of four equations: two equations of system (10.17) and two equations of the system (10.18) for $l = 0$.

Proof. The following notation is introduced:

$$\text{I: (10.9) } \operatorname{Im} \sum_{n=0}^{\infty} (a_n + ib_n) g'(n, 0) = p,$$

$$\text{II: (10.18)}_1, l = 0 \operatorname{Im} \sum_{n=0}^{\infty} (a_n + ib_n) t_3(n, 0) = 0,$$

$$\text{III: (10.18)}_2, l = 0 \operatorname{Im} \sum_{n=0}^{\infty} (a_n + ib_n) t_4(n, 0) = 0,$$

$$\text{IV: (10.17)}_1 \operatorname{Im} \sum_{n=0}^{\infty} (a_n + ib_n) g(n, 1) = -p/4,$$

$$\text{V: (10.17)}_2 \operatorname{Im} \sum_{n=0}^{\infty} (a_n + ib_n) g'(n, 1) = -p/2.$$

The following fact is asserted:

$$4\beta^2[I + V + 2IV] = II + III.$$

Equality for the right-hand sides is obvious. For the left-hand sides, we need to prove that $\forall n \in \mathbb{Z}_+$:

$$4\beta^2[g'(n, 0) + g'(n, 1) + 2g(n, 1)] = i(g''(n, 0) + g'''(n, 0) - g'(n, 0)). \quad (10.19)$$

Consider the linear differential operator

$$\mathcal{L}y = y'' + \frac{y'}{z} + \left(1 - \frac{n^2}{z^2}\right)y.$$

Lemma 10.1. *Let $u, v \in \text{Ker } \mathcal{L}$, i.e. u, v – Bessel function of index n , $G(z) = u(z)v(z)$. So*

$$G'''(z) + \frac{3}{z}G''(z) + \left(4 - \frac{4n^2 - 1}{z^2}\right)G'(z) + \frac{4}{z}G(z) = 0.$$

The proof of the lemma is derived from the relations for the Bessel functions. If we apply the assertion of the lemma to

$$u(z) = (-1)^{\lfloor \frac{n}{2} \rfloor} \frac{2}{H_n^{(1)}((1+i)\beta)} H_n^{(1)}(z), \quad v(z) = J_n(z), \quad G(z) = u(z)v(z),$$

then we prove the Eq. (10.19).



Chapter 11

Analysis of Solutions for Elliptic Boundary Layer in Cylindrical Shells at Edge Shock Loading

Irina V. Kirillova and Leonid Y. Kossovich

Abstract This paper is devoted to analysis of the asymptotic solution behaviour for the elliptic boundary layer in cylindrical shells in small vicinities of the surface Rayleigh wave front under normal edge shock loading. The boundary layer is described by the elliptic equations along the thickness of shells and the hyperbolic equations which are defined boundary conditions on the faces. These boundary conditions on cylindrical faces characterise wave motion on them.

The sought for solution is presented by the composite ones. The first one is the particular solution, satisfying only the boundary conditions on the shell edge. The boundary value problem for the second one is reduced to the problem for shock loading on the faces of the infinite cylindrical shell. This one is solved with the help of the Laplace transform on time and the Fourier transform on the longitudinal coordinate.

Inversion of the Laplace and Fourier transforms allows us represent the solution on the base of elementary function arctg of the complicated arguments. Analysis of this solution in a small quasifront vicinity by the asymptotic method defined properties of them at moving from the quasifront along the longitudinal coordinate. Numerical calculations confirmed this quality analysis of the solution.

Key words: Elliptic boundary layer, Cylindrical shell, Rayleigh wave front, Laplace transform, Fourier transform

11.1 Introduction

The solution scheme of the problem for transient waves in shells of revolution on the basis of asymptotic methods is described in Kirillova and Kossovich (2015). This

Irina V. Kirillova · Leonid Y. Kossovich
Saratov State University, 83 Astrakhanskaya Street, Saratov, 410012, Russian Federation
e-mail: nano-bio@info.sgu.ru, president@info.sgu.ru

scheme is based on representation of the solution with the help of components with different variability and dynamicity indices. There are the bending component (the low-frequency approximation corresponding to the bending component on the base of the Kirchhoff-Love shell theory), the Saint-Venant quasi-static boundary layer in a small vicinity of shell edge, the quasi-antiplane high-frequency, short wave component and two types of boundary layers: the hyperbolic boundary layer in the vicinity of shear wave front and the elliptic boundary layer in a small vicinity of the Rayleigh surface wave front. The asymptotic equations for the bending component Kirchhoff-Love shell theory, the Saint-Venant boundary layer, high frequency, short wave component and hyperbolic boundary layer were derived in Kossovich (1986); Kaplunov et al (1998).

The elliptic boundary layer has place in a small vicinity of the Rayleigh surface wave front and is described by the elliptic equations along the shell thickness with the boundary conditions on the faces which are defined by the hyperbolic equations. The asymptotic equations of this boundary layer in shells of revolution under normal shock surface loading were reduced in Kirillova and Kossovich (2017). The asymptotic equations of this boundary layer in shells of revolution under normal edge shock loading were constructed in Kirillova and Kossovich (2021). In this case the sought for solution is presented in the form of the composition of the particular one and some solution for the infinite shell with shock loading on the faces. The particular solution satisfies the boundary conditions on the shell edge. The problem for this boundary layer in the case of a cylindrical shell was considered in Kirillova and Kossovich (2020).

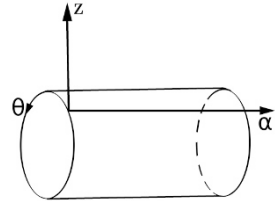
Present paper is devoted to the analysis of the solution for the elliptic boundary layer in cylindrical shells at edge shock loading, represented by the shear stress. The problem formulation is given in Sect. 11.2. Section 11.3 describes the particular solution for cylindrical shells, obtained on the basis of the particular solution for shells of revolution Kirillova and Kossovich (2020). Construction of the solution for the elliptic boundary layer is described in Sect. 11.4 and it is based on using the Laplace transform on time and the Fourier transform on the longitudinal coordinate. Numerical calculations and asymptotic analysis of the solution in the small vicinity of the Rayleigh surface wave front completely define the properties of this boundary layer.

11.2 Statement of the Problem

Consider a cylindrical shell (see Fig. 11.1), where α is the longitudinal coordinate on the midsurface, θ is the angular coordinate, z is the distance from the midsurface along the normal. Consider the following boundary conditions on the cylindrical shell faces defining axisymmetric case of the SSS (stress strain state)

$$\sigma_{33} = \sigma_{13} = 0, \quad z = \pm h \quad (11.1)$$

Fig. 11.1 Cylindrical shell.



and on the edge $\alpha = 0$

$$\sigma_{13} = IH(t), \quad v_1 = 0, \quad \alpha = 0, \tag{11.2}$$

where σ_{ij} and v_i ($i, j = 1, 2, 3$) denote stresses and displacements, h is the shell thickness, t is time, I is the amplitude of the load, $H(t)$ is Heaviside unit function. Let us consider the homogeneous initial conditions

$$v_i = \frac{\partial v_i}{\partial t} = 0 \quad (i = 1, 2, 3) \text{ at } t = 0. \tag{11.3}$$

Now we introduce the dimensionless variables, setting

$$\xi = \frac{\alpha}{h}, \quad \zeta = \frac{z}{h}, \quad \tau = \frac{tc_2}{h}, \quad c_2 = \sqrt{\frac{E}{2\rho(1+\nu)}}, \tag{11.4}$$

where E, ν, ρ are the Young's modulus, the Poisson's ratio and the mass density of the body; c_2 is the shear wave speed. Let us introduce the small parameter η :

$$\eta = \frac{h}{R}, \tag{11.5}$$

where R is the radius of the cylindrical midsurface. We assume that differentiation with respect to the dimensionless variables ξ and τ does not change the asymptotic order of unknown quantities with respect to small parameter $\eta \ll 1$. Then the dimensionless equations in displacements can be written as follows

$$\begin{aligned} \kappa^{-2} \frac{\partial^2 v_1}{\partial \xi^2} + \frac{\partial^2 v_1}{\partial \zeta^2} + \frac{1}{1-2\nu} \frac{\partial^2 v_1}{\partial \xi \partial \zeta} - \frac{\partial^2 v_1}{\partial \tau^2} + \eta \frac{\partial v_1}{\partial \zeta} + \eta \frac{1}{1-2\nu} \frac{\partial v_1}{\partial \xi} &= 0, \\ \frac{1}{1-2\nu} \frac{\partial^2 v_1}{\partial \xi \partial \zeta} + \frac{\partial^2 v_3}{\partial \xi^2} + \kappa^{-2} \frac{\partial^2 v_3}{\partial \zeta^2} - \frac{\partial^2 v_3}{\partial \tau^2} + \eta \frac{3-4\nu}{1-2\nu} \frac{\partial v_1}{\partial \xi} + \eta \kappa^{-2} \frac{\partial v_3}{\partial \zeta} &= 0, \end{aligned} \tag{11.6}$$

and

$$\begin{aligned}
\sigma_{11} &= \frac{E}{2(1+\nu)\kappa^2 h} \left(\frac{\partial v_1}{\partial \xi} + \frac{\nu}{1-\nu} \frac{\partial v_3}{\partial \zeta} + \eta \frac{\nu}{1-\nu} v_3 \right), \\
\sigma_{33} &= \frac{E}{2(1+\nu)\kappa^2 h} \left(\frac{\nu}{1-\nu} \frac{\partial v_1}{\partial \xi} + \frac{\partial v_3}{\partial \zeta} + \eta \frac{\nu}{1-\nu} v_3 \right), \\
\sigma_{13} &= \frac{E}{2(1+\nu)h} \left(\frac{\partial v_1}{\partial \zeta} + \frac{\partial v_3}{\partial \xi} \right),
\end{aligned} \tag{11.7}$$

where $\kappa^2 = c_2/c_1$, c_1 is the dilatation wave speed. Similarly to the general case of shell of revolution (Kirillova and Kossovich, 2021) we consider our SSS as short-wave SSS and represent it as combination of symmetric and antisymmetric parts. Similarly to Kirillova and Kossovich (2021) symmetric part of SSS is asymptotical main and governing equations can be written in the following form

$$\begin{aligned}
\kappa^{-2} \frac{\partial^2 v_1}{\partial \xi^2} + \frac{\partial^2 v_1}{\partial \zeta^2} + \frac{1}{1-2\nu} \frac{\partial^2 v_3}{\partial \xi \partial \zeta} - \frac{\partial^2 v_1}{\partial \tau^2} &= 0, \\
\frac{1}{1-2\nu} \frac{\partial^2 v_1}{\partial \xi \partial \zeta} + \frac{\partial^2 v_3}{\partial \xi^2} + \kappa^{-2} \frac{\partial^2 v_3}{\partial \zeta^2} - \frac{\partial^2 v_3}{\partial \tau^2} &= 0,
\end{aligned} \tag{11.8}$$

and

$$\begin{aligned}
\sigma_{11} &= \frac{E}{2(1+\nu)\kappa^2 h} \left(\frac{\partial v_1}{\partial \xi} + \frac{\nu}{1-\nu} \frac{\partial v_3}{\partial \zeta} \right), \\
\sigma_{33} &= \frac{E}{2(1+\nu)\kappa^2 h} \left(\frac{\nu}{1-\nu} \frac{\partial v_1}{\partial \xi} + \frac{\partial v_3}{\partial \zeta} \right), \\
\sigma_{13} &= \frac{E}{2(1+\nu)h} \left(\frac{\partial v_1}{\partial \zeta} + \frac{\partial v_3}{\partial \xi} \right).
\end{aligned} \tag{11.9}$$

11.3 Equivalent Problem for the Infinite Shell

Represent the solution in the following form:

$$SSS = SSS^{(0)} + SSS^{(1)}, \tag{11.10}$$

where index "0" denote the particular solution of equations (11.8), which satisfy only boundary conditions (11.2) on the edge. It is obviously that this particular solution has following simple form:

$$\begin{aligned}
v_1^{(0)} = 0, v_3^{(0)} &= \frac{(1+\nu)h}{E} I(\tau-\xi) H(\tau-\xi), \\
\sigma_{11}^{(0)} = \sigma_{33}^{(0)} = 0, \sigma_{13}^{(0)} &= IH(\tau-\xi).
\end{aligned} \tag{11.11}$$

The boundary conditions for $SSS^{(1)}$ on the edge and surface are written as follows

$$\begin{aligned} \frac{\partial v_3^{(1)}}{\partial \xi} = 0, v_1^{(1)} = 0, \xi = 0, \\ \sigma_{33}^{(1)} = 0, \sigma_{13}^{(1)} = IH(\tau - \xi), \zeta = \pm 1. \end{aligned} \tag{11.12}$$

Boundary conditions (11.12) show (Kirillova and Kossovich, 2021) that the deformed edge section in the problem (11.12) remains rectilinear and perpendicular to the axis ξ . Hence, if the infinite cylindrical shell is taken, as shown in Fig. 11.2, deformation of each symmetric part is equivalent to deformation of the considered semi-infinite shell. Let us name such problem for the infinite shell by the equivalent problem for the semi-infinite one.

Accordingly to Kirillova and Kossovich (2021) we introduce the potential functions φ and ψ :

$$\varphi = \varphi_1 + \varphi_2, \quad \psi = \psi_1 + \psi_2, \tag{11.13}$$

where the index "1" denote the solution for the region $\xi \geq 0$ and the index "2" denote the solution for $\xi \leq 0$. Equations for the regions $\xi > 0$ can be written in the following form (the index "1" we omit):

$$\begin{aligned} a^2 \frac{\partial^2 \varphi}{\partial \xi^2} + \frac{\partial^2 \varphi}{\partial \zeta^2} = 0, \\ b^2 \frac{\partial^2 \psi}{\partial \xi^2} + \frac{\partial^2 \psi}{\partial \zeta^2} = 0 \end{aligned} \tag{11.14}$$

under the following boundary conditions

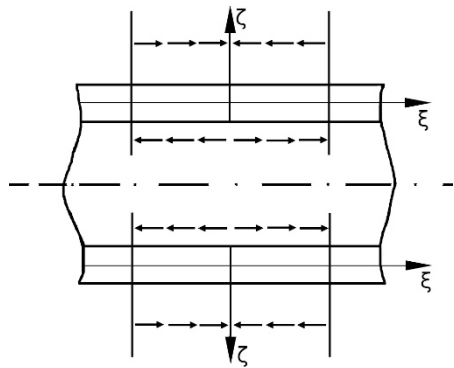


Fig. 11.2 Equivalent problem for semi-infinite shell.

$$\begin{aligned}
\kappa_R^2 \frac{\partial^2 \Psi}{\partial \xi^2} - \frac{\partial^2 \Psi}{\partial \tau^2} &= \frac{\kappa_R B_\omega}{g} IH(\tau - \xi), \quad \zeta = -1, \\
\kappa_R^2 \frac{\partial^2 \Psi}{\partial \xi^2} - \frac{\partial^2 \Psi}{\partial \tau^2} &= -\frac{\kappa_R B_\omega}{g} IH(\tau - \xi), \quad \zeta = 1, \\
\left(g + \frac{\kappa_R^2}{2}\right) \frac{\partial^2 \varphi}{\partial \xi^2} - \frac{1}{2} \frac{\partial^2 \varphi}{\partial \tau^2} + \left(b + \frac{\kappa_R^2}{2}\right) \frac{\partial^2 \psi}{\partial \xi^2} - \frac{1}{2b} \frac{\partial^2 \psi}{\partial \tau^2} &= 0, \quad \zeta = \mp 1,
\end{aligned} \tag{11.15}$$

where

$$\begin{aligned}
\Psi &= \frac{1}{b} \frac{\partial \psi}{\partial \zeta}, \quad B_\omega = 2 \left[\frac{\kappa_R}{1 - \kappa_R^2} + \frac{\kappa \kappa_R}{1 - \kappa^2 \kappa_R^2} - \frac{4\kappa_R}{2 - \kappa_R^2} \right]^{-1}, \\
a &= \sqrt{1 - \kappa^2 \kappa_R^2}, \quad b = \sqrt{1 - \kappa_R^2/2}, \quad g = 1 - \kappa_R^2/2, \quad \kappa_R = c_R/c_2,
\end{aligned} \tag{11.16}$$

c_R is the velocity of the surface Rayleigh waves.

Displacements and stresses are described through potential functions by the expressions

$$\begin{aligned}
v_1 &= h \left(\frac{\partial \varphi}{\partial \xi} + b \frac{\partial \psi}{\partial \xi} \right), \quad v_3 = h \left(\frac{\partial \varphi}{\partial \zeta} + \frac{1}{b} \frac{\partial \psi}{\partial \zeta} \right), \\
\sigma_{33} &= -\frac{Eh}{1+\nu} \left(g \frac{\partial^2 \varphi}{\partial \xi^2} + b \frac{\partial^2 \psi}{\partial \xi^2} \right), \\
\sigma_{13} &= \frac{Eh}{1+\nu} \left(\frac{1}{a^2} \frac{\partial^2 \varphi}{\partial \xi \partial \zeta} - \frac{\kappa^2 \kappa_R}{a^2} \frac{\partial^2 \varphi}{\partial \zeta \partial \tau} + \frac{g + \kappa_R^2}{b} \frac{\partial^2 \psi}{\partial \xi \partial \zeta} + \frac{\kappa_R}{b} \frac{\partial^2 \psi}{\partial \zeta \partial \tau} \right).
\end{aligned} \tag{11.17}$$

The expression for σ_{13} in (11.17) is not convenient at application of the Fourier transform on the longitudinal coordinate. In this case we can use the alternative form (Kirillova and Kossovich, 2020):

$$\begin{aligned}
\frac{\partial \sigma_{13}}{\partial \zeta} &= \frac{E}{(1+\nu)h} \left(\frac{2 - \kappa^2 \kappa_R^2}{2a} \frac{\partial^2 \Phi}{\partial \xi^2} - \frac{\kappa^2 \kappa_R}{2a} \frac{\partial^2 \Phi}{\partial \tau^2} + \frac{\partial^2 \Psi}{\partial \xi^2} - \frac{1}{2} \frac{\partial^2 \Psi}{\partial \tau^2} \right), \\
\Phi &= \frac{1}{a} \frac{\partial \varphi}{\partial \zeta}.
\end{aligned} \tag{11.18}$$

11.4 Solution of the Equivalent Problem for the Cylindrical Shell

Consider the equivalent problem on propagation of transient waves in the cylindrical shell at boundary conditions (11.15). The equations for the region $\xi < 0$ are written similarly to this case. Let us consider only the wave which is initiated by the face surface $\zeta = -1$. Then the governing equations for potential functions φ , ψ remain the form (11.14), but boundary conditions are described for regions $\xi > 0$ and $\xi < 0$ in the following form:

$$\begin{aligned} \kappa_R^2 \frac{\partial^2 \Psi}{\partial \xi^2} - \frac{\partial^2 \Psi}{\partial \tau^2} &= \frac{\kappa_R B \omega}{g} IH(\tau \mp \xi), \quad \zeta = -1, \\ \left(g + \frac{\kappa_R^2}{2}\right) \frac{\partial^2 \varphi}{\partial \xi^2} - \frac{1}{2} \frac{\partial^2 \varphi}{\partial \tau^2} + \left(b + \frac{\kappa_R^2}{2}\right) \frac{\partial^2 \psi}{\partial \xi^2} - \frac{1}{2b} \frac{\partial^2 \psi}{\partial \tau^2} &= 0, \quad \zeta = -1. \end{aligned} \quad (11.19)$$

The expressions for stresses and displacements at $\xi < 0$ remain the form (11.17) and (11.18). To solve this boundary value problem we apply the Laplace transform on time and the Fourier transform on the longitudinal coordinate. Then boundary conditions (11.19) and expression for the transformation of stress σ_{13} are represented as

$$\begin{aligned} (\kappa_R^2 \chi^2 + s^2) \Psi^{LF} &= -\sqrt{\frac{2}{\pi}} I \frac{\kappa_R B \omega}{g} \frac{\chi^2}{s(s^2 + \chi^2)}, \quad \zeta = -1, \\ \left[\left(g + \frac{\kappa_R^2}{2}\right) \chi^2 + \frac{1}{2} s^2\right] \varphi^{LF} + \left[\left(b + \frac{\kappa_R^2}{2b}\right) \chi^2 + \frac{1}{2b} s^2\right] \psi^{LF} &= 0, \quad \zeta = -1, \end{aligned} \quad (11.20)$$

$$\sigma_{13}^{LF} = -i \frac{E}{(1+\nu)h} \frac{1}{\chi} \left[\left(\frac{2 - \kappa^2 \kappa_R^2}{2a} \chi^2 + \frac{\kappa^2}{2a} s^2 \right) \Phi^{LF} + \left(\chi^2 + \frac{1}{2} s^2 \right) \Psi^{LF} \right], \quad (11.21)$$

where upper indices L and F denote Laplace and Fourier integral transforms consequently:

$$\varphi^F = \frac{1}{\sqrt{2\pi}} \int_{-\infty}^{\infty} \varphi e^{-i\chi\xi} d\xi, \quad \varphi^L = \int_0^{\infty} \varphi e^{-s\tau} d\tau \quad (11.22)$$

and χ , s are Fourier and Laplace transform parameter, and $i = \sqrt{-1}$.

Taking into account that the equations for the integral transform of potential functions φ and ψ have the form:

$$\begin{aligned} \frac{d^2 \varphi^{LF}}{d\zeta^2} - a^2 \chi^2 \varphi^{LF} &= 0, \\ \frac{d^2 \psi^{LF}}{d\zeta^2} - b^2 \chi^2 \psi^{LF} &= 0 \end{aligned} \quad (11.23)$$

we can obtain the solution for the transform of stress σ_{11}

$$\begin{aligned} \sigma_{13}^{LF} &= -i \sqrt{\frac{2}{\pi}} I \frac{\kappa_R B \omega}{g} \left[\left(g \frac{\chi^3}{s(\kappa_R^2 \chi^2 + s^2)(\chi^2 + s^2)} \right. \right. \\ &+ \left. \left(\frac{\kappa^2 g}{2a^2} + \frac{g}{2b^2} - \frac{1}{2} \right) \frac{\chi}{\chi^2 + s^2} \right) e^{\mp a\chi(1+\zeta)} \\ &- \left. \left(g \frac{\chi^3}{s(\kappa_R^2 \chi^2 + s^2)(\chi^2 + s^2)} + \frac{1}{2} \frac{\chi}{s(\chi^2 + s^2)} \right) e^{\mp \chi(1+\zeta)} \right], \end{aligned} \quad (11.24)$$

where signs " \mp " relate correspondingly to the regions $\xi > 0$ and $\xi < 0$.

Let us turn transform (11.24). Using the following formulae for turning the Laplace transform (Kirillova and Kossovich, 2020)

$$\frac{\chi}{s(\kappa_R^2\chi^2 + s^2)} \implies \frac{1}{\kappa_R^2\chi}(1 - \cos \kappa_R\tau\chi) \quad (11.25)$$

we obtain the formulae for the Fourier transform of our solution

$$\begin{aligned} \sigma_{13}^F = & -l \sqrt{\frac{2}{\pi}} I^{\kappa_R B_\omega} \left[\left(\frac{g}{b^2\kappa_R^2\chi} (1 - \cos \kappa_R\tau\chi) \right. \right. \\ & + \left. \left(\frac{\kappa^2 g}{2a^2} - \frac{g}{2b^2} - \frac{1}{2} \right) \frac{1}{\chi} (1 - \cos \tau\chi) \right) e^{\mp a\chi(1+\zeta)} \\ & - \left(\frac{g}{b^2\kappa_R^2\chi} (1 - \cos \kappa_R\tau\chi) \right. \\ & \left. \left. + \left(-\frac{g}{b^2} + \frac{1}{2} \right) \frac{1}{\chi} (1 - \cos \tau\chi) \right) e^{\mp b\chi(1+\zeta)} \right]. \end{aligned} \quad (11.26)$$

Now we return the Fourier transform with the help of following integral

$$\int_0^\infty \frac{1 - \cos \tau\chi}{\chi} e^{-a\chi} \sin \xi\chi d\chi = \arctan\left(\frac{\xi}{a}\right) - \frac{1}{2} \arctan\left(\frac{2\xi a}{a^2 - \xi^2 + \tau^2}\right) \quad (11.27)$$

and obtain the expression for σ_{13} :

$$\begin{aligned} \sigma_{13} = & \frac{2}{\pi} I^{\kappa_R B_\omega} \left[\left(\frac{g}{b^2\kappa_R^2} + \frac{\kappa^2 g}{2a^2} - \frac{g}{2b^2} - \frac{1}{2} \right) \arctan\left(\frac{\xi}{a(1+\zeta)}\right) \right. \\ & + \left(-\frac{g}{b^2\kappa_R^2} + \frac{g}{b^2} - \frac{1}{2} \right) \arctan\left(\frac{\xi}{b(1+\zeta)}\right) - \\ & - \frac{g}{2b^2\kappa_R^2} \arctan\left(\frac{2a\xi(1+\zeta)}{a^2(1+\zeta)^2 - \xi^2 + \kappa_R^2\tau^2}\right) - \\ & - \frac{1}{2} \left(\frac{\kappa^2 g}{2a^2} - \frac{g}{2b^2} - \frac{1}{2} \right) \arctan\left(\frac{2a\xi(1+\zeta)}{a^2(1+\zeta)^2 - \xi^2 + \tau^2}\right) \\ & + \frac{g}{2b^2\kappa_R^2} \arctan\left(\frac{2b\xi(1+\zeta)}{b^2(1+\zeta)^2 - \xi^2 + \kappa_R^2\tau^2}\right) \\ & \left. + \frac{1}{2} \left(-\frac{g}{b^2} + \frac{1}{2} \right) \arctan\left(\frac{2b\xi(1+\zeta)}{b^2(1+\zeta)^2 - \xi^2 + \tau^2}\right) \right]. \end{aligned} \quad (11.28)$$

Our boundary layer has place in small vicinity of the surface Rayleigh wave front $\xi = \kappa_R\tau$. Here:

$$\xi \gg 1, \tau \gg 1, \tau - \xi \gg 1 \text{ and } |\kappa_R\tau - \xi| \ll 1, \quad (11.29)$$

therefore we can consider the next estimation of the functions in (11.28)

$$\arctan\left(\frac{\xi}{a(1+\zeta)}\right) = \frac{\pi}{2}, \quad \arctan\left(\frac{\xi}{b(1+\zeta)}\right) = \frac{\pi}{2},$$

$$\arctan\left(\frac{2a\xi(1+\zeta)}{a^2(1+\zeta)^2 - \xi^2 + \tau^2}\right) = 0, \quad \arctan\left(\frac{2b\xi(1+\zeta)}{b^2(1+\zeta)^2 - \xi^2 + \tau^2}\right) = 0. \quad (11.30)$$

Then we obtain very simple expression for σ_{13} in a small vicinity of the Rayleigh wave front:

$$\sigma_{13} = I + \widetilde{\sigma}_{13},$$

$$\widetilde{\sigma}_{13} = I \frac{B_\omega}{\pi \kappa_R b^2} \left[-\arctan\left(\frac{2a\xi(1+\zeta)}{a^2(1+\zeta)^2 - \xi^2 + \kappa_R^2}\right) \right. \quad (11.31)$$

$$\left. + \arctan\left(\frac{2b\xi(1+\zeta)}{b^2(1+\zeta)^2 - \xi^2 + \kappa_R^2 \tau^2}\right) \right].$$

Now we consider the solution behaviour outside the small vicinity of the quasifront $|\xi - \kappa_R \tau| \gg 1$. This one is defined by the behaviour of the function arctan argument. We denote

$$y = \frac{2a\xi(1+\zeta)}{a^2(1+\zeta)^2 - \xi^2 + \kappa_R^2 \tau^2}. \quad (11.32)$$

This argument can be represented in the form for the asymptotic analysis

$$y = \frac{2a(1+\zeta)}{\frac{a^2(1+\zeta)^2}{\xi} - \frac{\xi + \kappa_R \tau}{\xi}(\xi - \kappa_R \tau)}. \quad (11.33)$$

In the region $\xi \gg 1$ (i.e. at $|\alpha - \kappa_R \tau| \gg h$, $x \gg h$) we have $a^2(1+\zeta)^2/\xi \ll 1$, $(\xi + \kappa_R \tau)/\xi = O(1)$ and consequently $y \ll 1$. Thus we have next values for the functions in (11.25)

$$\arctan\left(\frac{2a\xi(1+\zeta)}{a^2(1+\zeta)^2 - \xi^2 + \kappa_R^2 \tau^2}\right) \ll 1,$$

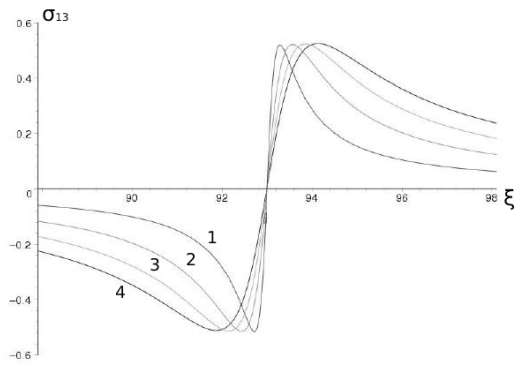
$$\arctan\left(\frac{2b\xi(1+\zeta)}{b^2(1+\zeta)^2 - \xi^2 + \kappa_R^2 \tau^2}\right) \ll 1 \quad (11.34)$$

and $\widetilde{\sigma}_{13}$ tends to zero at moving off quasifront. Dependence of the stress σ_{13} on longitudinal coordinate ξ in small vicinity of Rayleigh wave front is shown at Fig. 11.3.

References

- Kaplunov JD, Kossovich LY, Nolde EV (1998) Dynamics of Thin Walled Elastic Bodies. Academic Press, San-Diego
- Kirilova IV, Kossovich LY (2015) Asymptotic theory of waves in thin walled shells at shock edge loading of tangential, bending and normal types. In: Proceeding of the XI Russian conference

Fig. 11.3 Stress σ_{13} at time $\tau = 100$ for $\zeta = -0.5; 0; 0.5; 1$ (numbers 1 – 4 correspondingly).



on fundamental problems of theoretical and applied mechanics, Kazan University Press, Kazan, pp 2008–2015

Kirillova IV, Kossovich LY (2017) Refined equations of elliptic layer in shells of revolution under normal shock surface loading. *Vestnik of St Petersburg University, Mathematics* 50(1):68–73

Kirillova IV, Kossovich LY (2020) Asymptotic methods for studying an elliptical boundary layer in shells of revolution under normal type shock end impacts. *Mechanics of Solids* 55(5):710–715

Kirillova IV, Kossovich LY (2021) Elliptic boundary layer in shells of revolution under normal edge shock loading. In: Altenbach H, Eremeyev VA, Igumnov LA (eds) *Multiscale Solid Mechanics - Strength, Durability, and Dynamics, Advanced Structured Materials*, vol 141, Springer, Cham, pp 249–260

Kossovich LY (1986) *Non-Stationary Problems in Theory of Elastic Thin Shells*. Saratov University Press, Saratov



Chapter 12

Dimension Reduction in the Plate with Tunnel Cuts

Alexander G. Kolpakov and Sergei I. Rakin

Abstract We carry out dimension reduction in the homogenization theory 3D periodicity cell problem for the plate with a unidirectional system of channel cuts. We demonstrate that the original 3D problem may be reduced to several 2D problems. The main attention is paid to the solution near the top and the bottom surfaces of the plate. Our numerical analysis indicates the existence of a new type of boundary layer at the upper and lower surfaces of the plate. We estimate the thickness of the found boundary layer. We also find a wrinkling effect on the top and bottom surfaces of the plate.

Key words: Plate with channel cuts, Dimension reduction, Top/bottom face boundary layers, Wrinkling effect

12.1 Introduction

The homogenization problem for the elastic bodies with holes/pores attracted the attention of numerous researchers. One can mention the pioneering paper of Cioranescu and Paulin (1979). Relevant references may be found in Cioranescu and Donato (1999); Cioranescu et al (2018) (mathematics) and Kalamkarov and Kolpakov (1997); Kolpakov and Kolpakov (2009) (applications to composite materials). The

Alexander G. Kolpakov

SysAn, A. Nevskogo str., 12a, 34, Novosibirsk, 630075 & Novosibirsk state university of architecture and civil engineering (Sibstrin), 113 Leningradskay str., Novosibirsk, 630008, Russian Federation

e-mail: algk@ngs.ru

Sergei I. Rakin

SysAn, A. Nevskogo str., 12a, 34, Novosibirsk, 630075 & Siberian Transport University, 191 Dusi Kovalchuk str., Novosibirsk, 630049, Russian Federation

e-mail: rakinsi@ngs.ru

papers on the homogenization problem for plates with holes/pores/channels are not so numerous as the papers devoted to the homogenization problem for solids with holes/pores/channels.

The boundary layers in plates and shells were intensively discussed in literature after Rayleigh, Love, Lamb, and Basset (Sendekyj, 1974). In the 1970s-1980s, boundary layers were intensively discussed for laminated composite materials (van Dyke, 1994; Pipes and Pagano, 1970), later - for fiber-reinforced composite materials see, e.g., Kalamkarov and Kolpakov (1997); Andrianov et al (2011). Numerous experimental, theoretical, and numerical results were reported. Note that the boundary layers in the plates and shells were associated exclusively with the transverse cut surface.

When considering the plates with channel cuts, we meet the new type of boundary layers associated with the top and the bottom surfaces of the plate. The boundary layers of this type never occur in the homogeneous or in the laminated plates.

12.2 Statement of the Problem

We consider a plate with a periodic system of cylindrical geometry channels. Suppose the cylinders are parallel to the $0x$ -axis and form a periodic structure in the $0xz$ -plane. The periodicity cell (PC) of such a structure is shown in Fig. 12.1a, and the cross-section is displayed in Figs. 12.1b. The choice of the length of the PC in Fig. 12.1a is voluntary.

Since the plate under consideration is invariant with respect to translation in the direction $0y$ -axis, there is a reason to look for two-dimensional models to the plate. The dimension reduction procedures are known for the solids with periodic systems of fibers or holes (Grigolyuk et al, 1991; Grigolyuk and Fil'shtinskij, 1992; Lu, 1995; Mityushev and Rogozin, 2000; Drygaś et al, 2020). To the best knowledge of the authors, the first paper devoted to the dimension reduction in the bending problem for an elastic layer with tunnel cuts was Grigolyuk et al (1991). The mentioned paper was based on the double periodic function technique, thus treated the layer

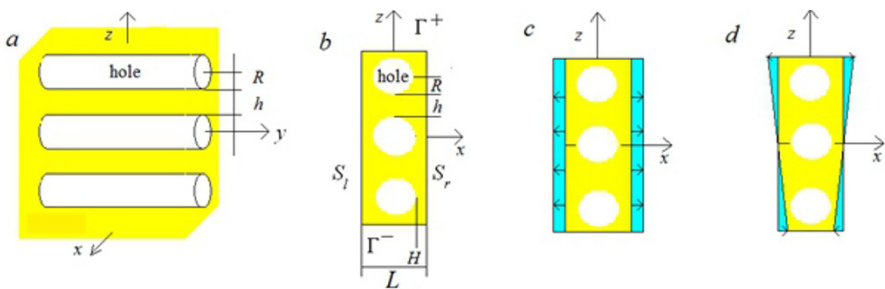


Fig. 12.1 Periodicity cell (a) and the cross-section (b) of the plate with the channel cuts and the deformation modes of PC: (c) - tension, (d) - bending.

of "infinite" thickness. It means that Grigolyuk et al (1991) can be used to predict the stress-strain state (SSS) inside the plate, but not near-surface phenomena. But the plate has a finite thickness. The aim of this paper is the dimension reductions for plates of finite thickness. Our research indicates the existence of a new range of boundary layers - boundary layers at the upper and lower surfaces of the plate. We also find a wrinkling effect on the top and bottom surfaces of the plate. The results of Grigolyuk et al (1991) can be used to describe the stress-strain state (SSS) inside the plate, but not near-surface phenomena.

The starting point of our research is the periodicity cell problem (PCP) of the homogenization theory as applied to plates (Caillerie, 1984; Kohn and Vogelius, 1984), which has the following form:

$$\begin{aligned} (a_{ijkl}N_{k,l}^{AB\mu} + (-1)^\mu a_{ijAB}z^\mu)_{,j} &= 0 \quad \text{in } P, \\ (a_{ijkl}N_{k,l}^{AB\mu} + (-1)^\mu a_{ijAB}z^\mu)n_j &= 0 \quad \text{on } \Gamma \cup H, \\ \mathbf{N}^{AB\mu}(\mathbf{y}) &\text{ periodic in } x, y. \end{aligned} \quad (12.1)$$

with the superscript μ taking the values 0 or 1. In the plate PCP, the top Γ^+ and bottom Γ^- surfaces are free. The PC may be subjected to in-plane ($\mu = 0$) or bending/torsion ($\mu = 1$) macroscopic deformation. These features distinguish the plates from the solids PCP. In the plate with channel cuts, the surfaces H_i of the channels are also free. Denoted: $\Gamma = \Gamma^+ \cup \Gamma^-$ and $H = \bigcup_{i=1}^n$, where n is the number of channels per one PC. The variables notation correspondence: $x \leftrightarrow 1, y \leftrightarrow 2, z \leftrightarrow 3$; the index $\mu = 0, 1$.

In the general case (Caillerie, 1984; Kohn and Vogelius, 1984), the local stresses in the PC are computed with the following formula:

$$\sigma_{ij} = a_{isjkl}N_{k,j}^{AB\mu} + (-1)^\mu a_{ijAB}z^\mu,$$

and the macroscopic stiffnesses of the plate are computed as

$$S_{\alpha\beta AB}^{\nu+\mu} = \frac{1}{|\text{Pr}P|} \int_P (a_{\alpha\beta kl}N_{k,j}^{AB\nu} + (-1)^\nu z^\nu a_{\alpha\beta AB}) (-1)^\mu z^\mu dx dz,$$

where $\text{Pr}P$ is projection of the PCP to the $0xy$ -plane. The superscript ν can take the values 0 or 1.

The PCP is a cylinder parallel to the $0y$ -axis, see Fig. 12.1, and the elastic constants a_{ijkl} are constants (we assume the plate is made of a homogeneous isotropic material). In this case, the solution to the problem (12.1) does not depend on the variable y and has the form $\mathbf{N}^{AB\mu} = \mathbf{N}^{AB\mu}(x, z)$. Substituting $\mathbf{N}^{AB\mu} = \mathbf{N}^{AB\mu}(x, z)$ into (12.1), we arrive at the following 2D PCP:

$$\begin{cases} (a_{i\alpha k\beta}N_{k,\beta}^{AB\mu} + (-1)^\mu a_{i\alpha AB}z^\mu)_{,\alpha} = 0 & \text{in } P, \\ (a_{i\alpha k\beta}N_{k,\beta}^{AB\mu} + (-1)^\mu a_{i\alpha AB}z^\mu)n_\alpha = 0 & \text{on } \Gamma, \\ \mathbf{N}^{AB\mu}(x, z) & \text{periodic in } x. \end{cases} \quad (12.2)$$

Hereafter $\alpha, \beta = 1, 3 : i, k = 1, 2, 3; A, B = 1, 1; 2, 2; 1, 2; 2, 1$. We use the same notation for the PC and its cross-sections, as well as for the boundaries of the plate and the boundaries of the channels. In (12.2)

$$a_{i\alpha k\beta} N_{k,\beta}^{AB\mu}(\mathbf{y}) + (-1)^\mu a_{i\alpha AB} z = a_{i\alpha\theta\beta} N_{\theta,\beta}^{AB\mu}(x, z) + a_{i\alpha 2\beta} N_{2,\beta}^{AB\mu}(x, z) + (-1)^\mu a_{i\alpha AB} z^\mu. \quad (12.3)$$

Equation (12.3) makes it possible to decompose the boundary-value problem (12.1) into several 2D problems. The form of the 2D problems is determined by the index i in (12.2). For this reason, we consider problem (12.2) for $i = 2$ and $i = \xi = 1, 3 = x, z$, separately.

12.3 Problem 12.1 with Index $i = 2$

We assume the plate is made of homogeneous isotropic material. We will use the tensor notations a_{ijkl} (it is convenient in our computations) for the elastic constants keeping into mind the relation of the elastic constants with Young's modulus E and Poisson's ratio ν (Love, 2013)

$$a_{1111} = a_{3333} = \frac{E(1-\nu)}{(1+\nu)(1-2\nu)}, \quad a_{1133} = a_{3311} = a_{1122} = a_{3322} = \frac{E\nu}{(1+\nu)(1-2\nu)}. \quad (12.4)$$

In the case under consideration, $a_{2\alpha\theta\beta} = 0, a_{2\alpha AB} = 0$ (Love, 2013) and expression in (12.3) takes the form ($\alpha = 1, 3$)

$$a_{2\alpha\theta\beta} N_{\theta,\beta}^{AB\mu} + a_{2\alpha 2\beta} N_{2,\beta}^{AB\mu} + (-1)^\mu a_{2\alpha AB} z^\mu = a_{2\alpha 2\alpha} N_{2,\alpha}^{AB\mu} + \begin{cases} (-1)^\mu a_{2121} z^\mu \\ \text{if } AB = 21, 12 \\ 0 \quad \text{else} \end{cases} \quad (12.5)$$

By virtue of (12.5), the solution to (12.2) $N_2^{AB\nu}(x, z) = 0$ if $AB \neq 21$. Only the component $N_2^{21\nu}(x, z)$ is non-zero. It is the case of in-plane shift ($\mu = 0$) or torsion ($\mu = 1$). The in-plane shift is also called anti-plane deformation (Love, 2013).

The problem for $N_2^{21\nu}(x, z)$ takes the form

$$\begin{cases} (a_{2\alpha 2\alpha} N_{2,\alpha}^{21\mu} + (-1)^\mu a_{2121} z^\mu \delta_{\alpha 1}),_{\alpha} = 0 & \text{in } P, \\ (a_{2\alpha 2\alpha} N_{2,\alpha}^{21\mu} + (-1)^\mu a_{2121} z^\mu \delta_{\alpha 1}) n_\alpha = 0 & \text{on } \Gamma \cup H, \\ N_2^{21\mu}(x, z) \text{ periodic in } x. \end{cases} \quad (12.6)$$

The term $(-1)^\mu a_{2121} z^\mu \delta_{\alpha 1}$ in (12.6) may be eliminated. There exists a function $w(x, z)$, such that ($\nu = 0, 1$)

$$a_{2\delta 2\delta} w_{,\delta} = (-1)^\nu a_{2121} z^\nu. \quad (12.7)$$

For $\delta = 2$ and $\delta = 3$, we obtain from (12.7) $a_{2121}w_{,1} = (-1)^{\nu}a_{2121}z^{\nu}$ and $a_{2323}w_{,3} = 0$. From these equalities, we obtain the following system of differential equations

$$w_{,1} = (-1)^{\nu}z^{\nu}, \quad w_{,3} = 0. \quad (12.8)$$

12.3.1 In-plane Shift

For $\nu = 0$, the system (12.8) takes the form $w_{,1} = 1, w_{,3} = 0$. The solution to this system is $w(x, z) = x$. We introduce function $M(x, z) = N_2^{120}(x, z) + x$ and rewrite (12.6) in the form of the following boundary-value problem for the Laplace equation:

$$\begin{cases} \Delta M = 0 & \text{in } P, \\ \frac{\partial M}{\partial \mathbf{n}} = 0 & \text{on } \Gamma \cup H, \\ M(x, z) - x & \text{periodic in } x \in [-L, L]. \end{cases} \quad (12.9)$$

After some algebra we obtain the following formula for the computation of the local stresses:

$$\sigma_{ij} = a_{ij2\alpha}N_{2,\alpha}^{120} + a_{ij21} = a_{ij2\alpha}M_{,\alpha},$$

and the following formula for the computation of homogenized shift stiffness:

$$S_{2121}^0 = \langle a_{212\alpha}N_{2,\alpha}^{120} + a_{2121} \rangle = \langle a_{212\alpha}M_{,\alpha} \rangle.$$

Hereafter

$$\langle \dots \rangle = \frac{1}{L} \int_P \dots dx dz$$

means the ‘‘average value’’, where L is the width of the 2D periodicity cell, Fig. 12.1b.

12.3.2 Torsion

For $\mu = 1$, (12.6) takes the form

$$\begin{cases} (a_{2\alpha 2\alpha}N_{2,\alpha}^{211} - a_{2121}z\delta_{\alpha 1})_{,\alpha} = 0 & \text{in } P, \\ (a_{2\alpha 2\alpha}N_{2,\alpha}^{211} - a_{2121}z\delta_{\alpha 1})n_{\alpha} = 0 & \text{on } \Gamma \cup H, \\ N_2^{211}(x, z) & \text{periodic in } x. \end{cases} \quad (12.10)$$

For $\nu = 1$, the system (12.8) takes form $w_{,1} = -z, w_{,3} = 0$. It is a not integrable system of differential equations. For this system, the necessary integrability condition (Sedov, 1971) is not satisfied because $w_{,13} = -z_{,3} = -1 \neq w_{,31} = 0$. As a result, it is

impossible to eliminate the term $a_{2121}z\delta_{\alpha 1}$ in (12.10) in a simple way as above. The problem (12.10) may be written in a compact form in the following way. Introduce function $\varphi(x, z)$ as

$$\varphi_{,3} = a_{2121}(N_{2,1}^{211} - z), \quad \varphi_{,1} = -a_{2323}N_{2,3}^{211} \quad (12.11)$$

The definition (12.11) uses the idea of the conjugate functions (Sedov, 1971). The existence of the function $\varphi(x, z)$ follows from the equality

$$\varphi_{,31} = (a_{2121}(x, z)(N_{2,1}^{211} - z))_{,1} + (a_{2323}(x, z)N_{2,3}^{211})_{,3} = 0,$$

which is the consequence of (12.10).

Express $N_2^{211}(x, z)$ from (12.11)

$$N_{2,1}^{211} = \frac{1}{a_{2121}}\varphi_{,3} + z, \quad N_{2,3}^{211} = -\frac{1}{a_{2121}}\varphi_{,1}. \quad (12.12)$$

Differentiation of (12.12) yields

$$0 = N_{2,13}^{211} - N_{2,31}^{211} = \left(\frac{1}{a_{2121}}\varphi_{,3} + z \right)_{,3} + \left(\frac{1}{a_{2121}}\varphi_{,1} \right)_{,1}.$$

Grouping the terms in the last equation, we arrive at the following Poisson equation:

$$\Delta\varphi = a_{2121}. \quad (12.13)$$

Consider the boundary conditions on the top and the bottom boundaries Γ^+, Γ^- and the holes H_i (12.6). With the use of the function $\varphi(x, z)$, these conditions can be written as follows:

$$(a_{2121}N_{2,1}^{21v} - a_{2121})n_1 + a_{2323}N_{2,3}^{21v}n_3 = \varphi_{,3}n_1 - \varphi_{,1}n_3 = \frac{\partial\varphi}{\partial s} = 0 \quad \text{on } \Gamma^+, \Gamma^- \text{ or } H_i, \quad (12.14)$$

where $\partial/\partial s$ is the derivative along the boundary Γ^+, Γ^- or H_i . In view of (12.14), the function $\varphi(x, z)$ is constant on the top and bottom boundaries Γ^+, Γ^- and H_i :

$$\varphi = \text{const} \quad \text{on } \Gamma^+, \Gamma^-, H_i. \quad (12.15)$$

Without loss of generality, we can fix one constant. Let us assume that at the bottom boundary Γ^- , $\varphi(x, z) = 0$.

Integrating the first equation in (12.11) over S_i , see Fig. 12.1b, we can have

$$\varphi(h, -L) = \varphi(-h, -L) + \int_{-h}^h a_{2121}(N_{2,1}^{211} - z)dz. \quad (12.16)$$

The asymmetric (out-of-plane) stiffness

$$S_{2121}^1 = \frac{1}{L} \int_P a_{2121} (N_{2,1}^{211} - z) dx dz.$$

Multiplying the differential equation in (12.10) by x and integrating by parts, we have

$$\int_P a_{2121} (N_{2,1}^{211} - z) dx dz = 2 \frac{L}{2} \int_{-h}^h a_{2121} (N_{2,1}^{211} dz - z) dx.$$

Then Eq. (12.16) becomes $\varphi(h, -L) = \varphi(-h, -L) + S_{2121}$. We have assumed that $\varphi(x, z) = 0$ on the bottom boundary Γ^- , thus, $\varphi(-h, -L) = 0$. Then $\varphi(h, -L) = S_{2121}$ and $\varphi(x, z) = S_{2121}$ on the top boundary Γ^+ . As a result, we arrive at the following boundary value problem:

$$\begin{cases} \Delta \varphi = a_{2121} & \text{in } P_0, \\ \varphi = 0 & \text{on } \Gamma^-, \quad \varphi = S_{2121}^1 & \text{on } \Gamma^+, \quad \varphi = C_1 & \text{on } H_i, \\ \varphi(x, z) & \text{periodic in } x \in [-L, L]. \end{cases} \quad (12.17)$$

The local stresses are expressed in the form

$$\sigma_{ij} = a_{ij2\alpha} N_{2,\alpha}^{211} + a_{ij21} z = \frac{a_{ij21}}{a_{2121}} (\varphi_{,3} - \varphi_{,1}) \quad (12.18)$$

and the homogenized torsion stiffness is expressed in the form

$$S_{2121}^2 = - \langle \varphi_{,3} - \varphi_{,1} \rangle.$$

12.4 Problem 12.2 with Indices $i = \xi = 1, 3 = x, z$. Deformation in the Direction Perpendicular to the Fibers

In this case, $a_{\xi\alpha\alpha 2\beta}(\mathbf{y}) = 0$ and (12.3) takes the following form:

$$a_{i\alpha k\beta} N_{k,\beta}^{AB\mu}(\mathbf{y}) + a_{\xi\alpha 2\beta} z^\mu N_{2,\beta}^{AB\mu}(\mathbf{y}) + (-1)^\mu a_{\xi\alpha AB} z^\mu = a_{\xi\alpha\theta\beta} N_{\theta,\beta}^{AB\mu}(\mathbf{y}) + (-1)^\mu a_{\xi\alpha AB} z^\mu.$$

Here $AB = 11; 22; 12; 21; \alpha, \beta, \theta, \xi = 1, 3$. Then the PCP (12.2) takes the form

$$\begin{cases} (a_{\xi\alpha\theta\beta} N_{\theta,\beta}^{AB\mu} + (-1)^\mu a_{\xi\alpha AB} z^\mu)_{,\alpha} = 0 & \text{in } P, \\ (a_{\xi\alpha\theta\beta} N_{\theta,\beta}^{AB\mu} + (-1)^\mu a_{\xi\alpha AB} z^\mu) n_\alpha = 0 & \text{on } \Gamma \cup H, \\ (N_1^{AB\mu}, N_3^{AB\mu})(x, z) & \text{periodic in } x. \end{cases} \quad (12.19)$$

In the case under consideration elastic constants $a_{\xi\alpha 12} = 0$ and $a_{\xi\alpha 21} = 0$ for $i = \xi = 1, 3$, then $(N_1^{21\mu}, N_3^{21\mu} = N_1^{12\mu}, N_3^{12\mu} = 0$. The problem is non-trivial only for $AB = 11; 22$. Let us demonstrate the term $(-1)^\mu a_{\xi\alpha AB} z^\mu$ in (12.19) may be represented in

the form $(-1)^\mu a_{\xi\alpha AB} e_{\theta\beta}^{AB\mu}$ ($\delta = 2, 3$) with the strains $e_{\theta\beta}^{AB\mu} = v_{\theta\beta}^{AB\mu}$ ($\mu = 0, 1$):

$$a_{\xi\alpha AB}(x, z)z^\mu = a_{\xi\alpha\theta\beta}(x, z)e_{\theta\beta}^{AB\mu} \quad (12.20)$$

12.4.1 Index $AB = 22$. Tension-compression and Bending Along the Fibers (in the $0xz$ -plane)

The typical overall deformations of the PC are shown in Figs. 12.1c, d. In the case under consideration, Eq. (12.20) takes the form $a_{\xi\alpha\theta\beta}e_{\theta\beta} = a_{\xi\alpha 22}z^\mu$. Be written in the coordinate-wise form, it becomes

$$\begin{aligned} a_{1111}e_{11} + a_{1133}e_{33} &= -a_{1122}z^\mu, \\ a_{3311}e_{11} + a_{3333}e_{33} &= -a_{3322}z^\mu, \\ a_{1313}e_{13} = -a_{1322}z^\mu &= 0, a_{3131}e_{31} = -a_{3122}z^\mu = 0. \end{aligned} \quad (12.21)$$

Substituting into (12.21) the elastic constants (12.4), we obtain from the first two equations in the following system:

$$\begin{cases} (1-\nu)e_{11} + \nu e_{33} = -\nu(x, z)z^\mu, \\ \nu e_{11} + (1-\nu)e_{33} = -\nu(x, z)z^\mu. \end{cases} \quad (12.22)$$

Solution to (12.22) is

$$e_{11} = e_{33} = -\nu z^\mu. \quad (12.23)$$

In addition, $e_{13} = e_{31} = 0$. Then

$$\frac{\partial v_1}{\partial x} = -\nu z^\mu, \quad \frac{\partial v_3}{\partial z} = -\nu z^\mu, \quad \frac{\partial v_1}{\partial z} + \frac{\partial v_3}{\partial x} = 0. \quad (12.24)$$

The solution to (12.24) may be obtained in the explicit form. For $\mu = 0$ from the first two equations in (12.24), we have $v_1 = -\nu x + f(z)$ and $v_3 = -\nu z + g(x)$. Substituting into the third equation in (12.24), we have $f'(z) + g'(x) = 0$, then $f(z) = 0$ and $g(x) = 0$.

For $\mu = 1$, we have from (12.24) $v_1 = -\nu z x + f(z)$ and $v_3 = -\frac{\nu}{2}z^2 + g(x)$. Substituting into the third equation in (12.24), we arrive at $-\nu x + f'(z) + g'(x) = 0$, and obtain $f'(z) = 0$, $g'(x) = \nu x$. Then $f(z) = 0$ and $g(x) = \frac{\nu}{2}x^2$. Finally, we have

$$v_1^{22\mu} = \begin{cases} -\nu x & \text{if } \mu = 0, \\ -\nu z x & \text{if } \mu = 1, \end{cases} \quad v_3^{22\mu} = \begin{cases} -\nu z & \text{if } \mu = 0, \\ -\frac{\nu}{2}z^2 + \frac{\nu}{2}x^2 & \text{if } \mu = 1. \end{cases} \quad (12.25)$$

Introduce $(M_1^{AB\mu}, M_3^{AB\mu}), (N_1^{AB\mu}, N_3^{AB\mu}) + (v_1^{AB\mu}, v_3^{AB\mu})$. For $(M_1^{22\mu}, M_3^{22\mu})$, the third condition in (12.19) takes the form: $(M_1^{22\mu} - v_1^{22\mu}, M_3^{22\mu} - v_3^{22\mu})$ is periodic in x , or $[M_1^{22\mu}]_x = -\nu z^\mu [x]_x, [M_3^{22\mu}]_x = 0$ (the square brackets $[\dots]_x$ mean the difference of

the function on the opposite sides of the periodicity cell in the direction Ox). Here we use that

$$[v_1^{22\mu}]_x = \begin{cases} -v[x]_x & \text{if } \mu = 0, \\ -vz[x]_x & \text{if } \mu = 1, \end{cases} \quad v_3^{22\mu} = \begin{cases} 0 & \text{if } \mu = 0, \\ -\frac{v}{2}[x^2]_x = 0 & \text{if } \mu = 1 \end{cases}$$

and

$$N_1^{220} = M_1^{220} + vx, N_3^{220} = M_3^{220} + vx, N_1^{221} = M_1^{221} + vz, N_3^{2201} = M_3^{221} + v\frac{z^2}{2} - v\frac{x^2}{2}.$$

The problem (12.19) takes the form

$$\begin{cases} (a_{\xi\alpha\theta\beta}M_{\theta,\beta}^{22\nu})_{,\alpha} = 0 & \text{in } P, \\ (a_{\xi\alpha\theta\beta}M_{\theta,\beta}^{22\nu}n_\alpha = 0 & \text{on } \Gamma \cup H, \\ [M_1^{22\nu}]_x = -vz^\nu[x]_x, [M_3^{22\nu}]_x = 0. \end{cases} \quad (12.26)$$

The local stresses are computed with the formula

$$\sigma_{ij} = a_{ij21}M_{1,1}^{220} + a_{ij21}v + a_{ij23}M_{1,3}^{220} + a_{ij22} \quad (12.27)$$

for $\nu = 0$ - the tension along Ox -axis; and with the formula

$$\sigma_{ij} = a_{ij21}M_{1,1}^{221} + a_{ij21}vz + a_{ij23}M_{1,3}^{221} + a_{ij23}vz + a_{ij22}z \quad (12.28)$$

for $\nu = 1$ - the bending in Oxz -plane. The homogenized in-plane stiffnesses are computed with the formula

$$S_{ij22}^0 = \langle a_{ij21}M_{1,1}^{220} + a_{ij21}v + a_{ij23}M_{1,3}^{220} + a_{ij22} \rangle \quad (12.29)$$

and the homogenized bending/torsion stiffnesses are computed with the formula

$$S_{ij22}^2 = \langle (a_{ij21}M_{1,1}^{221} + a_{ij21}vz + a_{ij23}M_{1,3}^{221} + a_{ij22})z \rangle.$$

12.4.2 Index $AB = 11$. Tension-compression and Bending Perpendicular to the Fibers (in the Oyz -plane)

In this case, Eq. (12.20) takes the form $a_{\xi\alpha\theta\beta}e_{\theta\beta} = a_{\xi\xi\alpha 11}z^\nu$ or, in the coordinate-wise form

$$\begin{aligned} a_{1111}e_{11} + a_{1133}e_{33} &= -a_{1111}z^\mu, \\ a_{3311}e_{11} + a_{3333}e_{33} &= -a_{3311}z^\mu, \\ a_{1313}e_{13} &= -a_{1311}z^\mu = 0, a_{3131}e_{31} = -a_{3111}z^\mu = 0. \end{aligned} \quad (12.30)$$

Writing in (12.30) the elastic tensor components in the terms of Young's modulus and Poisson ratio, see (12.4), we obtain from the first two equations in (12.30) the

following system of equations:

$$\begin{aligned}(1 - \nu)e_{11} + \nu e_{33} &= -(1 - \nu)z^\mu, \\ \nu e_{11} + (1 - \nu)e_{33} &= -\nu z^\mu.\end{aligned}$$

The solution to this system is $e_{11} = -z\nu, e_{33} = 0$. Taking into account that $e_{13} = e_{31} = 0$, we arrive at

$$\frac{\partial v_1}{\partial x} = -z^\mu, \quad \frac{\partial v_3}{\partial z} = 0, \quad \frac{\partial v_1}{\partial z} + \frac{\partial v_3}{\partial x} = 0. \quad (12.31)$$

The problem (12.31) may be solved in the explicit form. For $\mu = 0$, from the first two equations in (12.22), we have $v_1 = -x + f(z)$ and $v_3 = g(x)$. Substituting into the third equation in (12.22), we arrive at $f'(z) + g'(x) = 0$, then $f(z) = 0$ and $g(x) = 0$. For $\mu = 1$, we have $v_1 = -zx + f(z)$ and $v_3 = g(x)$. Substituting into the third equation in (12.22), we arrive at $-x + f'(z) + g'(x) = 0$, and obtain $f'(z) = 0, g'(x) = \nu x$. Then $f(z) = 0$ and $g(x) = \frac{x^2}{2}$. Finally,

$$v_1^{11} = z^\mu x, \quad v_3^{11} = \mu z^{\mu-1} \frac{x^2}{2} = \frac{x^2}{2} \begin{cases} 0 & \text{if } \mu = 0, \\ 1 & \text{if } \mu = 1. \end{cases} \quad (12.32)$$

The third condition for $(M_1^{11\nu}, M_3^{11\nu})$ in (12.19) takes the form: $(M_1^{11\nu} - \nu_1^{11}, M_3^{11\nu} - \nu_2^{11},)$ periodic in x . With regard to (12.32), it can be written as $[M_1^{11\nu}]_x = -\nu z^\mu [x]_x, [M_3^{11\nu}]_x = 0$. Then (12.19) takes the form

$$\begin{cases} (a_{\xi\alpha\theta\beta} M_{\theta,\beta}^{11\nu})_{,\alpha} = 0 & \text{in } P, \\ (a_{\xi\alpha\theta\beta} M_{\theta,\beta}^{11\nu} n_\alpha = 0 & \text{on } \Gamma \cup H, \\ [M_1^{11\nu}]_x = -\nu z^\nu [x]_x, [M_3^{11\nu}]_x = 0. \end{cases} \quad (12.33)$$

The boundary displacements in (12.33) are similar to one displayed in Fig. 12.1d.

12.4.3 Index $AB = 12, 21$. Shift/Torsion Perpendicular to the Fibers (in the Oyz -plane)

For $AB = 12$, Eq. (12.20) takes the form $a_{\xi\alpha\theta\beta} e_{\theta\beta} = a_{\xi\alpha 12} z^\nu = 0, \xi, \alpha = 1, 3$. Its solution is $e_{\theta\beta} = 0$. Then $\nu_1^{12} = \nu_3^{12} = 0$ and solution to (12.19) is $(M_1^{12\nu}, M_3^{12\nu}) = 0$. The non-trivial $M_2^{21\nu} \neq 0$ was discussed in Sect. 12.2.

12.5 Numerical Solutions

We present numerical solutions to several PCPs. In our computations Young's modulus $E_b = 2$ GPa and Poisson's ratio $\nu_b = 0.36$. The periodicity cell dimensions are

$h_1 = 1.1, h_2 = 2, h_3 = 1.1, h = 0.1$ and $2H = 0.1$. The radius of the fiber is 0.45. These values are indicated in the non-dimensional "fast" variables y . The corresponding actual dimensional values are computed by multiplying by the characteristic size ε . The programs we developed by using the APDL programming language of the ANSYS FEM software (Thompson and Thompson, 2017). The finite elements PLANE183 are used for the fibers and the matrix, the characteristic size of the finite elements is 0.03. The total number of finite elements is about 11000.

12.5.1 The Boundary Layers

The deformed PC and the local von Mises stress are displayed in Fig. 12.2. Figure 12.2a corresponds to the tension in $0x$ -direction and Fig. 12.2b corresponds to the bending. The boundary layers at the top and the bottom surfaces of the PC are seen. The boundary layer thickness is less the thickness of one structural layer $2R + h$ (diameter of hole + surrounding material). In the core of plate the solution is periodic in the in-plane tension/shift modes. In the bending/torsion mode, the solution in the core of plate coincides with solution in the plate of "infinite" thickness Grigolyuk et al (1991).

If the plate is thick, these boundary layers do not influence the effective stiffness of the plate. But the boundary layers do influence the local SSS in the plate of any thickness. In particular, the boundary layers influence the strength of the plate. In the tension mode, the maximum von Mises stress $\sigma_{vM} = 0.196 \cdot 10^9$ in the core of the plate occurs between the holes, see Fig. 12.2a. The maximum von Mises stress in the boundary layer is $\sigma_{vM} = 0.252 \cdot 10^9$. The ratio of the maxima is 1.29.

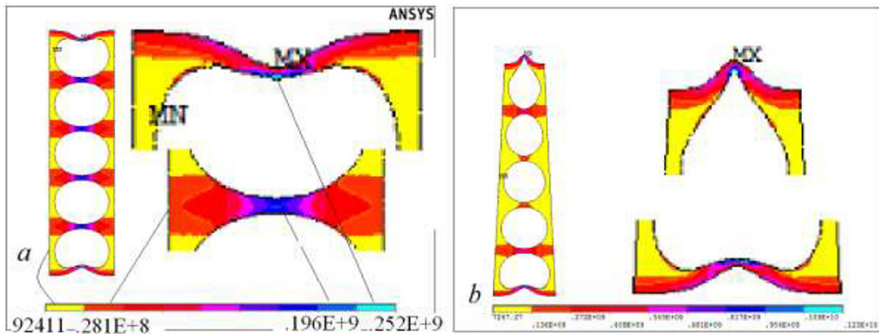


Fig. 12.2 5-hole PC and the top and the bottom surfaces of the PC (zoomed): a - tension and b - bending modes.

12.5.2 Wrinkling of the Top and Bottom Surfaces of the Plate

Figure 12.2 displays the top and bottom surfaces of the plate with channel cuts subjected to the overall tension - Fig. 12.2a, the overall bending - Fig. 12.2b. It is seen that the top and bottom surfaces are not flat in the case of the tension and not cylindrical in the case of bending. They are wavy. This is the wrinkling effect. The amplitude and period of the wrinkling are small (have the order of the PC dimension) but the corresponding change of the total length of the surfaces is not small. The wrinkling never occurs in the homogeneous or in the laminated plates. For the homogeneous or laminated plates, top and bottom surfaces are flat in the case of the tension and cylindrical in the case of bending.

12.6 The Macroscopic SSS of General Form

Solutions to a partial PCP corresponds to the basis macroscopic SSS: $e_{AB}^\nu = \delta_{AB}$, where δ_{AB} is Kronecker delta. For plate, we distinguish six basic macroscopic SSSs: two in-plane tensions and shift e_{AB}^0 , and two bending and torsion ρ_{AB} . In accordance with the homogenization theory (Caillerie, 1984; Kohn and Vogelius, 1984), the local strains are computed as

$$e_{kl} = [\delta_k^A \delta_l^B + N_{k,l}^{AB0}(x, z)]e_{AB}^0 + [-\delta_k^A \delta_l^B z + N_{k,l}^{AB1}(x, z)]\rho_{AB},$$

and the local stresses are computed as

$$\sigma_{ij} = [a_{ijAB}(x, z) + a_{ijAB}(x, z)N_{k,l}^{AB0}]e_{AB}^0 + [-a_{ijAB}(x, z)z + a_{ijAB}(x, z)N_{k,l}^{AB1}]\rho_{AB}.$$

These formulas may be used for prospective analysis of the behavior of plates of unidirectional structures subjected to the macroscopic SSS $\{e_{AB}^0, e_{AB}^1\}$ of general form, for example, the investigation of the strength of such kind plates.

12.7 Conclusions

The original 3D PCP (12.1) is reduced to several 2D boundary-value problems. The boundary-value problems for Laplace (12.9) and Poisson (12.17) equations correspond to the anti-plane elasticity problems. The boundary-value problems (12.26) and (12.33) are the planar elasticity problems.

The obtained 2D problems may be analyzed numerically with high accuracy. Our numerical solutions demonstrate the existence of boundary layers near the top and the bottom surfaces of PC. The boundary layer thickness is less the thickness of one structural. The wrinkling effect takes place for the plates with a system of tunnel cuts.

References

- Andrianov IV, Danishevskyy VV, Weichert D (2011) Boundary layers in fibre composite materials. *Acta Mechanica* 216(1):3–15
- Caillerie D (1984) Thin elastic and periodic plates. *Mathematical Methods in the Applied Sciences* 6(1):159–191
- Cioranescu D, Donato P (1999) *An Introduction to Homogenization*. Oxford University Press, Oxford
- Cioranescu D, Paulin JSJ (1979) Homogenization in open sets with holes. *Journal of Mathematical Analysis and Applications* 71(2):590–607
- Cioranescu D, Damlamian A, Griso G (2018) *The Periodic Unfolding Method*, Series in Contemporary Mathematics, vol 3, Springer, Singapore, chap Homogenization in perforated domains, pp 199–235
- Drygaś P, Gluzman S, Mityushev V, Nawalaniec W (2020) *Applied Analysis of Composite Media Analytical and Computational Results for Materials Scientists and Engineers*. Elsevier, Amsterdam
- van Dyke M (1994) Nineteenth-century roots of the boundary-layer idea. *SIAM Review* 36(3):415–424
- Grigolyuk EI, Fil'shtinskij LA (1992) *Periodic Piecewise Homogeneous Elastic Structures* (in Russ.). Nauka, Moscow
- Grigolyuk EI, Kovalev YD, Fil'shtinskii LA (1991) Bending of a layer weakened by through tunnel cuts. *Doklady Akademii Nauk SSSR* 317(1):51–53
- Kalamkarov AL, Kolpakov AG (1997) *Analysis, Design and Optimization of Composite Structures*. Wiley, Chichester
- Kohn RV, Vogelius M (1984) A new model for thin plates with rapidly varying thickness. *International Journal of Solids and Structures* 20(4):333–350
- Kolpakov AA, Kolpakov AG (2009) *Capacity and Transport in Contrast Composite Structures: Asymptotic Analysis and Applications*. CRC Press, Boca Raton, FL
- Love AEH (2013) *A treatise on the Mathematical Theory of Elasticity*. Cambridge University Press, Cambridge
- Lu JK (1995) *Complex Variable Methods in Plane Elasticity*. World Scientific, Singapore
- Mityushev V, Rogozin SV (2000) *Constructive Methods for Linear and Nonlinear Boundary Value Problems of Analytic Function Theory*. Chapman & Hall/CRC, Boca Raton, FL
- Pipes RB, Pagano N (1970) Interlaminar stresses in composite laminates under uniform axial extension. *Journal of Composite Materials* 4(4):538–548
- Sedov LI (1971) *A Course in Continuum Mechanics*. Wolters-Noordhoff
- Sendeckyj GP (1974) *Mechanics of Composite Materials*, vol 2, Academic Press, New York, London, chap Elastic behavior of composites, pp 45–83
- Thompson MK, Thompson JM (2017) *ANSYS Mechanical APDL for Finite Element Analysis*. Butterworth-Heinemann, Oxford



Chapter 13

Topological Optimization of Multilayer Structural Elements of MEMS/NEMS Resonators with an Adhesive Layer Subjected to Mechanical Loads

Anton V. Krysko, Jan Awrejcewicz, Pavel V. Dunchenkin, Maxim V. Zhigalov, and Vadim A. Krysko

Abstract The paper considers the problem of topological optimization of multilayer structural elements of MEMS/NEMS resonators with an adhesive layer under the action of mechanical loads. The purpose of this work is to obtain a design solution that is least susceptible to destruction due to an increase in the rigidity of the elements to be joined and, as a consequence, providing smoothing of stress peaks in the adhesive layer. To demonstrate the operation of the topological optimization algorithm for this class of problems, several examples are given that show significant improvements in the set target indicators. The problems were solved by the finite element method with the application of the sliding asymptotes method.

Key words: Topological optimization, Shear stresses, Adhesive, Method of sliding asymptotes

13.1 Introduction

Adhesive bonding technology, alone or in combination with mechanical fastening, can significantly improve the mechanical performance of a structure, both in terms

Anton V. Krysko

Scientific and Educational Center of Department of Mathematics and Modelling, Saratov State Technical University, Politekhnikeskaya 77, Saratov 410054, Russian Federation
e-mail: antonkrysko@gmail.com

Jan Awrejcewicz

Department of Automation, Biomechanics and Mechatronics, Lodz University of Technology, 1/15 Stefanowskiego Str., 90-924 Łódź, Poland
e-mail: jan.awrejcewicz@p.lodz.pl

Pavel V. Dunchenkin · Maxim V. Zhigalov · Vadim A. Krysko

Department of Mathematics and Modelling, Saratov State Technical University, Politekhnikeskaya, 77, Saratov 410054, Russian Federation
e-mail: dunchenkin.pasha@yandex.ru, zhigalovm@ya.ru, tak@san.ru

of rigidity and in terms of strength and fatigue (Hart-Smith, 1982; Kelly, 2006; da Silva et al, 2018). Adhesive joints have advantages over alternative bonding methods (bolted or riveted), as they provide stress distribution over a wider area of the joints, minimal thermal effect (as opposed to welding), high rigidity and high strength-to-weight ratio. In addition, adhesives have better corrosion resistance as well as good damping performance. In contrast to the uneven distribution of loads when joining fasteners, the transfer of load between glued or soldered components is continuous throughout the entire layer. This allows simpler and lighter connections to be used. In other words, the adhesive bond provides the ability to reduce the weight of the structure while providing mechanical strength. Based on this, such connections are increasingly used in the design of mechanical systems (Adams et al, 1997; Dixon, 2005; Watson, 2005).

Quite a lot of studies have been devoted to the problem of increasing the strength of adhesive joints. Most of them were based on parametric optimization, where it was assumed that the design variables were changed in a selected range using specified intervals Groth and Nordlund (1991); Hildebrand (1994); Rispler et al (2000); Taib et al (2006). For example, in da Silva et al (2011), such factors influencing the strength of the joint, as the adhesive properties of the material, the thickness of the intermediate layer, the contact area, and residual stresses, were determined.

In recent years, a number of works have been devoted to the problem of improving and researching structures with an adhesive layer, including research based on analytical formulations (Spaggiari and Dragoni, 2014; da Silva and Lopes, 2009), numerical modeling (Pires et al, 2003; Nimje and Panigrahi, 2014) or a combination of these two methods (das Neves et al, 2009; das Neves et al, 2009; Carbas et al, 2014). In all the studies considered, modifications were made to the shape of the elements to be joined or the shape and location of the adhesive layer.

Awrejcewicz et al (2020) developed a technique based on a combination of topological optimization methods (moving asymptotes method) and a finite element method for obtaining an optimal structure to reduce the stress level in a soldered joint. Krysko et al (2019) constructed a mathematical model and a technique for solving a wide class of problems of topological optimization of the adhesive layer under the action of both mechanical and thermal loads to obtain an optimal microstructure and gradient properties in order to reduce the stress level in it. It is shown that it is possible to achieve almost uniform shear stresses in the solder, arising due to the difference in the coefficients of linear thermal expansion. Krysko et al (2018) investigated the nonlinear dynamics of inhomogeneous beams with an optimal distribution of material over thickness and length. Comparison of static and dynamic results of optimal and homogeneous beams for different values of the scale parameter of material length and temperature was carried out. The influence of the scale parameter of the length of the material on the chaotic behavior of the beam was investigated. Scenarios of transition to chaos were constructed for various values of temperature, both for a homogeneous beam and for a beam with an optimal microstructure.

Zhu et al (2017) presented a systematic approach to the design of membrane structures for a piezoresistive pressure sensor using topology optimization. The

design problem was interpreted as the problem of optimizing a three-dimensional topology with calculated dependent loads, in which the dependence was considered due to the transferred loads. The topological optimization problem was solved using the popular SIMP (Solid Isotropic Material with Penalization) method.

A topological optimization method for a local resonator was presented in Jung et al (2020) to adapt flexural band gaps in plate structures. Topological optimization was performed with simulated annealing (SA) and using the finite element method. Numerical examples demonstrated the effectiveness of the presented method of creating a band gap at frequencies below 500 Hz. The above studies show that, under the action of mechanical loads, the destruction of structures occurs mainly due to peak stresses in the adhesive layer.

This paper poses the problem of topological optimization of the shape of the connected elements under the action of mechanical loads in order to obtain a design solution that is least susceptible to destruction. The solution was achieved by increasing the rigidity of the elements to be joined, which ensures the smoothing of stress peaks in the adhesive layer.

13.2 Statement of the Topological Optimization Problem

At present, the most widely used approaches to solving problems of topological optimization of structures are methods of explicit parameterization, which work on a fixed domain of finite elements; however, instead of a set of elastic properties of the microstructure, each finite element contains only one design variable. This variable is often understood as the density of the element material, ρ_e . To determine the defining characteristics of the material, one of the most well-known methods was chosen - the SIMP method. Power-law interpolation is used; in the case of setting the problem on a region containing a void and one phase of the material, it has the following form (Bendsøe and Sigmund, 2004)

$$E_e(\rho_e) = \rho_e^p; \quad 0 \leq \rho_{\min} \leq \rho_e \leq 1, \quad (13.1)$$

where ρ stands for amount of penalty. Design variable ρ is bounded from below by a small positive constant ρ_{\min} , which is introduced in order to prevent the degeneracy of the finite element matrix. Note that for the values $\rho_{\min} \leq \rho \leq 1$ and positive ρ , modulus $E_e(\rho_e)$ are limited to small value at density $\rho_e = \rho_{\min}$ and the value of Young modulus of the phase of the base material E_0 , for $\rho_e = 1$.

Here, the optimization problem relies on achieving a structure with maximum rigidity by modifying the structure of the elements connected by the adhesive layer while maintaining a given amount of modeling material. The redistribution of the material should ensure a decrease in stresses both in the elements to be joined and in the adhesive layer, which is the most susceptible to destruction.

Here, the algorithm minimizes strain energy W_s by increasing density in areas of higher sensitivity

$$\min \left(\frac{1}{W_{s0}} \int_{\Omega} W_s(x) d\Omega \right), \quad (13.2)$$

where: Ω - area of the structure under consideration, W_{s0} - normalizing factor. At the same time, restrictions on the amount of material used for modeling must be met in the area of solving the optimization problem

$$0 \leq \int_{\Omega} \rho_i(x) d\Omega_{\text{opt}} \leq \gamma_i A, \quad (13.3)$$

where: A - optimized area Ω_{opt} , γ - material volumetric ratio. To eliminate the checkerboard effect in the optimal structure, a penalty function is introduced in the form

$$\frac{h_0 h_{\max}}{A} \int_{\Omega} |\nabla \rho(x)|^2 d\Omega, \quad (13.4)$$

where: h_0 - initial grid size, which controls the size of the elements in the split, h_{\max} - the current size of the element at the given level. The penalty function is dimensionless and has a value of the order of unity for the worst possible solution. Dimensionless target function (13.2) and penalty function (13.4) must be consistent, for example, in the form of a linear combination (13.2) and (13.4) with a given parameter q , i.e. we have

$$f = \frac{1-q}{W_{s0}} \int_{\Omega} W(x) d\Omega + q \int_{\Omega} |\nabla \rho(x)|^2 d\Omega. \quad (13.5)$$

Below we will consider several examples for the problems of topological optimization of multilayer structures with an adhesive layer under the action of mechanical loads. The problems are solved by the finite element method, and linear triangular elements are used. The optimization algorithm is based on the sliding asymptote method.

13.3 Case Study 1

Consider a three-layer elastic structure, the dimensions and boundary conditions for which are shown in Fig. 13.1. Area Ω_1 filled with aluminium 2024-T3 with Young modulus equal to $E_1 = 73.1$ GPa, and Ω_2 stands for the area for solving the problem of topological optimization, in which it is necessary to find the optimal microstructure of the distribution of a given amount of aluminium 2024-T3, while Ω_3 is the area of evenly distributed adhesive FM73-M solder with $E_2 = 2260$ MPa. Mechanical load acting on the right $F = 100 \frac{\text{kN}}{\text{m}^2}$, the left border is fixed. The material data are taken from Mubashar et al (2011).

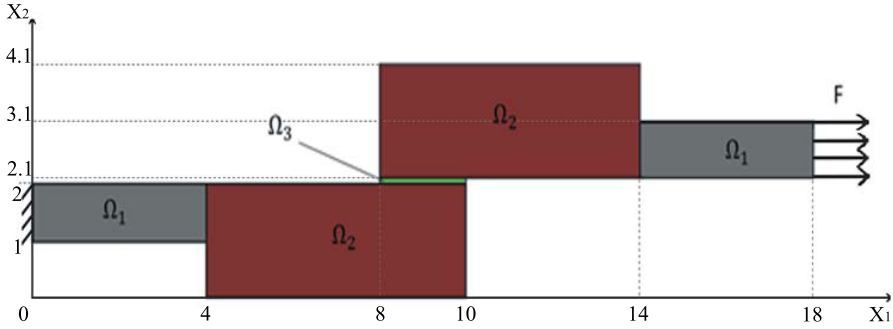


Fig. 13.1 Design and boundary conditions.

When overlapping, there are tears at the ends of the adhesive line. These inhomogeneities lead to bending moments due to eccentric loading as well as uneven distribution of moments around the adhesive layer. These moments create breaking stresses in the adhesive layer. Geometric rupture also creates high shear stresses in the adhesive. There are ways to reduce this eccentric load in lap joints. For example, it has been shown to be effective for this to taper the edges of the layers to be joined. A decrease in the maximum shear and peel stresses can be achieved by increasing the length of the joint, the thickness of the solder, and the thickness of the layers to be brazed. In this example, all geometrical and physical parameters of the solder remain constant, and a decrease in the maximum stress values at the ends of the solder is achieved due to the topological optimization of the microstructure of the layers to be joined.

Figure 13.2 shows three-layer constructions commonly found in practical applications (Fig. 13.2 (A, B)) and the optimal design obtained as a result of solving the problem of topological optimization (Fig. 13.2 (C)). The construction in Fig. 13.2 (B) features beveled corners of the elements to be joined, which is a classic engineering technique for reducing shear stresses. Note that the amount of duralumin and silver solder material in structures (Fig. 13.2 (A, B, C)) is the same, while solving the optimization problem, the coefficient γ should be taken equal to 0.5.

The Table 13.1 shows the numerical results: maximum values of von Mises stresses in the solder layer, maximum values of shear stresses in the solder layer, and total strain energy throughout the structure. For main stresses $\sigma_1, \sigma_2, \sigma_3$ the von Mises stress formula is defined as follows:

$$\sigma_{VM} = \frac{1}{\sqrt{2}} \sqrt{(\sigma_1 - \sigma_2)^2 + (\sigma_2 - \sigma_3)^2 + (\sigma_1 - \sigma_3)^2} \quad (13.6)$$

It can be seen from the table that when using the classical design option to reduce shear stresses (b), there is a slight improvement in this parameter. However, in terms of von Mises stresses σ_{VM} and deformation energy W_s this design is slightly inferior to the original one. For a topologically optimal design in solder, the maximum values

Fig. 13.2 Three-layer constructions (A, B, C) with an adhesive layer.

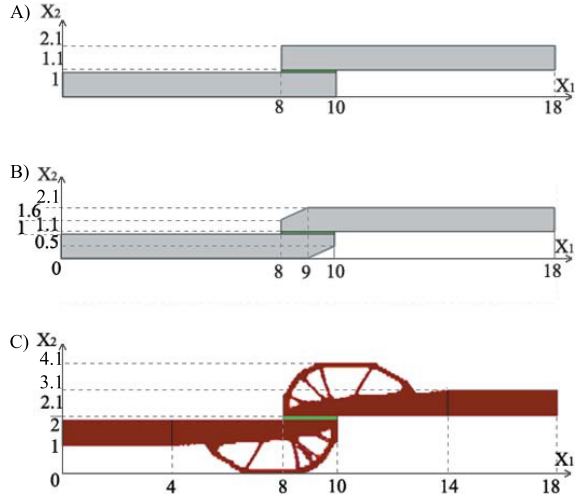


Table 13.1 Values of maximum stresses and strain energy.

| Construction | Maximum value of σ_{vM} (Pa) in the solder | Maximum shear stress (Pa) in the solder | Maximum shear stress W_s (Nm) by construction |
|--|---|---|---|
| Straight (original construction) (a) | 196620 | 97941 | 9118,3 |
| Bevel (Classic design for reducing shear stresses) (b) | 217390 | 93368 | 9383,9 |
| Topologically optimal design (c) | 100356 | 56308 | 456,0 |

are as σ_{vM} and the maximum values of shear stresses decrease by more than 2 times. The strain energy target for the entire structure has improved more than 20 times.

The graphs in Figs. 13.3, 13.4 show distribution σ_{vM} and shear stresses, respectively, in the adhesive layer for the cases of structures A, B, C. Here and further

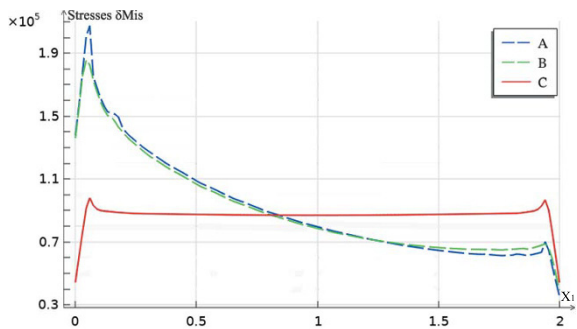
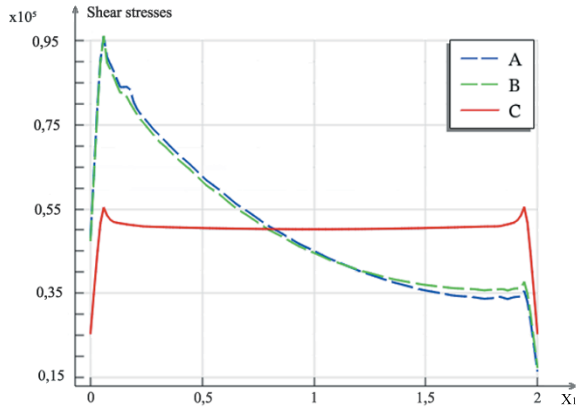


Fig. 13.3 Stresses σ_{vM} (Pa) for structures A, B, C.

Fig. 13.4 Shear stresses (Pa) for structures A, B, C.



in the work, the graphs are given for the coordinate axes passing through the center of the adhesive layer (as shown in Fig. 13.5). These plots confirm the previous conclusions, and also demonstrate the uniformity of stress distribution in the adhesive layer for a topologically optimal design.

13.4 Case Study 2

Consider the construction shown in Fig. 13.6 having two uniform overlapping adhesive joints. The physical properties of the materials are similar to the previous case.

Problems were solved for four different cases of load action:

- Symmetrical action of loads on the top and bottom of the structure $F = 100 \frac{\text{kN}}{\text{m}^2}$;
- Symmetrical action of loads on the top and bottom of the structure $F = 150 \frac{\text{kN}}{\text{m}^2}$;

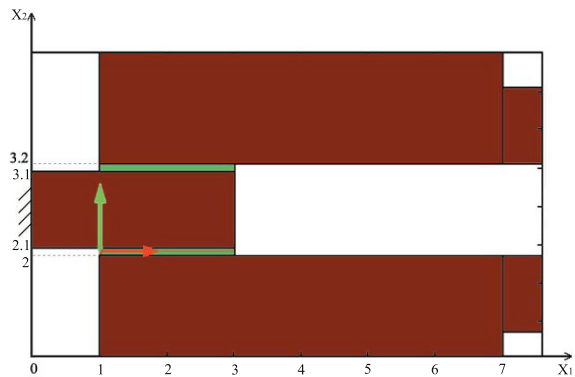
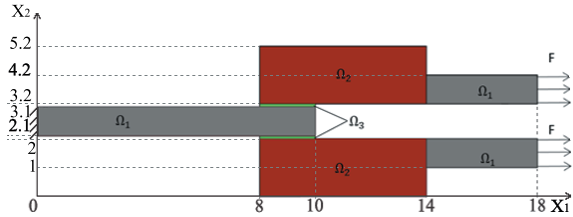


Fig. 13.5 Location of coordinate axes for graphs.

Fig. 13.6 Construction and boundary conditions.



- Load on the top of the structure $F = 100 \frac{\text{kN}}{\text{m}^2}$, to the bottom $F = 150 \frac{\text{kN}}{\text{m}^2}$;
- Load on the top of the structure $F = 100 \frac{\text{kN}}{\text{m}^2}$, to the bottom $F = 200 \frac{\text{kN}}{\text{m}^2}$.

Table 13.2 shows the numerical results for each of these load cases. Figure 13.7 shows the optimal topology of structures under symmetric loading (cases 1, 2). The optimal topologies of structures for different load intensities are almost identical, however, with a stronger impact (case 2), the result has a finer structure, which can be explained by the higher sensitivity of the objective function.

The graphs in Figs. 13.8 and 13.9 show the distribution σ_{vM} and shear stress for load case 2 at the center of the upper adhesive layer. In the case of a symmetric action of loads, the distribution graphs are symmetrical, but have different signs.

For example, in Fig. 13.10 the optimal topology of the structure with an asymmetric action of loads, for the case of loading 3, is reported.

Table 13.2 Numerical results for different loading cases.

| Load case | Construction | Adhesive layer | Maximum σ_{vM} (Pa) in the solder | Maximum shear stress (Pa) in the solder | Integral von Mises stress (Pa) over the solder area | W_s (Nm) designs |
|-------------|--------------|----------------|--|---|---|--------------------|
| First case | elementary | - | 134870 | 62601 | 17892 | 4019,7 |
| | optimized | - | 98299 | 56604 | 17423 | 961,6 |
| Second case | elementary | - | 202310 | 93902 | 26838 | 9044,3 |
| | optimized | - | 147390 | 84884 | 26137 | 2164,4 |
| Third case | elementary | top | 120030 | 53499 | 17931 | 8298,9 |
| | | bottom | 237550 | 109640 | 26837 | |
| | optimized | top | 98824 | 56968 | 17455 | 1552,6 |
| | | bottom | 147190 | 84827 | 26093 | |
| Fourth case | elementary | top | 132430 | 58057 | 18016 | 17117,0 |
| | | bottom | 340430 | 156390 | 35795 | |
| | optimized | top | 99920 | 56914 | 52145 | 4722,2 |
| | | bottom | 296110 | 17046 | 17553 | |

Fig. 13.7 Optimal topologies for two load cases.

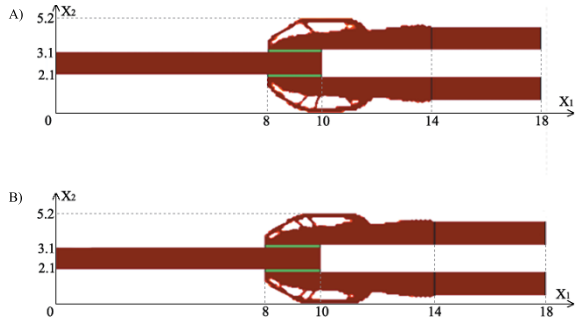


Fig. 13.8 Shear stress (Pa) along the central axis of the solder region for loading case 2 (A - not optimal, B - optimal).

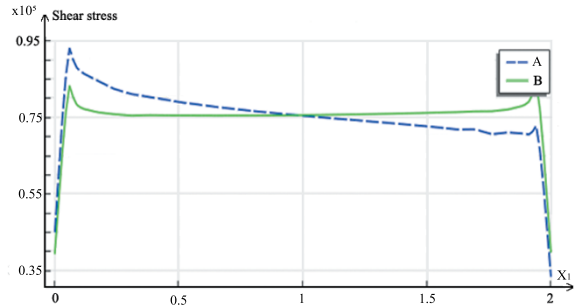


Fig. 13.9 Von Mises stress (Pa) along the central axis of the solder region for loading case 2 (A - not optimal, B - optimal).

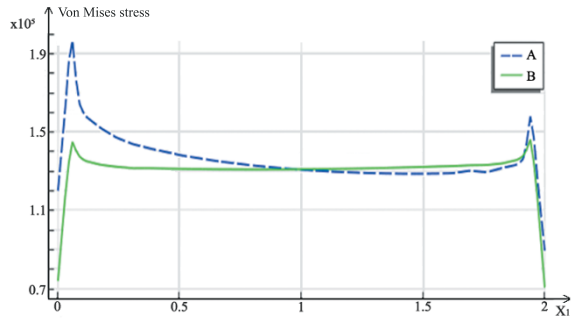
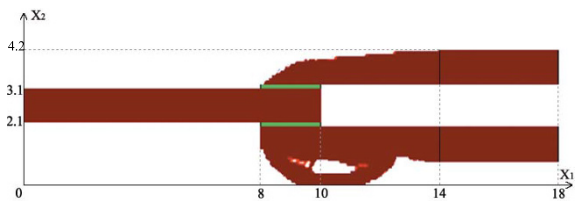


Fig. 13.10 Optimal topology with asymmetric loads.



In Figs. 13.11 and 13.12 shear stresses along the central axis of the region of the solder for the case of loading 3 along the upper and lower layers of the adhesive are shown.

For optimal structures, the stresses in all cases are distributed almost evenly, in contrast to the original structures. The optimization process makes it possible to reduce the stress drops for both symmetrical action of loads and for different intensities of loads in different parts of the structure.

13.5 Concluding Remarks

In this paper, the topological optimization algorithm was used to optimize sandwich structures with an adhesive layer under the action of mechanical loads in order to reduce peak stresses. The results show that the obtained optimal structures significantly reduce the peak shear and von Mises stresses in the solder layer in comparison with other common engineering solutions for this class of problems.

As a result of solving the problem of topological optimization, a design solution was obtained that is least susceptible to destruction due to an increase in the rigidity of the elements being connected and, as a consequence, provides smoothing of stress

Fig. 13.11 Shear stress (Pa) along the central axis of the solder region for the case of loading 3 (A - not optimal, B - optimal) along the upper layer.

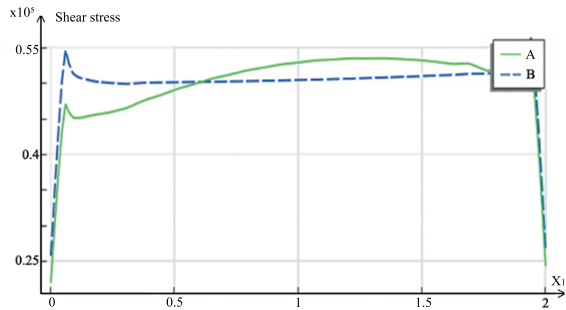
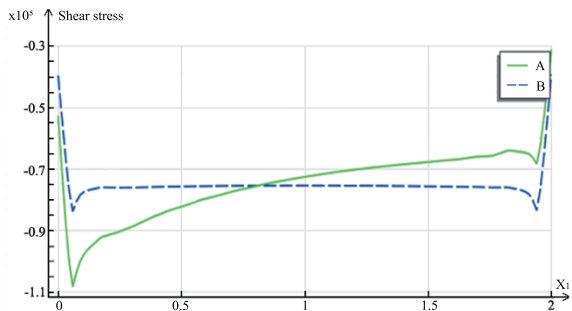


Fig. 13.12 Shear stress (Pa) along the central axis of the solder region for loading case 3 (A - not optimal, B - optimal) along the bottom layer.



peaks in the adhesive layer. This was achieved by modifying the optimization area with the same amount of material.

Acknowledgements This work was supported by the Russian Science Foundation (Grant No. 19-19-00215).

References

- Adams RD, Comyn J, Wake WC (1997) *Structural Adhesive Joints in Engineering*. Springer Netherlands
- Awrejcewicz J, Pavlov SP, Krysko AV, Zhigalov MV, Bodyagina KS, Krysko VA (2020) Decreasing shear stresses of the solder joints for mechanical and thermal loads by topological optimization. *Materials* 13(8):1862
- Bendsøe MP, Sigmund O (2004) *Topology Optimization: Theory, Methods and Applications*. Springer, Berlin, Heidelberg
- Carbas RJC, da Silva LFM, Madureira ML, Critchlow GW (2014) Modelling of functionally graded adhesive joints. *The Journal of Adhesion* 90(8):698–716
- da Silva LFM, Lopes MJCQ (2009) Joint strength optimization by the mixed-adhesive technique. *International Journal of Adhesion and Adhesives* 29(5):509–514
- das Neves PJC, da Silva LFM, Adams RD (2009) Analysis of mixed adhesive bonded joints. Part I: Theoretical formulation. *Journal of Adhesion Science and Technology* 23(1):1–34
- Dixon DG (2005) Aerospace applications of adhesives. In: Packham DE (ed) *Handbook of Adhesion*, 2nd ed., John Wiley & Sons, Chichester, pp 40–42
- Groth HL, Nordlund P (1991) Shape optimization of bonded joints. *International Journal of Adhesion and Adhesives* 11(4):204–212
- Hart-Smith LJ (1982) Design methodology for bonded-bolted composite joints. Technical Report AFWAL-TR-81-3154, Douglas Aircraft Company, Long Beach, California
- Hildebrand M (1994) Non-linear analysis and optimization of adhesively bonded single lap joints between fibre-reinforced plastics and metals. *International Journal of Adhesion and Adhesives* 14(4):261–267
- Jung J, Goo S, Kook J (2020) Design of a local resonator using topology optimization to tailor bandgaps in plate structures. *Materials & Design* 191:108,627
- Kelly G (2006) Quasi-static strength and fatigue life of hybrid (bonded/bolted) composite single-lap joints. *Composite Structures* 72(1):119–129
- Krysko AV, Awrejcewicz J, Pavlov SP, Bodyagina KS, Zhigalov MV, Krysko VA (2018) Non-linear dynamics of size-dependent Euler–Bernoulli beams with topologically optimized microstructure and subjected to temperature field. *International Journal of Non-Linear Mechanics* 104:75–86
- Krysko AV, Awrejcewicz J, Pavlov SP, Bodyagina KS, Krysko VA (2019) Topological optimization of thermoelastic composites with maximized stiffness and heat transfer. *Composites Part B: Engineering* 158:319–327
- Mubashar A, Ashcroft I, Critchlow G, Crocombe A (2011) Strength prediction of adhesive joints after cyclic moisture conditioning using a cohesive zone model. *Engineering Fracture Mechanics* 78(16):2746–2760
- das Neves PJC, da Silva LFM, Adams RD (2009) Analysis of mixed adhesive bonded joints. Part II: Parametric study. *Journal of Adhesion Science and Technology* 23(1):35–61
- Nimje SV, Panigrahi SK (2014) Numerical simulation for stress and failure of functionally graded adhesively bonded tee joint of laminated frp composite plates. *International Journal of Adhesion and Adhesives* 48:139–149

- Pires I, Quintino L, Durodola JF, Beevers A (2003) Performance of bi-adhesive bonded aluminium lap joints. *International Journal of Adhesion and Adhesives* 23(3):215–223
- Rispler AR, Tong L, Steven GP, Wisnom MR (2000) Shape optimisation of adhesive fillets. *International Journal of Adhesion and Adhesives* 20(3):221–231
- da Silva LFM, Öchsner A, Adams RD (eds) (2011) *Handbook of Adhesion Technology*. Springer, Berlin, Heidelberg
- da Silva LFM, Öchsner A, Adams RD (eds) (2018) *Handbook of Adhesion Technology*, 2nd edn. Springer, Heidelberg
- Spaggiari A, Dragoni E (2014) Regularization of torsional stresses in tubular lap bonded joints by means of functionally graded adhesives. *International Journal of Adhesion and Adhesives* 53:23–28
- Taib AA, Boukhili R, Achiou S, Gordon S, Boukehili H (2006) Bonded joints with composite adherends. Part I. Effect of specimen configuration, adhesive thickness, spew fillet and adherend stiffness on fracture. *International Journal of Adhesion and Adhesives* 26(4):226–236
- Watson C (2005) Engineering design with adhesives. In: Packham DE (ed) *Handbook of Adhesion*, 2nd ed., John Wiley & Sons, Chichester, pp 138–143
- Zhu B, Zhang X, Zhang Y, Fatikow S (2017) Design of diaphragm structure for piezoresistive pressure sensor using topology optimization. *Structural and Multidisciplinary Optimization* 55(1):317–329



Chapter 14

Forced Vibration Analysis of Laminated Piezoelectric Plates by a Strong Sampling Surfaces Formulation

Gennady M. Kulikov and Svetlana V. Plotnikova

Abstract This paper focuses on implementation of the sampling surfaces (SaS) method for the 3D vibration analysis of laminated piezoelectric plates. The SaS formulation is based on choosing inside the layers the arbitrary number of SaS parallel to the middle surface to introduce the displacements and electric potentials of these surfaces as basic plate variables. Such choice of unknowns allows the presentation of the laminated piezoelectric plate formulation in a very compact form. The feature of the proposed approach is that all SaS are located inside the layers at Chebyshev polynomial nodes that improves the convergence of the SaS method significantly. The use of outer surfaces and interfaces is avoided that makes possible to minimize uniformly the error due to Lagrange interpolation. Therefore, the strong SaS formulation based on direct integration of the equations of motion and the charge equation can be applied efficiently to the obtaining of exact solutions for laminated piezoelectric plates, which asymptotically approach the 3D solutions of piezoelectricity as the number of SaS tends to infinity.

Key words: Piezoelectricity, 3D vibration analysis, Laminated piezoelectric plate, Sampling surfaces method

14.1 Introduction

The exact vibration analysis of laminated piezoelectric plates was first carried out by Heyliger and Brooks (1995); Heyliger and Saravanos (1995) using the Pagano approach. The most popular state space approach was utilized for the free vibration of simply supported electroelastic plates in Chen et al (1998); Haojiang et al

Gennady M. Kulikov · Svetlana V. Plotnikova
Laboratory of Intelligent Materials and Structures, Tambov State Technical University, Sovetskaya Street, 106, Tambov 392000, Russian Federation
e-mail: gmkulikov@mail.ru

(1999); Chen and Ding (2002); Deü and Benjeddou (2005); Zhong and Yu (2006). Messina and Carrera (2015) proposed to employ the transfer matrix method to solve the ordinary differential equations in terms of the displacements and electric potential derived from the system of partial differential equations through the separating variable procedure. The dynamic response of laminated piezoelectric plates by a Taylor series expansion through the thickness was studied in Gao et al (1998); Vel et al (2004); Baillargeon and Vel (2005). The sampling surfaces (SaS) approach was also used for the free vibration analysis of piezoelectric laminated plates (Kulikov and Plotnikova, 2017a).

The SaS method (Kulikov and Plotnikova, 2012) has been applied effectively to the 3D stress analysis of laminated piezoelectric structures by Kulikov and Plotnikova (2013a,b). According to this method, we choose the arbitrary number of SaS throughout the layers parallel to the middle surface and located at Chebyshev polynomial nodes in order to introduce the displacements and electric potentials of these surfaces as basic plate unknowns. Such choice of unknowns with the consequent use of Lagrange polynomials in the through-thickness distributions of displacements, strains, electric potential and electric field leads to a robust laminated piezoelectric plate formulation. The above works are based on the variational SaS formulation, which requires including the interfaces into a set of SaS. However, it is important to take all SaS located at Chebyshev polynomial nodes due to the convergence criterion (Bakhvalov, 1977).

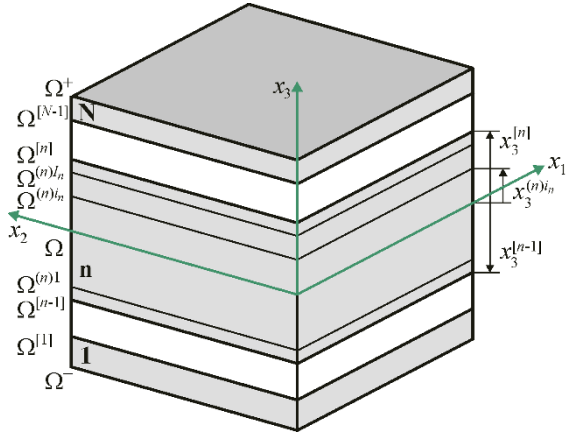
The present paper is intended to extend the variational SaS formulation for the free vibration of laminated piezoelectric plates (Kulikov and Plotnikova, 2017a) to the strong SaS formulation. The latter is based on the choice of all SaS inside the layers at Chebyshev polynomial nodes and direct integration of the equations of motion and the charge equation. The use of interfaces is avoided that allows one to minimize uniformly the error due to the higher-order Lagrange interpolation (Kulikov and Plotnikova, 2017b,c; Kulikov et al, 2017, 2019). Thus, the strong SaS formulation can be applied efficiently to the 3D vibration analysis of piezolaminated plates.

14.2 Basic Assumptions

Consider a laminated piezoelectric plate of the thickness h . Let the middle surface Ω be described by Cartesian coordinates x_1 and x_2 . The coordinate x_3 is oriented in the thickness direction. According to the SaS concept, we choose inside the n th layer I_n SaS $\Omega^{(n)1}, \Omega^{(n)2}, \dots, \Omega^{(n)I_n}$ parallel to the middle surface (see Fig. 14.1), where $n = 1, 2, \dots, N$; N is the number of layers and $I_n \geq 3$. The transverse coordinates of SaS of the n th layer located at Chebyshev polynomial nodes (roots of the Chebyshev polynomial of order I_n) are written as

$$x_3^{(n)i_n} = \frac{1}{2}(x_3^{[n-1]} + x_3^{[n]}) - \frac{1}{2}h_n \cos\left(\pi \frac{2i_n - 1}{2I_n}\right), \quad (14.1)$$

Fig. 14.1 Geometry of the laminated plate.



where $x_3^{[0]} = -h/2$, $x_3^{[N]} = h/2$; $x_3^{[m]}$ are the transverse coordinates of interfaces $\Omega^{[m]}$; $h_n = x_3^{[n]} - x_3^{[n-1]}$ is the thickness of the n th layer; the index $m = 1, 2, \dots, N - 1$ identifies the belonging of any quantity to the interface; the indices $i_n, j_n = 1, 2, \dots, I_n$ identify the belonging of any quantity to the SaS of the n th layer.

The through-thickness SaS approximations can be expressed as

$$[u_i^{(n)}, \varepsilon_{ij}^{(n)}, \sigma_{ij}^{(n)}, \varphi^{(n)}, E_i^{(n)}, D_i^{(n)}] = \tag{14.2}$$

$$\sum_{i_n} L^{(n)i_n} [u_i^{(n)i_n}, \varepsilon_{ij}^{(n)i_n}, \sigma_{ij}^{(n)i_n}, \varphi^{(n)i_n}, E_i^{(n)i_n}, D_i^{(n)i_n}],$$

where $u_i^{(n)}, \varepsilon_{ij}^{(n)}, \sigma_{ij}^{(n)}, \varphi^{(n)}, E_i^{(n)}, D_i^{(n)}$ are the displacements, strains, stresses, electric potential, electric field and electric displacements of the n th layer; $u_i^{(n)i_n}, \varepsilon_{ij}^{(n)i_n}, \sigma_{ij}^{(n)i_n}, \varphi^{(n)i_n}, E_i^{(n)i_n}, D_i^{(n)i_n}$ are the displacements, strains, stresses, electric potential, electric field and electric displacements of SaS of the n th layer $\Omega^{(n)i_n}$; $L^{(n)i_n}(x_3)$ are the Lagrange basis polynomials of degree $I_n - 1$ corresponding to the n th layer:

$$L^{(n)i_n} = \prod_{j_n \neq i_n} \frac{x_3 - x_3^{(n)j_n}}{x_3^{(n)i_n} - x_3^{(n)j_n}}. \tag{14.3}$$

14.3 Strong SAS Formulation

For simplicity, we consider the case of linear piezoelectric materials given by

$$\sigma_{ij}^{(n)} = C_{ijkl}^{(n)} \varepsilon_{kl}^{(n)} - e_{kij}^{(n)} E_k^{(n)}, \tag{14.4}$$

$$D_i^{(n)} = e_{ikl}^{(n)} \varepsilon_{kl}^{(n)} + \epsilon_{ik}^{(n)} E_k^{(n)}, \tag{14.5}$$

where $C_{ijkl}^{(n)}$, $e_{kij}^{(n)}$ and $\epsilon_{ik}^{(n)}$ are the elastic, piezoelectric and dielectric constants of the n th layer. Here, the summation on repeated Latin indices is implied.

The equations of motion and the charge equation of the laminated piezoelectric plate are written as

$$\sigma_{ij,j}^{(n)} = \rho_n \ddot{u}_i^{(n)}, \quad (14.6)$$

$$D_{i,i}^{(n)} = 0, \quad (14.7)$$

where ρ_n is the mass density of the n th layer; $\ddot{u}_i^{(n)}$ is the second order derivative of displacements with respect to time t ; the symbol $(\dots)_{,i}$ stands for the partial derivatives with respect to coordinates x_i .

The boundary conditions on bottom and top surfaces are defined as

$$u_i^{(1)}(-h/2) = w_i^- \text{ or } \sigma_{i3}^{(1)}(-h/2) = p_i^-, \quad \varphi^{(1)}(-h/2) = \phi^- \text{ or } D_3^{(1)}(-h/2) = Q^-, \quad (14.8)$$

$$u_i^{(N)}(h/2) = w_i^+ \text{ or } \sigma_{i3}^{(N)}(h/2) = p_i^+, \quad \varphi^{(N)}(h/2) = \phi^+ \text{ or } D_3^{(N)}(h/2) = Q^+, \quad (14.9)$$

where w_i^- , p_i^- , ϕ^- , Q^- and w_i^+ , p_i^+ , ϕ^+ , Q^+ are the prescribed displacements, surface tractions, electric potentials and electric charges at the bottom and top surfaces.

The continuity conditions at interfaces are

$$u_i^{(m)}(x_3^{[m]}) = u_i^{(m+1)}(x_3^{[m]}), \quad \sigma_{i3}^{(m)}(x_3^{[m]}) = \sigma_{i3}^{(m+1)}(x_3^{[m]}), \quad (14.10)$$

$$\varphi^{(m)}(x_3^{[m]}) = \varphi^{(m+1)}(x_3^{[m]}), \quad D_3^{(m)}(x_3^{[m]}) = D_3^{(m+1)}(x_3^{[m]}). \quad (14.11)$$

Satisfying equations of motion (14.6) and charge equation (14.7) at inner layer points $x_3^{(n)m_n}$ by using the SaS approximations (14.2), the following differential equations are obtained:

$$\sigma_{i1,1}^{(n)m_n} + \sigma_{i2,2}^{(n)m_n} + \sum_{i_n} M^{(n)i_n}(x_3^{(n)m_n}) \sigma_{i3}^{(n)i_n} = \rho_n \ddot{u}_i^{(n)m_n}, \quad (14.12)$$

$$D_{1,1}^{(n)m_n} + D_{2,2}^{(n)m_n} + \sum_{i_n} M^{(n)i_n}(x_3^{(n)m_n}) D_3^{(n)i_n} = 0, \quad (14.13)$$

where $M^{(n)i_n} = L_{,3}^{(n)i_n}$ are the derivatives of the Lagrange basis polynomials whose values at SaS $Q^{(n)m_n}$ are presented in Kulikov and Plotnikova (2013a,b); $m_n = 2, 3, \dots, I_n - 1$.

Next, we satisfy the boundary conditions on bottom and top surfaces

$$\sum_{i_1} L^{(1)i_1}(-h/2) u_i^{(1)i_1} = w_i^- \text{ or } \sum_{i_1} L^{(1)i_1}(-h/2) \sigma_{i3}^{(1)i_1} = p_i^-, \quad (14.14)$$

$$\sum_{i_1} L^{(1)i_1}(-h/2) \varphi^{(1)i_1} = \phi^- \text{ or } \sum_{i_1} L^{(1)i_1}(-h/2) D_3^{(1)i_1} = Q^-,$$

$$\sum_{i_N} L^{(N)i_N}(h/2) u_i^{(N)i_N} = w_i^+ \text{ or } \sum_{i_N} L^{(N)i_N}(h/2) \sigma_{i3}^{(N)i_N} = p_i^+, \quad (14.15)$$

$$\sum_{i_N} L^{(N)i_N}(h/2)\varphi^{(1)i_N} = \phi^+ \text{ or } \sum_{i_N} L^{(N)i_N}(h/2)D_3^{(N)i_N} = Q^+,$$

and the continuity conditions at interfaces

$$\begin{aligned} \sum_{i_m} L^{(m)i_m}(x_3^{[m]})u_i^{(m)i_m} &= \sum_{i_{m+1}} L^{(m+1)i_{m+1}}(x_3^{[m]})u_i^{(m+1)i_{m+1}}, \\ \sum_{i_m} L^{(m)i_m}(x_3^{[m]})\sigma_{i3}^{(m)i_m} &= \sum_{i_{m+1}} L^{(m+1)i_{m+1}}(x_3^{[m]})\sigma_{i3}^{(m+1)i_{m+1}}, \\ \sum_{i_m} L^{(m)i_m}(x_3^{[m]})\phi^{(m)i_m} &= \sum_{i_{m+1}} L^{(m+1)i_{m+1}}(x_3^{[m]})\phi^{(m+1)i_{m+1}}, \\ \sum_{i_m} L^{(m)i_m}(x_3^{[m]})D_3^{(m)i_m} &= \sum_{i_{m+1}} L^{(m+1)i_{m+1}}(x_3^{[m]})D_3^{(m+1)i_{m+1}}. \end{aligned} \quad (14.16)$$

Thus, the proposed strong SaS formulation deals with $4N_{\text{SaS}}$ governing equations (14.12)-(14.16) for obtaining the same number of SaS displacements $u_i^{(n)i_n}$ and SaS electric potentials $\varphi^{(n)i_n}$, where $N_{\text{SaS}} = I_1 + I_2 + \dots + I_N$ is the total number of SaS. These differential and algebraic equations have to be solved to describe the dynamic response of the laminated piezoelectric plate.

14.4 Free Vibrations of Simply Supported Piezoelectric Plates

In this section, we consider a laminated piezoelectric rectangular plate with simply supported edges. The boundary conditions on the edges are written as

$$\sigma_{11}^{(n)} = u_2^{(n)} = u_3^{(n)} = \varphi^{(n)} = 0 \text{ at } x_1 = 0 \text{ and } x_1 = a, \quad (14.17)$$

$$\sigma_{22}^{(n)} = u_1^{(n)} = u_3^{(n)} = \varphi^{(n)} = 0 \text{ at } x_2 = 0 \text{ and } x_2 = b,$$

where a and b are the length and width of the plate.

To satisfy boundary conditions (14.17), we seek the analytical solution of the problem in the following form:

$$\begin{aligned} u_1^{(n)i_n} &= u_{1rs}^{(n)i_n} e^{i\omega_{rs}t} \cos \bar{r}x_1 \sin \bar{s}x_2, & u_2^{(n)i_n} &= u_{2rs}^{(n)i_n} e^{i\omega_{rs}t} \sin \bar{r}x_1 \cos \bar{s}x_2, \\ u_3^{(n)i_n} &= u_{3rs}^{(n)i_n} e^{i\omega_{rs}t} \sin \bar{r}x_1 \sin \bar{s}x_2, & \varphi^{(n)i_n} &= \varphi_{rs}^{(n)i_n} e^{i\omega_{rs}t} \sin \bar{r}x_1 \sin \bar{s}x_2, \end{aligned} \quad (14.18)$$

where $\bar{r} = r\pi/a$, $\bar{s} = s\pi/b$; r and s are the half-wave numbers in x_1 and x_2 directions; $u_{irs}^{(n)i_n}$ and $\varphi_{rs}^{(n)i_n}$ are the amplitudes of displacements and electric potentials of SaS; ω_{rs} is the circular frequency; $i = \sqrt{-1}$ is the imaginary unit.

Using (14.18) in relations between the SaS variables (Kulikov and Plotnikova, 2017a), one finds

$$(\varepsilon_{11}^{(n)i_n}, \varepsilon_{22}^{(n)i_n}, \varepsilon_{33}^{(n)i_n}, \sigma_{11}^{(n)i_n}, \sigma_{22}^{(n)i_n}, \sigma_{33}^{(n)i_n}) =$$

$$\begin{aligned}
& (\varepsilon_{11rs}^{(n)i_n}, \varepsilon_{22rs}^{(n)i_n}, \varepsilon_{33rs}^{(n)i_n}, \sigma_{11rs}^{(n)i_n}, \sigma_{22rs}^{(n)i_n}, \sigma_{33rs}^{(n)i_n}) e^{i\omega_{rs}t} \sin \bar{r}x_1 \sin \bar{s}x_2, \\
& (E_3^{(n)i_n}, D_3^{(n)i_n}) = (E_{3rs}^{(n)i_n}, D_{3rs}^{(n)i_n}) e^{i\omega_{rs}t} \sin \bar{r}x_1 \sin \bar{s}x_2, \quad (14.19) \\
& (\varepsilon_{13}^{(n)i_n}, \sigma_{13}^{(n)i_n}, E_1^{(n)i_n}, D_1^{(n)i_n}) = (\varepsilon_{13rs}^{(n)i_n}, \sigma_{13rs}^{(n)i_n}, E_{1rs}^{(n)i_n}, D_{1rs}^{(n)i_n}) e^{i\omega_{rs}t} \cos \bar{r}x_1 \sin \bar{s}x_2, \\
& (\varepsilon_{23}^{(n)i_n}, \sigma_{23}^{(n)i_n}, E_2^{(n)i_n}, D_2^{(n)i_n}) = (\varepsilon_{23rs}^{(n)i_n}, \sigma_{23rs}^{(n)i_n}, E_{2rs}^{(n)i_n}, D_{2rs}^{(n)i_n}) e^{i\omega_{rs}t} \sin \bar{r}x_1 \cos \bar{s}x_2, \\
& (\varepsilon_{12}^{(n)i_n}, \sigma_{12}^{(n)i_n}) = (\varepsilon_{12rs}^{(n)i_n}, \sigma_{12rs}^{(n)i_n}) e^{i\omega_{rs}t} \cos \bar{r}x_1 \cos \bar{s}x_2,
\end{aligned}$$

where

$$\begin{aligned}
& \varepsilon_{11rs}^{(n)i_n} = -\bar{r}u_{1rs}^{(n)i_n}, \quad \varepsilon_{22rs}^{(n)i_n} = -\bar{s}u_{2rs}^{(n)i_n}, \quad 2\varepsilon_{12rs}^{(n)i_n} = \bar{s}u_{1rs}^{(n)i_n} + \bar{r}u_{2rs}^{(n)i_n}, \\
& 2\varepsilon_{13rs}^{(n)i_n} = \bar{r}u_{3rs}^{(n)i_n} + \beta_{1rs}^{(n)i_n}, \quad 2\varepsilon_{23rs}^{(n)i_n} = \bar{s}u_{3rs}^{(n)i_n} + \beta_{2rs}^{(n)i_n}, \quad \varepsilon_{33rs}^{(n)i_n} = \beta_{3rs}^{(n)i_n}, \\
& \beta_{irs}^{(n)i_n} = \sum_{j_n} M^{(n)j_n}(x_3^{(n)i_n}) u_{irs}^{(n)j_n}, \quad (14.20) \\
& E_{1rs}^{(n)i_n} = -\bar{r}\varphi_{rs}^{(n)i_n}, \quad E_{2rs}^{(n)i_n} = -\bar{s}\varphi_{rs}^{(n)i_n}, \quad E_{3rs}^{(n)i_n} = -\sum_{j_n} M^{(n)j_n}(x_3^{(n)i_n}) \varphi_{rs}^{(n)j_n}.
\end{aligned}$$

In the case of the piezoelectric material with $4mm$ symmetry, the constitutive equations (14.4) and (14.5) can be written in terms of SaS variables

$$\sigma_{ijrs}^{(n)i_n} = C_{ijkl}^{(n)} \varepsilon_{klrs}^{(n)i_n} - e_{kij}^{(n)} E_{krs}^{(n)i_n}, \quad (14.21)$$

$$D_{irs}^{(n)i_n} = e_{ikl}^{(n)} \varepsilon_{klrs}^{(n)i_n} + \varepsilon_{ik}^{(n)} E_{krs}^{(n)i_n}. \quad (14.22)$$

For the vibration analysis of piezoelectric plates with stress-free and voltage-free external surfaces, the boundary conditions (14.14) and (14.15) are used with $p_i^\pm = 0$ and $\phi^\pm = 0$. Substituting (14.18)-(14.22) in governing equations (14.12)-(14.16), we arrive at the homogeneous system of linear equations

$$\left(\begin{bmatrix} \mathbf{K}_{rs}^{uu} & \mathbf{K}_{rs}^{u\varphi} \\ \mathbf{K}_{rs}^{\varphi u} & \mathbf{K}_{rs}^{\varphi\varphi} \end{bmatrix} - \omega_{rs}^2 \begin{bmatrix} \mathbf{M}_{rs} & \mathbf{0} \\ \mathbf{0} & \mathbf{0} \end{bmatrix} \right) \begin{bmatrix} \mathbf{U}_{rs} \\ \Phi_{rs} \end{bmatrix} = \mathbf{0}, \quad (14.23)$$

where \mathbf{K}_{rs}^{uu} , $\mathbf{K}_{rs}^{u\varphi}$, $\mathbf{K}_{rs}^{\varphi u} = (\mathbf{K}_{rs}^{u\varphi})^T$ and $\mathbf{K}_{rs}^{\varphi\varphi}$ are the mechanical, piezoelectric and dielectric stiffness matrices; \mathbf{M}_{rs} is the mass matrix; \mathbf{U}_{rs} is the SaS displacement vector of order $3N_{\text{SaS}}$; Φ_{rs} is the SaS electric potential vector of order N_{SaS} given by

$$\mathbf{U}_{rs} = \left[\mathbf{U}_{1rs}^T \quad \mathbf{U}_{2rs}^T \quad \mathbf{U}_{3rs}^T \right]^T, \quad (14.24)$$

$$\mathbf{U}_{irs} = \left[u_{irs}^{(1)1} \quad u_{irs}^{(1)2} \quad \dots \quad u_{irs}^{(1)I_1} \quad u_{irs}^{(2)1} \quad u_{irs}^{(2)2} \quad \dots \quad u_{irs}^{(2)I_2} \quad \dots \quad u_{irs}^{(N)1} \quad u_{irs}^{(N)2} \quad \dots \quad u_{irs}^{(N)I_N} \right]^T,$$

$$\Phi_{rs} = \left[\varphi_{rs}^{(1)1} \quad \varphi_{rs}^{(1)2} \quad \dots \quad \varphi_{rs}^{(1)I_1} \quad \varphi_{rs}^{(2)1} \quad \varphi_{rs}^{(2)2} \quad \dots \quad \varphi_{rs}^{(2)I_2} \quad \dots \quad \varphi_{rs}^{(N)1} \quad \varphi_{rs}^{(N)2} \quad \dots \quad \varphi_{rs}^{(N)I_N} \right]^T. \quad (14.25)$$

Eliminating the vector Φ_{rs} from (14.23), one gets

$$\Phi_{rs} = -(\mathbf{K}_{rs}^{\varphi\varphi})^{-1} \mathbf{K}_{rs}^{\varphi u} \mathbf{U}_{rs}. \quad (14.26)$$

Inserting (14.26) in the first row of (14.23), the following reduced homogeneous system is obtained

$$(\mathbf{K}_{rs} - \omega_{rs}^2 \mathbf{M}_{rs}) \mathbf{U}_{rs} = \mathbf{0}, \quad (14.27)$$

which has a non-trivial solution only if

$$\det(\mathbf{K}_{rs} - \omega_{rs}^2 \mathbf{M}_{rs}) = 0, \quad (14.28)$$

where $\mathbf{K}_{rs} = \mathbf{K}_{rs}^{uu} - \mathbf{K}_{rs}^{u\varphi} (\mathbf{K}_{rs}^{\varphi\varphi})^{-1} \mathbf{K}_{rs}^{\varphi u}$ is the stiffness matrix of order $3N_{\text{SaS}} \times 3N_{\text{SaS}}$.

The polynomial equation (14.28) has to be solved to obtain the circular frequencies $0 < \omega_{rs}^{(1)} < \omega_{rs}^{(2)} < \dots < \omega_{rs}^{(3N_{\text{SaS}}-6N)}$ arranged in an increasing order. The number of frequencies $\omega_{rs}^{(q)}$ for each set of SaS depends on the number of zero rows in a mass matrix \mathbf{M}_{rs} , where the superscript $q = 1, 2, \dots, 3N_{\text{SaS}} - 6N$ stands for the number of through thickness modes. The eigenvectors $\mathbf{U}_{rs}^{(q)}$ associated with the corresponding eigenvalues $\lambda_{rs}^{(q)} = (\omega_{rs}^{(q)})^2$ can be evaluated by using the linear system (14.27).

14.5 Forced Vibrations of Simply Supported Piezoelectric Plates

Here, we study forced vibrations of the simply supported laminated piezoelectric rectangular plate with boundary conditions on the bottom and top surfaces

$$\sigma_{13}^{(1)} = \sigma_{23}^{(1)} = \sigma_{33}^{(1)} = \varphi^{(1)} = 0 \text{ at } x_3 = -h/2, \quad (14.29)$$

$$\sigma_{13}^{(N)} = \sigma_{23}^{(N)} = 0, \quad \sigma_{33}^{(N)} = p_3^+, \quad \varphi^{(N)} = \phi^+ \text{ at } x_3 = h/2.$$

Consider time-harmonic loading distributed on the top surface as follows:

$$\text{Problem A: } p_3^+ = p_0 e^{i\omega t} \sin \frac{\pi x_1}{a} \sin \frac{\pi x_2}{b}, \quad \phi^+ = 0; \quad (14.30)$$

$$\text{Problem B: } p_3^+ = 0, \quad \phi^+ = \phi_0 e^{i\omega t} \sin \frac{\pi x_1}{a} \sin \frac{\pi x_2}{b}, \quad (14.31)$$

where $p_0 = 1 \text{ Pa}$, $\phi_0 = 1 \text{ V}$ and ω is the forcing frequency.

To satisfy boundary conditions (14.17), we seek the analytical solution of the problem in the following form:

$$\begin{aligned} u_1^{(n)i_n} &= u_{10}^{(n)i_n} e^{i\omega t} \cos \frac{\pi x_1}{a} \sin \frac{\pi x_2}{b}, & u_2^{(n)i_n} &= u_{20}^{(n)i_n} e^{i\omega t} \sin \frac{\pi x_1}{a} \cos \frac{\pi x_2}{b}, \\ u_3^{(n)i_n} &= u_{30}^{(n)i_n} e^{i\omega t} \sin \frac{\pi x_1}{a} \sin \frac{\pi x_2}{b}, & \varphi^{(n)i_n} &= \varphi_0^{(n)i_n} e^{i\omega t} \sin \frac{\pi x_1}{a} \sin \frac{\pi x_2}{b}, \end{aligned} \quad (14.32)$$

where $u_{i0}^{(n)i_n}$ and $\varphi_0^{(n)i_n}$ are the amplitudes of displacements and electric potentials of SaS of the n th layer.

The described algorithm was performed with the Symbolic Math Toolbox, which incorporates symbolic computations into the numeric environment of MATLAB. This makes it possible to obtain the analytical solutions for free and forced vibra-

tions of the simply supported laminated piezoelectric rectangular plate in the framework of the SaS formulation, which asymptotically approach the 3D exact solutions of electroelasticity as the number of SaS goes to infinity.

As a numerical example, we consider a simply supported two-ply square plate [0/90] made of the graphite epoxy composite and covered with PZT-4 piezoelectric layers at the bottom and at the top. Therefore, we deal here with a hybrid four-layer plate [PZT/0/90/PZT] with ply thicknesses $[0.25h/0.25h/0.25h/0.25h]$. The material properties of the PZT-4 (Kulikov and Plotnikova, 2017a) polarized in the thickness direction are $E_1=E_2=81.3$ GPa, $E_3=64.5$ GPa, $G_{12}=30.6$ GPa, $G_{13}=G_{23}=25.6$ GPa, $\nu_{12}=0.329$, $\nu_{13}=\nu_{23}=0.432$, $e_{311}=e_{322}=-5.2$ C/m², $e_{333}=15.08$ C/m², $e_{113}=e_{223}=12.72$ C/m², $\epsilon_{11}=\epsilon_{22}=13.06$ nF/m, $\epsilon_{33}=11.51$ nF/m and $\rho=7600$ kg/m³. The material properties of the graphite epoxy (Kulikov and Plotnikova, 2017a) are $E_1=172.5$ GPa, $E_2=E_3=6.9$ GPa, $G_{12}=G_{13}=3.45$ GPa, $G_{23}=1.38$ GPa, $\nu_{12}=\nu_{13}=0.25$, $\nu_{23}=0.35$, $\epsilon_{11}=\epsilon_{22}=0.031$ nF/m, $\epsilon_{22}=\epsilon_{33}=0.027$ nF/m and $\rho=1800$ kg/m³.

To evaluate the results effectively, we introduce the dimensionless frequency (Kulikov and Plotnikova, 2017a)

$$\bar{\omega} = \omega a^2 \sqrt{\rho_0/E_0}/h \quad (14.33)$$

and dimensionless basic variables at crucial points as functions of the thickness coordinate

$$\begin{aligned} \bar{u}_3 &= 10^9 u_3(a/2, a/2, z)/h, \quad \bar{\sigma}_{11} = \sigma_{11}(a/2, a/2, z)/\sigma_0, \\ \bar{\sigma}_{13} &= \sigma_{13}(0, a/2, z)\sigma_0, \quad \bar{\sigma}_{33} = \sigma_{33}(a/2, a/2, z)/\sigma_0, \\ \bar{\varphi} &= \varphi(a/2, a/2, z)/\varphi_0, \quad \bar{D}_3 = 10^9 \varphi_0 D_3(a/2, a/2, z)/a\sigma_0, \quad z = x_3/h, \end{aligned} \quad (14.34)$$

where $a=1$ m, $h=0.1$ m, $E_0=81.3$ GPa, $\rho_0=7600$ kg/m³, $\sigma_0=1$ Pa and $\varphi_0=1$ V.

Figures 14.2 and 14.3 display the distributions of displacements, stresses, electric potential and electric displacement (14.34) through the thickness of the plate for the forcing frequencies $\bar{\omega} = 0, 0.8\bar{\omega}_0, 0.95\bar{\omega}_0$ and $1.05\bar{\omega}_0$ using seven SaS inside each layer, where $\bar{\omega}_0=6.0932$ is the fundamental frequency in the case of stress-free and voltage-free external surfaces (Kulikov and Plotnikova, 2017a). It is seen that the boundary conditions on bottom and top surfaces for the transverse stresses and the continuity conditions at interfaces for the transverse stresses and electric displacement are satisfied correctly. Note also that the displacements and stresses become larger as the forcing frequency approaches the fundamental frequency.

14.6 Conclusions

An efficient strong SaS formulation is developed for the 3D vibration analysis of laminated piezoelectric plates with the SaS located at Chebyshev polynomial nodes within the layers. It is based on direct integration of the equations of motion of piezoelectricity. The use of interfaces and outer surfaces is avoided that makes it

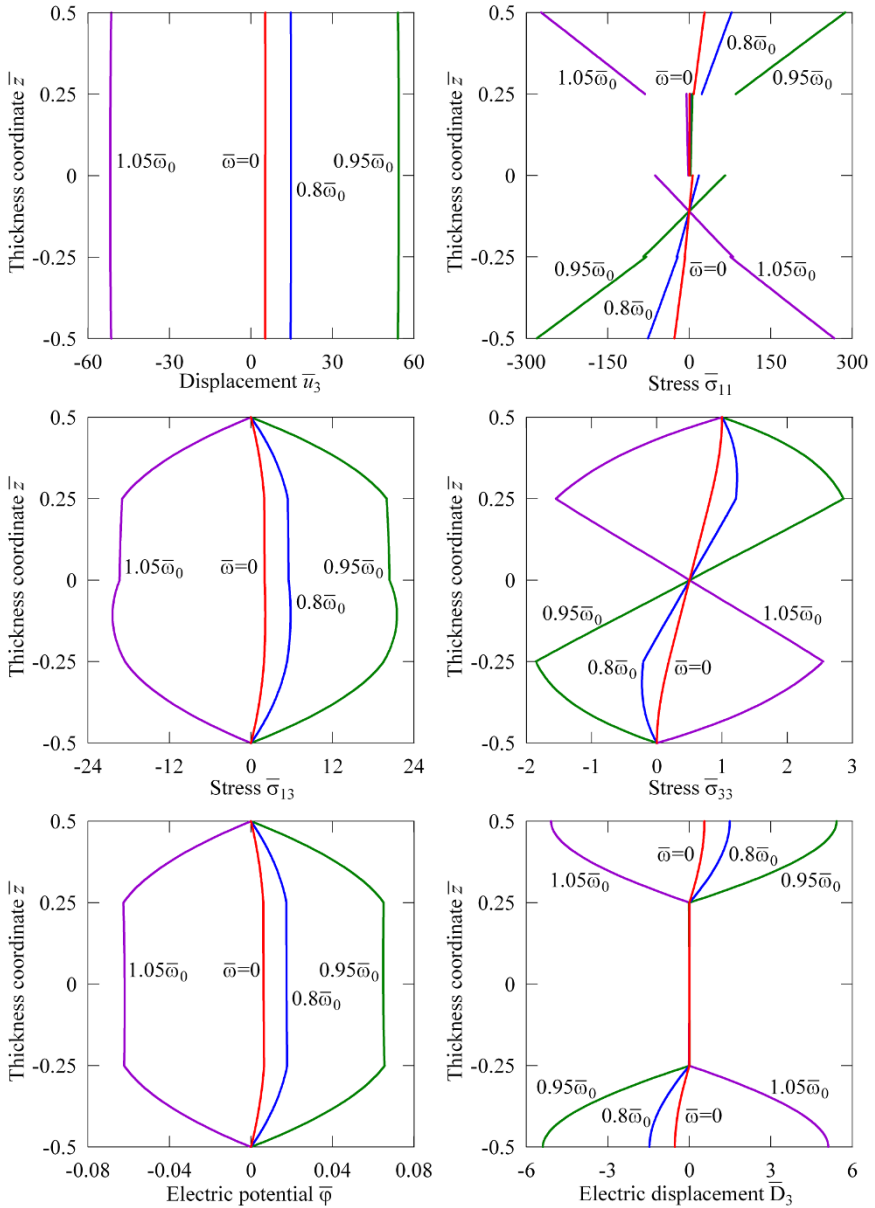


Fig. 14.2 Through-thickness distributions of transverse displacement, stresses, electric potential and electric displacement for the four-layer plate subjected to mechanical loading (problem A).

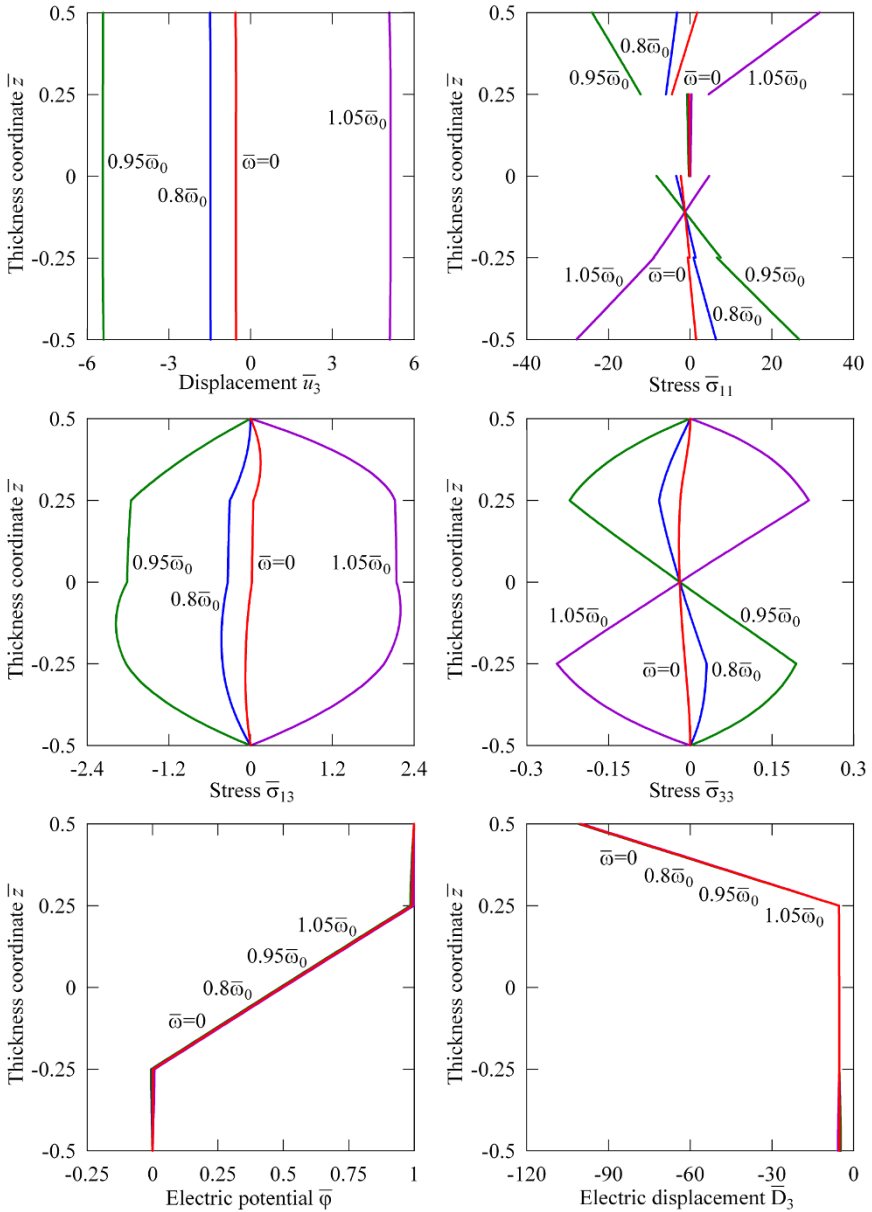


Fig. 14.3 Through-thickness distributions of transverse displacement, stresses, electric potential and electric displacement for the four-layer plate subjected to electric loading (problem B).

possible to minimize uniformly the error due to Lagrange interpolation. Therefore, the proposed strong SaS formulation allows one to obtain the analytical solutions for free and forced vibrations of laminated piezoelectric plates with a prescribed accuracy, which asymptotically approach the exact solutions of electroelasticity as the number of SaS goes to infinity.

Acknowledgements This work was supported by the Russian Science Foundation under Grant No. 22-21-00030.

References

- Baillargeon BP, Vel SS (2005) Exact solution for the vibration and active damping of composite plates with piezoelectric shear actuators. *Journal of Sound and Vibration* 282(3):781–804
- Bakhvalov NS (1977) Numerical methods: Analysis, algebra, ordinary differential equations. MIR Publishers, Moscow
- Chen WQ, Ding HJ (2002) On free vibration of a functionally graded piezoelectric rectangular plate. *International Journal of Solids and Structures* 153(3):207–216
- Chen WQ, Xu RQ, Ding HJ (1998) On Free Vibration of a Piezoelectric Composite Rectangular Plate. *Journal of Sound and Vibration* 218(4):741–748
- Deü JF, Benjeddou A (2005) Free-vibration analysis of laminated plates with embedded shear-mode piezoceramic layers. *International Journal of Solids and Structures* 42(7):2059–2088
- Gao JX, Shen YP, Wang J (1998) Three dimensional analysis for free vibration of rectangular composite laminates with piezoelectric layers. *Journal of Sound and Vibration* 213(2):383–390
- Haojiang D, Rongqiao X, Yuwei C, Weiqui C (1999) Free axisymmetric vibration of transversely isotropic piezoelectric circular plates. *International Journal of Solids and Structures* 36(30):4629–4652
- Heyliger P, Brooks S (1995) Free vibration of piezoelectric laminates in cylindrical bending. *International Journal of Solids and Structures* 32(20):2945–2960
- Heyliger P, Saravanos DA (1995) Exact free-vibration analysis of laminated plates with embedded piezoelectric layers. *The Journal of the Acoustical Society of America* 98(3):1547–1557
- Kulikov G, Plotnikova S (2013a) A sampling surfaces method and its application to three-dimensional exact solutions for piezoelectric laminated shells. *International Journal of Solids and Structures* 50(11):1930–1943
- Kulikov G, Plotnikova S (2013b) Three-dimensional exact analysis of piezoelectric laminated plates via a sampling surfaces method. *International Journal of Solids and Structures* 50(11):1916–1929
- Kulikov GM, Plotnikova SV (2012) On the use of sampling surfaces method for solution of 3D elasticity problems for thick shells. *ZAMM - Journal of Applied Mathematics and Mechanics / Zeitschrift für Angewandte Mathematik und Mechanik* 92(11-12):910–920
- Kulikov GM, Plotnikova SV (2017a) Benchmark solutions for the free vibration of layered piezoelectric plates based on a variational formulation. *Journal of Intelligent Material Systems and Structures* 28(19):2688–2704
- Kulikov GM, Plotnikova SV (2017b) Strong sampling surfaces formulation for laminated composite plates. *Composite Structures* 172:73–82
- Kulikov GM, Plotnikova SV (2017c) Strong sampling surfaces formulation for layered shells. *International Journal of Solids and Structures* 121:75–85
- Kulikov GM, Plotnikova SV, Kulikov MG (2017) Strong SaS formulation for free and forced vibrations of laminated composite plates. *Composite Structures* 180:286–297

- Kulikov GM, Plotnikova SV, Kulikov MG (2019) Three-dimensional vibration analysis of simply supported laminated cylindrical shells and panels by a strong SaS formulation. *ZAMM - Journal of Applied Mathematics and Mechanics / Zeitschrift für Angewandte Mathematik und Mechanik* 99(1):e201800,100
- Messina A, Carrera E (2015) Three-dimensional free vibration of multi-layered piezoelectric plates through approximate and exact analyses. *Journal of Intelligent Material Systems and Structures* 26(5):489–504
- Vel SS, Mewer RC, Batra RC (2004) Analytical solution for the cylindrical bending vibration of piezoelectric composite plates. *International Journal of Solids and Structures* 41(5):1625–1643
- Zhong Z, Yu T (2006) Vibration of a simply supported functionally graded piezoelectric rectangular plate. *Smart Materials and Structures* 15(5):1404–1412



Chapter 15

Asymptotic Analysis of Buckling of Layered Rectangular Plates Accounting for Boundary Conditions and Edge Effects Induced by Shears

Gennadi Mikhasev and Rovshen Ataev

Abstract Based on the equivalent single layer theory for laminated shells, buckling of layered rectangular plate under uniaxial compression with different variant of boundary conditions is studied. Equations in terms of the displacement, shear and stress functions, which take into account transverse shears inside the plate and near the edges with and without diaphragms, are used as the governing ones. Using the asymptotic approach, the buckling modes are constructed in the form of a superposition of the outer solution and the edge effect integrals induced by shears in the vicinity of the edges with or without diaphragms. Closed form relations for the critical buckling force accounting for shears are obtained for different variants of boundary conditions. It is detected that within one group of boundary conditions, the critical buckling forces can differ significantly depending on whether the edge is supplied with the diaphragm or not.

Key words: layered rectangular plate, shears, uniaxial compression, buckling, asymptotic approach, edge diaphragm, edge effects

15.1 Introduction

Buckling of thin plates is one of the extensive problems in the theory of thin-walled structures subjected to loading, which includes problems on buckling of single layer isotropic plates with various boundary conditions and under different schemes of loading, of composite and laminated plates based on different kinematic hypotheses, and others. Apparently, the first study on the stability of thin single layer isotropic rectangular plates in the framework of the classical Kirchhoff theory, was carried out by Bryan (1890). Applying the energy method, he obtained a simple formula for

G.I. Mikhasev · R.M. Ataev
Belarusian State University, 4 Nezavisimosti Avenue, 220030 Minsk, Belarus
e-mail: mikhasev@bsu.by, at.rovshan@gmail.com

the critical force resulting in buckling of an uniaxially loaded rectangular plate with simply supported edges. Soon, following the Euler approach, Timoshenko (1907, 1910) and Reissner (1909) independently considered similar problems for a plate in which two edges loaded by a compressive force are simply supported, and the other ones have arbitrary boundary conditions. Later, Bubnov (1912) solved the problem on buckling of a rectangular plate, in which a pair of opposite sides is loaded by forces linearly varying along these sides. There was also considered a rectangular simply supported plate under the action of shear stresses uniformly distributed along the contour of the plate.

The above closed form classical solutions together with many others (e.g., see Timoshenko, 1936; Donell, 1976; Alfutov, 2000), obtained for isotropic plates obeying Kirchhoff's hypotheses, became a benchmark for subsequent investigations on buckling of layered plates. Solutions of problems on buckling of laminated plates with different boundary conditions and under various scheme of loading, using the equivalent single layer (ESL) theories based on the Kirchhoff assumptions, can be found in Ashton and Whitney (1970); Reddy (2004). Obviously, similar solutions, ignoring shears and the transverse normal stresses, are not sufficiently accurate for laminated plates (Khdeir, 1989a,b). Therefore, the next contribution to the theory of buckling of layered plates was the use of the first-order shear deformation theory (FSDT) first proposed by Reissner (1945, 1952); Mindlin (1951) and then improved by other researches, see, e.g., the review papers Altenbach (1998); Qatu et al (2010). The series of studies based on this approach (see, among many others, Khdeir et al, 1987; Reddy and Khdeir, 1989; Nosier and Reddy, 1992) showed that taking transverse shears into account may give a large correction to the critical buckling force estimated within the classical shells theory for layered plates. The main drawback of the FSDT is that it does not allow satisfying the traction-free boundary conditions at the top and bottom surfaces of a laminated plate and so, it requires to introduce the shear correction factors (Mindlin, 1951). The next step in the development of more accurate approaches for modeling mechanical behavior of laminated plates is associated with the higher-order shear deformation theories (HSDT)s. They are based on quadratic, cubic and higher-order expansions at least of the in-plane displacements as functions of the transverse coordinate and comply with the traction-free boundary conditions on the face planes of a laminated plate, see relatively early papers Whitney and Sun (1973, 1974); Reddy (1984); Librescu et al (1987); Grigoliuk and Kulikov (1988), and also some more recent (Swaminathan and Ragounadin, 2004; Tovstik and Tovstik, 2007; Aydogdu, 2009; Amabili, 2015; Shi et al, 2018, to name a few). Using the developed HSDT)s, many buckling problems of rectangular laminated plates were analyzed for various boundary conditions and schemes of loading, taking into account anisotropy of layers composing the plate. A lot of examples on buckling of laminated plates with symmetric and antisymmetric, cross- and angle-ply orientation of fibres can be found in Reddy (2004). An extensive literature on early studies of buckling of laminated plates can be also found there.

Due to the widespread use of composite plates and shells in engineering practice, the number of papers devoted to the buckling of laminated and functionally graded material plates, based on using HSDT)s and high accurate layer-wise theo-

ries accounting the zig-zage effects, has increased dramatically, e.g., see the review article by Swaminathana et al (2015). These studies carried out, as a rule, using numerical methods, are characterized by high accuracy, but at the same time they are numerically highly-cost and do not allow obtaining closed form solutions and simple assessments for the critical buckling loads. In particular, a review of the available literature indicates the absence of any research of the transverse shear effects near the plate edges, induced by the edge diaphragms, on a value of the critical buckling load. At the same time, it should be noted that the asymptotic analysis of free vibration of a laminated cylindrical shell performed in Mikhasev and Botogova (2017); Mikhasev and Altenbach (2019c) displayed the strong dependence of the lowest eigenfrequencies on whether the shell edge is supplied with a diaphragm or not.

Motivated by the outcomes of Mikhasev and Botogova (2017); Mikhasev and Altenbach (2019c), we aim to investigate the influence of the transverse shears near edges on the value of the critical buckling force for rectangular plates which are pliable to shears. As the model we will use the ESL theory developed by Grigoliuk and Kulikov (1988) which is based on the generalized kinematical hypotheses of Timoshenko for the in-plane displacements and the parabolic distribution of transverse shear stresses through the plate thickness. This model complies with the traction-free boundary conditions on the top and bottom surfaces of a laminated plate and was verified by finite element simulation (Mikhasev and Altenbach, 2019a). In the framework of this theory, the full system of differential equations w.r.t. five unknowns is readily simplified and reduced to three equations for the displacement, stress and shear functions. These equations have more higher order than similar equations like Timoshenko-Reissner and, in a particular case, completely coincide with equations derived by Tovstik and Tovstik (2017a,b) from the 3D theory of elasticity. The higher order of this equations allows differing boundary conditions belonging to the same group (e.g., the clamped support group) depending on whether an edge has a diaphragm or not.

The asymptotic solutions of equations governing buckling of a rectangular laminated plate with various boundary conditions are constructed in the form of a superposition of the outer solution and the edge effect integrals induced by shears in the vicinity of an edge with or without a diaphragm. The corrections to classical relations for the critical buckling forces are derived.

15.2 Governing Equations

Consider a rectangular laminated plate with the sides a, b consisting of N transversally isotropic elastic layers. Each layer is characterized by the thickness h_k , Young's modulus E_k , the shear modulus G_k and Poisson's ratio ν_k , where $k = 1, 2, \dots, N$. The plate is referred to an orthogonal Cartesian coordinate system $Ox_1x_2x_3$ with the original plane Ox_1x_2 coinciding with the middle surface of any layer.

Let the plate be loaded with edges forces which generally generate the stress resultants $T_{11}^\circ, T_{22}^\circ, T_{12}^\circ$ in the original plane Ox_1x_2 , where $T_{11}^\circ, T_{22}^\circ$ are the membrane

forces acting in the x_1 - and x_2 - directions, respectively, and T_{22}° is the membrane shear force. Then the governing equations describing buckling of the plate based on the ESL theory by Grigoliuk-Kulikov can be written as follows:

$$D\left(1 - \frac{\theta h^2}{\beta} \Delta\right) \Delta^2 \chi - \left(T_{11}^\circ \frac{\partial^2}{\partial x_1^2} + 2T_{12}^\circ \frac{\partial^2}{\partial x_1 \partial x_2} + T_{22}^\circ \frac{\partial^2}{\partial x_2^2}\right) w = 0, \quad (15.1)$$

$$w = \left(1 - \frac{h^2}{\beta} \Delta\right) \chi, \quad \frac{1 - \nu}{2} \frac{h^2}{\beta} \Delta \phi = \phi. \quad (15.2)$$

Here Δ is the Laplace operator, $h = \sum_{k=1}^N h_k$ is the total plate thickness, w is the normal displacement, χ and ϕ are the displacement and shear functions, respectively, E , D and ν are the reduced Young's modulus, bending stiffness and Poisson's ratio, respectively, and θ, β are the reduced shear parameters determined by equations:

$$D = \frac{Eh^3}{12(1-\nu^2)} \eta_3, \quad E = \frac{1-\nu^2}{h} \sum_{k=1}^N \frac{E_k h_k}{1-\nu_k^2}, \quad \nu = \sum_{k=1}^N \frac{E_k h_k \nu_k}{1-\nu_k^2} \left(\sum_{k=1}^N \frac{E_k h_k}{1-\nu_k^2} \right)^{-1},$$

$$\theta = 1 - \frac{\eta_2^2}{\eta_1 \eta_3}, \quad \beta = \frac{12(1-\nu^2)}{Eh\eta_1} \left\{ \frac{\left[\sum_{k=1}^N \left(r_k - \frac{r_{k0}^2}{r_{kk}} \right) \right]^2}{\sum_{k=1}^N \left(r_k - \frac{r_{k0}^2}{r_{kk}} \right) G_k^{-1}} + \sum_{k=1}^N \frac{r_{k0}^2}{r_{kk}} G_k \right\}. \quad (15.3)$$

Parameters η_i, r_k, r_{kn} , where $i = 1, 2, 3; n = 0, k$, appearing in (15.3) are introduced by the following relations:

$$r_k = \int_{z_{k-1}}^{z_k} f_0^2(z) dz, \quad r_{kn} = \int_{z_{k-1}}^{z_k} f_k(z) f_n(z) dz, \quad \eta_1 = \sum_{k=1}^N \xi_k^{-1} \pi_{1k} \gamma_k - 3c_{12}^2, \quad (15.4)$$

$$\eta_2 = \sum_{k=1}^N \xi_k^{-1} \pi_{2k} \gamma_k - 3c_{12} c_{13}, \quad \eta_3 = 4 \sum_{k=1}^N \left(\xi_k^2 + 3\zeta_{k-1} \zeta_k \right) \gamma_k - 3c_{13}^2,$$

where

$$\gamma_k = \frac{E_k h_k}{1-\nu_k^2} \left(\sum_{k=1}^N \frac{E_k h_k}{1-\nu_k^2} \right)^{-1} \quad (15.5)$$

is the in-plane reduced stiffness of the k -th lamina, and

$$\begin{aligned}
 c_{12} &= \sum_{k=1}^N \xi_k^{-1} \pi_{3k} \gamma_k, & c_{13} &= \sum_{k=1}^N (\zeta_{k-1} + \zeta_k) \gamma_k, \\
 \frac{1}{12} h^3 \pi_{1k} &= \int_{z_{k-1}}^{z_k} g^2(x_3) dx_3, & \frac{1}{12} h^3 \pi_{2k} &= \int_{z_{k-1}}^{z_k} x_3 g(x_3) dx_3, \\
 \frac{1}{2} h^2 \pi_{3k} &= \int_{z_{k-1}}^{z_k} g(x_3) dx_3, & \eta_1 &= \sum_{k=1}^N \xi_k^{-1} \pi_{1k} \gamma_k - 3c_{12}^2, \\
 \eta_2 &= \sum_{k=1}^N \xi_k^{-1} \pi_{2k} \gamma_k - 3c_{12} c_{13}, & \eta_3 &= 4 \sum_{k=1}^N (\xi_k^2 + 3\zeta_{k-1} \zeta_k) \gamma_k - 3c_{13}^2, \\
 h\xi_k &= h_k, & h\zeta_n &= z_n \quad (n = 0, k).
 \end{aligned}
 \tag{15.6}$$

Functions f_0, f_k, g are taken in the polynomial form:

$$\begin{aligned}
 f_0(x_3) &= \frac{1}{h^2} (x_3 - z_0)(z_N - x_3) \quad \text{for } x_3 \in [z_0, z_N], \\
 f_k(x_3) &= \frac{1}{h_k^2} (x_3 - z_{k-1})(z_k - x_3) \quad \text{for } x_3 \in [z_{k-1}, z_k], \\
 f_k(x_3) &= 0 \quad \text{for } x_3 \notin [z_{k-1}, z_k], \quad g(x_3) = \int_0^{x_3} f_0(z) dz.
 \end{aligned}
 \tag{15.7}$$

In Eqs. (15.4), (15.6), (15.7), $x_3 = z_k$ is the coordinate of the upper bound of the k^{th} layer, and $x_3 = z_0$ is the coordinate of the bottom face.

The dimensionless parameter θ depends on a number of layers and thickness of each lamina. For instance, for a single layer isotropic plate, $\theta = 1/85$. The estimates of this parameter for layered plates and panels depending on a number of layers and their mechanical properties can be found in Mikhasev et al (2019); Mikhasev and Altenbach (2019d). If $\theta = 0$, then Eq. (15.1) together with the first equation from (15.2) degenerates into the fourth-order differential one which coincides with the equation like Timoshenko-Reissner obtained by Tovstik and Tovstik (2017a,b); Morozov et al (2016a,b) for plates inhomogeneous in the thickness direction. However, the shear parameter β is calculated in other way. We note that the parameter $G = E\eta_1\beta/[12(1 - \nu^2)]$ can be here treated as the effective (or reduced) shear modulus for laminated plate (Mikhasev and Altenbach, 2019b; Mikhasev and Tovstik, 2020).

We consider two groups of boundary conditions, the simple support group, and the clamped support group, which will be denoted by the letters S and C, respectively. Each of these groups consists of two variants boundary conditions which differ in the presence or absence of a diaphragm that prevents shears in the edge plane. To distinguish these condition in the framework of one fixed group, we will use the signs $^+$ and $^-$ for the edges with and without a diaphragm, respectively:

- S^+ – conditions,

$$\chi = \Delta\chi = \Delta^2\chi = \frac{\partial\phi}{\partial x_i} = 0; \quad (15.8)$$

- S^- – conditions,

$$\begin{aligned} \left(1 - \frac{h^2}{\beta}\Delta\right)\chi &= \frac{\partial^2}{\partial x_i^2} \left(1 - \frac{h^2}{\beta}\Delta\right)\chi = 0, \\ \left(\frac{\partial^2}{\partial x_i^2} + \nu \frac{\partial^2}{\partial x_j^2}\right)\chi - (1-\nu)\frac{\partial^2\phi}{\partial x_1\partial x_2} &= 0, \\ 2\frac{\partial^2\chi}{\partial x_1\partial x_2} + \frac{\partial^2\phi}{\partial x_i^2} - \frac{\partial^2\phi}{\partial x_j^2} &= 0; \end{aligned} \quad (15.9)$$

- C^- – conditions,

$$\left(1 - \frac{h^2}{\beta}\Delta\right)\chi = \frac{\partial\chi}{\partial x_i} = \frac{\partial}{\partial x_i}(\Delta\chi) = \phi = 0; \quad (15.10)$$

- C^+ – conditions,

$$\begin{aligned} \left(1 - \frac{h^2}{\beta}\Delta\right)\chi &= \frac{\partial}{\partial x_i} \left(1 - \frac{h^2}{\beta}\Delta\right)\chi = 0, \\ \frac{\partial\chi}{\partial x_i} - \frac{\partial\phi}{\partial x_j} &= \frac{\partial\chi}{\partial x_j} + \frac{\partial\phi}{\partial x_i} = 0 \end{aligned} \quad (15.11)$$

for $x_i = 0, x_i^*$, where $i, j = 1, 2; i \neq j$, and $x_1^* = a, x_2^* = b$.

There are 9 essentially different combinations of boundary conditions. In what follows, we consider only the following variants:

$$S^\pm S^\pm S^+ S^+, \quad S^\pm C^\pm S^+ S^+, \quad C^\pm C^\pm S^+ S^+,$$

where the first pair of letters denotes the boundary conditions at the edges $x_1 = 0, x_1 = a$, while the second one corresponds to conditions for $x_2 = 0, x_2 = b$. For instance, $S^+ S^+ S^+ S^+$ stands for the plate with simply supported edges supplied with the diaphragms, while the combination $C^- C^- S^+ S^+$ denotes a clamped support of the edges $x_1 = 0, x_1 = a$ without diaphragms.

As a rule, the plate loading is assumed to be one-parametric, so that

$$T_{ij}^\circ = -\lambda \frac{D}{a^2} t_{ij}^\circ, \quad (15.12)$$

where t_{ij}° is the dimensionless counterpart of T_{ij}° , and λ is the dimensionless load parameter. It is important that at least one of the parameters t_{ij}° be positive, that corresponds to the plate compression. The problem is to find the minimum positive value of a parameter λ for which the governing Eqs. (15.1), (15.2) with some speci-

fied variant of boundary conditions (15.8)-(15.11) have a non-trivial solution. Here, the case $t_{12}^{\circ} \neq 0$ is not considered.

15.3 Simply Supported Plate with the Edge Diaphragms

Consider the simplest case denoted as $S^+S^+S^+S^+$ when all edges are simply supported and supplied with the diaphragms. The corresponding boundary conditions are given by Eqs. (15.8). This case is probably the only one that allows us to construct a solution in the explicit simple form and analyse the effect of shears on the critical load. Without loss of generality, we assume that $t_{22}^{\circ} = 1$, and $t_{11}^{\circ} = t_1$ is any constant.

In this case the unique solution of the last equation from (15.2) satisfying the boundary conditions (15.8) is the trivial function, $\phi = 0$, while the displacement function can be represented as

$$\chi = c_0 \sin \frac{\pi m x_1}{a} \sin \frac{\pi n x_2}{b}, \quad (15.13)$$

where n, m are natural numbers, and c_0 is a nonzero constant. The substitution of (15.13) into Eqs. (15.1), (15.2) results in the simple formula for the eigenvalue

$$\lambda = \frac{\pi^2 (n^2 + l^2 m^2)^2 [1 + \theta K (n^2 + l^2 m^2)]}{l^2 (n^2 + t_1 l^2 m^2) [1 + K (n^2 + l^2 m^2)]}, \quad (15.14)$$

where $l = b/a$, and

$$K = \frac{\pi^2 h^2}{\beta b^2} \quad (15.15)$$

is the dimensionless shear parameter. The required critical value

$$\lambda^* = \min_{n,m} \lambda(n, m) = \lambda(n^*, m^*) \quad (15.16)$$

is the function of θ and K , where the dimensionless shear parameter K depends on the reduced shear modulus G , see Eq. (15.3). Because θ is a small value, the shear parameter K is the main one affecting the critical buckling force.

If all edges are uniformly loaded ($t_1 = 1$), then

$$n^* = m^* = 1, \quad \lambda^* = \lambda_{cl}^* \frac{1 + \theta K (1 + l^2)}{1 + K (1 + l^2)}, \quad (15.17)$$

where the eigenvalue

$$\lambda_{cl}^* = \frac{\pi^2 (1 + l^2)}{l^2} \quad (15.18)$$

corresponds to the classical value of the buckling force for a single layer isotropic plate (Alfutov, 2000).

Equation (15.17) shows that an increase in the shear parameter K (i.e., a decrease in the effective shear modulus G) leads to a decrease in the critical buckling force for a multilayer plate pliable to transverse shears. Because $\phi = 0$, then the edge effect in the case under consideration is absent. In other words, the presence of the diaphragms at simply supported edges does not generate shears localized near these edges.

15.4 Buckling Modes Accounting for the Edge Effects

In this section we consider the plates with boundary conditions belonging to the group $Y^\pm Z^\pm S^+ S^+$, where Y and Z denote either S or C conditions. In what follows, we assume that $t_{22}^\circ = 1$ and $t_{11}^\circ = 0$, i.e., the plate is compressed only in the x_2 - direction. For these combinations of boundary conditions the general solution of Eqs. (15.1), (15.2) can be represented in the form:

$$\chi = X(x) \sin \delta_n y, \quad \phi = \Phi(x) \cos \delta_n y, \quad (15.19)$$

where

$$x = \frac{x_1}{a}, \quad y = \frac{x_2}{a}, \quad \delta = \frac{\pi n}{l}. \quad (15.20)$$

Then Eqs. (15.1), (15.2) can be rewritten as follows:

$$(1 - \theta \kappa \Delta_1) \Delta_1^2 X - \lambda \delta^2 (1 - \kappa \Delta_1) X = 0, \quad (15.21)$$

$$\frac{1 - \nu}{2} \kappa \Delta_1 \Phi - \Phi = 0, \quad (15.22)$$

where $\Delta_1 = \frac{d^2}{dx^2} - \delta^2$ is the differential operator, and $\kappa = \frac{h^2}{\beta a^2}$ is the dimensionless shear parameter.

Accounting for (15.19), the boundary conditions for an unloaded edge ($x = 0$ or $x = 1$) read:

- S^+ - conditions,

$$X = 0, \quad \left(\frac{d^2}{dx^2} - \delta^2 \right) X = 0, \quad \left(\frac{d^2}{dx^2} - \delta^2 \right)^2 X = 0, \quad \frac{d\Phi}{dx} = 0. \quad (15.23)$$

- S^- - conditions,

$$\begin{aligned} (1 - \kappa \Delta_1) X = 0, \quad \frac{d^2}{dx^2} (1 - \kappa \Delta_1) X = 0, \\ \left(\frac{d^2}{dx^2} - \nu \delta^2 \right) X + (1 - \nu) \delta \frac{d\Phi}{dx} = 0, \\ 2\delta \frac{dX}{dx} + \frac{d^2 \Phi}{dx^2} + \delta^2 \Phi = 0, \end{aligned} \quad (15.24)$$

- C^- – conditions,

$$\begin{aligned} (1 - \kappa\Delta_1)X &= 0, & \frac{dX}{dx} &= 0, \\ \Delta_1 \frac{dX}{dx} &= 0, & \Phi &= 0; \end{aligned} \tag{15.25}$$

- C^+ – conditions,

$$\begin{aligned} (1 - \kappa\Delta_1)X &= 0, & \frac{d}{dx}(1 - \kappa\Delta_1)X &= 0, \\ \frac{dX}{dx} + \delta\Phi &= 0, & \delta X + \frac{d\Phi}{dx} &= 0. \end{aligned} \tag{15.26}$$

Depending on the orders of the shear parameters κ and θ , there are the following two distinctive cases:

- Case (A) $\kappa = \varepsilon^2$ is a small parameter, and $\theta = O(1)$ as $\varepsilon \rightarrow 0$;
- Case (B) θ is a small parameter, and $\kappa = O(1)$ as $\theta \rightarrow 0$.

Case (A) corresponds to very thin plates with the reduced Young's and shear moduli of the same order ($E \sim G$), and case (B) is related to thin plates for which $G \ll E$.

15.4.1 Layered Plates with the Reduced Young's and Shear Moduli of the same Order

Consider case (A). Regardless of the type of boundary conditions, the general solution of Eq. (15.22) is the function

$$\Phi = \varepsilon^{t_1} c_1 e^{-\frac{1}{\varepsilon} \sqrt{\frac{2+\varepsilon^2\delta^2(1-\nu)}{1-\nu}} x} + \varepsilon^{t_2} c_2 e^{\frac{1}{\varepsilon} \sqrt{\frac{2+\varepsilon^2\delta^2(1-\nu)}{1-\nu}} (x-1)}, \tag{15.27}$$

where t_i are the indices of intensity of the function Φ , and c_1, c_2 are constants of the order $O(1)$ to be determined from appropriate boundary conditions.

Consider Eq. (15.21). Its solution can be constructed in the form of the superposition of a solution, $X^{(m)}$, valid in the plate interior (the so-called "outer solution"), with a pair of boundary layers, $X_1^{(e)}$ and $X_2^{(e)}$, fading off away from the left and from the right plate ends, respectively:

$$X = X^{(m)}(x, \varepsilon) + \varepsilon^{\alpha_1} X_1^{(e)}(x, \varepsilon) + \varepsilon^{\alpha_2} X_2^{(e)}(x, \varepsilon), \tag{15.28}$$

where α_1, α_2 are indices of intensity of the edge effect integrals. We assume also that the following order relations hold:

$$\frac{\partial X^{(m)}}{\partial x} \sim X^{(m)}, \quad \frac{\partial X_i^{(e)}}{\partial x} \sim \varepsilon^{-s_i} X_i^{(m)} \quad \text{as } \varepsilon \rightarrow 0. \tag{15.29}$$

The positive parameters ς_i are named the indices of variation of the edge effect integrals. The indices α_1, α_2 depends on the boundary conditions and should be specified for each edge.

To derive an edge effect equation describing behaviour of the solution in the neighbourhood of the left and right ends, we scale in the vicinity of both edges. For instance, for the left edge we assume $x = \varepsilon^{\varsigma_1} \zeta$ and compare the main term in Eq. (15.21) containing the six-order derivative with others. As a result, we obtain $\varsigma_i = 1$ for both ends, and the edge effect equation reads

$$\begin{aligned} \theta \frac{d^6 X_i^{(e)}}{d\zeta^6} - (1 + 3\varepsilon^2 \theta \delta^2) \frac{d^4 X_i^{(e)}}{d\zeta^4} + \varepsilon^2 \delta^2 (2 + 3\varepsilon^2 \theta \delta^2 - \varepsilon^2 \lambda) \frac{d^2 X_i^{(e)}}{d\zeta^2} \\ - \varepsilon^4 \delta^2 [\delta^2 + \varepsilon^2 \theta \delta^4 - \lambda (1 + \varepsilon^2 \delta^2)] X_i^{(e)} = 0. \end{aligned} \tag{15.30}$$

Its solution is sought in the form of asymptotic series

$$X_i^{(e)} = \sum_{j=1}^{\infty} \varepsilon^j \chi_{ij}^{(e)}(\zeta).$$

Here we give only the leading terms of these expansions, returning to the original argument x :

$$X_1^{(e)} = a_1 e^{-\frac{x}{\varepsilon \sqrt{\theta}}} + O\left(\varepsilon e^{-\frac{x}{\varepsilon \sqrt{\theta}}}\right), \quad X_2^{(e)} = a_2 e^{\frac{x-1}{\varepsilon \sqrt{\theta}}} + O\left(\varepsilon e^{\frac{x-1}{\varepsilon \sqrt{\theta}}}\right), \tag{15.31}$$

where a_i are constants to be determined from the boundary conditions.

The outer solution $X^{(m)}$ as well as the eigenvalue λ are also sought in the form of series

$$X^{(m)} = \chi_0(x) + \varepsilon \chi_1(x) + \dots, \quad \lambda = \lambda_0 + \varepsilon \lambda_1 + \dots \tag{15.32}$$

Substituting (15.32) into Eq. (15.21) and grouping coefficients of the same powers of ε leads to the sequence of differential equations:

$$\sum_{j=0}^k \mathbf{L}_j \chi_{k-j} = 0, \tag{15.33}$$

where

$$\mathbf{L}_0 = \frac{d^4}{dx^4} - 2\delta^2 \frac{d^2}{dx^2} + \delta^2 (\delta^2 - \lambda_0), \quad \mathbf{L}_1 = -\lambda_1 \delta^2, \dots \tag{15.34}$$

To specify the boundary conditions for the functions $\chi_k(x)$, we substitute expansions (15.28), (15.31), (15.32) into appropriate conditions from (15.23)-(15.26), equate coefficients at the same powers of ε and impose the following requirements:

- in the leading approximation ($k = 0$), the boundary conditions for $\chi_0(x)$ should be homogeneous;
- the leading approximation generates equations coupling constants c_i with the function $\chi'_0(x)$ evaluated at the boundaries;

- the k th-order ($k \geq 1$) approximation results in the inhomogeneous boundary conditions for $\chi_k(x)$ and relations for a_i as well.

We note that indices α_i, t_i depend on the type of boundary conditions and can be different on the left and right edges.

15.4.1.1 Plate with S⁻S⁻S⁺S⁺ - Boundary Conditions

Let the unloaded edges be simply supported and not supplied with diaphragms. The corresponding boundary conditions are given by relations (15.24). Here, we obtain $\alpha_i = 3, t_i = 2$ for $i = 1, 2$.

In the leading approximation, one obtains the homogeneous boundary conditions,

$$\chi_0(0) = \chi_0(1) = 0, \quad \chi_0''(0) = \chi_0''(1) = 0, \quad (15.35)$$

and the pair of relations:

$$2\delta\chi_0'(0) + \frac{2}{1-\nu}c_1 = 0, \quad 2\delta\chi_0'(1) + \frac{2}{1-\nu}c_2 = 0. \quad (15.36)$$

The first-order approximation leads to the inhomogeneous boundary conditions,

$$\chi_1(0) = \chi_1(1) = 0, \quad (15.37)$$

$$\chi_1''(0) - \frac{\theta-1}{\theta^2}a_1 = 0, \quad \chi_1''(1) - \frac{\theta-1}{\theta^2}a_2 = 0, \quad (15.38)$$

and generates two the equations coupling constants a_i, c_i with the function $\chi_1''(x)$ evaluated at $x = 0$ and $x = 1$:

$$\begin{aligned} \chi_1''(0) + \frac{a_1}{\theta} - \delta(1-\nu) \frac{\sqrt{2}}{\sqrt{1-\nu}}c_1 &= 0, \\ \chi_1''(1) + \frac{a_2}{\theta} + \delta(1-\nu) \frac{\sqrt{2}}{\sqrt{1-\nu}}c_2 &= 0. \end{aligned} \quad (15.39)$$

Interrupting the process of finding the boundary conditions for functions $\chi_k(x)$, we consider the boundary-value problems arising in the first two approximations.

In the leading approximation ($k = 0$), one has the homogeneous differential equation $\mathbf{L}_0\chi_0 = 0$ with the homogeneous boundary conditions (15.35). The solution of this classical boundary-value problem is the eigenfunction $\chi_0 = c_0 \sin \pi m x$ with the associated eigenvalue

$$\lambda_0 = \lambda_0(n, m) = \frac{[(\pi m)^2 + \delta^2]^2}{\delta^2}. \quad (15.40)$$

The critical buckling force is evaluated as

$$\lambda_0^* = \min_{n,m} = \lambda(n^*, m^*) = \lambda(n^*, 1) = \frac{\pi^2 (l^2 + n^{*2})^2}{l^2 n^{*2}}, \quad (15.41)$$

where $n^* = 1$, if $l = b/a \leq 1$, and $n^* = \text{In}(l)$ for $l > 1$. Here $\text{In}(z)$ stands for the integer part of a number z . Then χ_0^* is the associated eigenfunction. Below, the asterisk $*$ is omitted for all parameters and the eigenfunction.

Now we can calculate

$$c_1 = -\pi\delta(1-\nu)c_0, \quad c_2 = \pi\delta(1-\nu)c_0, \quad (15.42)$$

where c_0 is an arbitrary constant that remains undefined in the framework of the linear problem. Here and below, the parameter $\delta = \delta_n$ is calculated at $n = n^*$.

Subtracting Eqs. (15.39) from Eqs. (15.38) and accounting for (15.42), we obtain the relations for constants

$$a_1 = a_2 = \sqrt{2}\pi\delta^2(1-\nu)^{3/2}\theta^2 c_0. \quad (15.43)$$

Then the pair of boundary conditions (15.39) can be rewritten as

$$\chi_1''(0) = \chi_1''(1) = \kappa c_0, \quad (15.44)$$

where

$$\kappa = \sqrt{2}\pi\delta^2(1-\nu)^{3/2}(1-\theta)c_0. \quad (15.45)$$

Consider the inhomogeneous differential equation (15.33) in the first-order approximation:

$$\frac{d^4\chi_1}{dx^4} - 2\delta^2\frac{d^2\chi_1}{dx^2} + \delta^2(\delta^2 - \lambda_0)\chi_1 = \lambda_1\delta^2\chi_0. \quad (15.46)$$

We note that the operator \mathbf{L}_0 is self-conjugated. Therefore, regardless of the type of boundary conditions imposed on the function $\chi_1(x)$, the condition for the existence of a solution to Eq. (15.46) will be as follows:

$$\begin{aligned} & \chi_1'''(1)\chi_0(1) - \chi_1'''(0)\chi_0(0) - \chi_1''(1)\chi_0'(1) + \chi_1''(0)\chi_0'(0) \\ & + \chi_1'(1)\chi_0''(1) - \chi_1'(0)\chi_0''(0) - \chi_1(1)\chi_0'''(1) + \chi_1(0)\chi_0'''(0) \\ & - 2\delta^2[\chi_1'(1)\chi_0(1) - \chi_1'(0)\chi_0(0) - \chi_1(1)\chi_0'(1) + \chi_1(0)\chi_0'(0)] \\ & - \lambda_1\delta^2 \int_0^1 \chi_0^2(x)dx = 0. \end{aligned} \quad (15.47)$$

Returning to the case of $S^-S^-S^+S^+$ – boundary conditions specified by relations (15.35), (15.37) and (15.44), we arrive at the parameter correcting the eigenvalue:

$$\lambda_1 = \frac{4\kappa\pi}{\delta^2}. \quad (15.48)$$

Then an approximate relations for the required eigenvalue and eigenmode can be written as follows:

$$\lambda = \frac{(\pi^2 + \delta^2)^2}{\delta^2} \left[1 + \varepsilon \Lambda_1 + O(\varepsilon^2) \right], \tag{15.49}$$

$$\chi \approx c_0 \sin \delta_n y \left[\sin \pi x + \varepsilon \chi_1(x) + \varepsilon^3 \sqrt{2} \pi \delta^2 \theta^2 (1 - \nu)^{3/2} \left(e^{-\frac{x}{\varepsilon \sqrt{\theta}}} + e^{\frac{x-1}{\varepsilon \sqrt{\theta}}} \right) \right],$$

where

$$\Lambda_1 = \frac{4 \sqrt{2} \pi^2 (1 - \nu)^{3/2} \delta^2 (1 - \theta)}{(\pi^2 + \delta^2)^2} > 0, \tag{15.50}$$

and $\chi_1(x)$ is the partial solution of Eq. (15.46) with the boundary conditions (15.37), (15.44).

We note that although the correction of the edge effect integrals to the eigenmode is of the order $\varepsilon^3 \left(e^{-\frac{x}{\varepsilon \sqrt{\theta}}}, e^{\frac{x-1}{\varepsilon \sqrt{\theta}}} \right)$, the error of relation (15.49) for χ has the order $O(\varepsilon^2)$.

We compare eigenvalue (15.49) with the analogous value given by relations (15.14), (15.16), corresponding to the simply supported plate with diaphragms at all edges. Note that $m^* = 1$ for $t_1 = 0$ in (15.14), (15.16). Since Eqs. (15.49), (15.49) are asymptotic, we expand formula (15.14) also into the series in a small parameter ε keeping in mind that $K = \varepsilon^2 \pi^2 l^{-2}$:

$$\lambda = \frac{(\pi^2 + \delta^2)^2}{\delta^2} \left[1 + \varepsilon^2 \Lambda_2 + O(\varepsilon^4) \right], \quad \Lambda_2 = (1 - \theta) (\pi^2 + \delta^2) > 0. \tag{15.51}$$

It can be seen that in the leading approximation the classical eigenvalues λ_0^* evaluated by Eqs. (15.49) and (15.51), which ignore the shear effects in a plate, are the same. The effect of shears on the buckling force turns to be different in plates with and without diaphragms. In the plate with simply supported edges with the diaphragms, the edge effects induced by shears are absent, and shears, taking place in the interior region of the plate, leads to a minor reduction of the buckling force with respect to the classical value λ_0^* , the normalized correction being a value of the order $O(\varepsilon^2)$.

Conversely, if there are no diaphragms at the simply supported edges, then near these edges shears occur, which lead to edge effects in the buckling form and increase the critical force with a normalized correction of the order $O(\varepsilon)$. It is interesting to note that similar reinforcing effect of the edge shears takes place in a cylindrical shell without diaphragms at the simply supported edges when the shell is under external pressure (Mikhasev and Botogova, 2017).

15.4.1.2 Plate with $C^\pm C^\pm S^+ S^+$ - Boundary Conditions

Consider a plate with the clamped unloaded edges without diaphragms ($C^- C^- S^+ S^+$ – conditions). The corresponding boundary conditions are given by relations (15.25). In this case $\alpha_1 = \alpha_2 = 3$, and $c_1 = c_2 = 0$ so that $\Phi = 0$.

In the leading approximation, the boundary conditions read

$$\chi_0(0) = \chi_0(1) = 0, \quad \chi'_0(0) = \chi'_0(1) = 0. \quad (15.52)$$

In addition, one obtains constants

$$a_1 = -a_2 = \theta^{3/2} \chi_0'''(0). \quad (15.53)$$

Consider the homogeneous differential equation $\mathbf{L}_0 \chi_0 = 0$ with the boundary conditions (15.52). This boundary-value problem has a straightforward exact solution

$$\chi_0(x, \delta) = c_1 e^{-\alpha x} + c_2 e^{\alpha(x-1)} + c_3 \sin \gamma x + c_4 \cos \gamma x, \quad (15.54)$$

where c_j are constants determined from conditions (15.52), and

$$\alpha = \sqrt{\delta \lambda_0^{1/2} + \delta^2}, \quad \gamma = \sqrt{\delta \lambda_0^{1/2} - \delta^2}, \quad \delta^2 < \lambda_0. \quad (15.55)$$

Let $\lambda(\delta)$ be the minimum positive eigenvalue for a fixed δ . The required eigenvalue λ_0^* corresponding to the plate buckling is determined as follows:

$$\lambda_0^* = \min_n \lambda_0(\delta(n)) = \lambda_0(\delta(n^*)) = \lambda_0(\delta^*).$$

The procedure to determine n^* , δ^* , λ_0^* will be described below (for different variants of boundary conditions).

In the first-order approximation, one has the inhomogeneous differential equation (15.46) with the homogeneous boundary conditions (15.52) for χ_1 . This inhomogeneous boundary-value problem implies $\lambda_1 = 0$, and the eigenfunction χ_1 is given with accuracy up to a constant by Eq. (15.54).

The second-order approximation, taking into account (15.53), generates the inhomogeneous boundary-value problem:

$$\mathbf{L}_0 \chi_2 = \mathbf{N} \chi_0 + \lambda_2 \delta^2 \chi_0, \quad (15.56)$$

$$\chi_2(0) = \chi_2''(0), \quad \chi_2(1) = \chi_2''(1),$$

$$\chi_2'(0) = \frac{a_1}{\sqrt{\theta}} = \theta \chi_0'''(0), \quad \chi_2'(1) = -\frac{a_2}{\sqrt{\theta}} = \theta \chi_0'''(1), \quad (15.57)$$

where \mathbf{N} is the differential operator introduced as follows:

$$\mathbf{N} = \theta \frac{d^6}{dx^6} - 3\theta \delta^2 \frac{d^4}{dx^4} + \delta^2 (3\theta \delta^2 - \lambda_0) \frac{d^2}{dx^2} + \delta^4 (\lambda_0 - \theta \delta^2).$$

The condition for existence of a solution of this problem results in the correction for the eigenvalue λ_0^* :

$$\lambda_2 = \{(\theta - 1)[\chi_0''(1)\chi_0'''(1) - \chi_0''(0)\chi_0'''(0)] - Z_N\}Z_1^{-1}, \quad (15.58)$$

where

$$Z_N = \int_0^1 \chi_0(x) \mathbf{N} \chi_0(x) dx, \quad Z_1 = \delta^2 \int_0^1 \chi_0^2(x) dx. \quad (15.59)$$

We note that the correction λ_2 is evaluated for $\lambda_0 = \lambda_0^*$, $\delta = \delta^*$.

Breaking the process of constructing the buckling mode, we write the approximate formulas for the critical load parameter λ^* and the corresponding bucking mode:

$$\lambda^* = \lambda_0^* \left[1 + \varepsilon^2 \Lambda_2 + O(\varepsilon^3) \right], \quad (15.60)$$

$$\chi \approx \sin \delta_n y \left\{ \chi_0(x) + \varepsilon^2 \chi_2(x) - \varepsilon^3 \theta^{3/2} \left[\chi_0'''(0) e^{-\frac{x}{\varepsilon \sqrt{\theta}}} + \chi_0'''(1) e^{\frac{x-1}{\varepsilon \sqrt{\theta}}} \right] \right\},$$

where $\Lambda_2 = \lambda_2 / \lambda_0^*$.

Now, let the unloaded edges be clamped and supplied with diaphragms ($C^+C^+S^+S^+$ – conditions). This case is not much different from the previous one (for $C^-C^-S^+S^+$ – conditions, see Eqs. (15.26)). Here, $\alpha_1 = \alpha_2 = 3$, and the boundary-value problems arising in the first three approximations are the same, so that all equations from (15.52) to (15.60) are valid. The only difference is that the function Φ defined by Eq. (15.27) is nonzero here. The asymptotic analysis of the boundary-value problems (15.33), (15.26) implies $\iota_1 = \iota_2 = 3$ and constants

$$c_1 = \sqrt{\frac{1-\nu}{2}} \delta \chi_0''(0), \quad c_2 = -\sqrt{\frac{1-\nu}{2}} \delta \chi_0''(1). \quad (15.61)$$

Thus, the presence of diaphragms on the clamped edges does not influence on the critical parameter λ^* , see Eq. (15.60), found from the first three approximations. An additional correction for the eigenvalue λ^* can be determined from considering the highest approximations.

15.4.1.3 Plate with $S^\pm C^- S^+ S^+$ - Boundary Conditions

Let the left edge be simply supported and the right one be clamped, with both edges free of diaphragms ($S^-C^-S^+S^+$ – conditions, see Eqs. (15.24), (15.25)). In this case $\alpha_1 = \alpha_2 = 3$, $\iota_1 = 2$, $c_2 = 0$. In the leading approximation, one has the homogeneous boundary conditions

$$\chi_0(0) = \chi_0''(0) = 0, \quad \chi_0(1) = \chi_0'(1) = 0. \quad (15.62)$$

The first approximation implies

$$c_1 = -\delta(1-\nu)\chi'_0(0), \quad a_1 = -\sqrt{2}(1-\nu)^{3/2}\theta^2\delta^2\chi'_0(0), \quad a_2 = -\theta^{3/2}\chi'''_0(1), \quad (15.63)$$

and the boundary conditions for $\chi_1(x)$ become as follows:

$$\chi_1(0) = 0, \quad \chi''_1(0) = -\sqrt{2}(1-\nu)^{3/2}(1-\theta)\delta^2\chi'_0(0), \quad \chi_1(1) = \chi'_1(1) = 0. \quad (15.64)$$

Condition (15.47) for the existence of a solution of the inhomogeneous boundary-value problem (15.33), (15.64) at $k = 1$ results in the following correction

$$\lambda_1 = -\frac{\sqrt{2}(1-\nu)^{3/2}(1-\theta)[\chi'_0(0)]^2}{\int_0^1 \chi_0^2(x) dx}. \quad (15.65)$$

Hence, we arrive at the following relations for the critical value of the load parameter and associated buckling mode:

$$\begin{aligned} \lambda^* &= \lambda_0^* \left[1 + \varepsilon \Lambda_1 + O(\varepsilon^2) \right], \\ \chi &\approx \sin \delta_n y \{ \chi_0(x) + \varepsilon \chi_1(x) \\ &\quad - \varepsilon^3 \left[\sqrt{2}(1-\nu)^{3/2}\theta^2\delta^2\chi'_0(0)e^{-\frac{x}{\varepsilon}\sqrt{\theta}} + \theta^{3/2}\chi'''_0(1)e^{\frac{x-1}{\varepsilon}\sqrt{\theta}} \right] \}, \end{aligned} \quad (15.66)$$

where $\Lambda_1 = \lambda_1/\lambda_0^*$.

Now we consider the variant of $S^+C^-S^+S^+$ – conditions, see Eqs. (15.23) and (15.25). In contrast to the previous case, here the left simply supported edge is supplied with the diaphragm. The asymptotic analysis of the sequence of Eqs. (15.33) with corresponding boundary conditions implies $\alpha_1 = 4, \alpha_2 = 3, \Phi = 0$.

The homogeneous boundary conditions for the leading approximation are as in the previous case and specified by Eqs. (15.62). Considering the first-order approximation gives $\lambda_1 = 0, \chi_1 = 0$, and the second-order approximation implies parameters

$$a_1 = -\theta^2\chi_0^{IV}(0), \quad a_2 = -\theta^{3/2}\chi_0'''(1), \quad (15.67)$$

and the boundary conditions for χ_2 :

$$\begin{aligned} \chi_2(0) &= 0, \quad \chi_2''(0) = \theta\chi_0^{IV}(0), \\ \chi_2(1) &= \chi_2''(1), \quad \chi_2'(1) = \theta\chi_0'''(1). \end{aligned} \quad (15.68)$$

A solution of the inhomogeneous boundary-value problem (15.56), (15.68) exists if and only if

$$\lambda_2 = \frac{\theta \left[\chi_0^{IV}(0) \chi_0'(0) + \chi_0'''(1) \chi_0''(1) \right] - \chi_0''(1) \chi_0'''(1) - \int_0^1 \chi_0 \mathbf{N} \chi_0 dx}{\delta^2 \int_0^1 \chi_0^2(x) dx}. \tag{15.69}$$

Thus, for the $S^-C^-S^+S^+$ – boundary conditions the critical value of the load parameter is calculated by the first relation from (15.60), the associated buckling mode being the function

$$\chi \approx \sin \delta_n y \left[\chi_0(x) + \varepsilon^2 \chi_2(x) - \varepsilon^3 \theta^{3/2} \chi_0'''(1) e^{\frac{x-1}{\varepsilon \sqrt{\theta}}} - \varepsilon^4 \theta^2 \chi_0^{IV}(0) e^{-\frac{x}{\varepsilon \sqrt{\theta}}} \right]. \tag{15.70}$$

15.4.2 Layered Plates with Small Reduced Shear Modulus

Consider case (B), where θ is a small parameter, and $\kappa = O(1)$ as $\theta \rightarrow 0$. The procedure of constructing the asymptotic solution remains the same with the following modifications. A solution of Eq. (15.21) is sought in the form:

$$X = X^{(m)}(x, \theta) + \theta^{\alpha_1} X_1^{(e)}(x, \theta) + \theta^{\alpha_2} X_2^{(e)}(x, \theta), \tag{15.71}$$

where

$$X^{(m)} = \chi_0(x) + \theta^{1/2} \chi_1(x) + \theta \chi_2(x) + \dots, \quad \lambda = \lambda_0 + \theta^{1/2} \lambda_1 + \theta \lambda_2 + \dots \tag{15.72}$$

and

$$X_1^{(e)} = a_1 e^{-\frac{x}{\sqrt{\theta}}} + O\left(\theta^{1/2} e^{-\frac{x}{\sqrt{\theta}}}\right), \quad X_2^{(e)} = a_2 e^{\frac{x-1}{\sqrt{\theta}}} + O\left(\theta^{1/2} e^{\frac{x-1}{\sqrt{\theta}}}\right), \tag{15.73}$$

The differential equation of the leading approximation reads

$$\mathbf{L}_0 \chi_0 \equiv \frac{d^4 \chi_0}{dx^4} - (2\delta^2 - \lambda_0 \delta^2 \kappa) \frac{d^2 \chi_0}{dx^2} + [\delta^4 - \lambda_0 \delta^2 (1 + \kappa \delta^2)] \chi_0 = 0. \tag{15.74}$$

Its general solution is defined by Eq. (15.54), where

$$\alpha = \frac{\sqrt{2}}{2} \sqrt{\delta^2 (2 - \lambda_0 \kappa) + \sqrt{\delta^2 \lambda_0 (4 + \lambda_0 \kappa^2 \delta^2)}}, \tag{15.75}$$

$$\gamma = \frac{\sqrt{2}}{2} \sqrt{-\delta^2 (2 - \lambda_0 \kappa) + \sqrt{\delta^2 \lambda_0 (4 + \lambda_0 \kappa^2 \delta^2)}},$$

and $\lambda_0 > \frac{\delta^2}{1 + \kappa \delta^2}$.

Here we restrict ourselves to the consideration of the $C^-C^-S^+S^+$ – boundary conditions. In this case, $\Phi = 0$, $\alpha_1 = \alpha_2 = 3/2$, and the boundary conditions in the

leading approximation read

$$\begin{aligned}\kappa\chi_0''(0) - (1 + \kappa\delta^2)\chi_0(0) &= 0, & \chi_0'(0) &= 0, \\ \kappa\chi_0''(1) - (1 + \kappa\delta^2)\chi_0(1) &= 0, & \chi_0'(1) &= 0\end{aligned}\tag{15.76}$$

In what follows, λ_0 is the minimum positive eigenvalue of the boundary-value problem (15.74), (15.76).

The next approximation yields the inhomogeneous boundary-value problem

$$\begin{aligned}\mathbf{L}_0\chi_1(x) &= \lambda_1\delta^2\left[(1 + \kappa\delta^2)\chi_0(x) - \kappa\chi_0''(x)\right], \\ \kappa\chi_1''(0) - (1 + \kappa\delta^2)\chi_1(0) &= -\kappa\chi_0'''(0), & \chi_1'(0) &= 0, \\ \kappa\chi_1''(1) - (1 + \kappa\delta^2)\chi_1(1) &= \kappa\chi_0'''(1), & \chi_1'(1) &= 0\end{aligned}\tag{15.77}$$

and the pair of constants, $a_1 = \chi_0'''(0)$, $a_2 = -\chi_0'''(1)$ for the edge effect integrals (15.73).

We note that the boundary-value problem (15.74), (15.76) is not self-conjugated. Let the function $\chi_*(x)$ be a solution of the homogeneous Eq. (15.74) with the following conjugated boundary conditions:

$$\begin{aligned}\kappa\chi_*'''(0) - (\kappa\delta^2 - \lambda_0\kappa^2\delta^2 - 1)\chi_*'(0) &= 0, & \chi_*(0) &= 0, \\ \kappa\chi_*'''(1) - (\kappa\delta^2 - \lambda_0\kappa^2\delta^2 - 1)\chi_*'(1) &= 0, & \chi_*(1) &= 0.\end{aligned}\tag{15.78}$$

Then the comparability conditions for the inhomogeneous boundary-value problem (15.77) results in the following correction for the eigenvalue λ_0 :

$$\lambda_1 = -\frac{\chi_0'''(0)\chi_*'(0) + \chi_0'''(1)\chi_*'(1)}{\delta^2(1 + \kappa\delta^2)\int_0^1\chi_0(x)\chi_*(x)dx - \delta^2\kappa\int_0^1\chi_0''(x)\chi_*(x)dx}.\tag{15.79}$$

15.5 Analysis of Influence of Boundary Conditions and Edge Effects on Critical Force

At first, we consider case (A). In the leading approximation ($k = 0$), the homogeneous boundary-value problems represented by Eq. (15.33) and by corresponding boundary conditions coincide with similar classical problems for single layer plates when shear effect is ignored. The careful analysis of the influence of boundary conditions on buckling of single layer isotropic rectangular plates can be found in Alfutov (2000). In particular, diagrams of the critical compressive force versus the side ratio $l = b/a$ are presented for all possible variants of boundary conditions. Here, we give similar plots of the load parameter λ_0 as of the function of a param-

eter $\delta = \pi n/l$. The minimum positive eigenvalue $\lambda_0(\delta)$ versus a fixed parameter δ is depicted in Fig. 15.1 for the three distinctive variants of boundary conditions, $S^\pm S^\pm S^+ S^+$, $S^\pm C^\pm S^+ S^+$ and $C^\pm C^\pm S^+ S^+$ – conditions (as a reminder, the value of λ_0 does not depend on whether the edges are equipped with diaphragms or not).

Let δ_m be a value at which the function $\lambda_0(\delta)$ takes a minimum value λ_m . Here, $\delta_m = \pi$, $\lambda_m \approx 39.478$ for $S^\pm S^\pm$ – boundary conditions at the unloaded edges, $\delta_m \approx 3.95$, $\lambda_m \approx 53.392$ for $S^\pm C^\pm$ – conditions and $\delta_m \approx 4.75$, $\lambda_m \approx 68.800$ for $C^\pm C^\pm$ – conditions. The required eigenvalue λ_0^* corresponding to the plate buckling strongly depends on the sides ratio $l = b/a$ and is determined as follows. If $l < \pi/\delta_m$, then $n^* = 1$, $\delta^* = \pi n^*/l = \pi/l$, and for $l \geq \pi/\delta_m$, one obtains $n^* = \text{In}(\delta_m l/\pi)$, where the sign $\text{In}(z)$ as above denotes the integer part of a number z . In both cases, $\lambda_0^* = \lambda_0(\delta^*)$.

The correction $\varepsilon^k \lambda_k$, taking into account shears, strongly depends on the type of boundary conditions. For the plates with $S^- S^-$, $S^- C^-$ – conditions at the unloaded edges $x = 0, 1$, we obtain the correction $\varepsilon \lambda_1$ of order $O(\varepsilon)$, while for the plates with $S^+ S^+$, $C^\pm C^\pm$, $S^+ C^-$ – conditions this correction becomes smaller and is a value of order $O(\varepsilon^2)$. Other words, if even one simply supported edge is free of a diaphragm, then the effect of shears on the critical buckling force increases.

A sign of the correction as well as its value depend on the ratio $\delta = b/a$ and the shear parameter θ . We remind that a parameter θ is the function of many magnitudes such as a number of layer, thickness and Young’s modulus of each layer. A parameter θ is generally small (Mikhasev et al, 2019). In Figs. 15.2 - 15.4, the relative corrections $\Lambda_1 = \lambda_1/\lambda_0$ and $\Lambda_2 = \lambda_2/\lambda_0$ are depicted as functions of δ for $\theta = 0.01, 0.1, 0.5, 0.8$.

It is seen that for $S^- S^-$ – conditions at the unloaded edges, the correction Λ_1 is always positive. When θ is infinitely small, then the correction is maximum for any δ . Note that $\theta = 0$ corresponds to the Timoshenko-Reissner model (Tovstik and Tovstik, 2017a) when the edge effects are ignored and only the transverse shears inside the plate are taken into account. Hence, accounting for shears near the simply supported edges without diaphragms reduces the positive correction and, as consequence, the critical buckling force. For any fixed θ , the correction Λ_1 reaches the

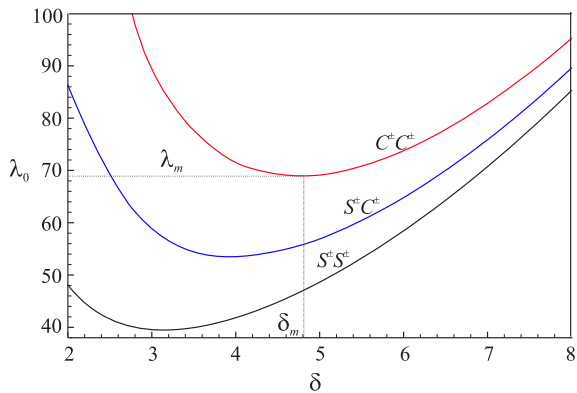


Fig. 15.1 The first positive eigenvalue $\lambda_0(\delta)$ vs. a parameter δ for $S^\pm S^\pm$, $S^\pm C^\pm$, $C^\pm C^\pm$ – boundary conditions at the unloaded edges. Case (A).

Fig. 15.2 The relative correction $\Lambda_1 = \lambda_1/\lambda_0$, taking into account shears, vs. parameter δ at various $\theta = 0.01, 0.1, 0.5, 0.8$ (curves 1, 2, 3, 4, respectively) for plates with S^-S^- – boundary conditions at the unloaded edges.

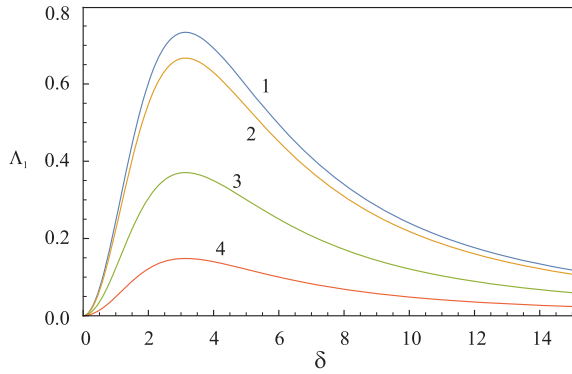


Fig. 15.3 The relative correction $\Lambda_1 = \lambda_1/\lambda_0$, taking into account shears, v.s parameter δ at various $\theta = 0.01, 0.1, 0.5, 0.8$ (curves 1, 2, 3, 4, respectively) for plates with S^-C^- – boundary conditions at the unloaded edges.

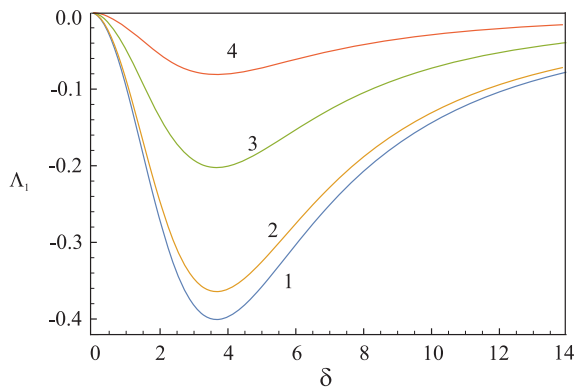
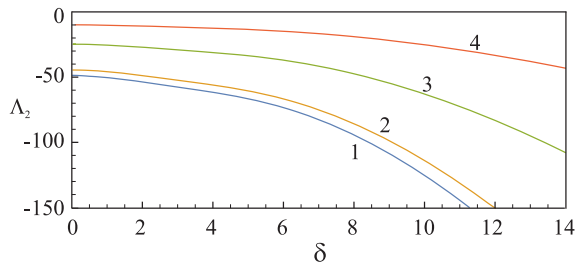


Fig. 15.4 The relative correction $\Lambda_2 = \lambda_2/\lambda_0$, taking into account shears, vs. parameter δ at various $\theta = 0.01, 0.1, 0.5, 0.8$ (curves 1, 2, 3, 4, respectively) for plates with $C^\pm C^\pm$ – boundary conditions at the unloaded edges.



maximum value at $\delta = \pi$. When $\delta \rightarrow 0$ or $\delta \rightarrow \infty$ (that corresponds to the degeneration of a plate into an infinitely narrow stripe or beam, respectively), the correction Λ_1 vanishes.

For S^-C^- – boundary conditions at the unloaded edges, the relative correction Λ_1 becomes negative. The maximum absolute value of Λ_1 is achieved at $\delta \approx 3.95$ for any θ ; the smaller the parameter δ , the greater the value of $|\Lambda_1|$.

Finally, for $C^\pm C^\pm$ – conditions, the correction is always negative for any δ and its absolute value increases together with δ . We note that relations (15.58), (15.60) for $C^\pm C^\pm$ – conditions as well as Eq. (15.69) for S^+C^- – conditions are asymptotically correct if $\varepsilon^2 \Lambda_2 \ll 1$.

Now we analyze case (B) for C^-C^- – conditions at the unloaded edges. Here, θ is assumed to be a small parameter, while κ is a finite value of the order $O(1)$ as $\theta \rightarrow 0$. In this case, in contrast to case (A), the eigenvalue λ_0 evaluated in the leading approximation takes into account the transverse shear inside the plate. In Fig. 15.5, the first positive eigenvalue λ_0 of the boundary-value problem (15.74), (15.76) is shown as the function of a parameter δ for different values of the shear parameter κ . The minimum value λ_m of the function $\lambda_0(\delta)$ and the associated argument δ_m are shown in Table 15.1 for various κ . We note the following limit relation $\lim_{\kappa \rightarrow 0} \lambda_m = 68.80$, where $\lambda_m = 68.80$ corresponds to the $C^\pm C^\pm$ – boundary conditions for case (A), see Fig. 15.1. The required critical buckling force λ_0^* is evaluated in accordance with the rule described above for case (A).

In Fig. 15.6, the relative corrections Λ_1 are depicted as functions of δ for different κ . In contrast to case (A) considered for $C^\pm C^\pm$ – boundary conditions (see Eq. (15.58) and Fig. 15.4), the positive correction $\varepsilon\Lambda_1$ takes into account only the edge effect integrals induced by the transverse shears in the neighborhood of the clamped edges $x = 0, x = 1$ without diaphragms. Thus, accounting for shears in the vicinity of the clamped edges results in the increase of the critical buckling force evaluated in the framework of the Timoshenko-Reissner model. It can be seen that the correction Λ_1 falls down when the shear parameter κ decreases. For each fixed κ , there exists such value of δ for which this correction takes the maximum value. It is also interesting to note that the correction Λ_1 becomes weakly dependent on the shear parameter for large δ (when a plate is degenerated into a beam) and vanishes as $\delta \rightarrow \infty$ for any κ .

Fig. 15.5 The first positive eigenvalue $\lambda_0(\delta)$ vs. a parameter δ for C^-C^- – boundary conditions at the unloaded edges for different values of the shear parameter $\kappa = 0.005, 0.07, 0.01, 0.02, 0.05, 0.1$ (curves 1, 2, 3, 4, 5, 6, respectively). Case (B).

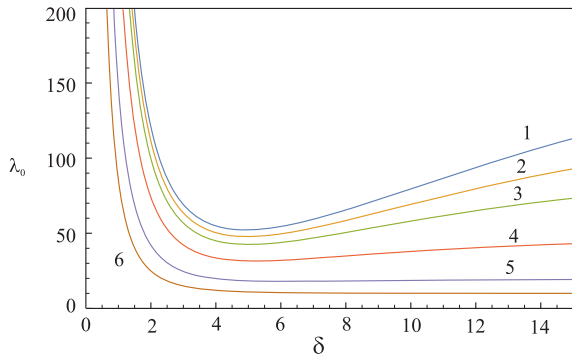
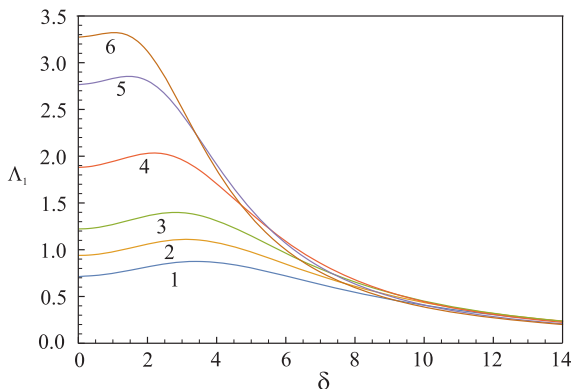


Table 15.1 Parameters λ_m, δ_m for different values of the shear parameter κ .

| | | | | | | |
|-------------|-------|-------|-------|-------|-------|-------|
| κ | 0.005 | 0.007 | 0.01 | 0.02 | 0.05 | 0.1 |
| δ_m | 4.92 | 4.96 | 5.02 | 5.21 | 6.25 | 15.00 |
| λ_m | 52.21 | 47.81 | 42.56 | 31.54 | 18.00 | 10.01 |

Fig. 15.6 The relative correction $\Lambda_1 = \lambda_1/\lambda_0$, taking into account shears in the vicinity of the unloaded edges with C^-C^- – boundary conditions, vs. a parameter δ for different values of the shear parameter $\kappa = 0.005, 0.07, 0.01, 0.02, 0.05, 0.1$ (curves 1, 2, 3, 4, 5, 6, respectively). Case (B).



15.6 Conclusions

Based on the ESL theory for laminated shells, buckling of layered rectangular plates uniaxially compressed by in-plane forces was studied. The loaded edges were assumed to be simply supported and supplied with diaphragms while for other edges two groups of boundary conditions, the clamped and simple support groups, with or without diaphragm(s) were considered. The solutions of governing equations were constructed in the form of a superposition of the outer solution and the edge effect integrals accounting shears in the neighbourhood of the unloaded edges. It was found out that the effect of boundary conditions on the critical buckling load depends on whether one of the unloaded edges is equipped with the diaphragm or not. In particular, if there are no diaphragms at all unloaded simply supported edges, then a correction to the classical buckling force turns out to be an order of magnitude higher than for a plate equipped with a diaphragm at least on one of the unloaded simply supported edges.

References

- Alfutov NA (2000) Stability of Elastic Structures. Foundations of Engineering Mechanics, Springer, Berlin, Heidelberg
- Altenbach H (1998) Theories for laminated and sandwich plates. a review. Mechanics of Composite Materials 34(3):243–252
- Amabili M (2015) A new third-order shear deformation theory with non-linearities in shear for static and dynamic analysis of laminated doubly curved shells. Compos Struct 128(0):260 – 273
- Ashton JE, Witney JM (1970) Theory of Laminated Plates. Technomic, Stamford, CT
- Aydogdu M (2009) A new shear deformation theory for laminated composite plates. Compos Struct 89(0):94–101
- Bryan GH (1890) On the stability of a plane plate under thrusts in its own plane, with applications to the buckling of the sides of a ship. Proc London Math Soc s1-22(1):54–67

- Bubnov I (1912) *Stroitel'naya mekhanika korablia* (in Russ.). Tip. Morskogo ministerstva, S.-Petersburg
- Donell LH (1976) *Beams, Plates and Shells*. McGraw-Hill Inc., New York
- Grigoliuk EI, Kulikov GM (1988) *Multilayered Reinforced Shells. Calculation of Pneumatic Tires* (in Russ.). Mashinostroenie, Moscow
- Khdeir AA (1989a) Comparison between shear deformable and kirchhoff theories for bending, buckling and vibration of antisymmetric angle-ply laminated plates. *Composite Structures* 13:159–172
- Khdeir AA (1989b) Free vibration and buckling of unsymmetric cross-ply laminated plates using a refined theory. *Journal of Sound and Vibration* 128(3):377–395
- Khdeir AA, Librescu L, Reddy JN (1987) Analytical solution of a refined shear deformation theory for rectangular composite plates. *International Journal of Solids and Structures* 23(10):1447–1463
- Librescu L, Khdeir AA, Reddy JN (1987) A comprehensive analysis of state of stress of elastic anisotropic flat plates using refined theories. *Acta Mech* 70(0):57–81
- Mikhasev G, Altenbach H (2019a) Elastic buckling of laminated beams, plates and cylindrical shells. In: *Thin-walled Laminated Structures, Advanced Structured Materials*, vol 106, Springer, Cham, pp 85–156
- Mikhasev G, Altenbach H (2019b) Equivalent single layer model for thin laminated cylindrical shells. In: *Thin-walled Laminated Structures, Advanced Structured Materials*, vol 106, Springer, Cham, pp 29–84
- Mikhasev G, Altenbach H (2019c) Free vibrations of elastic beams, plates and cylindrical shells. In: *Thin-walled Laminated Structures, Advanced Structured Materials*, vol 106, Springer, Cham, pp 157–198
- Mikhasev G, Altenbach H (2019d) Vibrations of laminated structures composed of smart materials. In: *Thin-walled Laminated Structures, Advanced Structured Materials*, vol 106, Springer, Cham, pp 199–272
- Mikhasev G, Botogova M (2017) Effect of edge shears and diaphragms on buckling of thin laminated medium-length cylindrical shells with low effective shear modulus under external pressure. *Acta Mech* 228(0):2119–2140
- Mikhasev G, Ereemeev V, Wilde K, Maevskaya S (2019) Assessment of dynamic characteristics of thin cylindrical sandwich panels with magnetorheological core. *Journal of Intelligent Material Systems and Structures* 30(18–19):2748–2769
- Mikhasev GI, Tovstik PE (2020) *Localized Dynamics of Thin-Walled Shells*. CRC Press, Boca Raton
- Mindlin RD (1951) Influence of rotatory inertia and shear on flexural motions of isotropic elastic plates. *Trans ASME J Appl Mech* 18:31–38
- Morozov NF, Tovstik PE, Tovstik TP (2016a) Generalized Timoshenko-Reissner model for a multilayer plate. *Mechanics of Solids* 51(5):527–537
- Morozov NF, Tovstik PE, Tovstik TP (2016b) The Timoshenko-Reissner generalized model for a plate highly nonuniform in thickness. *Doklady Physics* 61(8):394–398
- Nosier A, Reddy JN (1992) On vibration and buckling of symmetric laminated plates according to shear deformation theories. *Acta Mechanica* 94(3, 4):123–170
- Qatu MS, Sullivan RW, Wang W (2010) Recent research advances on the dynamic analysis of composite shells:2000-2009. *Comp Struct* 93(1):14–31
- Reddy JN (1984) A simple higher-order theory for laminated composite plates. *Trans ASME J Appl Mech* 51(4):745–752
- Reddy JN (2004) *Mechanics of Laminated Composite Plates and Shells: Theory and Analysis*, 2nd edn. CRC Press, Boca Raton
- Reddy JN, Khdeir AA (1989) Buckling and vibrations of laminated composite plates using various plate theories. *AIAA Journal* 27(12):1808–1817
- Reissner E (1945) The effect of transverse shear deformation on the bending of elastic plates. *Trans ASME J Appl Mech* 12(11):A69–A77

- Reissner E (1952) Stress-strain relations in the theory of thin elastic shells. *J Math Phys* 31:109–119
- Reissner H (1909) Über die Knicksicherheit ebener Bleche. *Zentralblatt der Bauverwaltung* 29(151):93–96
- Shi P, Dong C, Sun F, Liu W, Hu Q (2018) A new higher order shear deformation theory for static, vibration and buckling responses of laminated plates with the isogeometric analysis. *Compos Struct* 204(0):342–358
- Swaminathan R, Ragounadin D (2004) Analytical solutions using a higher-order refined theory for the static analysis of antisymmetric angle-ply composite and sandwich plates. *Compos Struct* 64(0):405–417
- Swaminathana K, Naveenkumara DT, Zenkourbc AM, Carrera E (2015) Stress, vibration and buckling analyses of fgm plates – a state-of-the-art review. *Compos Struct* 120(0):10–31
- Timoshenko SP (1907) On the question of the stability of compressed plates (in Russ.). *Bull of the Polytechnical Institute at Kiev* (2):35–94
- Timoshenko SP (1910) Einige Stabilitätsprobleme der Elastizitätstheorie. *Z Math Physik* 58(4):337–385
- Timoshenko SP (1936) *Theory of Elastic Stability*. McGraw-Hill Inc., New York
- Tovstik PE, Tovstik TP (2007) On the 2D models of plates and shells including the transversal shear. *ZAMM - Journal of Applied Mathematics and Mechanics / Zeitschrift für Angewandte Mathematik und Mechanik* 87(2):160–171
- Tovstik PE, Tovstik TP (2017a) An elastic plate bending equation of second-order accuracy. *Acta Mech* 228(10):3403–3419
- Tovstik PE, Tovstik TP (2017b) Generalized Timoshenko-Reissner models for beams and plates, strongly heterogeneous in the thickness direction. *ZAMM - Journal of Applied Mathematics and Mechanics / Zeitschrift für Angewandte Mathematik und Mechanik* 97(3):296–308
- Whitney JM, Sun CT (1973) A higher order theory for extensional motion of laminated anisotropic shells and plates. *Journal of Sound and Vibration* 30:85–97
- Whitney JM, Sun CT (1974) A refined theory of laminated anisotropic cylindrical shells. *Journal of Applied Mechanics* 41(2):471–476



Chapter 16

Semi-analytical Model for the Close-range Stress Analysis of Transverse Cracks in Composite Plates

Clemens Peiler, Andreas Kappel, and Christian Mittelstedt

Abstract In this paper, an efficient method for the computation of the stress state in the vicinity of transverse cracks in symmetric fibre-reinforced composite laminated plates under tensile load is presented. To determine the stress field, the solution of the Classical Lamination Theory (CLT) of the uncracked structure is superimposed with a so-called “internal solution” which is based on a subdivision of the layers into an arbitrary number of numerical plies. The displacement field of the composite laminated plate is approximated by introducing a priori unknown interface displacement functions. By employing the principle of minimum total potential energy, the governing equations are obtained in a closed-form manner and yield a quadratic eigenvalue problem, which is solved numerically. In order to obtain a full description of the state variables, the underlying boundary conditions as well as the continuity conditions have to be utilized. Comparisons with two-dimensional finite element studies indicate that the semi-analytical method is able predict the stress field with similar accuracy while only using a fraction of the underlying computational effort.

Key words: Composite plates, Transverse cracks, Interlaminar stresses, Layerwise analysis, Semi-analytical method

16.1 Introduction

Fibre-reinforced plastics are increasingly being used in a wide variety of engineering applications. Due to their favorable strength-to-weight ratio and the possibility to

Clemens Peiler · Andreas Kappel · Christian Mittelstedt
Technische Universität Darmstadt, Department of Mechanical Engineering, Institute for Lightweight Construction and Design, Germany
e-mail: clemens.peiler@klub.tu-darmstadt.de, andreas.kappel@klub.tu-darmstadt.de, christian.mittelstedt@klub.tu-darmstadt.de

optimize the material properties by tailoring the stacking sequence, they especially offer a great potential for lightweight construction applications. However, in order to ensure the integrity of those kinds of structural elements, potential flaws, such as transverse cracks, have to be considered in the development process or during maintenance work. Therefore, it is crucial to gain knowledge about the underlying stress state in close proximity of transverse cracks. At this point, one can refer to the finite element computations wherein especially the detailed discretization leads to computational efforts which in most cases turn out to be inefficient. An alternative approach is the method of complex potentials. Wang and Chen (1993) as well as Sator (2010) utilized this approach in order to determine the stress state in the vicinity of a transverse crack in a laminated plate wherein they assumed isotropic material behavior for each laminate layer. Hosoi and Kawada (2008), on the other hand, presented an analysis method in which the transverse cracks were specified as boundary effects while the potential stress concentrations at the tips of the cracks were neglected during the modelling process. Another approach is the scaled boundary finite element method, which was utilized by Lindemann (2013) in order to determine the stress field in composite laminated plates with transverse cracks which were subjected to thermomechanical loading conditions. Semi-analytical modelling techniques for similar structural situations were introduced by McCartney (1995), McCartney and Piers (1997b,a), as well as Schoeppner and Pagano (1998). A detailed overview on the topic of the stress analysis of transverse cracks in laminated structures is given by McCartney et al (2000). Concerning crack initiation and crack growth, the interested reader is referred to García et al (2014).

The objective of this contribution is to present an efficient method which enables the computation of the state variables in symmetric cross-ply laminated plates with transverse cracks by utilizing a layerwise approach which also has been employed in the works of Mittelstedt and Becker (2006, 2007) in order to analyze the free-edge stress fields in composite laminates. At first, the layers of the composite plate have to be subdivided into a number of numerical layers. Further on, for each of the numerical plies, a displacement field is introduced in which a closed-form CLT solution is combined with a layerwise approach. By virtue of the minimum total potential energy principle, the governing equations as well as the boundary conditions can be obtained in a closed-form manner. Modification of the equilibrium equations yields a quadratic eigenvalue problem which has to be solved numerically. Finally, by employing the boundary conditions at the transverse cracks, the analysis method enables a prediction of the state variables in the symmetric cross-ply laminated plate. The results of the semi-analytical approach are compared to highly detailed two-dimensional finite element computations. They reveal that the developed semi-analytical method is able to predict the stress field with high accuracy although using only a fraction of the underlying computational effort coming of full-scale numerical finite element analyses.

16.2 Structural Situation

The presented analysis method considers symmetric cross-ply laminated plates with transverse cracks. Due to the assumption of plane strain with respect to the y -direction, the model can be reduced to two dimensions as shown in Fig. 16.1. Further on, the composite plate has to be divided into two sections which are characterized by two coordinate systems. In this regard, the x_I, z - as well as the x_{II}, z -coordinate system originate in the middle plane of the laminated plate at the cross-section of the transverse cracks. The length of each section is defined in terms of l_1 and l_2 . The thickness of each laminate layer, on the other hand, is specified as h_i . The considered structure is fixed at its right edge, while the left edge is subjected to a tensile load in x -direction characterized by the initial displacement u_{init} . The fibres of a 0° layer are parallel to the x_I - and x_{II} -directions while of a 90° layer, the fibres run along the y -axis. The underlying material properties are displayed in Table 16.1.

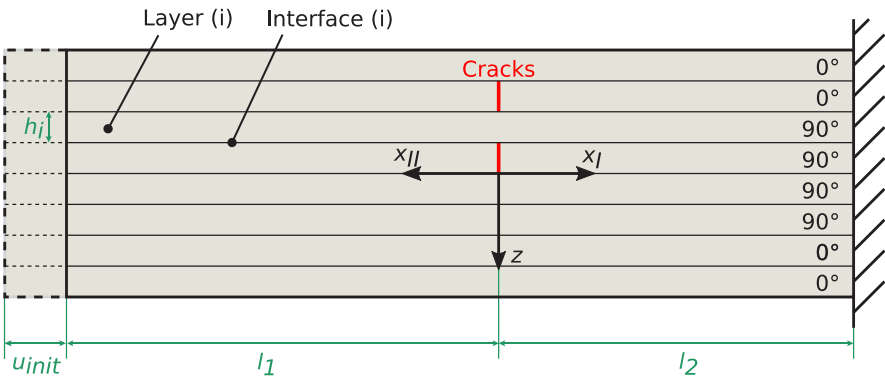


Fig. 16.1 Structural situation of the considered symmetric $[0_2^{\circ}/90_2^{\circ}]_S$ -laminated plate with transverse cracks in the fifth and seventh laminate layer.

Table 16.1 Considered dimensions as well as material properties (T300/Epoxy).

| Dimensions | | | |
|---|--------|-------|--------------------------------|
| l_1 | 10 | [mm] | Length of structure section I |
| l_2 | 10 | [mm] | Length of structure section II |
| h_i | 0.125 | [mm] | Thickness of individual layers |
| u_{init} | 0.004 | [mm] | Initial displacement |
| Material properties for a 0° layer | | | |
| $E_y = E_z$ | 10800 | [MPa] | Young's modulus |
| E_x | 132000 | [MPa] | Young's modulus |
| G_{yz} | 3360 | [MPa] | Shear modulus |
| $G_{xz} = G_{xy}$ | 5650 | [MPa] | Shear modulus |
| $\nu_{yz} = \nu_{xz} = \nu_{xy}$ | 0.238 | [-] | Poisson's ratio |

16.3 Semi-analytical Approach

The presented analysis method is based on the superposition of a closed-form analytical solution and a layerwise approach. In this context, the CLT solution is describing the intact areas of the composite laminated plate, while the internal solution is utilized in order to consider the influence of the transverse cracks onto the state variables. In the following, the derivation of both solution procedures will be developed.

16.3.1 CLT Solution

Based on the plane stress assumption with regard to the thickness direction z , the CLT solution for a symmetric cross-ply laminated plate is characterized as:

$$\begin{pmatrix} N_{xx,0} \\ N_{yy,0} \\ N_{xy,0} \\ M_{xx,0} \\ M_{yy,0} \\ M_{xy,0} \end{pmatrix} = \begin{bmatrix} A_{11} & A_{12} & 0 & 0 & 0 & 0 \\ A_{12} & A_{22} & 0 & 0 & 0 & 0 \\ 0 & 0 & A_{66} & 0 & 0 & 0 \\ 0 & 0 & 0 & D_{11} & D_{12} & 0 \\ 0 & 0 & 0 & D_{12} & D_{22} & 0 \\ 0 & 0 & 0 & 0 & 0 & D_{66} \end{bmatrix} \begin{pmatrix} \varepsilon_{xx,0} \\ \varepsilon_{yy,0} \\ \gamma_{xz,0} \\ \kappa_{xx,0} \\ \kappa_{yy,0} \\ \kappa_{xy,0} \end{pmatrix} \quad (16.1)$$

Furthermore, by considering the structural situation as illustrated in Fig. 16.1, the following assumptions can be made:

$$\begin{aligned} \varepsilon_{yy,0}^I &= \varepsilon_{yy,0}^{II} = 0, & \gamma_{xy,0}^I &= \gamma_{xy,0}^{II} = 0, \\ \kappa_{yy,0}^I &= \kappa_{yy,0}^{II} = 0, & \kappa_{xy,0}^I &= \kappa_{xy,0}^{II} = 0, \\ N_{yy,0}^I &= N_{yy,0}^{II} = 0, & N_{xy,0}^I &= N_{xy,0}^{II} = 0, \\ M_{xx,0}^I &= M_{xx,0}^{II} = 0, & M_{yy,0}^I &= M_{yy,0}^{II} = 0, \\ M_{xy,0}^I &= M_{xy,0}^{II} = 0, & N_{xx,0}^I &= N_{xx,0}^{II} = 0, \end{aligned} \quad (16.2)$$

Concerning the continuity and boundary conditions, the displacement functions of both structural areas are formulated as:

$$\begin{aligned} u_0^I(x_I) &= \frac{x_I - l_1}{l_1 + l_2} u_{init}, \\ u_0^{II}(x_{II}) &= \frac{x_{II} + l_1}{l_1 + l_2} u_{init} \end{aligned} \quad (16.3)$$

16.3.2 Internal Solution

The CLT solution considers a two-dimensional stress state with respect to the x,y -plane without taking any transverse cracks into account. Since for the underlying structural situation, two-dimensional stress concentrations in close proximity to the introduced transverse cracks are expected, the CLT solution has to be upgraded by a layerwise displacement-based approach. Herein, each of the n physical layers in the composite plate is subdivided into m numerical plies with respect to the thickness direction z . This can be carried out in the form of an equidistant distribution of the mathematical layers, or by concentrating the numerical plies at the interfaces of the laminate layers by utilizing a space ratio function α in z -direction which, in this regard, characterizes the ratio of two adjacent layers (Kappel and Mittelstedt, 2020). Nonetheless, both approaches lead to $n_L = m \cdot n$ mathematical layers and $n_L + 1$ mathematical interfaces which are displayed in Fig. 16.2. It should be noted that in the following, only the solution procedure for section I is derived, since section II can be described analogously. To attain a formulation for the resulting displacements in z -direction for each numerical layer, Hooke’s generalized law has to be utilized:

$$\begin{pmatrix} \sigma_{xx}^{(k)} \\ \sigma_{yy}^{(k)} \\ \sigma_{zz}^{(k)} \\ \tau_{yz}^{(k)} \\ \tau_{xz}^{(k)} \\ \tau_{xy}^{(k)} \end{pmatrix} = \begin{bmatrix} \bar{C}_{11}^{(k)} & \bar{C}_{12}^{(k)} & \bar{C}_{13}^{(k)} & 0 & 0 & 0 \\ \bar{C}_{12}^{(k)} & \bar{C}_{22}^{(k)} & \bar{C}_{23}^{(k)} & 0 & 0 & 0 \\ \bar{C}_{13}^{(k)} & \bar{C}_{23}^{(k)} & \bar{C}_{33}^{(k)} & 0 & 0 & 0 \\ 0 & 0 & 0 & \bar{C}_{44}^{(k)} & 0 & 0 \\ 0 & 0 & 0 & 0 & \bar{C}_{55}^{(k)} & 0 \\ 0 & 0 & 0 & 0 & 0 & \bar{C}_{66}^{(k)} \end{bmatrix} \begin{pmatrix} \varepsilon_{xx}^{(k)} \\ \varepsilon_{yy}^{(k)} \\ \varepsilon_{zz}^{(k)} \\ \gamma_{yz}^{(k)} \\ \gamma_{xz}^{(k)} \\ \gamma_{xy}^{(k)} \end{pmatrix} \tag{16.4}$$

Taking (16.2) and the assumption of plane strain with regard to the y -direction into account, the displacement $w_0^{I,(k)}$ can be formulated as:

$$w_0^{I,(k)} = -\frac{\bar{C}_{13}^{(k)}}{\bar{C}_{33}^{(k)}} \int_{z^{(k)}}^{z^{(k+1)}} \frac{\Delta u_0^{I,(k)}}{\Delta x_I} \Delta z \tag{16.5}$$

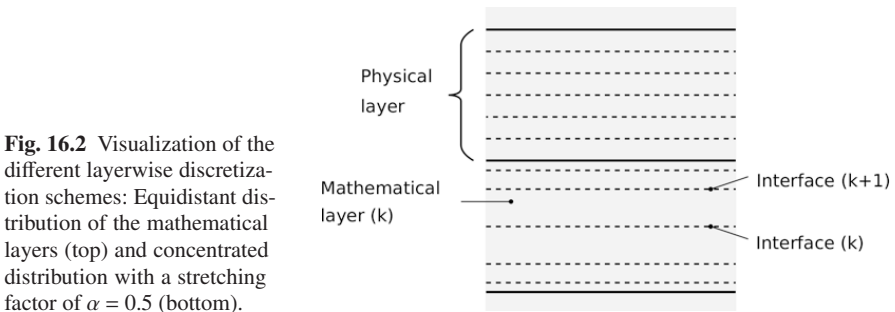


Fig. 16.2 Visualization of the different layerwise discretization schemes: Equidistant distribution of the mathematical layers (top) and concentrated distribution with a stretching factor of $\alpha = 0.5$ (bottom).

In order to include transverse cracks for each numerical layer, the displacements of the CLT solution have to be upgraded by a priori unknown displacement functions:

$$\begin{aligned} u^{I,(k)} &= u_0^{I,(k)}(x_I) + U_{VAR}^{I,(k)}(x_I, z) \\ w^{I,(k)} &= w_0^{I,(k)}(z) + W_{VAR}^{I,(k)}(x_I, z), \end{aligned} \quad (16.6)$$

wherein U_{VAR} and W_{VAR} are linearly approximated for all layers by means of Lagrangian interpolation functions $\psi_1^{(k)}$ and $\psi_2^{(k)}$ with respect to the thickness direction z from the neighboring displacement functions $U^{I,(k)}$ and $W^{I,(k)}$ in the interfaces. Consequently, the internal displacements displayed in Fig. 16.3 can be formulated as:

$$\begin{aligned} U_{VAR}^{I,(k)} &= U^{I,(k)}(x_I)\psi_1^{(k)}(z) + U^{I,(k+1)}(x_I)\psi_2^{(k)}(z), \\ W_{VAR}^{I,(k)} &= W^{I,(k)}(x_I)\psi_1^{(k)}(z) + W^{I,(k+1)}(x_I)\psi_2^{(k)}(z) \end{aligned} \quad (16.7)$$

By virtue of (16.6) and the underlying kinematics, the layerwise strain field can be specified as:

$$\begin{aligned} \varepsilon_{xx}^{I,(k)} &= \frac{\Delta u_0^{I,(k)}}{\Delta x_I} + \frac{\partial U^{I,(k)}}{\partial x_I} \psi_1^{(k)} + \frac{\partial U^{I,(k+1)}}{\partial x_I} \psi_2^{(k)}, \\ \varepsilon_{zz}^{I,(k)} &= \frac{\Delta w_0^{I,(k)}}{\Delta z} + W^{I,(k)} \frac{\partial \psi_1^{(k)}}{\partial z} + W^{I,(k+1)} \frac{\partial \psi_2^{(k)}}{\partial z}, \\ \gamma_{xz}^{I,(k)} &= U^{I,(k)} \frac{\partial \psi_1^{(k)}}{\partial z} + U^{I,(k+1)} \frac{\partial \psi_2^{(k)}}{\partial z} + \frac{\partial W^{I,(k)}}{\partial x_I} \psi_1^{(k)} + \frac{\partial W^{I,(k+1)}}{\partial x_I} \psi_2^{(k)} \end{aligned} \quad (16.8)$$

which, further on, can be employed in order to gain an insight into the stress state by consideration of (16.4). To obtain a formulation for the unknown interface displacements $U^{I,(k)}$ and $W^{I,(k)}$, the minimum total potential energy principle will be employed:

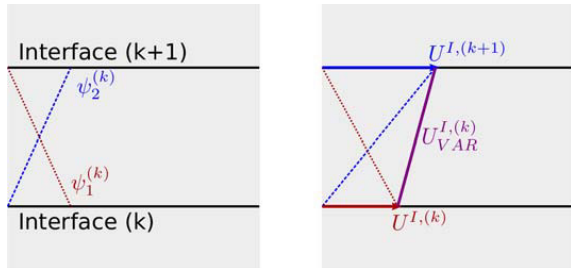


Fig. 16.3 Illustration of the linear shape functions (left) and displacements (right) of the k -th mathematical layer.

$$\begin{aligned} \Pi = \Pi_i^I + \Pi_i^{II} + \Pi_a = & \frac{1}{2} \sum_{k=1}^{n_L} \underbrace{\int_{V^{I,(k)}} \varepsilon^{I,(k)T} \bar{\mathbf{C}}^{I,(k)} \varepsilon^{I,(k)} \Delta V^{I,(k)} +}_{\Pi_i^I} \\ & \frac{1}{2} \sum_{k=1}^{n_L} \underbrace{\int_{V^{II,(k)}} \varepsilon^{II,(k)T} \bar{\mathbf{C}}^{II,(k)} \varepsilon^{II,(k)} \Delta V^{II,(k)} - N_{xx}^0 u_{int}}_{\Pi_i^{II}} = \text{Min} \quad (16.9) \end{aligned}$$

Since the external potential has a constant value, it will vanish due to the variation of the total potential energy. Thus, only the internal potentials of the two sections remain, each of which must fulfill the requirement to become minimal. Therefore the minimum total potential energy principle for section I can be reduced to:

$$\int_{z_k}^{z_{k+1}} \varepsilon^{I,(k)T} \bar{\mathbf{C}}^{I,(k)} \varepsilon^{I,(k)} \Delta z = \text{Min} \quad (16.10)$$

Applying the Euler-Lagrange-equations eventually yields the governing equations:

$$\begin{aligned} \delta U^{I,(k+1)} : & -E_{1112}^{(k)} \frac{\Delta^2 U^{I,(k)}}{\Delta x_I^2} - \left(E_{1122}^{(k)} + E_{1111}^{(k+1)} \right) \frac{\Delta^2 U^{I,(k+1)}}{\Delta x_I^2} - E_{1112}^{(k+1)} \frac{\Delta^2 U^{I,(k+2)}}{\Delta x_I^2} \\ & + G_{5512}^{(k)} U^{I,(k)} + \left(G_{5522}^{(k)} + G_{5511}^{(k+1)} \right) U^{I,(k+1)} + G_{5512}^{(k+1)} U^{I,(k+2)} \\ & + \left(F_{5512}^{(k)} - F_{1321}^{(k)} \right) \frac{\Delta W^{I,(k)}}{\Delta x_I} \\ & + \left(F_{5522}^{(k)} + F_{5511}^{(k+1)} - F_{1322}^{(k)} - F_{1311}^{(k+1)} \right) \frac{\Delta W^{I,(k+1)}}{\Delta x_I} \\ & + \left(F_{5521}^{(k+1)} - F_{1312}^{(k+1)} \right) \frac{\Delta W^{I,(k+2)}}{\Delta x_I} = 0 \\ \delta W^{I,(k+1)} : & + \left(F_{1312}^{(k)} - F_{5521}^{(k)} \right) \frac{\Delta U^{I,(k)}}{\Delta x_I} \\ & + \left(F_{1322}^{(k)} + F_{1311}^{(k+1)} - F_{5522}^{(k)} - F_{5511}^{(k+1)} \right) \frac{\Delta U^{I,(k+1)}}{\Delta x_I} \\ & + \left(F_{1321}^{(k+1)} - F_{5512}^{(k+1)} \right) \frac{\Delta U^{I,(k+2)}}{\Delta x_I} \\ & - E_{5512}^{(k)} \frac{\Delta^2 W^{I,(k)}}{\Delta x_I^2} - \left(E_{5522}^{(k)} + E_{5511}^{(k+1)} \right) \frac{\Delta^2 W^{I,(k+1)}}{\Delta x_I^2} - E_{5512}^{(k+1)} \frac{\Delta^2 W^{I,(k+2)}}{\Delta x_I^2} \\ & + G_{3312}^{(k)} W^{I,(k)} + \left(G_{3322}^{(k)} + G_{3311}^{(k+1)} \right) W^{I,(k+1)} + G_{3312}^{(k+1)} W^{I,(k+2)} \\ & + D_{132}^{I,(k)} + D_{131}^{I,(k+1)} + F_{332}^{I,(k)} + F_{331}^{I,(k+1)} = 0 \end{aligned} \quad (16.11)$$

The abbreviations in (16.11) are provided in the Appendix. Summarizing the interface displacements into the vectors \mathbf{U}^I and \mathbf{W}^I , eventually leads to:

$$\begin{aligned} \mathbf{K}_1 \frac{\Delta^2}{\Delta x_I^2} \mathbf{U}^I + \mathbf{K}_2 \frac{\Delta}{\Delta x_I} \mathbf{W}^I + \mathbf{K}_3 \mathbf{U}^I = 0, \\ \mathbf{K}_4 \frac{\Delta^2}{\Delta x_I^2} \mathbf{W}^I + \mathbf{K}_5 \frac{\Delta}{\Delta x_I} \mathbf{U}^I + \mathbf{K}_6 \mathbf{W}^I = \mathbf{R}^I \end{aligned} \quad (16.12)$$

Herein, \mathbf{K}_j ($j = 1, 2, \dots, 6$) are $(n_L + 1) \times (n_L + 1)$ coefficient matrices, while \mathbf{R}^I represents the right-hand side vector. The vectors \mathbf{U}^I and \mathbf{W}^I specify the interface dis-

placements in x_I - and z -direction and, in the following, are assembled into a single displacement vector:

$$\mathbf{U}_{tot}^I = \begin{pmatrix} \mathbf{U}_I \\ \mathbf{W}_I \end{pmatrix} \quad (16.13)$$

Utilizing (16.13), the differential equation systems in (16.12) can be summarized as:

$$\underbrace{\begin{bmatrix} \mathbf{K}_1 & 0 \\ 0 & \mathbf{K}_4 \end{bmatrix}}_{\mathbf{K}_{1,tot}} \frac{\Delta^2}{\Delta x_I^2} \mathbf{U}_{tot}^I + \underbrace{\begin{bmatrix} 0 & \mathbf{K}_2 \\ \mathbf{K}_5 & 0 \end{bmatrix}}_{\mathbf{K}_{2,tot}} \frac{\Delta}{\Delta x_I} \mathbf{U}_{tot}^I + \underbrace{\begin{bmatrix} \mathbf{K}_3 & 0 \\ 0 & \mathbf{K}_6 \end{bmatrix}}_{\mathbf{K}_{3,tot}} \mathbf{U}_{tot}^I = \begin{pmatrix} 0 \\ \mathbf{R}_I \end{pmatrix} \quad (16.14)$$

The coefficient matrices $\mathbf{K}_{j,tot}$ ($j = 1, 2, 3$) are of the dimension $2(n_L + 1) \times 2(n_L + 1)$. Equation (16.14) is a inhomogeneous ordinary differential equation system of second order and can be solved by means of the following approach:

$$\mathbf{U}_{hom}^I = \mathbf{A}^I e^{\lambda^I x_I} \quad (16.15)$$

Substituting \mathbf{U}_{tot}^I in (16.14) with (16.15) yields a quadratic eigenvalue problem that can be solved numerically:

$$\left(\lambda^{I2} \mathbf{K}_{1,tot} + \lambda^I \mathbf{K}_{2,tot} + \mathbf{K}_{3,tot} \right) \mathbf{A}^I = \mathbf{0} \quad (16.16)$$

Herein, \mathbf{A}^I is the eigenvector for the corresponding eigenvalue λ^I . In total, there are $4(n_L + 1)$ eigenvalues. It can be expected, that the transverse cracks only influence the stress field of the composite plate in close proximity. In order to be able to depict the decaying behavior remote from the transverse cracks, only the negative eigenvalues and their corresponding eigenvectors are considered. Thus $2(n_L + 1)$ eigenvalues remain. To avoid zero eigenvalues, the coefficient matrices \mathbf{K}_j ($j = 1, 2, \dots, 6$) are modified as:

$$\mathbf{K}_{j,mod} = \mathbf{K}_j - k_k \mathbf{K}_A \quad (16.17)$$

The definition of \mathbf{K}_A can be found in the Appendix, while k_k is set to $k_k = -10^{-3}$. Eventually, by solving (16.16), the unknown displacement functions can be formulated as:

$$\mathbf{U}_{hom}^I = \sum_{r=1}^{2(n_L+1)} b_r^I \mathbf{A}_r^I e^{\lambda_r^I x_I} \quad (16.18)$$

The particular solution of (16.14) is neglected in order to avoid rigid-body displacements and due to the fact that the additional displacements are already incorporated by the global CLT solution. Note that the so-called weight factors b_r^I are still unknown. To determine them, boundary and continuity conditions for each numerical layer have to be utilized which are obtained by virtue of the minimum total potential energy principle. The continuity conditions are used for intact mathematical layers to connect the sections I and II:

$$\begin{aligned}
& \int_{z^{(k-1)}}^{z^{(k)}} \sigma_{xx}^{I,(k-1)}(x_I = 0) \psi_2^{(k-1)} \Delta z + \int_{z^{(k)}}^{z^{(k+1)}} \sigma_{xx}^{I,(k)}(x_I = 0) \psi_1^{(k)} \Delta z = \\
& \int_{z^{(k-1)}}^{z^{(k)}} \sigma_{xx}^{II,(k-1)}(x_{II} = 0) \psi_2^{(k-1)} \Delta z + \int_{z^{(k)}}^{z^{(k+1)}} \sigma_{xx}^{II,(k)}(x_{II} = 0) \psi_1^{(k)} \Delta z, \\
& \int_{z^{(k-1)}}^{z^{(k)}} \tau_{xz}^{I,(k-1)}(x_I = 0) \psi_2^{(k-1)} \Delta z + \int_{z^{(k)}}^{z^{(k+1)}} \tau_{xz}^{I,(k)}(x_I = 0) \psi_1^{(k)} \Delta z = \\
& - \int_{z^{(k-1)}}^{z^{(k)}} \tau_{xz}^{II,(k-1)}(x_{II} = 0) \psi_2^{(k-1)} \Delta z - \int_{z^{(k)}}^{z^{(k+1)}} \tau_{xz}^{II,(k)}(x_{II} = 0) \psi_1^{(k)} \Delta z, \\
& U^{I,(k)}(x_I = 0) = -U^{II,(k)}(x_{II} = 0), \\
& W^{I,(k)}(x_I = 0) = W^{II,(k)}(x_{II} = 0) \quad (16.19)
\end{aligned}$$

For layers with a transverse crack, following boundary conditions are employed:

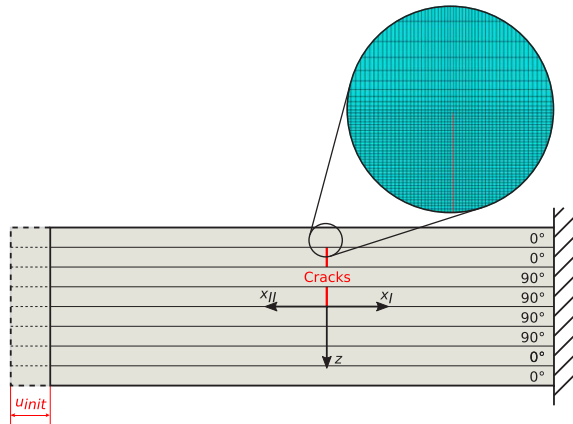
$$\begin{aligned}
& \int_{z^{(k-1)}}^{z^{(k)}} \sigma_{xx}^{I,(k-1)}(x_I = 0) \psi_2^{(k-1)} \Delta z + \int_{z^{(k)}}^{z^{(k+1)}} \sigma_{xx}^{I,(k)}(x_I = 0) \psi_1^{(k)} \Delta z = 0, \\
& \int_{z^{(k-1)}}^{z^{(k)}} \tau_{xz}^{I,(k-1)}(x_I = 0) \psi_2^{(k-1)} \Delta z + \int_{z^{(k)}}^{z^{(k+1)}} \tau_{xz}^{I,(k)}(x_I = 0) \psi_1^{(k)} \Delta z = 0, \\
& \int_{z^{(k-1)}}^{z^{(k)}} \sigma_{xx}^{II,(k-1)}(x_{II} = 0) \psi_2^{(k-1)} \Delta z + \int_{z^{(k)}}^{z^{(k+1)}} \sigma_{xx}^{II,(k)}(x_{II} = 0) \psi_1^{(k)} \Delta z = 0, \\
& \int_{z^{(k-1)}}^{z^{(k)}} \tau_{xz}^{II,(k-1)}(x_{II} = 0) \psi_2^{(k-1)} \Delta z + \int_{z^{(k)}}^{z^{(k+1)}} \tau_{xz}^{II,(k)}(x_{II} = 0) \psi_1^{(k)} \Delta z = 0 \quad (16.20)
\end{aligned}$$

16.4 Results

The stress field of a $[0^\circ/90^\circ]_S$ -laminate with two transverse cracks in the fifth and seventh physical layer (as illustrated in Fig. 16.1) is computed using the previously derived analysis method. In this regard, linear interpolation functions, 16 mathematical layers per physical layer and a space ratio of $\alpha = 0.8$ are utilized. The results are compared with those of a highly detailed two-dimensional finite element computation, as displayed in Fig. 16.4. Note that the semi-analytically calculated stresses at the mathematical interfaces are averaged from those of their neighboring layers.

Figure 16.5 displays the stresses in the cracked cross-section over the z -axis. In Fig. 16.6, the stresses over the x_I -axis are illustrated on the left starting from the crack tip of the cracked 0° layer at $z = -0.375\text{mm}$, while the right diagrams display the stresses at the middle of the crack ($z = -0.0625\text{mm}$) in the 90° layer over x_I . The results indicate, that the semi-analytical approach shows an adequate prediction of the underlying stress field.

Fig. 16.4 Discretization of the finite element model at the tips of the transverse cracks.



16.5 Summary and Conclusions

In the present work, a semi-analytical method for the computation of the intra- and interlaminar stresses in close proximity of transverse cracks in a symmetric cross-ply laminated plate subjected to a tensile load was developed. The results of the semi-analytical approach were compared with those of finite element computations. It was revealed that the proposed method yields results of similar accuracy while being highly efficient in terms of the computational effort. Therefore, the semi-analytical method can be confidently used in order to predict the stress state in transversely cracked composite laminated plates and thus help to evaluate the behavior of such components in preliminary design conceptualizations or during parametric studies.

References

- García IG, Mantič V, Blázquez A, París F (2014) Transverse crack onset and growth in cross-ply [0/90]_s laminates under tension. application of a coupled stress and energy criterion. *International Journal of Solids and Structures* 51(23-24):3844–3856
- Hosoi A, Kawada H (2008) Stress analysis of laminates of carbon fiber reinforced plastics, containing transverse cracks, considering free-edge effect and residual thermal stress. *Materials Science and Engineering* 498(1-2):69–75
- Kappel A, Mittelstedt C (2020) Free-edge stress fields in cylindrically curved cross-ply laminated shells. *Composites Part B: Engineering* 183:107,693
- Lindemann J (2013) Der Laminatrandeffekt und seine Analyse, insbesondere mit der Rand-Finite-Elemente-Methode. PhD thesis / Forschungsbericht Vol. 30, Studienbereich Mechanik, Technische Universität Darmstadt, Darmstadt
- McCartney L (1995) Comparison of models for transverse ply cracks in composite laminates. a recursive method of calculating stress transfer in multiple-ply cross-ply laminates subject to biaxial loading. NPL report DMMA(A)

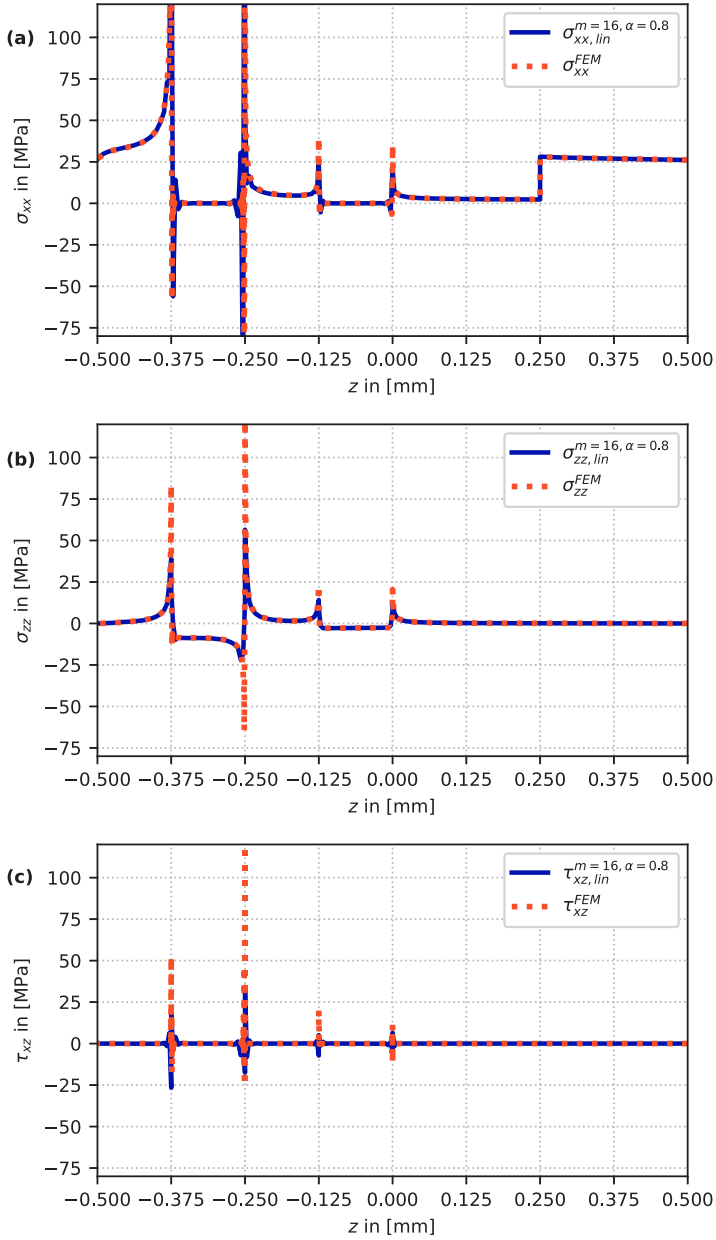


Fig. 16.5 Stress components (a) σ_{xx} , (b) σ_{zz} and (c) τ_{xz} in the cross section at $x_I = 0$ displayed in z -direction.

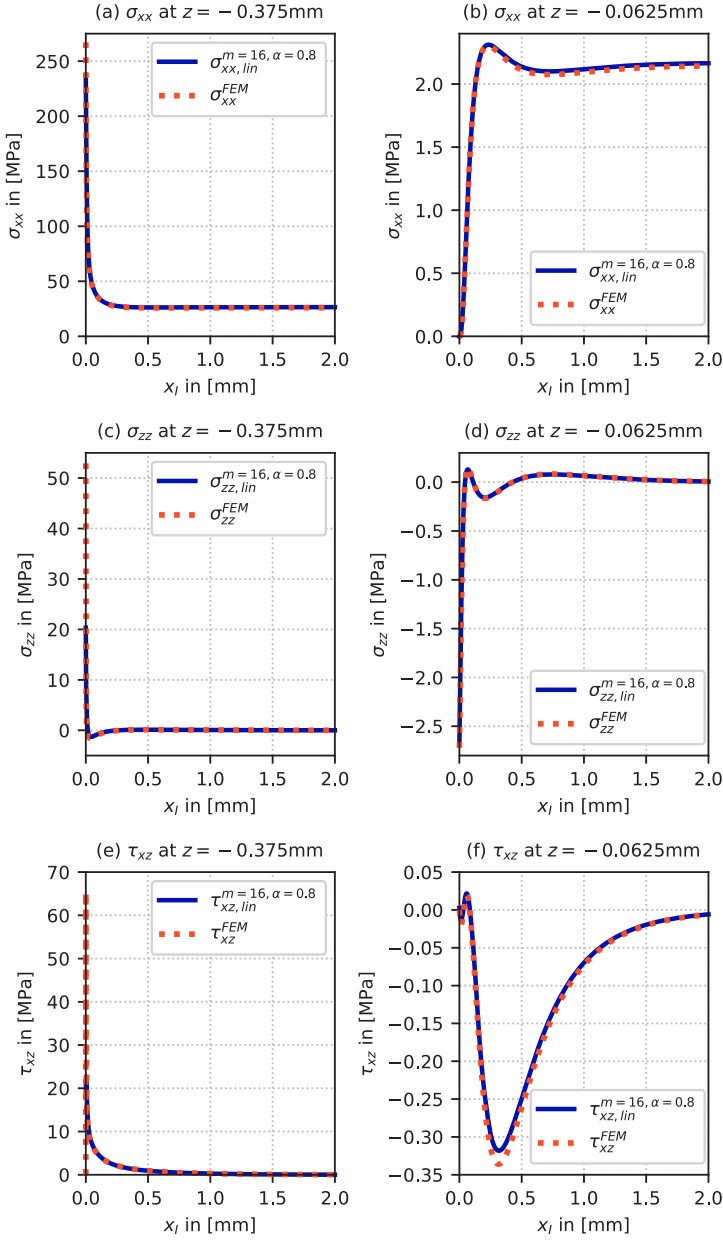


Fig. 16.6 Stresses at the crack tip of the transverse crack at $z = -0.375\text{mm}$ (left) and in the middle at $z = -0.0625\text{mm}$ (right) illustrated over the x_j -axis.

- McCartney LN, Piers C (1997a) Stress transfer mechanics for multiple ply laminates for axial loading and bending. In: Proceedings of the 11th International Conference on Composite Materials, vol V: Textile Composites and Characterisation, pp V662–V671
- McCartney LN, Piers C (1997b) Stress transfer mechanics for multiple ply laminates subject to bending. NPL Report, National Physical Laboratory, Centre for Materials Measurement & Technology, Teddington
- McCartney LN, Schoepner GA, Becker W (2000) Comparison of models for transverse ply cracks in composite laminates. *Composites Science and Technology* 60(12):2347–2359
- Mittelstedt C, Becker W (2006) Fast and reliable analysis of free-edge stress fields in a thermally loaded composite strip by a layerwise laminate theory. *International Journal for Numerical Methods in Engineering* 67(6):747–770
- Mittelstedt C, Becker W (2007) Free-edge effects in composite laminates. *Applied Mechanics Reviews* 60(5):217–245
- Sator C (2010) Asymptotische Nahfeldanalysen ebener Multi-Materialverbindungsstellen mit der Methode komplexer Potentiale. PhD thesis / Forschungsbericht Vol. 21, Studienbereich Mechanik, Technische Universität Darmstadt, Darmstadt
- Schoepner GA, Pagano NJ (1998) Stress fields and energy release rates in cross-ply laminates. *International Journal of Solids and Structures* 35(11):1025–1055
- Wang WC, Chen JT (1993) Theoretical and experimental re-examination of a crack perpendicular to and terminating at the bimaterial interface. *The Journal of Strain Analysis for Engineering Design* 28(1):53–61

Appendix

$$\begin{aligned}
 E_{opqr}^{(k)} &= \int_{z^{(k)}}^{z^{(k+1)}} \bar{C}_{op}^{(k)} \psi_q^{(k)} \psi_r^{(k)} \Delta z, \\
 F_{opqr}^{(k)} &= \int_{z^{(k)}}^{z^{(k+1)}} \bar{C}_{op}^{(k)} \psi_q^{(k)} \frac{\partial \psi_r^{(k)}}{\partial z} \Delta z, \\
 G_{opqr}^{(k)} &= \int_{z^{(k)}}^{z^{(k+1)}} \bar{C}_{op}^{(k)} \frac{\partial \psi_q^{(k)}}{\partial z} \frac{\partial \psi_r^{(k)}}{\partial z} \Delta z, \\
 D_{opq}^{(k)} &= \int_{z^{(k)}}^{z^{(k+1)}} \bar{C}_{op}^{(k)} \varepsilon_{xx,CLT}^{(k)} \frac{\partial \psi_q^{(k)}}{\partial z} \Delta z, \\
 F_{opq}^{(k)} &= \int_{z^{(k)}}^{z^{(k+1)}} \bar{C}_{op}^{(k)} \varepsilon_{zz,CLT}^{(k)} \frac{\partial \psi_q^{(k)}}{\partial z} \Delta z, \\
 \Delta_{qr}^{(k)} &= \int_{z^{(k)}}^{z^{(k+1)}} \psi_q^{(k)} \psi_r^{(k)} \Delta z
 \end{aligned} \tag{16.21}$$

$$K_{\Delta} = \begin{bmatrix} \Delta_{11}^{(1)} & \Delta_{12}^{(1)} & 0 & \cdots & 0 & 0 & 0 \\ \Delta_{12}^{(1)} & \Delta_{22}^{(1)} + \Delta_{11}^{(2)} & \Delta_{12}^{(2)} & \cdots & 0 & 0 & 0 \\ \vdots & \vdots & \vdots & \ddots & \vdots & \vdots & \vdots \\ 0 & 0 & 0 & \cdots & \Delta_{12}^{(n_L-1)} & \Delta_{22}^{(n_L-1)} + \Delta_{11}^{(n_L)} & \Delta_{12}^{(n_L)} \\ 0 & 0 & 0 & \cdots & 0 & \Delta_{12}^{(n_L)} & \Delta_{22}^{(n_L)} \end{bmatrix} \quad (16.22)$$



Chapter 17

Shear Deformable Elastic Beam Models in Vibration and Sensitivity of Natural Frequencies to Warping Effects

Castrenze Polizzotto, Isaac Elishakoff, and Paolo Fuschi

Abstract A theory of shear deformable beams in vibration is formulated using a shear-warping theory whereby the cross section is allowed to warp according to a parametrically specified warping rule (parametric warping). A continuous family of beams is generated which is controlled by a warping parameter $s \geq 0$ spanning from $s = 0$ (Timoshenko-Ehrenfest beam) to $s = \infty$ (Euler-Bernoulli beam) and intersecting the Levinson-Reddy model for $s = 0.5$. This enables one to express any response parameter as a function of s useful to describe the sensitivity of the beam's behavior to warping effects. The governing transverse displacement differential equation (DE) - of the fourth order in the case of no warping - is instead of the sixth order in the presence of warping effects, but remarkably the maximum order of time derivatives is still four. The vibration motion of the family's general beam is characterized by two basic macroscopic space and time scales, which make it possible to ascertain that the terms of the governing DE with the fourth order time derivative are negligible with respect to the others. The simplified governing DE without fourth order time derivatives is applied to a beam case to derive the physically meaningful spectrum with warping effects and to assess the sensitivity of natural frequencies to the warping effects. Every frequency as a function of s exhibits a waved pattern featured by softening for $0 < s < s_h$ (with smaller frequencies therein), by hardening for $s > s_h$ (with larger frequencies therein), s_h varying with the vibration mode.

Castrenze Polizzotto

Department of Engineering, University of Palermo, I-90128 Palermo, Italy
e-mail: castrenze.polizzotto@unipa.it

Isaac Elishakoff

Department of Ocean and Mechanical Engineering, Florida Atlantic University, Boca Raton, FL 33431-0991, USA
e-mail: elishako@fau.edu

Paolo Fuschi

Department PAU, University Mediterranea of Reggio Calabria, I-89124 Reggio Calabria, Italy
e-mail: paolo.fuschi@unirc.it

Key words: Shear deformable elastic beams, Parametric warping theory, Free vibration analysis, Sensitivity of natural frequencies to warping effects

17.1 Introduction

Historically, Timoshenko (1916, 1921, 1922), in cooperation with Ehrenfest, proposed his beam model as an improvement of the Euler–Bernoulli (EB) and Bresse–Rayleigh (BR) beam models, whereby the cross section is allowed to remain plane, but not necessarily orthogonal to the deflected axis of the beam. Contrary to the EB-beam, which is shear undeformable, the Timoshenko–Ehrenfest (TE) beam is fully shear deformable in the sense that the shear strain is uniformly distributed through the whole thickness of the beam, thus contradicting the requirement of zero shear stress at the lower and upper free surfaces of the beam. Shear deformable beams were subsequently proposed, in which this requirement was satisfied by allowing the beam cross section to warp according to specified warping rules, thus making superfluous the shear correction introduced by Timoshenko (1921) (see also Engesser, 1891; Föppl, 1897; Cowper, 1966; Kaneko, 1978; Elishakoff, 2020). For this purpose the axial displacement, say u_x , of the generic point was enriched by the addition of suitable terms varying through the thickness as $f(z)\phi(x)$, with $\phi(x)$ being the cross section rotation at the abscissa x , $f(z)$ a warping function of the thickness co-ordinate z . This function has been chosen in a variety of forms, either as a polynomial (Levinson, 1981; Bickford, 1982; Heyliger and Reddy, 1988; Subramanian, 2006; Reddy, 2007; Shi and Voyiadjis, 2011; Carrera and Giunta, 2010; Giunta et al., 2013), or trigonometric functions (Arya, 2003; Jun and Hongxing, 2009; Touratier, 1991; Sayyad and Ghugal, 2014), or hyperbolic functions (Soldatos, 1992), or exponential functions (Karama et al., 2003; Aydogdu, 2008; Mantari et al., 2011). For more details about these shear warping theories, see the papers by Eltaher et al. (2016) and Sayyad and Ghugal (2018) and the literature therein.

All the above shear warping theories adopt each a fixed warping profile of the beam's cross section with which the motion analysis is pursued. A mention is due to the unified formulation by Carrera and Giunta (2010) and Giunta et al. (2013) by Carrera and his associates, of which almost all the other models are particular cases.

Of particular interest for our purposes are the theories proposed by Levinson (1981); Reddy (1984); Heyliger and Reddy (1988) in which the added term is of the form $\Delta u_x = z^3\phi(x)$. In this way, mainly through the research work by Reddy and co-workers (Reddy, 2004, 2007), a third order theory (usually referred to as Reddy, or Levinson-Reddy (LR beam), theory) was constructed, in contrast to the first order (EB beam) and second order (TE beam) theories. The interested reader can consult with the book of Reddy (2004) for applications of this third order theory to various engineering problems and in particular to composite structural models in statics and dynamics.

In a recent paper (Polizzotto, 2015), the above theory was generalized by considering additional displacement terms of the form $\Delta u_x = z^N f(x)$, with $N = 1 + 2n$, ($n = 0, 1, \dots$). In this way a discrete numerable family of shear deformable beam models was introduced, which spans from the EB beam ($n = 0$) to the TE beam ($n \rightarrow \infty$). Every beam model in the family is governed by the same differential equations and boundary conditions, hence the solution for the generic beam holds good for the whole family. In a subsequent study (Polizzotto, 2017) this theory was extended to plate models, but using additional displacement terms of the form $\Delta u_\alpha = |z|^\omega f(x_\alpha)$, ($\alpha = 1, 2$), with $\omega \geq 0$ being a real scalar *warping parameter*. In the latter form, this shear warping theory has been extended to nonlocal beam models (Pisano et al., 2020).

The above *parametric* shear warping theory is substantially different from all other analogous theories. Whereas with every other theory a precise warping rule is used for the analysis of a specific beam model, instead with the parametric theory the governing equations incorporate the warping parameter. This implies that with the parametric theory the sensitivity analysis of any output of interest (maximum deflection, buckling load, natural frequencies) to the warping effect can be achieved for use within the inherent designing purposes.

In the present paper, the parametric warping theory is applied to shear deformable beams in free vibration in the purpose to evaluate the sensitivity of the natural frequencies to the warping effects. The obtained results will be illustrated by graphically reporting a few natural frequencies each as a function of the warping parameter. It will be shown that - at least for the examples here considered- the sensitivity exhibits a waved pattern, more pronounced for higher orders of every natural frequency.

The paper is organized as follows. In Sect. 17.2, the kinematics and stress-strain relations for a shear deformable beam with warping are reported together with the inherent shear-warping function. Also, the relations between bending moments M, \widehat{M} , shear forces Q, \widehat{Q} and the beam distributed degrees of freedom (deflection w and shear angle γ) are reported. In Sect 17.3, the equilibrium equations are employed to derive the two basic governing DEs, of which one is a sixth order space/time DE in the deflection w , the other is a differential relation between the shear angle γ and w . In Sect. 17.4, an alternative form of the sixth order governing DE is derived, in which the beam's geometrical characteristics (A, I) and the inertia ones ($\rho A, \rho I$) are incorporated into two basic space and time scale parameters, i.e. r (radius of inertia of the cross section) and τ (time interval for a wave to travel the distance r). The time scale τ , as small as $\approx 10^{-4}$ sec, is a basis to ascertain that the fourth order time derivatives can be disregarded from the governing DE. In Sect. 17.5, an application to a simply supported beam is addressed in which the frequencies sensitivity to warping effect is stated. Sect. 17.6 is devoted to the conclusions.

17.2 Kinematics, Stresses, and Warping Function

Let us consider a prismatic beam of length L and uniform rectangular cross section of height h and width b , constrained at the ends such as to impede global rigid motions, but with constraints that remain unspecified for the moment. The undeformed beam is referred to a Cartesian orthogonal co-ordinate system, say x, y, z , with the x axis coinciding with the centroid line, such that the beam ends are located at $x = 0$ and $x = L$, respectively, whereas the z axis is downward oriented in the thickness direction, the y axis in the width direction. The axes y and z are parallel to the inertia axes of the cross section. The beam finds itself in a free vibration state, whereby it experiences (infinitesimal) transverse displacements $w(x, t)$ of the centroids in the z direction, along with (absolute, infinitesimal) rotations $\phi(x, t)$ of the cross sections around the y axis, positive in the anticlockwise sense. The symbol t denotes the time variable. The usual simplifying assumptions of EB beam theory are valid, except that the cross sections are allowed to warp according to warping rules specified hereafter.

Following the axiomatic approach, let the beam's displacements be taken as

$$\begin{aligned} u_x &= -z w'(x, t) + \underbrace{\theta(z) \gamma(x, t)}_{\Delta u_x} \\ u_z &= w(x, t), \quad u_y \equiv 0 \end{aligned} \quad (17.1)$$

where $\theta(z)$ is the warping function also depending on the warping parameter s ; whenever it is appropriate, we shall write $\theta(z, s)$ instead of $\theta(z)$. The notation $w'(x, t) := \partial_x w(x, t)$ and $\dot{w}(x, t) := \partial_t w(x, t)$ is used hereinafter. The symbol γ denotes the *shear angle*, that is, the (relative, anticlockwise) rotation of the cross section with respect to the plane orthogonal to the deflected beam axis; it is related to the absolute rotation of the same cross section through the relation

$$\gamma(x, t) = w'(x, t) + \phi(x, t) \quad (17.2)$$

According to (17.1)₁, the displacement increment $\Delta u_x = \theta(z) \gamma(x, t)$ produced by warping is measured from the plane normal to the deflected axis. In the deformed state, the cross section finds itself rotated of the shear angle γ measured at the centroid c , but its profile is an antisymmetric curve like a-c-b, which has the slope γ at c , but slopes zero at the ends a, b , see Fig. 17.1.

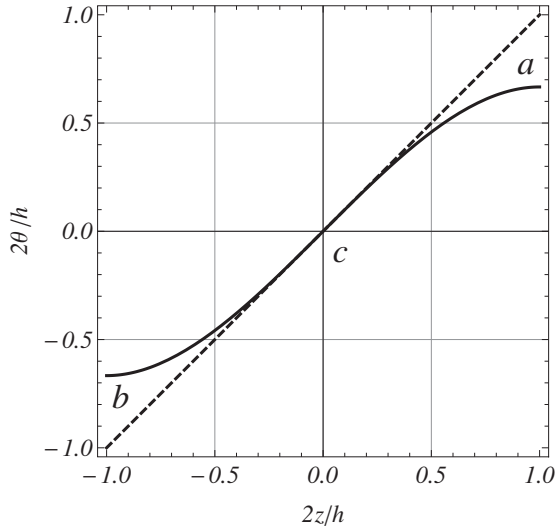
The only not identically vanishing strain components are

$$\begin{aligned} \varepsilon_{xx} &= -z w''(x, t) + \theta(z) \gamma'(x, t) \\ 2\varepsilon_{xz} &= \theta'(z) \gamma(x, t) \end{aligned} \quad (17.3)$$

For simplicity, isotropic material is considered. Denoting E, G the Young and shear elastic moduli, respectively, the stresses corresponding to the strains (17.3) are

$$\begin{aligned} \sigma_{xx} &= -E z w''(x, t) + E \theta(z) \gamma'(x, t) \\ \sigma_{xz} &= G \theta'(z) \gamma(x, t) \end{aligned} \quad (17.4)$$

Fig. 17.1 Profile of the warped cross section for some value of $s > 0$ and $\gamma = 1$ with the related non-dimensional axial displacement increment $2\theta(z)/h$.



The function $\theta(z)$ is the *shear-warping function* (Polizzotto, 2015, 2017), which is here chosen in the form

$$\theta(z) := z - \frac{|z|^{1+1/s} \text{sign}(z)}{(1 + 1/s)(h/2)^{1/s}}, \tag{17.5}$$

where $s \geq 0$ is a specified non-negative real number, here called *warping parameter*.

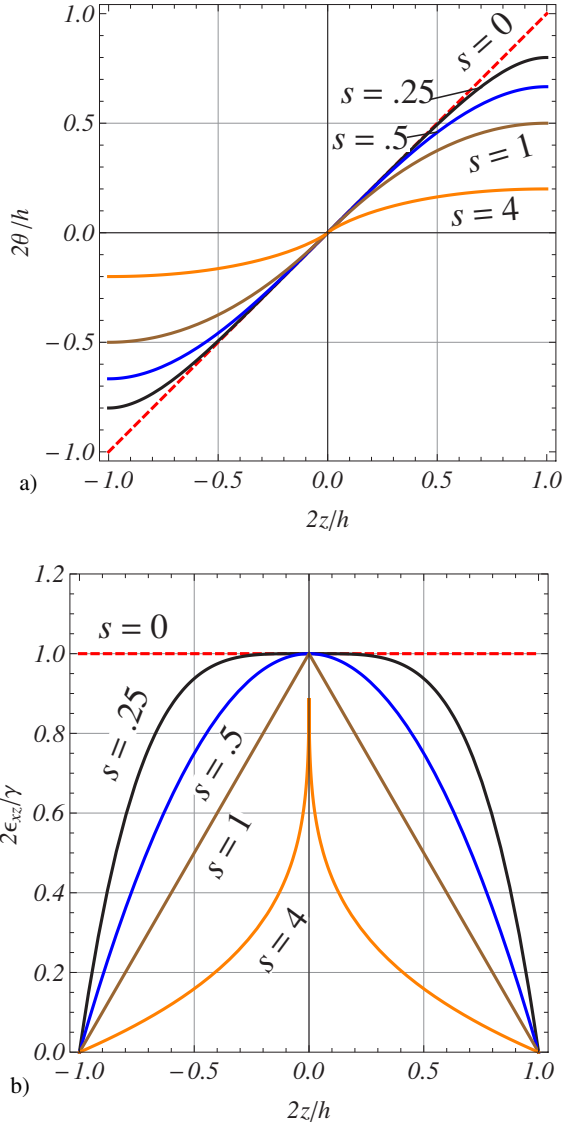
Since

$$\theta'(z) = 1 - \left(\frac{2|z|}{h}\right)^{1/s}, \quad \forall s \geq 0 \tag{17.6}$$

and thus $\theta'(\pm h/2) = 0$, it follows by (17.3)₂ that the shear strain ε_{xz} , along with the corresponding shear stress σ_{xz} , is vanishing at the lower and upper free surfaces of the beam, no matter the values of γ and s . The function $\theta(z)$ of (17.5) is suitable to rectangular cross sections with the elastic centroid at the middle of the thickness, but it may be somewhat changed such as to deal with anisotropic material whereby generally the elastic centroid finds itself at different distances from the lower and upper surfaces.

It may be useful to have a graphical representation of the warping effects. In Fig. 17.2(a) a small segment of a deformed beam around a generic cross section is considered, in which the dashed straight line is tangent to the cross section profile having a slope $\gamma = 1$ at the centroid. The exact shape of the cross section profile depends on the chosen value of s , but it is always an antisymmetric curve which - at parity of γ - is in between the dashed straight line (with which it coincides for $s = 0$, that is, in the TE beam case) and the normal to the deflected axis (with which it coincides for $s = \infty$, that is, in the EB beam case). In Fig. 17.2(b) the shear

Fig. 17.2 Warping effects with increasing the warping parameter s : a) Evolution of the warped cross section profile for $s = 0, 0.25, 0.5, 1, 4$; b) Analogous evolution of the shear strain distribution through the thickness.



strain distribution over the thickness is reported for a few values of s , which shows a symmetric convex shape for $s > 1$, a bi-linear shape for $s = 1$, a two-branch concave shape for $s < 1$. For $s = 0$ the strain is constant equal to γ (TE beam), for $s = \infty$ the strain is vanishing (EB beam).

It is noted that the shear-warping function of (17.5) is similar to functions proposed in Polizzotto (2015, 2017) for beam and plate models, respectively, and in Pisano et al. (2020) for nonlocal beam models, with the difference that in the latter

quoted works the warping parameter was taken in the form $\omega = 1/s$, so as $\omega = 0$ corresponds to the EB beam, $\omega = \infty$ to the TE beam. Instead, with the warping parameter s as in (17.5), $s = 0$ corresponds to the fully shear deformable TE beam, whereas values $s > 0$ correspond to consistently shear deformable beams, with shear deformability decreasing as s increases, till $s = \infty$ corresponding to the shear undeformable EB beam. The value $s = 0.5$ corresponds to the Levinson-Reddy model.

The following stress resultants are needed for the following developments (Polizzotto, 2015), namely, the bending moment M and warping bending moment \widehat{M} as

$$\begin{aligned} M &:= \int_A z\sigma_{xx}(x,t) dA = EI[-w''(x,t) + a_1\gamma'(x,t)] \\ \widehat{M} &:= \int_A \theta(z)\sigma_{xx}(x,t) dA = EI[-a_1w''(x,t) + a_2\gamma'(x,t)] \end{aligned} \quad (17.7)$$

along with the shear force Q and the warping shear force \widehat{Q} as

$$\begin{aligned} Q &:= \int_A \sigma_{xz} dA = k_1GA\gamma(x,t) \\ \widehat{Q} &:= \int_A \theta'(z)\sigma_{xz} dA = k_2GA\gamma(x,t) \end{aligned} \quad (17.8)$$

Here above, A, I denote the area and the second area moment of the cross section, whereas a_1, a_2, k_1, k_2 denote shear-warping coefficients defined as

$$\begin{aligned} (a_1, a_2) &= \frac{1}{I} \int_A (z\theta(z), \theta^2(z)) dA \\ (k_1, k_2) &= \frac{1}{A} \int_A (\theta'(z), \theta'^2(z)) dA \end{aligned} \quad (17.9)$$

These all are functions of s , but for simplicity of notation this dependence is not explicitly indicated. The analytical expressions of the above coefficients for a rectangular cross section are reported (with a different notation) in Polizzotto (2015) in terms of the discrete parameter $2n = 1/s$, ($n = 0, 1, 2, \dots$), and in Polizzotto (2017) in terms of the real continuous parameter $\omega = 1/s$. In the following the (non-negative) coefficient a_0 defined as

$$a_0 := a_2 - (a_1)^2 \quad (17.10)$$

will be also required.

17.3 Equilibrium Equations and Governing Differential Equations

The equilibrium equations for a shear deformable beam with warping effects read as (Polizzotto, 2015)

$$\begin{aligned} M''(x, t) + p_z(x, t) + m'(x, t) &= 0 \\ \widehat{M}'(x, t) - \widehat{Q}(x, t) + \widehat{m}(x, t) &= 0 \end{aligned} \quad (17.11)$$

where p_z, m, \widehat{m} denote applied transverse distributed loads and distributed (anticlockwise) couples, all of them being here generated by inertia forces. Denoting by b_x, b_z the inertia body forces given by

$$\begin{aligned} b_x &= -\rho \ddot{u}_x = -\rho \left[-z \ddot{w}'(x, t) + \theta(z) \ddot{\gamma}(x, t) \right] \\ b_z &= -\rho \ddot{u}_z = -\rho \ddot{w}(x, t) \end{aligned} \quad (17.12)$$

then we obtain

$$\begin{aligned} p_z &= \int_A b_z \, dA = -\rho A \ddot{w}(x, t) \\ m &= \int_A z b_x \, dA = -\rho I \left[-\ddot{w}'(x, t) + a_1 \ddot{\gamma}(x, t) \right] \\ \widehat{m} &= \int_A \theta(z) b_x \, dA = -\rho I \left[-a_1 \ddot{w}'(x, t) + a_2 \ddot{\gamma}(x, t) \right] \end{aligned} \quad (17.13)$$

The boundary conditions for a shear deformable simple beam under warping effects - to be used later on - are as follows (Polizzotto, 2015):

$$\begin{aligned} &\text{Either } w, \text{ or } M' \text{ specified} \\ &\text{Either } w', \text{ or } M \text{ specified} \\ &\text{Either } \gamma, \text{ or } \widehat{M} \text{ specified} \end{aligned} \quad (17.14)$$

Next, substituting (17.7), (17.8) and (17.13) into (17.11) results in the equations

$$\begin{aligned} EI(-w^{iv} + a_1 \gamma''') - \rho A \ddot{w} + \rho I(\ddot{w}' - a_1 \ddot{\gamma}') &= 0 \\ EI(-a_1 w'''' + a_2 \gamma'') - k_2 GA \gamma + \rho I(a_1 \ddot{w}' - a_2 \ddot{\gamma}) &= 0 \end{aligned} \quad (17.15)$$

On differentiating (17.15)₂ once more with respect to x and multiplying it by a_1 , then subtracting the obtained relation from (17.15)₁ multiplied by a_2 , we get

$$a_1 k_2 GA \gamma' = \underbrace{a_0 EI w^{iv}}_{\text{bending}} + \underbrace{a_2 \rho A \ddot{w}}_{\text{EB inertia}} - \underbrace{a_0 \rho I \ddot{w}''}_{\text{BR inertia}} \quad (17.16)$$

where a_0 is defined by (17.10).

Equation (17.16) constitutes a differential relation between the shear angle γ and the deflection w within an equilibrium configuration of the beam. It states that the shear curvature γ' is formed up by three different contributions of which the first one comes from the bending deformation (first addend on the r.h.s. of (17.16)), the other two arise from the Euler–Bernoulli (EB) transverse inertia and, respectively, the Bresse–Rayleigh (BR) rotary inertia.

Equation (17.16) can be used to eliminate γ from (17.15). Therefore, after a further double differentiation of (17.16) either in space, or in time, then substituting into (17.15)₁ gives

$$\begin{aligned}
 &-\frac{a_0 EI}{k_2 GA} EI w^{vi} + EI w^{iv} + \rho A \ddot{w} - \rho I \left(1 + \frac{a_2 E}{k_2 G}\right) \ddot{w}'' \\
 &+ \frac{2a_0 EI}{k_2 GA} \rho I \ddot{w}^{iv} + \frac{\rho^2 I}{k_2 G} \partial_t^4 \left(a_2 w - \frac{a_0 I}{A} w''\right) = 0
 \end{aligned} \tag{17.17}$$

Equation (17.17) is the governing DE in terms of deflection $w(x, t)$. We note the following:

- For $s = 0$ (TE beam) it is $a_0 = 0, a_1 = a_2 = k_2 = 1$, hence (17.17) identifies with the Bresse–Rayleigh/Timoshenko–Ehrenfest equation (taken with the shear correction coefficient equal to 1, see Challamel and Elishakoff, 2019), namely,

$$EI w^{iv} + \rho A \ddot{w} - \rho I \left(1 + \frac{E}{G}\right) \ddot{w}'' + \frac{\rho^2 I}{G} \partial_t^4 w = 0 \tag{17.18}$$

- For $s \rightarrow \infty$ (EB beam) it is $a_0 = a_1 = a_2 = 0$, hence (17.17) identifies with the Bresse–Rayleigh (BR) equation, that is,

$$EI w^{iv} + \rho A \ddot{w} - \rho I \ddot{w}'' = 0 \tag{17.19}$$

Let us also observe that a notable feature of the beam undergoing warping deformation is that the governing displacement equation is a space/time DE of the sixth order, but with time derivatives up to the fourth order like with the Bresse–Rayleigh (BR) beam. This means that the existence of a second spectrum of natural frequencies does occur also in the presence of warping effect (Stephen, 2006; Elishakoff et al., 2015).

17.4 An Alternative Form of the Motion Equation

An alternative more expressive form of the governing Eq. (17.17) is obtained by multiplying it by the factor $(\frac{I}{A})^2/(EI)$. By a re-ordering we obtain the following equation

$$\begin{aligned}
 &\underbrace{\left(\frac{I}{A}\right)^2 w^{iv} + \frac{\rho I}{EA} \ddot{w}}_{\text{EB beam}} - \underbrace{\left(1 + \frac{a_2 E}{k_2 G}\right) \frac{\rho I}{EA} \frac{I}{A} \ddot{w}''}_{\text{BR and TE corrections}} + \underbrace{\frac{a_2 E}{k_2 G} \left(\frac{\rho I}{EA}\right)^2 \partial_t^4 w}_{\text{h.o. TE correction}} + \\
 &+ \frac{a_0 E}{k_2 G} \left[\underbrace{-\left(\frac{I}{A}\right)^3 w^{vi} + 2 \frac{\rho I}{EA} \left(\frac{I}{A}\right)^2 \ddot{w}^{iv}}_{\text{warping correction}} - \underbrace{\left(\frac{\rho I}{EA}\right)^2 \frac{I}{A} \partial_t^4 w''}_{\text{h.o. warping correction}} \right] = 0
 \end{aligned} \tag{17.20}$$

in which “h.o.” stands for higher order. Next, let us introduce the notation:

$$r := \sqrt{\frac{I}{A}} \quad (\text{radius of inertia of cross section})$$

$$c := \sqrt{\frac{E}{\rho}} \quad (\text{velocity of propagation of a wave in isotropic elastic medium})$$

$$\tau := \frac{r}{c} = \sqrt{\frac{\rho I}{EA}} \quad (\text{time interval for a wave to travel a distance } r)$$

With this notation, Eq. (17.20) takes on a notable form as

$$\begin{aligned} & \underbrace{r^4 w^{iv}(x,t) + \tau^2 \ddot{w}(x,t)}_{\text{EB beam}} - \underbrace{\left(1 + \frac{a_2 E}{k_2 G}\right) \tau^2 r^2 \ddot{w}''(x,t)}_{\text{BR and TE corrections}} + \underbrace{\frac{a_2 E}{k_2 G} \tau^4 \partial_t^4 w(x,t)}_{\text{h.o. TE correction}} \\ & + \frac{a_0 E}{k_2 G} \left[\underbrace{-r^6 w^{vi}(x,t) + 2\tau^2 r^4 \ddot{w}^{iv}(x,t)}_{\text{warping correction}} - \underbrace{\tau^4 r^2 \partial_t^4 w''(x,t)}_{\text{h.o. warping correction}} \right] = 0 \end{aligned} \quad (17.21)$$

This latter time/space DE is cast in a form whereby the various addends of the first line represent the bending effect of the EB beam and the BR/TE corrections, whereas those of the second line provide the warping corrections. The notable aspect of (17.21) is that the equation coefficients are expressed in terms of a few essential physical/geometrical parameters. These include, beside the warping coefficients a_0, a_2, k_2 and the elastic moduli through the ratio E/G , two novel parameters, namely r and τ , having the meaning of *macroscopic space and time scales of the vibrating beam*. These novel coefficients carry in the essential pieces of information needed by the vibrating beam problem concerning the geometrical (A, I) and the inertial ($\rho A, \rho I$) characteristics of the vibrating beam.

17.4.1 A Simplification: From Double Spectrum to Single Spectrum

Assuming r and τ as unit space and time measures, that is, using the non-dimensional space and time co-ordinates $X = x/r, T = t/\tau$, and considering the deflection w as a function of (X, T) , then (17.21) becomes

$$\begin{aligned} & \partial_X^4 w + \partial_T^2 w - \left(1 + \frac{a_2 E}{k_2 G}\right) \partial_X^2 \partial_T^2 w + \frac{a_2 E}{k_2 G} \partial_T^4 w \\ & + \frac{a_0 E}{k_2 G} \left[-\partial_X^6 w + 2\partial_X^4 \partial_T^2 w - \partial_X^2 \partial_T^4 w \right] = 0 \end{aligned} \quad (17.22)$$

Equation (17.22) provides the vibration modes of a class of beams whose geometrical and inertial characteristics satisfy the scale conditions $r(A, I) = \bar{r}, \tau(\rho, A, I) = \bar{\tau}$, with $\bar{r}, \bar{\tau}$ being fixed values of r and τ .

It is obvious that Eq. (17.22), as well as Eq. (17.21), predicts two series of natural frequencies of the vibrating beam, due to the presence of the fourth order time derivative. However, considering e.g. $r = 10$ cm and $c = 5300$ m/second for steel (Eringen and Suhubi, 1975, p. 505) the time scale turns out to be as small as $\tau \approx 10^{-4}$ second. Therefore, the two additive terms on the l.h.s. of Eq. (17.21), which contain the fourth order time derivative (assumed to be each not excessively large by its own), both terms being affected by the factor $\tau^4 \approx 10^{-16}$, result to be negligible with respect to the other terms and they can thus be disregarded. This provision is in agreement with the findings of Stephen (2006); Elishakoff (2010) and Elishakoff et al. (2015). In the latter quoted paper a limit asymptotic analysis was accomplished to prove that only one of the two predicted series of natural frequencies of a vibrating Timoshenko–Ehrenfest beam has to be considered physically meaningful. With this provision Eq. (17.21) simplifies as

$$\begin{aligned} r^4 w^{iv}(x, t) + \tau^2 \ddot{w}(x, t) - \left(1 + \frac{a_2 E}{k_2 G}\right) \tau^2 r^2 \ddot{w}''(x, t) \\ + \frac{a_0 E}{k_2 G} \left[-r^6 w^{vi}(x, t) + 2\tau^2 r^4 \ddot{w}^{iv}(x, t)\right] = 0 \end{aligned} \quad (17.23)$$

which leads to the prediction of a single spectrum instead of two. Equation (17.23) is an extension of Eq. (24) of Elishakoff et al. (2015) (but the shear correction coefficient equal to 1), which takes into account warping effects on the vibrating beam. Indeed, taking $s = 0$ (TE beam), since then $a_0 = 0, a_2 = k_2 = 1$, (17.23) further simplifies as

$$r^4 w^{iv}(x, t) + \tau^2 \ddot{w}(x, t) - \left(1 + \frac{E}{G}\right) \tau^2 r^2 \ddot{w}''(x, t) = 0 \quad (17.24)$$

Apart the notation, this equation coincides with the mentioned Eq. (24) of Elishakoff et al. (2015) carrying in the *correction of Timoshenko–Ehrenfest correction*.

17.5 Application to a Simply Supported Beam

Let the vibrating beam be a simply supported beam of length L , with the ends located at $x = 0$ and $x = L$. The boundary conditions (17.14) applied to this beam can be expressed as:

$$\left. \begin{aligned} w(0, t) = w(L, t) = 0 \\ M(0, t) = M(L, t) = 0 \\ \widehat{M}(0, t) = \widehat{M}(L, t) = 0 \end{aligned} \right\} \quad \forall t \geq 0 \quad (17.25)$$

This implies that both the bending rotation $-w'$ and the shear angle γ play each the role of free variable. By the constitutive Eqs. (17.7) we write

$$\left. \begin{aligned} -w''(0, t) + a_1 \gamma'(0, t) = -w''(L, t) + a_1 \gamma'(L, t) = 0 \\ -a_1 w''(0, t) + a_2 \gamma'(0, t) = -a_1 w''(L, t) + a_2 \gamma'(L, t) = 0 \end{aligned} \right\} \quad \forall t \geq 0 \quad (17.26)$$

which are satisfied if, and only if, the following conditions are met:

$$\left. \begin{aligned} w''(0,t) = w''(L,t) = 0 \\ \gamma'(0,t) = \gamma'(L,t) = 0 \end{aligned} \right\} \forall t \geq 0 \quad (17.27)$$

Also, by (17.16) the conditions (17.27)₂ require that

$$w^{iv}(0,t) = w^{iv}(L,t) = 0 \quad \forall t \geq 0 \quad (17.28)$$

Next, let the solution to (17.23) be sought in the form

$$w(x,t) = \sum_{m=1}^{\infty} C_m \sin \frac{m\pi x}{L} e^{i\omega_m t}, \quad (i = \sqrt{-1}) \quad (17.29)$$

which guarantees that (17.25)₁, (17.27) and (17.28) be identically satisfied. Here the ω_m , ($m = 1, 2, \dots$), constitute a discrete numerable set of natural frequencies. Then, substituting (17.29) into (17.23) and using the notation $\Omega_m := \tau\omega_m$, ($m = 1, 2, \dots$), we obtain

$$\begin{aligned} \sum_{m=1}^{\infty} \left\{ \left[1 + \frac{a_0 E}{k_2 G} \left(\frac{m\pi r}{L} \right)^2 \right] \left(\frac{m\pi r}{L} \right)^4 + \right. \\ \left. -\Omega_m^2 \left[1 + \left(1 + \frac{a_2 E}{k_2 G} \right) \left(\frac{m\pi r}{L} \right)^2 + \frac{2a_0 E}{k_2 G} \left(\frac{m\pi r}{L} \right)^4 \right] \right\} C_m \sin \frac{m\pi x}{L} = 0 \end{aligned} \quad (17.30)$$

Therefore the non-dimensional natural frequencies Ω_m (measuring each the number of waves in the scale time interval τ) turn out to be expressed as

$$\Omega_m = \frac{\left(\frac{m\pi}{\lambda} \right)^2 \sqrt{1 + \frac{a_0 E}{k_2 G} \left(\frac{m\pi}{\lambda} \right)^2}}{\sqrt{1 + \left(1 + \frac{a_2 E}{k_2 G} \right) \left(\frac{m\pi}{\lambda} \right)^2 + \frac{2a_0 E}{k_2 G} \left(\frac{m\pi}{\lambda} \right)^4}}, \quad (m = 1, 2, \dots), \quad (17.31)$$

where $\lambda = L/r$ denotes the *slenderness ratio* of the beam. Since the warping coefficients a_0, a_2, k_2 are (continuous) functions of the warping parameter s , then the natural frequencies Ω_m turn out to be functions of s , $\Omega_m = \Omega_m(s)$.

Equation (17.31) is the extension to the present theory of the result given by Elishakoff et al. (2015), see Eq. (25) of the latter quoted paper, with which it identifies taking $s = 0$, that is,

$$\Omega_m(0) = \frac{\left(\frac{m\pi}{\lambda} \right)^2}{\sqrt{1 + \left(1 + \frac{E}{G} \right) \left(\frac{m\pi}{\lambda} \right)^2 + \frac{2E}{G} \left(\frac{m\pi}{\lambda} \right)^4}}. \quad (m = 1, 2, \dots) \quad (17.32)$$

For comparison, a few other shear warping theories from the literature have been considered and the corresponding natural frequencies have been computed. The following warping functions, say $f(z)$, representative of polynomial, trigonometric, hyperbolic and exponential warping functions, respectively, have been considered:

1. Levinson (1981); Reddy (1984, 2007) $f(z) = \theta(z, 0.5) = z - (4z^3/3h^2)$
2. Touratier (1991); Sayyad and Ghugal (2014, 2018) $f(z) = (h/\pi) \sin(\pi z/h)$
3. Soldatos (1992) $f(z) = z \cosh(1/2) - h \sinh(z/h)$
4. Karama et al. (2003) $f(z) = ze^{-2(z/h)^2}$

In Figs. 17.3(a,b), the first natural frequency computed with the parametric warping theory is plotted as a function of s (solid lines) against the analogous frequencies computed using the above other shear warping theories (straight discontinuous lines), using the slenderness ratio $\lambda = 10$ in a) and $\lambda = 50$ in b).

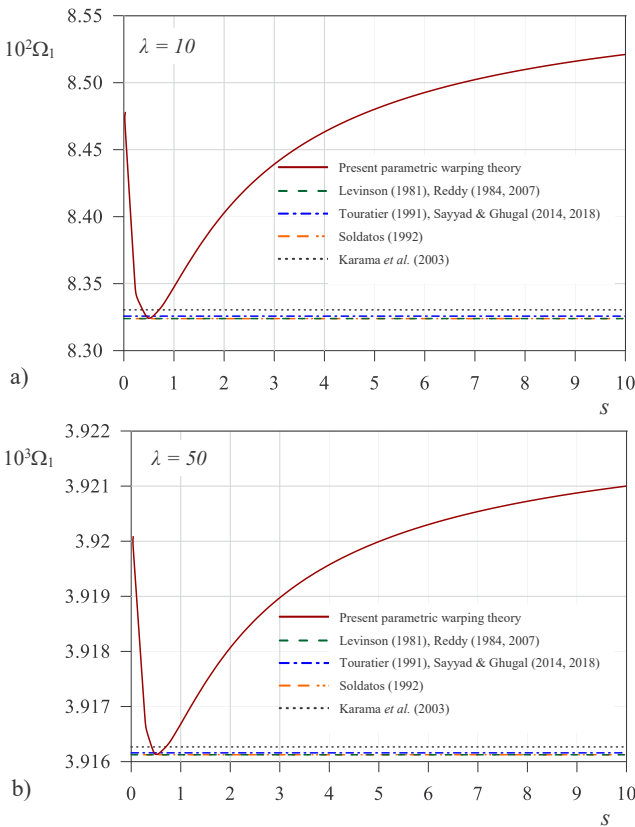


Fig. 17.3 First and fourth nondimensional natural frequencies $\Omega_m(s) = \tau\omega_m(s)$ of the simply supported beam versus the warping parameter s , computed with the parametric theory (solid lines), Levinson-Reddy theory (dashed lines), Touratier-Sayyad & Ghugal theory (dash-dot lines), Soldatos theory (double dash-dots lines), Karama et al. theory (dotted lines): a) $m = 1, \lambda = 10$; b) $m = 1, \lambda = 50$.

Analogous results are reported in Figs. 17.4(a,b) for the fourth natural frequency. Every curve $\Omega_m(s)$ exhibits a waved pattern whereby for every s the natural frequency of a particular beam in the family is represented, namely, the TE beam for $s = 0$, the LR beam for $s = 0.5$, the EB beam for $s \rightarrow \infty$. For every $m = 1, 2, \dots$, a particular value of s exists, namely $s = s_h(m)$, such that $\Omega_m(s) < \Omega_m(0) \forall s : 0 < s < s_h(m)$ (softening), whereas $\Omega_m(s) > \Omega_m(0) \forall s > s_h(m)$ (hardening). For easy reference, the numbers $s_h(m)$ are called *separation s_h numbers*, whereas the corresponding beam models are called *neutral frequency beams, exhibiting neither softening nor hardening*. The main salient feature emerging from these plots is that the frequencies determined with warping theories different from the proposed one are all below $\Omega_m(0)$, that is in the softening zone, more or less in the vicinity of $\Omega_m(0.5)$.

The values of $\Omega_m(s) (m = 1, 2, 3, 4)$ related to the TE ($\Omega_m(0)$), LR ($\Omega_m(0.5)$) and EB ($\Omega_m(\infty)$) beam models, as well as to the neutral frequency beam ($\Omega_m(s_h)$), are

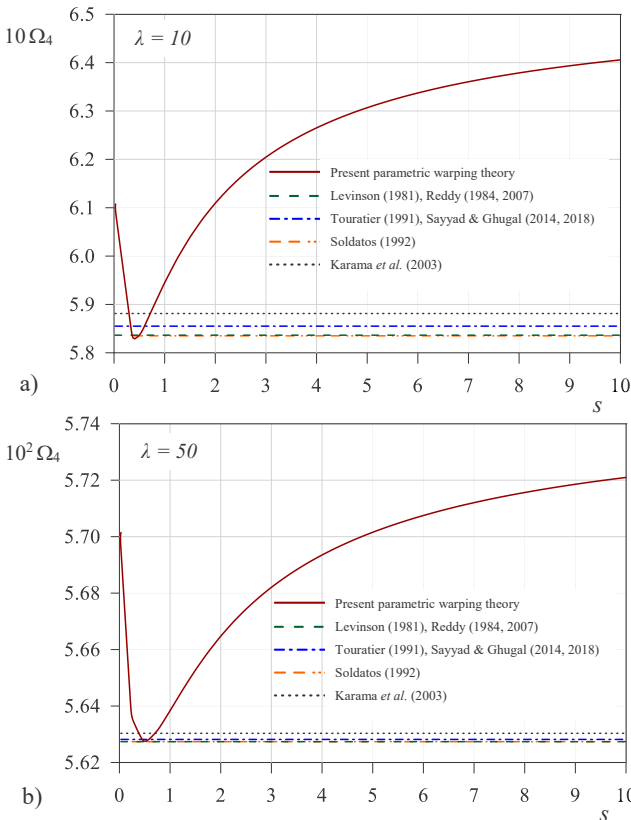


Fig. 17.4 First and fourth nondimensional natural frequencies $\Omega_m(s) = \tau\omega_m(s)$ of the simply supported beam versus the warping parameter s , computed with the parametric theory (solid lines), Levinson-Reddy theory (dashed lines), Touratier-Sayyad & Ghugal theory (dash-dot lines), Soldatos theory (double dash-dots lines), Karama et al. theory (dotted lines): a) $m = 4, \lambda = 10$; b) $m = 4, \lambda = 50$.

reported in Tables 17.1 and 17.2 for $\lambda = 10$ and $\lambda = 50$, respectively. The first four natural frequencies, Ω_m ($m = 1, 2, 3, 4$), computed with the four different shear warping theories borrowed from the literature are also reported in Tables 17.3 and 17.4, for $\lambda = 10$ and $\lambda = 50$, respectively.

Two more plots are finally given to highlight the above discussed effects of the parametric warping on the natural frequencies of the simply supported beam. Precisely, in Figs. 17.5(a,b) the ratio $\Omega_m(s)/\Omega_m(0)$ versus the warping parameter s and for $m = 1, 2, 3, 4$, is plotted for $\lambda = 10$ and $\lambda = 50$, respectively. Apart from the above mentioned waved pattern of the curves, a sensitivity of the natural frequencies to the slenderness ratio $\lambda = L/r$ can also be observed.

17.5.1 Other Comments on the Obtained Numerical Results

The curves $\Omega_m(s)$ plotted in Figs. 17.3(a,b), 17.4(a,b) and 17.5(a,b) show some features worthy of mention. Namely, every curve has a minimum for some $s = s^*(m) \approx 0.5$, which means that the LR beam model is characterized by natural frequencies close to the minimum. The value $s = s_h(m)$ that separates, for every $m = 1, 2, \dots$, the softening/hardening zones from each other corresponds to a particular beam of the family which has *natural frequency equal to the m -th frequency of the TE beam*.

Table 17.1 Nondimensional frequencies Ω_m ($m = 1, 2, 3, 4$) of the simply supported beam for particular beams in the family: TE beam ($s = 0$); LR beam ($s = 0.5$); Neutral frequency beam ($s = s_h$); EB beam ($s = \infty$), computed with the parametric warping theory and for slenderness $\lambda = L/r = 10$.

| $\Omega_m(s)$ | TE beam $s = 0$ | LR beam $s = 0.5$ | Neutral frequency beam $(s_h); s = s_h$ | EB beam $s = \infty$ |
|---------------|--------------------|----------------------|--|-------------------------|
| Ω_1 | 0.0848 | 0.0832 | (4.75); 0.0848 | 0.0941 |
| Ω_2 | 0.2537 | 0.2441 | (3.75); 0.2537 | 0.3343 |
| Ω_3 | 0.4335 | 0.4142 | (2.75); 0.4335 | 0.6464 |
| Ω_4 | 0.6108 | 0.5836 | (2.00); 0.6108 | 0.9833 |

Table 17.2 Nondimensional frequencies Ω_m ($m = 1, 2, 3, 4$) of the simply supported beam for particular beams in the family: TE beam ($s = 0$); LR beam ($s = 0.5$); Neutral frequency beam ($s = s_h$); EB beam ($s = \infty$), computed with the parametric warping theory and for slenderness $\lambda = L/r = 50$.

| $\Omega_m(s)$ | TE beam $s = 0$ | LR beam $s = 0.5$ | Neutral frequency beam $(s_h); s = s_h$ | EB beam $s = \infty$ |
|---------------|--------------------|----------------------|--|-------------------------|
| Ω_1 | 0.0039 | 0.0039 | (5.50); 0.0039 | 0.0039 |
| Ω_2 | 0.0154 | 0.0153 | (5.25); 0.0154 | 0.0157 |
| Ω_3 | 0.0334 | 0.0332 | (5.25); 0.0334 | 0.0349 |
| Ω_4 | 0.0570 | 0.0563 | (5.00); 0.0570 | 0.0613 |

Table 17.3 Nondimensional frequencies Ω_m ($m = 1, 2, 3, 4$) of the simply supported beam, with slenderness $\lambda = L/r = 10$, using four different shear warping theories from the literature.

| Shear warping theory | $10^2\Omega_1$ | $10^1\Omega_2$ | $10^1\Omega_3$ | $10^1\Omega_4$ |
|---|----------------|----------------|----------------|----------------|
| 1. Levinson (1981); Reddy (1984, 2007) | 8.3239 | 2.4416 | 4.1418 | 5.8364 |
| 2. Touratier (1991); Sayyad and Ghugal (2014); Sayyad and Ghugal (2018) | 8.3257 | 2.4437 | 4.1495 | 5.8551 |
| 3. Soldatos (1992) | 8.3239 | 2.4415 | 4.1413 | 5.8351 |
| 4. Karama et al. (2003) | 8.3304 | 2.4477 | 4.1617 | 5.8812 |

Table 17.4 Nondimensional frequencies Ω_m ($m = 1, 2, 3, 4$) of the simply supported beam, with slenderness $\lambda = L/r = 50$, using four different shear warping theories from the literature.

| Shear warping theory | $10^3\Omega_1$ | $10^2\Omega_2$ | $10^2\Omega_3$ | $10^2\Omega_4$ |
|---|----------------|----------------|----------------|----------------|
| 1. Levinson (1981); Reddy (1984, 2007) | 3.9161 | 1.5301 | 3.3186 | 5.6274 |
| 2. Touratier (1991); Sayyad and Ghugal (2014); Sayyad and Ghugal (2018) | 3.9161 | 1.5302 | 3.3189 | 5.6282 |
| 3. Soldatos (1992) | 3.9161 | 1.5301 | 3.3186 | 5.6274 |
| 4. Karama et al. (2003) | 3.9163 | 1.5304 | 3.3196 | 5.6303 |

Also, for every other warping theory considered in Tables 17.3 and 17.4, there exist two differently warped beams in the family which possess the same natural frequencies. Though the numerical investigation is not sufficiently wide for a safe judgement on the sensitivity of the natural frequencies to the warping effects, nevertheless it clearly appears that these effects may be notable and that further studies would be hoped for. The plots of Figs. 17.5(a,b) show that the natural frequencies $\Omega_m(s)$ exhibit some sensitivity to the slenderness ratio $\lambda = L/r$. Though this outcome may be considered self-intuitive, further investigation is needed on this point.

17.6 Conclusion

A class of shear deformable beams in vibration has been presented whereby a warping theory (called *parametric warping*) is used to make the cross section to warp according to a fixed warping rule controlled by a *warping parameter* $s \geq 0$. On letting s vary from zero to infinite, a continuous family of shear deformable beams models is generated, which spans from the TE beam for $s = 0$ (no warping is active, full shear deformability), to the EB beam for $s \rightarrow \infty$ (again no warping is active, but zero shear deformation). Remarkable feature of this formulation is that what-

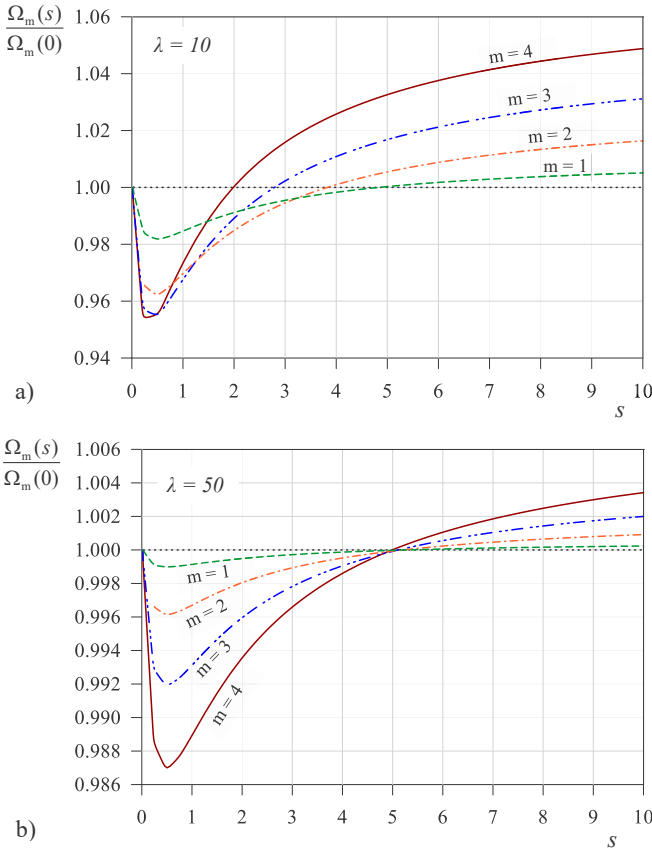


Fig. 17.5 Ratios of nondimensional natural frequencies of the simply supported beam $\Omega_m(s)$ over $\Omega_m(0)$ (TE-beam nondimensional frequencies), plotted for $m = 1, 2, 3, 4$, versus warping parameter s and obtained with the parametric theory: a) for slenderness ratio $\lambda = L/r = 10$; b) for $\lambda = 50$.

ever may be the chosen (non-negative) value of s , the shear stress is vanishing at the bottom and top surfaces of the beam. Another remarkable property is that no shear correction coefficient is needed.

The differential equation of the generic shear deformable beam in vibration has been found to be of the sixth order in the spacial variable, but still of fourth order in the time variable, it therefore predicts two distinct series of natural frequencies like for the TE beam. It is also found that the vibration motion of the beam is controlled by two basic scale parameters, namely r (radius of inertia of the cross section) and τ (time interval for a wave to travel the distance r). As in practice τ takes on small values, then the term of the differential equation with the fourth order time derivative can be disregarded. In this way a simpler differential equation is obtained which is still of the sixth order in the spacial variable, but of the second order in the time variable, hence it predicts only a single spectrum.

The simplified differential equation has been used to derive the natural frequencies of a simply supported beam. The first four frequencies were reported graphically as functions of the warping parameter $s \geq 0$, so evaluating the sensitivity of the natural frequencies to the warping effects. This sensitivity is smaller for the first order frequency, but increases with the frequency order. The natural frequencies were also computed using other shear warping theories from the literature for comparison.

The main original contributions of the present research work can be summarized as follows:

- Extension to vibrating beams of a parametric warping theory previously advanced in Polizzotto (2015, 2017).
- Formulation of the governing sixth order time/space differential equation for shear deformable vibrating beams taking into account the warping effect.
- Introduction of two parameters with the meaning of macroscopic space and time scales of the vibrating beam, which carry in the basic pieces of information regarding the inherent geometrical and inertial features of the vibrating system.
- Exploitation of these scale parameters to ascertain that the addends of the governing differential equation incorporating the (upmost) fourth order time derivatives are negligible with respect to the others, which extends previous results by Elishakoff et al. (2015) and Elishakoff (2020) to shear deformable beams.
- Assessment of the sensitivity of natural frequencies to the warping effects.

References

- Arya, H., (2003). A new zig-zag model for laminated composite beams: free vibration analysis. *Jour. Sound Vib.* 264(2):485–490.
- Aydogdu, M., (2008). Vibration of multi-walled carbon nanotubes by generalized shear deformation theory. *Int. J. Mech. Sci.* 50(4):837–844.
- Bickford, W.B., (1982). A consistent higher order beam theory. *Developments in Theor. Appl. Mech., SECTAM*, 11:137–150.
- Carrera, E., Giunta, G., (2010). Refined beam theories based on a unified formulation. *Int. J. Appl. Mech.* 2(21):117–143.
- Challamel, N., Elishakoff, I., (2019). A brief history of first-order shear deformable beam and plate models. *Mech. Res. Commun.* 102(103389), 1-8.
- Cowper, G.R., (1966). The shear coefficient in Timoshenko's beam theory. *Int. J. Appl. Mech.* 33(2):335–340.
- Elishakoff, I., (2010). An equation both more consistent and simpler than the Bresse–Timoshenko equation. In: Gilat R., Banks-Sills L. (eds.), *Advances in Mathematical Modeling and Experimental Methods for Materials and Structures, Solid Mechanics and Its Applications* 168, DOI 10.1007/978-90-481-3467-0-19.
- Elishakoff, I., (2020). *Handbook on Timoshenko-Ehrenfest Beam and Uflyand-Mindlin Plate Theories*. Singapore, World Scientific.
- Elishakoff, I., Kaplunov, J., Nolde, E., (2015). Celebrating the centenary of Timoshenko's study of effects of shear deformation and rotary inertia. *Appl. Mech. Rev.* 67(6), 060802-1–11.

- Eltaher, M.A., Khater, M.E., Emam, S.A., (2016). A review on nonlocal elastic models for bending, buckling, vibrations and wave propagation of nanoscale beams. *Appl. Math. Modelling*. 40(5):4109–4128.
- Engesser, F., (1891). Über die Knickfestigkeit gerader Stäbe. *Zeitschrift des Architekten und Ingenieur Vereins zu Hannover*. 35(4):455–462 (in German).
- Eringen, A.C., Şuhubi, E.S., (1975). *Elastodynamics, Vol. II: Linear Theory*. Academic Press, New York.
- Föppl, A., (1897). *Vorlesungen über Technische Mechanik, Dritter Band, Festigkeitslehre*, Leipzig, Druck und Verlag Von B.G. Teubner (in German).
- Giunta, G., Biscani, F., Belouettar, S., Ferreira, A.J.M., Carrera, E., (2013). Free vibration analysis of composite beams via refined theories. *Compos. Part B*. 44(1):540–552.
- Heyliger, P.R., Reddy, J.N., (1988). A higher order beam finite element for bending and vibration problems. *J. Sound Vib*. 126(2):309–326.
- Jun, L., Hongxing, H., (2009). Dynamic stiffness analysis of laminated composite beams using trigonometric shear deformation theory. *Compos. Struct*. 89(3):433–442.
- Kaneko, T., (1978). An experimental study of the Timoshenko's shear coefficient for flexurally vibrating beams. *Journal of Physics D: Applied Physics* 11(14):1979–1988.
- Karama, M., Afaq, K.S., Mistou, S., (2003). Mechanical Behaviour of laminated composite beam by the new multi-layered laminated composite structures model with transverse shear stress continuity. *Int. J. Solids Struct*. 40(6):1525–1546.
- Levinson, M., (1981). A new rectangular beam theory. *J. Sound Vib*. 74(1):81–87.
- Mantari, J.L., Oktem, A.S., Soares, C.G., (2011). Static and dynamic analysis of laminated composite and sandwich plates and shells by using a new higher-order shear deformation theory. *Compos. Struct*. 94(1):37–49.
- Pisano, A.A., Fuschi, P., Polizzotto, C., (2020). A strain-difference based nonlocal elasticity theory for small-scale shear-deformable beams with parametric warping. *Int. J. for Multiscale Computational Engineering* 18(1):83–102.
- Polizzotto, C., (2015). From the Euler–Bernoulli beam to the Timoshenko one through a sequence of Reddy-type shear deformable models of increasing order. *Eur. J. Mech. A/Solids* 53:62–74.
- Polizzotto, C., (2017). A class of shear deformable isotropic elastic plates with parametrically variable warping shapes. *ZAMM, Z. Angew. Math. Mech.* 1–27, DOI 10.1002/zamm.201700070.
- Reddy, J.N., (1984). A simple higher-order theory for laminated composite plates. *J. Appl. Mech*. 51(4):745–752.
- Reddy, J.N., (2007). Nonlocal theories for bending, buckling and vibration of beams. *Int. J. Eng. Sci.* 45:288–307.
- Reddy, J.N., (2004). *Mechanics of Laminated Composite Plates and Shells. Theory and Analysis*, 2nd edition, CRC Press, Boca Raton, New York, Washington D.C.
- Sayyad, A.S., Ghugal, Y.M., (2014). Flexure of cross-ply laminated plates using equivalent single layer trigonometric shear deformation theory. *Struct. Eng. Mech.* 51(5):867–891.
- Sayyad, A.S., Ghugal, Y.M., (2018). Modeling and analysis of functionally graded sandwich beams: A review. *Mechanics of Advanced Materials and Structures*. doi:10.1080/15376494.2018.1447178.
- Shi, G., Voyiadjis, G.Z., (2011). A sixth order theory of shear deformable beams with variational consistent boundary conditions. *J. Appl. Mech.* 78:1–11.
- Soldatos, K.P., (1992). A transverse shear deformation theory for homogeneous monoclinic plates. *Acta Mech*. 94(3–4):195–200.
- Stephen, N.G., (2006). The second spectrum of Timoshenko beam theory —Further assessment. *Journal Sound Vib*. 292:372–389.
- Subramanian, P., (2006). Dynamic analysis of laminated composite beams using higher order theories and finite elements. *Compos. Struct*. 73(3):342–353.
- Touratier, M., (1991). An efficient standard plate theory. *Int. J. Eng. Sci.* 29(8):901–916.
- Timoshenko, S.P., (1916). *Course of Elasticity Theory. Part 2 —Columns and Plates*. A.E. Collins Publishers, St. Petersburg (in Russ.), (2nd Ed. Naukova Dumka, Kiev, 1972).

- Timoshenko, S.P., (1921). On the correction for shear of the differential equation for transverse vibrations of prismatic bars. *Phil. Mag. Ser. 6*(41):744–746.
- Timoshenko, S.P., (1922). On the transverse vibrations of bars of uniform cross-section. *Phil. Mag. Ser. 6*(43):125–131.



Chapter 18

Conceptual Approaches to Shells. Advances and Perspectives

Oksana R. Polyakova and Tatiana P. Tovstik

Abstract The history of scientific discoveries in elasticity theory that preceded the creation of the theory of shells is described. The way of finding solutions and the logic of scientific discoveries are indicated, including the history of the question of the position of the neutral line of a loaded beam and the history of the derivation of the equations of elasticity theory. Some applied questions of analytical methods, including the method of asymptotic expansions, are discussed. The prospects and current use of methods of mechanics and the concept of shells in interdisciplinary research are described.

Key words: History of shell theory, Elastic plates and shells, Analytical methods, Asymptotic methods

18.1 Introduction

At present, many questions of the theory of shells, which were open several generations ago, are solved and considered as classical results of the theory. Hence the more interesting and important it is to see the prospects for the development of the mechanics of shells and shell media. The historical perspective of the future is more clearly seen with a scientific view of the perspective of the past, and the deeper and

Oksana R. Polyakova
St. Petersburg State University of Architecture and Civil Engineering, 2ya Krasnoarmejskaya ul.,
4, St. Petersburg, 190005, Russian Federation,
e-mail: ksenpolyaor@yandex.ru

Tatiana P. Tovstik
Institute for Problems in Mechanical Engineering RAS, Bolshoy pr. V. O., 61, St. Petersburg,
199178, Russian Federation,
e-mail: tovstik_t@mail.ru

more accurately we understand it, the greater and more diverse will be the vision of further directions of development.

In addition, on the example of the theory of shells over the centuries one can clearly see the stages of development of mechanics as a whole in its many sections, as well as mathematics, without which mechanics would not have taken place as a science.

It is difficult to say when the shells first appeared in science. According to the available medieval references, there was a work by Archimedes dedicated to finding the center of gravity of plates. One should also mention the mechanisms invented by Leonardo da Vinci, in which shells were used. They include

- wings allowing to rise into the air,
- fans for fanning the fire, and
- underwater spacesuit for humans.

Already at the beginning of the Renaissance, many phenomena of mechanics necessary for the beginning of research in the mechanics of shells were discovered. They ranged from the simplest ones, capable of providing data on the elastic properties of matter such as experiments on the breaking of a wire, experiments on measuring the deflection of a beam freely supported at its ends, to more complex and beautiful experiments related, for example, to the phenomenon of resonance. Here is how Leonardo da Vinci (1452–1519) describes the resonance: "The stroke given in the bell will cause response and some slight movement in another bell similar to itself; and the string of a lute as it sounds will cause response and movement in another similar string of like tone in another lute; and this you will see by placing a straw on the string similar to that which has sounded" (Timoshenko, 1953; Ravaisson-Mollien, 1881, p. 22).

As Charles-Augustin de Coulomb (1736–1806) wrote in 1773, giving his work for publication in the French Academy of Science: "The sciences are monuments consecrated to the public good. Each citizen ought to contribute to them according to his talents" (Timoshenko, 1953). What path did the scientists of the XVI–XXI century have to go from the descriptive works of the Renaissance to the modern differential and integral and differential equations describing, for example, the same resonance!

It is clear that the development of mechanics could not have taken place without the development of the corresponding branches of mathematics. As Leonardo da Vinci wrote in his Paris notebook in 1513–1514: "Mechanics is the paradise of mathematical science because here we come to the fruits of mathematics" (Timoshenko, 1953; Ravaisson-Mollien, 1891, p. 8). Let us outline the most beautiful and significant achievements in the theory of shells.

18.2 Historical Perspective

18.2.1 *On the Tension-torsion Test of Beams*

One of the first issues with which the practice of shell research began was the strength testing of shells and membranes, beams, and wires. The history of searching for models of mechanics shows us that the correct solutions to problems were not achieved immediately. For example, consider in this regard a simple tension of a body. After making a series of tensile tests for iron wire, Leonardo da Vinci concludes that the shorter the wire, the greater tensile stress it can withstand. Perhaps this answer was due to various defects distributed along the length of wires manufactured at that time. Already Galileo Galilei (1564–1642) finds that the tensile strength of a copper sample is proportional to the cross-sectional area and does not depend on its length. Robert Hooke (1635–1703) established a linear relationship between force and strain and in 1678 published the first ever printed work on the theory of elasticity "De Potentia Restitutiva, or of Spring".

In 1784, Charles Coulomb conducted experiments on wire torsion and observed torsional vibrations of a weight suspended on it. He was able, similarly to the well-known Hooke formula for rod tension, to experimentally establish a formula that relates the angle of rotation of the rod φ to the torque M (Timoshenko, 1953)

$$M = \frac{\mu d^4}{l} \varphi, \quad (18.1)$$

where l and d are the length and diameter of the rod, respectively, μ is the material constant. In addition, Coulomb discovered the existence of another value that characterizes the elastic limit for a given material — the critical torsion up to which the deformation remains elastic and beyond which the accumulation of residual deformation occurs. For example, the elastic limit of a rod increases if it is twisted far beyond its elastic limit, but the modulus of elasticity μ does not change in this case. And further, the elastic limit again decreases if the wire obtained in this way is annealed. On the contrary, the elastic limit increases when the metal is quenched. Explaining this result, Coulomb made the assumption that each elastic material is characterized by a certain arrangement of molecules, and with a deformation beyond the limits of elasticity these molecules begin to slip relative to each other, which ultimately leads to an increase in the molecular coupling forces and an increase in the elastic limit. However, small elastic deformations do not change the relative position of the molecules. The English scientist Thomas Young (1773–1829) finds an additional term for the torque in (18.1). This is the resistance to torque, proportional to the cube of the twist angle and caused by the longitudinal stresses of the fibers bending along the helical lines. In this case, the outer fibers are stretched, and the inner fibers are compressed.

18.2.2 Beam Bending and Neutral Line Detection History

The first studies of bending of freely supported and cantilevered beams were performed by Leonardo da Vinci and Galileo: Leonardo investigated the influence of the length and width of the beam on its deflection, while Galileo investigated also the effect of its thickness. The existence of a neutral beam line was not addressed by Galileo, since he assumed that the bending load is distributed uniformly over the transversal section.

In engineering calculations, the question of the location of the neutral line in the beam bending problem was treated differently throughout the 17–18th centuries, and partly even the 20th century. For brittle materials, such as stone beams, the Galilean hypothesis of the uniform stress distribution over the beam thickness was accepted. For flexible materials, for example, wooden beams, a later model was used in the calculations, according to which the beam is not stressed on the inner side, and the tensile stresses of the fibers are maximal on the outer side.

Many mechanical scientists like Edme Mariotte (1620–1684), Robert Hooke, Antoine Parent (1666–1716), Leonhard Euler (1707–1783) devoted their time to the search for a formula for calculating the beam strength during bending. During the initial consideration of the problem, all of them first placed the neutral unstressed line of the curved beam tangentially to the contour of the cross-section of the beam from its concave side, and only then solved the problem by placing the neutral line inside the beam. With this statement of the problem, the stress pattern and the calculation formulas undergo changes, for example, the fibers stretch on the convex side of the beam and shrink on the concave side.

When comparing the problems of bending and stretching, Thomas Young determined the most advantageous shape of a rectangular beam if it is cut from a beam with a given circular cross-section. If we need to minimize the deflection, then the ratio of the height of the beam to its width should be $\sqrt{3} : 1$, if we need the maximum bending strength, then the ratio should be $\sqrt{2} : 1$, for the most rigid beam in tension, the cross-section shape will be $1 : 1$.

18.2.3 To the History of the Derivation of the Shell Equations

After Isaac Newton (1643–1727) in England and Gottfried Leibniz (1646–1716) in Europe laid the foundation of the calculus of infinitesimals, this new mathematical apparatus began to be used by mathematicians in the study of mechanical problems. Daniel Bernoulli (1700–1782) and Leonhard Euler became interested in the equilibrium problems of elastic rods and found the shape of an elastic line (elastica) for a number of various problems. They then derived the differential equation of transverse vibrations of a prismatic beam. Daniel Bernoulli sets up experiments, which he shares in a letter with Leonhard Euler: "These oscillations arise freely, and I have determined various conditions, and have performed a great many beautiful experiments on the position of the knot points and the pitch of the tone, which

agree beautifully with the theory" (Fuss, 1843). Leonhard Euler found a solution to the 4th order differential equation of beam oscillation for various conditions at the ends: cantilever rod, freely supported ends, rigidly fixed ends, and completely free ends. Euler noted that the obtained result can be used not only for experimental verification of the theory, but also for determination of the elastic constant of the rod material.

Next, Leonhard Euler obtains a partial differential equation for the vibration of a membrane. Here it takes the model of a membrane in the form of two mutually perpendicular systems of strings. He applies the same method for the problem of bell oscillations. Jacob Bernoulli (1759–1789) deduced the formula of vibrations of a plate, which he also modeled as two systems of cross beams. However, he notes that this is only the first attempt to derive these equations, and if the beams are taken at different angles, the form of the equations will change. In its modern form, the equations of vibrations of a plate were derived by Sophie Germain (1776–1831) via the Euler equation.

Since the beginning of the 19th century, the European scientific community has become interested in the forms of plate vibrations thanks to the amazing experiments of Ernst Chladni (1756 – 1827), see Chladni (1802, 2015); Faraday (1837). Pouring a thin layer of fine-grained sand on a glass plate and passing a violin bow along the edge of the plate, Chladni excited vibrations of the plate with sand at different frequencies. As a result, sand nodal lines were formed as a consequence of plate vibrations.

After Chladni's presentation of his experiments at the French Academy, a competition was announced and, at the suggestion of Napoleon, a prize was awarded for the development of a mathematical theory of plate vibrations and for a comparison of theoretical and experimental results. Sophie Germain submitted her work to this competition three times (there were no other contestants), and on the third time she received the prize, although the commission was not completely satisfied with her justification of the formula of the integral of the deformation energy of the plate (Euler's formula), from which the equation of plate vibrations was obtained.

Simeon Denis Poisson (1781–1840), Louis-Marie Henri Navier (1785–1836), and Augustin Louis Cauchy (1789–1857) worked on the derivation of the equilibrium equations of an isotropic elastic body. To derive the equations of elasticity theory, Cauchy considers the equilibrium of an elementary tetrahedron, introduces the concept of stress for the first time, describing it as the pressure on the plane, but not perpendicular to the plane, unlike the pressure in gas theory. Navier and Poisson used a model of a body consisting of molecules interacting with each other (molecular theory). The equations of the molecular theory gave only one elastic constant of the material for an isotropic body and 15 constants (for in the general an anisotropic linear model). Cauchy's theory gave 2 and 21 independent constants, respectively. In the middle of the 19th century, the increased accuracy of experiments showed the need of taking into account the Poisson ratio as the second constant of an isotropic material.

George Green (1793–1841) considered both ways of deriving the equations of elasticity and derived them in a third way, not using the assumption about the struc-

ture of the matter, but rather relying on the law of conservation of energy and introducing the potential function, which for small displacements was found to be a homogeneous function of the second degree of the six components of deformation.

18.3 Analytical Methods in the Shell Theory

The solution of the problem of elasticity theory for a shell as a three-dimensional body in the spatial formulation is an involved problem of mathematical physics. Taking into account the geometric and elastic (or rheonomic) characteristics of the shell, as well as the loading conditions and other factors, various approaches were developed to simplify the problem. There are four main analytical methods for studying the stress-strain state of beams, plates, and shells — the method of hypotheses, decomposition with respect to the parameter, the asymptotic method and the direct method:

1. The method of hypotheses is based on the acceptance of hypotheses about the nature of the distribution of stresses, deformations or displacements over the thickness. This is the so-called semi-inverse method of elasticity theory. This method of solution is transparent and allows one to obtain simple resolution relations. The disadvantage of this method is the lack of criteria for evaluating the error. To refine the results obtained, it is necessary to move on to more general hypotheses and solve a virtually different problem. This method is used in models of the Bernoulli–Euler beam and the Kirchhoff–Love shell. The Timoshenko–Ehrenfest beam and Uflyand–Mindlin plate theories (Elishakoff, 2020), the theories of E. Reissner, S.A. Ambartsumian, and Timoshenko-type theories were constructed on the basis of relaxed hypotheses.
2. For an expansion in terms of the thickness parameter, all the desired functions are represented as the product of two functions, one of which depends on the coordinates of the median surface and the second one is selected as a series of the transverse coordinate. In this case, to refine the results, it is necessary to take a larger number of terms of the series and increase the order of the system being solved.
3. When solving problems by the method of asymptotic integration, all the desired values are represented as an asymptotic series in the powers of some dimensionless physical or geometric small (or large) parameter. The solution is sought in the form of recurrent formulas for unknown functions. This method gives the asymptotic order of error of the solution.

The results obtained by asymptotic methods provide approximate solutions that can be used directly in technical applications as well as analytical solutions; they are indispensable for verification of numerical results. The main value of asymptotic solutions is because they are capable of given a qualitative description of the behavior of the shell as its parameters change. The idea of asymptotic expansions is a very deep idea in science, which reflects the cognitive capabilities

of a person, when more and more hierarchical complexity levels are consistently comprehended starting from the simple ones.

The asymptote is translated from Greek as "not coincident"; in other words, it does not coincide, but it brings us closer to the fullness of knowledge of the picture of the world. And if it is not yet possible to solve the problem in full, there is a possibility to build its approximations, grasping in them the most fundamental and important features. The question of what to pay attention to and what "features" will be important in this task is decided by the scientist.

Initially, asymptotic methods were used for regularly perturbed equations. Starting from the 1960s, asymptotic methods have also been used for singularly perturbed equations. In a regularly perturbed problem the asymptotic solution is constructed by a single representation, but in a singularly perturbed problem there may be several such representations, which leads to the problem of merging these expansions.

Justification of the classical theory of shells, including the derivation of two-dimensional shell equations from the three-dimensional equations of the theory of elasticity using asymptotic analysis, is contained in the fundamental monograph (Goldenveizer, 1961), which includes justifications of the classical theory of shells based on the hypotheses of Kirchhoff–Love and Timoshenko–Reissner, the nonlinear theory of shells, and the theories of anisotropic and multilayer shells. A great contribution to the solution of involved problems of vibrations and stability of shells and to the development of asymptotic methods was made by Professor Peter E. Tovstik of St. Petersburg University.

Consideration of the anisotropy and inhomogeneity of shells provides a huge field for the application of asymptotic methods in the development and refinement of classical theories. The situation arises when one needs to choose a model for solving the problem with the corresponding small parameters. Here, the most important phenomenon and the basis for success is the scientist himself, with his or her immersion in the study. "To successfully find something, it is always desirable to know at least approximately what is being looked for" (Blekhman et al, 1983).

The second necessary characteristic of a scientist is intuition, which should help to find a way to solution. The choice can be made in many ways, but achievement of simplicity and accuracy of constructions requires subtlety, sensitivity and insight as some necessary components of intuition. Professor P.E. Tovstik had this remarkable talent of having deep scientific "asymptotic intuition". This is evidenced by his works. For singularly perturbed equations, algorithms were obtained for solving problems on the oscillations and stability of shells, when the merging of asymptotic expansions is required. In particular, for the shells of zero curvature, when one of the coefficients of the equation of oscillations vanishes. For integrals in the vicinity of the rotation points, the solutions are constructed using reference functions that do not depend on the shape of the shell and the oscillation frequency. An effective asymptotic method was constructed and critical loads of shell stability loss were found for many classes of problems interesting

for practice, for which only numerical results were previously known (Tovstik and Smirnov, 2001; Bauer et al, 2015; Mikhasev and Tovstik, 2020).

4. A direct method for deriving of equations of plates and shells was developed by Zhilin (1976); Altenbach and Zhilin (1988, 2004); Zhilin (2006c). This method does not rely on any hypotheses, but directly deduces the equations of the shell as a two-dimensional body with the use of the fundamental law of energy balance and the two principles: the principle of momentum and the principle of moment of momentum. Both principles results in the Eulerian laws of motion (Truesdell, 1964). Under this approach, the principle of material objectivity is satisfied automatically. Concrete forms of the tensors of elastic modules of the medium are obtained by applying the Curie-Neumann principle. The direct tensor calculus is used for writing down the laws of mechanics and describing the characteristics of the medium. The problem in application of the direct approach is the establishment of the constitutive equations and the identification procedure for the effective stiffness properties. Recently, new applications of this method were found due to the appearance of new materials, in particular, nanomaterials, and in view of the increasing requirements for the accuracy of calculation (Altenbach and Eremeyev, 2008, 2009).

A number of directions of the nonclassical theory of elastic media and shells have appeared with the advent of advanced technologies pertaining to shells of involved structure. For a survey and discussion of generalized Cosserat-type theories of plates and shells, see Altenbach et al (2010). The Cosserat continuum is used as a model for inhomogeneous materials with granular structure and for composite materials consisting of sufficiently rigid grains that can both move and rotate inside the material under load (superplastic media, acoustic metamaterials).

18.4 A Mathematical View of Shells

Almost four centuries have passed since the discovery of the Newton–Leibniz formula, the most important formula of integral calculus, which gives a connection between two operations: the operator taking the Riemann integral and the operator of determination the primitive. In calculus, this formula is generalized, via Fubini’s theorem, to problems of higher dimension. In general, the formula reads as

$$\int_{\sigma} d\omega = \int_{\partial\sigma} \omega, \quad (18.2)$$

where σ is an orientable p -dimensional submanifold defined on an oriented manifold M of dimension n , ($p < n$); ω is the differential form of degree $p - 1$; $d\omega$ is the exterior derivative of the form; $d\sigma$ is the positive oriented boundary of the submanifold. For proofs and derivations of such formulas, see, for example, Zorich (2016).

For two-dimensional spaces, this formula becomes the Green formula, for three-dimensional spaces, this is the Gauss–Ostrogradsky formula, and in general space, this is the Stokes formula. These formulas are have great value and are used in the theory of elasticity, hydro- and aerodynamics, electrodynamics, and many other sciences. These formulas relate mathematically the things happening "inside" and "on the boundary", where a philosophical understanding of this fact leads to the assumption of the "limit" of the boundary of a submanifold, which concentrates certain parameters of the submanifold itself.

For closed shell forms let us show some interesting points supporting the thesis that the shell is related to the internal content of the vol that it restricts. A clear illustration of this fact is given in the Gauss–Ostrogradsky formula, which states that the integral of the divergence of a vector field \bar{A} over a volume G is equal to the flow of the vector through the surface,

$$\iiint_G \operatorname{div} \bar{A} dV = \iint_S \bar{A} d\bar{S}. \quad (18.3)$$

Just like the Green formula for the two-dimensional case, the Gauss–Ostrogradsky formula relates integrals of different dimensions.

Recall the concept of the linear hull from linear algebra. The linear hull can be defined in a linear space of any dimension. The linear hull in an N -dimensional space X over a field F (real or complex) is defined for a family x_1, x_2, \dots, x_m of elements of the space. For a linear space, the operations of vector addition and multiplication by a number are defined, and so by taking the linear combination of elements x_j with coefficients c_j form the field F , we get the set of linear combinations of elements x_1, x_2, \dots, x_m of the space X ; that is, the linear hull

$$\operatorname{Lin}\{x_1, x_2, \dots, x_m\} = \left\{ \sum c_j x_j, \quad c_j \in F \right\}. \quad (18.4)$$

So, for m , strictly smaller than the dimension of the space X , it is possible to interpret the shell as the shape of a body for which at least one of the dimensions significantly smaller than the others.

18.5 On Forms of Shells

Reticulated shells provide an interesting modern example of shells in construction. As building structures, they have a relatively short history due to the complexity of the calculation and the high requirements for the materials from which they are made. However, one cannot but admire their architectural elegance. Shell towers, shell overlaps, reticulated shell structures of complex geometric shapes have a piercing aesthetic effect on a person with a plexus of their "one-dimensional linear shells".

The American design engineer Paul Weidinger, who wrote about hyperbaric structures (forms of hyperbolic paraboloids) accurately conveyed the essence of the inner beauty of such architectural: "The beauty of forms is not achieved by means of "cosmetics", but follows from the essence of the structures. The form itself is almost an epitome of the effort it must take in" (Voloshinov, 1992).

Of all the forms of shells, the most remarkable is the sphere as a form that has maximum symmetry. The problems of elasticity of spherical shells were studied by such scientists as Louis Navier, Simeon Poisson, Gabriel Lamé (1795–1870) and Benoît Clapeyron (1799–1864). Philosophically speaking, Isaac Newton chose an apple-shaped object for his legend of the discovery of the law of gravity.

Mathematicians and mechanics in complex problems always tend to first investigate the reference (canonical) form, which usually has the undeniable advantages of obtaining explicit solutions. In this sense, the advantages of the spherical shape of shell, as well as of the objects modeled by spherical manifolds, are obvious. The concept of sphericity, which is equivalent to the diameter, is introduced for the study of complex objects. The equivalent diameter of a nonspherical particle is equal to the diameter of a spherical particle that exhibits the same properties (for example, aerodynamic, hydrodynamic, optical, electrical) as the nonspherical particle under study. Sphericity is a measure of how spherical an object is.

Let us see where similar spherical shells can occur. The human body and all living organisms consist of cells covered with a cytoplasmic membrane. In terms of mechanical properties, the cell membrane ensures the integrity of the cell and separates the contents of the cell from the external environment. On the example of a cell, one can see the philosophical foundations and the functionality that any closed shell carries — these being the wholeness and integrity of what the shell "envelops" with simultaneous protection and separation from what is happening outside.

The variety of functions of biomembranes includes:

1. The barrier shell with selective permeability,
2. Transport shell with the specifics of passive and active transport,
3. Matrix shell, which ensures optimal interaction of membrane proteins, and so on.

The mechanical properties of the shell, on the one hand, can be distinguished separately, but on the other hand, they cannot but reflect the complexity of the processes occurring in the cell (Gennis, 1989).

Perhaps the first steps in the study of the mechanical properties of cell shells will begin with the study of cell walls. The cell wall, which is the cell envelope located outside of the cytoplasmic shell, is found in most bacteria and plants. A strong cell wall is the most important feature of a plant cell, and its main component is cellulose. Higher plants have a cell wall, which is a complex, mostly polymeric, extracellular matrix that surrounds each cell. The cells of animals and humans do not have such a structure, being more highly organized matter in comparison with plants.

Let us consider an interesting aspect of approaches to the study of objects belonging to different realms of nature. Here we mean the realms of plants, animals, and human being. The typology of matter in these royal forms has different specifics and

features. If we look at scientific research from this angle, then the evolution of the development of science involves a consistent complication of the objects of research, starting with the kingdom of minerals, which includes all "deformable solids", and further to the objects of the plant and animal kingdoms. The pinnacle of research is the study of the human realm, which consists of the most complexly organized matter. Modern participants in this direction are such sciences as biophysics and biomechanics. Here it is appropriate to recall the words of Isaac Newton, which in many ways have not lost their relevance in our time: "I do not know what I may appear to the world; but to myself I seem to have been only like a boy playing on the sea-shore, and diverting myself in now and then finding a smoother pebble or a prettier shell than ordinary, whilst the great ocean of truth lay all undiscovered before me" (Brewster, 2010).

18.6 Problems of Modern Biomechanics

Biomechanics considers, in particular, problems for analysis and modeling of shells. Biomechanics of the hearing organs sets the task of evaluation of parameters of the tympanic membrane (tympanic membrane). This problem arises when planning surgical operations to restore the integrity of the tympanic membrane and improve auditory conductivity. To solve this problem, experimental studies are conducted for identification of the amplitude-frequency characteristics of the tympanic membrane of the ear in the normal mode and after the installation of cartilage grafts of various configurations.

Analysis involve mathematical models of the middle ear. Finite element modeling is used to calculate the forced vibrations of the middle ear with a cartilage graft. One finds the mechanical rigidity of the tympanic membrane, the motion of the points of the middle ear, and the principal forms of vibration. To improve the auditory conductivity it is necessary to meet the condition of equality of free vibration frequencies for the corresponding principal forms of oscillations of the middle ear in normal mode and of the middle ear with an installed cartilage graft of optimal thickness and configuration.

Analysis of the shells of the eye is a new direction in biomechanics, which makes use of almost all modern achievements of the theory of shells. Performance of the eye is governed by the laws of hydromechanics, thermodynamics, mechanics, and optics. At the turn of the 20th and 21st centuries, fundamental studies of the mechanics of the eye were initiated with the use of the theory of shells and the mechanics of deformable solids.

The outer shell of the eye is multi-layered and consists of the sclera, choroid, and retina. Detachment of some layers can occur in the process of injury or disease. An important issue is the study of the conditions under which such detachment can occur and the study of treatment methods. Mathematical models of the theory of shells make more clear the mechanisms and processes of retinal detachment, detachment of the vascular membrane. When simulating the effect of intraocular pressure on

the sclera, the problem of equilibrium of the transversally isotropic or even the orthotropic shell under the action of internal pressure is considered. The anisotropy is due to the fact that the shells of the eye (sclera and cornea) have elastic modulus in the direction of the thickness of the shell significantly smaller than in the tangential directions. Currently, it is known that often myopia of the eye is associated with the fact that the modulus of elasticity along the meridian becomes less than the modulus of elasticity along the parallel and the eye becomes ellipsoidal.

New knowledge in the field of biomechanics of the eye allows one to individualize the diagnosis, to study the influence of the parameters of the eyeball on the indicators of measuring devices, and to predict changes in the eye pressure after injections and surgeries. Thus, there is a constant search for new techniques and methods of treatment, where mathematical models are important to help predict the results of therapeutic and surgical treatment.

The collection of papers (Altenbach and Mikhasev, 2015) contains the result of long-time fruitful international cooperation in the field of shell structures in biomechanics.

18.7 Micro- and Macro-scale Shells

Everyone knows the concept of the electron shell of an atom. This concept combines the electrons and the nucleus and determines the place of the atom in the periodic table.

There is a conjecture that the electron shells, which have been studied by physicists for more than a decade, can later be described in the framework of the etheric form of matter (Zhilin, 2006b, 2013). (These studies are discussed in more detail in the next section). We can expect that the next stages of the development of exact sciences will lead to new conceptual approaches in relation to any elementary particles, where each particle will necessarily have a shell, and hence the "elastic" properties of the shells.

The study of shells will expand to macroscales as well. So, with the new mathematical apparatus, it will be possible to study the geographical shell of the Earth, not only in the form of studying its individual layers by individual sciences, but also as a whole, as a complete shell, including the lithosphere, the lower part of the atmosphere (troposphere, stratosphere), hydrosphere, biosphere, anthroposphere or noosphere. All spheres are in continuous interpenetration and interaction, in which the exchange of matter, energy and other components is carried out. The list of spheres can be supplemented by singling out the Earth's magnetosphere and ionosphere separately. An integrated approach requires taking into account the effects of the Sun, Moon, planets, and matter of the Solar System.

On the scale of the macrocosm, let us consider the ultimate (at present) shell of the universe. In analogy with the known shells that exist around the Planet, the Solar System and the Milky Way galaxy, we can assume the existence of a shell around the entire metagalaxy, the relic radiation from which has been studied for more than

half a century (Doroshkevich and Novikov, 1964, 2018). It is known that the relic radiation in the metagalaxy, which is observed nowadays, was formed during the transition of the original plasma to the gaseous state of neutral particles. The region of space in which the relic radiation was formed is called the surface of the last scattering. Since the degree of uniformity of the relic radiation is extremely high, it is represented as a sphere within which the universe or metagalaxy is transparent. In the future, studies of the processes of macroscale phenomena of nature will lead to the description of the shell of the surface of the last scattering by a system of differential equations with the possibility of directly calculating the natural frequencies that cause certain cosmic phenomena.

18.8 The Role of Mechanics in the Development of Science

Mechanics is developed in two directions. On the one hand, with the development of new branches of mathematics, scientists are able to model and describe in the language of mathematics more and more complex natural phenomena. On the other hand, physics provides mechanical scientists with the results of experiments waiting for their scientific explanation.

So, many equations of physics that were written by trial and error, bypassing the stage of derivation of formulas, were later derived by mechanics using tensor calculus. Professor Pavel Andreevich Zhilin derived (Zhilin, 2006b, p. 71) the equation for the Kelvin medium, which at one limit transition gives the well-known Schrodinger equation, and in the other limit case passes into the equally well-known Klein–Gordon equation.

In Zhilin (2006a, p. 32), Zhilin showed that the Maxwell equations are a special case of the well-known and strictly mathematically obtained equations of the theory of elasticity describing the oscillations of the elastic continuum. Moreover, the Maxwell equations are obtained from the equations of the theory of elasticity by the limit transition as the velocity of longitudinal waves tends to infinity. The speed of light is the speed of transverse waves. Note that for the equations of the theory of elasticity, the existence and uniqueness theorems of the solution are proved, which cannot be said about the Maxwell equations in their classical version. Maxwell himself also noted (Maxwell, 1873, p. 784) that his equations describe a transverse wave in an incompressible medium. In turn, it is known that the incompressibility of the medium in the limit leads to an infinite velocity of propagation of the longitudinal wave.

Zhilin's models of mechanics of multi-spin particles (Zhilin, 2013, 2006a, p. 112), which are capable of providing mechanical interpretations of the concepts of temperature, entropy, and chemical potential, are developed by his pupils (Gavrilov and Krivtsov, 2020; Grekova and Zhilin, 2001; Grekova, 2019a,b; Ivanova, 2015, 2019, 2021; Kuzkin and Krivtsov, 2021; Shishkina and Gavrilov, 2017; Shishkina et al, 2020; Tovstik, 2008, 2011; Vilchevskaya and Müller, 2021). Thus, mechanics, which deals with precise theories with strict derivation of formulas, provides a

deeper look at the structure of the world and completes the missing bricks in the building of science.

Acknowledgements The authors express are greatly indebted to S.M. Bauer, S.B. Filippov, E.A. Ivanova and A.L. Smirnov for their help and valuable advice given during the preparation of the article.

This research was carried out with the financial support of the Russian Foundation for Basic Research (grant no. 19.01.00208-a, 16.51.52025 MHT-a).

References

- Altenbach H, Eremeyev VA (2008) Direct approach based analysis of plates composed of functionally graded materials. *Archive of Applied Mechanics* 78(10):775–794
- Altenbach H, Eremeyev VA (2009) On the bending of viscoelastic plates made of polymer foams. *Acta Mechanica* 204(3–4):137–154
- Altenbach H, Mikhasev GI (eds) (2015) *Shell and Membrane Theories in Mechanics and Biology, Advanced Structured Materials*, vol 45. Springer, Cham
- Altenbach H, Zhilin PA (1988) A general theory of elastic simple shells (in Russ.). *Uspeki Mekhaniki* 11(4):1–12
- Altenbach H, Zhilin PA (2004) The theory of simple elastic shells. In: Kienzler R, Altenbach H, Ott I (eds) *Critical Review of the Theories of Plates and Shells*, Springer, Berlin, *Lecture Notes in Applied and Computational Mechanics*, vol 16, pp 1–12
- Altenbach J, Altenbach H, Eremeyev VA (2010) On generalized Cosserat-type theories of plates and shells: a short review and bibliography. *Archive of Applied Mechanics* 80(1):73–92
- Bauer SM, Filippov SB, Smirnov AL, Tovstik PE, Vaillancourt R (2015) *Asymptotic Methods in Mechanics of Solids*. Birkhäuser, Basel
- Blekhman II, Myshkis AD, Panovko YG (1983) *Mechanics and applied mathematics, Logic and features of mathematics applications (in Russ.)*. Nauka, Moscow
- Brewster D (2010) *Memoirs of the Life, Writings, and Discoveries of Sir Isaac Newton*, Cambridge Library Collection - Physical Sciences, vol 2, Cambridge University Press, Cambridge, chap XXVII, p 303–322
- Chladni EFF (1802) *Die Akustik*. Breitkopf und Härtel, Leipzig
- Chladni EFF (2015) *Treatise on Acoustics. The First Comprehensive English Translation of E.F.F. Chladni's Traité d'Acoustique*. Springer, Leipzig
- Doroshkevich AG, Novikov ID (1964) Republication of: Mean density of radiation in the Metagalaxy and certain problems in relativistic cosmology. *Soviet Physics-Doklady*, 9(2):111–113
- Doroshkevich AG, Novikov ID (2018) Republication of: Mean density of radiation in the Metagalaxy and certain problems in relativistic cosmology. *General Relativity and Gravitation* 50(11):138 (1–6)
- Elishakoff I (2020) *Handbook of the Timoshenko-Ehrenfest Beam and Uflyand-Mindlin Theories*. World Scientific, Singapore
- Faraday M (1837) On a peculiar class of acoustical figures; and on certain forms assumed by groups of particles upon vibrating elastic surfaces. *Abstracts of the Papers Printed in the Philosophical Transactions of the Royal Society of London* 3:49–51
- Fuss PH (1843) *Correspondance Mathématique et Physique De Quelques Célèbres Géomètres Du XVIIIeme Siecle, Précédée d'une notice sur les travaux de Léonard Euler*, vol II. St.-Petersbourg
- Gavrillov SN, Krivtsov AM (2020) Steady-state kinetic temperature distribution in a two-dimensional square harmonic scalar lattice lying in a viscous environment and subjected to a point heat source. *Continuum Mechanics and Thermodynamics* 32(1):41–61

- Gennis RB (1989) *Biomembranes. Molecular Structure and Function*. Springer Advanced Texts in Chemistry, Springer, New York
- Goldeneizer AL (1961) *Theory of elastic thin shells*, translation from the Russian, edited by G. Herrmann. Pergamon Press, New York
- Grekova E, Zhilin P (2001) Basic equations of Kelvin's medium and analogy with ferromagnets. *Journal of Elasticity* 64(1):29–70
- Grekova EF (2019a) Nonlinear isotropic elastic reduced and full cosserat media: waves and instabilities. *Continuum Mechanics and Thermodynamics* 31(6):1805–1824
- Grekova EF (2019b) Reduced enhanced elastic continua as acoustic metamaterials. In: Altenbach H, Belyaev A, Eremeyev V, Krivtsov A, Porubov A (eds) *Dynamical Processes in Generalized Continua and Structures*, Springer, Cham, *Advanced Structured Materials*, vol 103, pp 253–268
- Ivanova EA (2015) A new model of a micropolar continuum and some electromagnetic analogies. *Acta Mechanica* 226(3):697–721
- Ivanova EA (2019) On a micropolar continuum approach to some problems of thermo- and electro-dynamics. *Acta Mechanica* 230(5):1685–1715
- Ivanova EA (2021) Modeling of electrodynamic processes by means of mechanical analogies. *ZAMM - Journal of Applied Mathematics and Mechanics / Zeitschrift für Angewandte Mathematik und Mechanik* 101(4):e202000,076
- Kuzkin VA, Krivtsov AM (2021) Unsteady ballistic heat transport: linking lattice dynamics and kinetic theory. *Acta Mechanica* 232(5):1983–1996
- Maxwell JC (1873) *A treatise on electricity and magnetism*, vol I & II. Clarendon Press, Oxford
- Mikhasev GI, Tovstik PE (2020) *Localized Dynamics of Thin-Walled Shells*. CRC Press. Taylor & Francis
- Ravaisson-Mollien C (ed) (1881) *Les manuscrits de Leonardo da Vinci, publes en fac-similes photographiques avec transcriptions litterales etc.*, vol 1. A. A. Quantin, Paris
- Ravaisson-Mollien C (ed) (1891) *Les manuscrits de Leonardo da Vinci, publes en fac-similes photographiques avec transcriptions litterales etc.*, vol 3. E. A. Quantin, Paris
- Shishkina EV, Gavrilov SN (2017) Stiff phase nucleation in a phase-transforming bar due to the collision of non-stationary waves. *Archive of Applied Mechanics* 87(6):1019–1036
- Shishkina EV, Gavrilov SN, Mochalova YA (2020) Passage through a resonance for a mechanical system, having time-varying parameters and possessing a single trapped mode. the principal term of the resonant solution. *Journal of Sound and Vibration* 481:115,422
- Timoshenko SP (1953) *History of Strength of Materials*. McGraw-Hill, New York
- Tovstik PE, Smirnov AL (2001) *Asymptotic Methods in the Buckling Theory of Elastic Shells, Series on Stability, Vibration and Control of Systems, Series A*, vol 4. World Scientific, Singapore et al.
- Tovstik TP (2008) Elastic and dynamical properties of the graphite crystal lattice model. In: *Fourth European Conference on Structural Control*, IPME RAS, St. Petersburg, pp 811–818
- Tovstik TP (2011) Propagation of longitudinal waves along a two-layer rod (in Russ.). In: *Simulation of Dynamic Systems*, Interservice Publishing House, Nizhny Novgorod, pp 91–98
- Truesdell C (1964) Die Entwicklung des Drallsatzes. *ZAMM - Journal of Applied Mathematics and Mechanics / Zeitschrift für Angewandte Mathematik und Mechanik* 44(4-5):149–158
- Vilchevskaya EN, Müller WH (2021) Modeling of orientational polarization within the framework of extended micropolar theory. *Continuum Mechanics and Thermodynamics* n/a(n/a):n/a
- Voloshinov AV (1992) *Mathematics and Art (in Russ.)*. Prosveschenie, Moscow
- Zhilin PA (1976) Mechanics of deformable directed surfaces. *International Journal of Solids and Structures* 12(9–10):635–648
- Zhilin PA (2006a) *Advanced Problems in Mechanics*. In: Indeitsev DA, Ivanova EA, Krivtsov AM (eds) *Selection of articles presented at the Annual International Summer School – Conference Advanced Problems in Mechanics*, Institute for Problems in Mechanical Engineering of Russian Academy of Sciences, St. Petersburg, vol 2
- Zhilin PA (2006b) *Advanced Problems in Mechanics (in Russ.)*. In: Indeitsev DA, Ivanova EA, Krivtsov AM (eds) *Selection of articles presented at the Annual International Summer School*

- Conference Advanced Problems in Mechanics, Institute for Problems in Mechanical Engineering of Russian Academy of Sciences, St. Petersburg, vol 1
- Zhilin PA (2006c) Applied Mechanics. Foundations of the Theory of Shells (in Russ.). St. Petersburg State Polytechnical University, St. Petersburg
- Zhilin PA (2013) Construction of a model of an electromagnetic field from the standpoint of rational mechanics (in Russ.). RENSIT 5(1):77–97
- Zorich VA (2016) Mathematical Analysis, Universitext, vol II, 2nd edn. Springer, Berlin-Heidelberg



Chapter 19

Necessary Conditions for Energy Minimizers in a Cosserat Model of Fiber-reinforced Elastic Solids

Milad Shirani and David J. Steigmann

Abstract Pointwise necessary conditions for energy minimizers are derived in the context of a Cosserat model of fiber-reinforced elastic solids in which the Cosserat rotation field accounts for the kinematics of the embedded fibers, modelled as spatial Kirchhoff rods. The analysis requires careful consideration of constraints associated with the fact that fibers are convected by the continuum deformation field as material curves.

Key words: Cosserat elasticity, Fiber-reinforced materials, Legendre-Hadamard conditions

19.1 Introduction

Our aim in this work is to obtain pointwise necessary conditions of the Legendre-Hadamard type for energy minimizing states of fiber-reinforced solids in which the fibers are regarded as continuously distributed Kirchhoff rods (Landau and Lifshitz, 1986; Dill, 1992; Antman, 2005) that convect with the underlying continuum deformation. The kinematics of these rods are controlled by a rotation field and its gradient. Accordingly, Cosserat elasticity furnishes the appropriate conceptual framework for this model (Steigmann, 2012, 2015). Unlike conventional Cosserat elasticity (Cosserat and Cosserat, 1909; Truesdell and Noll, 1965; Reissner, 1975, 1987; Neff, 2006; Pietraszkiewicz and Eremeyev, 2009), the fibers induce a directional Cosserat effect associated with the trajectories of the fibers. A complicating feature of the present model *vis a vis* the derivation of the Legendre-Hadamard condition is the materiality of the embedded fibers. This entails non-standard constraints in-

Milad Shirani · David Steigmann

Department of Mechanical Engineering, University of California, Berkeley, CA. 94720, USA
e-mail: milad_shirani@berkeley.edu, dsteigmann@berkeley.edu

volution of the deformation and rotation fields. A derivation of the Legendre-Hadamard condition for unconstrained Cosserat continua is given in Shirani et al (2020).

We present a brief resumé of Cosserat elasticity in Sect. 19.2, together with its adaptation to materials reinforced by a single family of continuously distributed fibers. Conservative problems are discussed in Sect. 19.3, where the Legendre-Hadamard conditions for energy minimizers are derived.

We use standard notation such as \mathbf{A}^t , \mathbf{A}^* , $\text{Skw}\mathbf{A}$ and $\det\mathbf{A}$. These are respectively the transpose, the cofactor, the skew part and the determinant of a tensor \mathbf{A} , regarded as a linear transformation from a three-dimensional vector space to itself. The axial vector $\text{ax}(\text{Skw}\mathbf{A})$ of $\text{Skw}\mathbf{A}$ is defined by $\text{ax}(\text{Skw}\mathbf{A}) \times \mathbf{v} = (\text{Skw}\mathbf{A})\mathbf{v}$ for any vector \mathbf{v} . The tensor product of three-vectors is indicated by interposing the symbol \otimes , and the Euclidean inner product of tensors \mathbf{A}, \mathbf{B} is denoted and defined by $\mathbf{A} \cdot \mathbf{B} = \text{tr}(\mathbf{A}\mathbf{B}^t)$, where $\text{tr}(\cdot)$ is the trace; the induced norm is $|\mathbf{A}| = \sqrt{\mathbf{A} \cdot \mathbf{A}}$. The symbol $|\cdot|$ is also used to denote the usual Euclidean norm of three-vectors. Latin and Greek indices take values in $\{1, 2, 3\}$ and $\{2, 3\}$ respectively, and, when repeated, are summed over their ranges. Finally, bold subscripts are used to denote derivatives of scalar functions with respect to their vector or tensor arguments.

19.2 Cosserat Elasticity of Fiber-reinforced Materials

Cosserat elasticity theory furnishes the natural setting for elastic solids with embedded fibers - modelled as continuously distributed Kirchhoff rods - that support bending and twisting moments. The fibers are assumed to be perfectly bonded to an underlying matrix material and aligned locally with a unit-vector field $\mathbf{D}(\mathbf{X})$, where \mathbf{X} is the position of a material point in a fixed reference configuration κ . If a fiber is sufficiently stiff relative to the matrix then its deformation gradient is approximated by a rotation field $\mathbf{R}(\mathbf{X})$. In Dill's interpretation of the Kirchhoff theory (Dill, 1992) this is accompanied by a small axial strain. Moreover, the fiber is convected as a material curve with respect to the underlying matrix deformation. Thus,

$$\mathbf{F}\mathbf{D} = \lambda\mathbf{d}, \quad \text{where } \mathbf{d} = \mathbf{R}\mathbf{D} \quad \text{and} \quad \lambda = |\mathbf{F}\mathbf{D}|, \quad (19.1)$$

where λ is the fiber stretch and \mathbf{F} is the gradient of a deformation field $\boldsymbol{\chi}(\mathbf{X})$. The fields \mathbf{F} and \mathbf{R} are otherwise independent. Equivalently, $\mathbf{R}^t\mathbf{F}\mathbf{D} = \lambda\mathbf{D}$ and this entails two constraints

$$\mathbf{D}_\alpha \cdot \mathbf{R}^t\mathbf{F}\mathbf{D} = 0; \quad \alpha = 2, 3, \quad (19.2)$$

involving the fiber rotation and matrix deformation, where \mathbf{D}_α are cross-sectional vectors embedded in the fiber but not in the matrix. Accordingly, their images, $\mathbf{d}_\alpha = \mathbf{R}\mathbf{D}_\alpha$, in the current configuration are free to shear relative to the matrix while remaining mutually orthogonal and perpendicular to \mathbf{d} .

19.2.1 Kinematical and Constitutive Variables in Cosserat Elasticity

The constitutive response of an elastic Cosserat continuum is embodied in a strain-energy density $U(\mathbf{F}, \mathbf{R}, \nabla \mathbf{R}; \mathbf{X})$, per unit volume of κ , where $\nabla \mathbf{R}$ is the rotation gradient. In Cartesian index notation, these are

$$\mathbf{F} = F_{iA} \mathbf{e}_i \otimes \mathbf{E}_A, \quad \mathbf{R} = R_{iA} \mathbf{e}_i \otimes \mathbf{E}_A \quad \text{and} \quad \nabla \mathbf{R} = R_{iA,B} \mathbf{e}_i \otimes \mathbf{E}_A \otimes \mathbf{E}_B \quad (19.3)$$

with

$$F_{iA} = \chi_{i,A}, \quad (19.4)$$

where

$$(\cdot)_{,A} = \frac{\partial(\cdot)}{\partial X_A}$$

and where $\{\mathbf{e}_i\}$ and $\{\mathbf{E}_A\}$ are fixed orthonormal bases associated with the Cartesian coordinates x_i and X_A , with $x_i = \chi_i(X_A)$.

We assume the strain energy to be Galilean invariant and thus require

$$U(\mathbf{F}, \mathbf{R}, \nabla \mathbf{R}; \mathbf{X}) = U(\mathbf{Q}\mathbf{F}, \mathbf{Q}\mathbf{R}, \mathbf{Q}\nabla \mathbf{R}; \mathbf{X}), \quad (19.5)$$

where \mathbf{Q} is an arbitrary spatially uniform rotation with

$$(\mathbf{Q}\nabla \mathbf{R})_{iAB} = (Q_{ij}R_{jA})_{,B} = Q_{ij}R_{jA,B}.$$

The restriction

$$U(\mathbf{F}, \mathbf{R}, \nabla \mathbf{R}; \mathbf{X}) = W(\mathbf{E}, \mathbf{\Gamma}; \mathbf{X}), \quad (19.6)$$

with (Pietraszkiewicz and Eremeyev, 2009)

$$\mathbf{E} = \mathbf{R}^t \mathbf{F} = E_{AB} \mathbf{E}_A \otimes \mathbf{E}_B; \quad E_{AB} = R_{iA} F_{iB}, \quad (19.7)$$

$$\mathbf{\Gamma} = \mathbf{\Gamma}_{DC} \mathbf{E}_D \otimes \mathbf{E}_C; \quad \Gamma_{DC} = \frac{1}{2} e_{BAD} R_{iA} R_{iB,C}, \quad (19.8)$$

where W is the reduced strain-energy function and e_{ABC} is the permutation symbol, is both necessary and sufficient for Galilean invariance. Sufficiency is obvious, whereas necessity follows by choosing $\mathbf{Q} = \mathbf{R}_{|X}^t$, where X is the material point in question, and making use of the fact that, for each fixed $C \in \{1, 2, 3\}$, the matrix $R_{iA} R_{iB,C}$ is skew. This follows by differentiating $R_{iA} R_{iB} = \delta_{AB}$ (the Kronecker delta). The axial vectors $\mathbf{\Gamma}_C$ associated with this skew matrix have components

$$\Gamma_{D(C)} = \frac{1}{2} e_{BAD} R_{iA} R_{iB,C}, \quad (19.9)$$

yielding (Pietraszkiewicz and Eremeyev, 2009)

$$\mathbf{\Gamma} = \mathbf{\Gamma}_C \otimes \mathbf{E}_C. \quad (19.10)$$

19.2.2 Virtual Power and Equilibrium

We define equilibria to be states that satisfy the virtual-power statement

$$\dot{E} = P, \quad (19.11)$$

where P is the virtual power of the loads acting on the body,

$$E = S + \int_{\kappa} \Lambda_{\alpha} \mathbf{D}_{\alpha} \cdot \mathbf{E} \mathbf{D} dv, \quad (19.12)$$

is the extended energy, Λ_{α} are Lagrange multipliers accompanying the constraints (19.2),

$$S = \int_{\kappa} U dv \quad (19.13)$$

is the total strain energy, and superposed dots are used to denote variational derivatives. Thus,

$$\dot{U} = \dot{W} = \boldsymbol{\sigma} \cdot \dot{\mathbf{E}} + \boldsymbol{\mu} \cdot \dot{\boldsymbol{\Gamma}}, \quad (19.14)$$

where

$$\boldsymbol{\sigma} = W_{\mathbf{E}} \quad \text{and} \quad \boldsymbol{\mu} = W_{\boldsymbol{\Gamma}} \quad (19.15)$$

are evaluated at equilibrium. Further,

$$(\mathbf{D}_{\alpha} \cdot \mathbf{E} \mathbf{D})' = \mathbf{D}_{\alpha} \otimes \mathbf{D} \cdot \dot{\mathbf{E}} \quad (19.16)$$

so that

$$\dot{E} = \int_{\kappa} [(\boldsymbol{\sigma} + \boldsymbol{\Lambda} \otimes \mathbf{D}) \cdot \dot{\mathbf{E}} + \boldsymbol{\mu} \cdot \dot{\boldsymbol{\Gamma}} + \dot{\Lambda}_{\alpha} \mathbf{D}_{\alpha} \cdot \mathbf{E} \mathbf{D}] dv, \quad (19.17)$$

where

$$\boldsymbol{\Lambda} = \Lambda_{\alpha} \mathbf{D}_{\alpha}. \quad (19.18)$$

It follows easily from (19.7) that

$$\dot{\mathbf{E}} = \mathbf{R}' (\nabla \mathbf{u} - \boldsymbol{\Omega} \mathbf{F}), \quad \text{where} \quad \mathbf{u} = \dot{\boldsymbol{\chi}} \quad \text{and} \quad \boldsymbol{\Omega} = \dot{\mathbf{R}} \mathbf{R}' \quad (19.19)$$

We also have

$$\dot{\boldsymbol{\Gamma}} = \mathbf{R}' \nabla \boldsymbol{\omega}, \quad (19.20)$$

where $\boldsymbol{\omega} = \text{ax}\boldsymbol{\Omega}$. To demonstrate this we combine (19.8)₂ and (19.19)₃ to derive

$$\begin{aligned}
\dot{\Gamma}_{DC} &= \frac{1}{2} e_{BAD} (\dot{R}_{iA} R_{iB,C} + R_{iA} \dot{R}_{iB,C}) \\
&= \frac{1}{2} e_{BAD} [\Omega_{im} R_{mA} R_{iB,C} + R_{mA} (\Omega_{mj,C} R_{jB} + \Omega_{mj} R_{jB,C})] \\
&= \frac{1}{2} e_{BAD} R_{mA} [\Omega_{mi,C} R_{iB} + (\Omega_{mi} + \Omega_{im}) R_{iB,C}] \\
&= \frac{1}{2} e_{BAD} R_{iB} R_{mA} \Omega_{mi,C}.
\end{aligned} \tag{19.21}$$

Because $\det \mathbf{R} = 1$ we have $e_{BAD} R_{iB} R_{mA} R_{jD} = e_{imj}$, and hence $e_{BAC} R_{iB} R_{mA} = e_{imj} R_{jC}$, where use has been made of $R_{jD} R_{jC} = \delta_{DC}$. Altogether, we find

$$\dot{\Gamma}_{DC} = R_{jD} \omega_{jC}, \tag{19.22}$$

where

$$\omega_j = \frac{1}{2} e_{imj} \Omega_{mi},$$

and thus arrive at (19.20).

We these results elementary calculations (Shirani and Steigmann, 2020) deliver the virtual power (cf. (19.11)) in the form

$$P = \int_{\partial\kappa} (\mathbf{t} \cdot \mathbf{u} + \mathbf{c} \cdot \boldsymbol{\omega}) da + \int_{\kappa} (\mathbf{g} \cdot \mathbf{u} + \boldsymbol{\pi} \cdot \boldsymbol{\omega}) dv, \tag{19.23}$$

where

$$\mathbf{g} = -\text{Div}(\mathbf{R}\boldsymbol{\sigma} + \boldsymbol{\lambda} \otimes \mathbf{D}) \quad \text{and} \quad \boldsymbol{\pi} = -\text{Div}(\mathbf{R}\boldsymbol{\mu}) - 2\text{ax}\{\mathbf{R}\text{Skw}[(\boldsymbol{\sigma} + \boldsymbol{\Lambda} \otimes \mathbf{D})\mathbf{E}^t]\mathbf{R}^t\} \tag{19.24}$$

are volumetric densities of force and couple acting in κ , with

$$\boldsymbol{\lambda} = \mathbf{R}\boldsymbol{\Lambda} = \Lambda_\alpha \mathbf{d}_\alpha, \tag{19.25}$$

and where

$$\mathbf{t} = (\mathbf{R}\boldsymbol{\sigma} + \boldsymbol{\lambda} \otimes \mathbf{D})\boldsymbol{\nu} \quad \text{on} \quad \partial\kappa_t \quad \text{and} \quad \mathbf{c} = (\mathbf{R}\boldsymbol{\mu})\boldsymbol{\nu} \quad \text{on} \quad \partial\kappa_c \tag{19.26}$$

are surface densities of force and couple, where $\partial\kappa_t$ is a part of $\partial\kappa$ where position is not assigned and $\partial\kappa_c$ is a part where rotation is not assigned. Position is assigned on $\partial\kappa \setminus \partial\kappa_t$ ($\mathbf{u} = \mathbf{0}$) and rotation is assigned on $\partial\kappa \setminus \partial\kappa_c$ ($\boldsymbol{\omega} = \mathbf{0}$).

19.2.3 Fiber-matrix Interaction

We assume that Cosserat elasticity is conferred by the mechanical interaction between an elastomeric matrix and a single family of continuously distributed embedded fibers, regarded as spatial Kirchhoff rods that respond constitutively to a

bend-twist strain vector. The bend-twist strain of a fiber family initially tangential to the unit-vector field $\mathbf{D}(\mathbf{X})$ is $\boldsymbol{\gamma} = \text{ax}(\mathbf{R}'\mathbf{R}')$ (Shirani and Steigmann, 2020), where $(\cdot)'$ is the directional derivative along \mathbf{D} . This may be expressed in the form

$$\boldsymbol{\gamma} = \gamma_i \mathbf{D}_i \quad \text{with} \quad \gamma_i = \frac{1}{2} e_{ijk} \mathbf{D}_k \cdot \mathbf{R}'\mathbf{R}'\mathbf{D}_j, \quad (19.27)$$

oriented orthonormal triad with $\mathbf{D}_1 = \mathbf{D}$. Using $R'_{iA} = R_{iA,B} D_B$ we derive

$$\mathbf{R}'\mathbf{R}' = R_{iC} R_{iA,B} D_B \mathbf{E}_C \otimes \mathbf{E}_A = e_{ACD} \Gamma_{DB} D_B \mathbf{E}_C \otimes \mathbf{E}_A. \quad (19.28)$$

The Cosserat rotation field is given simply by

$$\mathbf{R} = \mathbf{d}_i \otimes \mathbf{D}_i, \quad (19.29)$$

where $\mathbf{d}_i = \mathbf{R}\mathbf{D}_i$ are the images of directors in the deformed body. Thus $\mathbf{d} = \mathbf{d}_1$ is the field of unit tangents to the deformed fibers and \mathbf{d}_α ($\alpha = 1, 2$) are embedded in the fiber cross sections, but *not* in the matrix material.

It follows from (19.27) and (19.28) that $\boldsymbol{\gamma}$ is determined by $\boldsymbol{\Gamma}$ via $\boldsymbol{\Gamma}\mathbf{D}$. In fact, we can show that

$$\boldsymbol{\gamma} = \boldsymbol{\Gamma}\mathbf{D}. \quad (19.30)$$

To see this we combine (19.27) and (19.28), reaching

$$\gamma_i = A_{iD}^* \Gamma_{DB} D_B, \quad (19.31)$$

where

$$A_{iD}^* = \frac{1}{2} e_{ijk} e_{DAC} A_{jA} A_{kC} \quad (19.32)$$

are the cofactors of the matrix with components $A_{jA} = \mathbf{D}_j \cdot \mathbf{E}_A$. The latter induce the tensor $\mathbf{A} = A_{iA} \mathbf{D}_i \otimes \mathbf{E}_A$. Using $\mathbf{D}_i = (\mathbf{D}_i \cdot \mathbf{E}_B) \mathbf{E}_B = A_{iB} \mathbf{E}_B$, we have

$$\mathbf{A} = A_{iA} A_{iB} \mathbf{E}_B \otimes \mathbf{E}_A, \quad (19.33)$$

with

$$A_{iA} A_{iB} = (\mathbf{D}_i \cdot \mathbf{E}_A)(\mathbf{D}_i \cdot \mathbf{E}_B) = \mathbf{I} \cdot \mathbf{E}_A \otimes \mathbf{E}_B = \delta_{AB}, \quad (19.34)$$

where $\mathbf{I} = \mathbf{D}_i \otimes \mathbf{D}_i$ is the identity for 3-space. It follows that $\mathbf{A} = \mathbf{I}$. Using the well known formula $\mathbf{A}'\mathbf{A}^* = (\det \mathbf{A})\mathbf{I}$, we conclude, from (19.31), that

$$A_{iC} \gamma_i = A_{iC} A_{iD}^* \Gamma_{DB} D_B = \delta_{CD} \Gamma_{DB} D_B = \Gamma_{CB} D_B. \quad (19.35)$$

Equation (19.27)₁, expressed in the form $\boldsymbol{\gamma} = A_{iC} \gamma_i \mathbf{E}_C$, then yields (19.30).

Because the Cosserat effect is attributed to the embedded fibers, it is appropriate to require that the strain energy depend on $\boldsymbol{\Gamma}$ via the combination $\boldsymbol{\gamma} = \boldsymbol{\Gamma}\mathbf{D}$, and hence that

$$W(\mathbf{E}, \boldsymbol{\Gamma}; \mathbf{X}) = w(\mathbf{E}, \boldsymbol{\gamma}; \mathbf{X}), \quad (19.36)$$

for some function w . Thus,

$$\boldsymbol{\sigma} = w_{\mathbf{E}}. \quad (19.37)$$

To obtain the couple stress $\boldsymbol{\mu}$ we vary (19.30), i.e.,

$$\dot{\boldsymbol{\gamma}} = \dot{\mathbf{I}}\mathbf{D}. \quad (19.38)$$

Varying the energy at fixed \mathbf{E} , we then have

$$\boldsymbol{\mu} \cdot \dot{\mathbf{I}} = \dot{W} = \dot{w} = w_{\boldsymbol{\gamma}} \cdot \dot{\boldsymbol{\gamma}} = \mathbf{M} \otimes \mathbf{D} \cdot \dot{\mathbf{I}}, \quad (19.39)$$

where

$$\mathbf{M} = w_{\boldsymbol{\gamma}}, \quad (19.40)$$

yielding

$$\boldsymbol{\mu} = \mathbf{M} \otimes \mathbf{D} \quad \text{and} \quad \mathbf{R}\boldsymbol{\mu} = \mathbf{m} \otimes \mathbf{D}, \quad \text{where} \quad \mathbf{m} = \mathbf{R}\mathbf{M}. \quad (19.41)$$

The force and couple traction conditions reduce to

$$\mathbf{t} = (\mathbf{R}\boldsymbol{\sigma})\boldsymbol{\nu} + (\mathbf{D} \cdot \boldsymbol{\nu})\boldsymbol{\lambda} \quad \text{on} \quad \partial\kappa_t, \quad \text{and} \quad \mathbf{c} = (\mathbf{D} \cdot \boldsymbol{\nu})\mathbf{m} \quad \text{on} \quad \partial\kappa_c, \quad (19.42)$$

and furnish the interpretation of $\boldsymbol{\lambda}$ and \mathbf{m} , respectively, as shear force and moment densities acting on fiber 'cross sections'; that is, on surfaces that intersect the fibers orthogonally ($\mathbf{D} \cdot \boldsymbol{\nu} = \pm 1$). We observe that no solution exists if a non-zero couple is specified on a part of $\partial\kappa_c$ containing \mathbf{D} as a tangent vector ($\mathbf{D} \cdot \boldsymbol{\nu} = 0$).

19.3 Conservative Problems, Energy Minimizers and the Legendre-Hadamard Conditions

We are concerned with conservative problems characterized by a potential energy. These are such that there exists a *load potential* L , say, the variational derivative of which is identical to the virtual power. Thus,

$$\dot{L} = P, \quad (19.43)$$

and the potential energy is $E - L$, apart from an unimportant constant. Equilibria are thus seen to be those states that render the potential energy stationary, i.e.,

$$(E - L)' = 0, \quad (19.44)$$

for all admissible \mathbf{u} and $\boldsymbol{\omega}$. Moreover, the existence of a load potential renders meaningful the consideration of energy minimizers.

An example of conservative loading is furnished by the dead-load problem with vanishing volumetric densities of force \mathbf{g} and couple $\boldsymbol{\pi}$. The associated load potential is

$$L = \int_{\partial\kappa_t} \mathbf{t} \cdot \boldsymbol{\chi} da + \int_{\partial\kappa_c} \mathbf{T} \cdot \mathbf{R} da \quad (19.45)$$

in which \mathbf{t} and \mathbf{T} respectively are assigned configuration-independent vector and tensor fields. Here \mathbf{t} is as in (19.42)₁, and the couple traction in (19.42)₂ is

$$\mathbf{c} = 2\alpha[\text{Skw}(\mathbf{T}\mathbf{R}^t)]. \quad (19.46)$$

Thus the couple traction is configuration *dependent* in the dead-load problem. Indeed, it is well known that configuration-independent couples are associated with non-conservative problems (Ziegler, 1977) for which no potential energy exists.

Our aim is to derive the relevant version of the Legendre-Hadamard necessary condition for energy minimizers. We shall see that boundary loading does not play a role in this derivation and thus we suppress the load potential at the outset. The potential energy then reduces to the strain energy

$$E = \int_{\kappa} w(\mathbf{E}, \boldsymbol{\gamma}) dv. \quad (19.47)$$

The associated first and second variations are

$$\dot{E} = \int_{\kappa} (w_{\mathbf{E}} \cdot \dot{\mathbf{E}} + w_{\boldsymbol{\gamma}} \cdot \dot{\boldsymbol{\gamma}}) dv \quad (19.48)$$

and

$$\begin{aligned} \ddot{E} = & \int_{\kappa} (w_{\mathbf{E}} \cdot \ddot{\mathbf{E}} + w_{\boldsymbol{\gamma}} \cdot \ddot{\boldsymbol{\gamma}}) dv \\ & + \int_{\kappa} \{ \dot{\mathbf{E}} \cdot w_{\mathbf{E}\mathbf{E}}[\dot{\mathbf{E}}] + (w_{\mathbf{E}\boldsymbol{\gamma}}) \dot{\boldsymbol{\gamma}} \cdot \dot{\mathbf{E}} + (w_{\boldsymbol{\gamma}\mathbf{E}}) \dot{\mathbf{E}} \cdot \dot{\boldsymbol{\gamma}} + \dot{\boldsymbol{\gamma}} \cdot (w_{\boldsymbol{\gamma}\boldsymbol{\gamma}}) \dot{\boldsymbol{\gamma}} \} dv. \end{aligned} \quad (19.49)$$

The second variation, evaluated at an equilibrium state, is necessarily non-negative if that state minimizes the energy.

The second variations of \mathbf{E} and $\boldsymbol{\gamma}$ follow by varying (19.19) and (19.38), respectively. Thus,

$$\ddot{\mathbf{E}} = \mathbf{R}^t(\nabla \mathbf{v} - \boldsymbol{\Phi}\mathbf{F}) - \mathbf{R}^t\boldsymbol{\Omega}(\nabla \mathbf{u} + \mathbf{R}\dot{\mathbf{E}}), \quad (19.50)$$

where $\mathbf{v} = \ddot{\boldsymbol{\chi}}$ and $\boldsymbol{\Phi} = \dot{\boldsymbol{\Omega}}$, and

$$\dot{\boldsymbol{\gamma}} = \mathbf{R}^t\boldsymbol{\varphi}' + \dot{\mathbf{R}}^t\boldsymbol{\omega}' = \mathbf{R}^t\boldsymbol{\varphi}' - \mathbf{R}^t\boldsymbol{\Omega}\mathbf{R}\dot{\boldsymbol{\gamma}}, \quad (19.51)$$

where

$$\boldsymbol{\varphi} = \dot{\boldsymbol{\omega}} = \alpha x \dot{\boldsymbol{\Phi}}. \quad (19.52)$$

Accordingly,

$$\int_{\kappa} (w_E \cdot \ddot{\mathbf{E}} + w_{\boldsymbol{\gamma}} \cdot \ddot{\boldsymbol{\gamma}}) dv = \int_{\kappa} [w_E \cdot \mathbf{R}'(\nabla \mathbf{v} - \boldsymbol{\Phi} \mathbf{F}) + w_{\boldsymbol{\gamma}} \cdot \mathbf{R}' \boldsymbol{\varphi}'] dv - \int_{\kappa} [w_E \cdot \mathbf{R}' \boldsymbol{\Omega}(\nabla \mathbf{u} + \mathbf{R} \dot{\mathbf{E}}) + w_{\boldsymbol{\gamma}} \cdot (\mathbf{R}' \boldsymbol{\Omega} \mathbf{R}) \dot{\boldsymbol{\gamma}}] dv. \quad (19.53)$$

Equilibria render the potential energy stationary:

$$0 = \dot{\mathbf{E}} = \int_{\kappa} [w_E \cdot \mathbf{R}'(\nabla \mathbf{u} - \boldsymbol{\Omega} \mathbf{F}) + w_{\boldsymbol{\gamma}} \cdot \mathbf{R}' \boldsymbol{\omega}'] dv \quad (19.54)$$

for all \mathbf{u} and $\boldsymbol{\omega}$ such that (cf. (19.16))

$$0 = \mathbf{D}_{\alpha} \cdot \dot{\mathbf{E}} \mathbf{D} = \mathbf{D}_{\alpha} \cdot \mathbf{R}'(\nabla \mathbf{u} - \boldsymbol{\Omega} \mathbf{F}) \mathbf{D} = \mathbf{d}_{\alpha} \cdot (\mathbf{u}' - \boldsymbol{\omega} \times \boldsymbol{\chi}'). \quad (19.55)$$

We have explained the consequences of (19.54) in Sect. 19.2 on the basis of an extension of the energy to unconstrained states combined with the use of Lagrange multipliers (Berdichevsky, 2009). Here we avoid Lagrange multipliers by operating directly on the manifold defined by the constraints.

The constraints (19.55) are equivalent to the requirement that $\mathbf{u}' - \boldsymbol{\omega} \times \boldsymbol{\chi}'$ be parallel to \mathbf{d} , and hence, with $\boldsymbol{\chi}' = \lambda \mathbf{d}$, that

$$\mathbf{d} \times (\boldsymbol{\omega} \times \mathbf{d}) = \lambda^{-1} \mathbf{d} \times \mathbf{u}'. \quad (19.56)$$

The identity $\boldsymbol{\omega} = (\boldsymbol{\omega} \cdot \mathbf{d}) \mathbf{d} + \mathbf{d} \times (\boldsymbol{\omega} \times \mathbf{d})$ then delivers the general solution to (19.55) as

$$\boldsymbol{\omega} = \sigma \mathbf{d} + \lambda^{-1} \mathbf{d} \times \mathbf{u}' \quad (19.57)$$

in which σ is an arbitrary scalar.

Varying (19.55), it follows that kinematically admissible second variations must be such that

$$\begin{aligned} 0 &= \mathbf{D}_{\alpha} \cdot \ddot{\mathbf{E}} \mathbf{D} = \mathbf{D}_{\alpha} \cdot \mathbf{R}'(\nabla \mathbf{v} - \boldsymbol{\Phi} \mathbf{F}) \mathbf{D} - \mathbf{D}_{\alpha} \cdot \mathbf{R}' \boldsymbol{\Omega}(\nabla \mathbf{u} + \mathbf{R} \dot{\mathbf{E}}) \mathbf{D} \\ &= \mathbf{d}_{\alpha} \cdot (\mathbf{v}' - \boldsymbol{\varphi} \times \boldsymbol{\chi}') - \mathbf{d}_{\alpha} \cdot \boldsymbol{\omega} \times (\mathbf{u}' + \mathbf{R} \dot{\mathbf{E}} \mathbf{D}). \end{aligned} \quad (19.58)$$

We confine attention to second variations satisfying

$$\mathbf{d}_{\alpha} \cdot (\mathbf{v}' - \boldsymbol{\varphi} \times \boldsymbol{\chi}') = 0. \quad (19.59)$$

For these it follows from (19.54) and (19.55) that the first integral on the right-hand side of (19.53) vanishes, and that the second variation of the energy reduces to

$$\begin{aligned} \ddot{\mathbf{E}} &= \int_{\kappa} \{ \dot{\mathbf{E}} \cdot w_{EE} [\dot{\mathbf{E}}] + (w_{E\boldsymbol{\gamma}}) \dot{\boldsymbol{\gamma}} \cdot \dot{\mathbf{E}} + (w_{\boldsymbol{\gamma}E}) \dot{\mathbf{E}} \cdot \dot{\boldsymbol{\gamma}} + \dot{\boldsymbol{\gamma}} \cdot (w_{\boldsymbol{\gamma}\boldsymbol{\gamma}}) \dot{\boldsymbol{\gamma}} \} dv \\ &\quad - \int_{\kappa} [w_E \cdot \mathbf{R}' \boldsymbol{\Omega}(\nabla \mathbf{u} + \mathbf{R} \dot{\mathbf{E}}) + w_{\boldsymbol{\gamma}} \cdot (\mathbf{R}' \boldsymbol{\Omega} \mathbf{R}) \dot{\boldsymbol{\gamma}}] dv, \end{aligned} \quad (19.60)$$

subject to the residual content of (19.58), namely,

$$\mathbf{d}_\alpha \cdot \boldsymbol{\omega} \times (\mathbf{u}' + \mathbf{R}\dot{\mathbf{E}}\mathbf{D}) = 0. \tag{19.61}$$

To solve these latter conditions we first note that

$$\boldsymbol{\chi}' = \mathbf{F}\mathbf{D} = \lambda\mathbf{d}, \tag{19.62}$$

where λ is the fiber stretch, the variation of which is

$$\mathbf{u}' = \dot{\lambda}\mathbf{d} + \boldsymbol{\omega} \times \boldsymbol{\chi}'. \tag{19.63}$$

We also have

$$\dot{\mathbf{E}}\mathbf{D} = \mathbf{R}'(\mathbf{u}' - \boldsymbol{\omega} \times \boldsymbol{\chi}'), \tag{19.64}$$

so that (19.61) reduces to

$$0 = \mathbf{d}_\alpha \cdot \boldsymbol{\omega} \times (2\dot{\lambda}\mathbf{d} + \boldsymbol{\omega} \times \boldsymbol{\chi}'). \tag{19.65}$$

Thus there is a scalar c such that

$$2\dot{\lambda}\boldsymbol{\omega} \times \mathbf{d} + \lambda\boldsymbol{\omega} \times (\boldsymbol{\omega} \times \mathbf{d}) = c\mathbf{d}. \tag{19.66}$$

Taking the inner product with $\boldsymbol{\omega} \times \mathbf{d}$ gives $\dot{\lambda} = 0$, i.e.,

$$\mathbf{u}' = \boldsymbol{\omega} \times \boldsymbol{\chi}', \tag{19.67}$$

which is compatible with (19.55) and yields $\boldsymbol{\omega} \times (\boldsymbol{\omega} \times \boldsymbol{\chi}') = c\mathbf{d}$.

Let $\mathbf{e} = \boldsymbol{\omega}/|\boldsymbol{\omega}|$. The identity $\boldsymbol{\chi}' = (\mathbf{e} \cdot \boldsymbol{\chi}')\mathbf{e} + \mathbf{e} \times (\boldsymbol{\chi}' \times \mathbf{e})$, applied to (19.66), results in

$$(c + \lambda|\boldsymbol{\omega}|^2)\mathbf{d} = \lambda|\boldsymbol{\omega}|^2(\mathbf{e} \cdot \mathbf{d})\mathbf{e}. \tag{19.68}$$

The possibilities are:

- (i) $\mathbf{e} \cdot \mathbf{d} = \pm 1$ and $c = 0$, or
- (ii) $\mathbf{e} \cdot \mathbf{d} = 0$ and $c = -\lambda|\boldsymbol{\omega}|^2$.

We conclude that (19.61) is satisfied at any $\mathbf{X} \in \kappa$ provided that

$$\boldsymbol{\omega} \in \text{Span}\{\mathbf{d}\} \quad \text{or} \quad \boldsymbol{\omega} \in (\text{Span}\{\mathbf{d}\})^\perp. \tag{19.69}$$

The first restriction is satisfied by taking $\mathbf{u}' = \mathbf{0}$ and the second requires that $\mathbf{u}' \neq \mathbf{0}$.

We are now in a position to prove

Theorem 19.1 (Legendre-Hadamard Theorem). *If the second variation is non-negative then it is necessary that*

$$\mathbf{D} \cdot \mathbf{K}\mathbf{D} \geq 0 \quad \text{and} \quad \mathbf{D} \times \boldsymbol{\alpha} \cdot \mathbf{K}(\mathbf{D} \times \boldsymbol{\alpha}) \geq 0 \quad \text{for all vectors } \boldsymbol{\alpha}, \tag{19.70}$$

and at every $\mathbf{X} \in \kappa$, where $\mathbf{D}(\mathbf{X})$ is the unit tangent to the fiber passing through \mathbf{X} and

$$\mathbf{K}(\mathbf{X}) = w_{\gamma\gamma}\mathbf{X} \tag{19.71}$$

is the symmetric 2nd-order fiber stiffness tensor, evaluated at the energy-minimizing state $\{\boldsymbol{\chi}(\mathbf{X}), \mathbf{R}(\mathbf{X})\}$.

Remark 19.1. Inequalities (19.70) are identical to restrictions derived in Steigmann (2015), where they are shown to imply the non-negativity of the torsional and flexural stiffnesses of the embedded fibers. The method of proof discussed here is different, however. It is similar to that employed in Shirani et al (2020) to derive the Legendre-Hadamard condition for unconstrained Cosserat continua.

Proof. Consider the variations

$$\mathbf{u}(\mathbf{X}) = \epsilon^2 \boldsymbol{\xi}(\mathbf{Y}) \quad \text{and} \quad \boldsymbol{\omega}(\mathbf{X}) = \epsilon \boldsymbol{\eta}(\mathbf{Y}), \quad \text{with} \quad \mathbf{Y} = \epsilon^{-1}(\mathbf{X} - \mathbf{X}_0), \tag{19.72}$$

where \mathbf{X}_0 is an interior point of κ , ϵ is a positive constant, and $\boldsymbol{\xi}, \boldsymbol{\eta}$ are differentiable vector-valued functions compactly supported in a region D - the image of a strictly interior neighborhood $\kappa' \subset \kappa$ of \mathbf{X}_0 under the map $\mathbf{Y}(\cdot)$. Accordingly \mathbf{u} and $\boldsymbol{\omega}$ vanish on $\partial\kappa$, and it is for this reason that the loading terms in (19.45) are not relevant to our present considerations.

Substituting (19.72) in (19.60), dividing by ϵ^3 , passing to the limit $\epsilon \rightarrow 0$ and invoking the Dominated Convergence Theorem, we reduce the inequality $\ddot{E} \geq 0$ to

$$\int_D \mathbf{R}'_0(\nabla \boldsymbol{\eta}) \mathbf{D}_0 \cdot \mathbf{K}_0 \mathbf{R}'_0(\nabla \boldsymbol{\eta}) \mathbf{D}_0 dv \geq 0, \tag{19.73}$$

where the subscript $_0$ indicates evaluation at \mathbf{X}_0 , and, here and henceforth, ∇ is the gradient with respect to \mathbf{Y} . This holds for all $\boldsymbol{\eta}(\mathbf{Y})$ subject to (cf. (19.69) and (19.72)₂)

$$\boldsymbol{\eta} \in \text{Span}\{\mathbf{d}_0\} \quad \text{or} \quad \boldsymbol{\eta} \in (\text{Span}\{\mathbf{d}_0\})^\perp. \tag{19.74}$$

In the course of deriving (19.73) from (19.60) we have used (19.19) and (19.72) with $|\boldsymbol{\Omega}| = |\boldsymbol{\omega}| = O(\epsilon)$ to infer that $|\dot{\mathbf{E}}| = O(\epsilon)$ and $|\dot{\boldsymbol{\gamma}}| = O(1)$ after the change of variable.

We extend $\boldsymbol{\eta}$ to complex-valued vector fields as

$$\boldsymbol{\eta} = \boldsymbol{\eta}_1 + i\boldsymbol{\eta}_2, \tag{19.75}$$

where $\boldsymbol{\eta}_{1,2}$ are real-valued and i is the complex unit ($i^2 = -1$). It follows from the symmetry of \mathbf{K}_0 that

$$\begin{aligned} & \mathbf{R}'_0(\nabla \boldsymbol{\eta}) \mathbf{D}_0 \cdot \mathbf{K}_0 \mathbf{R}'_0(\nabla \bar{\boldsymbol{\eta}}) \mathbf{D}_0 \\ &= \mathbf{R}'_0(\nabla \boldsymbol{\eta}_1) \mathbf{D}_0 \cdot \mathbf{K}_0 \mathbf{R}'_0(\nabla \boldsymbol{\eta}_1) \mathbf{D}_0 + \mathbf{R}'_0(\nabla \boldsymbol{\eta}_2) \mathbf{D}_0 \cdot \mathbf{K}_0 \mathbf{R}'_0(\nabla \boldsymbol{\eta}_2) \mathbf{D}_0, \end{aligned} \tag{19.76}$$

in which the overbar identifies the complex conjugate, so that if (19.73) holds for real-valued $\boldsymbol{\eta}$ subject to (19.74), then

$$\int_D \mathbf{R}'_0(\nabla \boldsymbol{\eta}) \mathbf{D}_0 \cdot \mathbf{K}_0 \mathbf{R}'_0(\nabla \bar{\boldsymbol{\eta}}) \mathbf{D}_0 dv \geq 0 \tag{19.77}$$

for complex-valued $\boldsymbol{\eta}$ subject to the same restrictions.

Restriction (19.74)₁ is satisfied by taking

$$\boldsymbol{\eta} = \phi(\mathbf{Y})\mathbf{d}_0 \quad (19.78)$$

with ϕ a complex-valued differentiable scalar function compactly supported in D . Then, $\nabla\boldsymbol{\eta} = \mathbf{d}_0 \otimes \nabla\phi$ and

$$\mathbf{R}'_0(\nabla\boldsymbol{\eta})\mathbf{D}_0 = (\mathbf{D}_0 \cdot \nabla\phi)\mathbf{D}_0. \quad (19.79)$$

Consider

$$\phi(\mathbf{Y}) = f(\mathbf{Y})\exp(ik\mathbf{N} \cdot \mathbf{Y}), \quad (19.80)$$

with \mathbf{N} a fixed real vector, k a non-zero real number and f a real-valued differentiable function compactly supported in D . This gives

$$\mathbf{R}'_0(\nabla\boldsymbol{\eta})\mathbf{D}_0 = \exp(ik\mathbf{N} \cdot \mathbf{Y})(ikf\mathbf{D}_0 \cdot \mathbf{N} + \mathbf{D}_0 \cdot \nabla f)\mathbf{D}_0 \quad (19.81)$$

and

$$\mathbf{R}'_0(\nabla\boldsymbol{\eta})\mathbf{D}_0 \cdot \mathbf{K}_0\mathbf{R}'_0(\nabla\bar{\boldsymbol{\eta}})\mathbf{D}_0 = [k^2f^2(\mathbf{D}_0 \cdot \mathbf{N})^2 + (\mathbf{D}_0 \cdot \nabla f)^2]\mathbf{D}_0 \cdot \mathbf{K}_0\mathbf{D}_0, \quad (19.82)$$

and (19.77) reduces to

$$\mathbf{D}_0 \cdot \mathbf{K}_0\mathbf{D}_0[k^2(\mathbf{D}_0 \cdot \mathbf{N})^2 \int_D f^2 dv + \int_D (\mathbf{D}_0 \cdot \nabla f)^2 dv] \geq 0, \quad (19.83)$$

for arbitrary \mathbf{N} . This is equivalent to

$$\mathbf{D}_0 \cdot \mathbf{K}_0\mathbf{D}_0 \geq 0, \quad (19.84)$$

which is just (19.70)₁ on account of the arbitrariness of \mathbf{X}_0 .

It remains to analyze the second possibility (19.74)₂. The antecedent of this restriction is (19.69)₂, which requires that $\sigma = 0$ in (19.57) and thus $\boldsymbol{\omega} = \lambda^{-1}\mathbf{d} \times (\nabla\mathbf{u})\mathbf{D}$ in which $\nabla\mathbf{u}(\mathbf{X}) = \epsilon\nabla\xi(\mathbf{Y})$. Accordingly, with reference to (19.72)₂ we satisfy (19.74)₂ by taking

$$\boldsymbol{\eta} = \lambda_0^{-1}\mathbf{d}_0 \times (\nabla\xi)\mathbf{D}_0. \quad (19.85)$$

Consider

$$\xi(\mathbf{Y}) = f(\mathbf{Y})\exp(ik\mathbf{N} \cdot \mathbf{Y})\mathbf{a}, \quad (19.86)$$

where \mathbf{a} and \mathbf{N} are fixed real vectors, k is a real constant and f is a differentiable real-valued function with f and ∇f vanishing on ∂D (to ensure that $\boldsymbol{\eta}$ is compactly supported in D). With some effort we obtain

$$\boldsymbol{\eta} = \lambda_0^{-1}\exp(ik\mathbf{N} \cdot \mathbf{Y})[\mathbf{D}_0 \cdot (\nabla f + ikf\mathbf{N})]\mathbf{d}_0 \times \mathbf{a} \quad (19.87)$$

and

$$(\nabla\eta)\mathbf{D}_0 = \lambda_0^{-1} \exp(ik\mathbf{N} \cdot \mathbf{Y})F(\mathbf{Y})\mathbf{d}_0 \times \mathbf{a}, \quad (19.88)$$

with

$$F(\mathbf{Y}) = \mathbf{D}_0 \cdot \nabla(\mathbf{D}_0 \cdot \nabla f) - k^2 f(\mathbf{N} \cdot \mathbf{D}_0)^2 + 2ik(\mathbf{N} \cdot \mathbf{D}_0)\mathbf{D}_0 \cdot \nabla f. \quad (19.89)$$

Because \mathbf{R}_0^t is a rotation we have

$$\mathbf{R}_0^t(\mathbf{d}_0 \times \mathbf{a}) = \mathbf{R}_0^t \mathbf{d}_0 \times \mathbf{R}_0^t \mathbf{a} = \mathbf{D}_0 \times \boldsymbol{\alpha},$$

where $\boldsymbol{\alpha} = \mathbf{R}_0^t \mathbf{a}$, and thus reduce (19.77) to

$$\lambda_0^{-2} \mathbf{D}_0 \times \boldsymbol{\alpha} \cdot \mathbf{K}_0(\mathbf{D}_0 \times \boldsymbol{\alpha}) \int_D |F|^2 dv \geq 0 \quad (19.90)$$

for arbitrary \mathbf{N} and $\boldsymbol{\alpha}$, where $|F|^2 = F\bar{F}$. This in turn is equivalent to

$$\mathbf{D}_0 \times \boldsymbol{\alpha} \cdot \mathbf{K}_0(\mathbf{D}_0 \times \boldsymbol{\alpha}) \geq 0 \quad \text{for all } \boldsymbol{\alpha}, \quad (19.91)$$

and this yields (19.70)₂ because of the arbitrariness of $\mathbf{X}_0 \in \kappa$.

□

Acknowledgements This work was supported by the US National Science Foundation through grant CMMI-1931064. The work of MS was also supported by the P.M. Naghdi and B. Steidel Fellowships, administered by the Department of Mechanical Engineering at UC Berkeley

References

- Antman SS (2005) *Nonlinear Problems of Elasticity*. Springer, Berlin
- Berdichevsky VL (2009) *Variational Principles of Continuum Mechanics, vol I: Fundamentals*. Springer, Berlin
- Cosserat E, Cosserat F (1909) *Théorie des Corps Déformables*. Hermann, Paris
- Dill EH (1992) Kirchhoff's theory of rods. *Archive for History of Exact Sciences* 44(1):1–23
- Landau LD, Lifshitz EM (1986) *Theory of Elasticity*, 3rd edn. Pergamon, Oxford
- Neff P (2006) Existence of minimizers for a finite-strain micromorphic elastic solid. *Proceedings of the Royal Society of Edinburgh: Section A Mathematics* 136(5):997–1012
- Pietraszkiewicz W, Eremeyev VA (2009) On natural strain measures of the non-linear micropolar continuum. *International Journal of Solids and Structures* 46(3):774–787
- Reissner E (1975) Note on the equations of finite-strain force and moment stress elasticity. *Studies in Applied Mathematics* 54(1):1–8
- Reissner E (1987) A further note on finite-strain force and moment stress elasticity. *Zeitschrift für angewandte Mathematik und Physik ZAMP* 38(5):665–673
- Shirani M, Steigmann DJ (2020) A Cosserat model of elastic solids reinforced by a family of curved and twisted fibers. *Symmetry* 12(7):1133
- Shirani M, Steigmann DJ, Neff P (2020) The Legendre–Hadamard condition in Cosserat elasticity theory. *The Quarterly Journal of Mechanics and Applied Mathematics* 73(4):293–303
- Steigmann DJ (2012) Theory of elastic solids reinforced with fibers resistant to extension, flexure and twist. *International Journal of Non-Linear Mechanics* 47(7):734–742

- Steigmann DJ (2015) Effects of fiber bending and twisting resistance on the mechanics of fiber-reinforced elastomers. In: Dorfmann L, Ogden RW (eds) *Nonlinear Mechanics of Soft Fibrous Tissues*, Vienna and New York, CISM Courses and Lectures, vol 559, pp 269–305
- Truesdell C, Noll W (1965) The non-linear field theories of mechanics. In: Flügge S (ed) *Handbuch der Physik*, Springer, Berlin, vol III/3
- Ziegler H (1977) *Principles of Structural Stability*. Springer, Basel



Chapter 20

Vibration Control of a Non-homogeneous Circular Thin Plate

Andrei L. Smirnov and Grigory P. Vasiliev

Abstract Transverse vibrations of an inhomogeneous circular thin plate are studied. The plates, which geometric and physical parameters slightly differ from constant and depend only on the radial coordinate, are analyzed. After separation of variables the obtained homogeneous ordinary differential equations together with homogeneous boundary conditions form a regularly perturbed boundary eigenvalue problem. For frequencies of free vibrations of a plate, which thickness and/or Young's modulus nonlinearly depend on the radial coordinate asymptotic formulas are obtained by means of the perturbation method. The effect of the small perturbation parameter on behavior of frequencies is analyzed under special conservation conditions:

- i) for a plate, the mass of which is fixed, if the thickness is variable, and
- ii) for a plate with the fixed average stiffness, if Young's modulus is variable.

Asymptotic results for the lower vibration frequencies well agree with the results of finite element analysis with COMSOL Multiphysics 5.4.

Key words: Free vibrations of plates, Inhomogeneous circular plate, Perturbation method

20.1 Introduction

Plates of various shapes and of non-uniform thickness are widely used in engineering structures and study of the vibration of a thin circular plate is basic in structural mechanics. Many papers have been written on the vibration of plates covering various shapes, thickness variations according to different laws and different

Andrei L. Smirnov · Grigory P. Vasiliev
St. Petersburg State University, 7/9 Universitetskaya nab., St. Petersburg, Russian Federation
e-mail: a.l.smirnov@spbu.ru, vasiliev.gregory@gmail.com

boundary conditions, vibrations non-uniform circular plates. The natural frequencies of circular plates have been studied extensively for more than a century and the results of these studies have been summarized in Leissa (1969). Different methods have been applied by the authors to analyze circular plate vibrations. Here we mention just a few research papers those deal with small transverse vibrations of circular thin shells. Many researchers have used Rayleigh-Ritz method to solve the problem numerically (Singh and Saxena, 1996). Chakraverty et al (1994) have surveyed the research on vibration of plates using boundary characteristic polynomials in the Rayleigh-Ritz method. Wang et al (1995) used the differential quadrature method to obtain solution for linear variation of thickness. Conway (1958) analyzed the axisymmetric vibration of thin circular plates with a power function thickness variation in terms of Bessel functions. Wang (1997) used the power series method for free vibration analysis of circular thin plates of power varying thickness. Jaroszewicz (2017) examined the circular plate whose thickness decreases with the distance from the centre of symmetry according to the hyperbolic law with the index $m < 0$. Jaroszewicz and Zoryj (2006) studied free vibration of circular thin plates of variable distribution of parameters using the method of partial discretization (MPD). Prasad et al (1972) studied the free axisymmetric vibrations of linearly varying thickness have been studied on the basis of classical theory of plates using by Frobenius method and the solution has been represented as an infinite series of radial coordinate. Eisenberger and Jabareen (2001) have found the exact axisymmetric vibration frequencies of circular variable thickness plates using the exact element method that allows for the exact solution of problems with general polynomial variation in thickness using infinite power series. They obtained the values for the natural frequencies for linear, parabolic and cubic variations of the plate thickness. Knowledge about the distribution of variable values of mass and stiffness can allow to affect the behavior of structural elements such us circular plates. In the current research we concentrate on the question: to which extent the small radial variation of thickness and/or stiffness parameters may affect the spectrum of transverse vibration of a circular plate and which type of the perturbation function affect greatly on the frequencies of vibrations provided that the average values of the parameters of the inhomogeneous are equal to the values of the parameters of the uniform plate. For example, if the thickness varies, the plate mass is assumed to remain constant. The perturbation method described in Bauer et al (2015) is applied to solve the obtained boundary eigenvalue problem and the results are checked by means of the finite element method. The current resurch continues the study of vibrations of nonuniform circular plates by means of asymptotic methods started in Vasiliev and Smirnov (2020).

20.2 Statement of the Problem

Here we consider free nonaxisymmetric transverse vibrations of a circular thin plate of radius R , variable thickness h and/or Young's modulus E (see Fig. 20.1) The

variable parameters depend only on the radial coordinate r . The other physical parameters are assumed to be constant. Non-dimensional equations of transverse vi-

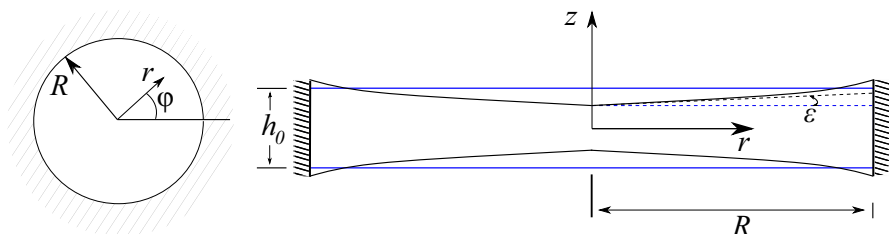


Fig. 20.1 Circular plate with the variable cross-section.

brations based on the Kirchhoff-Love plate model after separation of variables are the following

$$L(w_m(r)) - h(r)\lambda_m^4 w_m(r) = 0, \quad L(w_m(r)) = \sum_{i=0}^4 b_i \frac{d^i}{dr^i} w_m(r). \quad (20.1)$$

Here

$$w(r, \varphi) = \sum_{m=0}^{\infty} w_m(r) \cos(m\varphi)$$

is the deflection, m — the circumferential wave number, λ_m — the eigenvalue. The coefficients of differential operator L are given by formulas

$$b_0 = \frac{m^4 - 4m^2}{r^4} D - \frac{\nu m^2}{r^2} D'' + \frac{3m^2}{r^3} D', \quad b_2 = -\frac{2m^2 + 1}{r^2} D + \frac{2 + \nu}{r} D' + D'',$$

$$b_1 = -\frac{2m^2 + 1}{r^2} D' + \frac{2m^2 + 1}{r^3} D + \frac{\nu}{r} D'', \quad b_3 = \frac{2}{r} D + 2D', \quad b_4 = D.$$

Here $D = D(r)$ — the cylindrical stiffness, ν — Poisson ratio and the relations between dimensional and non-dimensional (with $(\tilde{\cdot})$) values are the following

$$D(r) = D_0 \tilde{D}(\tilde{r}), \quad h(r) = h_0 \tilde{h}(\tilde{r}), \quad E(r) = E_0 \tilde{E}(\tilde{r}), \quad w(r) = R w(\tilde{r}),$$

$$r = R \tilde{r}, \quad \lambda^4 = \frac{12(1 - \nu^2) R^4 \omega^2 \rho}{E_0 h_0^2}, \quad D_0 = \frac{E_0 h_0^3}{12(1 - \nu^2)}, \quad 0 \leq \tilde{r} \leq 1,$$

where D_0, h_0, E_0 are unperturbed bending stiffness, thickness and Young's modulus respectively and ω is the free frequency. Below the sign $(\tilde{\cdot})$ and subscript $(\dots)_m$ are omitted. For the plate with constant parameters $D(r) = 1$ and $h(r) = 1$.

20.3 Boundary Eigenvalue Problem

To study the effect of small variability of the plate thickness and stiffness on the spectrum of free vibrations we apply the perturbation method. Assume the shell parameters in the form

$$h(r) = 1 + \sum_{i=1}^{\infty} \varepsilon^i h_i(r), \quad E(r) = 1 + \sum_{i=1}^{\infty} \varepsilon^i E_i(r),$$

and seek of solution and eigenvalue as

$$\lambda(r) = \sum_{i=0}^{\infty} \varepsilon^i \lambda_i(r), \quad w(r) = \sum_{i=0}^{\infty} \varepsilon^i w_i(r), \quad (20.2)$$

Substituting (20.2) in (20.1) we get the system of equations:

$$\begin{aligned} \varepsilon^0 : \Delta^2 w_0(r) - \lambda_0^4 w_0(r) &= 0, \\ \varepsilon^1 : \Delta^2 w_1(r) - \lambda_0^4 w_1(r) &= F_{11}(\lambda_0, w_0(r)) + F_{12}(\lambda_0, w_0(r)) \cdot \lambda_1, \\ \varepsilon^2 : \Delta^2 w_2(r) - \lambda_0^4 w_2(r) &= F_{21}(\lambda_0, w_0(r), \lambda_1, w_1(r)) + F_{22}(\lambda_0, w_0(r), \lambda_1, w_1(r)) \cdot \lambda_2, \\ \varepsilon^3 : & \dots, \end{aligned} \quad (20.3)$$

which together with the boundary conditions provide the series of boundary value problems. Later we consider only homogeneous boundary conditions of two types: clamped edge and free supported edge. The solvability conditions for system (20.3) is the orthogonality of the right sides of equations to solution $w_0(r)$ (Bauer et al, 2015), i.e.

$$\int_0^1 (F_{i1}(\lambda_j, w_j(r)) + F_{i2}(\lambda_j, w_j(r)) \cdot \lambda_i) w_0(r) r dr = 0, \quad j = 0, \dots, i-1; \quad i = 1, 2, \dots, \quad (20.4)$$

where the scalar product of functions $f(r)$ and $g(r)$ is defined as

$$(f(r) \cdot g(r)) = \int_0^1 f(r)g(r)rdr.$$

As a result we get the formulas for the eigenvalues corrections λ_i

$$\lambda_i = -\frac{I_{i1}}{I_{i2}}, \quad I_{ik} = \int_0^1 F_{ik} w_0(r) r dr, \quad k = 1, 2 \quad i = 1, 2, \dots \quad (20.5)$$

Here we show only the structure of operators F_{1k} and F_{1k} in (20.4)

$$\begin{aligned} F_{11} &= ((3H_1 + E_1) \cdot R_1 + CH_{01}) \cdot W_0^T, & F_{12} &= F_{12} = 4\lambda_0^3 w_0(r), \\ F_{21} &= ((3H_2 + E_2) \cdot R_1 + B_1 + (H_1 \cdot (3R_1, R_2, R_3)))^T \cdot E_1^T + \end{aligned}$$

$$+ \sum_{i=1}^5 H_1 \cdot A_i \cdot H_1^T + CH_{11}) \cdot W_0^T + ((3H_1 + E_1) \cdot R_1 + B_2 + CH_{01}) \cdot W_1^T,$$

where H_k, E_k — are vectors of the length 3, CH_{11}, CH_{01}, B_k — are vectors of the length 5, R_i — 3×5 matrices and A_i — 3×3 matrices. Vectors W_k of the length 5 contain the derivatives $d^l w_k / dr^l$ for $l = 0, \dots, 4$. The terms containing letters H and E depend on the thickness and stiffness variations correspondingly. The explicit formulas for vectors and matrices are included in the Appendix. The sequence of the moves to find the solution $w(r)$ is the following. For given boundary conditions we find the unperturbed solution $w_0(r)$ and eigenvalue λ_0 . Then find λ_1 from formula (20.5) and solution of the equation of the first approximation $w_1(r)$ and so on. Only freely supported plates are considered below in examples. As it was shown in Vasiliev and Smirnov (2020) there is no big qualitative difference between thickness or stiffness variation effect for plates with different boundary conditions.

20.4 Results

We are interested in which extent free frequencies of the plate can be controlled by a small perturbation of its parameter, provided that the average value of the parameter remains constant.

20.4.1 Plate with the Variable Thickness

Consider the plate with variable thickness $h(r)$. We assume that the thickness varies monotonously according the linear, quadratic or exponential laws

1. $h_l = h(r) = 1 + \varepsilon(1 + ar)$,
2. $h_q = h(r) = 1 + \varepsilon(1 + ar^2)$,
3. $h_e = h(r) = 1 + \varepsilon(1 + a(\exp(r) - 1))$.

If the plate mass is fixed, then the values of a must satisfy the condition

$$\int_0^1 h(r)rdr = \int_0^1 rdr = 1/2,$$

from which we get

1. $h_l = h(r) = 1 + \varepsilon(1 - 3/2r)$,
2. $h_q = h(r) = 1 + \varepsilon(1 - 2r^2)$,
3. $h_e = h(r) = 1 + \varepsilon(2 - \exp(r))$. Note that in all cases $h(0) = 1 + \varepsilon$.

Firstly, we calculate the first terms in the asymptotic expansion for three lower frequencies $\lambda_1^{(m,n)}$, due to Eq. (20.5). The results are listed in Table 20.1. In Fig. 20.2 the dependence of the lower frequencies on small parameter ε is plotted. The dotted

Table 20.1 Values of the first correction for different types of the thickness variation.

| (m,n) | Linear | Quadratic | Exponential |
|---------|---------|-----------|-------------|
| (0,0) | 0.1956 | 0.3087 | 0.2402 |
| (1,0) | 0.1437 | 0.3087 | 0.2156 |
| (2,0) | 0.1038 | 0.1839 | 0.1395 |
| (0,1) | 0.4779 | 0.7805 | 0.6034 |
| (3,0) | -0.0495 | -0.0227 | -0.0349 |

line are the values calculated numerically with the COMSOL Multiphysics 5.4, the straight solid lines are two term approximations due to (20.3). For small values of $|\varepsilon|$ the straight lines corresponding to two term approximations practically coincide with the curves obtained numerically, the quadratic variation provides slightly larger change of frequencies compared to the other variations in consideration. The thickness variation greatly effect the axisymmetric frequencies, $\lambda^{(0,n)}$, whereas the effect on non-axisymmetric frequencies $\lambda^{(m,n)}$ ($m > 0$) is insignificant and it decreases as wave numbers increase. All frequencies monotonously decrease for large $|\varepsilon|$, except the fundamental frequency for negative ε .

20.4.2 Plate with the Variable Stiffness

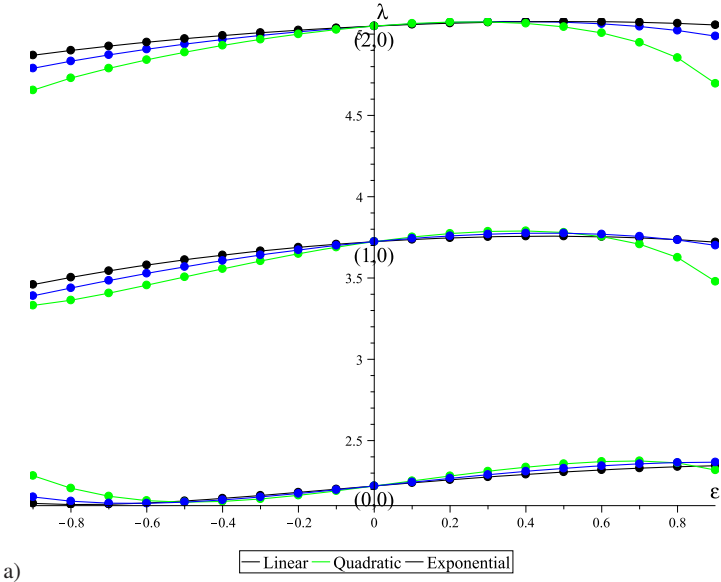
Finally consider the plate with variable Young’s modulus $E(r)$. We assume that Young’s modulus varies monotonously according the linear, quadratic or exponential laws, and its average value is fixed. These assumptions yield

1. $E_l = E(r) = 1 + \varepsilon(1 - 3/2r)$,
2. $E_q = E(r) = 1 + \varepsilon(1 - 2r^2)$,
3. $E_e = E(r) = 1 + \varepsilon(2 - \exp(r))$.

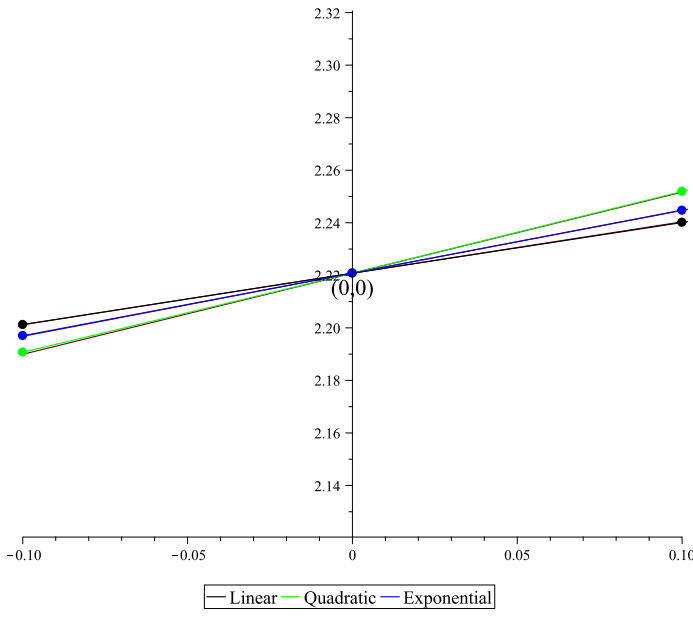
Firstly, we calculate the first terms in the asymptotic expansions for the lower frequencies, $\lambda_1^{(m,n)}$, due to Eq. (20.5). The results are listed in Table 20.2. In Fig. 20.3 the dependence of the lower frequencies on small parameter ε is plotted. The dotted

Table 20.2 Values of the first correction for different types of the thickness variation.

| (m,n) | Linear | Quadratic | Exponential |
|---------|---------|-----------|-------------|
| (0,0) | 0.1300 | 0.2041 | 0.1592 |
| (1,0) | 0.0982 | 0.2041 | 0.1423 |
| (2,0) | 0.0597 | 0.1331 | 0.0919 |
| (0,1) | 0.2870 | 0.4331 | 0.3467 |
| (3,0) | -0.0206 | 0.0251 | 0.0016 |

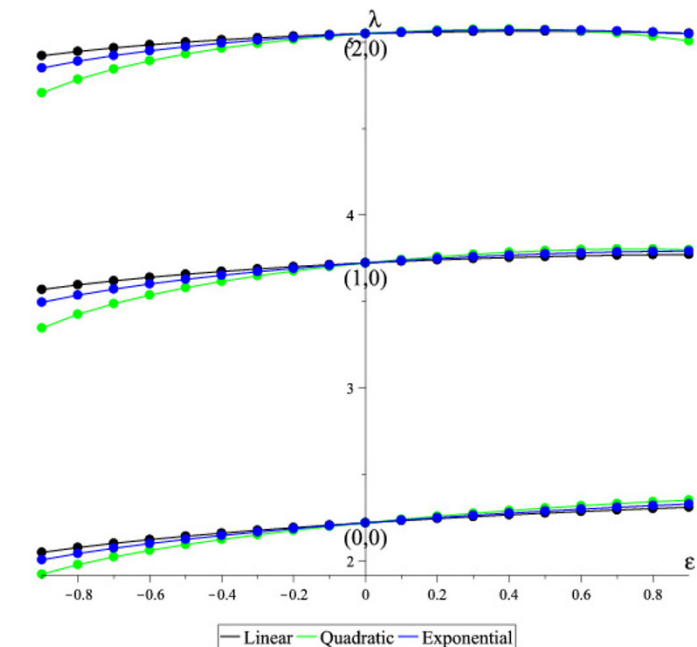


a)

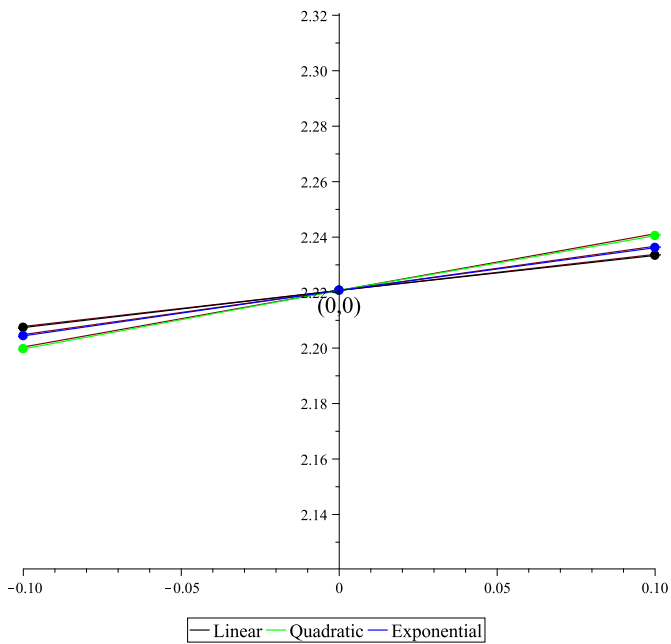


b)

Fig. 20.2 Lower frequencies vs. small parameter ϵ for different thickness variation laws: a) three lower frequencies vs. the thickness perturbation parameter ϵ for different perturbation functions, b) effect of different thickness perturbation functions on the lowest frequency.



a)



b)

Fig. 20.3 Lower frequencies vs. small parameter ϵ for different stiffness variation laws: a) three lower frequencies vs. the stiffness perturbation parameter ϵ for different perturbation functions, b) effect of different stiffness perturbation functions on the lowest frequency.

line are the values calculated numerically with the COMSOL Multiphysics 5.4, the straight solid lines are two term approximations due to (20.5). Similar to the case of thickness variation the axisymmetric frequencies, $\lambda^{(0,n)}$, are the most sensitive to the stiffness variation and the quadratic stiffness variation comparatively is the most significant, especially for negative values of ε .

20.5 Conclusions

For the plates of equal masses (average stiffness) the spectrum of free transverse vibration frequencies may be shifted slightly with small variation of the plate thickness (stiffness). For a wide enough range of values of the variation parameter the frequency change is linear and the corresponding relation may be obtained with the perturbation method.

Acknowledgements The research was supported in parts by the RFBR (grants Nos. 18-01-00832 and 19-01-00208).

References

- Bauer SM, Filippov SB, Smirnov AL, Tovstik PE, Vaillancourt R (2015) *Asymptotic Methods in Mechanics of Solids*. Birkhäuser, Basel
- Chakraverty S, Bhat RB, Stiharu I (1994) Recent research on vibration of structures using boundary characteristic orthogonal polynomials in the rayleigh–ritz method. *The Shock and Vibration Digest* 173(2):157–178
- Conway HD (1958) Some special solutions for the flexural vibrations of discs of varying thickness. *Ingenieur-Archiv* 26(6):408–410
- Eisenberger M, Jabareen M (2001) Axisymmetric vibrations of circular and annular plates with variable thickness. *International Journal of Structural Stability and Dynamics* 1(2):195–206
- Jaroszewicz J (2017) Natural frequencies of axisymmetric vibrations of thin hyperbolic circular plates with clamped edges. *International Journal of Applied Mechanics and Engineering* 22(2):451–457
- Jaroszewicz J, Zoryj L (2006) The method of partial discretization in free vibration problems of circular plates with variable distribution of parameters. *International Applied Mechanics* 42(3):364–373
- Leissa AW (1969) *Vibration of Plates*. US Government Printing Office, Washington
- Prasad C, Jain RK, Soni SR (1972) Axisymmetric vibrations of circular plates of linearly varying thickness. *ZAMP* 23:941–948
- Singh B, Saxena V (1996) Axisymmetric vibration of a circular plate with exponential thickness variation. *Journal of Sound and Vibration* 31(3):187–194
- Vasiliev GP, Smirnov AL (2020) Free vibration frequencies of a circular thin plate with variable parameters. *Vestnik of St Petersburg University: Mathematics* 53(3):351–357
- Wang J (1997) General power series solution of the vibration of classical circular plates with variable thickness. *Journal of Sound and Vibration* 202(4):593–599

Wang X, Yang J, Xiao J (1995) On free vibration analysis of circular annular plates with non-uniform thickness by the differential quadrature method. *Journal of Sound and Vibration* 184(3):547–551

Appendix

$$W_i = \left(\frac{d^k w_i(r)}{dr^k} \right), H_i = \left(\frac{d^j h_i(r)}{dr^j} \right), E_l = \left(\frac{d^l e_l(r)}{dr^l} \right), CH_{il} = (C_i \cdot H_l^T, 0, 0, 0, 0),$$

$$k = 0, \dots, 4; \quad j = 0, 1, 2; \quad i = 0, 1; \quad l = 1, 2,$$

$$C_0 = (\lambda_0^4, 0, 0), C_1 = (4\lambda_0^3\lambda_1, 0, 0), B_1 = (6\lambda_0^2\lambda_1^2, 0, 0, 0, 0), B_2 = (4\lambda_0^3\lambda_1, 0, 0, 0, 0),$$

$$R_1 = \begin{pmatrix} -\frac{m^2(m^2-4)}{r^4} & -\frac{2m^2+1}{r^3} & \frac{2m^2+1}{r^2} & -\frac{2}{r} & -1 \\ -\frac{3m^2}{r^3} & \frac{2m^2+1}{r^2} & -\frac{\nu+2}{r} & -2 & 0 \\ \frac{m^2\nu}{r^2} & -\frac{\nu}{r} & -1 & 0 & 0 \end{pmatrix},$$

$$R_2 = \begin{pmatrix} -\frac{9m^2}{r^3} & \frac{6m^2+3}{r^2} & -\frac{3(\nu+2)}{r} & -6 & 0 \\ \frac{6m^2\nu}{r^2} & -\frac{6\nu}{r} & -6 & 0 & 0 \\ 0 & 0 & 0 & 0 & 0 \end{pmatrix}, R_3 = \begin{pmatrix} \frac{3m^2\nu}{r^2} & -\frac{3\nu}{r} & -3 & 0 & 0 \\ 0 & 0 & 0 & 0 & 0 \\ 0 & 0 & 0 & 0 & 0 \end{pmatrix},$$

$$A_1 = \begin{pmatrix} \frac{3m^2(4-m^2)}{r^4} & -\frac{9m^2}{r^3} & \frac{3m^2\nu}{r^2} \\ -\frac{9m^2}{r^3} & \frac{6m^2r^2\nu}{r^4} & 0 \\ \frac{3m^2\nu}{r^2} & 0 & 0 \end{pmatrix}, A_2 = \begin{pmatrix} -\frac{6m^2}{r^3} - \frac{3}{r^3} & \frac{6m^2}{r^2} + \frac{3}{r^2} & -\frac{3\nu}{r} \\ \frac{6m^2}{r^2} + \frac{3}{r^2} & -\frac{6\nu}{r} & 0 \\ -\frac{3\nu}{r} & 0 & 0 \end{pmatrix},$$

$$A_3 = \begin{pmatrix} \frac{3(2m^2+1)}{r^2} & -\frac{3\nu}{r} - \frac{6}{r} & -3 \\ -\frac{3\nu}{r} - \frac{6}{r} & -6 & 0 \\ -3 & 0 & 0 \end{pmatrix}, A_4 = \begin{pmatrix} -\frac{6}{r} & -6 & 0 \\ -6 & 0 & 0 \\ 0 & 0 & 0 \end{pmatrix}, A_5 = \begin{pmatrix} -3 & 0 & 0 \\ 0 & 0 & 0 \\ 0 & 0 & 0 \end{pmatrix}.$$



Chapter 21

Modeling of an Inhomogeneous Circular Timoshenko Plate with an Elastically Supported Boundary

Alexander O. Vatulyan, Olga A. Potetyunko, and Ivan V. Bogachev

Abstract The deformation of a circular elastic plate of variable stiffness is studied in the present paper. The problem is considered in the framework of Timoshenko's hypotheses with various conditions of support at the boundary, including the presence of elastic bonds. One of the applications of this model is the problem of modeling a lamina cribrosa sclerae (LC) of an eyeball. Timoshenko's hypotheses are used in view of the necessity to take into account in modeling shear deformations of a LC. Elastic constraints in boundary conditions are characterized by two coefficients of subgrade resistance. An energy functional is presented with the use of the variational Lagrange principle for an inhomogeneous plate. It also takes into account the potential energy of bonds at the edge. Deflection of the plate and rotation angle of the normal are found using the Ritz method, which makes it possible to derive a solution based on the energy functional. The influence of the number of coordinate functions on the accuracy of the obtained solution is investigated. A comparison is made with the results obtained earlier in the framework of Kirchhoff's plates.

Key words: Lamina cribrosa, Sclera, Heterogeneity, Elastic binding, Ritz method, Reconstruction

21.1 Introduction

Plates are one of the main structural elements of many engineering structures, such as bridge decks, turbine disks, base plates, tanks, structural elements for diaphragms, measuring systems. In addition, various models of plates are used to solve problems of biomechanics, for example, to optimize orthopedic surgeries of bone osteosynthesis and to model a lamina cribrosa of the sclera in ophthalmology. Over time,

Alexander O. Vatulyan · Olga A. Potetyunko · Ivan V. Bogachev
SFU, Russia, 344006, Rostov-on-Don, Bolshaya Sadovaya str., 105/42
e-mail: vatulyan@aaanet.ru, ol_potet73@mail.ru, bogachev89@yandex.ru

more and more demanding requirements are imposed on the diagnostics of such systems. Currently, non-destructive methods for detecting cracks, determining the shapes and sizes of regions and objects have been developed quite well. Electronic diagnostics of defects in mechanical systems is actively developing. At the same time, the problems of diagnostics of the state of fastenings and loading of objects began to be investigated relatively recently (Akhtyamov, 2006). So, in Vybornov (1985); Uglov et al (2009), the theoretical foundations of low-frequency acoustic control methods are presented, which is one of the most common and most accessible way of monitoring structural elements.

One of the actively developing areas of biomechanics is the biomechanics of the sclera of an human eye (Iomdina et al, 2015). One of its urgent task is to study the causes of glaucoma and diagnose its stage. It has been proven that one of such reasons is the deformation of a lamina cribrosa sclerae (LC) under the influence of intraocular pressure (IOP), as a result of which the nerve fibers passing through a LC are squeezed. The factor of significant inhomogeneity of a LC, weakened by a multitude of holes, which affects its deformation characteristics, must be taken into account when modeling (Bauer and Voronkova, 2014). It is also important to take into account the boundary conditions describing the attachment of a LC to the sclera. This is indicated by Sigal et al (2005), which states that the deformation of a LC largely depends on the elastic modulus and the thickness of the sclera. It was previously shown (Vatulyan and Potetyunko, 2017) that modeling the contact of a LC and a sclera as an elastic fixation characterized by compliance coefficients in the boundary conditions is more accurate with respect to the condition of a rigidly embedded edge.

One of the main hypotheses of the occurrence of glaucoma is the hypothesis of "mechanical damage" of glaucomatous optic neuropathy. It is assumed that IOP-induced deformation of a LC exposes the nerve fiber bundles to increased stresses, which lead to axonal damage (Yan et al, 1998). In addition, with glaucoma and increased IOP, the deflections of a LC are comparable in order. All of the aforementioned makes it relevant to consider geometrically nonlinear models of plates for these problems, which make it possible to take into account shear deformation.

A lot of works by A.S. Volmir, K.F. Chernykh, I.I. Vorovich, S.A. Kabrits, E.I. Grigolyuk and many others are devoted to questions of nonlinear models of shells. For example, Kabrits et al (2002) gives a systematic presentation of the general nonlinear theory of shells and presents modified nonlinear equations of K.F. Chernykh taking into account the "kinematic compression". One of the most common non-classical models is the Timoshenko model (Timoshenko and Woinowsky-Krieger, 1959). Tovstik (2008) compares the Timoshenko-Reissner plate and shell model, taking into account shear, with the classical Kirchhoff-Love model and with the three-dimensional theory of elasticity.

21.2 Statement of the Problem

This paper presents the further development of a study carried out in Vatulyan and Potetyunko (2017) within the framework of Kirchhoff's hypotheses for an axisymmetric inhomogeneous circular plate, to the case of Timoshenko's hypotheses, taking into account the shear deformation characteristic of a LC. As in Vatulyan and Potetyunko (2017), we assume that a uniformly distributed load q acts on a plate of radius R and thickness h . The edge of the plate is elastically supported, which is modeled by two elastic constraints with the coefficients C_1 and C_2 . Within the framework of Timoshenko's hypotheses, in the case under consideration, the components of the displacement vector in a cylindrical coordinate system have the form:

$$u_r = z\theta, \quad u_z = w, \quad (21.1)$$

where w is the plate deflection function, θ is the angle of normal's rotation along the radial coordinate axis.

A variational approach is used to construct a scheme for calculating the deformation of a plate. The Lagrange functional is derived within the framework of this approach and it takes into account the hypotheses (21.1). This functional contains an expression for the potential energy of elastic bonds at the edge; below is its general dimensionless form:

$$F^* = \frac{1}{2} \int_0^1 \left[f(\xi) \left(\theta'^2 + \frac{2\nu}{\xi} \theta \theta' + \frac{\theta^2}{\xi^2} \right) + \gamma g(\xi) (\theta + w')^2 \right] \xi d\xi - \int_0^1 q w \xi d\xi + \frac{g_1}{2} w^2(1) + \frac{g_2}{2} \theta^2(1) \quad (21.2)$$

Here we have introduced the dimensionless parameters and variables by the formulas:

- $\xi = R^{-1} r$ – a dimensionless radial coordinate whose derivative in (21.2) is indicated by a stroke;
- $f(\xi) = D_0^{-1} D$, $g(\xi) = B_0^{-1} B$ – dimensionless plate stiffness functions, where $D = Eh^3/[12(1-\nu^2)]$, $B = Eh/[2(1+\nu)]$, $D_0 = D(0)$, $B_0 = B(0)$;
- $\gamma = D_0^{-1} B_0 = 6(1-\nu)R^2h^{-2}$ – dimensionless parameter;
- $g_1 = D_0^{-1} R^2 C_1$, $g_2 = C_2$ – stiffness parameters of the elastic support;
- $q = q_0(ar)a^{-3}$ – dimensionless parameter characterizing the level of distributed loading; it was assumed to be 1 in the calculations.

Note that if we put $\theta = -w'$, which leads to Kirchhoff's conjectures, then the functional (21.2) takes the form obtained in Vatulyan and Potetyunko (2017).

21.3 Direct Problem Solving Method

From (21.2) by varying functional and equating to zero the coefficients of the independent variations we can obtain the equilibrium equation and boundary conditions. However, in this study, the Ritz method was used to calculate the deflection functions $w(\xi)$ and the angle of normal's rotation $\theta(\xi)$. It allows constructing a solution based on the functional (21.2). Within the framework of the Ritz method, we represent the sought functions in the form:

$$w(\xi) = a_1\phi_{11} + \sum_{k=2}^N a_k\phi_{1k}, \quad \theta(\xi) = \sum_{k=1}^N b_k\phi_{2k}, \quad (21.3)$$

where a_k and b_k are coefficients and ϕ_{jk} are basis functions satisfying homogeneous boundary conditions:

$$\phi_{11} = 1, \quad \phi_{1k} = \sin\left(\frac{\pi}{2}\xi k\right), \quad \phi_{2k} = \sin(\pi\xi k), \quad k = 1..N. \quad (21.4)$$

Substituting the expressions (21.3) into the functional (21.2) and finding its stationary value from the conditions

$$\frac{\partial F^*}{\partial a_j} = 0, \quad \frac{\partial F^*}{\partial b_j} = 0, \quad j = 1..N, \quad (21.5)$$

we obtain a system of linear algebraic equations for the unknown expansion coefficients a_k and b_k . Its matrix has a block form:

$$\begin{vmatrix} \mathbf{A}_1 & \mathbf{A}_2 \\ \mathbf{A}_3 & \mathbf{A}_4 \end{vmatrix} \cdot \begin{vmatrix} \mathbf{X}_1 \\ \mathbf{X}_2 \end{vmatrix} = \begin{vmatrix} \mathbf{F}_1 \\ \mathbf{F}_2 \end{vmatrix}, \quad (21.6)$$

where $\mathbf{X}_1 = (a_1, a_2, \dots, a_N)$, $\mathbf{X}_2 = (b_1, b_2, \dots, b_N)$, $\mathbf{F}_1 = (f_1, f_2, \dots, f_N)$, $\mathbf{F}_2 = (0, 0, \dots, 0)$. The sought functions $w(\xi)$ and $\theta(\xi)$ are determined from the solution of the system (21.6), according to (21.3).

21.4 Computational Experiments

A series of computational experiments was carried out for various laws of plate inhomogeneity and embedding parameters. The program was written using Maple package and tested on the problem of bending a plate with constant stiffness in the static case, which has an exact analytical solution (Timoshenko and Woinowsky-Krieger, 1959). Tables 21.1 – 21.2 demonstrate the change in the coefficients of the expression (21.3) for the deflection w and the angle of rotation θ depending on the number of coordinate functions for a homogeneous plate at $g_1 = g_2 = 10^4$, which simulates a rigid restraint. A decrease in the coefficients with an increase in the

Table 21.1 Deflection coefficients w at $f(\xi) = 1$.

| w | $N = 3$ | $N = 4$ | $N = 5$ |
|-------|---------|---------------------|---------------------|
| a_1 | 0.0200 | 0.0200 | 0.0200 |
| a_2 | 0.0356 | 0.0356 | 0.0356 |
| a_3 | 0.0156 | 0.0156 | 0.0156 |
| a_4 | | $-5 \cdot 10^{-17}$ | $-4 \cdot 10^{-15}$ |
| a_5 | | | $2 \cdot 10^{-15}$ |

Table 21.2 Coefficients for the angle of rotation θ at $f(\xi) = 1$.

| θ | $N = 3$ | $N = 4$ | $N = 5$ |
|----------|---------------------|---------------------|-----------------------|
| b_1 | 0.0625 | 0.0625 | 0.0625 |
| b_2 | -0.0625 | -0.0625 | -0.0625 |
| b_3 | $-2 \cdot 10^{-16}$ | $-3 \cdot 10^{-16}$ | $1.1 \cdot 10^{-13}$ |
| b_4 | | $-4 \cdot 10^{-18}$ | $-1.3 \cdot 10^{-12}$ |
| b_5 | | | $5 \cdot 10^{-14}$ |

number of functions is observed, which indicates the convergence of the method.

Tables 21.3 – 21.4 show the coefficients of the expression (21.3) for the deflection w and the angle of rotation θ depending on the number of coordinate functions for an inhomogeneous plate at $g_1 = g_2 = 10^4$ and the law of distribution of stiffness, most typical for a LC, i.e. $f(\xi) = e^{-\xi}$. Here, one can see a decrease in the coefficients with an increase in the number of functions, which indicates the convergence of the method.

Table 21.5 shows the deflection w and the angle of rotation θ for an inhomogeneous plate with the stiffness distribution law $f(\xi) = e^{-\xi}$ for 7 coordinate functions depending on the radius plates ξ and for different values of the coefficients of elastic sealing g_1, g_2 : $g_1 = g_2 = 10^4$ and $g_1 = g_2 = 10^6$, which can simulate rigid sealing, $g_1 = g_2 = 10^2$, which is closer to the loose edge, $g_1 = 10^5, g_2 = 10$ can sim-

Table 21.3 Deflection coefficients for w at $f(\xi) = e^{-\xi}$.

| w | $N = 3$ | $N = 4$ | $N = 5$ | $N = 6$ | $N = 7$ |
|-------|---------|---------|---------|---------|---------|
| a_1 | 0.0067 | 0.0210 | 0.0352 | 0.0371 | 0.0372 |
| a_2 | 0.0027 | -0.0160 | -0.0361 | -0.0406 | -0.0424 |
| a_3 | 0.0066 | 0.0209 | 0.0411 | 0.0472 | 0.0521 |
| a_4 | | -0.0076 | -0.0196 | -0.0261 | -0.0326 |
| a_5 | | | 0.0058 | 0.0101 | 0.0159 |
| a_6 | | | | -0.0019 | -0.0052 |
| a_7 | | | | | 0.0011 |

Table 21.4 Coefficients of the angle of rotation θ for $f(\xi) = e^{-\xi}$.

| θ | $N = 3$ | $N = 4$ | $N = 5$ | $N = 6$ | $N = 7$ |
|----------|---------|---------|---------|---------|---------|
| b_1 | 0.0154 | 0.0253 | 0.0419 | 0.0431 | 0.0434 |
| b_2 | -0.0151 | -0.0165 | -0.0105 | -0.0107 | -0.0105 |
| b_3 | -0.0017 | 0.0032 | 0.0031 | 0.0026 | 0.0028 |
| b_4 | | -0.0003 | -0.0023 | -0.0015 | -0.0014 |
| b_5 | | | 0.0006 | 0.0008 | 0.0006 |
| b_6 | | | | -0.0004 | -0.0003 |
| b_7 | | | | | 0.0003 |

Table 21.5 Deflection and angle of rotation at different points of the plate, depending on the parameters of the embedding.

| ξ | $g_1 = g_2 = 10^2$ | | $g_1 = g_2 = 10^6$ | | $g_1 = g_2 = 10^4$ | | $g_1 = 10^5, g_2 = 10$ | | $g_1 = 10^2, g_2 = 10^5$ | |
|-------|--------------------|----------|--------------------|----------|--------------------|----------|------------------------|----------|--------------------------|----------|
| | w | θ | w | θ | w | θ | w | θ | w | θ |
| 0 | 0.0353 | 0 | 0.0298 | 0 | 0.0298 | 0 | 0.0343 | 0 | 0.0348 | 0 |
| 0.25 | 0.0325 | 0.0081 | 0.0270 | 0.0067 | 0.0271 | 0.0068 | 0.0313 | 0.0078 | 0.0320 | 0.0080 |
| 0.5 | 0.0241 | 0.0121 | 0.0187 | 0.0094 | 0.0188 | 0.0094 | 0.0223 | 0.0111 | 0.0237 | 0.0119 |
| 0.75 | 0.0125 | 0.0094 | 0.0073 | 0.0055 | 0.0074 | 0.0055 | 0.0095 | 0.0071 | 0.0123 | 0.0092 |
| 0.95 | 0.0056 | 0.0053 | 0.0005 | 0.0005 | 0.0006 | 0.0006 | 0.0010 | 0.0010 | 0.0055 | 0.0053 |

ulate hinged support along the contour. In addition, the choice of the parameters $g_1 = 10^2, g_2 = 10^5$ simulates a floating termination, however, due to the small influence of the coefficient g_2 , the results obtained will be qualitatively close to a rigid termination. In Figs. 21.1 – 21.2 table data 21.5 is shown. If we estimate the influ-

Fig. 21.1 Dependence of the deflection on the radius of the plate at different values of the embedding parameters. $N = 7, f(\xi) = e^{-\xi}$.

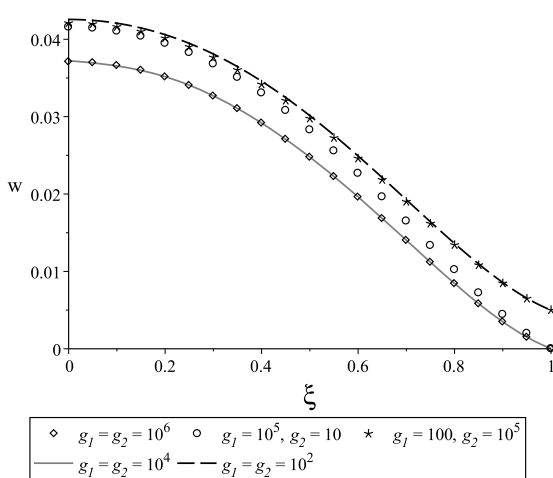
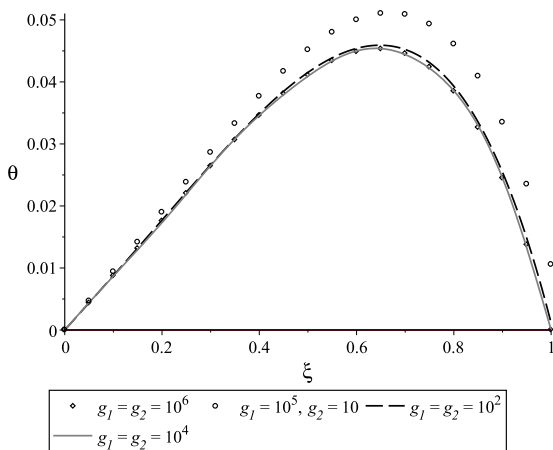


Fig. 21.2 Dependence of the angle of rotation on the radius of the plate for different values of the embedding parameters. $N = 7, f(\xi) = e^{-\xi}$.



ence of the parameters g_1 and g_2 on the deformability of the plate, it turns out that the influence of g_1 is much more significant than g_2 . Table 21.6 shows the deflection w and the angle of rotation θ for an inhomogeneous plate with elastic sealing coefficients $g_1 = g_2 = 10^4$ at 7 coordinate functions depending on the radius of the plate ξ and for different distribution laws of stiffness $f(\xi)$. Figure 21.3 graphically shows the deflection values w from Table 21.5. Figures 21.4 - 21.7 compare the deflection w for plates in the framework of the Timoshenko and Kirchhoff hypotheses. Kirchhoff's hypotheses can be obtained from Timoshenko's hypotheses, as shown above, if we put $\theta = -w'$ in the functional (21.2). Figures 21.4 - 21.5 present w for homogeneous ($f(\xi) = 1$) and inhomogeneous ($f(\xi) = e^{-\xi}$) plates, respectively, within the framework of the Timoshenko and Kirchhoff hypotheses at different coefficients of elastic sealing g_1, g_2 . Figures 21.6 - 21.7 compare w for homogeneous

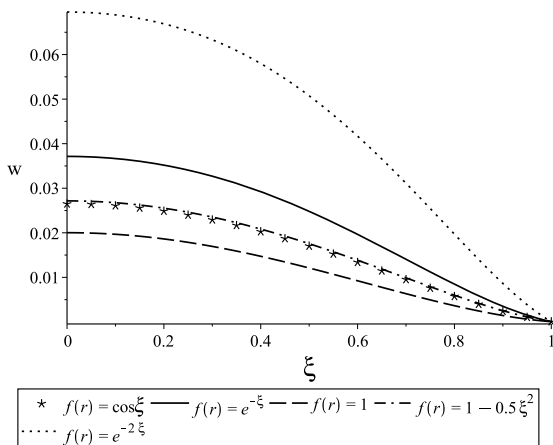


Fig. 21.3 Comparison of plate deflection shapes for different laws of stiffness distribution. $N = 7, g_1 = g_2 = 10^{-4}$.

Table 21.6 Deflection and angle of rotation at different points of the plate depending on the distribution law of stiffness.

| ξ | $f(\xi) = 1$ | | $f(\xi) = 1 - 0.5\xi^2$ | | $f(\xi) = e^{-\xi}$ | | $f(\xi) = \cos(\xi)$ | | $f(\xi) = e^{-2\xi}$ | |
|-------|--------------|----------|-------------------------|----------|---------------------|----------|----------------------|----------|----------------------|----------|
| | w | θ | w | θ | w | θ | w | θ | w | θ |
| 0 | 0.0259 | 0 | 0.0221 | 0 | 0.0298 | 0 | 0.0216 | 0 | 0.0542 | 0 |
| 0.25 | 0.0228 | 0.0057 | 0.0198 | 0.0049 | 0.0271 | 0.0068 | 0.0193 | 0.0048 | 0.0503 | 0.0126 |
| 0.5 | 0.0148 | 0.0074 | 0.0135 | 0.0067 | 0.0188 | 0.0094 | 0.0131 | 0.0065 | 0.0373 | 0.0186 |
| 0.75 | 0.0053 | 0.0039 | 0.0053 | 0.0039 | 0.0074 | 0.0055 | 0.0050 | 0.0038 | 0.0161 | 0.0120 |
| 0.95 | 0.0004 | 0.0004 | 0.0004 | 0.0004 | 0.0006 | 0.0006 | 0.0004 | 0.0004 | 0.0014 | 0.0013 |

Fig. 21.4 Comparison of the deflection w within the hypotheses of Timoshenko and Kirchhoff. $f(\xi) = 1$.

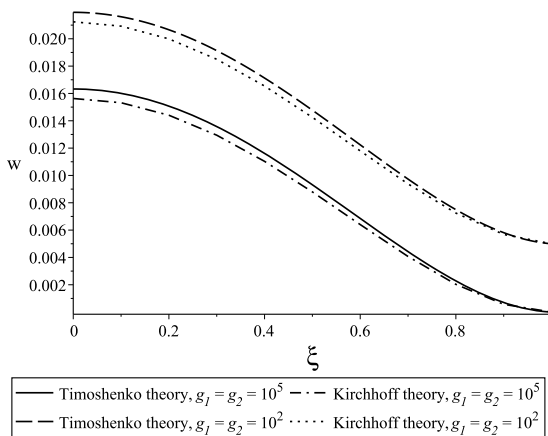


Fig. 21.5 Comparison of the deflection w within the hypotheses of Timoshenko and Kirchhoff. $f(\xi) = e^{-\xi}$.

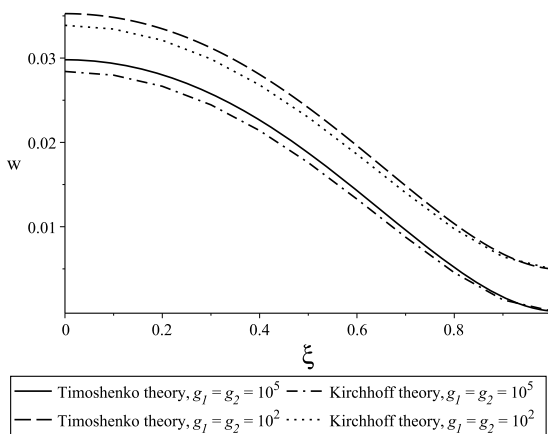


Fig. 21.6 Comparison of the deflection w within the hypotheses of Timoshenko and Kirchhoff. $h = 2.5 \cdot 10^{-4}$, $r = 10^{-3}$, $f(\xi) = 1$.

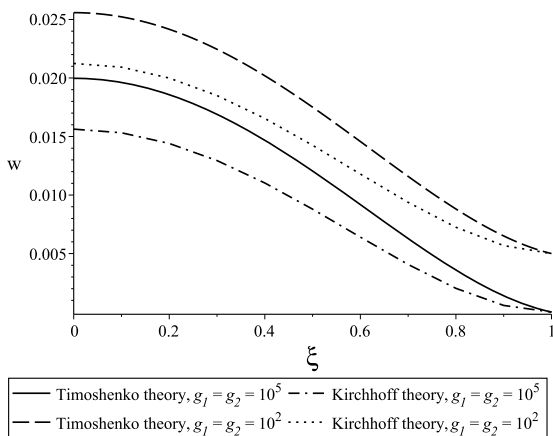
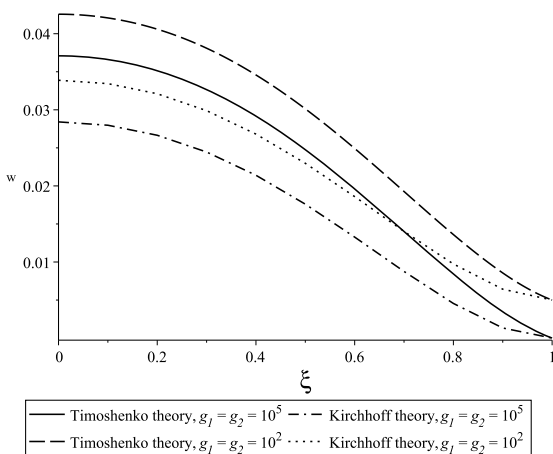


Fig. 21.7 Comparison of the deflection w within the hypotheses of Timoshenko and Kirchhoff, $f(\xi) = e^{-\xi}$.



($f(\xi) = 1$) and inhomogeneous ($f(\xi) = e^{-\xi}$) plates of thickness $h = 2.5 \cdot 10^{-4}$ and radius $\xi = 10^{-3}$ within the framework of the Timoshenko and Kirchhoff hypotheses at different coefficients of elastic sealing g_1, g_2 . Note that such parameters of thickness and radius correspond to the real physiological dimensions of a LC.

21.5 Conclusion

On the basis of the proposed approach, the problems of calculating the deflection for various laws of plate inhomogeneity were solved within the framework of Timoshenko's hypotheses and the values of the material parameters of an elastic support. Calculations have shown that to ensure the required accuracy, it is enough to take 6-8 coordinate functions. It is also shown that the greatest deflection values

are achieved with a decreasing exponential law of modulus change. The results of calculating the deflection function are compared with ones obtained earlier in the framework of Kirchhoff's hypotheses, in particular, with the solution in the case of a rigid sealing. It is shown that in the case of thin plates, the deflection functions differ insignificantly (less than 1%), and in the case of thick plates, the difference is more significant (more than 5%), which corresponds to the results obtained by Tovstik (2008).

Acknowledgements The reported study was funded by RFBR, project number 20-31-90066.

References

- Akhtyamov AM (2006) Identification of the boundary conditions of a rectangular membrane from its natural frequencies (in Russ.). *Akusticheskiy zhurnal* 52(3):293–296
- Bauer SM, Voronkova EB (2014) Models of shells and plates in the problems of ophthalmology. *Vestnik St Petersburg University: Mathematics* Vestnik St Petersburg University: Mathematics 47(3):123–139
- Iomdina EN, Bauer SM, Kotlyar KE (2015) Biomechanics of the human: theoretical aspects and clinical applications (in Russ.). Real Time, Moscow
- Kabrits SA, Mikhailovsky EI, Tovstik PE, Chernykh KF, Shamina VA (2002) General nonlinear theory of elastic shells (in Russ.). St. Petersburg University Publishing House, St. Petersburg
- Sigal IA, Flanagan JG, Ethier CR (2005) Factors Influencing Optic Nerve Head Biomechanics. *Investigative Ophthalmology & Visual Science* 46(11):4189–4199, DOI 10.1167/iovs.05-0541
- Timoshenko SP, Woinowsky-Krieger S (1959) *Theory of Plates and Shells*. McGraw-Hill, New York
- Tovstik PE (2008) Non-classical models of beams, plates and shells (in Russ.). *Izvestiya Saratov University Series Mathematics, Mechanics, Computer science* 8(3):72–85
- Uglov AL, Erofeev VI, Smirnov AN (2009) Acoustic control of equipment during manufacture and operation (in Russ.). Nauka, Moscow
- Vatulyan AO, Potetyunko OA (2017) On the assessment of deformability of the ethmoid plate of the eye (in Russ.). *Russian Journal of Biomechanics* 21(1):8–16
- Vybornov BI (1985) Ultrasonic flaw detection (in Russ.). Metallurgy, Moscow
- Yan D, Flanagan J, Flanagan J, Farra T, Trope G, Ethier C (1998) Study of regional deformation of the optic nerve head using scanning laser tomography. *Current Eye Research* 17(9):903–916



Chapter 22

Effect of Distributed Dislocations on Large Deformations of Cylindrical Tube made of Micropolar Elastic Material

Leonid M. Zubov and Evgeniya V. Goloveshkina

Abstract The generalized Lamé problem for an elastic hollow circular cylinder at large deformations is considered. The cylinder is made of micropolar material and contains continuously distributed dislocations. The dislocation density tensor contains four nonzero components and describes the distribution of both screw and edge dislocations. Under the assumption that the material is isotropic, the problem is reduced to a system of nonlinear ordinary differential equations. For a special material model and an axisymmetric distribution of edge dislocations, an exact solution in an explicit analytical form is found.

Key words: Nonlinear elasticity, Micropolar medium, Hollow circular cylinder, Screw and edge dislocations, Exact solution

22.1 Introduction

The most common mathematical model of elastic bodies is the model of a simple material (Truesdell and Noll, 1965), for which deformation of a medium is described as a smooth mapping of one region of three-dimensional Euclidean space to another. Within the framework of the simple material model, each particle of the body has three degrees of freedom, i.e. is considered as a material point. The desire to take into account a microstructure in a structure of deformable bodies led to the creation of mathematical models of generalized media. One of these models is the micropolar medium or the Cosserat continuum. This theory finds application in describing the properties of composites, nanostructured materials, geophysical media, metamaterials, liquid crystals, magnetic materials, tissues of living organisms, etc.

Leonid M. Zubov · Evgeniya V. Goloveshkina
Institute of Mathematics, Mechanics, and Computer Science of Southern Federal University,
Milchakova Str. 8a, Rostov-on-Don, 344090, Russian Federation,
e-mail: zubovl@yandex.ru, evgeniya.goloveshkina@yandex.ru

The Cosserat continuum is a material body, each particle of which has six degrees of freedom of an absolutely rigid body, and besides the particle rotation field is kinematically independent of the displacement field. The contact interaction of parts of a micropolar body is carried out not only by ordinary (force) stresses, but also by moment stresses. For this reason, the theory of elasticity of a micropolar medium is often called the moment theory of elasticity.

A large number of publications are devoted to the linear moment theory of elasticity, of which we note Aero and Kuvshinskij (1961); Pal'mov (1964); Nowacki (1986); Eringen (1999). The nonlinear theory of micropolar elasticity is presented in Toupin (1964); Shkutin (1988); Zubov (1997); Nikitin and Zubov (1998) and Pietraszkiewicz and Eremeyev (2009). Experimental methods for identifying material parameters of micropolar media are discussed in Lakes (1995).

A two-dimensional analogue of the Cosserat continuum is one of the variants of the theory of elastic shells (Altenbach et al, 2010; Chróscielewski et al, 2004; Eremeyev and Zubov, 2008; Libai and Simmonds, 1998; Zhilin, 1976). Note that the theory of elastic shells is an important part of the scientific activity of prof. P.E. Tovstik (see, for example, Tovstik, 1997; Tovstik et al, 2002).

In this paper, we consider nonlinear deformations of an elastic hollow cylinder made of a micropolar material, loaded with external and internal pressures, taking into account distributed dislocations. The linear theory of continuously distributed dislocations and disclinations for micropolar media was developed in De Wit (1977); Zelenina and Zubov (2017); Zubov (2017), and the nonlinear theory in Zubov (2004, 2011). The nonlinear spherically symmetric problem of the theory of dislocations for a micropolar elastic medium is solved in Zubov (2020).

22.2 Input Relations

The system of equilibrium equations for a micropolar nonlinear elastic medium consists of Toupin (1964); Shkutin (1988); Zubov (1997); Nikitin and Zubov (1998) the balance equations for forces and moments

$$\operatorname{div} \mathbf{D} + \rho \mathbf{f} = 0, \quad (22.1)$$

$$\operatorname{div} \mathbf{G} + \left(\mathbf{C}^T \cdot \mathbf{D} \right)_x + \rho \mathbf{l} = 0, \quad (22.2)$$

constitutive equations

$$\begin{aligned} \mathbf{D} &= \mathbf{P} \cdot \mathbf{H}, \quad \mathbf{G} = \mathbf{K} \cdot \mathbf{H}, \\ \mathbf{P} &= \frac{\partial W}{\partial \mathbf{E}}, \quad \mathbf{K} = \frac{\partial W}{\partial \mathbf{L}}, \quad W = W(\mathbf{E}, \mathbf{L}), \end{aligned} \quad (22.3)$$

and geometric relations

$$\mathbf{E} = \mathbf{C} \cdot \mathbf{H}^T, \tag{22.4}$$

$$\mathbf{L} = \frac{1}{2} \mathbf{r}^n \otimes \left(\frac{\partial \mathbf{H}}{\partial q^n} \cdot \mathbf{H}^T \right)_{\times} = \frac{1}{2} \mathbf{I} \text{tr} \left[\mathbf{H} \cdot (\text{curl } \mathbf{H})^T \right] - \mathbf{H} \cdot (\text{curl } \mathbf{H})^T, \tag{22.5}$$

$$\mathbf{C} = \text{grad } \mathbf{R}(\mathbf{r}). \tag{22.6}$$

Here \mathbf{D} and \mathbf{G} are the stress and couple stress tensors of the first Piola–Kirchhoff type, respectively, while \mathbf{P} and \mathbf{K} are these of the second Piola–Kirchhoff type, \mathbf{C} is the deformation gradient, \mathbf{H} is the proper orthogonal tensor describing the rotational degree of freedom of micropolar continua called often the microrotation tensor (Zubov, 1997; Nikitin and Zubov, 1998; Pietraszkiewicz and Eremeyev, 2009), \mathbf{E} and \mathbf{L} are the strain tensors in the nonlinear micropolar continuum called stretch and wryness tensors, respectively (Zubov, 1997; Nikitin and Zubov, 1998; Pietraszkiewicz and Eremeyev, 2009), \mathbf{I} is the unit tensor, ρ is the material density in the reference configuration, \mathbf{f} is the external distributed mass force, \mathbf{l} is the external distributed mass moment, W is the strain energy density, $\mathbf{r} = x_s \mathbf{i}_s$, $\mathbf{R} = X_k \mathbf{i}_k$, x_s , and X_k are the position vectors and the Cartesian coordinates in the reference and actual configurations, respectively, \mathbf{i}_k are the corresponding constant base vectors, $k, s = 1, 2, 3$. The gradient, curl, and divergence operators in curvilinear coordinates of the reference configuration $q^n = q^n(x_1, x_2, x_3)$, $n = 1, 2, 3$, are expressed by the formulas

$$\text{grad } \Phi = \mathbf{r}^n \otimes \frac{\partial \Phi}{\partial q^n}, \quad \text{curl } \Phi = \mathbf{r}^n \times \frac{\partial \Phi}{\partial q^n}, \quad \text{div } \Phi = \mathbf{r}^n \cdot \frac{\partial \Phi}{\partial q^n}, \quad \mathbf{r}^n = \mathbf{i}_k \frac{\partial q^n}{\partial x_k}, \tag{22.7}$$

where Φ is an arbitrary differentiable tensor field of any order. The symbol \mathbf{T}_{\times} denotes the vector invariant of the second rank tensor $\mathbf{T} = t_{mn} \mathbf{r}^m \otimes \mathbf{r}^n$:

$$\mathbf{T}_{\times} = t_{mn} \mathbf{r}^m \times \mathbf{r}^n.$$

The property of isotropy of a micropolar medium imposes the following restrictions on the dependences of the specific energy, stresses, and moment stresses on the strain tensors \mathbf{E} and \mathbf{L} (Nikitin and Zubov, 1998)

$$\begin{aligned} W(\mathbf{S}^T \cdot \mathbf{E} \cdot \mathbf{S}, (\det \mathbf{S}) \mathbf{S}^T \cdot \mathbf{L} \cdot \mathbf{S}) &= W(\mathbf{E}, \mathbf{L}), \\ \mathbf{P}(\mathbf{S}^T \cdot \mathbf{E} \cdot \mathbf{S}, (\det \mathbf{S}) \mathbf{S}^T \cdot \mathbf{L} \cdot \mathbf{S}) &= \mathbf{S}^T \cdot \mathbf{P}(\mathbf{E}, \mathbf{L}) \cdot \mathbf{S}, \\ \mathbf{K}(\mathbf{S}^T \cdot \mathbf{E} \cdot \mathbf{S}, (\det \mathbf{S}) \mathbf{S}^T \cdot \mathbf{L} \cdot \mathbf{S}) &= (\det \mathbf{S}) \mathbf{S}^T \cdot \mathbf{K}(\mathbf{E}, \mathbf{L}) \cdot \mathbf{S}. \end{aligned} \tag{22.8}$$

In (22.8), \mathbf{S} denotes an arbitrary orthogonal tensor and it is taken into account that the tensors \mathbf{E} and \mathbf{P} are true tensors of the second rank, and \mathbf{L} and \mathbf{K} are pseudotensors of the second rank.

If dislocations with tensor density α are distributed in the body, then the vector field $\mathbf{R}(\mathbf{r})$ does not exist, the tensor \mathbf{C} is called the distortion tensor, and the equality (22.6) is replaced by the incompatibility equation (Zubov, 2004, 2011)

$$\text{curl } \mathbf{C} = \alpha, \tag{22.9}$$

in which the tensor α must satisfy the solenoidality condition

$$\operatorname{div} \alpha = 0. \quad (22.10)$$

The complete system of equilibrium equations for a micropolar elastic body with distributed dislocations contains, as unknown functions, the tensor fields of distortion \mathbf{C} and microrotation \mathbf{H} and consists of the balance equations for forces and moments (22.1) and (22.2), the incompatibility equation (22.9), the constitutive equations (22.3), and the geometric relations (22.4) and (22.5).

22.3 Cylindrical Tube with Distributed Dislocations

Introduce in the reference configuration of the micropolar medium the cylindrical coordinates r , φ , and z associated with the Cartesian coordinates by the relations $x_1 = r \cos \varphi$, $x_2 = r \sin \varphi$, and $x_3 = z$. Consider an elastic body in the form of a hollow circular cylinder with an external radius r_0 , an internal radius r_1 , and an axis parallel to the vector \mathbf{i}_3 . As a vector basis, we will use the unit vectors \mathbf{e}_r , \mathbf{e}_φ , and \mathbf{i}_3 that are directed tangentially to the coordinate lines. The following formulas hold:

$$\mathbf{e}_r = \mathbf{i}_1 \cos \varphi + \mathbf{i}_2 \sin \varphi, \quad \mathbf{e}_\varphi = -\mathbf{i}_1 \sin \varphi + \mathbf{i}_2 \cos \varphi.$$

Let us assume that the dislocation density tensor is given in the following form:

$$\alpha = \alpha_{11}(r)\mathbf{e}_r \otimes \mathbf{e}_r + \alpha_{22}(r)\mathbf{e}_\varphi \otimes \mathbf{e}_\varphi + \alpha_{32}(r)\mathbf{i}_3 \otimes \mathbf{e}_\varphi + \alpha_{33}(r)\mathbf{i}_3 \otimes \mathbf{i}_3. \quad (22.11)$$

The functions $\alpha_{11}(r)$, $\alpha_{22}(r)$, and $\alpha_{33}(r)$ are the scalar densities of screw dislocations in the radial, azimuthal, and axial directions, respectively, and the function $\alpha_{32}(r)$ is the scalar density of edge dislocations. The solenoidality requirement (22.10) applied to (22.11) leads to one equation

$$\alpha_{22} = \frac{d}{dr}(r\alpha_{11}). \quad (22.12)$$

It follows from (22.12) that the solenoidality condition for the dislocation density tensor does not impose any restrictions on the functions $\alpha_{32}(r)$ and $\alpha_{33}(r)$ that can be arbitrary, including the Dirac delta function.

We will seek the tensor fields of distortion and microrotation in the following form:

$$\mathbf{C} = C_{11}(r)\mathbf{e}_r \otimes \mathbf{e}_r + C_{22}(r)\mathbf{e}_\varphi \otimes \mathbf{e}_\varphi + C_{23}(r)\mathbf{e}_\varphi \otimes \mathbf{i}_3 + C_{32}(r)\mathbf{i}_3 \otimes \mathbf{e}_\varphi + \lambda \mathbf{i}_3 \otimes \mathbf{i}_3, \quad (22.13)$$

$$\mathbf{H} = \mathbf{e}_r \otimes \mathbf{e}_r + (\mathbf{e}_\varphi \otimes \mathbf{e}_\varphi + \mathbf{i}_3 \otimes \mathbf{i}_3) \cos \chi(r) + (\mathbf{e}_\varphi \otimes \mathbf{i}_3 - \mathbf{i}_3 \otimes \mathbf{e}_\varphi) \sin \chi(r), \quad (22.14)$$

where λ is a real value. The geometric interpretation of the expression (22.14) is that the particles of the cylinder rotate around the vector \mathbf{e}_r at the angle $\chi(r)$ upon deformation.

Due to (22.11) and (22.13), the tensor incompatibility equation (22.9) is reduced to the system of ordinary differential equations

$$C_{32} = -r\alpha_{11}, \quad \frac{\Delta C_{32}}{\Delta r} = -\alpha_{22}, \quad (22.15)$$

$$\frac{\Delta}{\Delta r}(rC_{23}) = r\alpha_{33}, \quad (22.16)$$

$$\frac{\Delta C_{22}}{\Delta r} + \frac{C_{22} - C_{11}}{r} = \alpha_{32}. \quad (22.17)$$

The first equation in (22.15) defines the distortion component C_{32} . The second equation in (22.15) should be discarded, since it follows from the first one and the solenoidality condition (22.12). Integrating Eq. (22.16), we find the distortion component C_{23} :

$$C_{23}(r) = \frac{1}{r} \int_{r_1}^r \alpha_{33}(r') \Delta r' + \frac{b}{2\pi r}. \quad (22.18)$$

Here b is the length of the Burgers vector of an isolated screw dislocation which can be contained in a hollow cylinder (Zubov, 1997). The function $C_{11}(r)$ is expressed in terms of $C_{22}(r)$ using (22.17):

$$C_{11} = \frac{\Delta}{\Delta r}(rC_{22}) - r\alpha_{32}. \quad (22.19)$$

Thus, after fulfilling the incompatibility equations, only the distortion component C_{22} remains an unknown function. Another unknown function is the microrotation angle $\chi(r)$. To find the functions $C_{22}(r)$ and $\chi(r)$, one should refer to the equilibrium equations (22.1), (22.2). To compose the expressions of the stresses \mathbf{D} and \mathbf{G} , we first compute the tensors \mathbf{E} and \mathbf{L} of strains arising in a cylindrical tube. Based on (22.4), (22.5), (22.13), (22.14), and (22.15), we get

$$\begin{aligned} \mathbf{E} = & C_{11} \mathbf{e}_r \otimes \mathbf{e}_r + (C_{22} \cos \chi + C_{23} \sin \chi) \mathbf{e}_\varphi \otimes \mathbf{e}_\varphi + (C_{23} \cos \chi - C_{22} \sin \chi) \mathbf{e}_\varphi \otimes \mathbf{i}_3 \\ & + (\lambda \sin \chi - r\alpha_{11} \cos \chi) \mathbf{i}_3 \otimes \mathbf{e}_\varphi + (r\alpha_{11} \sin \chi + \lambda \cos \chi) \mathbf{i}_3 \otimes \mathbf{i}_3, \end{aligned} \quad (22.20)$$

$$\mathbf{L} = \frac{\Delta \chi}{\Delta r} \mathbf{e}_r \otimes \mathbf{e}_r + \frac{\sin \chi}{r} \mathbf{e}_\varphi \otimes \mathbf{e}_\varphi + \frac{\cos \chi - 1}{r} \mathbf{e}_\varphi \otimes \mathbf{i}_3. \quad (22.21)$$

Considering the micropolar material of the cylinder isotropic, we assume

$$\mathbf{S} = \mathbf{S}_1 = 2\mathbf{e}_r \otimes \mathbf{e}_r - \mathbf{I}, \quad \det \mathbf{S}_1 = 1$$

in the relations (22.8). From (22.20) and (22.21), the equalities follow:

$$\mathbf{S}_1^T \cdot \mathbf{E} \cdot \mathbf{S}_1 = \mathbf{E}, \quad \mathbf{S}_1^T \cdot \mathbf{L} \cdot \mathbf{S}_1 = \mathbf{L},$$

whence we have

$$\mathbf{P} \cdot \mathbf{S}_1 = \mathbf{S}_1 \cdot \mathbf{P}, \quad \mathbf{K} \cdot \mathbf{S}_1 = \mathbf{S}_1 \cdot \mathbf{K}. \quad (22.22)$$

A consequence of the relations (22.22) is the equalities

$$\begin{aligned} \mathbf{e}_r \cdot \mathbf{P} \cdot \mathbf{e}_\varphi = 0, \quad \mathbf{e}_r \cdot \mathbf{P} \cdot \mathbf{i}_3 = 0, \quad \mathbf{e}_\varphi \cdot \mathbf{P} \cdot \mathbf{e}_r = 0, \quad \mathbf{i}_3 \cdot \mathbf{P} \cdot \mathbf{e}_r = 0, \\ \mathbf{e}_r \cdot \mathbf{K} \cdot \mathbf{e}_\varphi = 0, \quad \mathbf{e}_r \cdot \mathbf{K} \cdot \mathbf{i}_3 = 0, \quad \mathbf{e}_\varphi \cdot \mathbf{K} \cdot \mathbf{e}_r = 0, \quad \mathbf{i}_3 \cdot \mathbf{K} \cdot \mathbf{e}_r = 0. \end{aligned} \quad (22.23)$$

The equalities (22.23) mean that the stress tensors \mathbf{P} and \mathbf{K} in the basis of cylindrical coordinates have the following expansions:

$$\begin{aligned} \mathbf{P} &= P_{11} \mathbf{e}_r \otimes \mathbf{e}_r + P_{22} \mathbf{e}_\varphi \otimes \mathbf{e}_\varphi + P_{23} \mathbf{e}_\varphi \otimes \mathbf{i}_3 + P_{32} \mathbf{i}_3 \otimes \mathbf{e}_\varphi + P_{33} \mathbf{i}_3 \otimes \mathbf{i}_3, \\ \mathbf{K} &= K_{11} \mathbf{e}_r \otimes \mathbf{e}_r + K_{22} \mathbf{e}_\varphi \otimes \mathbf{e}_\varphi + K_{23} \mathbf{e}_\varphi \otimes \mathbf{i}_3 + K_{32} \mathbf{i}_3 \otimes \mathbf{e}_\varphi + K_{33} \mathbf{i}_3 \otimes \mathbf{i}_3. \end{aligned} \quad (22.24)$$

Because the energy density W is an isotropic function of the tensor arguments \mathbf{E} and \mathbf{L} , it can be represented as a function of a certain number of polynomial invariants of these tensors (Zubov and Karyakin, 2006; Eremeyev et al, 2018). Since these invariants are fully expressed through the components of the tensors \mathbf{E} and \mathbf{L} in the orthonormal basis \mathbf{e}_r , \mathbf{e}_φ , and \mathbf{i}_3 , by virtue of (22.13), (22.14), (22.20), and (22.21) they will be functions only of the coordinate r . Hence, based on (22.3), we conclude that for a homogeneous medium the components of the stress tensors \mathbf{P} and \mathbf{K} in (22.24) do not depend on the coordinates φ and z . Using the formulas (22.3), (22.13), (22.14), and (22.24), we get

$$\mathbf{D} = D_{11}(r) \mathbf{e}_r \otimes \mathbf{e}_r + D_{22}(r) \mathbf{e}_\varphi \otimes \mathbf{e}_\varphi + D_{23}(r) \mathbf{e}_\varphi \otimes \mathbf{i}_3 + D_{32}(r) \mathbf{i}_3 \otimes \mathbf{e}_\varphi + D_{33}(r) \mathbf{i}_3 \otimes \mathbf{i}_3, \quad (22.25)$$

$$\mathbf{G} = G_{11}(r) \mathbf{e}_r \otimes \mathbf{e}_r + G_{22}(r) \mathbf{e}_\varphi \otimes \mathbf{e}_\varphi + G_{23}(r) \mathbf{e}_\varphi \otimes \mathbf{i}_3 + G_{32}(r) \mathbf{i}_3 \otimes \mathbf{e}_\varphi + G_{33}(r) \mathbf{i}_3 \otimes \mathbf{i}_3, \quad (22.26)$$

$$\begin{aligned} D_{11} = P_{11}, \quad D_{22} = P_{22} \cos \chi - P_{23} \sin \chi, \quad D_{23} = P_{23} \cos \chi + P_{22} \sin \chi, \\ D_{32} = P_{32} \cos \chi - P_{33} \sin \chi, \quad D_{33} = P_{32} \sin \chi + P_{33} \cos \chi, \end{aligned} \quad (22.27)$$

$$\begin{aligned} G_{11} = K_{11}, \quad G_{22} = K_{22} \cos \chi - K_{23} \sin \chi, \quad G_{23} = K_{23} \cos \chi + K_{22} \sin \chi, \\ G_{32} = K_{32} \cos \chi - K_{33} \sin \chi, \quad G_{33} = K_{32} \sin \chi + K_{33} \cos \chi. \end{aligned} \quad (22.28)$$

Thus, for any isotropic micropolar material, it has been proved that for deformation of a circular cylinder, given by the relations (22.13) and (22.14) the Piola-type stress and moment stress tensors have the same zero components as the distortion tensor. The nonzero components of the stress tensors depend only on the radial coordinate.

Based on (22.13), (22.15), (22.25), and (22.26), we have

$$\begin{aligned} \operatorname{div} \mathbf{D} &= \left(\frac{\Delta D_{11}}{\Delta r} + \frac{D_{11} - D_{22}}{r} \right) \mathbf{e}_r, \\ \operatorname{div} \mathbf{G} &= \left(\frac{\Delta G_{11}}{\Delta r} + \frac{G_{11} - G_{22}}{r} \right) \mathbf{e}_r, \end{aligned} \quad (22.29)$$

$$(\mathbf{C}^T \cdot \mathbf{D})_{\mathbf{x}} = (C_{22} D_{23} - C_{23} D_{22} - r \alpha_{11} D_{33} - \lambda D_{32}) \mathbf{e}_r. \quad (22.30)$$

Suppose that the mass force and moment loads are given as $\mathbf{f} = f(r)\mathbf{e}_r$, $\mathbf{l} = l(r)\mathbf{e}_r$. Then, according to (22.29) and (22.30), the vector equilibrium equations (22.1) and (22.2) are reduced to two scalar equations

$$\frac{\Delta D_{11}}{\Delta r} + \frac{D_{11} - D_{22}}{r} + \rho f = 0, \quad (22.31)$$

$$\frac{\Delta G_{11}}{\Delta r} + \frac{G_{11} - G_{22}}{r} + C_{22}D_{23} - C_{23}D_{22} - r\alpha_{11}D_{33} - \lambda D_{32} + \rho l = 0. \quad (22.32)$$

We assume that the cylindrical tube is subjected to external hydrostatic pressure p_0 and internal pressure p_1 . In addition, uniformly distributed tracking moment loads m_0 and m_1 can be applied to the cylindrical surfaces. The vectors of these moments have the direction of the normal vector to the surface of the deformed body. Then the boundary conditions for the system of equations (22.31) and (22.32) will be as follows

$$\begin{aligned} D_{11}(r_0) &= -p_0 [\lambda C_{22}(r_0) + r_0 \alpha_{11}(r_0) C_{23}(r_0)], \\ G_{11}(r_0) &= m_0 [\lambda C_{22}(r_0) + r_0 \alpha_{11}(r_0) C_{23}(r_0)], \end{aligned} \quad (22.33)$$

$$\begin{aligned} D_{11}(r_1) &= -p_1 [\lambda C_{22}(r_1) + r_1 \alpha_{11}(r_1) C_{23}(r_1)], \\ G_{11}(r_1) &= m_1 [\lambda C_{22}(r_1) + r_1 \alpha_{11}(r_1) C_{23}(r_1)]. \end{aligned} \quad (22.34)$$

The constant λ can be determined by specifying the resulting longitudinal force

$$Q = 2\pi \int_{r_1}^{r_0} D_{33}(r)r \Delta r$$

applied to the ends of the tube.

So, the problem of large deformations of a cylindrical tube with distributed dislocations of the form (22.11) is reduced to a nonlinear boundary value problem (22.31)–(22.34) for a system of two ordinary differential equations. The unknown functions in this problem are $C_{22}(r)$ and $\chi(r)$.

22.4 Distribution of Straight Edge Dislocations

Consider equilibrium of a cylindrical tube in the case when $\alpha_{11} = \alpha_{22} = \alpha_{33} = 0$, $b = 0$. The dislocation density tensor now has the form $\alpha = \alpha_{32}(r)\mathbf{i}_3 \otimes \mathbf{e}_\varphi$ and describes the distribution of edge dislocations whose axes are parallel to the cylinder axis \mathbf{i}_3 . The scalar dislocation density $\alpha_{32}(r)$ is an arbitrary function. From (22.15) and (22.18) it follows that the distortion tensor will be as follows:

$$\mathbf{C} = C_{11}(r)\mathbf{e}_r \otimes \mathbf{e}_r + C_{22}(r)\mathbf{e}_\varphi \otimes \mathbf{e}_\varphi + \lambda \mathbf{i}_3 \otimes \mathbf{i}_3. \quad (22.35)$$

As will be shown below, in this case the moment equilibrium equation (22.32) will be satisfied for $l = 0$ for any isotropic material if the function $\chi(r)$ is chosen such that $\sin\chi(r) \equiv 0$. Then $\cos\chi(r) = \eta$, $\eta = \pm 1$.

Based on (22.14), (22.20), (22.21), and (22.35), for $\sin\chi(r) \equiv 0$, we have

$$\begin{aligned}\mathbf{H} &= \mathbf{e}_r \otimes \mathbf{e}_r + \eta(\mathbf{e}_\varphi \otimes \mathbf{e}_\varphi + \mathbf{i}_3 \otimes \mathbf{i}_3), \\ \mathbf{E} &= C_{11}\mathbf{e}_r \otimes \mathbf{e}_r + \eta C_{22}(r)\mathbf{e}_\varphi \otimes \mathbf{e}_\varphi + \eta \lambda \mathbf{i}_3 \otimes \mathbf{i}_3, \\ \mathbf{L} &= \frac{\eta - 1}{r} \mathbf{e}_\varphi \otimes \mathbf{i}_3.\end{aligned}\tag{22.36}$$

Assume in the isotropy condition (22.8) $\mathbf{S} = \mathbf{S}_2 = \mathbf{I} - 2\mathbf{e}_\varphi \otimes \mathbf{e}_\varphi$. From (22.36) the equalities follow:

$$\mathbf{S}_2^T \cdot \mathbf{E} \cdot \mathbf{S}_2 = \mathbf{E}, \quad \mathbf{S}_2^T \cdot \mathbf{L} \cdot \mathbf{S}_2 = -\mathbf{L}.\tag{22.37}$$

Since $\det \mathbf{S}_2 = -1$, from (22.8) and (22.37) we have

$$\mathbf{P} \cdot \mathbf{S}_2 = \mathbf{S}_2 \cdot \mathbf{P}, \quad \mathbf{K} \cdot \mathbf{S}_2 = -\mathbf{S}_2 \cdot \mathbf{K}.\tag{22.38}$$

The first equality of (22.38) gives $\mathbf{e}_\varphi \otimes \mathbf{e}_\varphi \cdot \mathbf{P} = \mathbf{P} \cdot \mathbf{e}_\varphi \otimes \mathbf{e}_\varphi$. Multiplying the last relation on the left by \mathbf{e}_φ and on the right by \mathbf{i}_3 we get $\mathbf{e}_\varphi \cdot \mathbf{P} \cdot \mathbf{i}_3 = 0$, and multiplying on the left by \mathbf{i}_3 and on the right by \mathbf{e}_φ we get $\mathbf{i}_3 \cdot \mathbf{P} \cdot \mathbf{e}_\varphi = 0$. Therefore, in (22.26), $P_{23} = P_{32} = 0$, and the Piola stress tensor \mathbf{D} due to (22.27) takes the form

$$\mathbf{D} = D_{11}(r)\mathbf{e}_r \otimes \mathbf{e}_r + D_{22}(r)\mathbf{e}_\varphi \otimes \mathbf{e}_\varphi + D_{33}(r)\mathbf{i}_3 \otimes \mathbf{i}_3.\tag{22.39}$$

Multiplying the second equality of (22.38) on the left and right by the vector \mathbf{e}_φ we get $K_{22} = 0$. Setting in (22.8) $\mathbf{S} = \mathbf{S}_3 = \mathbf{I} - 2\mathbf{i}_3 \otimes \mathbf{i}_3$, $\det \mathbf{S}_3 = -1$, in a similar way we prove that $K_{33} = 0$.

The pseudoscalar quantity $\Gamma = \text{tr} \mathbf{K} = K_{11} + K_{22} + K_{33}$ in an isotropic body is an isotropic function of the tensors \mathbf{E} and \mathbf{L} , that is, it obeys the requirement

$$\Gamma(\mathbf{S}^T \cdot \mathbf{E} \cdot \mathbf{S}, (\det \mathbf{S})\mathbf{S}^T \cdot \mathbf{L} \cdot \mathbf{S}) = (\det \mathbf{S})\Gamma(\mathbf{E}, \mathbf{L}).\tag{22.40}$$

Setting $\mathbf{S} = \mathbf{S}_2$ in (22.40) we get $\Gamma(\mathbf{E}, \mathbf{L}) = -\Gamma(\mathbf{E}, \mathbf{L})$, i. e. $\Gamma = 0$. Therefore, $K_{11} = 0$, and by virtue of (22.28) we have

$$\mathbf{G} = G_{23}(r)\mathbf{e}_\varphi \otimes \mathbf{i}_3 + G_{32}(r)\mathbf{i}_3 \otimes \mathbf{e}_\varphi.\tag{22.41}$$

Thus, for any isotropic elastic micropolar material, it is proved that if in a cylinder the distortion tensor \mathbf{C} and the microrotation tensor \mathbf{H} have the form (22.35) and (22.36), then the tensor stress and moment stress fields are described by the relations (22.39) and (22.41).

From (22.35), (22.39), and (22.41), it follows that for $l = 0$ the moment equilibrium equation (22.32) is satisfied identically, and the force equilibrium equation (22.31), taking into account (22.19), serves to determine the function $C_{22}(r)$. According to (22.33), (22.34), and (22.41), to implement this solution in which

$\sin\chi(r) \equiv 0$, it is not required to apply a moment load to the tube surfaces $r = r_0$ and $r = r_1$.

22.5 Exact Solution

As a specific model of an elastic material, we take an isotropic physically linear micropolar continuum (Pal'mov, 1964; Zubov, 1997). This model is given by the quadratic function of the specific strain energy

$$2W = \frac{2\mu\nu}{1-2\nu} \text{tr}^2(\mathbf{E} - \mathbf{I}) + (\mu + \tau) \text{tr}[(\mathbf{E} - \mathbf{I}) \cdot (\mathbf{E}^T - \mathbf{I})] \\ + (\mu - \tau) \text{tr}(\mathbf{E} - \mathbf{I})^2 + \gamma_1 \text{tr}^2 \mathbf{L} + \gamma_2 \text{tr}(\mathbf{L} \cdot \mathbf{L}^T) + \gamma_3 \text{tr} \mathbf{L}^2,$$

where μ , ν , τ , γ_1 , γ_2 , and γ_3 are material constants.

The stress and moment stress tensors \mathbf{P} and \mathbf{K} for the given material are linear functions of the strain tensors $(\mathbf{E} - \mathbf{I})$ and \mathbf{L} :

$$\mathbf{P} = \frac{2\mu\nu}{1-2\nu} \mathbf{I} \text{tr}(\mathbf{E} - \mathbf{I}) + (\mu + \tau)(\mathbf{E} - \mathbf{I}) + (\mu - \tau)(\mathbf{E}^T - \mathbf{I}), \quad (22.42)$$

$$\mathbf{K} = \gamma_1 \mathbf{I} \text{tr} \mathbf{L} + \gamma_2 \mathbf{L} + \gamma_3 \mathbf{L}^T. \quad (22.43)$$

For $\mathbf{E} = \mathbf{E}^T$, the constitutive equation (22.42) coincides with Hooke's law for an isotropic material with shear modulus μ and Poisson's ratio ν .

In the equilibrium problem for a tube with straight edge dislocations, based on (22.3), (22.35), (22.36), (22.42), and (22.43), we obtain the following formulas for the stress components in the expressions (22.39) and (22.41):

$$D_{11} = \frac{2\mu}{1-2\nu} [(1-\nu)C_{11} + \eta\nu(C_{22} + \lambda) - 1 - \nu], \\ D_{22} = \frac{2\mu}{1-2\nu} [\eta\nu C_{11} + (1-\nu)C_{22} + \nu\lambda - (1+\nu)\eta], \quad (22.44) \\ D_{33} = \frac{2\mu}{1-2\nu} [\eta\nu C_{11} + \nu C_{22} + (1-\nu)\lambda - (1+\nu)\eta], \\ G_{23} = \frac{2(1-\eta)}{r} \gamma_2, \quad G_{32} = \frac{2(1-\eta)}{r} \gamma_3.$$

Using (22.44) we express the distortion components through the stresses D_{11} and D_{22} :

$$C_{11} = \frac{1-\nu}{2\mu} D_{11} - \frac{\eta\nu}{2\mu} D_{22} + 1 + \nu - \eta\nu\lambda, \\ C_{22} = -\frac{\eta\nu}{2\mu} D_{11} + \frac{1-\nu}{2\mu} D_{22} + (1+\nu)\eta - \nu\lambda. \quad (22.45)$$

Let us express the stress D_{22} in terms of D_{11} using the equilibrium equation (22.31) and assuming that the mass forces are absent:

$$D_{22} = \frac{\Delta}{\Delta r}(rD_{11}). \quad (22.46)$$

Substituting the relations (22.45) into the incompatibility equation (22.19) and taking into account (22.46) we arrive at a differential equation for the function $D_{11}(r)$:

$$r^2 \frac{\Delta^2 D_{11}}{\Delta r^2} + 3r \frac{\Delta D_{11}}{\Delta r} = \frac{2\mu}{1-\nu} [(1+\nu+\nu\lambda)(1-\eta) + r\alpha_{32}(r)]. \quad (22.47)$$

The solution to the equation (22.47) has the form

$$D_{11}(r) = \frac{1}{2} \int_{r_1}^r \rho h(\rho) \Delta \rho - \frac{1}{2r^2} \int_{r_1}^r \rho^3 h(\rho) \Delta \rho + A + \frac{B}{r^2}, \quad (22.48)$$

where A and B are constants, and $h(r)$ denotes the right-hand side of the equation (22.47)

$$h(r) = \frac{2\mu}{1-\nu} [(1+\nu+\nu\lambda)(1-\eta) + r\alpha_{32}(r)].$$

The constants A and B are found from the boundary conditions (22.33), (22.34) that are linear. In (22.33) and (22.34) one should set $\alpha_{11} = 0$, and the value C_{22} should be expressed in terms of D_{11} using (22.45) and (22.46).

In general, the value η is not necessarily considered to be constant. It can be a discontinuous piecewise constant function taking the value 1 on some segments of the region $r_1 \leq r \leq r_0$ and the value (-1) on other segments. If $\alpha_{32}(r) = \alpha_0 r^{-1}$ and $\eta = \text{const}$, then the function $h(r)$ will be constant, which we denote by h_0 . Then the solution to the equation (22.47) is written as

$$D_{11} = A + \frac{B}{r^2} + \frac{1}{2} h_0 \ln \frac{r}{r_0}.$$

For the cylinder $r_0 = 1$, $r_1 = 0.9$ with the scalar dislocation density $\alpha_{32} = \beta_0 r^\kappa$ (we take $\beta_0 = 1$) in the case $\eta = 1$, $\nu = 0.3$, $\mu = 1$ the eigenstresses and the distortions are shown in Figs. 22.1–22.3 and Figs. 22.4 and 22.5, respectively. The case $\eta = -1$ corresponds to the eigenstresses in Figs. 22.6 and 22.7. Figures 22.8 and 22.9 show the dependence of the longitudinal force Q on the parameter λ for $\eta = 1$ and $\eta = -1$. The dependence is the same for different κ .

In the case of the scalar density $\alpha_{32} = \alpha_0 r^{-1}$, for different values of α_0 , the stresses and the distortions are presented in Figs. 22.10–22.12 and Figs. 22.13 and 22.14, respectively.

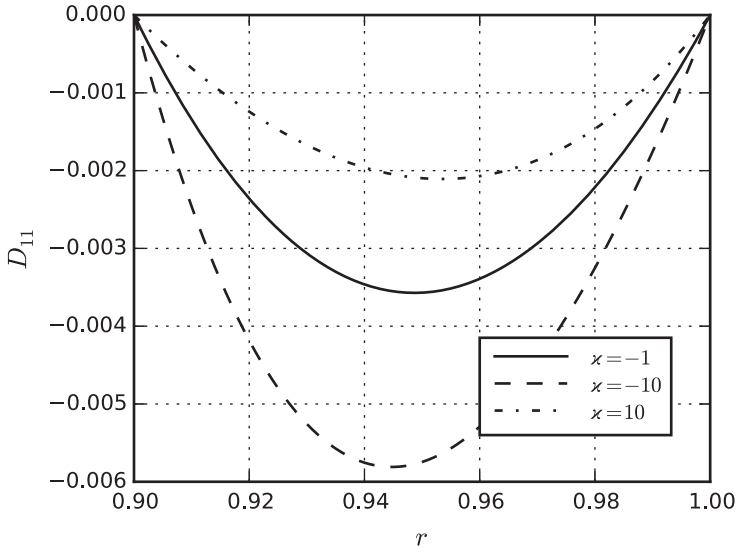


Fig. 22.1 Eigenstress D_{11} , $\eta = 1$, $\lambda = 1$.

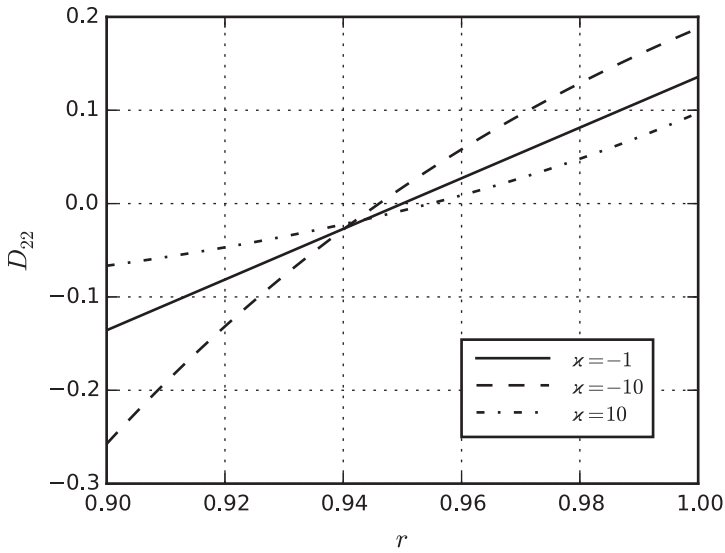


Fig. 22.2 Eigenstress D_{22} , $\eta = 1$, $\lambda = 1$.

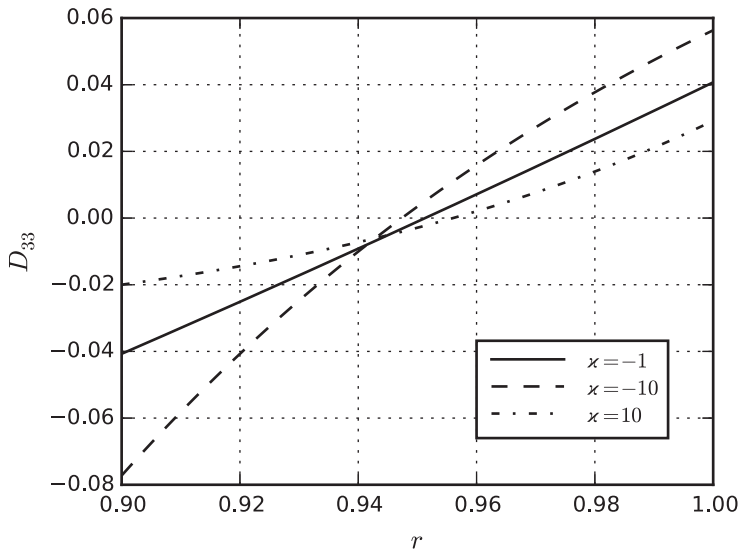


Fig. 22.3 Eigenstress D_{33} , $\eta = 1$, $\lambda = 1$.

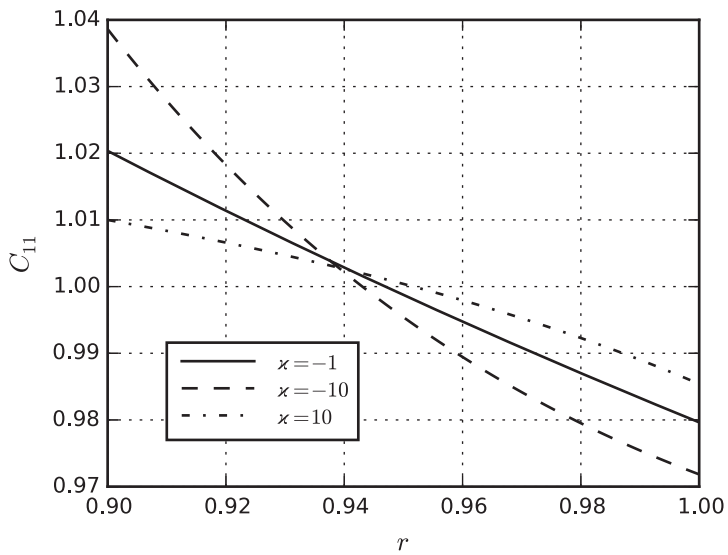


Fig. 22.4 Distortion C_{11} , $\eta = 1$, $\lambda = 1$.

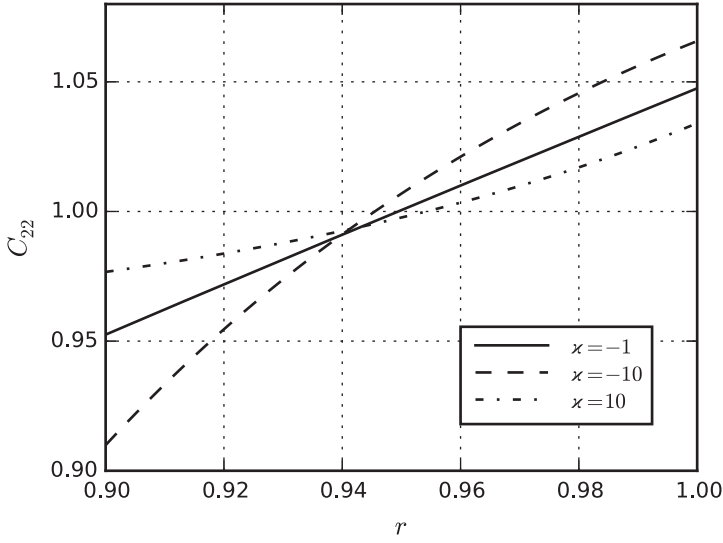


Fig. 22.5 Distortion C_{22} , $\eta = 1$, $\lambda = 1$.

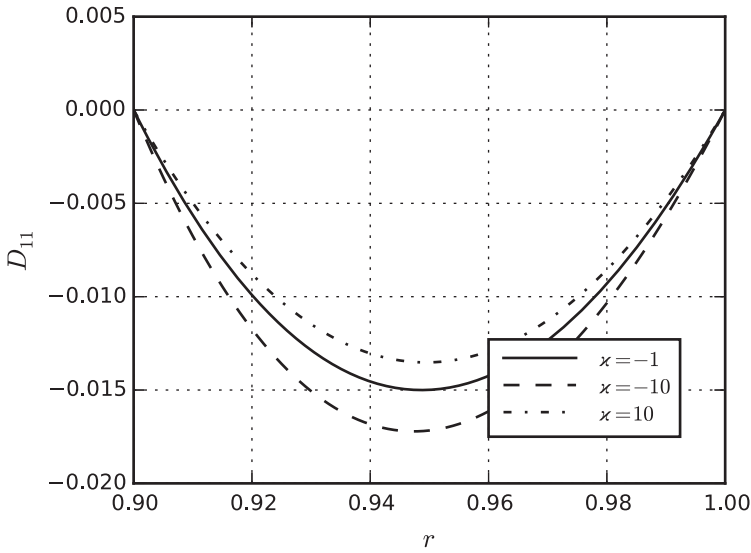


Fig. 22.6 Eigenstress D_{11} , $\eta = -1$, $\lambda = 1$.

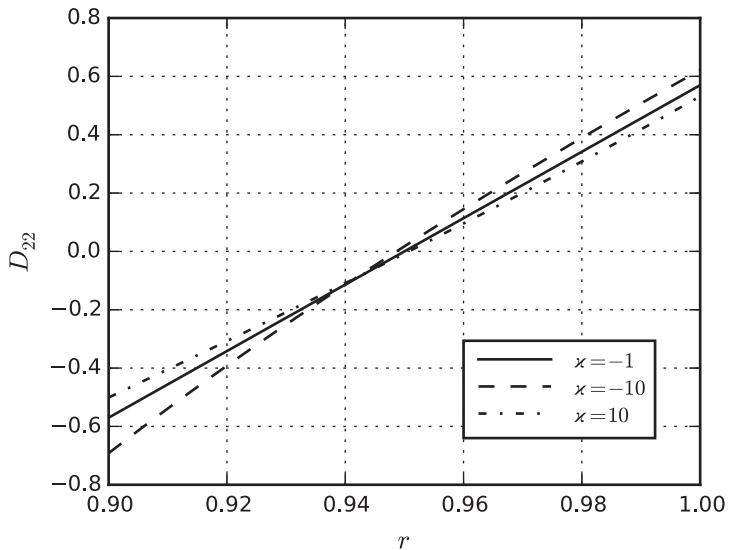


Fig. 22.7 Eigenstress D_{22} , $\eta = -1$, $\lambda = 1$.

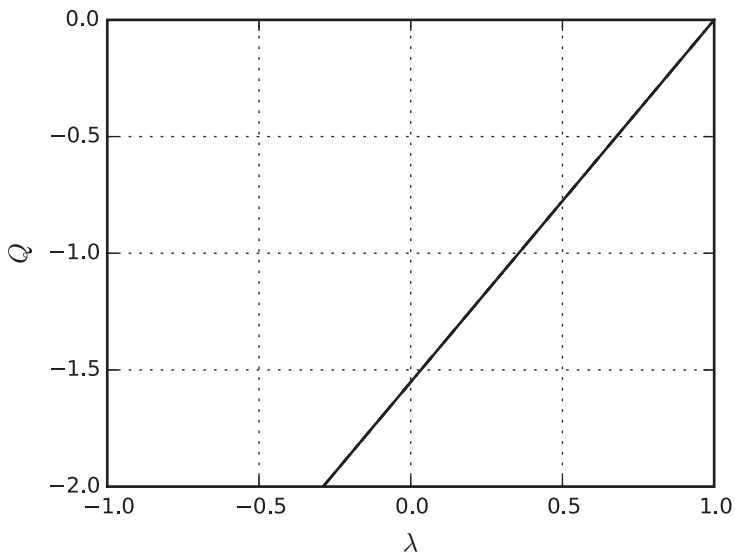


Fig. 22.8 Dependence of longitudinal force Q on parameter λ , $\eta = 1$.

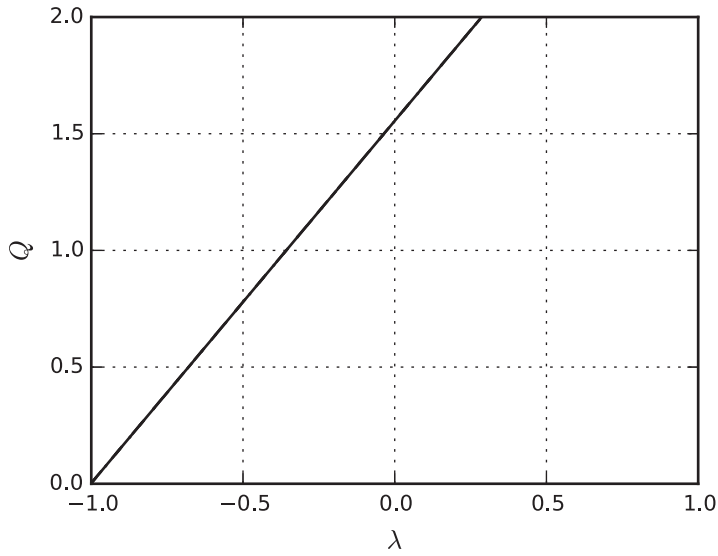


Fig. 22.9 Dependence of longitudinal force Q on parameter λ , $\eta = -1$.

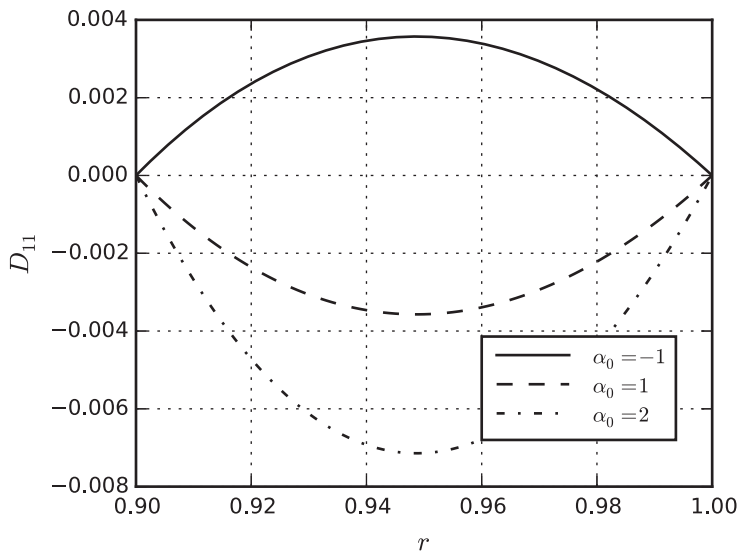


Fig. 22.10 Eigenstress D_{11} , $\eta = 1$, $\lambda = 1$, $\alpha = -1$ for different α_0 .

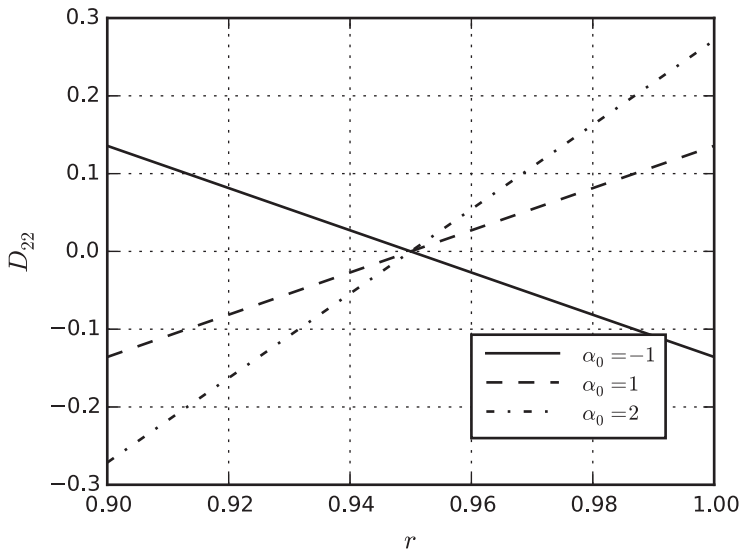


Fig. 22.11 Eigenstress D_{22} , $\eta = 1$, $\lambda = 1$, $\varkappa = -1$ for different α_0 .

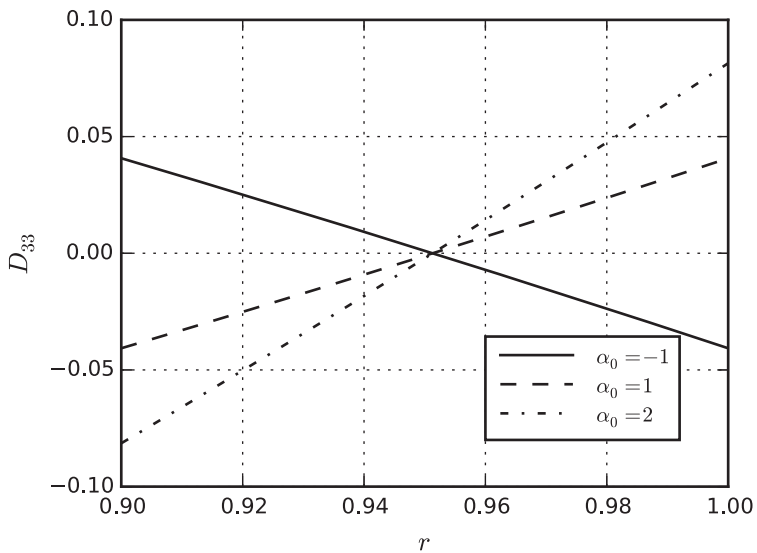


Fig. 22.12 Eigenstress D_{33} , $\eta = 1$, $\lambda = 1$, $\varkappa = -1$ for different α_0 .

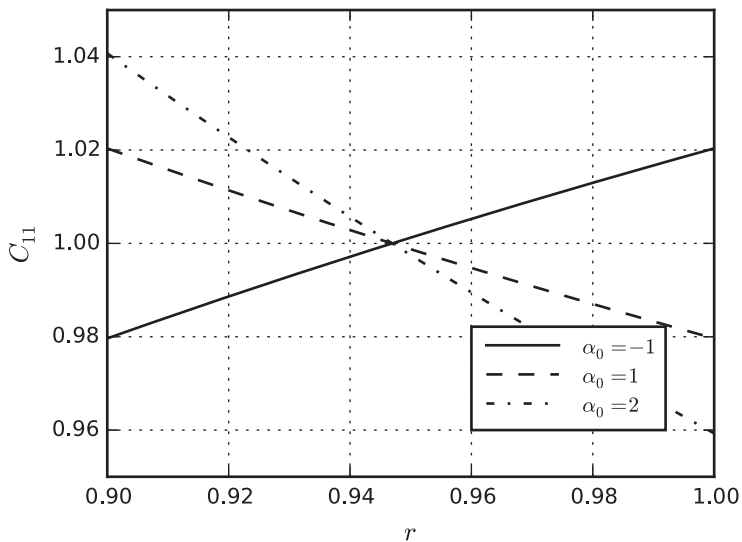


Fig. 22.13 Distortion C_{11} , $\eta = 1$, $\lambda = 1$, $\varkappa = -1$ for different α_0 .

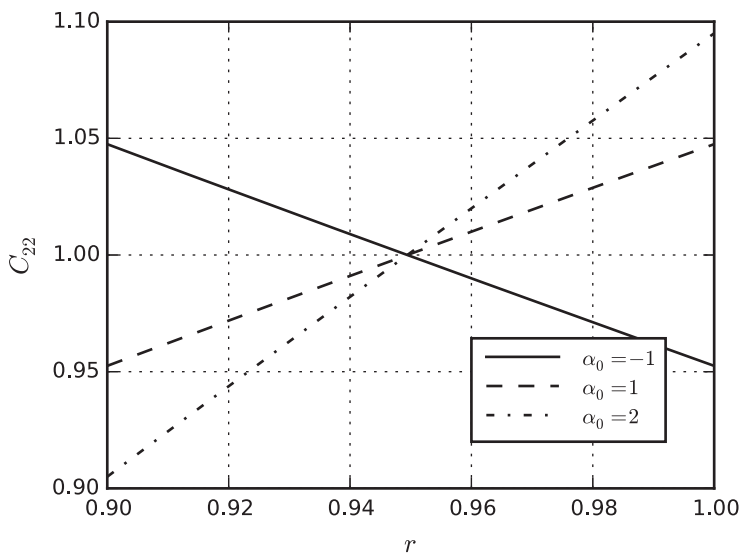


Fig. 22.14 Distortion C_{22} , $\eta = 1$, $\lambda = 1$, $\varkappa = -1$ for different α_0 .

22.6 Conclusion

In this work, we have solved the problem of large deformations of an elastic hollow cylinder made of a micropolar material, taking into account distributed dislocations. The stress state due to external and internal hydrostatic pressures is investigated, that is, the generalized Lamé problem is considered. The dislocations in the cylinder were assumed to be continuously distributed. The dislocation density tensor described the distribution of screw and edge dislocations, for which it was shown that the scalar densities of edge dislocations, as well as screw dislocations of the axial direction, can be arbitrary, including the Dirac delta function.

When solving the problem, we used a property of isotropy of the material. It is proved that for any isotropic micropolar material at the considered deformation of the cylinder, the nonzero components of the Piola-type stress tensors depend only on the radial coordinate, and the zero components are the same as for the distortion tensor. A system of equations describing equilibrium of a micropolar elastic body with distributed dislocations consists of balance equations for forces and moments, an incompatibility equation, constitutive equations, and geometric relations. The unknown functions are distortion and microrotation tensor fields. Under the assumption that the material is isotropic, the problem is reduced to a system of nonlinear ordinary differential equations.

An exact solution for a physically linear micropolar continuum and an axisymmetric distribution of edge dislocations is found.

Acknowledgements The reported study was funded by the Russian Foundation of Basic Research, project number 19-31-90045.

References

- Aero J, Kuvshinskij E (1961) Fundamental equations of the theory of elastic media with rotationally interacted particles. *Sov Phys SolidState* 2(7):1272–1281
- Altenbach J, Altenbach H, Eremeyev VA (2010) On generalized Cosserat-type theories of plates and shells: a short review and bibliography. *Archive of Applied Mechanics* 80(1):73–92
- Chróścielewski J, Makowski J, Pietraszkiewicz W (2004) Statyka i dynamika powłok wielopłatkowych. Nieliniowa teoria i metoda elementów skończonych (In Polish). Wydawnictwo IPPT PAN, Warszawa
- De Wit R (1977) *Continual Theory of Disclinations* (in Russian). Mir, Moscow
- Eremeyev VA, Zubov LM (2008) *Mechanics of elastic shells* (In Russian). Nauka, Moscow
- Eremeyev VA, Cloud MJ, Lebedev LP (2018) *Applications of Tensor Analysis in Continuum Mechanics*. World Scientific, New Jersey
- Eringen A (1999) *Microcontinuum Fields Theories. I. Foundations and Solids*. Springer, New York
- Lakes RS (1995) Experimental methods for study of cosserat elastic solids and other generalized continua. In: Mühlhaus HB (ed) *Continuum Models for Materials with Microstructure*, 6, Wiley, N.Y., pp 1–22
- Libai A, Simmonds JG (1998) *The Nonlinear Theory of Elastic Shells*, 2 edn. Cambridge University Press

- Nikitin E, Zubov L (1998) Conservation laws and conjugate solutions in the elasticity of simple materials and materials with couple stress. *J Elast* 51(1):1–22
- Nowacki W (1986) *Theory of Asymmetric Elasticity*. Pergamon Press, Oxford
- Pal'mov V (1964) Fundamental equations of the theory of asymmetric elasticity. *J Appl Math Mech* 28(6):1341–1345
- Pietraszkiewicz W, Eremeyev V (2009) On natural strain measures of the non-linear micropolar continuum. *Int J Solids Struct* 46(34):774–787
- Shkutin L (1988) *Mechanics of Deformations of Flexible Bodies* (In Russian). Nauka, Novosibirsk
- Toupin R (1964) Theories of elasticity with couple-stress. *Arch Ration Mech Anal* 17(2):85–112
- Tovstik P, Smirnov AL, Steele C (2002) Asymptotic methods in the buckling theory of elastic shells. *Appl Mech Rev* 55
- Tovstik PE (1997) Axially symmetric deformation of thin shells of revolution made of a non-linearly elastic material. *PMM* 61(4):660–673
- Truesdell C, Noll W (1965) The non-linear field theories of mechanics. In: Flügge S (ed) *Handbuch der Physik*, vol 3, Springer, Berlin, pp 1–602
- Zelenina AA, Zubov LM (2017) Quasi-solid states of micropolar elastic bodies. *Doklady Physics* 62(1):30–33
- Zhilin PA (1976) Mechanics of deformable directed surfaces. *International Journal of Solids and Structures* 12(9–10):635–648
- Zubov LM (1997) *Nonlinear Theory of Dislocations and Disclinations in Elastic Bodies*. Springer, Berlin
- Zubov LM (2004) Continuously distributed dislocations and disclinations in nonlinearly elastic micropolar media. *Dokl Phys* 49(5):308–310
- Zubov LM (2011) The continuum theory of dislocations and disclinations in nonlinearly elastic micropolar media. *Mech Solids* 46(3):348–356
- Zubov LM (2017) Static-geometric analogy in the micropolar theory of elasticity. *Dokl Phys* 62(9):434–437
- Zubov LM (2020) Nonlinear deformations of an elastic sphere with couple stresses and distributed dislocations. *Advanced Struct Mater* 136:175–187
- Zubov LM, Karyakin MI (2006) *Tensor calculus* (in Russian). Vuzovskaya kniga, M.